Investigation on Wildfire Flashovers in The Mediterranean Climate Regions with Emphasis on VOCs Contributions

Rawaa Jamaladdeen

THESE

Pour l'obtention du Grade de

DOCTEUR DE L'ECOLE NATIONALE SUPERIEURE DE MECANIQUE ET D'AEROTECHNIQUE

(Diplôme National – Arrêté du 25 mai 2016 Modifié par l'Arrêté du 26 Août 2022)

Ecole Doctorale :

MIMME_ Mathématiques, Informatique, Matériaux, Mécanique, Energétique

Secteur de Recherche : Fluides, Thermique et Combustion

Présentée par:
Rawaa JAMALADDEEN

****

Investigation on Wildfire Flashovers in The Mediterranean Climate Regions with Emphasis on VOCs Contributions

****

Directeur de thèse : GARO Jean-Pierre

Co-directeur: WANG Hui Ying

Co-encadrant: COUDOUR Bruno

****

Soutenance prevue le le 22/12/2023

devant la Commission d'Examen

****

JURY

Président :
SANTONI Paul-Antoine, Professeur, Université de Corse, Corte.
Rapporteurs :
CHETEHOUNA Khaled, Professeur, INSA Centre Val de Loire, Bourges.
MITRI George, Full Professor, University of Balamand, Koura, Liban.
Membres du jury :
LEMEE Laurent, Ingénieur de Recherche (HDR), IC2MP, Université de Poitiers.
B. COUDOUR, Maître de Conférences, Université de Poitiers.
DEDALDECHAMP Fabienne, Maître de Conférences (HDR), Université de Poitiers.
GARO Jean-Pierre, Professeur, Université de Poitiers.
SANTONI Paul-Antoine, Professeur, Université de Corse, Corte.
WANG Hui-Ying, Directeur de Recherche CNRS, Institut P', Poitiers.

Dedication

This thesis is dedicated to the soul of my gone mother. For all the love, support, and sacrifice you have embellished my life with. Without your continuous encouragement I would never have been able to complete this thesis. I hope I made you proud. Till we meet again, I miss you and I love you endlessly.

Acknowledgements

I would like to acknowledge and give my warmest thanks to my supervisors, Pr. Jean Pierre GARO, Dir. Hui Ying WANG, and Dr. Bruno COUDOUR who made this work possible. Thank you for your patience, your understanding, and support through all the stages of this thesis.

I am indebted to my father Hamada, my brothers Ali and Adnan, my sister Rola, my uncle Ahmad JAMAL EDDINE, and my dearest friend Lahna ACHERAR. Your constant support, guidance, and encouragement have been invaluable throughout the entire process.

I would also like to thank my committee members for their efforts, comments, and suggestions, to make this thesis more professional and concrete. The remarkable participation of Pr. Khaled CHETEHOUNA, and Pr. Paul-Antoine SANTONI is an added value to any PhD dissertation due to their outstanding contribution in the scientific research and academic fields. A special thanks to Pr. George MITRI from Lebanon for taking the time and effort to become a valuable member of the jury. Many thanks to Dr. Christelle ROUDAUT, and Dr. Fabienne DEDALDECHAMP for their appreciated collaboration, your insights have greatly enriched the quality of my work. Last but not least, a special thanks and deepest gratitude to Eng. Laurent LEMEE for generously sharing his extensive academic knowledge and expertise, and for playing a pivotal role in helping me in the experimental work of this thesis, and improving my analytical skills. I am also thankful for his significant contributions to my publications during my PhD.

I am grateful to the staff and administration of ENSMA for their valuable support, especially to its former director Pr. Denis LEMONNIER for granting me a partial fund for my PhD thesis. A big thanks is also to the director of the doctoral school, Pr. Damien HALM, who has never saved an effort to support all the doctoral students in ENSMA and respond to all their concerns with the most professional yet friendly attitude, confirming once again his persistent dedication and honorable suitability to his position.

Finally, this work is inspired by the original work and acheivements of Richard C. ROTHERMEL who produced a 50-year milestone for the prediction of fire spread in wildland fuels since 1972. Although the ensuing years have brought many technological innovations, Rothermel fire-spread model is still the engine of the predictive tools used by fire behavior investigators today. As Gail WELLS once said, “The Rothermel fire-spread model is still running like a champ”.

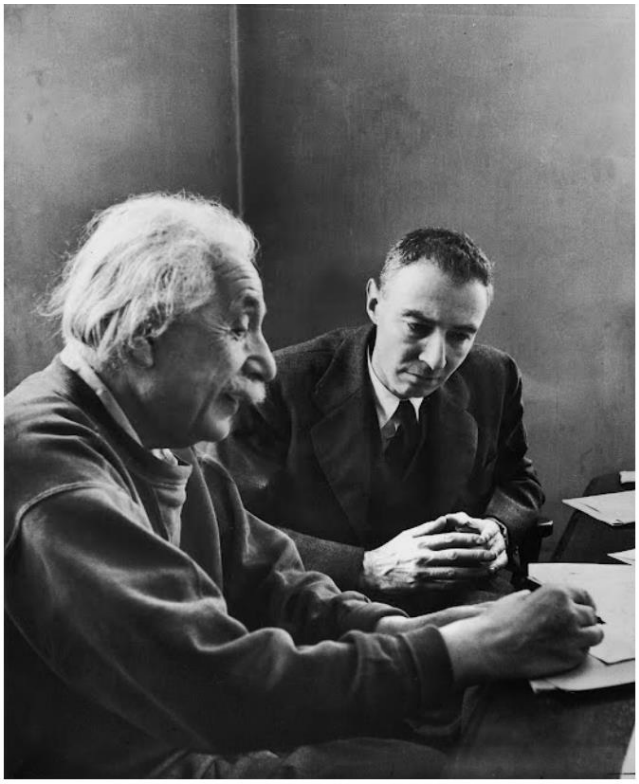

Look deep into nature, and then you will understand everything better –

Albert Einstein

Le monde est dangereux à vivre ! Non pas tant à cause de ceux qui font le mal, mais à cause de ceux qui regardent et laissent faire –

Albert Einstein

Abstract

Requests from the firefighting communities are increasing urging the scientific communities to create operational protective and preventive tools that help them understand extreme wildfire behaviors considering not only the atmospheric conditions but also topography, and vegetation characteristics. Thus, our objective was to provide answers to such requests by investigating the probable factors responsible for intensifying wildfire regimes to flashovers using numerical, and thermobiochemical experimental approaches. The numerical model is a gas dispersion model validating experimental data from wind tunnel tests to resolve the controversy of whether or not the volatile organic compounds (VOCs) accumulations in confined topographies end up inducing wildfire flashovers. It comprises a propagating fire front calculated using the Rothermel semi-empirical steady-state surface fire model, and Van Wagner transition to crown fire behavior criteria, with an integrated unsteady rate of VOC emissions simulating the ones evolving from the vegetation burning in the firefront. To synchronize our work with field input, thermochemical experiments were conducted on various Mediterranean vegetation species to examine their VOC emission rates in normal and stressful environmental conditions as they may end up defining different flammability scenarios in wildfires. First, two Mediterranean shrub species: Cistus albidus and Rosmarinus officinalis are explored for their VOC emissions and physiological changes after being subjected to abiotic stresses (drought and heat), using pyrolysis-gas chromatography and mass spectrometry (Py-GC/MS) analyses. Two other Mediterranean forest species: Quercus suber L. and Cupressus sempervirens horizontalis L. were investigated for their distinctive flammability characteristics using thermo-gravimetric and differential thermal analyses (TG/DTA), coupled with Py-GC/MS analysis to identify the gases emitted during the exo-thermic peaks. This step aims to better understand the flammability descriptors of these species as a part of a more efficient forest management strategy by which, favoring the plantation of certain lesser flammable species in silviculture measures may protect other more flammable but economically valuable species, from the dangers of wildfires and their extreme behaviors. Mediterranean vegetation species are important VOC emitters especially when provoked by external stresses during wildfires however, some biogenic VOCs (BVOCs), more particularly sesquiterpenes, are still not thoroughly covered for their flammability characteristics, such as their lower and upper flammability limits, auto-ignition temperatures, flashpoints, etc. Such a scientific lack we found it necessary to enrich by studying the flammability limits of β-Caryophyllene, one of the most important sesquiterpenes emitted from Mediterranean vegetation. Preliminary tests for measuring the vapor pressures of β-Caryophyllene are conducted in preparation for experimenting its flammability limits in a spherical bomb as future plans. The work in this thesis should be considered as the first step in a more global approach that should provide operational firefighting staff, with a comprehensive decision-making tool capable of shaping their forest management strategies from wildfire characteristics themselves and protecting wildlands and firefighters equally from the dangers and extreme behaviors of wildfire flashovers.

Key words:

Adsorption, wood distillation, cellulose--effect of fires on, oak, chemisorption, cistaceae, volatile organic compounds, cypress, fire testing, forest fires--prevention and control, pyrolysis, rosmarinus, sesquiterpenes--flammability.

Résumé

Cette thèse apporte des réponses aux demandes de la communauté des pompiers d'étudier les facteurs probables responsables de l'intensification des régimes de feux de forêt jusqu'aux flashovers en utilisant des approches expérimentales numériques et thermochimiques. Le modèle numérique est un modèle de dispersion de gaz validant les données expérimentales des essais en soufflerie pour résoudre la controverse quant à savoir si les accumulations de composés organiques volatils (COV) dans des topographies confinées finissent par induire des incendies de forêt. Il comprend un front de feu se propageant calculé à l'aide du modèle semi-empirique de feu de surface en régime permanent de Rothermel et de la transition de Van Wagner vers les critères de comportement des feux de cime, avec un taux instable intégré d'émissions de COV simulant ceux évoluant à partir de la combustion de la végétation dans le front de feu. Pour synchroniser nos travaux avec les données de terrain, des expériences thermochimiques ont été menées sur diverses espèces de végétation méditerranéenne afin d'examiner leurs taux d'émission de COV dans des conditions environnementales normales et stressantes, car elles pourraient finir par définir différents scénarios d'inflammabilité lors d'incendies de forêt. Premièrement, deux espèces d'arbustes méditerranéens : Cistus albidus et Rosmarinus officinalis sont explorées pour leurs émissions de COV et leurs changements physiologiques après avoir été soumises à des stress abiotiques (sécheresse et chaleur), à l'aide d'analyses par chromatographie en phase gazeuse par pyrolyse et par spectrométrie de masse (Py-GC/MS). Deux autres espèces forestières méditerranéennes : Quercus suber L. et Cupressus sempervirens horizontalis L. ont été étudiées pour leurs caractéristiques d'inflammabilité distinctives à l'aide d'analyses thermogravimétriques et thermiques différentielles (TG/DTA), couplées à une analyse Py-GC/MS pour identifier les gaz émis. lors des pics exothermiques. Cette étape vise à mieux comprendre les descripteurs d'inflammabilité de ces espèces dans le cadre d'une stratégie de gestion forestière plus efficace par laquelle, en favorisant la plantation de certaines espèces moins inflammables dans les mesures sylvicoles, on pourrait protéger d'autres espèces plus inflammables mais économiquement précieuses, des dangers des incendies de forêt et leurs comportements extrêmes. Les espèces de la végétation méditerranéenne sont d'importants émetteurs de COV, en particulier lorsqu'ils sont provoqués par des stress externes lors d'incendies de forêt. Cependant, certains COV biogènes (COBV), plus particulièrement les sesquiterpènes, ne sont pas encore complètement couverts pour leurs caractéristiques d'inflammabilité, telles que leurs limites inférieure et supérieure d'inflammabilité, leur auto-inflammation, températures, points d'éclair, etc. Une telle lacune scientifique qu'il a fallu enrichir en étudiant les limites d'inflammabilité du β-Caryophyllène, l'un des plus importants sesquiterpènes émis par la végétation méditerranéenne. Des tests préliminaires pour mesurer les pressions de vapeur du β-Caryophyllène sont menés en vue d'expérimenter ses limites d'inflammabilité dans une bombe sphérique comme plans futurs. Les travaux de cette thèse doivent être considérés comme la première étape d'une approche plus globale qui devrait fournir aux personnels opérationnels de lutte contre les incendies un outil d'aide à la décision complet, capable de façonner leurs stratégies de gestion forestière pour protéger les milieux naturels et les pompiers des dangers des comportements extrêmes des incendies de forêt.

Mots Clés :

Adsorption, bois--distillation, cellulose--effets du feu, chênes, chimisorption, cistacées**,** composés organiques volatils/ volatile organic compounds**,** cyprès, dépolymérisation réductrice**,** essais de comportement au feu**,** forêts--incendies--lutte contre, pyrolyse, rosmarinus**,** sesquiterpènes—inflammabilité.

Table of Contents

***

List of Figures

***

List of Tables

****

Nomenclature

Abbreviations

BVOCs	Biogenic Volatile Organic Compounds
CBD	Canopy Bulk Density
CBH	Crown Base Height
DFMC	Dead Fuel Moisture Content
DMAPP	Dimethylallyl Diphosphate
DTA/TGA	Differential Thermal Analysis/Thermogravimetric Analysis
ER	Emission Ratio
FAO	Food and Agriculture Organization
FMC	Fuel Moisture Content
GHG	Green-House Gas
GLV	Green Leaf Volatiles
IPCC	Intergovernmental Panel on Climate Change
IPP	Isopentenyl diphosphate
LDMC	Leaf Dry Matter Content
LFL	Lower Flammability Limit
MCE	Modified Combustion Efficiency
MCR	Mediterranean Climate Region
MT	Monoterpenes
MTC	Mediterranean Type Climate
NFPA	National Fire Protection Association
NMBVOC	Non-Methane Biogenic Volatile Organic Compounds
Py-GC/MS	Pyrolysis-Gas Chromotography/Mass Spectrometry
R'	Non-Dimensional Rate of Spread of the Fire Front
SAV	Surface Area to Volume Ratio
SH	Stand Height
SLA	Specific Leaf Area
ST	Sesquiterpenes
UFL	Upper Flammability Limit
UWI	Urban-Wildland Interface
VOCs	Volatile Organic Compounds

Latin Symbols

Q_{ig}^{*}	Heat absorbed by a volume of fuelbed	$Btu.ft^{-3}$ or $W.h.m^{-3}$
c_{pf}	Fuel bed specific heat capacity	$kJ.kg^{-1}.\ K^{-1}$
E	Activation energy	$kJ.mol^{-1}$
EF	Emission Factor	$g.kg^{-1}$
Gw	stomatal conductance	$mmolH_2O.\ m^{-2}.\ s^{-1}$
h	Heat content of fuel	$Btu.lb^{-1}$ or $MJ.\ kg^{-1}$
h_c	Convective heat transfer coefficient	$W.m^{-2}.\ K^{-1}$
h_{vap}	Enthalpy of vaporization	$kJ.mol^{-1}$
I	Fireline intensity	$kW.m^{-1}$
K	Turbulence kinetic energy	$m^2.s^{-2}$
K_0	frequency factor	s^{-1}
K_b	Ember temperature	Kelvin °C

K_b	Thermal conductivity of ember	$W.m^{-1}.K^{-1}$
K_h	Henry's law constant	$Pa\ m^3\ mol^{-1}$
L_{fl}	Flame length	m
P_r	Prandtl number	-
Q_{ig}	Heat required to bring unit mas of fuel	$Btu.lb^{-1}$
R	Gas constant	$J.mol^{-1}.K^{-1}$
Re_D	Reynolds' number	-
ROS	Rate of Spread	$m.s^{-1}$
T_a	Ambient temperature	Kelvin, °C
T_{fl}	Flame temperature	Kelvin, °C
T_{fs}	Fuelbed surface temperature	Kelvin, °C
T_{ig}	Temperature of ignition	Kelvin
U	numerical horizontal wind velocity	$m.\ s^{-1}$
U_x	experimental horizontal wind velocity	$m.\ s^{-1}$
U_z	experimental vertical wind velocity	$m.\ s^{-1}$
V	numerical vertical wind velocity	$m.\ s^{-1}$

Greek Symbols

σ	Stefan Boltzman constant	$W.m^{-2}.K^{-4}$
ε	Kinetic energy dissipation rate	$kg.m^2.s^{-3}$
σ	Surface area to volume ratio	ft^{-1} or m^{-1}
ε_{fl}	flame emissivity	
α_w	Flame tilt angle due to wind	
$\sigma_{x,\,z}$	standard deviation	
a	Heating rate	$K.min^{-1}$ or $°C.min^{-1}$
Φ	Equivalence ratio	
δ	Fuel depth	m or ft
β	Fuelbed packing ratio	
ξ	Propagating flux ratio	
α	Valley angle	
θ	Flame tilt angle	
ρ	Density	$kg.m^{-3}$
ρ_f	Fuel particle density	$kg.m^{-3}$
τ_R	Flame residence Time	min
Ω_s	Slope angle	
μ	Air molecular viscosity	$kg.m^{-1}.s^{-1}$

General Introduction

Wildfires are one of the main natural hazards facing humans, ecology, environment, and socioeconomics worldwide. In certain countries and certain regions, such as the ones characterized by Mediterranean climate, it is even the most significant natural risk to vegetation lands mainly dense forests, which are hard to recover in the long term and often face irreversible damage. Despite the considerable efforts deployed in prevention and extinction actions, large wildfires with extreme behaviors remain recurring events. These behaviors produce outrageous fires bursting out of control and threatening not only the lives of the firefighters but also large sections of the population especially since the interaction between forests, infrastructure, and homes is growing rapidly in the Mediterranean regions. This thesis is divided into 5 parts with a common objective: to investigate the causes and to evaluate the contributing factors of a common phenomenon of extreme wildfire behaviors, wildfire flashovers. The thesis manuscript will begin by presenting an overview of wildfires, their causes, their heat transfer mechanisms, their phases, and some statistics about their distributions worldwide with emphasis on the Mediterranean climate regions. Then, it's structured and outlined in five chapters, as follows:

In Chapter I, a literature review addresses the behavior of wildfires in Mediterranean-type climate (MTC) regions, the know-how, and their effects on vegetation structures and distribution. Information is also provided on the Mediterranean climate vegetation diversity and their BVOC synthesis in response to environmental stressors. The quantification of volatile emissions is also expressed in relationship to vegetation thermal degradation under fire heat stressors. Finally, the extreme fire behaviors of wildfires are described and explained to be further investigated in detail in the following chapters as part of our aims to provide information to decision tools of the firefighting communities.

In Chapter II, we present a numerical approach to trace the dispersion of wildfire front gases in a porous forest incorporating valleys with different internal angles. This chapter makes use of the data provided in Chapter I about the fire phases and emission factors of the corresponding VOC emissions, and former experimental results confirming gas accumulation inside confined topographies. Rothermel mathematical formulations are used to calculate a steady state propagating firefront combined with an unsteady VOC emission profile to investigate the controversial debate on whether VOC emissions from vegetation in wildfires are direct contributors to wildfire flashovers in confined topographies.

After investigating the role of VOC emissions in provoking wildfire flashovers, it is important to investigate more about VOCs and how they are linked to vegetation flammability. Continuing to provide information for decision tools to firefighting and forest management communities, Chapter III addresses the possibility of using certain forest species in silviculture measures to protect other endangered and valuable forest species from devastating wildfires and flashovers. To this end, the flammability characteristics of two Mediterranean forest species, Cupressus sempervirens L. and Quercus suber L. are investigated using thermogravimetric and differential thermal analyses (TGA/DTA). Their flammability is further linked to their volatile contents and emission rates under thermal stresses using pyrolysis-gas chromatography and mass spectrometry analysis (Py-GC/MS). These emissions are categorized by source, i.e., from holocellulose or lignin degradation. We will also investigate the presence or absence of volatile

reserves in coniferous and deciduous species and how such characteristics affect vegetation flammability.

In Chapter IV, we will address the effect of the environmental stresses on two Mediterranean shrub species that have been involved in wildfire flashovers; Rosmarinus officinalis and Cistus albidus. The most threatening environmental stresses in the Mediterranean climate regions are prolonged droughts and high temperatures, would these stresses affect the VOC reserves and emissions of the vegetation, and consequently their flammability descriptors? These concerns will be addressed with experimental conduct on the two species.

Sesquiterpenes' flammabilities are rarely addressed in literature. After concluding from the previous chapters, the importance of sesquiterpenes' reserves and emission rates in Mediterranean vegetation, and their influence to the intrinsic flammability of vegetation, the last chapter of this thesis, chapter V, addresses the flammability limits of one of the main sesquiterpenes emitted by common Mediterranean vegetation species: β-caryophyllene. The vapor pressure of β-caryophyllene is investigated numerically and experimentally at different temperatures as part of the experimental prospects to measure its flammability limits in a spherical bomb. We end this thesis by giving our general conclusions and prospects.

Wildfires: An Overview

****

1 Wildfires

Wildfires, also referred to as wildland fires or rural fires, are unpredicted forms of fires that burst wildly in combustible vegetation complexes and landscapes and become hard to be controlled by conventional fire extinguishing methods (Krawchuk et al. 2009, Bowman et al. 2011). Vegetation complexes are parts of earth's ecosystems and they form the main energy drives of wildfires. In fact, wildfires are classified as ground, surface or crown fires according to the type of vegetation complexes they consume (Wane et al. 2009). These last are classified into; forests with tree stands, shrub and bush fields, grasslands, peatlands, litter (timber and dead leaves), and logging slash. Ground fires consume the parts of the plants that are embedded in soils such as roots which may smolder for long periods of time, rarely the conditions favor their evolvement to surface fires. Most wildfires begin with surface fires. Surface fires consume mainly litter, shrubs and small plants growing just above ground. Upon meeting certain criteria surface fires may initiate forest crown fires consuming tree stand canopies in active, passive or independent behaviors (Alexander and Cruz 2010).

In many regions of the world, in fact, wildfires are becoming increasingly frequent and violent (Camia et al. 2013; Sharples et al. 2016). However, it seems that beyond certain environmental conditions, the characterization tradition of wildfires and their behavior is no longer relevant and a new strategy must prevail. First it is essential to understand that there are three factors forming the triangle of fire; fuel, heat, and oxygen (Figure I.1). Eliminate any of these last and fire flame will no longer ignite nor persist.

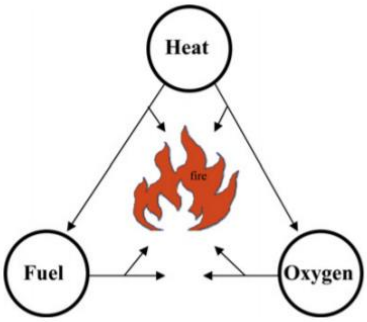

Figure I.1. The classical fire triangle. **(**Innes et al. 2011**).**

In a wildfire the components of the fire triangle are interpreted as follows: fuel is the vegetation complex with a certain spatial arrangement and chemical content that favor combustion, and is characterized by a percentage of moisture content (%), surface area to volume ratio (m^{-1}), load (kg/m^2), and total thickness (m). Heat, the fire ignition and sustainable energy source, can be in the form of a flame, a spark, or heat flux. The last component, oxygen, which is abundant at 21% in atmospheric air, works as an oxidizing agent for the combustion reaction which only needs 16%. Fire will burn as long as the three components are available, in fact, fire extinguishing operations are based on removing one of these components to suppress a wildfire. However, further fire research has added a fourth component to the fire triangle, an uninhibited chemical chain reaction. Fire is described as a rapid oxidation exothermic reaction where fuel works as the reducing agent and oxygen as the oxidizing agent. Part of the heat released from the combustion reaction is responsible for fire spread in a self-sustaining mechanism. When the

fuel burns or heats it produces flammable vapors which in turn combust and release more heat to the nearby fuel enough to remove its moisture content, release its share of combustible vapors, and raise its temperature to ignition temperature. Therefore; the chain reaction is described by the continuous supply of combustible vapors evolving from the heated fuel to the flame front. With this fourth component added, the fire triangle can now be more accurately represented by a tetrahedron (Figure I.2).

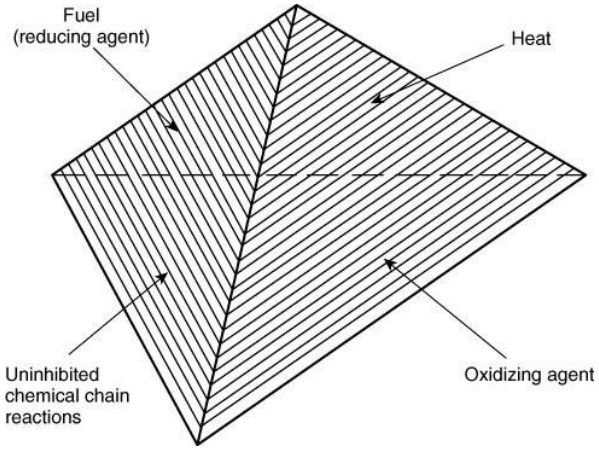

Figure I.2. Fire tetrahedron with uninhibited chemical chain reaction. (National Fire Protection Association).

1.1 Wildfires Ignition Sources

Wildfires ignition causes should be differentiated from wildfire spread causes, by which these last are going to be discussed in a later section. Wildfire ignitors are hard to be identified mostly due to lack of skilled personnel, logistics, or for reasons of evasions from judicial responsibility. Uncertainties in identifying the ignitors classify causes as unknown, certain or known but uncertain (Camia et al. 2014). Research on wildfire occurrences had been largely undertaken on spatial and temporal scales in order to better understand and predict the factors influencing ignitions (Pulcinski 2012). Oxygen and dry vegetation (fuel) always exist in nature, making them natural unremitting factors to wildfires ignitions (Pausas and Keeley 2009). However, the heat source is what classifies the wildfire into a naturally occurring or a human-caused wildfire (direct and indirect).

1.2 Natural Causes of Wildfires:

Wildfires caused by natural events exclude any direct or indirect human intervention and they are identified as follows:

1.2.1 Lightning

Dry lightning strikes that are accompanied by little to no rainfalls in stormy weather are the most probable natural causes of wildfires. Indeed, biomass fuel of critical load and moisture content located at high elevation sites will be at higher risks to be ignited by lightning strikes (Muller et al. 2013; Nash and Johnson 1996). Although the probabilities of wildfires igniting by lightning strikes are less than those igniting by human activities; however, underestimating them will undervalue the risk assessment studies of wildfires occurrences. For instance, the causes of 80% of the total areas burned by naturally ignited wildfires in northern Canada are attributed to lightning strikes (Stocks et al. 2003). What's more, lightning fires that occurred in

cerrado vegetation of the Brazilian forests (Figure I.3), formed 91% of the 45 fire events registered from June 1995 to May 1999 (Pevillo 2011).

Figure I.3. Wildfire in cerrado vegetation, in Brazil. **(**Pevillo 2011**)**

1.2.2 Volcanic Eruptions and Meteorite Strikes

The recorded ignitions of wildfires caused by volcanoes are rare especially that they are linked to active volcanic eruptions. For example, in Chile volcanic fires account for about 1% of wildfires (Úbeda and Sarricolea 2016). On the other hand, only one large wildfire was recorded due to a meteorite strike in Russia, in 1908 (FAO 1999).

1.2.3 Natural Gas Emissions

Peatlands, the forgotten fossil fuels, are major storage pools of one-third of sequestered soils carbon but also a primary source of vegetation greenhouse gas emissions such as methane, which has a lower flammability limit (LFL) of 4.4%, (Cashdollar et al. 2000). The drainage of these peat bogs due to warmer atmospheric temperatures or excessive exploitation of groundwaters, increases their methane emissions and consequently enhances their rank as wildfires' natural stimulants (Furukawa et al. 2005). Luckily, they do not occupy a large land cover and are mostly located in northern hemisphere countries as Greenland and Siberia (Ucla 2006).

1.3 Human Causes of Wildfires

Humans caused the largest percentages of recorded wildfires around the globe with a total of 95% (Camia et al. 2010), above 85% in the Mediterranean regions (Keeley et al. 2012) and 85% in the US alone (Wildfire Management Information, WFMI, 2000-2017). The human impact may be direct through acts of vandalism or negligence, or indirect by global warming and the random expansion of the urban-wildland interface (UWI) where residential communities intermingle with wildland vegetation.

1.3.1 Direct Human Causes

Wildfires were deliberately ignited (arson) mostly in the Mediterranean basin regions (Figure I.4a), US, and Australia (Figure I.4b) compared to central and Northern Europe (Figure I.4c), Canada, and New Zealand (Figure I.4d), respectively (Ganteaume & Syphard 2018). Negligence also accounts for a big percentage of human-caused wildfires. For example, by far, fire has been used by indigenous people of the Amazonian forests in Brazil (Pevillo 2011), the USA, Australia, and many countries of the Mediterranean regions (FAO 1990), as a land management tool, for purposes of transforming forests into agricultural lands and grasslands

for livestock, or even for wildfire research by prescribed burning (Bonora et al. 2002). The absence of professional planned monitoring of such activities surely results in uncontrolled wildfire spread accidents. Negligence acts in modern countries are most probably referred to leisure or recreational activities, powerlines fall or equipment failures.

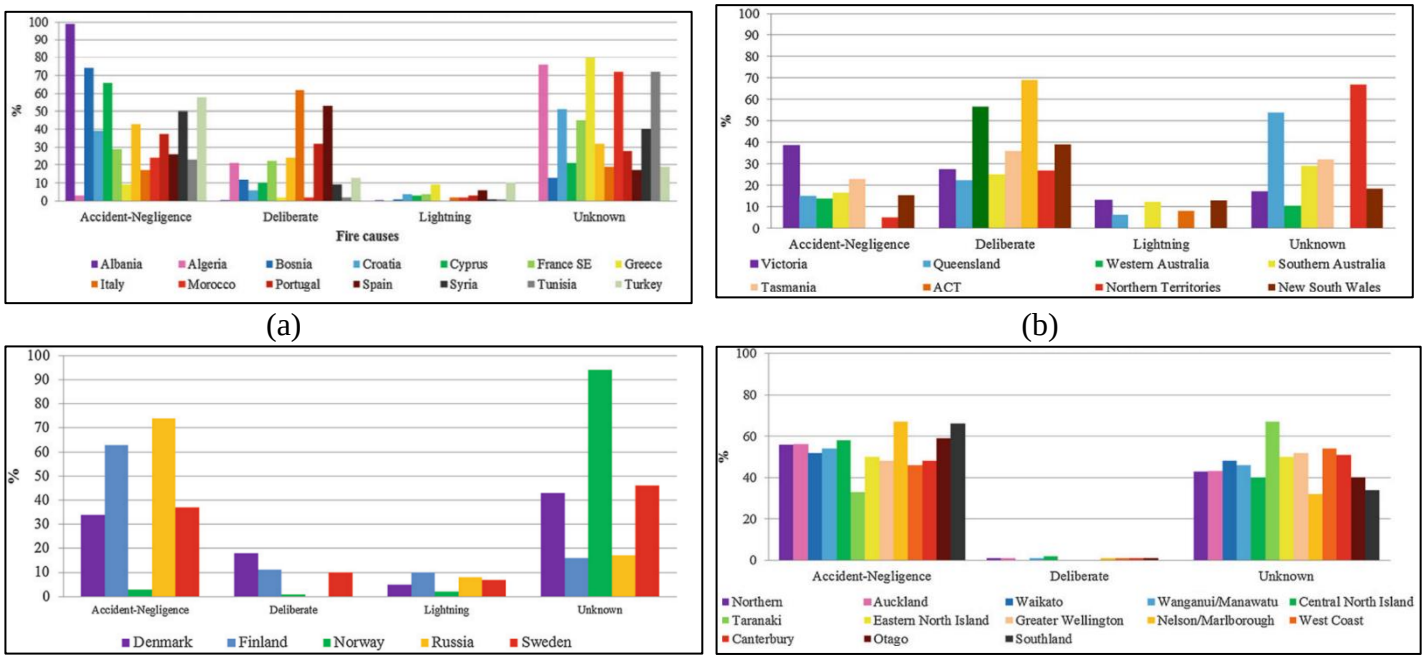

Figure I.4. Occurrence of fires due to natural, deliberate, accident-negligence and unknown causes in (a) Mediterranean basin, (b) Australia, (c) Northern Europe, (d) New Zealand. (Ganteaume & Syphard 2018).

1.3.2 Indirect Human Causes

1.3.2.1 Global warming

Anthropogenic factors like burning fossil fuels, deforestation, releasing chemical emissions from heavy industrial facilities, and farming livestock have increased the emissions of greenhouse gases into the atmosphere and aggravated the global warming problem. Based on the intergovernmental data on climate change (IPCC, 2013), global warming has created conductive conditions to wildfires, such as, raising the average temperature of Earth and increasing the frequency and severity of heatwaves and drought periods. For example, during the 20th century, the mean temperature of Earth has increased by 0.4 - 0.8 °C (Viola et al. 2010). In the Amazonia, the effect of drought on the frequencies of wildfires started emerging in the 90's (Abatzoglou et al. 2019). Such effect was reflected by the decrease in the frequencies of deforestation as nature has already been doing the job since 2000, (Aragao et al. 2018). Climate change has imposed favorable fire weather conditions translated in increased burned areas especially in warm periods in the Mediterranean basin and Southern Europe (Abatzoglou et al. 2019, Parente et al. 2019), as well as in the Western US and Canada (Williams et al. 2019), and finally Siberia and Australia (Flannigan et al. 2013, Dowdy 2018). 1.5 °C to 3°C increase in earth temperature above pre-industrial levels will increase the wildfires burned areas in the Mediterranean climate regions, by 40% and 200%, respectively (Turco et al. 2014).

Diminishing anthropogenic greenhouse gases emissions to limit global warming to 2 °C above pre-industrial levels will reduce wildfires ignition risks around the globe. However, solar radiation management by stratospheric SO_2 injections must also be carefully considered in order to further reduce the warming to the safest level of 1.5°C (Burton et al. 2018).

1.3.2.2 Wildland-Urban Interface (WUI)

The wildland-urban interface (WUI) is the spatial zone where residential communities and wildland vegetation meet or interact (Radeloff et al. 2018). WUI term is now used exclusively in the context of wildland fire (Stewart et al. 2007) and lately modified to HUI (human-wildland interface), (Viegas et al. 2009). Indeed, human activities at these interfaces increase the risks of wildfires' ignition and put more human lives in danger. In the decade of the nineties, the west coast of the United States saw an increase in the size of wildfires by 11% and an increase in the number of houses impacted by these fires by 17% (Hammer et al. 2007). Every year, more than 50,000 wildland fires affect 500,000 hectares of wildland vegetation in the Mediterranean southern European countries where extensive WUIs exist (Lampin-Maillet et al. 2010). Over 90% of these fires were caused by human activities at these interfaces, mainly by agricultural practices, followed by 'negligence' and 'arson' (Camia et al 2013). There has been an excellent body of literature to identify and map WUI patterns and relate them to wildfire ignition risks in many countries such as France (Lampin-Maillet et al. 2010), Spain (Chas-Amil 2013), the United States (Radeloff et al. 2018), Canada (Hirsch & Fuglem 2006) and Australia (Kornakova & Glavovic 2018). To assess the components of wildfire ignition risks at the wildland-urban interfaces, these last were classified into 12 types according to the spatial density of the habitation sites (homes) and the surrounding vegetation (aggregation index), (Figure I.5).

In his study on WUI and wildfires risks (Lampin-Maillet et al. 2010) investigated the area located in the proximity of Marseille and Aix-en-Province in France and found that scattered and isolated WUI with low to high vegetation aggregation indices represented a high wildfire ignition density. Although wildfires spread may be limited in dense WUIs due to loss of connectivity in burnable vegetation however, their occurrences pose a significant effect on human lives, property, and infrastructure. Nevertheless, the cost of suppressing these fires will be about 10 times that of wildland fires (Hirsch and Fuglem 2006).

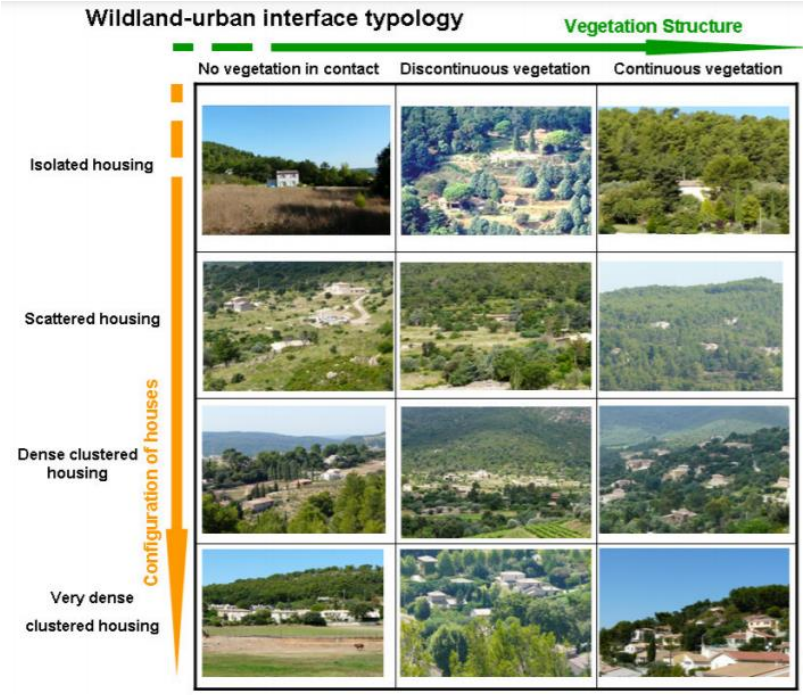

Figure I.5. Twelve types of wildland urban interfaces. (Lampin-Maillet et al. 2010).

2 Heat Transfer Mechanisms in Wildfires

A heat transfer is a process of energy exchange between two points in space occurring when a temperature difference exists between these two points. In wildfires, fire propagation is guaranteed when the fuel bed is heated to a point where its moisture content is evaporated and its temperature is raised to the temperature of ignition. The physical processes of heat transfer contributing to wildfire propagation are conduction, radiation and convection (Figure I.6).

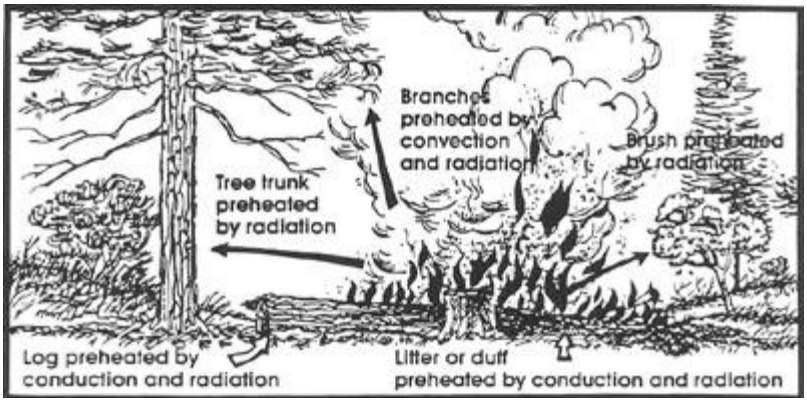

Figure I.6. Forms of heat transfer in wildfire, conduction, convection and radiation.

2.1 Energy Conservation

A wildfire starts as a surface fire consuming surface fuels and propagating with a surface rate of spread, ROS ($m.s^{-1}$) and fire line intensity I ($kW.m^{-1}$), (Byram 1959). Later and upon meeting certain criteria the surface fire transition into a crown fire (Reinhardt and Scott 2001). A successful fire rate of spread depends on an energy conservation equation stating that the latent and sensible heats required to evaporate the fuel moisture content and raise it to ignition temperature (T_{ig}), respectively, are equal to the sum of the conductive, convective and radiative

heat fluxes received by a fuel element in a forest fuel bed (Equation 2) (Koo et al 2005). Conduction is usually neglected in the energy equation, although it's considered in studies at plant scale level (see below, section 2.2), which leaves us with the surface and internal radiation and convection terms (Figure I.7).

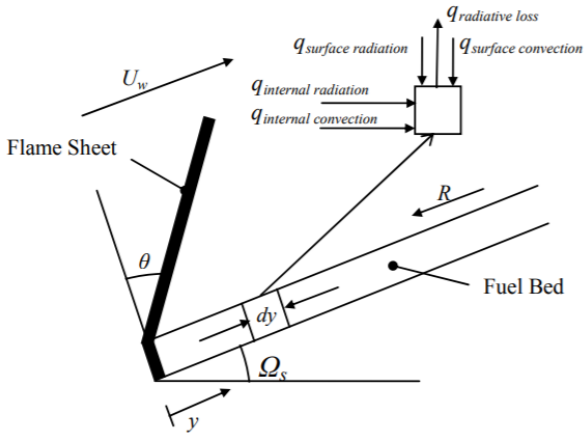

Figure I.7. Flame spread schematic in a fuel bed upslope. dy: fuel element length, Uw: wind velocity Ωs: slope angle, R: rate of spread, θ: flame tilt angle, fuel bed is assumed to be porous medium. (Koo et al 2005).

$q_{sensible} + q_{latent} = q_{sr}$ (surface radiation) + q_{ir} (internal radiation) + q_{rl} (radiative loss)

+ q_{sc} (surface convection) + q_{ic} (internal convection) *(2)*

$$q_{sensible} = \begin{cases} -\rho_f \, c_{pf} \, R \, \phi \, \dfrac{dT}{dy}, & at\ T \neq 373\ K \\ 0, & at\ T = 373\ K \end{cases}$$

$$q_{latent} = \begin{cases} \rho_f \, h_{vap} \, R \, \phi \, \dfrac{dM_w}{dy}, & at\ T = 373\ K \\ 0, & at\ T \neq 373\ K \end{cases}$$

Where,

ρ_f is the fuel particle density (kg.m^{-3}), c_{pf} is fuel bed specific heat capacity (kJ.kg^{-1}.K^{-1}), ϕ is the volume of solid fuel per unit fuel bed volume (i.e., packing ratio), T is the fuel temperature at y (K), h_{vap} is the specific enthalpy of change of water to vapor at 373K (kJ.mol^{-1}). (Koo et al 2005).

2.2 Conduction:

Conduction is the result of molecular agitation, itself linked to the constitution and temperature of the environment. It can therefore only occur in a medium material, whether solid, liquid or gas. The heat diffuses from the hot body to the cold body. In practice, conduction is usually

neglected in the propagation models of vegetation fires, with the exception of ground or peat bog (duff) fires, by which it is the preponderant process of heat transfer through the soil layers in the fire smoldering phase. The thermal properties that govern the conductive heat transfer in the soil vary according to its mineral composition, structure, the volume fractions of organic matter, mineral matter and water (Michaletz and Johnson 2007). On the other hand, conduction within the solid material in the fuel bed explains the differences in behavior between fuel elements depending on their thickness and thermal conductivity i.e. tree trunk or bole (bark, inner bark…), stems, needle, branches, …etc. Heat transfer from a forest fire into the tree bole occur through convection and radiation while heat transfer inside the bole is governed by conduction. Conductive heat transfers have been addressed in the physical and biophysical models in the literature. The physical models describe the process of heat transfer in an element of combustible plant material (stem) which is responsible for its pyrolysis and evolution of volatiles (Baranovskiy and Demikhova 2019) whereas the biophysical models describing tree mortality due to heat transfer inside the tree bole leading to vascular cambium necrosis (Michaletz and Johnson 2007).

2.3 Convection

Convection is heat transfer by macroscopic movements of a fluid (gas in the case of a fire) whose mass transports the heat that it contains. If the flow of the fluid is imposed, we speak of forced convection. On the other hand, if the movement is due to differences in density (density gradient) caused by differences in temperature (temperature gradient) creating buoyancy forces, we speak of free convection. In wildland fires, combustion produces hot gases which mix with ambient air which gets heated in turn. These hot gases are lighter and rise rapidly. They bring a lot of heat to the fuels above (crowns), dry them out and raise their temperature to the point of ignition. The wind, pushing the hot gases ahead of the flame front, even within the lower strata of the vegetation (internal convection), accelerates the spread of fire. In addition, moving gases often transport ignited materials ("Fire brands"), which can fall several hundred meters ahead of the fire and form a source of new fire outbreaks. The basic formula of convection is as described in (Equation 3).

$$q = h_c A (T_{fs} - T_a) \qquad (3)$$

Where,

q is the heat transferred per unit time (W), A is the heat transfer area of the surface (m^2), h_c is the convective heat transfer coefficient of the process ($W.m^{-2}.K^{-1}$) or ($W.m^{-2}.C^{-1}$), T_{fs} is the fuelbed surface temperature and T_a is the ambient temperature both in K or °C.

Slope and wind factors, among others, were taken into consideration when calculating the heat transfer terms for their significant effect on changing fire behavior. According to literature, a 10° increase in slope will increase the fire rate of spread (ROS) by two folds (Butler et al. 2007) while wind velocity will lead to flame tilt towards the fuel bed increasing by that the surface convective and radiative (view factor) effects in flat terrain, upslope and downslope heading fires (Figure I.8). The tilt angle (θ) in (Figure I.7) is the sum of the flame tilt angle due to wind

(α_w) and the slope angle (Ω_s). The flame tilt angle due to wind is calculated by (Butler et al. 2004) in (Equation 4).

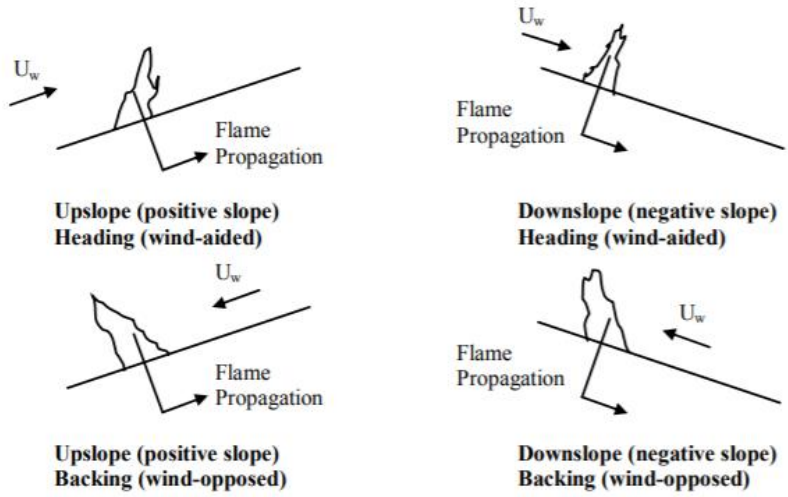

Figure I.8. Wind and slope configurations. (Koo et al. 2005)

$$tan^2\ \alpha_w\ = \frac{3\ U^2}{2gH} \qquad (4)$$

Where,

α_w is the flame tilt angle due to wind, U is usually referred to as the mean horizontal wind speed (m.s^{-1}) however, when willing to study the effect of the tilted flame on the unburned fuel bed, U will be the relative windspeed (U_{wind} − ROS), g is the acceleration due to gravity, and H is the flame length above the fuel bed (m), (Butler et al. 2004).

The flame is considered a permeable sheet where air passes through it. Convection from the flame with temperature (T_{fl}) to the fuel bed surface at distance y from the flame (T_y) is expressed in (Equation 5).

$$q_{surface\ convection} = \frac{0.565\ K_{fl} Re^{1/2} P_r{}^{1/2}}{y l_f} \left(T_{fl} - T(y)\right) e^{-0.3\frac{y}{L_{fl}}} \qquad (5)$$

Where,

K_{fl} is the thermal conductivity (W.m^{-1}. K^{-1}), Re is Reynolds number, P_r is Prandtl number, y is distance from the flame and l_f is the fuel bed thickness (both representing length scale), T_{fl} and $T(y)$ are the temperatures of the flame and fuel bed at distance y (K), respectively, and L_{fl} is the flame length (m).

2.3.1 Convection and Forest Porosity

Fuel beds can be considered as porous structures with the fuel elements (needles, branches, barks…etc.) considered as cylinders. (Koo et al. 2005) considered a fuel bed with big porosity such that a single cylinder will represent the convective heat transfers inside the fuel bed

calculated by (Equation 6). Noting that, the wind velocity inside the fuel bed is adapted to the inertial losses in the porous fuel bed.

$$q_{internal\ convection} = \frac{0.911 s K_b\ {Re_D}^{0.385} {P_r}^{1/3}}{D} (T_b - T(y)) e^{-0.25sy} \quad (6)$$

Where,

s is the total fuel-particle surface area per fuel bed volume (m^{-1}), K_b is the thermal conductivity of ember ($W.m^{-1}.K^{-1}$), Re_D is the Reynolds number (adapted to flow velocity inside fuel bed), Pr is Prandtl number, D is the branch diameter (length scale) (m), T_b and T_y are the temperatures (K) of the ember and a point in the fuel bed at distance y from the ember, respectively.

2.4 Radiation

Radiation is a mode of transfer of energy in the form of electromagnetic waves propagating with or without material support. Any object of which the absolute temperature is greater than 0 ° K, i.e. –273 ° C, emits electromagnetic radiation whose frequency is a function of this temperature. Thermal radiation can be characterized by the Stefan-Boltzman law (Equation 7), which states that the flux of energy emitted by a body (the emissive power) is proportional to the emissivity of the body and the forth power of the absolute temperature of the body's surface (Mechaletz et al. 2007). The radiant energy received from an emitter is proportionally absorbed and reflected by the recipient object depending on a view factor which depends on the geometries of the objects (emitter and recipient), and the distance separating them. (Howell and Mengüç 2011) provide a list of view factors for several geometries.

$$E_{fl} = \varepsilon_{fl} \sigma T_{fl}^4 \quad (7)$$

Where,

ε is the body emissivity (proportion of emissive power relative to a perfect emitter i.e., a black body), σ is Stefan Boltzman constant, and T_{fl} is the flame temperature.

The flame emissivity ε_{fl} is a function of gas and soot of wood fuel emissivity which can be calculated according to (Equation 8) with the flame mean beam length proportional to flame length (L_{fl}) and an effective total absorption coefficient of 0.6 m^{-1}, (Koo et al. 2005).

$$\varepsilon_{fl} = 1 - e^{-0.6 L_{fl}} \quad (8)$$

The surface radiation from the flame above the fuel bed to each point on the fuel bed surface is calculated in (Equation 9) and the internal radiation from the internal fire-fuel bed interface received by the unburned fuel inside the fuel bed is calculated as in (Equation 10). The radiant heat losses by the unburned fuel at the top surface of the fuel bed is calculated by (Equation 11). All the equations are referenced to (Koo et al. 2005).

$$q_{surface\ radiation} = \frac{a_{fb}\, E_{fl}}{2 l_f}\left(1 - \frac{Z}{(1+Z^2)^{\frac{1}{2}}}\right) \times \tanh^{-1}\left(\frac{2}{3}\left(\frac{w}{L_{fl}}\right)^{1/3}\right) \quad (9)$$

$$q_{internal\ radiation} = 0.25\ s\ E_b \exp(-0.25\ sy) \quad (10)$$

$$q_{radiative\ loss} = -\frac{\varepsilon_{fb}\ \sigma(T(y)^4 - T_\infty^4)}{l_f} \quad (11)$$

Where,

w is the width of the fuel bed, l_f is the thickness of the fuel bed, L_{fl} is the flame length, Z= (y/L_{fl} – sinθ)/cosθ determine the view factor and E_b is the ember emissivity. The rest of the parameters have been identified earlier.

The different heat transfer terms during a forest fire will classify the fire phases that the fuel bed undergo during a wildfire into four phases, pre-ignition, flaming combustion, smoldering combustion, and glowing combustion each with different BVOC emissions. These phases will be discussed in the next section.

3 Wildfire Phases and Corresponding Emissions

3.1 Combustion Phases

In a wildfire, vegetation fuel bed undergoes 4 combustion phases that in reality occur simultaneously: (1) pre-ignition phase (solid phase), (2) flaming phase (gas phase), (3) smoldering phase, and (4) glowing phase (Ottmar 2014) (Figure I.9). A brief description of the wildfire/fuel behavior in each combustion phase is presented in Table I.1.

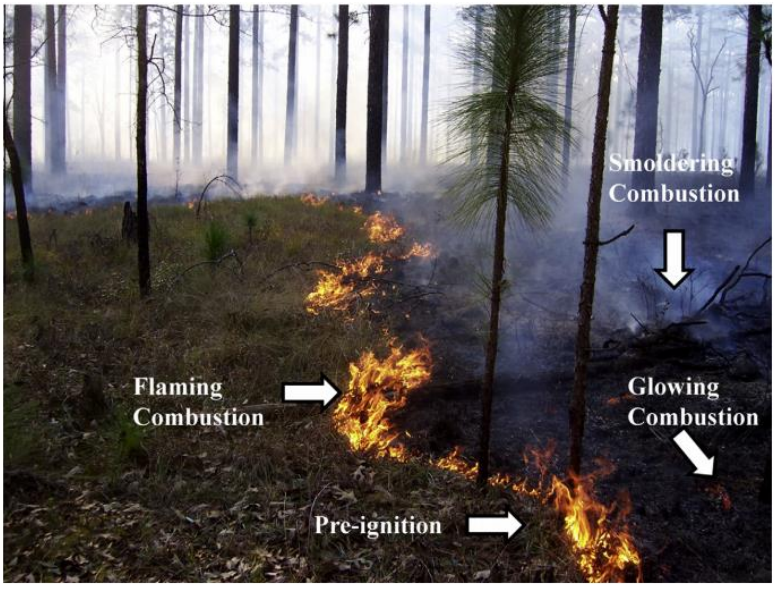

Figure I.9. Wildfire phases. (Ottmar 2014)

Table I.1. Wildfire/Fuel behavior at each combustion phase. (Ottmar 2014).

Wildfire Phase	Description
Pre-ignition	• Fuel bed ahead of the fire front is heated by radiation and convection (30 - 400°C). • Water vapor is driven to the surface of the fuels and expelled into the atmosphere. • Pyrolysis begins. Cellulose, hemicellulose, and lignin begin to decompose and release hot volatiles which rise and mix with oxygen to begin the flaming phase.
Flaming	• Volatiles mix with oxygen and combust and the temperature of the fuel rises rapidly (500 –1900°C). • Pyrolysis rate accelerates. • Combustion efficiency increases. • More fraction of the fuel carbon is converted to CO_2 and H_2O.
Smoldering	• Vapors are too low to support flaming combustion resulting in a temperature decrease (300-600°C). • Hot gases and vapors begin to condense due to a low convection column which make them appear as white smoke on ground level. • Oxygen supply is restricted to the burnt fuel and flaming ceases. • The remaining fuel that hasn't been consumed transforms into char.
Glowing	• Most of the volatile gases have been driven off from the fuel at temperature levels (300 – 600 °C). • Oxygen now can react with the surface of the fuel and oxidize the char layer. • CO, CO_2, and methane are the dominant emissions.

3.2 Solid Phase and Gaseous Phase

Literature has also classified wildfire into two phases: the solid phase and the gaseous phase (Lobert 1993). The solid phase consists of the fire phases that decompose the solid fuel matter while the gas phase involves the reactions that the emitted gases undergo to produce the flame (Table I.2).

Table I.2. Solid and gas phases of a wildfire. (Chan et al. 2011, Lobert 1993)

Combustion Phase	Process	Process Characteristics
Solid Phase	Drying and Distilling	Emissions of H_2O, alcohols, aldehydes and terpenes.
	Pyrolysis	Endothermic < 450K Exothermic > 450K Dehydrocellulose (high molecular weight) decomposition into (intermediate molecular weight) i.e., tar (forming 2/3 of volatiles calorific value) and char with H_2O, CO, and CO_2. Tar > char flaming occurs. Char > tar more H_2O and CO_2 flaming not possible.

	Smoldering	Takes place at concentrations of oxygen as low as 5%. Non-oxidized emissions proceed over days even under conditions of high moisture. $CO > CO_2$ emissions.
	Glowing	Char > tar. Oxygen oxidizes char to CO which later oxidizes to CO_2.
Gas Phase	Flaming	Intermediate molecular weight tars react with oxygen and burn to form low molecular weight compounds. $CO_2 > CO$ emissions. Hydrocarbons oxidize with OH to form small hydrocarbon radicals (CH_3, C_2H_5) which then oxidize to CO, CO_2 and H_2O (Figure I.10).

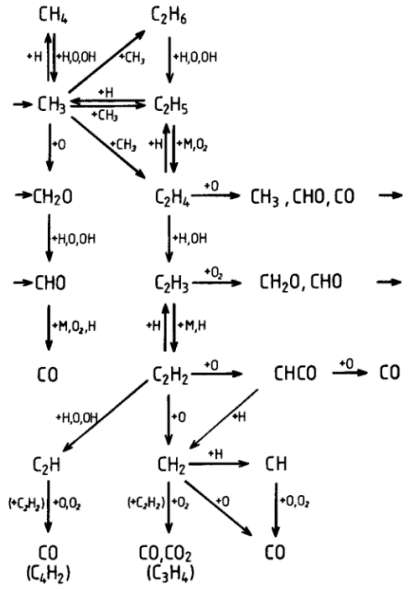

Figure I.10. Oxidation path of C1 and C2 hydrocarbons in the flame. (Lobert 1993)

4 Wildfires Statistics

4.1.1 Global Stats

When we talk about the most disastrous global events in the history of wildfires it's essential to mention the Great Black Dragon Fire that occurred in China in 1987 (Pyne 1989). The Chinese wildfire consumed 18 million acres of wildland where hundreds of thousands of pine trees were burned, more than 200 people were killed, other 250 were injured, and thousands of people were left homeless (Nath and Nath 2019).

In the last decade there were an average of 62,693 wildfires burning 7.5 million acres of land every year. In 2020, more than 58,250 wildfires (51,727 in 2019) burned 10.3 million acres of land in the US alone (Ijaz 2021).The worst wildfires relevant to the number of humans' lives lost, areas burned, and costs of material and property damage during the last two decades occurred in Australia, the USA (mainly California), Siberia, Canada, South Korea, Portugal, and the biomes of Brazil (Table I.3).

Table I.3. Global mega wildfires record in the last two decades: name, country, year, area burnt and post fire effects**.** (Igini 2022).

Fire Name/Country	Year	Area Burnt (Acres)	Fire Effects
Siberian Taiga fires, Russia	2003	47 million	No serious property damage or fatalities recorded due to low population.
Portugal wildfires	2003	879635	18 deaths 10% of the country's forests were burnt.
Black Tuesday Fire, Australia Eyre Peninsula bushfire	2005	192650	9 deaths, 115 injured 93 houses were destroyed
Australian Black Saturday bushfire	2009	1.1 million	173 deaths, 414 injured More than 3500 buildings worth 100 million dollars were destroyed
Northwest Territories fire, Canada	2014	8.4 million	Smoke traveled to western side of Europe. Smoke affected air quality in Canada Property damage No deaths
Siberian wildfires	2015&2019		Dozens of deaths Thousands of homes were destroyed
Portugal wildfires	2017	111120	100 deaths 5,6% of forests got burnt 1700 firefighters were deployed
Camp fire, Tubbs fire, Tunnel fire California, USA	2018	1.8 million	85 deaths 10 billion dollars' worth of damages
South Korean Gangwon wildfire	2019	1307	2 deaths, 30 injured 2000 Buildings worth millions of dollars were destroyed 15,000 soldiers and firefighters were deployed
Australian bushfires	2019-2020	46 million	34 deaths Over 10,000 buildings worth hundreds of millions of dollars were destroyed
Amazonas and Pantanal Brazil	2020	930144	4,5 million people exposed to polluted air

Brazil fires consume mostly the Cerrado biomes during the long dry equatorial season from May to October. California, the US state of breaking records in wildfires, is characterized by a Mediterranean climate with low rainfall and warm dry summer season (June -August). The majority of wildfires occur during the months from May to October, consuming a mosaic of California's vegetation cover of chaparral shrublands, oak woodlands, conifers (pine), coastal scrub and annual grasslands (Rogan & Franklin 2001). Significant wildfire intensities were recorded during the dry summer seasons (May-October) over forest covers of southeastern Australia and shrublands of eastern Australia attributed to highly combustible crown and

surface fuel loads, respectively (Kganyago & Shikwambana 2022). Canada and Russia share extreme weather conditions, although Russia wildfires are more common in spring than in summer, as in the case of Canada, wildfires in both countries consume mostly their deciduous and coniferous boreal forests which possess different flammability resistance among the two countries (De Groot et al. 2013).

4.1.2 Mediterranean Type Climate (MTC) Regions Stats

The Mediterranean climate regions are found to have the most wildfire-prone ecosystems because of their characteristic mild wet winters, warm dry summers, and fire-sensitive vegetation covers (Pausas et al. 2008, Keeley 2012, Moreira et al. 2020). Warming and severe drought periods of this climate, which have increased due to climate change, are enough driving forces to increase the numbers of wildfires (Turco et al. 2014). That's why it's essential to focus on and study the fire regimes in the regions of the Mediterranean climate in around the world. Five regions in the world share Mediterranean climate ecosystems and are referred to as Mediterranean climate regions (MCR) or Mediterranean-type climate (MTC) regions (Keeley et al. 2013).

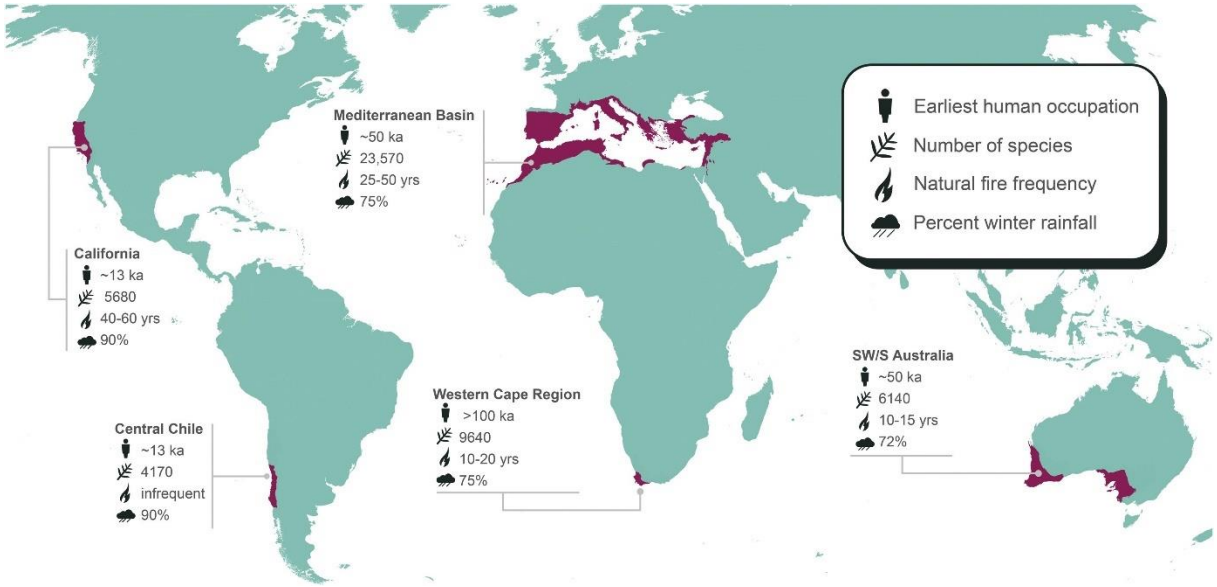

Figure I.11. Location of Mediterranean climate regions with environmental and cultural characteristics. Human occupation, approximate number of plants and vertebrate species, annual to decadal frequency of fires and rainfall percentages in winter seasons. (Rick et al. 2020)

The five MTC regions are located near the west coasts of continents between 30° and 40° latitude as California, Central Chile, the Mediterranean Basin, the Cape Region of South Africa, and Southwestern and South Australia (Figure I.11). The vegetation covers in these regions are diversified in a range of forests (coniferous, thermophilous deciduous), woodlands, savannas, shrublands and grasslands, all representing the perfect fuel for wildfires (Gauquelin et al. 2016, Safford & Vallejo 2019). The high amounts of precipitation in the rainy seasons of the MTC exceed the evapotranspiration potentials of the vegetation species, resulting in an increase in the soil water potential and boosting plant growth. Thus, these conditions produce contiguous fuel loads that are highly flammable in summer droughts (Keeley et al. 2013).

The MTC forests form about 1.8% of the world's total forest area with the vast majority existing in the Mediterranean basin (Gauquelin et al. 2016). The increased number of wildfires in the Mediterranean basin region during the 20th century have reached more than 5,000 fires which burned an estimated average of 600,000 to 800,000 hectares each year. 80% of the wildfires recorded in Europe are concentrated in the MTC regions (Viegas et al. 2009). In some countries as France, Spain, Greece, Italy, and Portugal forests represent at least half of their total land area. The annual report of the European Forest Fire Information System (EU EFFIS), provides annual statistics about the number of wildfires and the burnt areas in the Mediterranean basin of Europe, Middle East and North Africa. It is a platform for the involved countries to exchange knowledge and expertise about fire prevention strategies, firefighting practices, and other fire management policies. Among its European neighbors, France is in a good position in fire risk management through its effective fire prevention system that led to a relatively low number of wildfire records in the 2019 compared to Spain and Italy (Figure I.12). Portugal and Spain are reconsidering their fire management policies as they were hitting serious records of wildfires that burned areas larger than 40,000 ha in 2019 (Figure I.12). Up to May 2019, wildfire recorded were eleven times more than usual for this time of year, resulting in 40% increase of the area burnt, compared to the whole year 2018.

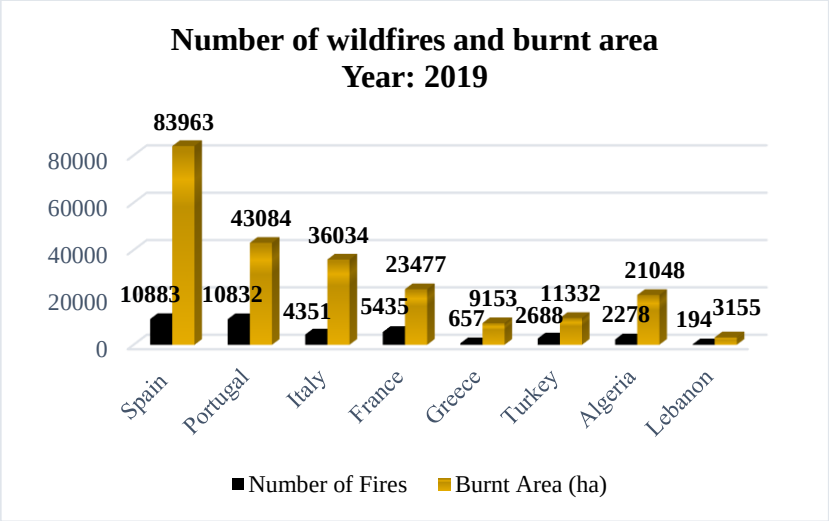

Figure I.12. Number of wildfires and the burnt area (ha) in selected Mediterranean countries in Europe, Middle East, and North Africa, in 2019. (EFFIS 2019).

The monthly distribution of burnt areas by wildfires in the MTC regions showed high values accompanied with the heat waves during the summer season (average May-September) with peaks rising in the month of August which experienced the most damage (Figure I.13). Exceptions for winter fires (February – March) such as the ones that burnt 3780 ha of the shrublands in Corsica, France.

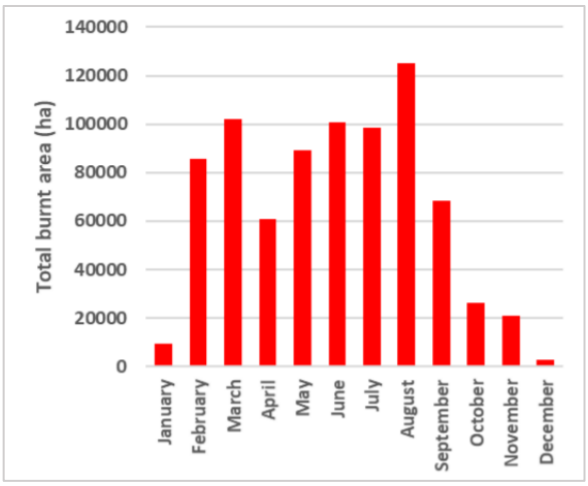

Figure I.13. Monthly distribution of total area burnt in the MTC regions in 2019. (EFFIS 2019).

The impact of the extended heat waves due to climate change was witnessed in the case of Lebanon in the month of October, 2019. In fact, more than 45 fires were recorded burning more than 1500 ha of forested area at a mean atmospheric temperature of 24°C, regardless of a notable high amount of precipitation (65 mm) compared to zero in the month of August (Figure I.14.a, b).

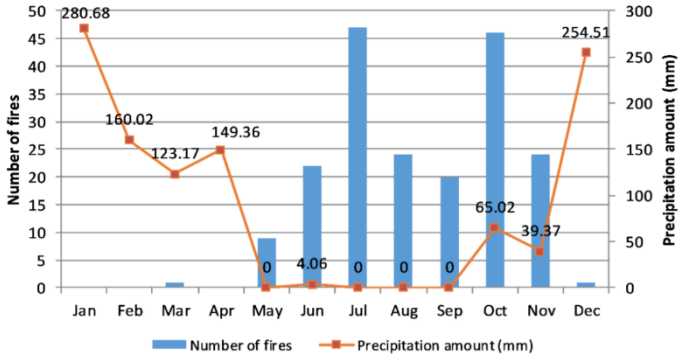

(a)

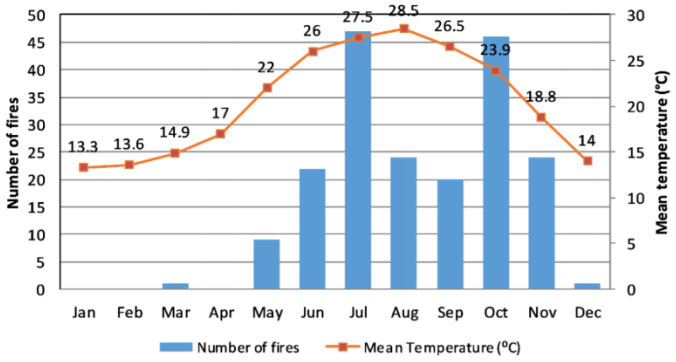

(b)

Figure I.14. Monthly distribution of wildfire occurrences and affected areas in Lebanon with plots of: (a). Mean temperatures and (b). Precipitation amounts. (EFFIS 2019).

Albeit wildfires form an essential part of the ecological balance in the Mediterranean ecosystems, their increasing frequencies are becoming beyond the coping capacities of these systems. Fueled with climate change, these ecosystems have scored dangerous events of wildfires with an ascending order in the past decades, for example in addition to the above records in 2019, more than 100 people were killed during the 2021 fire season, and it doesn't end there. Therefore, studies focusing on understanding wildfires' behaviors, coming out with strategies to reduce their risks, and saving lives should be prioritized in these Mediterranean climate regions. Our choice to study this region stems from these motives.

CHAPTER I

****

State of the Art on Wildfires of the Mediterranean Vegetation and their Extreme Behaviors

Résumé

Les feux de forêt et de végétation sont des incendies qui se déclarent dans des couverts végétaux. Dans les régions méditerranéennes, ils deviennent difficiles à contrôler par les méthodes d'extinction d'incendie conventionnelles si l'humain n'intervient pas rapidement. Ils sont classés en feux de sol, de surface et de cime selon le type de végétation qu'ils consomment (Wane et al. 2009). Cette dernière peut former : des forêts avec peuplements d'arbres, des champs d'arbustes et de buissons, des prairies, des tourbières, des litières (bois et feuilles mortes) et rémanents de coupe. Premièrement, il est essentiel de comprendre qu'il y a trois facteurs formant le triangle du feu ; combustible, chaleur et oxygène. Éliminez l'un de ces derniers et les flammes s'éteindront. Le triangle du feu peut également être remplacé par un tétraèdre où une quatrième composante appelée réaction en chaîne est ajoutée et est décrite comme l'apport continu de vapeurs combustibles évoluant du combustible chauffé au front de flamme permettant la propagation du feu à travers un lit de combustible végétal. Les incendies peuvent être causés par des causes naturelles telles que la foudre, les éruptions volcaniques et les impacts de météorites, ainsi que les émissions de gaz naturel. Cependant, la plupart des incendies de forêt dans le monde sont d'origine humaine par des actions volontaires (incendie criminel) ou involontaires, mégots, barbecues, engins agricoles par exemple. Dans le monde, au cours de la dernière décennie, il y a eu en moyenne 62 693 incendies de forêt qui ont brûlé 7,5 millions d'acres de terres chaque année. En 2020, plus de 58 250 incendies de forêt (51 727 en 2019) ont brûlé 10,3 millions d'acres de terres dans le monde (Ijaz 2021). Les régions au climat méditerranéen présentent les écosystèmes les plus assujettis aux incendies de forêt en raison de leurs hivers doux et humides caractéristiques, de leurs étés chauds et secs et des espèces pyrophytes qui se reproduisent par le feu (Pausas et al. 2008, Keeley 2012, Moreira et al. 2020). La répartition mensuelle des surfaces brûlées par les incendies de forêt dans les régions de climat méditerranéen a montré des valeurs élevées au moment des vagues de chaleur pendant la saison estivale (moyenne mai-septembre) avec des pics en hausse au mois d'août qui a subi le plus de dégâts ; à l'exception des feux d'hiver (février - mars) comme ceux qui ont brûlé 3780 ha de maquis en Corse, France. Une fois allumé, le comportement du feu de forêt est affecté par trois éléments principaux ; combustible (végétation combustible), conditions météorologiques et topographie qui forment les trois côtés du triangle de comportement du feu. Un changement critique de ces facteurs transformera le comportement du feu en un comportement extrême. Les feux de forêt dans les régions à climat méditerranéen (MCR) consomment trois types de forêts : les forêts de feuillus thermophiles, les forêts de feuillus sempervirentes et les forêts de conifères (Gauquelin et al. 2016). Les températures élevées et les périodes de sécheresse prolongées sont les indices météorologiques les plus critiques qui augmentent la probabilité d'incendie de forêt. La sécheresse est un stress abiotique et a augmenté en raison du réchauffement climatique causé par les gaz à effet de serre (GES) entraînant une augmentation des risques incendie en forêt. Par exemple, la sécheresse augmente la probabilité d'incendie en forêt en modifiant la structure et la continuité de la forêt, en augmentant le rapport entre combustible mort et -vivant. Ces changements spectaculaires dans les structures forestières ont entraîné une augmentation des taux de propagation des incendies de 30 %, (Nolan et al. 2020). La topographie, principalement les pentes (haut et bas), peut créer des changements spectaculaires dans le comportement de propagation du feu. Selon la littérature, une augmentation de 10° de la pente augmentera le taux de propagation du feu de

deux fois (Butler et al. 2007). D'autre part, la vitesse du vent entraînera une inclinaison de la flamme vers le lit de combustible, augmentant ainsi les effets convectifs et radiatifs de surface (facteur de vue) dans les feux de terrain plat, de pente ascendante et descendante. Un effet majeur de la sécheresse à l'échelle de la plante est de nuire à son activité photosynthétique. Un processus de photosynthèse altéré en raison d'un déséquilibre des concentrations de CO_2 dans le mésophylle des plantes modifiera la voie de production plastidiale des précurseurs responsables de la biosynthèse des composés organiques volatils biogéniques (COVB) et des taux d'émission dans les plantes (Bäck et al. 2005). Les parties feuillues des plantes ligneuses libèrent un mélange diversifié de terpénoïdes, notamment de l'isoprène (C_5H_8, 2-méthyl-1,3-butadiène), des monoterpènes ($C_{10}H_{16}$), des sesquiterpènes ($C_{15}H_{24}$) et des diterpènes ($C_{20}H_{32}$) (Owen et al. 2001, Keeling et Bohlman 2006). Les composés organiques volatils biogéniques (COVB) produits par les plantes sont impliqués dans la croissance, la reproduction, la défense et les moyens de communication des plantes au sein des communautés végétales (Peñuelas et Staudt 2010). Certaines espèces végétales telles que *Pinus*, *Abies*, *Eucalyptus* et celles de la famille des Rutacées et des Lamiacées ont des compartiments de stockage tels que des conduits de résine, des cavités, des glandes sébacées, des trichomes glandulaires, où les COVB sont stockés tandis que d'autres espèces telles que certains *chênes* (*Quercus spp.)* ne disposent pas de tels compartiments de stockage (Laothawornkitkul et al. 2009, Loreto et Schnitzler 2010). En ce qui concerne les émissions de ces COVB, il existe deux types ; émissions constitutives et induites. Les émissions constitutives de COVB (Holopainen 2004, Loreto et Schnitzler 2010) se produisent dans des conditions normales lorsque les terpénoïdes se libèrent des grands bassins de stockage dans les conduits de résine vers les bassins mésophylles. Leurs émissions sont en outre régies par les constantes de la loi de *Henry* (K_h) qui déterminent leurs volatilités. Les composés organiques volatils induits (COV) sont émis à partir de bassins de stockage ou de synthèse *de-novo* avec des proportions dépendant de la durée et de la sévérité des différents stress abiotiques (ozone (O_3), rayonnement, sécheresse, températures extrêmes, etc.) et biotiques (champignons, bactéries, herbivores, etc.) (Kleist et al. 2012, Niinemets et al. 2013). Les facteurs d'émissions (FE) sont utilisés pour mesurer la quantité d'émissions provenant de la végétation brûlée lors d'un feu de forêt par rapport à la quantité de combustible sec brûlé, mesurée en grammes d'émissions par kilogramme de combustible sec brûlé ($g.kg^{-1}$) (Andreae 2019). Les COVB émis par la végétation lors des incendies de forêt permettent la propagation du feu par des réactions chimiques en chaîne (quatrième élément du tétraèdre du feu). Cependant, leurs accumulations dans des topographies confinées (vallées, canyons) pourraient atteindre des concentrations inflammables (entre leurs limites inférieure et supérieure d'inflammabilité) pour provoquer la survenue de violentes éruptions de feu parfois appelées ′Flashovers′ dans la littérature (Dold 2010). De tels incidents sont soudains et pour l'instant imprévisibles, formant un lac de feu au-dessus de la couche de combustible qui a surprennent et mettent en danger les pompiers devant le front de feu même après l'extinction de l'incendie. Par conséquent, ce chapitre reprend les données concernant les incendies de forêt dans les régions climatiques méditerranéennes (RCM) pour être discutées et utilisées tout au long de cette thèse. Cette thèse aborde principalement l'une des formes les plus dangereuses d'éruptions de feu ; Flashovers de feux de forêt. Bien qu'ils aient causé de nombreux décès humains et par leurs comportements extrêmes et incontrôlables, leurs causes sont encore controversées dans la communauté scientifique travaillant sur les incendies de forêt. Notre recherche vise à mieux

comprendre les mécanismes de propagation pour fournir des outils de décision et d'informations pouvant être utilisés par la communauté des pompiers et les équipes de gestion forestière pour mettre en œuvre les meilleures mesures de prévention et de protection dans leurs opérations de lutte contre les incendies et leurs activités de reboisement, respectivement. Nous avons mis l'accent sur les émissions de COV de la végétation qui, selon nous, sont les principaux moteurs de l'initiation, de la propagation et principalement des flashovers d'incendies de forêt. Les émissions de COV (dont les COVB), sous les effets de la chaleur et des flammes des incendies de forêt, sont affectées par de nombreux facteurs atmosphériques et environnementaux, en plus des caractéristiques de la végétation elle-même. Or, les facteurs influençant les émissions sont eux aussi méconnus et variables en fonction des études. Le contenu des émissions va à son tour affecter les paramètres d'inflammabilité de la végétation. Le risque avec ces COVB provient de leur capacité à s'enflammer spontanément à des températures inférieures à 300°C et à leur densité leur permettant de s'accumuler au niveau du sol. Les régions au climat méditerranéen en Australie, au Brésil, aux États-Unis et dans le bassin méditerranéen ont été submergées ces dernières années par les énormes incendies de forêt qui ont détruit leur précieuse richesse forestière et réduit drastiquement un large éventail formes de vie écologiques et biologiques. Réduire les émissions de gaz à effets de serre pour limiter le réchauffement climatique pourrait réduire les températures et le risque d'incendies de forêt, mais jusqu'à ce que des résultats tangibles apparaissent, la communauté scientifique s'efforce de fournir les meilleurs outils à la communauté des pompiers pour contrôler et peut-être réduire les risques d'incendie de forêt. Sans compter que les feux de forêt participent fortement à l'augmentation des gaz à effet de serre et forment ce qu'on appelle une boucle de rétroaction.

1 Introduction

Wildfires do not have a defined area of impact. They spread freely over the territory as long as there is available fuel however, their ignition, propagation, and extinction are mostly influenced by the human factor. In all cases, a high risk of outbreak (generally of human origin) and a strong capacity for fire propagation, depend mainly on the fuel load, distribution, and volatile and moisture contents. Extreme changes in such traits alter the probability of the occurrence of fires. Therefore, anticipating as best as possible the type of fire and its strategic behavior that's going to develop in a vegetation bed, facilitates the design of specific prevention or extinguishing actions that are adapted to a common fire scenario but also account for any sudden changes in fire behavior. Considering fire spread as a series of ignitions in a fuel bed aids in the prediction of its behavior. The potential fuel ahead of the firefront is heated by the fire, the surface is dehydrated, and further heating raises the surface temperature until the fuel begins to pyrolyze and release combustible gases. Therefore, the theory of flame spreading over an igniting propellant surface is viewed as one of continuous, diffusive gas-phase ignition. This is why the main factor that is manageable to control wildfires and predict their behaviors is fuel and vegetation. Mediterranean nature would carry within itself the seeds of its own destruction: the recurring summer drought and the flammability of vegetation would lead to the inevitable reoccurrences of fire.

This state-of-the-art describes the current knowledge about the Mediterranean vegetation through the analysis of the published work about their BVOC biosynthesis and emission rates, their adaptations to climate change extremes (drought and extreme temperatures), and their direct relationship to wildfire phases and propagation. It provides a comprehensive overview to understand the degradation phases undergone by vegetation in wildfires and the resulting gaseous mixtures formed. Different quantification methods of these gases are also presented to support the novelty of our work in estimating extreme fire behaviors. Finally, this chapter ends up zooming on the forms of extreme wildfire behaviors documented in the literature with emphasis on one particular form related to VOC accumulations in confined forest topographies referred to as wildfire flashovers.

2 Wildfires Behaviors: Know-How

2.1 Fire Behavior Triangle: Fuel, Weather, & Topography

A wildfire is the result of a chemical reaction; combustion. Combustion is a strong exothermic oxidation reaction that produces heat due to the action of an oxidizer on a fuel; in the case of wildfires, oxygen in the air on vegetation. Combustion requires the presence of three elements: the fuel, the oxidizer, and an initial energy input. The combustion process is broken down into three stages: evaporation of the water contained in the fuel, emission of flammable gases by pyrolysis and finally ignition. The combustion is triggered by an external energy source, thus in order for the flame to propagate a part of the energy released by combustion is then reabsorbed by the fuel to maintain the combustion (chain reaction Figure I.2). Once ignited, the wildfire behavior is affected by three main elements; fuel (combustible vegetation), weather, and topography by which they form the sides of the fire behavior triangle (Figure I.15).

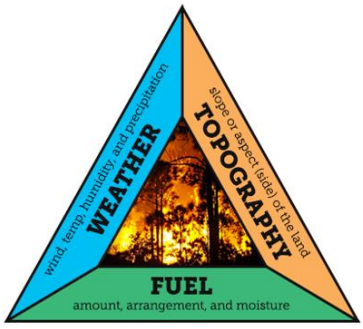

Figure I.15. Fire behavior triangle.

Fuels are all the living and dead plant material that can be ignited by a fire and they affect wildfire behavior through their amount, arrangement, and moisture content. Weather conditions such as wind, temperature and humidity or precipitation amounts also contribute to fire behavior. Slopes are the main landscape topographic features that may hinder or increase wildfires intensities and rates of spread pushing their behaviors to extremes. Wind, topographies, temperatures, and oxygen are fire parameters that can't be controlled before a wildfire ignition; however, fuel can. Fuel is the only parameter in the fire behavior triangle that can be controlled or managed to reduce the potential occurrences of wildfires and their post effects and behaviors.

Next, we will identify the main vegetation fuel characteristics that are ought to affect wildfire behaviors, coupled with weather indices such as drought and temperature. Wind speed and slope topographies effects on wildfire behaviors will be experimentally and numerically addressed in C*hapter 2*.

2.2 Fuel: MTC Vegetation

Identifying and quantifying vegetation structures and characteristics in wildfire vulnerable ecosystems, serve as future indicators to wildfire intensities and rates of spread. The absence/presence of different vertical stratification layers and the continuity/discontinuity between them will help predict the transitions that may occur in wildfire behaviors and accordingly set efficient fire management strategies (Morsdorf et al. 2010). In fact, depending on the type of the vertical vegetation stratum consumed in a wildfire, this last will be classified into a ground fire, a surface fire, or a crown fire with fuel being the common denominator for them all. Table I.4, classifies wildfires to ground, surface and crown according to the vegetation they consume, the combustion phase, and their transition mechanisms.

Table I.4. Classification of wildfires into ground, surface and crown fires.

	Type of Fuel Burnt	Fire Combustion Phase	Behavior Transition
Ground Fire[1]	Duff layer, decaying roots and decayed logs in soil	Smoldering	To surface fire if in contact with roots near soil surface
Surface Fire[2]	Needles, moss, lichen, herbaceous vegetation, shrubs, small trees, and saplings.	Flaming Smoldering (after passage of flame)	To crown fire (crown fire initiation criteria)[4]
Crown Fire[3]	Tree crowns (foliage and twigs<6mm)	Flaming Smoldering (after passage of flame)	Three types: Passive, Active, Independent

1: Sandhyavitri et al. 2016; 2: Baines 1990; 3: Scott 2006; 4: Scott and Reinhardt 2001.

2.2.1 Combustible Vegetation in MTC

Vegetation cover in MTC is one of the most biodiverse (Myers et al. 2000; Olson and Dinerstein 2002), it is composed of forests (canopy cover > 10%, height > 5m; FAO 2000) or woodlands (5% < canopy cover < 10%, height < 5m; FAO 2000), shrublands (chaparral, sage scrub), and grasslands and savannas (grasslands with spotted trees). Mosaic of complex vegetation structures in a Mediterranean forest are possible depending on topography, exposure to sunlight, and water abundance. A typical Mediterranean forest is divided into three vertical strata, litter and duff, understory (shrubs and grass), and crown.

2.2.2 Wildfire Effects on Vegetation Diversity in the MTC Regions

Disturbances created by wildfires have led to alterations in the original forest structures in the Mediterranean regions; South Africa, Australia, California, the Mediterranean Basin, and Chile (Acácio et al. 2009). 70% of the forests and shrublands were destroyed by 1990 in the MTC regions, while the remaining cover is considered in critical and endangered conditions (Acácio et al. 2008). Wildfires in the MTC regions consume three kinds of forests: thermophilous deciduous forests, broadleaved evergreen forests, and coniferous forests (Gauquelin et al. 2016). The consumption of these original forests resulted in the emergence of post-fire altered landscapes consisting of four main patch types of vegetation: forests, savannas, shrublands, and grasslands. For example, in the Iberian Peninsula (territory between Spain and Portugal), the excessive consumption of oak trees by wildfires over the last 45 years have resulted in the decrease of their persistence as a forest patch-type to 55% while the shrublands patch-type has increased to 59% and the savanna and grasslands to 33% and 15%, respectively (Acácio et al. 2008). The forest dominating species are changing from fire resilient species with thick bark insulation (eg. cork oak) into fire sensitive shrubland species (eg. *Cistus*) which are very flammable due to many factors among of which is the presence of resins on their leaves (Trabaud 1981), that result in generating extreme surface wildfire intensities. Other important transitions occurred in savannas, as they changed to shrublands (28%) or forests (23%) (Acácio et al. 2008). Pine forests in the Mediterranean basin are also witnessing changes in their post-fire regeneration patterns. In a study made on forest lands dominated by three types of pine species (*Pinus halepensis*, *P. nigra* and *P. sylvestris*) after 30 years of a fire, it was noticed that (77-93%) of the forest have changed into oak species and (7-16%) have changed into shrublands (Retana et al. 2002). This important increase in post-fire growth of understory shrublands with horizontal continuity and mid-story canopies with increased canopy bulk density (CBD), has to be viewed with concern as they could increase the risk of more frequent and recursive surface fires transitioning into high intensity crown fires.

2.3 Weather: Drought Indices in MTC Regions

Drought, referred to as abiotic stress occurs naturally however, climate change due to the induced global warming by greenhouse gas (GHG) has generally accelerated the process to make it set in quicker and become more intense with many consequences, not the least of which is increased wildfire risk. Large fires co-occur with extensive soil water deficit due to warming-induced increase in evaporative demand. Studies linking forest flammability and plant vulnerability to drought through a decrease in fuel moisture content (FMC) are diverse (Ruffault et al. 2018, Sharples et al. 2021, Pellizzaro et al. 2007, Chuvieco et al. 2004). It's essential first

to understand some plant traits that are affected by drought and enhance the bonds between vegetation and intensified wildfire regimes (Table I.5).

2.3.1 Effect of Drought on Forest Spatial Distribution Scale

Drought increases wildfire probability by changing forest structure and continuity (Figure I.16), i.e., decreasing the turgor pressure in the canopy foliage due to cavitation which impairs foliage growth and leads to death (Farooq et al. 2009, Wolfe et al. 2016). As the dead to live fuel ratio of the crown increases, shedding of the dead fuel increases and thickens the surface litter layer. The continuous foliage mortality increases the gap space in the forest canopy allowing for heat to dry more ground litter (dead FMC ~ 7-30%) and understory shrublands, these dramatic changes in forest structures lead to an increase in fire rates of spread by 30% (Nolan et al. 2020).

Table I.5. Drought related plant traits.

Plant Trait	Symbol	Definition	Source
Relative Water Content	RWC	Foliage moisture content expressed in drought literature. Quantifies the mass of water in foliage relative to saturated water content. Commonly modeled to as function of leaf water potential. $\Psi_{potential}$. $$RWC = \left(\frac{Fw - Dw}{Tw - Dw}\right) \times 100$$ Fw is the fresh weight (i.e. weight prior to rehydration). Dw is the dry weight of the fuel. Tw is the turgid (saturated) weight of the fuel	Nolan et al. 2020
Live Fuel Moisture Content	LFMC	Foliage moisture content expressed in wildfire literature. Quantifies the mass of water in foliage relative to foliar dry weight. $$LFMC = \left(\frac{Fw - Dw}{Dw}\right) \times 100$$	Nolan et al. 2020
Turgor pressure	Ψ_p	Pressure potential (typical = 0.6-0.8 MPa), pushes the plasma membrane against the cell wall of plant, caused by the osmotic flow of water from outside of the cell into the cell's vacuole. Responsible to keep the plant erect.	LibreTexts 2021
Osmotic Pressure		A hydrostatic pressure caused by difference in the amounts of solutes between solutions that are separated by a semi-permeable membrane. Osmosis is how plants are able to absorb water from soil. The roots of the plant have a higher solute concentration than the surrounding soil, so water flows into the roots.	LibreTexts 2021
Gravity potential	Ψ_g	The force of gravity pulls water downwards to the soil, which reduces the total amount of potential energy in the water in the plant (Ψ_{total}). More influential in tall plants (trees) than in shorter plants (shrubs) (≤ 0).	LibreTexts 2021
Cavitation		Occurs at stem or bole and leaf scale. With soil water deficit, air enters the conducting vessel not allowing the circulation of sap which causes the rupture of the water column and hydraulic failure. Vessels are filled with air bubbles (embolism). Leaves become unfunctional and therefore are shed.	Wolfe et al. 2016
Stomatal Conductance	g_l	Measure in degree of stomatal opening and can be used as indicator of plant water status. Reduction in stomatal openings prevent the decrease in turgor pressure by reducing transpiration.	Gimenez et al. 2013

2.3.2 Effect of Drought on Plant Scale: Photosynthesis

A major effect of drought on plant scale is impairing its photosynthetic activity. When drought decreases water availability in soil, plant leaf stomata close in order reduce excessive water loss through evapotranspiration (Farooq et al. 2009, Mansfield and Atkinson 1990). Stomatal closure reduces the CO_2 uptake necessary for the process of photosynthesis. During the last decade stomatal closure was generally accepted to be the main determinant for decreased photosynthesis under mild to moderate drought (Farooq et al. 2009). Severe droughts however, result in decreasing the secretion and activity of Rubisco enzyme which is responsible for CO_2 fixation in the process of photosynthesis (Bota et al. 2004). Less turgor pressure results in cellular shrinkage and volume decline which increases the viscosity of its contents and accumulates proteins. This results in boosting the cellular toxicity levels which weakens Rubisco enzyme functions and secretions (Farooq et al. 2009). Impaired photosynthesis process due to imbalance in CO_2 concentrations in plant mesopyll will alter the plastidial production pathway of the precursors responsible for biogenic volatile organic compounds (BVOC) biosynthesis and emission rates in plants (Bäck et al. 2005). What are these BVOCs and what are their roles in wildfires will be discussed in the next section.

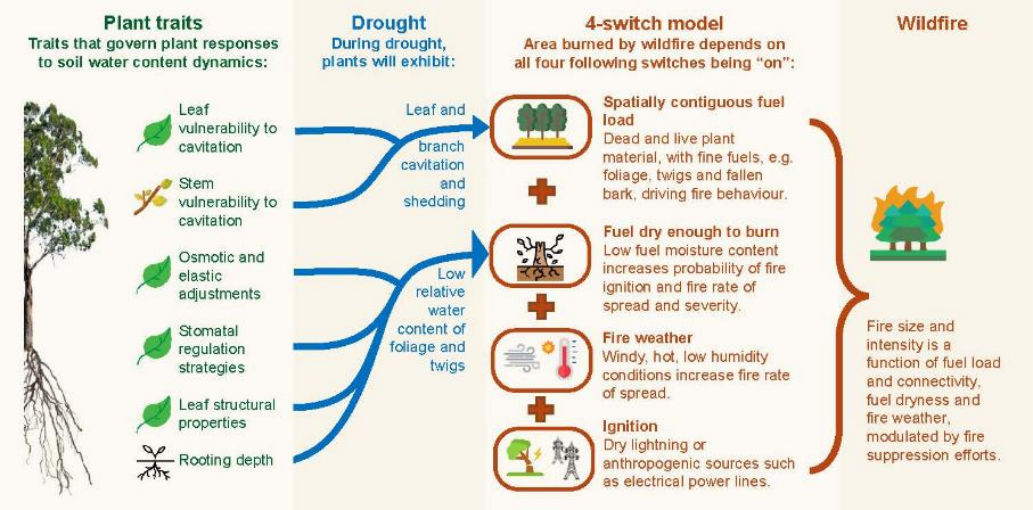

Figure I.16. Conceptual model illustrating linkages between drought-related plant traits and the likelihood of wildfire. (Nolan et al. 2020).

3 Biogenic Volatile Organic Compounds (BVOCs)

3.1 BVOCs Roles in Plant Communities and Urban Atmosphere

In addition to the well-known gases exchanged with atmosphere (oxygen, carbon dioxide and water vapor), plants, in particular trees, emit considerable amounts of different compounds known as biogenic volatile organic compounds (BVOCs) (Calfapietra et al. 2013). BVOCs are synthesized and released from below- and above- ground plant organs; however, vegetation leaves are the most emitting plant organs (Figure I.17). Leafy parts of woody plants release a diverse mixture of terpenoids, including isoprene (C_5H_8, 2-methyl-1,3-butadiene), monoterpenes ($C_{10}H_{16}$), sesquiterpenes ($C_{15}H_{24}$), and diterpenes ($C_{20}H_{32}$) (Owen et al. 2001, Keeling and Bohlman 2006), while grass species, emit large amounts of oxygenated BVOCs and some monoterpenes (Fukui and Doskey 2000, Laothawornkitkul et al. 2009). Biogenic volatile organic compounds (BVOCs) produced by plants are involved in plant growth,

reproduction, defense, and communication media within plant communities (Peñuelas and Staudt 2010, Laothawornkitkul et al. 2009, Iijima 2014). In urban atmosphere, the importance of BVOC emissions is related to their reactivity with anthropogenic pollutants especially nitrogen oxides (NO_x), to produce tropospheric ozone (O_3) (Figure I.18) (Schnitzler et al. 2004), aldehydes and ketones, secondary organic aerosols and particulate matter (Calfapietra et al. 2013, Sonwani et al. 2016).

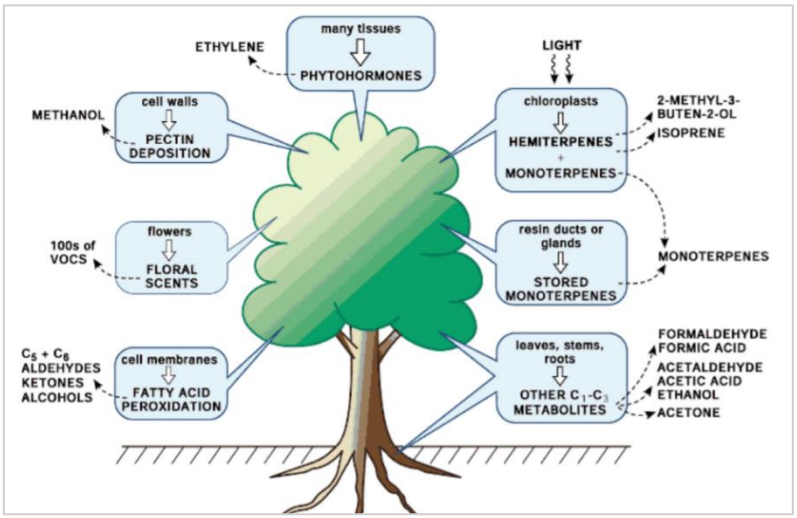

Figure I.17. Diagram illustrating storage and emissions of BVOCs from different plant organs.

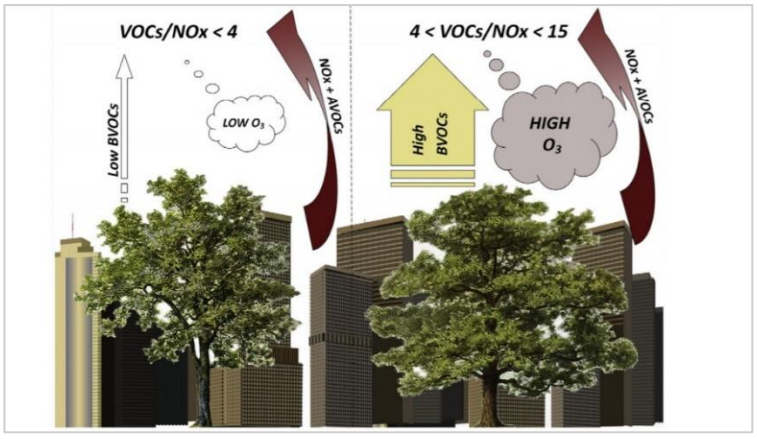

Figure I.18. Effect of BVOC emissions by urban trees on tropospheric ozone formation (O_3), AVOCs (anthropogenic VOCs). (Calfapietra et al. 2013).

3.2 Biosynthesis of BVOCs as Plant Secondary Metabolites

Primary metabolic processes of plants such as photosynthesis and respiration, form the production pathways of major secondary metabolites such as terpenoids, alkaloids, flavonoids and phenolic compounds (Solomon 2019).

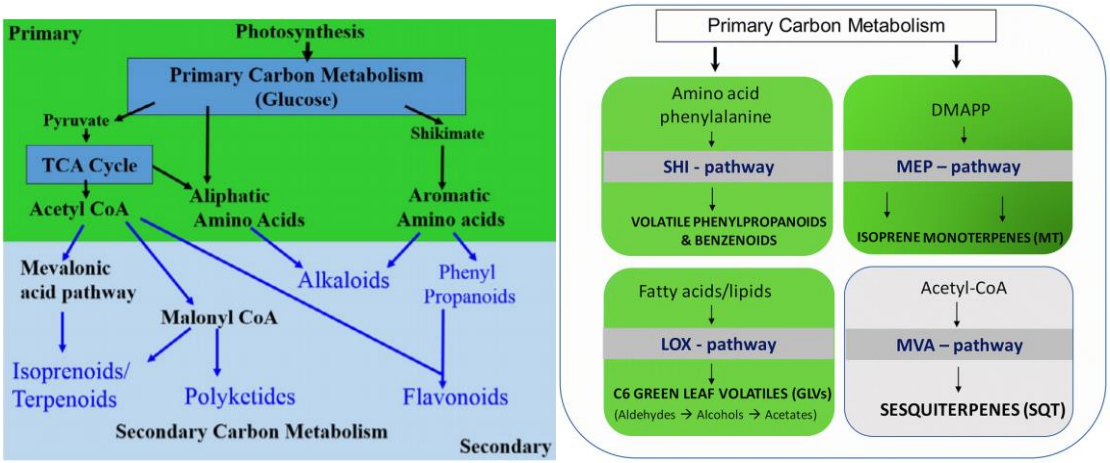

Figure I.19. Overview of the biosynthesis pathway of plant secondary metabolites from primary metabolites (photosynthesis). Left (Solomon 2019), right (Šimpraga et al.2019).

Pathways involved in primary and secondary metabolic processes to produce BVOCs are shown in Figure I.19 while their groups, precursors, and functional characteristics are tabulated in Table I.6.

Table I.6. Main group of plant-produced biogenic volatile organic compounds (BVOCs) and their functional characteristics. (Iijima 2014)

Compound Group	Typical BVOCs	Precursors (derived from)	Functional Characteristics
Isoprenoids	Isoprene	IDP	Tolerance to sunlight-induced heating
Monoterpenes	β-Ocimene, β-Myrcene, α-/β- Pinene, Limonene, Linalool, Geraniol	GDP	Harbivore-induced signal, Attractant to pollinator, Fragrance
Sesquiterpenes	β-Caryophellene, β-Farnesene, Farnesol, Nerolidol	FDP	Harbivore-induced signal, Antimicrobal Activity
Homoterpenes	TMTT DMNT	(E, E)-Geranyllinalool (E)- Nerolidol	Harbivore-induced signal
Phenylpropenes	Eugenol, Methylchavicol	Phenylalanine	Aroma, Antioxidative activity, Antimicrobial activity
Benzenoids	Phenylethanol, Vanillin Methyl salicylate	Phenylalanine Phenylalanine/Isochorismate	Aroma, Fragrance Aroma, Harbivore-induced signal
Lipid derivatives	Hexanal, Hexenals, Hexanol, Hexenols, (Z)-3-Hexenl acetate, Methyl jasmonate	Fatty Acids	Stress, damage, and herbivore-induced signal, Pathogen resistance
Aliphatic amino acid/lipid derivatives	Isonyl acetate, Isonyl alcohol Hexyl hexanoate	Leucine, Isoleucine Acyl CoA	Fruit Aroma
S, N - containning	Isothiocyanates Disulfides, Trisulfides	Glucosinolates S-alk(en)yl cysteine sulphoxides	Herbivore-induced signal, Antimicrobal activity, Flavor

DMNT: 4,8-dimethylnona-1,3,7-triene; FDP: Famesyl diphosphate; GDP: Geranyl diphosphate; IDP: Isopentenyl diphosphate; TMTT: 4,8,12-trimethyltrideca-1,3,7,11-tetraene.

3.2.1 Biosynthesis of Terpenoids

The most important terpenoid in earth system is isoprene (2-methyl-1,3-butadiene) (Faubert 2010), it's also an important commodity chemical used in a wide range of industrial applications such as the production of synthetic rubber, adhesives, and lubricants (Gao et al. 2016). Isoprene is the precursor of all other terpenoids by which they are formed from repeating units of isoprene. Isoprene is synthesized from two precursors, the two 5-carbon molecules: isopentenyl diphosphate (IPP) and its isomer dimethylallyl pyrophosphate (DMAPP; also called dimethylallyl diphosphate) (Chatzivasileiou et al. 2019). There are two synthesis pathways of these precursors, the mevalonate pathway (Figure I.20) and the non-mevalonate methyl-D-erythritol 4-phosphate (MEP) (Figure I.21). In the former, IPP and DMAPP originate from the six-carbon mevalonic acid through the condensation of three molecules of acetyl-coenzyme (acetyl-CoA) in the plant cytoplasm, while the latter originates from the condensation of equimolar quantities of pyruvate and glyceraldehyde 3-phosphate (G3P) in plant plastids (Gao et al. 2016). IPP and DMAP will later undergo condensation to provide a 10-Carbon skeleton of GPP (geranyl diphosphate); the immediate precursor of monoterpene. Adding 5-carbon unit to GDP leads to FPP (farnesyl pyrophosphate); the immediate precursor to sesquiterpene (15 carbon), then another 5-carbon unit added to FPP will give GGPP (geranylgeranyldiphosphate) which is the immediate precursor of diterpenes (20 carbon), (Solomon 2019).

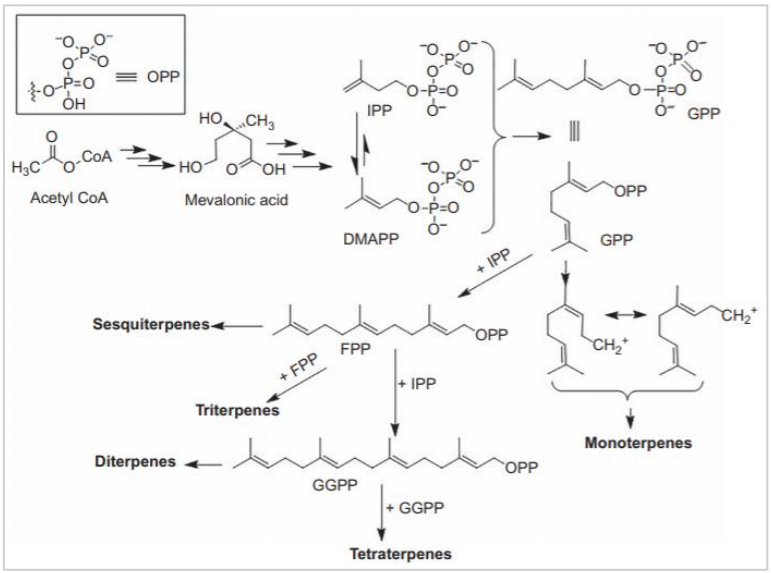

Figure I.20. Mevalonate pathway to isoprene production and the consequent biosynthesis of terpenoids. (Solomon 2019).

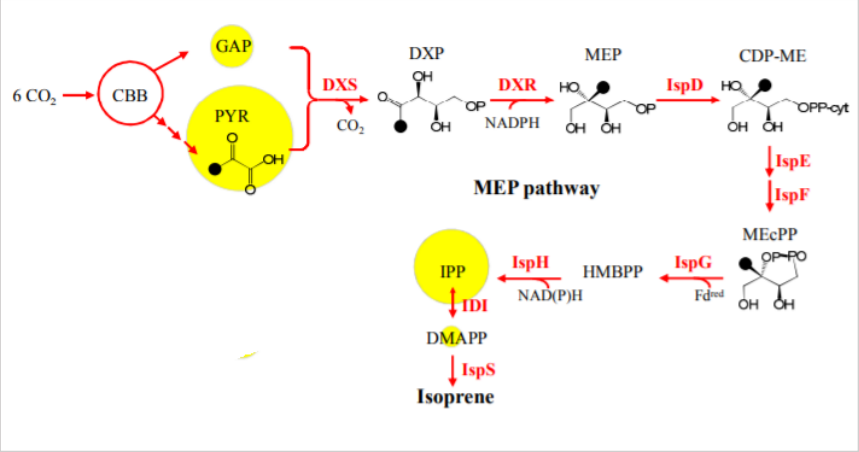

Figure I.21. MEP pathway for isoprene production. (Gao et al. 2016).

3.3 Storage and Emissions of Plant Terpenoids

3.3.1 Storage Pools of BVOCs in Mediterranean Plant Species

Some plant species as Pinus, Abies, Eucalyptus and those in family of Rutaceae and Lamiaceae, have storage compartments such as resin ducts, cavities, oil glands, glandular trichomes, where BVOCs are stored while other species such as some oaks (*Quercus spp*.) don't have such storage compartments (Laothawornkitkul et al. 2009, Loreto and Schnitzler 2010). There are two different types of monoterpenes storage pools in many BVOC emitting species including conifers; a first dynamic-fast responding temporary pool located in chloroplast and in the intercellular spaces of the mesophyll tissue, and a second larger permanent storage pool in the lumen of the thick-walled resin canals (Bäck et al. 2005).The terpenoids synthesized in the leucoplasts of the resin duct epithelial cells, are responsible for plant defense against biotic and abiotic stresses and are stored in the large size permanent storage pool which reduces in size significantly after foliar damage due to *de novo* synthesis and increased emissions (Holopainen 2004, Bäck et al. 2005).

3.3.2 Constitutive Emissions of BVOCs from Mediterranean Plant Species

The constitutive emissions of BVOCs (Holopainen 2004, Loreto and Schnitzler 2010) occur in normal conditions when terpenoids leak from the large storage pools in resin ducts to the mesophyll pools. These last, consist of two spatially separated sub-pools: a mesophyll pool and a surface pool among where there exists a gradient of terpenoids in their liquid phases from the pool with higher concentration, to the pool with lower concentration (Bäck et al. 2005). Mediterranean vegetation species have been described as high BVOC emitters (Fares et al. 2013, Owen et al. 1997). It has been found that conifer species such as Pinus pinea, Pinus sylvestris and Picea abies can emit significant amounts of monoterpenes while the broad-leaved trees such as Populus deltoids, Populus alba, Eucalyptus sp., Quercus cerris and Acacia cyanophylla emit large amounts of isoprene (Chen et al. 2020) between 400-600 $TgCyr^{-1}$ (Saunier et al. 2017). This is because these last species don't have storage pools and as isoprene has a very low boiling temperature (33°C) (Sharkey 1996) and high volatility due to a high Henry's law constant (K_h ~7500 Pa m^3 mol^{-1} at 25°C) (Harley 2013), it is not stored at all in large storage pools but readily emitted from *de novo* synthesis with a great dependence on light and temperature (Laothawornkitkul 2009, Lüpke et al. 2016). Isoprene help protect plant cell membranes involved in photosynthesis from thermal damage due to its hydrophobic

Table I.7. The major classes of biogenic volatile organic compounds (BVOCs), the major emitting plants, and current and future BVOC fluxes into atmosphere. (Laothawornkitkul et al. 2009)

BVOC Species	Present estimated annual global emission (10^{12} gC)	Future estimated annual global emission (10^{12} gC)	Atmospheric lifetime (d)	Example	Major emitting plants
Total	700 – 1000	1251 – 1288	-	-	-
Isoprene	412 – 601	638 – 689	0.2		Populus, Salix, Platanus, Cocos, Elaeis, Casaurina, Picea and Eucalyptus
Monoterpenes	33 – 480	265 – 316	0.1 – 0.2	β-Pinene, α-Pinene, limonene	Lycopersicon, Quercus, Cistus, Malus, Pinus, Cypressus, Trichostema
Other reactive BVOCs	~ 260	~ 56 – 159 (only for acetaldehyde and formaldehyde)	<1	Acetaldehyde, 2-methyl-3-buten-2-ol and hexanal family	Grassland (mix of C3 plants), Vitis, Brassica, Secale and Betula
Other less reactive BVOCs	~ 260	~ 292 – 514 (only for methanol, aceton, formic acid and acetic acid)	>1	Methanol, ethanol, formic acid, acetic acid, and aceton	Grassland (mix of C3 plants), Vitis, Brassica, Secale and Betula
Ethylene	8 – 25		1.9		

characteristics (Sharkey and Singsaas 1995, Sharkey 1996) and it is emitted from leaf stomata and cuticle (Saunier et al. 2017). The total amount of BVOCs emitted globally from living organisms are measured at 1 Pg per year, with plant BVOCs accounting in percentages of 44% isoprene, 11% monoterpenes, and 22.5% of oxygenated hydrocarbons and other leaf volatiles (Iijima 2014). BVOC emissions from forested areas are typically estimated by multiplying an emission factor expressed as micrograms of BVOC carbon per gram foliar dry mass per hour (μg-C. $g^{-1}.h^{-1}$), while for crops, emission rates are expressed as BVOC mass per unit time per land area (Geron et al. 1994). Table I.7, lists the current and predicted future fluxes of major groups of BVOCs emitted from major groups of BVOC emitting plants.

3.3.3 Induced BVOC Emissions from Mediterranean plant species

The induced volatile organic compounds (IVOCs) are emitted from storage pools or *de-novo* synthesis with proportions depending on the duration and severity of various abiotic stresses (Ozone (O_3), radiation, drought, extremes in temperatures, etc.) and biotic stresses (fungi, bacteria, herbivores, etc.) (Kleist et al. 2012, Niinemets et al. 2013). IVOCs include mainly terpenoids and C6 green leaf volatiles (GLVs) in addition to alkenes, alkanes, carboxylic acids, and alcohols (Laothawornkitkul 2009, Holopainen 2004) (see also Figure I.22).

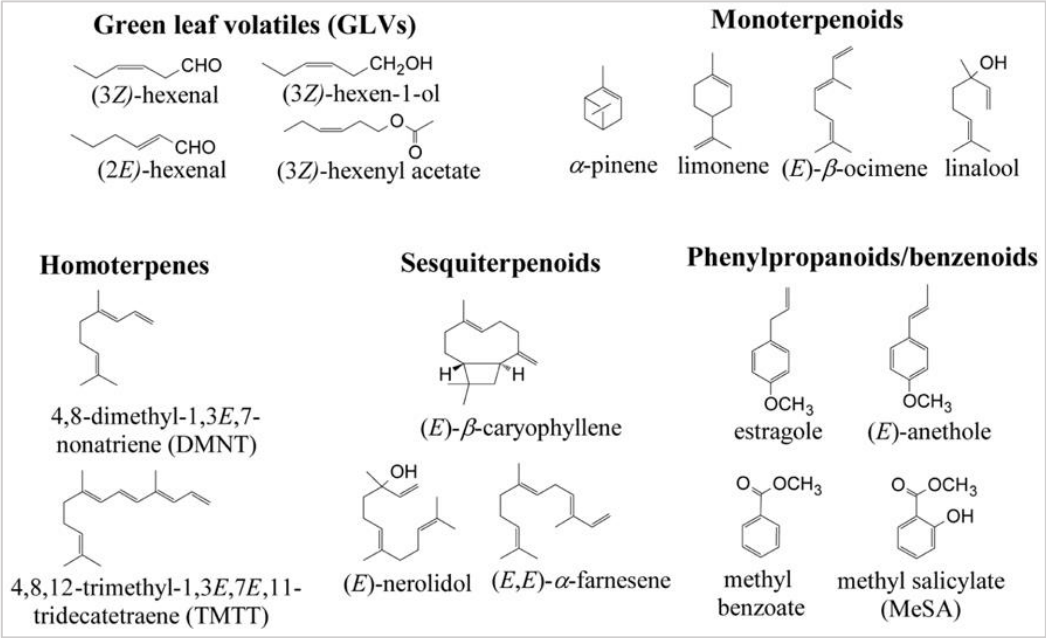

Figure I.22. Molecular Structures of selected plant volatiles (BVOC) emitted in response to a variety of stress factors, (Niinemets et al. 2013). GLV are mainly C_6 saturated or monosaturated aldehydes, alcohols and esters produced via the lipoxygenase (LOX) pathway, can account of >50% of emissions from damaged plant parts. (Holopainen 2004).

3.4 Effect of Abiotic Stresses on BVOCs Synthesis and Emission Rates

Abiotic stresses affect the biosynthesis rates of BVOCs by inhibiting photosynthesis due to the decrease of CO_2 uptake and diffusion inside leaves to the site of fixation hence inhibiting the carbon source of terpenes synthesis (Loreto and Schnitzler 2010). This effect on BVOC biosynthesis is also coupled to their emissions. We are going to focus on the environmental abiotic stressors on BVOC emissions in order to couple them to the main environmental factors affecting wildfires behavior (see Figure I.15), i.e. temperature and drought.

3.4.1 Temperature

The emission of BVOCs under the effect of temperature is related to the partition between their liquid and gas phases in the plant according to their volatility parameter, the Henry's law constant, k_h (Equation 1) also called the air-water partition coefficient. It's the ratio of a compound's partial pressure in air to its concentration in water at a given temperature (Katyal and Morrison 2007). Indeed, the compounds with a larger K_h, partition primarily to the gas phase whereas those with a low K_h, partition mainly to the aqueous phase (Niinemets et al. 2004, Katyal and Morrison 2007). At its simplest, volatilization is a function of the partial pressure of the BVOC to its concentration in the solution, the higher the Henry's law constant the higher the volatility. At rising temperatures more BVOCs will enter their gaseous phase and get emitted from the plant. The Henry's law constants for some common BVOCs at 25°C are listed in Table I.8, The values are augmented by 1.3- to 1.8- fold for every 10°C increase in temperature (Copolovici and Niinemets 2005).

$$K_h = \frac{P_a}{[c]} \qquad (1)$$

Where,

K_h is the Henry's law constant in Pa m^3 mol^{-1}.
P_a is the partial pressure of the gas (Pa).
[c] is the molar concentration of the gas in the aqueous solution $mol.m^{-3}$.

Table I.8. Henry's law constants (Kh) at 25°C of common BVOCs.

Compound Class	Compound Name	K_h (Pa m^3 mol^{-1})
Acyclic alcohol [a]	Linalool	2.078
Monocyclic alcohol [a]	α-Terpineol	0.244
Bicyclic ketone [a]	Camphor	0.900
Ethers [a]	1,4-Cineol	13.48
	1,8-Cineole	13.27
	α-Pinene oxide	42.2
Acyclic Hydrocarbons [a]	Isoprene	7789
	Myrcene	6300
	β-Ocimene	2507
Aromatic monocyclic hydrocarbons [a]	m-Cymene	1105
	p-Cymene	935
Bicyclic hydrocarbons [a]	Camphene	3238
	α-Pinene	13590
	3-Carene	13650
	β-Pinene	6826
Monocyclic Hydrocarbons [a]	Sabinene	6451
	Limonene	2850
	p-Menthane	179900
	α-Phellandrene	5496
	β-Phellandrene	5666
	α-Terpinene	3593
	γ-Terpinene	2601
	Terpinolene	2682
Sesquiterpenes [b]	β-Caryophyllene	2731
	α-Cedrene	3510
	α-Farnesene	2960
	α-Humulene	3410

[a] (Copolovici and Niinemets 2005), [b] (Copolovici and Niinemets 2015)

This direct effect of elevated temperatures on emissions of BVOCs is governed by the resistance to their diffusion track from their synthesis sites to the atmosphere. Evaporation rates of BVOCs are higher from the temporary storage pools in the leaf mesophyll governed by the stomata openings, rather than from the large storage pools in the resin ducts by which the emissions from these large concentrations are only affected if they were opened by external factors such as herbivores, wind or fires. Usually high temperatures are accompanied by droughts which affect the stomatal conductance *Gw* ($mmolH_2O.\ m^{-2}.\ s^{-1}$) by closing the stomatal openings to reduce the amount of water lost by transpiration. Isoprene and monoterpenes which easily transition to gaseous phases due to their high K_h are not affected by stomatal conductance

because they build up to increase their partial pressures which increase their diffusion gradient (ΔP) from the intercellular air space inside the leaves to the atmosphere (Loreto and Schnitzler 2010, Chen et al. 2020). However, the compounds which have high partition to liquid phase such as oxygenated VOCs (methanol, C_6 aldehydes, and alcohols) are strongly restrained by stomatal closure (Loreto and Schnitzler 2010). Monoterpene (MT) emissions in Mediterranean conifer species (Scots *pine*, Norway *Spruce*) under thermal stresses are mainly emitted from the resin ducts where they are stored, while other broadleaf species with no storage pools (European *beech*, Palestine *oak*) emit MT from *de novo* synthesis (Kleist et al. 2012). Kleist et al. (2012), studied the reversible and irreversible effects of raised temperatures (heat waves) on the constitutive emissions of MT from storing and non-storing Mediterranean species. They found that the emissions from non-storing species were reduced after application of thermal stresses (31 – 44°C for periods ranging from 1h to 5 days) (Table I.9), whereas for species with storage pools MT emissions increased with thermal stresses (31 - 51°C for 1- 48 hours) indicating their high diffusion from the resin ducts, and there were no irreversible impacts on their emissions after applying the heat stresses. It's notable that GLV (green leaf volatiles) emissions are indicators to a possible damage to the membrane surrounding the resin ducts due to severe thermal stresses (46 - 51°C for 3 hours) by which MT emissions remained at high values after the thermal stresses.

Table I.9. Monoterpene (MT) emissions (φ) from Palestine *oak* (*Quercus calliprinos*) measured at 24°C before and after thermal stress application. (Kleist et al. 2012)

MT	Φ BEFORE [PMOL M^{-2}. S^{-1}]	Φ AFTER [PMOL M^{-2}. S^{-1}]
α-thujene	8.3 ± 0.4	4.2 ± 0.8
α-pinene	260.0 ± 6.5	120.0 ± 15.2
sabinene	22.0 ± 0.8	14.0 ± 2.4
β-pinene	93.0 ± 2.7	50.0 ± 6.9
myrcene	11.0 ± 0.9	2.6 ± 0.4
α-phellandrene	5.4 ± 0.3	2.1 ± 0.4
α-terpinene	16.0 ± 1.0	2.3 ± 0.5
β-phellandrene	13.0 ± 0.6	6.4 ± 1.0
γ -terpinene	39.0 ± 1.9	1.6 ± 0.3

Most MT were emitted from storage pools in conifers; however, an exception was for 1,8-cineole (bicyclic ether) which was emitted from *de novo* synthesis by which its emission rates ceased after the application of heat stresses and the emergence of GLV compounds. The emissions only recovered after 3 days (Kleist et al. 2012). They also noticed that remarkable de novo emissions of sesquiterpenes (α-farnesene and β-farnesene) and phenolic BVOCs (methyl salicylate) due to biotic stress (insect infestation) which ceased after the heat stress treatment. (Chen et al. 2020) studied the effect of temperatures on the diurnal and seasonal emissions of BVOCs (isoprene, monoterpenes, sesquiterpenes) from five Mediterranean temperate forest species (conifers and broadleaf) and found the correlation factors between the emissions and physiological parameters such as temperatures, stomatal conductance, photosynthetic rates, … etc. In the diurnal measurements, they found that the highest emission rates of isoprene and

monoterpene were accompanied by the highest air temperatures and PAR (photosynthetically active radiation) usually during midday. Also, broad-leaf trees had higher emissions of isoprene compared to conifers which had higher emissions of MT with the high rates from spring-summer seasons peaking in August and decreasing from September to reach minimum levels in winter (Figure I.23).

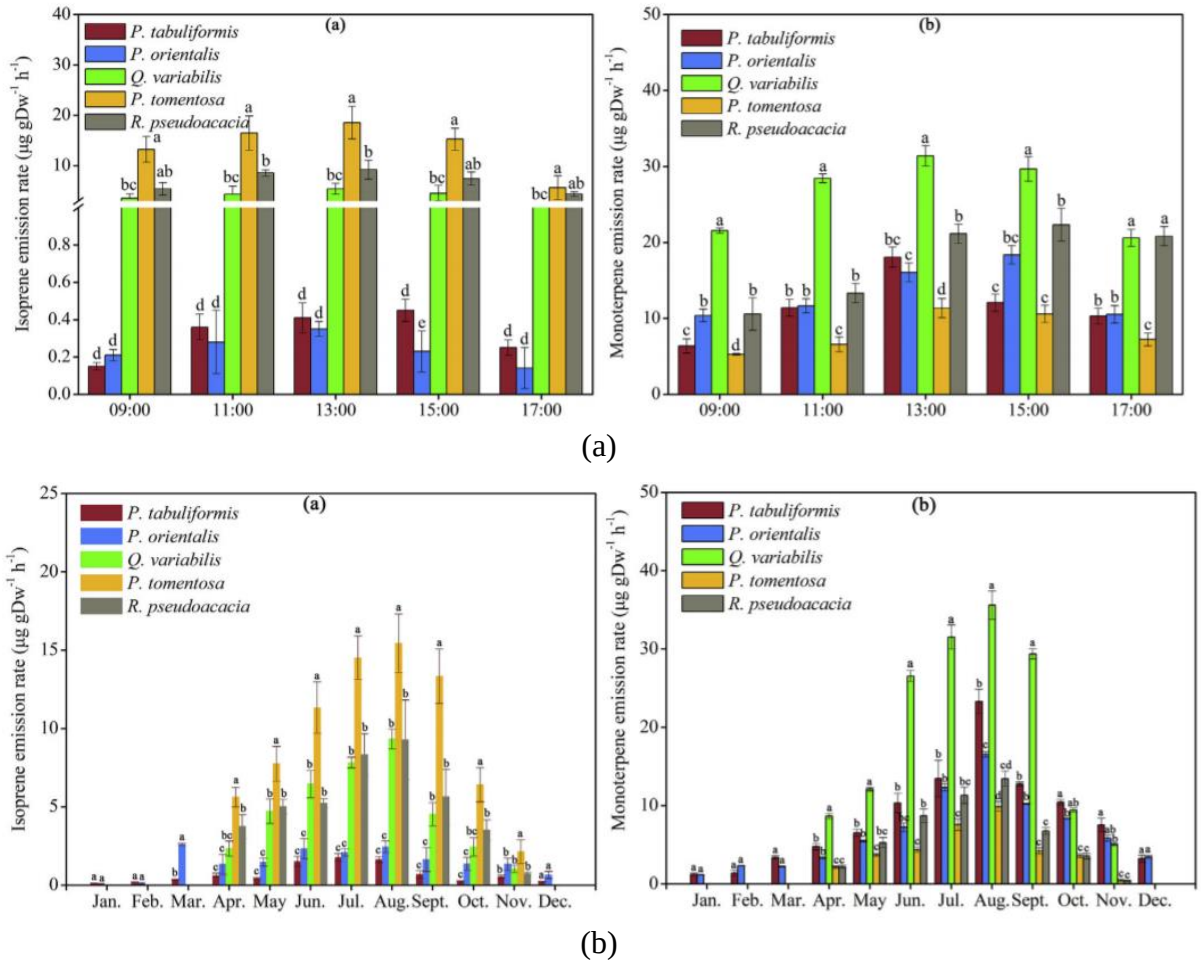

Figure I.23. (a) Diurnal and (b) seasonal measurements of isoprene and monoterpenes emissions from five temperate forest species (broadleaf and conifers), (Chen et al. 2020).

Such results were found by (Gernard-Zielinski et al. 2015), who found that isoprene emissions from the Mediterranean *Quercus pubescens* were more than 300 times the MT emissions, while the MT emissions were dominated by 67% α-pinene and 33% limonene contributed to light and temperature dependent *de novo* emissions. (Ghirardo et al. 2010) found the same results in his studies on conifers such as *Pinus sylvestris L.*, *Larix decidua L.* and deciduous *Holm oak* (*Q ilex L.*). Our focus on temperate deciduous and boreal conifer forests are because they are the dominating forest biomes in the Mediterranean climates (Naudts et al. 2016). Although grasslands and shrublands cover 45% of the Mediterranean region with species such as *Dehesa* and dry perennial grasslands, dwarf shrublands of *Cistus* and *Rosmarinus officinalis*, shrublands of *Thymus vulgaris* and *Lavandula pedunculata*, *Toledo*, and coastal *maquis* species (Marcenò et al. 2018) however, their emissions were humbly studied. *Sclerophyllous* shrub species such as *Cistus* (*Cistus monspeliensis*, *Cistus albidus*) and *Rosmarinus officinalis* are reported to be BVOC storing species in their glandular hairs and leaf glands, respectively. Their storage

includes different terpene mixtures i.e. monoterpenes in *Rosmarinus* and sesquiterpenes in *Cistus albidus* (Ormeno et al. 2008, Rivoal et al. 2010). *Cistus monspeliensis* store terpenes 10 folds less compared to *Cistus albidus*, and they emit BVOCs (α-pinene, camphene, β-pinene, limonene, … etc.) with highest rates (70% higher) during summer seasons (due to high temperatures) compared to winter seasons (Table I.10). Their stored BVOCs were composed of one oxygenated monoterpene (β-cyclocitral) and three sesquiterpenes (α-copaene, alloaromadendrene, δ-cadinene) while their emitted BVOCs due to temperature and light (highest in summer) were different, an evidence that they were emitted out of *de novo* synthesis (Rivoal et al. 2010). To this end, there exists two major algorithms that simulate emissions according to the presence or absence of storage compartments in vegetation species; the Tingey algorithm which uses only temperature for storing species and the Guenther's algorithm which uses temperature and light for non-storing species (Rivoal et al. 2010). *Rosmarinus officinalis* a wide spread shrubland species in the Mediterranean climate regions, possess external terpene storage organs (glandular trichomes) by which their concentrations decrease due to temperature augmentation and increase due to drought stress accompanied with remarkable synthesis of antioxidant mono and di - terpenes as defense to leaves oxidation (Lluisià et al. 2006). Seasonal concentrations of terpenoids in *Rosmarinus officinalis* coupled with effects of warming and drought were presented by (Lluisià et al. 2006).

Table I.10. Seasonal emission rates of terpenes from Cistus monspeliensis. (Rivoal et al. 2010)

			Emission rate (µg g^{-1} h^{-1})		
Compound	**Winter**	**Summer**	**Compound**	**Winter**	**Summer**
Monoterpenes			**Oxygenated monoterpenes**		
α-Pinene	0.064	6.576	1, 8 Cineole	0.001	0.178
Camphene	0.001	0.034	Camphor	0.001	0.006
β-Pinene	0.001	0.597	α-Terpineol	0.001	0.282
β-Myrcene	0.025	1.681	Monoterpene derivatives		
α-Phellandrene	0.007	0.016	Bornyl acetate	0.005	0.033
β-Cymene	0.005	0.065	**Sesquiterpenes**		
Limonene	0.038	0.176	B-Caryophyllene	0.004	0.003
Overall terpenes	0.153	9.873			

3.4.2 Drought

The average temperature of the planet will increase by 1.4 to 5.8 °C by the end of the century, with drought being the main consequences of this warming (Preston & Jones 2006). Drought effects on BVOC emissions from plants depend on its severity. Moderate drought can decrease, enhance, or has no effect on isoprene and monoterpene emissions, but a severe long-lasting water stress that leads to gross wilting or complete inhibition of photosynthesis, will significantly reduce BVOC emissions (Laothawornkitkul et al. 2009). Mediterranean vegetation species which have terpene storage compartments continue to emit BVOCs during drought periods, however, other species may compensate the absence of these compartments by the efficient use of their water content, so that they are classified into water savers or water spenders (Vilagrosa et al. 2003). For example, in a semi-arid climate such as the Mediterranean climate, common shrub species such as *Quercus coccifera* and *Pistacia lentiscus L*. have the ability to modify their above and under-ground biomass in order to accommodate to severe

droughts that would lead to the loss of their stomatal conductance *Gw* (mmol (H_2O) m^{-2}. s^{-1}). For example, *Q. coccifera* develop a sparse and deep root network in order to increase its leaf water content and photochemical efficiency while P. lentiscus develop a dense root system to take advantage of any Autumn rainfall (Vilagrosa et al. 2003). This strategy allowed *Q. coccifera* to continue emitting even when the soil moisture content decreased by 80%, while a species like *Quercus ilex* inhibited its emission after a reduction of 50% in soil moisture content (Laothawornkitkul et al. 2009). Table I.11. lists the drought effects on the BVOC emissions of some Mediterranean species with the references of the conducted studies.

Table I.11. Effect of drought on BVOC emissions from Mediterranean vegetation species. (Laothawornkitkul et al. 2009).

Source	Description	Plant species	Effect on BVOC emissions
Bertin & Staudt (1996)	18 days of drought period (severe drought). Soil moisture reduced by ~54%. Pot-grown plants. Young plants (age not specified).	*Quercus ilex L.*	100% decrease in monoterpenes
Pegoraro et al. (2004)	10–12 days of drought period (severe drought) Soil moisture reduced by ~80%. Pot-grown plants 2-yr-old plants.	*Quercus virginiana Mill.*	64% decrease in isoprene
Plaza et al. (2005)	Field observation 30-yr-old Mediterranean oak forest. Two growing seasons (2000–01) Natural drought (measured diurnal courses of emission rates).	*Quercus ilex spp. rotundifolia*	Inconsistent monoterpene emission over the 2 years
Pegoraro et al. (2006)	36 days of drought period (mild drought). Soil moisture reduced by ~50% from field capacity. ~15-yr-old plants.	Mixed isoprene-emitting and non-isoprene-emitting species with deep roots	No significant effect on isoprene
Llusia et al. (2006)	Field observation. Sliding plastic curtain (mild drought).	*Pinus halepensis L.*	Contrasting results depending on seasons, plant species, year and type of BVOC.
	Mediterranean scrubland (2002–04). Soil moisture reduced by 19% from field capacity.	*Globularia alypum L.* *Rosmarinus officinalis L.* *Erica multiflora L.*	
Ormeno et al. (2007)	Laboratory observation. 11 days of drought period (severe drought).	*Rosmarinus officinalis L.*	~ 20% decrease in total monoterpene and sesquiterpenes
	Pot-grown plants. Soil moisture reduced by ~82% from field capacity.		No sig. effect on total monoterpene
	3-yr-old plants		~ 70% decrease in total sesquiterpenes
		Pinus halepensis L.	~ 290% increase in total monoterpenes and sesquiterpenes
			~ 270% increase in total monoterpenes

			~ 28% decrease in total sesquiterpenes
		Cistus albidus L.	~ 107% increase in total monoterpenes and sesquiterpenes
			~ 285% increase in total monoterpenes
			~ 13% decrease in total sesquiterpenes
		Quercus coccifera L.	No sig. except day 7 ~ 265% increase in total monoterpenes + sesquiterpenes
			No sig. effect on total monoterpenes
			~ 1% decrease in total sesquiterpenes
Llusia et al. (2008)	Field observation. Sliding plastic curtain.	*Pinus halepensis L.*	~ 166.5% increase in selected monoterpenes
	Mediterranean scrubland. Long-term drought (mild drought).	*Globularia alypum L.*	75% increase in selected monoterpenes
	Two growing seasons (2003–05) (protect all rain events). Soil moisture reduced by ~16% from field capacity.	*Erica multiflora L.*	19% decrease in isoprene and 26.4% increase in selected monoterpene
Fortunati et al. (2008)	Laboratory observation. 35 days of drought period (severe drought).	*Populus nigra L.*	~ 71% decrease in isoprene
	Pot-grown plants. Soil moisture reduced by ~65% from field capacity		

3.5 Linking BVOC Emissions to Wildfires

It is proven in fire research that, it is not the solid fuel that burns but rather, when the solid matter is heated up sufficiently it degrades into smaller particles and produces fumes in the form of flammable pyrolysis gases which form the actual fire fuel (Figure I.24). Same concept applies for wildfires (Lambert 2013). Pyrolysis is not a phase change it's a chemical process, more correctly, it is the thermal degradation of a solid into smaller volatile molecules without interacting with oxygen or any other oxidants (Stauffer et al. 2008). After a wildfire is ignited, the mechanism that ensures wildfire propagation is described as the chemical chain reaction in the triangle of wildfire (Figure I.2), by which the gases emitted from the heated solid vegetation present at the fire front, get burnt and flame attachment takes place. However, the term "sufficient heat" in wildfire literature is called the heat of preignition (Q_{ig}), which includes is the heat required to bring a unit mass of fuel to ignition temperature (Rothermel 1972, Albini 1976). A part of this heat is consumed by the fuel to evaporate its moisture content defined as the latent heat of vaporization and another part is the sensible heat required to raise the temperature of the fuel to the point of flame attachment or pilot ignition, i.e. 325°C (Prabir 2018). The forms of this heat transfer in a wildfire is achieved through three mechanisms, conduction, convection, and radiation which will be discussed in the next section.

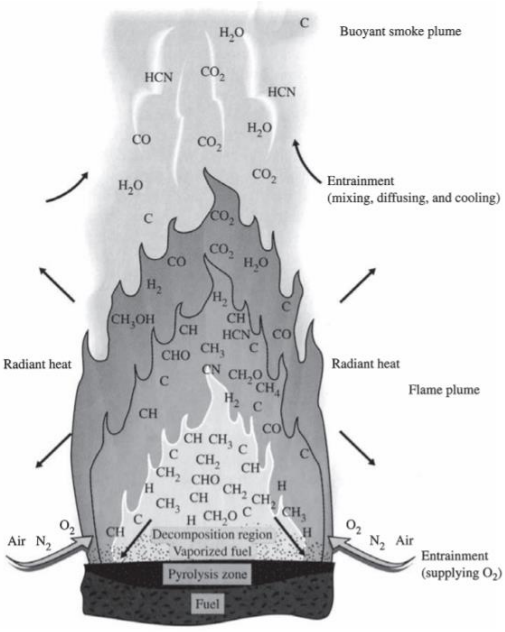

Figure I.24. Representation of the process of flaming combustion. (Stauffer et al. 2008)

4 Vegetation Biomass Polymer Structures and Thermal Degradation

Wildland vegetation matter consists of cellulose, hemicellulose, lignin, protein, nucleic acid, amino acid, and volatile extractables (Lobert and Warnatz 1993). The cellulose (41-53% of dry biomass) is a linear condensation polymer consisting of 7000-12000 D-glucose monomers while the hemicellulose (15-25% of dry biomass) is made of 100-200 sugar monomers composed of mixtures of carbohydrate polysaccharides (Liodakis et al. 2002). Lignin which comprises (16–33%) of the plant dry matter is a complex polymer, consisting of four or more phenylpropane monomers per molecule (Liodakis et al. 2002). The decomposition of these structures in the pyrolysis process result in the generation of combustible organic gases which mix with oxygen in air and produce the flame, of course the higher the cellulose and hemicellulose amounts compared to lignin the faster the pyrolysis process and the sooner the ignition (Ottmar 2014).

4.1 Pyrolysis and Char Formation

It's difficult to standardize pyrolysis processes and mechanisms among biomass species as the pyrolysis kinetics and activation energies (Jones et al. 2015), depend on the plant moisture content, lignin/cellulose/hemicellulose ratios, volatile oils or terpene content, and ash content and composition, sometimes even in specimens of the same plant (Diebold 1980). After evaporation (30-100°C) and volatilization (120-170°C), biomass pyrolysis starts at about 180°C when the hemicellulose begins decomposing until 350°C, followed by cellulose decomposition (275 – 350°C), and lignin (250 – 500°C), Table I.12, (Lowden and hull 2013, Liodakis et al. 2002b).

Table I.12. Temperature ranges of vegetation pyrolysis and combustion. (Lowden and Hull 2013).

Temperature range	Vegetation Decomposition Process
>100°C	The evaporation of chemically unbound water.
160-200°C	The three polymeric components of solid vegetation begin to decompose slowly. Gases formed at this stage are non-combustible (mainly H_2O).
200-225°C	Solid vegetation pyrolysis is still very slow, and most of the gases produced are non-combustible.
225-275°C	The main pyrolysis begins and flaming combustion will occur with the aid of a pilot flame.
280-500°C	Gases produced are now volatile (CO, methane etc.) and smoke particles are visible. Char forms rapidly as the physical structure of wood breaks down.
>500°C	Volatile production is complete. Char continues to smolder and oxidize to form CO, CO2 and H2O

4.2 Thermal Degradation of Cellulose: Laboratory Scale Analysis

Pyrolysis can be endothermic and exothermic at which char is formed. Two forms of gaseous (tar) products are produced from biomass pyrolysis, those that evaporate readily following the pyrolysis of lignocellulose which are rich in hydrogen and oxygen and those that don't. If these formed tar molecules do not evaporate quickly at a certain temperature of a thermal stress, they cross link to form larger thermally stable tar molecules which eventually form char. The relative ratios between volatile-char formation depends on temperature, at 300°C the volatile forming reaction is favored over the char formation reaction by a ratio of only two to one, while at 600°C the volatiles formation is favored by 50 to 1, i.e., if the biomass spends insignificant amount at lower temperatures, nearly all volatiles will be produced (Diebold 1980). If char forms on the vegetation surface it will act as a barrier between the volatiles and oxygen in air, especially that the carbon-carbon bond in the graphitic carbon structures are unbreakable by pyrolysis alone to temperatures beyond 3000 °C (Lowden and Hull 2013). On a laboratory scale, experimental thermal stresses with radiant heat fluxes on very thin two-dimensional cellulose samples, produced 33% by weight char at 6.3 W/cm^2, 3% at 46 W/cm^2, and 1% at 12500 W/cm^2 however, a 3-dimensional sample will require more heat fluxes in order to achieve these results due to heat sink effects (Copper and Mountain 1980). These results have led to the conclusion that in order to achieve a fast pyrolysis rate with maximum volatile emissions, a supply of a 2000 J/g pyrolysis activation energy (calculated by Arhenius, Equation 12) should be supplied to the biomass surface at about 500°C with a 50W/cm^2 heat flux.

$$\ln\left(\frac{a}{T^2}\right) = \ln\left(\frac{K_0 R}{E}\right) + 0.6705 - \frac{E}{RT} \qquad (12)$$

Where,

a is the heating rate (K.min^{-1} or °C.min^{-1}), T is the temperature of heating (K or °C), E is the activation energy (kJ.mol^{-1}), K_0 is the frequency factor corresponding to E (s^{-1}), R is gas constant (8.3145 J.mol^{-1}. K^{-1}). (Sonobe and Worasuwannarak 2008).

During the combustion, the cellulose molecules decompose by two pathways; in the first pathway at temperatures <300 °C, biofuels are depolymerized, fragmented and oxidized to char, while in the second pathway, i.e. > 300°C, bond cleavage by transglycosylation, fission and disproportionation reactions give rise to the formation of levoglucosan, a widely used molecular marker for biomass burning process (Chan et al. 2011). Laboratory experimental investigations on the thermal decomposition products of cellulose under different temperatures in vacuum and atmospheric pressure in nitrogen (inorganic catalyst) are listed in Table I.13 (Diebold 1980).

Table I.13. Effect of temperature and medium on the products of cellulose powder pyrolysis. (Diebold 1980).

Medium	Oven T (°C)	Pyrolysis time (min)	Percent yield from cellulose		
			Char	Tar	Levoglucosan
Vacuum	300	180	21	60	34
	325	60	10	70	38
	350	30	8	70	38
	375	10	6	70	38
	400	5	5	77	39
	425	4	4	78	40
	450	3	4	78	39
	475	3	3	80	38
	500	3	3	81	38
Nitrogen	300		34.2	19.1	3.57

An important note to take care of while conducting experimental thermal stressing on biomass, is that the oven temperatures are not necessarily the same temperatures developed at the stressed sample. In Figure I.25, the experimental pyrolysis tests ran at oven temperatures from 300-500°C raised the rate of heat transfer but didn't raise the temperature of the cellulose substrate at the same rate because the evaporation process and the pyrolysis of volatiles are endothermic reactions (Diebold 1980).

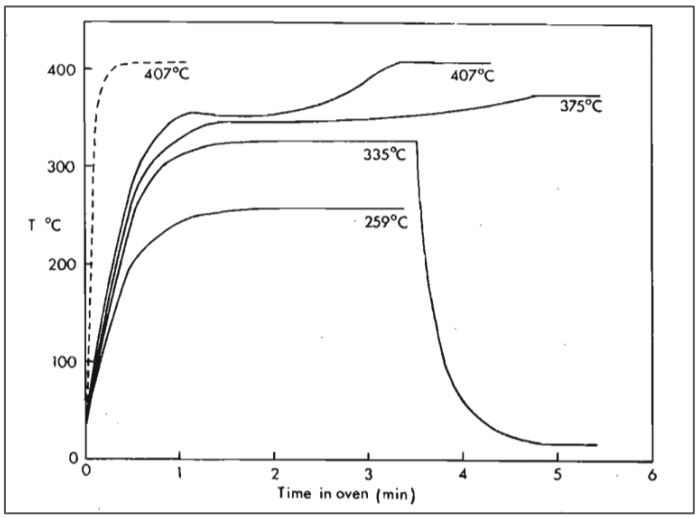

Figure I.25. Temperature of pyrolysis as measured by a thermocouple in cellulose sample versus an oven temperature from 300 – 500°C. The dotted line is a result of empty sampling. The drop is cooling after the removal of the specimen. (Diebold 1980)

4.3 Thermal degradation of lignin/laboratory scale analysis

The thermal decomposition of lignin starts at relatively low temperatures (200-275°C), the main process occurring around 400°C with the formation of aromatic hydrocarbons, phenolics, hydroxyphenolics and guaiacyl-/syringyl-type compounds (intermediate degradation products where their production decreases with increasing pyrolysis temperatures), most products having phenolic-OH groups (Brebu and Vasile 2009). The dehydration of lignin is harder than cellulose or hemicellulose and dehydration products are unsaturated side chains such as styrene derivatives, vanillin and vanillic acid and others. Further pyrolysis produces acetic acid, and non-condensable gases such as CO_2, CO and CH_4 which start at 230°C and reach a maximum at 500°C at which H_2 starts to emerge due to rearrangement and condensation of aromatic rings, beyond 600°C, char, C1-C3 hydrocarbons start to emerge (Brebu and Vasile 2009). The volatile yield from lignin varies from 61-74% wt depending on the nature and amount of lignin in the vegetation species, i.e., as the amount of lignin increases (with low methoxy groups in thermally stable softwood as coniferous species) bio char formation increases.

5 Quantification Methods of VOCs in Wildfires Smoke

Forest fires emissions depend on multiple and interdependent factors such as forest fuels characteristics, burning efficiency, burning phase, fire type, meteorology and geographical location (Miranda et al. 2009, Andreae 2019). Burning phases where emissions are differentiated are classified between pre-ignition, flaming, and smoldering. A modified combustion efficiency (MCE), is used to identify and differentiate two types of combustion phases flaming and smoldering according to the ratio between the carbon emitted from the fire as CO_2 and the carbon emitted as CO_2 and CO as a total in relation to background (ambient) values as illustrated in (Equation 13), where ([]) represents the concentration (Evtyugina et al. 2013, Andreae 2019).

$$MCE = \frac{\Delta CO_2}{\Delta CO_2 + \Delta CO} \qquad (13)$$

Where,

$\Delta CO_2 = [CO_2]_{plume} - [CO_2]_{background}$

and,

$\Delta CO = [CO]_{plume} - [CO]_{background}$

An MCE << 0.9 means [CO] > [CO_2] is an indication of smoldering fire, whereas an MCE = 0.99 means [CO_2] > [CO] is an indication of pure flaming (Evtyugina et al. 2013).

Quantification of emissions from vegetation fuels in wildfire events is done by two methods: emission ratios and emission factors. The former relates the emissions to a reference species such as CO_2 or CO while the latter relates the emissions to the amount of fuel burnt.

5.1 Emission ratio (ER)

Emission ratios (ERs) relate the emissions from burning vegetation during a wildfire to a reference species. It is calculated by dividing the excess of a particular species of interest by the excess of a reference species such as CH_4, C_2H_2 (acetylene), and mainly CO and CO_2. The choice for the reference species depends on their redundancy in the smoke of each fire phase,

i.e., CO is used to calculate the ER of the species emitted during the smoldering phase while CO_2 is used for those emitted during the flaming phase. The excess is calculated by subtracting the concentration of the species in the ambient from the concentration found in the smoke. (Equation 14) shows an example to calculate the emission ratio (ER) of methyl chloride CH_3Cl relative to CO (Andreae & Merlet 2001).

$$ER_{CH_3Cl/CO} = \frac{\Delta CH_3Cl}{\Delta CO} = \frac{(CH_3Cl)_{smoke} - (CH_3Cl)_{ambient}}{(CO)_{smoke} - (CO)_{ambient}} \quad (14)$$

5.2 Emission Factor (EF)

Emissions factors (EFs) are used to relate the emissions from burnt vegetation in a wildfire to the amount of the dry fuel burnt. The emission factor of a species has the unit of a gram of emissions per kilogram of dry fuel burnt ($g.kg^{-1}$), (Andreae 2019). Measuring the EF requires the knowledge of the carbon content of the biomass burned or the carbon budget of the fire. The carbon content can be measured by combining the emitted concentrations of CO_2, CO, hydrocarbons and particulate carbon when feasible, and when not, the fuel carbon budget can be estimated by multiplying the concentration of CO_2 in the smoke with an assumed factor to represent non-CO_2 such as (CO, hydrocarbons, aerosol carbon) however, when none of this information are available a 45% of biomass carbon content is usually assumed (Andreae and Marlet 2001). (Equation 15) represents the equation of EF as the ratio of concentration of species [X] by the total carbon concentration in the smoke, while (Equation 16) represents the calculation of emission factor EF of species [X] from its emission ratio (ER) (Andreae 2019).

$$EF_x = \frac{M_X}{M_{biomass}} = \frac{M_X}{M_C}[C]_{biomass} \quad (15)$$

$$\cong \frac{[X]}{\sum([C_{CO_2}] + [C_{CO}] + [C_{CH_4}] + [C_{VOC}] + \cdots)}[C]_{biomass}$$

Where,

M_c is the mass of the carbon emitted, $[C]_{biomass}$ is the carbon concentration in the biomass burnt and [X] is the concentration of species X in the smoke and $[CO_2]$ … are the concentrations of the various carbon species in the smoke (Andreae and Merlet 2001).

$$EF_X = ER_{(X/Y)} \frac{MW_X}{MW_Y} EF_Y \quad (16)$$

Where,

EF_X is the emission factor of species X, $ER_{(X/Y)}$ is the emission ratio of species X relative to reference species Y, MW_X and MW_Y are the molecular weights of the species X and the reference species Y, and EF_Y is the emission factor of reference species Y.

5.3 Emission Factors of VOCs from Wildfires

Out of non-methane biogenic volatile organic compounds (NMBVOCs) are terpenoids (isoprene, monoterpenes, sesquiterpenes…) which form 80% of the total VOCs released from undisturbed wildland vegetation (Loreto and Centritto 2008). However, the fire induced VOCs either from burning, heated (ahead of fire front), and smoldering vegetation are diverse and temperature dependent (Figure I.26). Global emissions annual estimates from biomass burning fall in the range of 4.3 to 12.9 Pg. a^{-1} (Andreae 2019). The nature of these emissions depends on the dominant fire phase for example in dry grasslands, flaming combustion dominates (high CO_2) while smoldering phase dominates (high CO) in boreal and temperate forests which have high fuel moisture content and large fuel diameters. Average emission factors of VOC emissions from global wildfires in different wildland vegetation covers, in addition to average of emissions from laboratory experiments are presented in Table I.14.

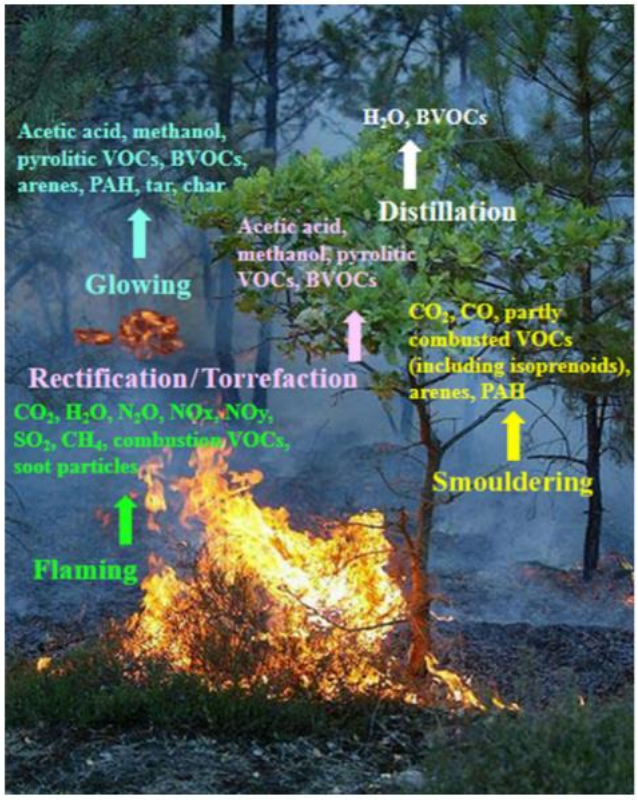

Figure I.26. VOC emissions from different combustion stages. (Ciccioli et al. 2014)

Table I.14. Average EFs ($g.kg^{-1}$ dry biomass burned) of pyrogenic species emitted from various types of biomass burning. (Andreae 2019)

	Average EFs			
Species	**Savanna and grassland**	**Temperate forest**	**Boreal forest**	**Lab studies**
MCE	0,94	0,9	0,89	0,9
CO2	1660	1570	1530	1590
CO	69	113	121	93
CH_4	2,7	5,2	5,5	5,9
VOC	5,1	13,4	6	18

Total NMVOCs, incl. unidentified	30	39	59	–
C_2H_2	0,31	0,31	0,28	0,35
C_2H_4	0,83	1,11	1,54	1,6
C_2H_6	0,42	0,69	0,97	1,12
C_3H_4	0,071	0,05	0,062	0,54
C_3H_6	0,46	0,6	0,67	0,85
C_3H_8	0,13	0,28	0,29	0,27
1-Butene	0,082	0,12	0,16	0,27
i-Butene	0,041	0,086	0,052	0,18
trans-2-Butene	0,02	0,037	0,03	0,123
cis-2-Butene	0,017	0,038	0,023	0,158
Butadiene	0,095	0,125	0,089	0,17
n-Butane	0,021	0,08	0,111	0,188
i-Butane	0,007	0,031	0,052	0,444
1-Pentene	0,022	0,048	0,046	0,136
2-Pentenes	0,014	0,043	0,011	0,09
n-Pentane	0,007	0,034	0,05	0,076
Methyl-butenes	0,025	0,056	0,051	0,202
2-Methyl-butane	0,008	0,017	0,032	0,096
n-Pentadienes	0,048	0,035	0,049	0,171
Isoprene	0,101	0,1	0,074	0,34
Cyclopentene	0,019	0,041	0,03	0,055
Cyclopentadiene	0,026	0,027	0,041	0,038
4-Methyl-1-pentene	0,049	0,04	0,043	0,005
2-Methyl-1-pentene	0,018	0,058	0,043	0,019
1-Hexene	0,043	0,084	0,109	0,045
Hexadienes	0,006	0,006	0,009	0,061
n-Hexane	0,018	0,032	0,054	0,026
Isohexanes	0,019	0,026	0,013	0,062
Heptanes	0,016	0,029	0,021	0,08
Octenes	0,021	0,036	0,021	0,044
Terpenes	0,104	1,17	1,53	0,46
Benzene	0,33	0,42	0,57	0,6
Toluene	0,19	0,27	0,35	0,4
Xylenes	0,086	0,16	0,11	0,14
Ethylbenzene	0,022	0,041	0,038	0,086
Styrene	0,056	0,066	0,13	0,064
PAHs	0,012	0,017	0,72	0,061
Methanol	1,35	2,2	2,33	2,17
Ethanol	0,036	0,076	0,058	0,084
1-Propanol	0,025	0,041	0,044	0,25
2-Propanol	0,08	0,13	0,14	0,11
Butanols	0,11	0,064	0,071	0,015
Cyclopentanol	0,033	0,035	0,038	–
Phenol	0,43	0,25	0,75	1,06

Formaldehyde	1,23	2,04	1,75	1,37
Acetaldehyde	0,84	1,21	0,81	1,62
Hydroxyacetaldehyde(glycolaldehyde)	0,13	0,39	0,38	0,63
Glyoxal	0,33	0,54	0,59	0,41
Methylglyoxal	0,4	0,27	0,57	0,33
Acolein (propenal)	0,48	0,34	0,33	0,55
Propanal	0,053	0,087	0,24	0,23
Butanals	0,11	0,11	0,15	0,09
Methacrolein	0,1	0,14	0,11	0,1
Crotonaldehyde (2-butenal)	0,24	0,39	0,42	0,09
Hexanals	0,048	0,038	0,038	0,009
Heptanals	0,003	0,005	0,005	0,007
Acetone	0,47	0,76	1,59	0,64
2-Butanone	0,13	0,23	0,16	0,22
2,3-Butanedione	0,35	0,89	0,34	0,51
1-Butene-3-one (methylvinyl ketone)	0,23	0,165	0,099	0,16
Pentanones	0,014	0,066	0,074	0,067
Hexanones	0,048	0,045	0,066	0,014
Heptanones	0,006	0,005	0,005	0,063
Octanones	0,015	0,023	0,025	0,005
Benzaldehyde	0,102	0,132	0,096	0,081
Acetol (hydroxyacetone)	0,56	1,13	2,1	0,7
Furan	0,29	0,41	0,36	0,53
2-Methyl-furan	0,2	0,34	0,42	0,29
3-Methyl-furan	0,01	0,034	0,052	0,13
2-Ethylfuran	0,005	0,016	0,008	0,011
2,4-Dimethyl-furan	0,008	0,011	0,012	0,013
2,5-Dimethyl-furan	0,063	0,07	0,1	0,11
Tetrahydrofuran	0,009	0,001	0,011	0,012
Benzofuran	0,045	0,094	0,06	0,029
Furfural (2-furaldehyde)	0,73	0,52	0,61	0,84
Methyl formate	0,073	0,024	0,024	0,043
Methyl acetate	0,159	0,095	0,087	0,054
Acetonitrile	0,17	0,22	0,31	0,21
Acrylonitrile	0,037	0,031	0,068	0,062
Propionitrile	0,027	0,011	0,11	0,12
Pyrrole	0,013	0,062	0,14	0,09
Trimethylpyrazole	–	–	–	0,124
Methylamine	–	–	–	0,057
Dimethylamine	–	–	–	0,062
Ethylamine	–	–	–	0,005
Trimethylamine	–	–	–	0,041
n-Pentylamine	–	–	–	0,44

2-Methyl-1-butylamine	–	–	–	0,14
Formic acid	0,21	0,91	1,04	0,34
Acetic acid	2,31	2,74	3,8	3,6
H2	0,97	2,1	1,6	–
NOx (as NO)	2,5	3	1,18	2,1
PM2.5	6,7	18,5	18,7	10,5
Levoglucosan	0,05	1,33	1,3	0,45

Table I.15 contains emissions factors (EFs) of two of the most abundant compounds in wildfires smoke plumes; α-pinene and benzene. Benzene a human carcinogen and a precursor of PAHs (polyaromatic hydrocarbons), is considered the dominant aromatic VOC in wildfire plumes with concentrations reaching 280 ppbv (Evtyugina et al. 2013). α-pinene is the second most abundant BVOC emitted in wildfires after isoprene, especially in vegetation species that contain isoprenoid storage compartments by which their emissions occur during vegetation distillation and pyrolysis processes. Oxygenated volatile organic compounds (OVOCs) such as methanol, acetic acid, formic acid, formaldehyde, phenol, furan, etc. are also emitted in large amounts in wildfires and their EFs can be found in (Akagi et al. 2011, and references therein), all other VOCs emitted in wildfires (prescribed and real) are present in the literature cited in Table I.15. EFs of total hydrocarbons (THC) depend on the MCE values which define the fire phase of the vegetation i.e., flaming or smoldering depending on the biomass properties, weather conditions and topographies (Evtyugina et al. 2013).

Table I.15. Emission factors in literature for α-pinene and benzene from different Mediterranean wildfires.

Description	**EF mg.kg^{-1} (g.kg^{-1})**		**Notes**	**Source**
	Benzene	α- pinene		
Savanna grass land	230 (0,23)		EFs of tropical and extra-tropical forests are also documented. Other debris types as well.	Lemieux et al. 2004
Florida debris	195 (0,195)			
Ponderosa pine slash	444 (0,44)			
Boreal forest	0,55 ± 0,11	0,81 ± 0,10	Average EF from five Canadian boreal forest fresh fire plumes from 29 June to 10 July 2008.	Simpson et al. 2011
Boreal and temperate forests	0,49 ± 0,08		EF from Andreae and Merlet 2001	
Boreal forests	1,1	1,64	EF from Akagi et al. 2011	
Long pine leaves	0,268	1,677	Ground base samples	Akagi et al. 2011
	0,251	0,086	Airborne samples	
Pine + Sparkleberry	0,429	0,026	Ground base samples	
	0,254	0,103	Airborne samples	
Pine + Oak	1,712	6,248	Ground base samples	
	0,284	0,069	Airborne samples	
Pine plantation	0,35	0,117	Airborne samples	

California Riversidian Sage Brush/Scrub	0,44			
California Sage Brush	0,81		Literature values.	Friedli et al. 2001
Temperate forests		0,0746	Calculated from the emission ratio (ER) of alpha pinene relative to CO. Emission ratios were similar for smoldering and flaming combustion	
Laboratory combustion experiments at 7m/s wind velocity on pine wood (Mediterranean vegetation)	2,929 ± 0,192	0,947 ± 0,037	Flaming combustion	Ciccioli et al. 2001
	1,542 ± 0,192	0,373 ± 0,003	Smoldering combustion	
Wheat straw (Mediterranean vegetation)	0,679 ± 0,132		Flaming combustion	
	0,607 ± 0,440		Smoldering combustion	
Initial smoke fires emissions from African savanna fuels	0,21		EF from Sinha et al. 2003	Christian et al. 2003
Indonesian fuels	0,94			

Coastal heathland fire Tropical savanna Australia	0,69 0,42, [0.23]		Information in brackets from Hurst et al (1994a) for same type of vegetation species.	Lawson et al. 2015
	0,29, [0,24]		Information in brackets from Hurst et al (1994b) for same type of vegetation species.	
	0,21, [0,02]		Information in brackets from Shirai et al (2003) for same type of vegetation species.	
Temperate Northern hemisphere (temperate forests and chaparral)	0,45 (0,29)		Information in brackets from Yokelson et al. (2013) for same vegetation species.	
Australian temperate forests, Eucalyptus	0,39 ± 0,07	0,5 ± 0,1	EF by Guérette et al. 2018	Guérette et al. 2018
	0,69	0,11	Lawson et al. (2015). Alpha-pinene are relevant to Monoterpenes emissions.	
	0,3	0,9	Akagi et al. (2011) Alpha-pinene are relevant to Monoterpenes emissions.	

Boreal forest	1,11	1,64	Akagi et al. (2011).	
Pinus pinea		67,2 ± 2,6 (0.067)	Ciccoli et al. (2001). Flaming Combustion.	Ciccioli et al. 2014
		6,3 (0,0063)	Ciccoli et al. (2001) Smoldering Combustion.	
Temperate forests	0,250 – 0,44			Urbanski et al. 2009
Temperate range land	0,22			
Boreal forests	0,55 ± 0,11	0,81 ± 0,10	Fresh fire smoke samples in Canadian boreal forests.	Simpson et al. 2011
Eucalyptus	0,811 ± 0,339	0,065 ± 0,035	Sampling: 1.5m above ground @ 10-200 m downwind during smoldering.	Evtyungina et al. 2013
Pinus pinaster forest and bush fires	0,609 ± 0,148	0,220 ± 0,096		
Boreal forest	0,55 ± 0,11	0,81 ± 0,10		
Almond pruning	0,03		EF of various VOCs from different wildland vegetation species classified between smoldering and flaming combustion are also present in source.	W. Battye and R. Battye 2002
Douglas fir slash	0,2			
Ponderosa pine	0,44			
Walnut pruning	0,016			
Grasses, wood, hay, pine needles	0,34			
Pine trees and bushes wildfires in Greece	84µg/m³ [a]		Sampling site: 100m from fire flame-front. Elapsed time: 30 min.	Statherpoulor and Karma 2007
	112µg/m³ [a]		Sampling site: 100m from fire flame-front. Elapsed time: 60 min.	
	696µg/m³ [a]		Sampling site: 70m from fire flame-front. Elapsed time: 30 min.	
	85µg/m³ [a]		Sampling site: 150m from fire flame-front. Elapsed time: 30 min.	

[a] Measurements in (µg. m^{-3}) are concentrations and not EF.

6 Extreme Wildfire Behaviors: Forms and Hypotheses

6.1 Blow Up or Flashover

The National Wildfire Coordinating Group's definition of extreme fire behavior (EFB) indicates a level of fire behavior characteristics that ordinarily precludes methods of direct control action (Werth et al. 2011). There are three types of extreme fire behaviors: eruptive fires, crown fires, and spot fires (Viegas and Simeoni 2011). Eruptive fire behaviors are of greater concern from a fire safety point of view because they impose a great threat to the safety

of the firefighters engaged in the firefighting operations. Fire eruptions were first named by (Viegas 2005) because of their characteristic behavior of sudden increase in fire intensity and rate of spread resulting in a big convection column similar to a volcanic eruption. Another definition states it as a transition from a steady state rate into a highly non-steady state rate of fire spread especially in confined topographies even without any ambient wind, as reported by (Viegas and Pita 2004). Literature also referred to extreme fire behaviors as "blow up" or "flashover" (Viegas and Simeoni 2011, Dold and Zinoviev 2009). To avoid misleading, care must be taken when using these last two terms to describe eruptive fire behaviors in confined topographies, because the term "blow up" was described by (Butler et al. 1998) as a transition from a surface fire with low intensity consuming litter and grass vegetation to a crown fire consuming tree crowns and developing higher flame heights and faster rates of spread. However, such a transition can occur in open terrains and not necessarily in confined topographies. On the other hand, the term "flashover" is described by (Dold 2010), as the spread of flame through unburnt pyrolysates and other combustible vapors, that might, due to certain circumstances accumulate in confined topographies (canyons) to form flammable gaseous mixtures. A schematic representing the fire environments that promote rapid changes in fire behavior and cause entrapments and fatalities in the lives of the firefighting teams in vicinity is shown in (Figure I.27).

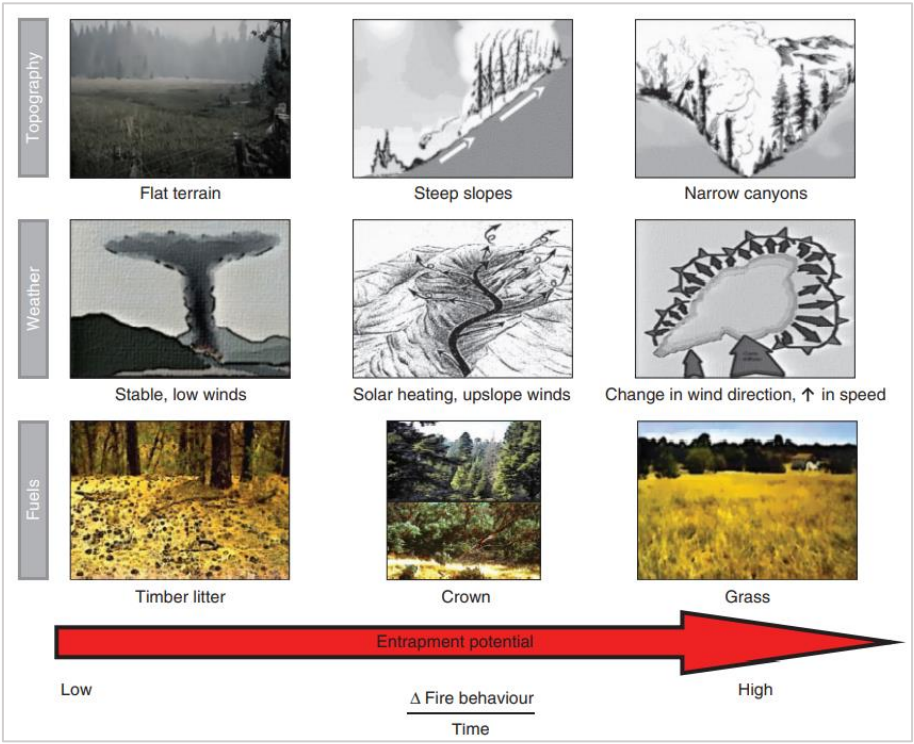

Figure I.27. Example characteristics of the fire environment (top to bottom) that promotes rapid changes in fire behavior. (Page et al 2019)

6.2 Fire Eruptions in Canyons

Fire eruptions associated to canyons are not rare but little is known on their circumstances and direct causes yet they have been reported to cause a great number of fatalities among the firefighting teams (Table I.16). Often these eruptions or flashovers have been commonly reported by surviving firefighters while they were attempting to suppress a wildfire spreading

down slope on a steep hill or canyon, that a sudden fire had developed below them and erupted uphill and killed a large part of the group (Viegas and Simeoni 2011). The big number of the fatalities due to fire eruption accidents in (Table I.16) should not be neglected although the occasional and unpredictable occurrences of these accidents have not permitted the implementation of empirical studies to explain their exact stimulators. So far, in the literature the fire rate of spread depends on the three factors that form the fire behavior triangle i.e., weather, topography and fuel. (Viegas 2006) has added the chronological time factor, which corresponds to the accumulation of energy during the interaction of the fire with its environment with time, until these accumulations become enough to cause fire eruption and accelerate the fire rate of spread.

Table I.16. Some accidents with multiple fatalities associated with extreme fire behaviors in canyons. (Viegas and Simoeni 2011)

Case	Year	Place	Country	Victims
1	1949	Mann Gulch	USA	13
2	1953	Rattlesnake	USA	15
3	1966	Sintra	Portugal	25
4	1984	La Gomera	Spain	20
5	1985	Armamar	Portugal	14
6	1986	A gueda	Portugal	16
7	1990	Dude	USA	6
8	1994	Storm King	USA	14
9	1996	Loop	USA	12
10	1999	Alajar	Spain	4
11	1999	Tabuaco	Portugal	2
12	2000	Palasca	France	2
13	2000	Mação	Portugal	2
14	2003	Cramer	USA	2
15	2003	Freixo	Portugal	2
16	2005	Guadalajara	Spain	11
17	2005	Mortagua	Portugal	4
18	2006	Famalicão	Portugal	6
19	2007	Kornati Island	Croatia	11
			Total:	181

6.3 Accelerating Forest Fires (AFF)

Two explanations of the drive of fire accelerations resulting from fire eruptions exist in the literature; the first depends on the sudden change in the external factors that form the fire behavior triangle i.e., weather, topography, and fuel and the second depends on the self-induced fire behavior (Viegas and Simoeni 2011). (Dold 2010) defined fire eruptions as fires that grow in spread rate and intensity without any change in external driving forces such as the ambient wind, temperature, aspect, moisture content, vegetation type, etc. Therefore, it's a local or internal dynamic connected with the fire that causes its acceleration. Mechanisms of fire accelerations due to internal fire dynamics are referred in the literature to convective feed-back from the fire, flow attachment, gas accumulation, and spotting (Viegas and Simoeni 2011, Dold 2010). Notably, gas accumulations and spotting are cross-linked.

6.3.1 Positive Feedback from the Fire

Viegas (2005), proposed a mathematical model to predict the rate of spread of the head of an eruptive fire due to wind and positive slope. The wind supplies more oxygen to the flame which increases its length and entraps more oxygen in the reaction zone ahead of it. The rate of change of a non-dimensional fire rate of spread with time is expressed in (Equation 17) depending on factors related to wind velocity and reaction time.

$$\frac{dR'}{dt} = a_1^{\frac{1}{b_1}} . b_1 . a_2 . (R' - 1)^{(1 - 1/b_1)} . R'^{b_2} \qquad (17)$$

Where,

R' is the non-dimensional rate of spread of the fire front, a_1, b_1, a_2, are constants related to the fire rate of spread change with wind velocity and reaction time of the fuelbed measured experimentally at laboratory and field scales. For example, the time lag for eruptive fire initiation in a shrub fuel was predicted by the model to be in the order of 15 to 20 mins similar to experimental results (Viegas and Simeoni 2011). The model was also used to predict the change in the fire rate of spread in the presence of slope for the eruptive fire (Freixo de Espada-a-Cinta) that occurred in Portugal in August 2003 (Viegas 2005).

6.3.2 Flow Attachment

In steady state fire spread, the vertical component of acceleration in the buoyant air and combustion products rising in the plume and causing a vertical momentum with height, entrain air flow from both sides of the flame (in front and behind), suffice to say that an eruptive fire behavior with unsteady rate of spread especially in upslopes would have a different plume behavior referred to as flame or plume attachment (Dold 2010, Grumstrup et al. 2017). Plume attachment occurs when an imbalance in the flow of air entrained into the plume in uphill direction causes its tilting which increases the convective and radiative (less role) heat transfer rates to the unburnt fuel ahead of the flame-front. The convective heat transfers to the unburnt fuel is significant from the hot combustion gases emitted from the burnt fuel (H_2O, CO_2, smoke, etc.) at which their temperatures can reach 1000-2000°C close to the flame temperature (Grumstrup et al. 2017). The critical slope angle beyond which flame attachment length increases dramatically is 24° (Grumstrup et al. 2017). (Dold and Zinoviev 2009) related the fire intensity and rate of spread of an eruptive fire mediated by flame attachment by 'Byram's number' defined as $B = Q.m.R/I$ which is equal to 1 for steady, and greater than one for unsteady fire spread rate. Q is the energy of combustion in $kJ.kg^{-1}$, m is the fuel load consumed in $kg.m^{-2}$, R is the fire rate of spread $m.s^{-1}$, and I is the fireline intensity in $kW.m^{-1}$.

6.3.3 Gas Accumulations with Spotting

Fire eruptions termed as flashovers are due to accumulations of gases and were suggested following some incidents that occurred during wildfires at which the firefighters got overwhelmed by sudden fire flashovers far ahead of them for example; the severe fire near Canberra, Australia (Dold et al. 2005) and the Palasca fire in Corsica, France (Dold et al 2009) and others (Peuch 2007). Gas accumulations in confined topographies are given two identities. The first identifies them as the unburned gaseous products in the fire plume and the gases

produced from the pyrolyzed vegetation elsewhere which migrate and concentrate in places ahead of the fire front. The second identifies these gases as the VOCs emitted from the heated vegetation ahead of the fire front (e.g. Mediterranean vegetation) at temperatures below their ignition point (~320°C) (Rothermel and Anderson 1966). Owen et al. (1997) and Owen et al. (2001) published the VOC emissions from 40 different Mediterranean vegetation species and correlated their various emission rates to temperatures. The higher the heating temperature the higher the emissions of VOCs (Barboni 2006). The densities of these emitted VOCs are higher than air so they migrate at ground level and flow downslope to concentrate deep inside a canyon especially if the slope was steep enough to cause air circulation inside it and prevent the VCOs from evacuation. The controversy in wildfire flashover is in whether these accumulations are going to form a flammable mixture with air (fuel/air ratio) under certain conditions, i.e., its concentration lays between its lower and upper flammability limits, at which any spark coming from the fire will ignite it or, if any of the gaseous mixture components will reach their autoignition conditions (Catoire and Naudet 2005). The high volatility of the VOCs (high Henry's constant, *cf.* Table I.8), means they have low enthalpy of vaporization h_{fg} (kJ.kg^{-1}), low boiling points, and high vapor pressure. If such characteristics of the gases are coupled with their characteristic low flammability limits (e.g. 0.76% of α-pinene at 100°C, Catoire and Naudet 2005), or low autoignition temperatures (e.g. 300°C for α-pinene, Coudour et al. 2014) and low flashpoints (e.g. 33°C for α-pinene, Chatelon et al. 2014), one can infer that the gas will not only evaporate but surely will ignite.

6.3.3.1 Temperatures Developed Ahead of Fire Front

The distance at which the fuel is heated and the temperatures developed on air and fuel bed scales ahead of the flame front depend among other factors on the radiative and/or convective heat transfer mechanisms developed in the absence or presence of wind, respectively. In the absence of wind, radiation dominates and the convective flow is towards the flame as in (Figure I.28a), while in the presence of wind (Figure I.28b) the flame tilts towards the fuelbed and the airflow is from the flame to the unburned fuel. If the temperature of the flame is greater than that of the fuel particles, convective heat transfer will dominate in addition to the radiation from the flame and flaming fuelbed.

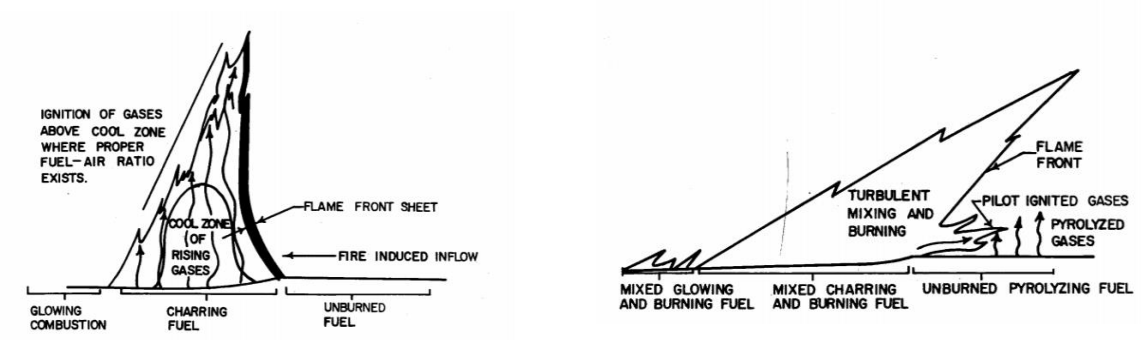

(a) (b)

Figure I.28. Flaming zone combustion characteristics (a) in the absence of wind and (b) in the presence of wind. (Rothermel and Anderson 1966)

The temperatures developed at the fuel bed present at a distance from 0.15 to 1.27 m will develop temperatures of 250 to 27°C, respectively. In (Figure I.29a), in the absence of wind, the radiation from a flame of 1.13 meters height can heat a fuel bed of pine needles (4% FMC), up to a two-flame length distance and the water boiling temperature will be reached when the flame is 0.3m away. While in (Figure I.29b) at a wind velocity of (~2.5 $m.s^{-1}$) the fuel is heated while the flame front is still more than 1.28m away and water boiling temperature was reached at 2.4m away from the fire (Rothermel and Anderson 1966).

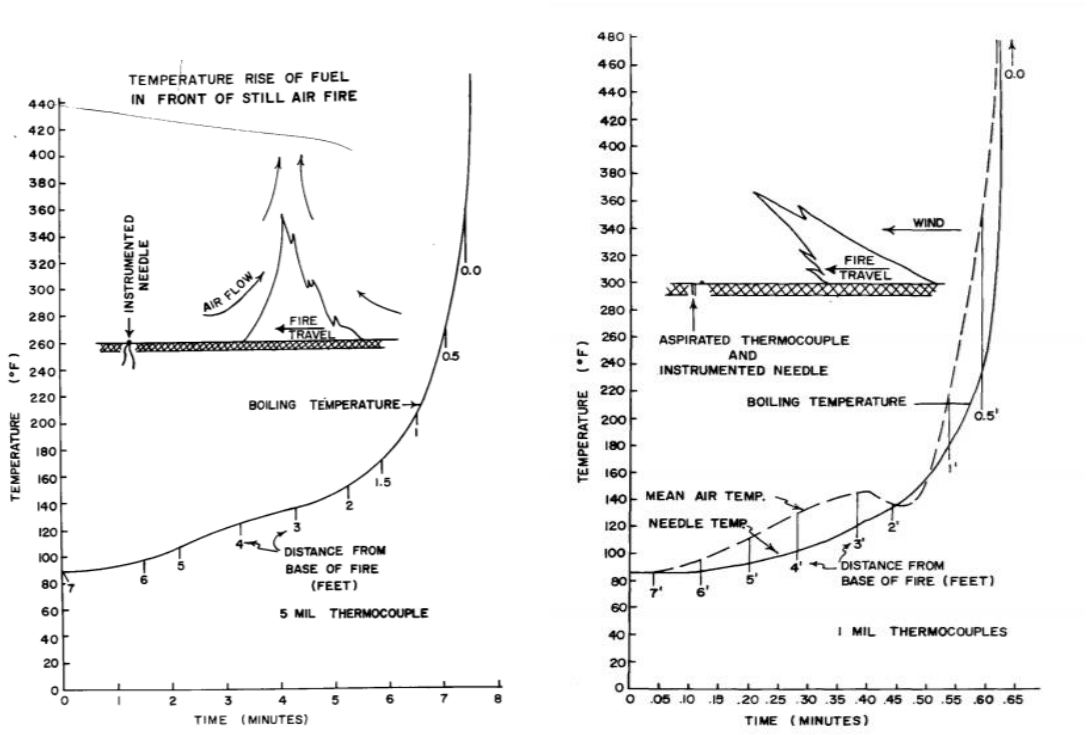

Figure I.29. Temperature rise profiles of air and fuel in front of a flame front for (a) still air fire and (b) wind-driven fire. (Rothermel and Anderson 1966)

6.3.3.2 BVOC Emissions from Heated Mediterranean Plants: Laboratory Scale

Laboratory experiments were done on Mediterranean vegetation to configure the identity of the VOC emissions (including BVOCs) under thermal stresses prior to their ignition temperatures. The critical temperature of maximum BVOC (terpenoids) emissions among of which α-pinene was the most abundant, from pine, cistus, heather, and arbutus was found at 175°C, while diterpenes (oxide 13-epi-manyole with 0.4%LFL) were mainly emitted at 200°C (Chatelon et al. 2014). However, the temperatures for maximum emission rates of BVOCs depend on three factors: their boiling temperatures that are easily reached ahead of the fire front as they are mostly less than 200°C (Table I.17), the type of the vegetation (Barboni 2006), and the maturity of the plant (Bracho-Nunez et al. 2011). (Zhao et al. 2011) conducted heating experiments on needles and twigs of Pinus Pumila at 200°C and found that terpenoids (especially monoterpenes) were the dominantly emitted among the VOC at a percentage of 72.93% (α-pinene at 59.6%) and 92.4% (α-pinene at 35.72%) from the needles and twigs, respectively (Table I.18). Variations in percentages are due to the presence of larger amounts of volatile oils in twigs than needles.

Table I.17. Formula, molecular weight and boiling temperature of the main terpenoids emitted by Pinus Pumilla (Zhao et al. 2011).

Compound	Formula	Molecular weight	Boiling point (°C)
santene	C_9H_{14}	122	140-141
fenchene	$C_{10}H_{16}$	136	142-143
tricyclene	$C_{10}H_{16}$	136	152-153
α-pinene	$C_{10}H_{16}$	136	155-156
camphene	$C_{10}H_{16}$	136	159-160
sabinene	$C_{10}H_{16}$	136	163-164
β-pinene	$C_{10}H_{16}$	136	165-167
α-terpinene	$C_{10}H_{16}$	136	173-175
trans-β-ocimene	$C_{10}H_{16}$	136	174-175
eucalyptol	$C_{10}H_{18}O$	154	174-177
D-limonene	$C_{10}H_{16}$	136	176-177
β-phellandrene	$C_{10}H_{16}$	136	178-179
γ-terpinene	$C_{10}H_{16}$	136	181-183
terpinolene	$C_{10}H_{16}$	136	183-185
neo-allo-ocimene	$C_{10}H_{16}$	136	188-189
2(10)-pinen-3-one	$C_{10}H_{14}O$	150	217-218
myrtenal	$C_{10}H_{14}O$	150	220-221
verbenone	$C_{10}H_{14}O$	150	227-228
sesquiterpenes	$C_{15}H_{24}$	204	250-280

Table I.18. Terpenoid emissions from heated needles of Pinus Pumilla at 200°C. (Zhao et al. 2011)

Compound	Emission ratio (µg. g)	Proportion of terpenoids (%)
Santene	1.017±0.075	1.63
α-pinene	37.223±2.136	59.60
Camphene	8.900±0.092	14.25
β-pinene	7.452±0.103	11.93
3-carene	1.801±0.112	2.88
β-ocimene	0.474±0.213	0.76
D-limonene	3.513±0.142	5.63
β-phellandrene	0.607±0.215	0.97
Eucalyptol	0.213±0.128	0.34
Neo-allo-ocimene	1.262±0.263	2.02
Total	61.200±2.569	100.00

It's not only the temperature which affects the total VOC emissions but also the type and the maturity of the plant depending on the developmental and functional composition. Mediterranean shrub species such as Cistus albidus, don't emit isoprene because they don't store it. Also, their monoterpene emissions decrease with maturity because their photosynthesis rates decrease with age (Table I.19). And as the defense mechanisms of the young leaves demand more sesquiterpenes emissions because they are more prone to herbivores, the

sesquiterpenes emission potential decrease for mature leaves (Bracho-Nunez et al. 2011). On the other hand, Rosmarinus officinalis monoterpene emissions weren't affected with maturity.

Table I.19. Emission quantities of Methanol and BVOCs in µg. $g^{-1}.h^{-1}$ from different young vs mature Mediterranean plant species (Bracho-Nunez et al. 2011)

Plant Species	Y/M	Methanol	Isoprene	Monoterpene	Sesquiterpene
Buxus sempervirens	Y (few days)	1.68 ± 0.3	5.06 ± 4.07	0.42 ± 0.10	<d.l.
	M (>1 year)	1.04 ± 0.63	21.46 ± 5.21	0.13 ± 0.06	0.07 ± 0.05
Ceratonia siliqua	Y (few days)	3.51 ± 1.00	<d.l.	0.33 ± 0.11	<d.l.
	M (>1 year)	0.79 ± 0.23	0.52 ± 0.17	7.94 ± 5.41	0.03 ± 0.02
Cistus albidus	Y (few days)	6.17 ± 3.11	<d.l.	1.44 ± 1.04	3.33 ± 1.41
	M (>1 year)	8.20 ± 4.61	<d.l.	0.30 ± 0.07	0.63 ± 0.32
Coronilla valentine	Y (few days)	29.35 ± 4.76	<d.l.	2.70 ± 1.05	0.42 ± 0.07
	M (>1 year)	13.48 ± 7.84	0.43 ± 0.08	0.75 ± 0.45	<d.l.
Olea europea	Y (few days)	1.56 ± 0.53**	0.19 ± 0.05	2.84 ± 2.44	0.28 ± 0.19
	M (>1 year)	1.03 ± 0.20	0.12 ± 0.09	1.21 ± 0.95	0.09 ± 0.01
Pinus halepensis	Y (few days)	5.70 ± 0.58	0.12 ± 0.01	1.95 ± 0.57	0.08 ± 0.13
	M (>1 year)	2.95 ± 0.09	0.10 ± 0.07	2.75 ± 0.94	<d.l.
Prunus persica	Y (few days)	14.23 ± 5.4	<d.l.	0.45 ± 0.10	<d.l.
	M (~one month)	4.01 ± 1.30	0.04 ± 0.03	0.36 ± 0.25	<d.l.
Rosmarinus officinalis	Y (few days)	21.3 ± 10.1	<d.l.	1.55 ± 0.51	<d.l.
	M (>1 year)	2.03 ± 0.61	<d.l.	1.97 ± 1.36	<d.l.
Spartium junceum	Y (few days)	22.77 ± 8.1	33.0 ± 14.79	0.44 ± 0.15	<d.l.
	M (>1 year)	3.74 ± 0.72	28.28 ± 6.13	<d.l.	<d.l.

<d.l.: under detection limit. Y means young leaves. M means mature leaves.

6.3.3.3 Lower and Upper Flammability Limits of Gaseous Mixtures

Gaseous mixtures evolving from vegetation in the events of wildfires whose accumulations are favored by atmospheric conditions and topography, will only become ignitable when they reach concentrations constrained between their lower and upper flammability limits. In a gas mixture consisting of a fuel gas, and an oxidizing gas or even possibly a diluent or inert gas, the lower flammability limit (LFL) is the minimum concentration of fuel gas likely to be ignited.

Similarly, the upper flammability limit (UFL) is the maximum concentration of fuel gas that can be ignited.

$$LFL\ OR\ UFL\ [g.m^{-3}] = \frac{LFL(\%) OR\ UFL(\%)}{V_m\ (l.mol^{-1})}\ M(g.mol^{-1}) \qquad (18)$$

Where,

LFL (%) and UFL (%) are the lower and upper flammability limits, respectively. M is the molar mass of the compound concerned ($g.mol^{-1}$) and V_m is the molar volume (24.8 $L.mol^{-1}$). The lower flammability limits of a mixture in nitrogen and/or air is given by Le Chatelier's equation as follows,

$$\frac{100}{LFL\ (mixture)} = \frac{A_1}{LFL_1} + \frac{A_2}{LFL_2} + \cdots + \frac{A_n}{LFL_n} \qquad (19)$$

Where,

LFL is the lower flammability limit in mol% of each gas.

A is the molar fraction in mol% of each gas.

Le Chatelier's equation is not recommended to be used to calculate UFLs. The UFLs found by experimental works have shown great variability with the values calculated using the formula, probably because the UFL is highly dependent on the flame propagation direction (Mendiburu et al. 2020). Other equations for finding the UFL of a mixture will be addressed throughout the course of this thesis. If the mixture exists in an inert atmosphere other than nitrogen, the formula should change to consider the nitrogen equivalency of the new inert gas, referred to as (K_k). The concentration of the inert gas in the mixture affects fuel gas concentration necessary for flame propagation (Schröder 2016).

The lower and upper flammability limits are temperature and pressure dependents. Increasing the temperature will decrease the lower flammability limit and increase the upper flammability limit therefore widening the range of flammability of a certain compound in air. Whereas, decreasing the pressure below the atmospheric pressure for example, will increase the lower flammability limit and decrease the upper flammability limit therefore, narrowing the flammability range of the compound.

7 Conclusion

This chapter summarized all the data concerning the wildfires in the Mediterranean climate regions (MCR) to be further discussed and utilized throughout this thesis. This thesis primarily addresses one of the most dangerous forms of fire eruptions; Wildfire Flashovers. Although they have caused many human fatalities and extremely uncontrollable fire behaviors, their causes are still controversial in wildfire research. Our research aims to provide the best decision tools and information that can be used by the firefighting community and the forest management teams to implement the best preventive and protective measures in their firefighting operations and forestation activities, respectively. We have emphasized vegetation VOC emissions which we believe are the main drivers of wildfire initiation, propagation, and mainly flashovers. The VOCs (including BVOCs) emissions under heat and fire effects of wildfires are affected by

many atmospheric and environmental factors, in addition surely to the vegetation characteristics themselves. Their percentages will in turn affect the flammability parameters of the vegetation which renders certain vegetation species more flammable than others. The risk with these VOCs is not only by their flammable emission rates but also by their ability to spontaneously ignite in an explosive manner forming a lake of indistinguishable flames without the mediation of any ignition source in the process, supposedly their ignition parameters are reached. The Mediterranean climate regions in Australia, Brazil, the USA, and the Mediterranean basin were overwhelmed in the past few years by the enormous wildfires destroying their valuable forest wealth and exterminating a wide range of their biological and ecological forms of life. A long-run plan that may reduce the risks of wildfires in MCR would be to reduce greenhouse effects and limit global warming which may reduce the temperatures but until tangible results appear, scientific research strives to provide the best tools to the firefighting community to control and possibly reduce wildfire risks.

CHAPTER II

****

Numerical Approaches to Investigate Fire-Front Gas Dispersion in Confined Valleys

Résumé

Etude Numérique de la Dispersion des Gaz du Front de Flamme de la Zone Encaissée

Les 'Flashovers' sont des phénomènes complexes qui se produisent dans des espaces clos et sont définis par la norme NFPA921 (2011) comme l'inflammation simultanée de gaz résultant de la dégradation thermique de matériaux combustibles exposés au rayonnement du feu. Les scientifiques ont tenté de relier les causes des 'Flashovers' aux observations des pompiers lors d'une éruption d'un feu de forêt dans une topographie confinée ou une dépression de relief. Les pompiers de l'incendie de Palasca (Dold et al. 2009), par exemple, ont signalé avoir remarqué un nuage de gaz avec des odeurs de COV observables avant que l'incendie n'éclate sous la forme d'un 'Flashover' qui a consumé 15 acres en 45 secondes. D'autres signalements ont fait état de flammes qui formaient un lac de feu homogène et prenaient une forme semblable à un feu de gaz d'hydrocarbures (Peuch 2007). D'autres témoignages de pompiers ont fait état d'une accélération de la vitesse de propagation du feu alors que le feu continuait de se propager vers le bas (Viegas 2009). Remarquablement, les comportements des incendies éruptifs étaient principalement couplés et à des pentes. En effet, une augmentation de 10° de la pente peut augmenter le taux de propagation du feu de deux fois tandis qu'une augmentation de 20° de la pente augmentera le taux de propagation du feu de 4 fois (Butler et al. 2007). Les incendies se propagent beaucoup plus rapidement vers le haut que vers le bas en raison de plusieurs facteurs et de plusieurs mécanismes qui ont été largement discutés dans la littérature tels que l'attachement de flamme (Dold et Zonviev 2009) sans aucun changement significatif dans la direction ou la vitesse du vent ambiant (Viegas et Pita 2004). Cependant, la plupart des éruptions de feu signalées comprenant des comportements d'accélération du feu vers le haut des pentes ont été précédées de formes d'inflammation de poches gazeuses, résultant en un lac ou une couverture de feu qui dure quelques secondes, parfois à deux mètres au-dessus une terre nue sans végétation comme l'incendie de Canberra (Williamson et al. 2022).

Hypothèses Scientifiques sur les Flashovers

Il existe deux hypothèses quant à l'origine des gaz qui s'accumulent à l'intérieur d'une vallée comme suggéré par (Carbonell et al. 2004). La première hypothèse est la génération d'émissions de la végétation pyrolysée en amont en raison du rayonnement du feu qui amorce et se propage en aval, tandis que la deuxième hypothèse fait référence aux accumulations de COV non brûlés qui ont échappé au front de feu en se propageant en avant de la vallée, ont migré et s'y sont concentrés.

Objectif de ce Travail

Les 'Flashovers' de feux de forêt constituent régulièrement une menace vitale pour les pompiers d'autant plus que leurs causes directes restent ambiguës et controversées. Apporter des éléments au débat quant à savoir si les poches de gaz COV contribuent aux 'Flashovers' a été l'objectif de cette étude numérique. Afin d'étudier la dispersion des COV émis sous le vent lors d'un incendie de forêt et leurs accumulations possibles dans une topographie confinée (c'est-à-dire une vallée), le logiciel STAR-CCM+ a été choisi, un outil de calcul multiphysique Logiciel de dynamique des fluides (DDF). Le modèle numérique de dispersion des gaz a d'abord été validé par rapport à des résultats issus d'un dispositif expérimental incorporant une maquette de forêt au sein d'une soufflerie qui sera présenté et décrit dans une première partie. Les résultats ont

montré l'accumulation de gaz à l'intérieur d'une vallée à à partir d'un certain angle intérieur, notamment dû à un phénomène de recirculation. Ensuite, deux modèles numériques turbulents seront présentés et discutés. Une fois le Le premier modèle numérique validé sur les profils expérimentaux basés sur des émissions d'éthane (C_2H_6) qui néglige les effets de flottabilité le deuxième modèle numérique a ensuite été adapté à des émissions de gaz d'une gamme de composés de différentes densités typiques de ceux émis lors d'un incendie de forêt. Les débits d'émission ont été choisis par rapport aux valeurs de la littérature.

Dispositif Experimental

Le dispositif expérimental a été mis en œuvre par (Coudour et al. 2014), qui ont étudié le transport et la dispersion des émissions gazeuses avec le vent à travers une forêt comprenant un relief topographique en forme de V pour modéliser une zone encaissée telle qu'un thalweg (ancien lit de rivière) où ont eu lieu plusieurs feux éruptifs. Dans leurs expériences, Coudour et al. (2014) ont utilisé une maquette de forêt avec deux angles de vallées différents et ont utilisé un système d'injection d'éthane à travers la forêt. La forêt a été divisée en différentes zones avant et après la vallée. L'objectif était de déterminer quelle zone émettrice aurait le plus grand effet sur la concentration de gaz dans la vallée selon les deux angles de vallée α = 50° et 80°, (Figure 1).

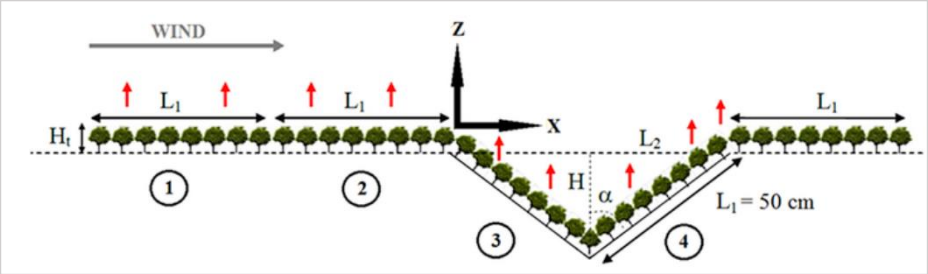

Figure 1. Géométrie du modèle forestier

Concepts d'Analyse Numérique

Notre étude numérique préliminaire visait à valider les profils expérimentaux de vitesse et de concentration obtenus avec la maquette de forêt présentés ci-dessus. Le modèle numérique a ensuite été amélioré pour étudier la dispersion de gaz issu d'un front de flamme se déplaçant sur les zones 1 et 2 jusqu'à l'entrée de la vallée (cf. Figure 1). Les débits d'émission ont été fixés en fonction des facteurs d'émission d'un front de flamme en grammes d'émission pour chaque kg de végétation brûlée que l'on peut trouver dans la littérature. Le concept d'émissions non stationnaires transitoires simule leur évolution et leur dispersion avec le front de feu en mouvement dans un incendie réel. Le modèle Rothermel depuis 1972 avec quelques ajustements de Frank Albini en 1976, est considéré comme une étape importante de chaque modèle de propagation de feu de surface. La combinaison de facteurs d'émission de COV collectés à partir de feux réels avec les méthodes de Rothermel et Van Wagner prédisant une transition de propagation d'un feu de surface vers un feu de cime peut être mise en œuvre dans un modèle CFD pour simuler les conditions réelles d'un feu de forêt. Avec des vitesses de vent suffisamment fortes pour contrer les effets thermiques, les densités des COV émis jouent un rôle important dans leur dispersion et leur accumulation dans les topographies confinées où ils sont le plus susceptibles d'atteindre leurs limites d'inflammabilité.

Résultats de ce Travail

Après avoir confirmé expérimentalement l'accumulation d'éthane dans une vallée confinée (α= 50°), nos simulations numériques ont montré que des COV aussi légers que le méthane s'accumulera et que des composés plus lourds tels que le benzène, le toluène et les monoterpènes atteindront même leurs limites d'inflammabilité dans une vallée en forme de V avec un angle interne de 50° pour un front de flamme se déplaçant pendant 13 min. Ceci. On peut imaginer que ces gaz favoriseront les apparitions de 'Flashovers', (Figure 2). Il y a donc des raisons de s'inquiéter de l'hypothèse d'accumulation de gaz avant un flashover. En rajoutant un modèle thermique et en étudiants des topographies du terrain avec des connaissances sur la structure de la forêt, c'est-à-dire la porosité, la topographie, le type et l'âge de la végétation, et les facteurs de ses émissions correspondantes couplées aux conditions atmosphériques, notre modèle peut devenir un outil de décision pour les pompiers afin de prédire la probabilité d'embrasements, de prendre des mesures préventives et leur sauver la vie. Il serait intéressant d'étudier différentes vitesses de vent et angles de vallée pour déterminer les vitesses et angles critiques pour lesquelles ont peut atteindre les limites inférieures d'inflammabilité (LII). Cependant, il faudrait plus de données sur les LII de mélanges gazeux issus d'un front de flamme pour pouvoir analyser l'inflammabilité des concentrations obtenues.

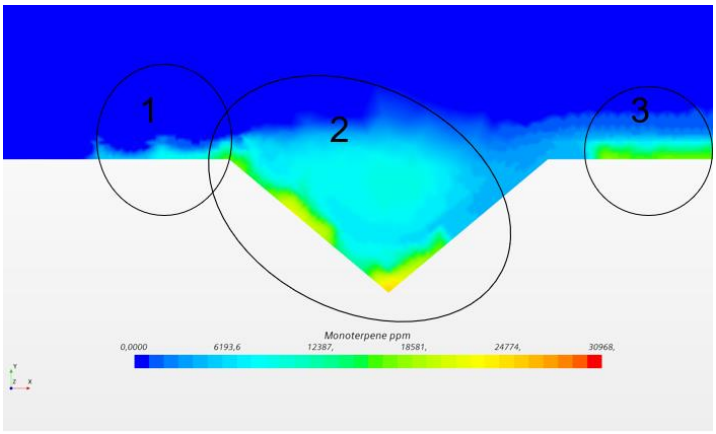

Figure 2. Profils de concentrations et vecteurs vitesses dans la vallée de α = 50° après 13 min de propagation du feu jusqu'en bord de vallée pour les monoterpènes. 1 : Indication de la position du front de feu à la pointe de la vallée. 2 : Indication des accumulations à l'intérieur de la vallée au moment où le front de feu est en position 1. 3 : Indication des accumulations dans la région forestière plate après la vallée avec zéro émission.

1 Introduction

The controversy of whether VOC accumulations in confined topographies will lay in their flammability ranges and ignite in an explosive manner, namely flashover, will be investigated in this chapter. However, these investigations exclude the thermal effects of a propagating firefront and depend on the atmospheric dispersions of VOCs governed by nothing other than their own densities. In order to investigate the dispersion of the emitted VOCs down a 6m. s^{-1} wind during a wildfire and their possible accumulations in a confined topography (i.e., a valley), a preliminary experimental setup was used to realize these investigations followed by a numerical validation using STAR-CCM+, a multiphysics Computational Fluid Dynamics (CFD) software. First, accumulation results from a pre-requisite experimental setup in a boundary-layer wind tunnel are discussed. It incorporates two forest models with two sharp- and wide-angled valleys, and a steady-state ethane gas (C_2H_6) emission mechanism simulating VOC emission above a forest canopy. Then, the experimental results are validated and improved with two numerical turbulent models that solve for the set of the different Favre averaged transport equations of mass, momentum, species, kinetic energy, and turbulence dissipation. The first numerical model investigates the concentration profiles of a steady-state emission of ethane gas (C_2H_6) throughout the forest volume, neglecting buoyancy effects. The second numerical model investigates the concentrations of a range of compounds with different densities emitted in a forest fire and follows a realistic unsteady emission profile with the steady-state propagating firefront. Rothermel's mathematical model is used to calculate the propagating surface firefront parameters using inputs of the physical and chemical makeup of the fuel and the environmental conditions during which the fire took place. The parameters are as such, fuel loading, fuel particle surface-area-to-volume ratio, fuel particle moisture content, moisture of extinction, etc. Van Wagner criteria are used to estimate the surface-to-crown fire transition and calculate the final fire behavior parameters. VOCs are implemented in the CFD simulations as emission factors (EFs) estimated by grams of emissions per kg of biomass burnt in the reaction zone of the moving firefront. Finally, VOC accumulations in ppm inside a porous forest geometry incorporating two valleys with different angles, are traced and calculated. The VOC concentrations calculated inside the valley are later compared to their flammability limits in favor of estimating the probability of wildfire flashover.

2 Eruptive Fire Behaviors

Terminologies used to describe wildfire eruptions varied in literature according to their causes, their behaviors, and coordinates of incidence (i.e., flat surface, upslopes, downslopes…) (Chatelon et al. 2014; Butler et al, 1998, Viegas 2004). Regardless of their causes, so far, fire eruptions in their different forms have been given a unique characteristic by the firefighters who were overwhelmed by their occurrences during a wildfire; their instantaneousness.

2.1 Definition

Fire eruptions change the rate of spread and intensity of the fire without any stimulus from external drivers such as wind speed or ambient temperature or the fuel bed characteristics such as moisture content or vegetation type.

2.2 Forms

2.2.1 Generalized Blaze Flash (GBF):

A Generalized Blaze flash (GBF), is the term used to describe a wildfire that has transitioned from a surface fire to a crown fire by which its fireline intensity, rate of spread, and flame length increase dramatically (Chatelon et al. 2014).

2.2.2 Fire Blowup

Fire blowup, was the term used by (Sharples & Dold 2010, Viegas 2004), who described it as a fire eruption with an increased rate of spread (ROS) of the fire front, and that occurs in a single layer of fuel with no transition nor a change in the fire spatial and temporal boundary conditions.

2.2.3 Fire Flashover

Flashovers are complex phenomena that occur in closed spaces and are defined by the NFPA921 (2011) as the simultaneous ignition of gases resulting from the thermal degradation of combustible materials exposed to radiation from the fire. Scientists tried to link the causes of flashovers with the firefighters' observations during an eruption of a wildfire in a confined topography or relief depression. Firefighters in the Palasca fire (Dold et al. 2009) for example, reported that they noticed a cloud of gases with observable VOC odors before the fire erupted in a form of a flashover that consumed 15 acres in 45 secs. Other reports came about the flames which formed a homogeneous lake of fire and took a shape similar to a hydrocarbon gas fire (Peuch 2007). Other firefighters' testimonies reported an upslope acceleration in the fire rate of spread while the fire was still spreading downhill (Viegas 2009). Remarkably, eruptive fire behaviors were mostly coupled with gaseous accumulations and slopes as shown in Table II.1. Indeed, a 10° increase in slope can increase the fire rate of spread by two folds while a 20° increase in slope will increase the fire rate of spread by 4 folds (Butler et al. 2007). Fires spread upslope much faster than downslope due to several factors and by several mechanisms which have been extensively discussed in literature such as flow attachment (Dold and Zonviev 2009) without any significant change in ambient wind direction or velocity (Viegas and Pita 2004). However, as shown in Table II.1, most of the reported fire eruptions comprising behaviors of upslope fire accelerations were preceded with forms of explosions of gaseous pockets, resulting in a lake or blanket of fire that last for seconds, sometimes elevated two meters above a bare land with no vegetation such as the Canberra fire (Williamson et al. 2022).

Table II.1. Wildfire eruption accidents reported in France and globally, which were related to explosions of accumulated gas pockets in confined wildland topographies.

Wildfire Eruption Accident	Year	Observations
France		
Forest fire suppression accident, South of France [(a)]	2004	Mediterranean scrub and pine trees. Sudden inflammation of gas pocket in canyon. Fire spread acceleration uphill.
Lambsec [(b)]	2003	Mediterranean pine, low vegetation and reforestation plots. Deep valley configurations. Sudden flare up of gas accumulations inside a valley as the fire front approaches its tip.

Cogolin [b]	2003	Mediterranean forest (Cork oaks, chestnut, Aleppo pines, maquis, cistus). Deep valley configurations. High intensity explosion of the accumulated gases ahead of the fire front creating a lake of fire that lasted few minutes.
Palasca Fire [c] [f]	2000	Mediterranean vegetation (scrub, shrub, pine plantation). Steep sided valley, sheltered from wind. Sudden fire eruption appeared in the middle of the canyon. Homogeneous lake of fire lasted for 50 secs. Hydrocarbon gas fire.
Cornillon Confoux [b]	2000	Mediterranean mixed high forest of Aleppo pine and oak covering litter and shrub. Narrow thalweg. Flame detachment at the tip of the canyon followed by an explosion in the thalweg of accumulated gases.
Lancon de Provence [b]	1995	Mediterranean scrubland (Kermes oak and thorny gorse). Narrow thalweg. Gas pocket explosion ahead of fire front accelerated due to wind venturi effect.
Cabasson [b]	1990	Mediterranean scrub. Thalweg comprising 19% slope. Presence of colder air layer above the thalweg. Sudden emergence of glowing gas bubble.
Pennes-Mirabeau [a] [b]	1989	Mediterranean vegetation (scrub, Kermes oak, Cistus, Argeiras, Rosmariums, and pine trees). Sheltered canyon prevented wind from affecting the fire spread. Fire spread downhill. High intensity fire explosion of inflammable. compounds (i.e. a-pinene, β-pinene, camphene, β-myrcene) concentrated in the bottom of the valley. Upslope flared up.
Sainte Maxime [b]	1982	Large leafy vegetation (Moors). Very steep inaccessible thalweg. Explosion of gases confined in the bottom of the thalweg when in contact with flame.
	Other Countries	
Canberra (Australia) [d]	Jan 2003	Mediterranean climate vegetation. Fire started in a valley behind the firefighters and continued upwards a bare land with no vegetation present to produce pyrolysis gases. Blanket of flames was 2 meters above ground level and 8 meters high. Trees only burned in the middle, sheeps of cottage present burnt only on their backs.

Guadalajara (Spain) [(c)]	2005	Pinus Pinaster plantations and shrubs. Complex topography comprising a canyon. Spotting fire started and progressed on the downslope and erupted upslope as soon as it reached the bottom of the canyon.
Famalicao de Serra (Portugal) [(c)]	2006	Initial part of the slope was covered with some herbaceous and other light fuel vegetation, the upslope part was covered by mature pine stand. Crown fire development. Fire started on downslope (right side of the canyon) and spread then upon reaching the bottom of the canyon it erupted and accelerated upslope (left side of the canyon). Flames and heavy smoke. No shift in wind direction contributed to the fire acceleration upslope but rather the fire induced convection.
Kornati (Croatia) [(c) (e)]	2007	Mediterranean vegetation dominated by grass fine fuel with FMC from 12-14%. Sipnate canyon of 500m in length, closed from three sides (east, north and west) opened from south. Slope 14%. Fire eruption occurred at the bottom of the canyon and accelerated upslope (flames and heavy smoke).
Artemida (Greece) [(c)]	2007	Mediterranean vegetation comprising olive trees, pines and grass. Deep valley. Fire eruption was due to transition from surface fire of the grass layer to crown fire consuming the pine crowns. This transition was accompanied by an acceleration in fire front upslope the valley.

[(a)] Puech 2007, [(b)] Carbonell et al. 2004, [(c)] Viegas 2009, [(d)]Williamson et al. 2022, [(e)] Viegas et al. 2008, [(f)] Dold et al. 2009.

2.2.3.1 Confinement of Gaseous Emissions Inside the Valley

There are two hypotheses for the origin of the gases which accumulate inside a valley as suggested by (Carbonell et al. 2004). The first hypothesis is the generation of emissions from the pyrolyzed vegetation upslope due to the radiation from the fire initiating and spreading downslope (Figure II.1a), while the second hypothesis refers to the accumulations of the unburned VOCs that escaped the fire front propagating ahead of the valley, migrated and concentrated in it (Figure II.1b). In both cases, above the site of the fire, there is an inversion of temperature where a layer of colder air covers the smoke and so the large volume of flammable gases gets retained in a confined situation. Besides, the densities of the VOCs which are greater than that of air even when heated, permit them to accumulate at ground levels and migrate with winds to concentrate in the bottom of canyon where they form a gas mixture pocket ready to ignite.

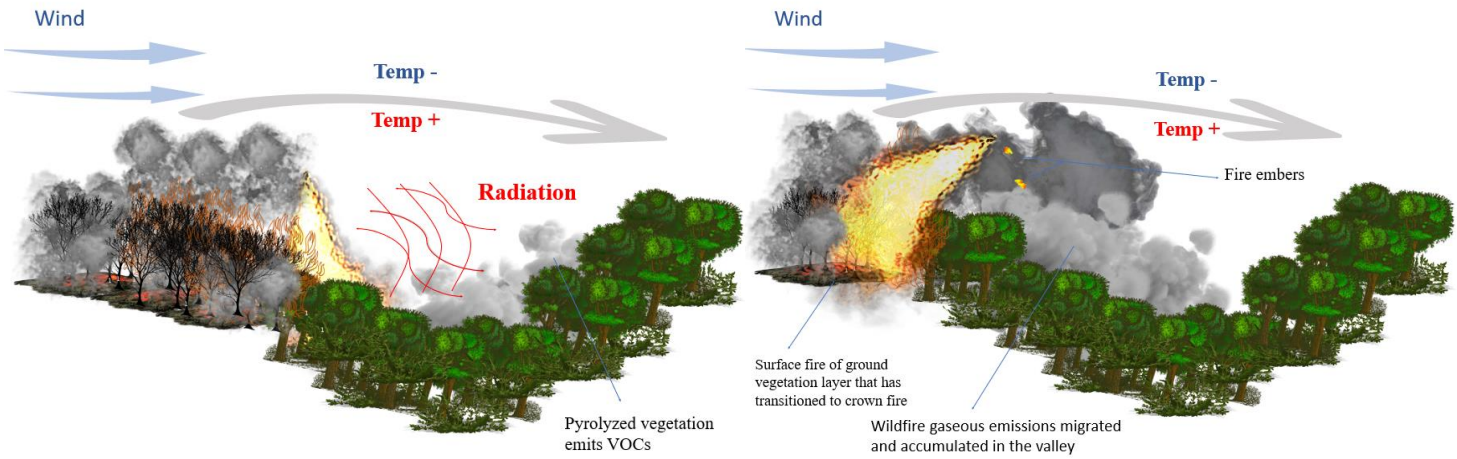

(a) (b)

Figure II.1. (a). Schemas representing accumulations of fire gases inside a valley from: (a) pyrolyzed vegetation upslope due to radiation from fire spreading downslope, (b). VOC migrated with the fire front ahead of the valley.

3 The Experimental Setup

The experimental setup was implemented by (Coudour et al. 2014), who attempted to investigate the transport and dispersion of gaseous emissions with wind flow across a forest landscape comprising topographic relief depressions. In their experiments, (Coudour et al. 2014) used a model mimicking a real forest geometry with two different V-shaped valleys of different angles and used a gas injection system supplying ethane (C_2H_6) gas through the forest. The forest was divided into different zones designating the different origins of the emissions either from smoldering, burning or pyrolyzing vegetation. The aim was to determine which emitting zone would have the greater effect on the concentration of gases throughout the forest with different valley angles.

3.1 Materials and Methods

3.1.1 Forest Model

The forest model was designed according to the work of (Conan et al. 2015) at a scale of 1/400 placed in an atmospheric boundary-layer wind tunnel in order to study the effect of the aerodynamic mechanisms (velocity and turbulence profiles) on the dispersion and accumulation of emissions inside and above the forest canopy. The trees were fabricated according to the work of (Auburn and Leitl 2004) to form a porous medium resisting the air flow and representing a typical deciduous forest with average tree height of 20 m and a leaf area index (LAI) of 3.6, a characteristic of a dense canopy. The trees were fabricated in the form of open cylinders 50 mm in height (H) with meshed walls (2.8 mm mesh size) formed from a steel wire (0,4 mm in diameter) rolled twice at the uppermost one third of the cylinder height (1/3 x H) to represent the denser tree crown (Figure II.2). The diameter of each cylinder was equal to ~ 30 mm, designed to be about two thirds of its height (2/3 x H). Metallic cylinders were then attached on boards of 12mm thickness, 2.5 m long in the wind direction and 1 m wide in the cross-wind direction and were arranged in a quadratic arrangement (Figure II.2) to represent a forest stand. However, such an arrangement was not meant to mimic the exact shape and

characteristics of a real forest, but rather to achieve the same aerodynamic properties inside and above the canopy.

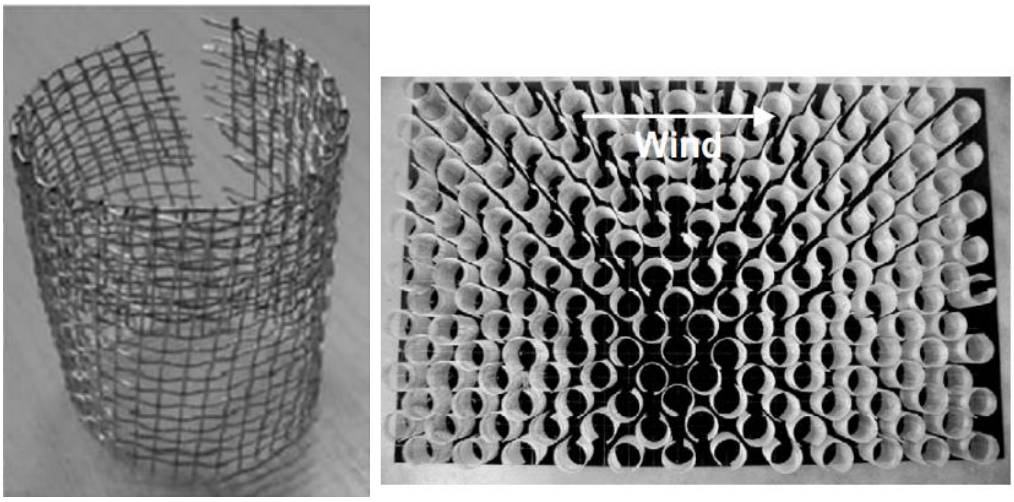

Figure II.2. Meshed cylinder representing a tree (left). Quadratic arrangement of the meshed cylinders representing a forest stand (right); (Aubrun and Leitl 2004)

The (2.5 x 1 m^2) boards were divided into five parts each of fixed length (L_1 = 0.5 m) and width (W = 1 m) with fixed metallic cylinders. However, the zones of interest to our study were four: the first two flat zones 1 and 2 each of (0.5 x 1 m^2) placed ahead of the valley, and the other two zones 3 and 4 (0.5 x 1m^2) formed the lee and wind sides of the valleys, respectively (Figure. II.3). The two valleys studied had two different half internal angles (α) representing a steep valley with α = 50° and a shallower valley with α = 80°.

3.1.2 Atmospheric Boundary-Layer Wind Tunnel

The forest model was placed in an atmospheric boundary layer wind tunnel to simulate the interaction of the wind and earth in the lowest layers of the atmosphere. A honeycomb turbulence generator was installed at the entrance of the wind tunnel to pre-form the boundary-layer. A 16 m long flow development section with roughness elements attached to it was used to generate a proper boundary-layer height at the forest model (Figure II.4). This last was placed far enough from the turbulence generator to achieve realistic full-scale boundary-layer characteristics. The wind tunnel inlet velocity was set at 6 m/s.

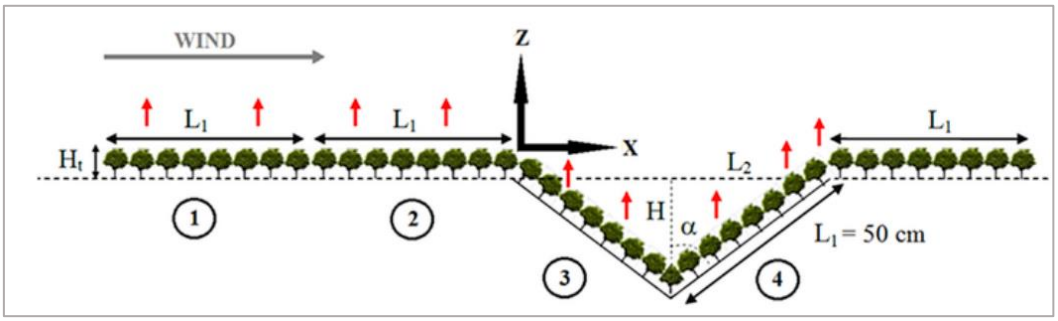

Figure II.3. Forest model geometry.

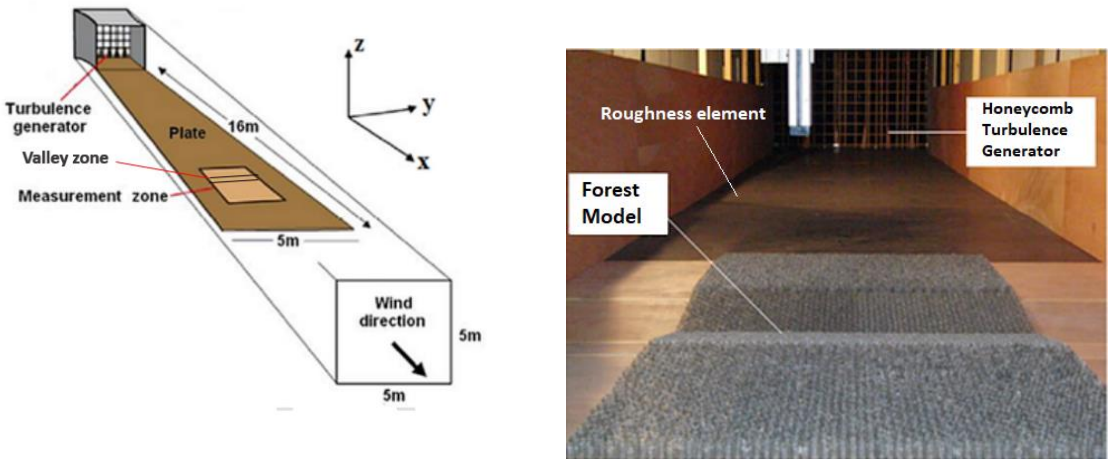

Figure II.4. Atmospheric boundary layer wind tunnel with the development section and forest model.

3.1.3 Gaseous Emissions

The emissions were achieved homogenously by C_2H_6 gas injection through 400 tubes distributed equally throughout the metallic cylinders throughout an area equal to (0,5m in width and 1m in length) of the four zones (100 tubes/zone). To identify the contribution of the emissions of each zone to the concentrations in the valley, each patch of 100 tubes were branched to a secondary distribution box with a flow controlling valve (on/off) independent from the main *Brooks*® mass flow controller. The tubes were positioned at a height equal to 80% of the cylinders heights (40mm) in order to simulate the emissions from the foliar elements of a canopy (Figure II.5). Since the investigations of the aerodynamic profiles were independent of the buoyancy effects of the emitted species (passive transport), ethane was chosen as the injection gas in the experimental work because its density (~1,282 kg/m^3) is very close to that of air, it is also a nontoxic gas and easily detectable by a Flame Ionization Detector FID. The volumetric flow rate of C_2H_6 gas was 2,09 l.min^{-1}.m^{-2}.

Figure II.5. Ethane (C_2H_6) distribution network.

3.1.4 Measuring Equipment

Velocity measurements were done using Laser-Doppler-Velocimeter (LDV) from Dantec® while C_2H_6 concentrations were measured by a fast Flame Ionization Detector (fast-FID) from Cambustion®. The FID measures the ionized carbon atoms of C_2H_6 by a hydrogen flame, after which they have created a current at the detector electrodes. The concentrations of molar

fraction were measured in parts per million (ppm) and were normalized by the volumetric flow rate per unit area and a reference air velocity (U_{ref}) measured above the canopy at a height equal to 10 times of its height (Coudour et al. 2014). Velocity (U) measurements were done in the horizontal x and vertical z direction to measure U_x and U_z. Velocity measurements were taken at 385 and 224 points for the 50° and 80° valleys, respectively. Velocity measurements were time-averaged over 120s for each point in order to establish a correct convergence of their mean and standard deviation values. With the standard deviation and mean values of the horizontal and vertical velocities at each point we were able to quantify the horizontal and vertical turbulence intensities I_x and I_z respectively (*Equation II.1*).

$$I_{x,z} = \frac{\sigma_{x,z}}{\bar{U}} \qquad (II.1)$$

Where,

σ is the standard deviation of the velocity measurements (horizontal and vertical) time-averaged over 120s at a particular point;

$\sigma_{x,\,z} = \sqrt{\frac{1}{n}\sum_{i=1}^{n}(u_i - \bar{U})^2} = \sqrt{\frac{2}{3}K}$, with K being the turbulent kinetic energy.

$\bar{U}$ is the mean velocity of the two velocity components (U_x and U_z) at a certain point;

$$\bar{U} = \sqrt{{U_x}^2 + {U_z}^2}$$

3.2 Experimental Results

The experimental velocity and concentration measurements showed important circulation in velocity profiles in the sharp angled valley of 50° due to the separation of the boundary layer explained by the null turbulence intensities, unlike the case of the relatively flat valley of 80° where no detachment of boundary layer nor velocity circulation profiles were observed, and the turbulence intensities inside the valley were very high (>1.4). Due to the re-circulation of the velocity profiles and the absence of turbulence in the valley of $\alpha = 50°$, concentrations reached significant values on the lee side of the valley with a value of 1790 ppm 3.5 times more than the concentrations measured above the canopy flat surface prior to the valley. On the other hand, for the valley of $\alpha = 80°$, C_2H_6 concentrations were humble and no re-circulation of the velocity profiles was noticed as there was no detachment of the boundary layer (Figure II.6).

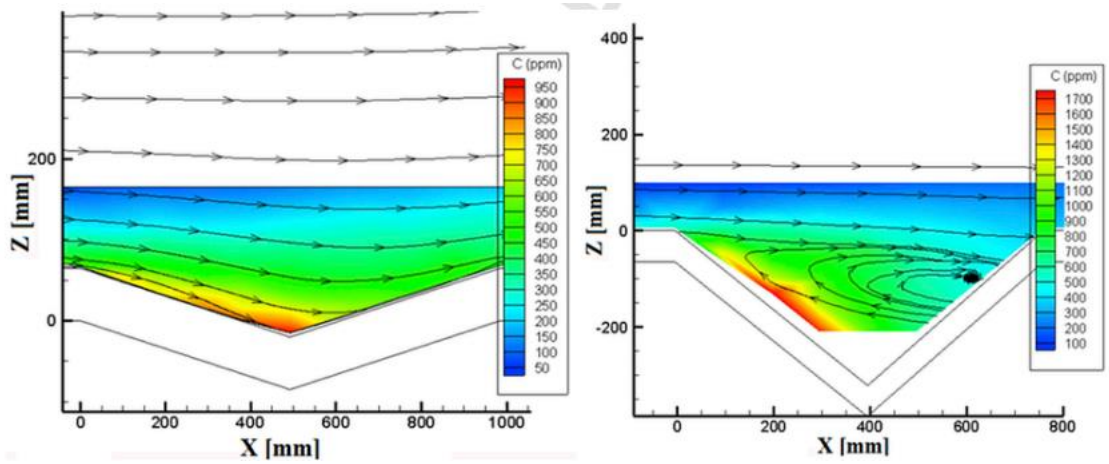

Figure II.6. Experimental results of concentrations with velocity streamlines for α= 80° (left) and α= 50° (right).

4 Numerical Model Simulations with STAR-CCM+

4.1 Why STAR-CCM+?

The CFD methods have been the most efficient for modeling the transport and dispersion of the compounds of gaseous mixture in space. STAR-CCM+ is not only a CFD solver but also a computational aided engineering (CAE) solution for solving multidisciplinary problems in both fluid and solid continuum mechanics with a single integrated user interface. It provides a choice between the different turbulence models form modeling different flow behaviors, including the K-epsilon (i.e., standard, realizable, two-layer, low-Reynolds number, etc…). STAR-CCM+ provides several methods including the Eulerian and Lagrangian methods, for predicting the dispersion of gaseous compounds in a space associated with air flow and turbulence. The software also incorporates the porous media model which represents a solid structure with porous parameters that can be used to simulate our forest model with the use of the physical velocity formulation. This formulation accounts for the increase in velocity when the flow enters the porous medium and the dominance of the structure and porosity in forming the turbulence scales inside the forest.

4.2 Numerical Model Preprocessing

4.2.1 Physical Model Choice

The steady flow of a gaseous species (C_2H_6 in our case) along the air streamline is represented by a 2D steady Euler-Euler approach to simulate its motion by solving the density-weighted averaged conservation equations of mass, momentum and species together with the transport equations of turbulence variables K and ε, without accounting for the buoyancy production and destruction terms as they are neglected in our study for the absence of temperature gradient or thermal convection.

The general equation of the transport of each scalar (K) where the convective flux is computed with the mass flow rate of the gas (C_2H_6) is:

$$\frac{\partial}{\partial x_i}\left(\rho u_i \Phi_k - \Gamma_k \frac{\partial \Phi_k}{\partial x_i}\right) = S_{\Phi_k} \qquad (II.2)$$

Where,

$\boldsymbol{\Gamma}_k$ and S_{Φ_k} are the diffusion and source terms, respectively of every scalar K. K = 1…., N for mass, momentum, kinetic energy of turbulence (K), rate of dissipation of K (ε), and the species mass fraction, in addition to buoyancy which is neglected in our simulation.

The terms of diffusion and production of mass and momentum are the same as the ones used by (Coudour et al. 2014) however, since the RNG K-Epsilon turbulence model is not supported by STAR-CCM+, the realizable K-Epsilon (RKE) model is used instead, with a different formulation for the transport equations of K and ε as follows:

$$\frac{\partial}{\partial x}(\rho k) + \nabla.(\rho K \bar{\nabla}) = \nabla.\left[\left(\mu + \frac{\mu_t}{\sigma_k}\right) \nabla k\right] + P_k - \rho(\varepsilon - \varepsilon_0) + S_k \qquad \textit{(II.3)}$$

$$\frac{\partial}{\partial x}(\rho \varepsilon) + \nabla.(\rho \varepsilon \bar{\nabla}) = \nabla.\left[\left(\mu + \frac{\mu_t}{\sigma_\varepsilon}\right) \nabla \varepsilon\right] + \frac{1}{T} C_{\varepsilon 1} P_\varepsilon - C_{\varepsilon 2} f_2 \rho \left(\frac{\varepsilon}{T_e} - \frac{\varepsilon_0}{T_0}\right) + S_\varepsilon \qquad \textit{(II.4)}$$

Where;

$\bar{\nabla}$ is the mean velocity.

μ is the dynamic viscosity.

σ_k, σ_ε, $C_{\varepsilon 1}$, $C_{\varepsilon 2}$ are model coefficients.

P_k and P_ε are the production terms for turbulent kinetic energy and its dissipation, respectively.

S_k and S_ε are the source terms for turbulent kinetic energy and its dissipation, respectively.

f_2 is a damping function.

μ_t is the turbulent eddy viscosity.

ε_0 is the ambient turbulence value in the source terms that counteracts turbulence decay. This term imposes to use the definition of a specific time-scale T_0.

In the realizable K-Epsilon (RKE) model is a variant of the standard K-Espilon model because it contains a new formulation for the turbulent viscosity where a damping function f_μ is applied to the critical coefficient of the model C_μ. The RKE model provides superior performance for flows involving boundary layers under strong adverse pressure gradients such as those developed in the porous region of the forest, the separation of the boundary layer, and recirculation. Such characteristics make the model outperform the standard and RNG K-Epsilon models.

Table II.2. RKE model coefficients, formulations and terms descriptions.

RKE Model Coefficients	Formulation	Description
$\mathbf{P_k}$	$f_c G_k + G_b - \Upsilon_M$	G_k: Turbulent Production. G_b: Buoyancy production. $C\varepsilon_3$: model coefficient. f_c: curvature correction factor. Υ_M: Compressibility Modification.
$\mathbf{P_\varepsilon}$	$f_c Sk + C_{\varepsilon 3} + G_b$	
$\mathbf{C_{\varepsilon 1}}$	$\max\left(0.43, \frac{\eta}{5+\eta}\right)$ where: $\eta = \frac{SK}{\varepsilon}$	S: Mean stress tensor.
$\mathbf{C_{\varepsilon 2}}$	1.9	
$\mathbf{C_{\varepsilon 3}}$	$\tanh\frac{\lvert v_b\rvert}{\lvert u_b\rvert}$	Ce3 = $\begin{cases}1 \ for\ G_b \geq 0\\ 2\ for\ G_b < 0\end{cases}$
$\boldsymbol{\sigma_\varepsilon}$	1.2	
$\boldsymbol{\sigma_k}$	1	
$\boldsymbol{f_2}$	$\frac{k}{k+\sqrt{\nu\varepsilon}}$	
$\mathbf{T_0}$	$\max\left(\frac{k_0}{\varepsilon_0}, C_t\sqrt{\frac{\nu}{\varepsilon_0}}\right)$	
$\mathbf{C_t}$	1	
$\boldsymbol{\mu_t}$	$\rho C_\mu \frac{k^2}{\varepsilon}$	
$\mathbf{C_\mu}$	0.09	

4.2.2 The Geometry

STAR-CCM+ contains its own feature-based parametric solid modeler called 3D-CAD which allows to draw the geometry in 3D domain. Simulations can be later run in 2D domain after converting the one-cell-thick 3D mesh into a 2D. Two geometries were drawn for the wind tunnel comprising the forests with two different internal valley angles; 50° and 80°. The forest dimensions are (2.5 x 1 x 0.062 m). However, since the emissions are released at 80% of the forest height the forest will be divided into two lower and upper regions of heights 0.05 m and 0.012m, respectively. The geometric parts are drawn and then are assigned to three regions (the wind tunnel, the forest, and the ethane zone) as shown in Figure II.7.

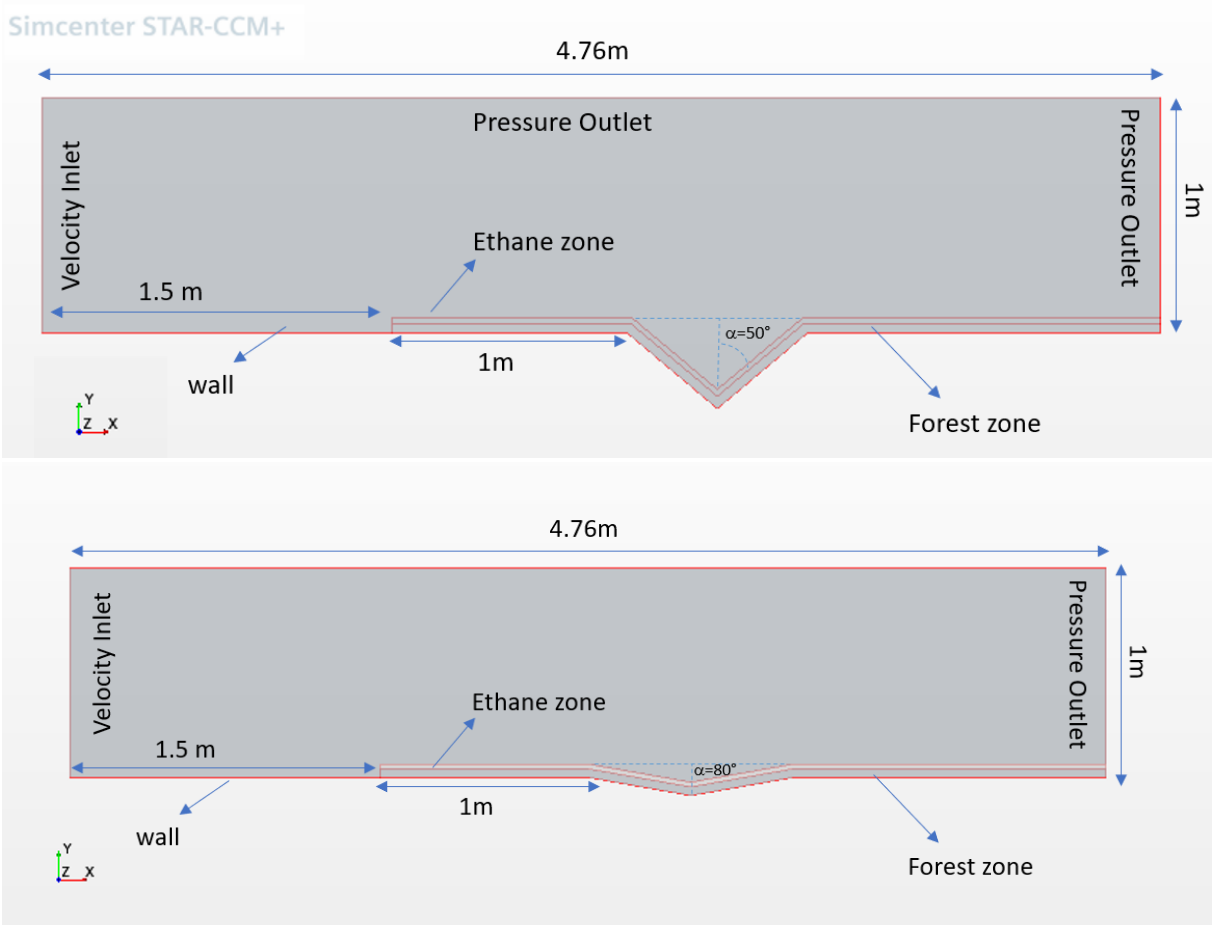

Figure II.7. Geometry of the computational domain with regions and boundary conditions for two valley internal angles α = 50° (up) and 80° (down).

4.2.3 Mesh Pre-Processing

4.2.3.1 Near Wall Region: Y⁺ Wall Function Approach

Walls are a source of vorticity, therefore an accurate prediction of the flow across the wall boundary layer is essential in order to get accurate results for our simulations. Unlike the Low Reynolds K-ω model, the RKE is a High Reynolds number model therefore, the near wall region cannot be modeled correctly with the last unless it is coupled with the wall function. The wall function is used to model the turbulence in the near wall region where "Low Reynolds" number dominates. The turbulent boundary layer is divided into two layers: the outlet layer and the inner layer. The outer layer is dominated by turbulent effects. The inner layer is split up into three more sublayers, the log and buffer layers, and the viscous sublayer (Figure II.8). In STAR-CCM+, wall functions are used to bridge the inner region between the wall and the turbulence fully developed region. Therefore, the mesh size and the computational domain in the near wall region will be reduced. The nondimensional wall distance y^+ is used to define the extents of the sublayers (Figure II.8).

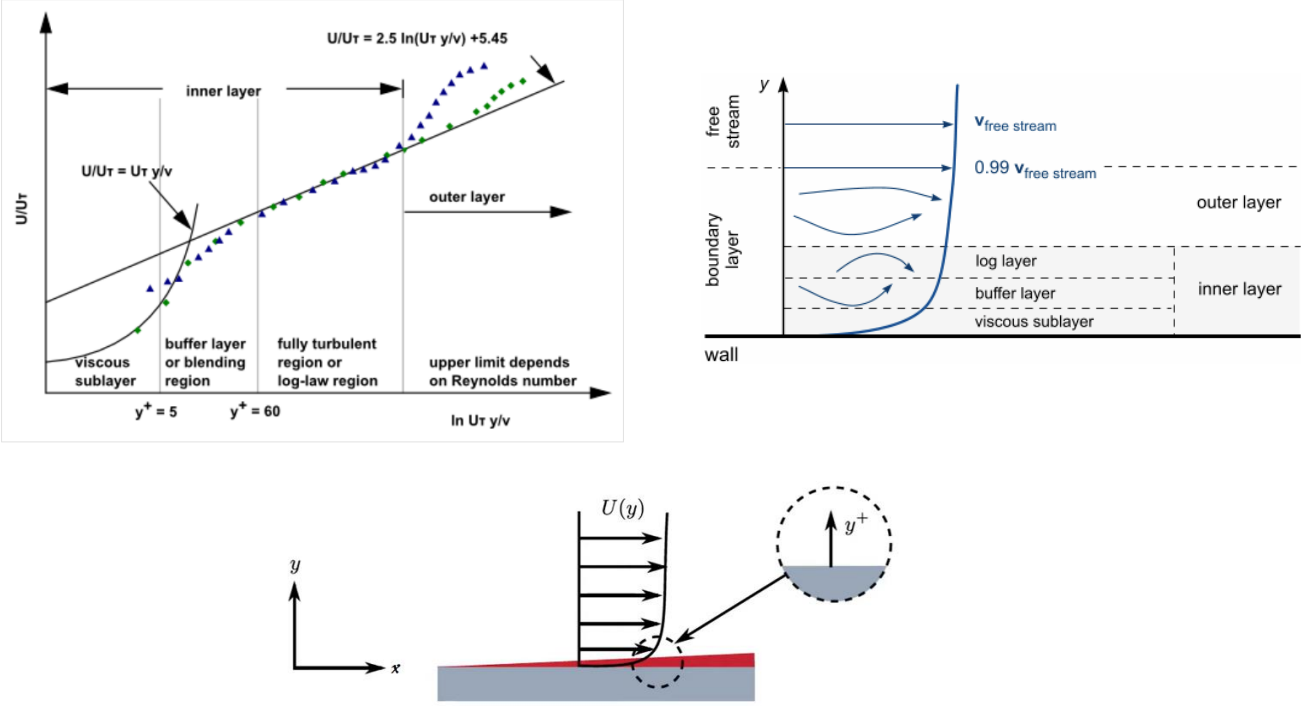

Figure II.8. Resolution of the boundary layer using y^+ wall function.

4.2.3.2 Inflation Layer

4.2.3.3 Predicting Near Wall First Cell Size

In meshing, with the RKE model, the first cell center needs to be placed in the log-law region i.e. $30 < y^+ < 100$ in order to ensure the accuracy of the simulation results. Notably with the K-ω the first cell center would have been put in the viscous sublayer i.e. $y^+<5$ therefore, the meshing and the computational domain will be very high.

The boundary layer is meshed with prism layers which is referred to as inflation layer in STAR-CCM+ (Figure II.9). In the preprocessing stage and to avoid remeshing, the height of the first layer (y_h) in the grid cells of the inflation layer (prism layers) should first be predicted so that y^+ lays in the desired range. It is an iteration procedure where the y^+ value is assumed for example ($\cong 50$) to calculate y_h and adapt it in the mesh parameters then the wall function is observed to check if it lays in the desired range ($30 < y^+ < 100$). The empirical correlation suggested by (section 10.6 in Cengel & Cimbala 2006) is used in the calculation of the following boundary layer parameters. The wind tunnel length (L) is 13m before the forest, and the inlet air velocity of the boundary layer wind tunnel is 6m. s^{-1}. For flat plate, Reynolds number ($Re_l = \frac{\rho V L}{\mu}$) gives $Re_l = 5.3 \times 10^6$, a turbulent regime ($> 5\times10^5$).

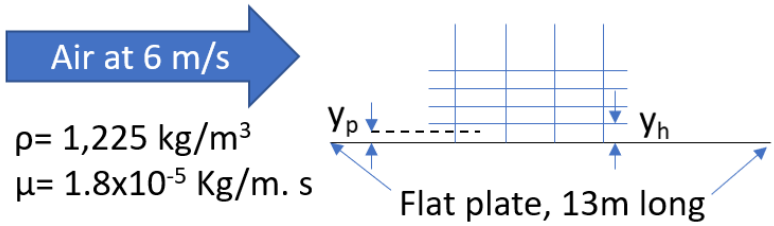

Figure II.9. Near-Wall cell central height (y_p) and total height (y_h).

The value of y+,

$$y^+ = \frac{\rho U_\tau y_p}{\mu} \leftrightarrow y = \frac{y^+ \mu}{U_\tau \rho} \qquad (II.5)$$

For $y^+ \cong 50$ for RKE as suggested in (Salim & Cheah 2009), the near wall velocity scale $U_\tau = \sqrt{\frac{\tau_w}{\rho}}$ where, the wall shear stress $\tau_w = \frac{1}{2} C_f \rho U_\infty^2$ with the skin friction coefficient $C_f = 0.027 Re_l^{-\frac{1}{7}} = 0.0029$. Therefore, $\tau_w = 0.065\ Kg.m^{-1}.s^2$ with U_∞ = 6 m. s^{-1}, $\therefore U_\tau$ = 0.230 m. s^{-1}.

Aiming for y^+ of 50 implies that $y_p = \frac{y^+ \mu}{U_\tau \rho}$ = 0.00367 m. Therefore, the first cell center height (y_p) in our meshing should be approximately 3.6 mm and the total first cell height (y_h) which is identified in STAR-CCM+ as "wall thickness" should be initially set to 7.2 mm.

4.2.3.4 Total Prism Layer Thickness

In the mesh preprocessing it is important to aim for an inflation layer (prism layer) with total thickness that contains the boundary layer δ_{99} (Figure II.8). The first cell size (yh) is calculated in the previous section, while the total height (y_T) is calculated according to

$$y_T = y_h + y_h G + y_h G^2 + y_h G^3 + \cdots + y_h G^{N-1} \qquad (II.6)$$

Where G, is the geometric growth ratio (G>1). Therefore, each consecutive layer is larger than the previous layer and N is the total number of the prism layers. In order to calculate G, y_T is assumed to be equal to the boundary layer (δ_{99}) (Figure II.10).

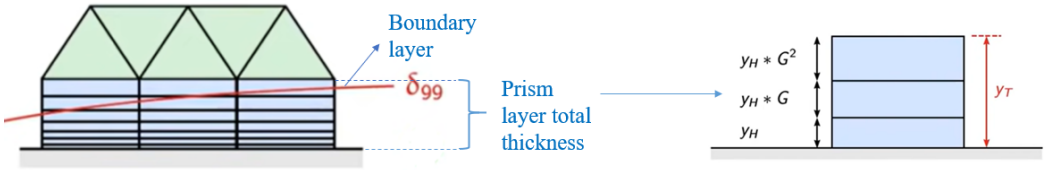

Figure II.10. Boundary layer δ_{99} contained in the inflation layer (prism layer) with growth rate G and total thickness y_T.

The formula of y_T can be simplified by using a geometric series formulation to become,

$$\sum_{k=0}^{N-1} y_h G^k = y_h \frac{1-G^N}{1-G} = y_T = \delta_{99} \qquad (II.7)$$

The boundary layer δ_{99} can be calculated as follows;

$$\delta_{99} = \frac{0.38 \times L}{(Re)^{1/5}} = \frac{0.38 \times 13}{(5.3 \times 10^6)^{1/5}} = 0.22\ m \qquad (II.8)$$

Assuming $y_T = \delta_{99} = 0.22$m and $y_h = 0.0072$ m, N and G can now be calculated. Forums and discussion posts suggest values for N >10 when y^+ is >30 therefore a value of 10 will be used as a first guess. Using the bisection method for N = 10, the growth ratio G = 1.09481 >1. Therefore, with the parameters of the inflation layer we can now size the prism layers of our selected mesh in STAR-CCM+.

4.2.4 The Meshing

The use of a one-cell-thick three-dimensional mesh is much less efficient than using a real two-dimensional mesh for two-dimensional simulations therefore, the geometry was badged for 2D mesh in STAR-CCM+. This operation identifies the parts surfaces that lay on the Z=0 plane to be parts of the automated 2D mesh (Figure II.11). There are two types of regions in the computational domain a fluid region (wind Tunnel) and a porous region (forest) connected with an interface. The mesh needs to be conformal across the interface therefore, the triangular mesh is used instead of the trimmer. The prism layer (inflation layer) mesh with the parameters calculated in the previous section is also used to fit the wall function accurately. Prism layers do not only provide near wall mesh density, they also allow high-aspect-ratio cells to be used, thus providing better cross-stream resolution without incurring an excessive stream-wise resolution.

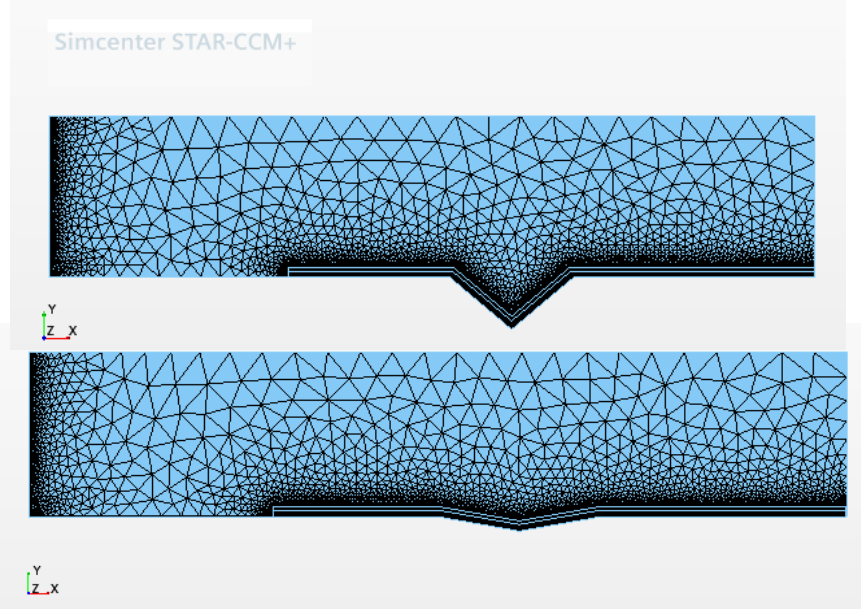

Figure II.11. Mesh visualization of the two valley internal angles α = 50° (up) and 80° (down).

4.2.5 The Physics Models

The physics models used for the simulations are shown in the tree of (Figure II.12). A multi-component gas was used with air and. The density of air and C_2H_6 are defined by default in STAR-CCM+ at standard conditions as 1.18 and 1.28 $kg.m^{-3}$, respectively.

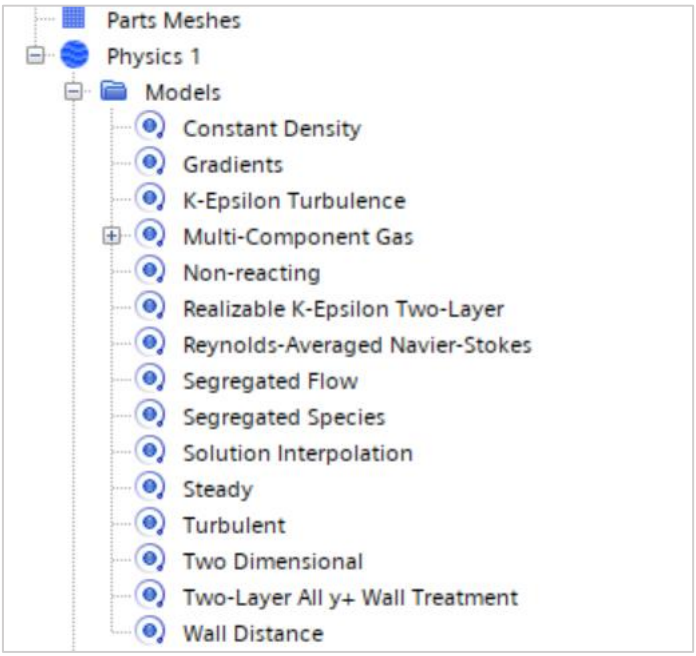

Figure II.12. Physics models of the numerical simulation in STAR-CCM+.

4.2.5.1 Initial Conditions

The following settings are common for 50° and 80°. After the physics models are chosen and the parts are assigned to regions, the boundaries of the regions are defined as shown in Figure II.7. The initial horizontal and vertical components of the velocities (U & V), are set to 6 $m.s^{-1}$ and zero. Reference pressure is set to atmospheric pressure at 101325Pa and the initial pressure is set to zero. Initial species mass fraction of C_2H_6 and air are equally set to 1.

4.2.5.2 Boundary conditions

The following settings are common for 50° and 80°. After the initial conditions are specified, the parts are assigned to regions and the boundary conditions are set. The wind tunnel region is set to fluid while the forest and ethane zone are set to porous regions.

- **Inlet velocity:** The experimental measurements of the horizontal and vertical velocity components (U & V) have shown uniform profiles up to 1.5 m prior to the forest. Therefore, these experimental values were added to the inlet velocity boundary while the turbulent kinetic energy (K) and turbulent dissipation rate (ε) were calculated accordingly and set for the turbulence specification (Table II.3). The inlet velocity profile is plotted in Figure II.13. The species mass fractions are set to 0 and 1 for C_2H_6 and air, respectively.
- **Pressure outlets:** The pressure specification at the pressure outlets boundaries are set to zero because the reference pressure in the initial conditions is already set to

atmospheric pressure, and the species mass fractions are set to one for both C_2H_6 and air.

- **Wall:** The wall is set to impermeable and the inflation (prism) layer heights (y_h & y_T), number of layers (N), and growth rate (G) were added as calculated (*cf. section* 4.2.3.4).
- **Ethane zone**: porous region with isotropic porosity parameters (explained below). C_2H_6 species source option is set at a mass flow rate of 0.001902 $kg.m^{-3}.\ s^{-1}$.
- **Interfaces:** The interfaces (forest zone/ethane zone & ethane zone/tunnel) are initialized and set to internal interfaces. The meshes were conformal at the interfaces after initialization.

Table II.3. The velocity inlet boundary conditions, velocity and turbulence specification for 50° and 80°.

X	Y	U	V	K	ε
0	0.005	2.56	0.04	0.167	0.213
0	0.01	2.8	0.05	0.172	0.224
0	0.02	3.15	0.06	0.207	0.296
0	0.03	3.29	0.06	0.208	0.297
0	0.04	3.46	0.06	0.208	0.297
0	0.05	3.6	0.04	0.208	0.297
0	0.06	3.71	0.04	0.225	0.335
0	0.07	3.76	0.06	0.197	0.274
0	0.08	3.85	0.06	0.197	0.274
0	0.09	3.94	0.06	0.223	0.329
0	0.1	4.02	0.07	0.197	0.274
0	0.15	4.2	0.08	0.197	0.274
0	0.2	4.45	0.09	0.168	0.216
0	0.25	4.6	0.09	0.139	0.162
0	0.3	4.76	0.1	0.116	0.125
0	0.35	4.96	0.11	0.116	0.125
0	0.4	5.04	0.11	0.106	0.108
0	0.45	5.07	0.11	0.095	0.092
0	0.5	5.24	0.12	0.082	0.074
0	0.55	5.29	0.13	0.083	0.075
0	0.6	5.4	0.12	0.071	0.060

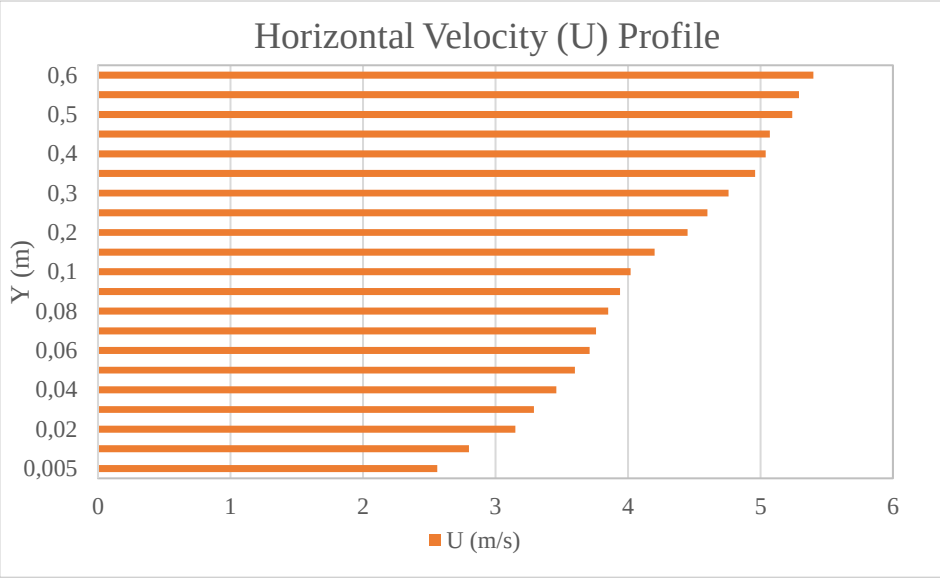

Figure II.13. Inlet horizontal velocity profile (U).

4.2.5.3 Setting Porous Resistance Properties for Forest Region

The flow of a fluid (air in our case) through a porous medium is governed by the relationship between the velocity and the pressure gradient caused by the packed bed. Darcy's law describes this relation for low Reynold's number by the following equation,

$$-\nabla p = \frac{\mu Vs}{Kp} \qquad (II.9)$$

Where μ is the fluid (air) molecular viscosity, K_p is the permeability, and V_s is the superficial velocity through the medium. For high Reynolds number (our case), the relation becomes nonlinear and Forchheimer updated it to contain a quadratic term in a general form as follows,

$$-\nabla p = \frac{\mu}{Kp} Vs + b\rho|Vs|Vs \qquad (II.10)$$

One example of the Forchheimer equation for a particular class of flow is the Ergun equation. This equation is an empirical model for the pressure drop (d_p) over a length (L) of fluid (air) flowing through a packed bed:

$$\frac{-dp}{L} = Pv + Pi = \frac{150\mu(1-X)^2 Vs}{X^3 Dp^2} + \frac{1.75\rho(1-X)Vs^2}{X^3 Dp} \qquad (II.11)$$

Where;

Pv and Pi are the viscous and inertial terms.

ρ is air density = 1.25 Kg.m$^{-3.}$

D_p is the diameter of the pore = 0.006m.

X is the volume porosity = 0.7.

Comparing the two equations we get the permeability (viscous term) as:

$$\frac{1}{Kp} = \frac{150(1-X)^2}{X^3 Dp^2} \qquad (II.12)$$

And the b factor (inertial term) as:

$$b = \frac{1.75(1-X)}{X^3 Dp} \qquad (II.13)$$

In order to implement this model in STAR-CCM+, it is necessary to define the above terms in user field functions. First the pore diameter and the volume porosity are defined in field functions as constants, then they are used in the field functions of the above terms. The porosity is set to 0.7(dimensionless) and the pore diameter D_p is set to 0.006m. The field functions for the permeability and the b factor are respectively:

150.0*$DynamicViscosity*pow((1-$BedPorosity),2)/(pow($BedPorosity,3) * pow($BedSphereDiameter,2))

and

(1.75*$Density*(1-$BedPorosity))/(pow($BedPorosity,3) * ($BedSphereDiameter)

4.2.6 Post-processing

In analyzing the simulation results we are interested in the velocity and C_2H_6 concentration profiles for $\alpha = 50°$ and $\alpha = 80°$. Therefore, postprocessing objects are created to gain these results. Vector scenes are created to observe the velocity profiles inside the valleys and scalar scenes are created to observe the spatial concentration profiles of C_2H_6 and compare them with the experimental results. A field function was created to calculate the concentrations of C_2H_6 in ppm using the following equation from Wikipedia.

$$ppmv = mg/m^3 \times \frac{(0.082057338 \times T)}{M} \qquad (II.14)$$

Where,

ppmv is the concentration of C_2H_6 in parts per million by volume.

mg/m^3 is the mass concentration per cubic meter of air at standard conditions.

M is the molecular mass of C_2H_6 30.7 $g.mol^{-1}$.

T is the ambient temperature in K = 273 +°C.

0.082057338 is the universal gas constant in $L.atm.mol^{-1}. K^{-1}$.

The spatial concentrations of C_2H_6 were measured at different locations inside the valley similar to the positions used in the experimental setups. y-z plane sections were created in the derived parts of the two geometries of $\alpha = 50°$ and $\alpha = 80°$. After creating a user defined coordinate system which origin is at the beginning of the forest zone, the positions of the sections for $\alpha = 50°$ were at x= 1.195m, 1.295m, 1.395m, and 1.495m and for 80° at x = 1.382m, 1.492m, and 1.582m (Figure II.14). C_2H_6 concentrations are traced at each x position along the total height (y-axis) of the computational domain.

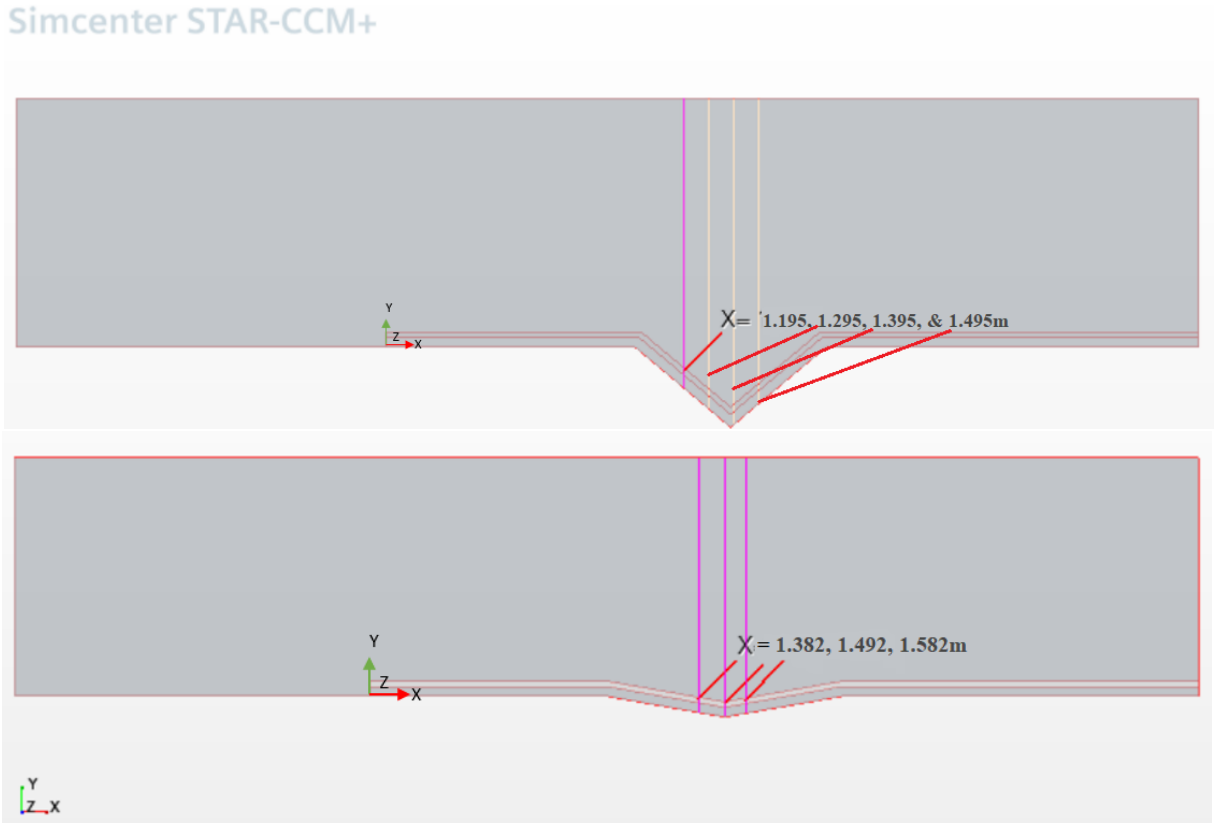

Figure II.14. Plane sections at different locations inside of the valleys of α= 50° (up) and α = 80° (down).

4.3 Results

4.3.1 Numerical Velocity and C_2H_6 Spatial Concentration Profiles for α = 50° & 80°

After initializing the solution and running the simulation, we were able to visualize the numerical results of the velocity and C_2H_6 concentration profiles through the vector and scalar scenes and the graphical plots available in the post-processing features of STAR-CCM+.

4.3.1.1 $\alpha = 50°$

The vector scene of the velocity profiles (Figure II.15) allowed us to trace the velocity vectors throughout the fluid region and the porous region. The superficial velocity values outside the porous region are the same as inside the porous region (Equation II.15). However, to maintain an accurate representation of the velocity values which normally increase due to porosity, STARCCM+ solves for the physical true velocity throughout the flow field. Contrary to the superficial velocity, the physical velocity is discontinuous throughout the interface between the two regions (porous and fluid).

$$\vec{v}_{superficial} = \vec{Xv}_{physical} \qquad (II.15)$$

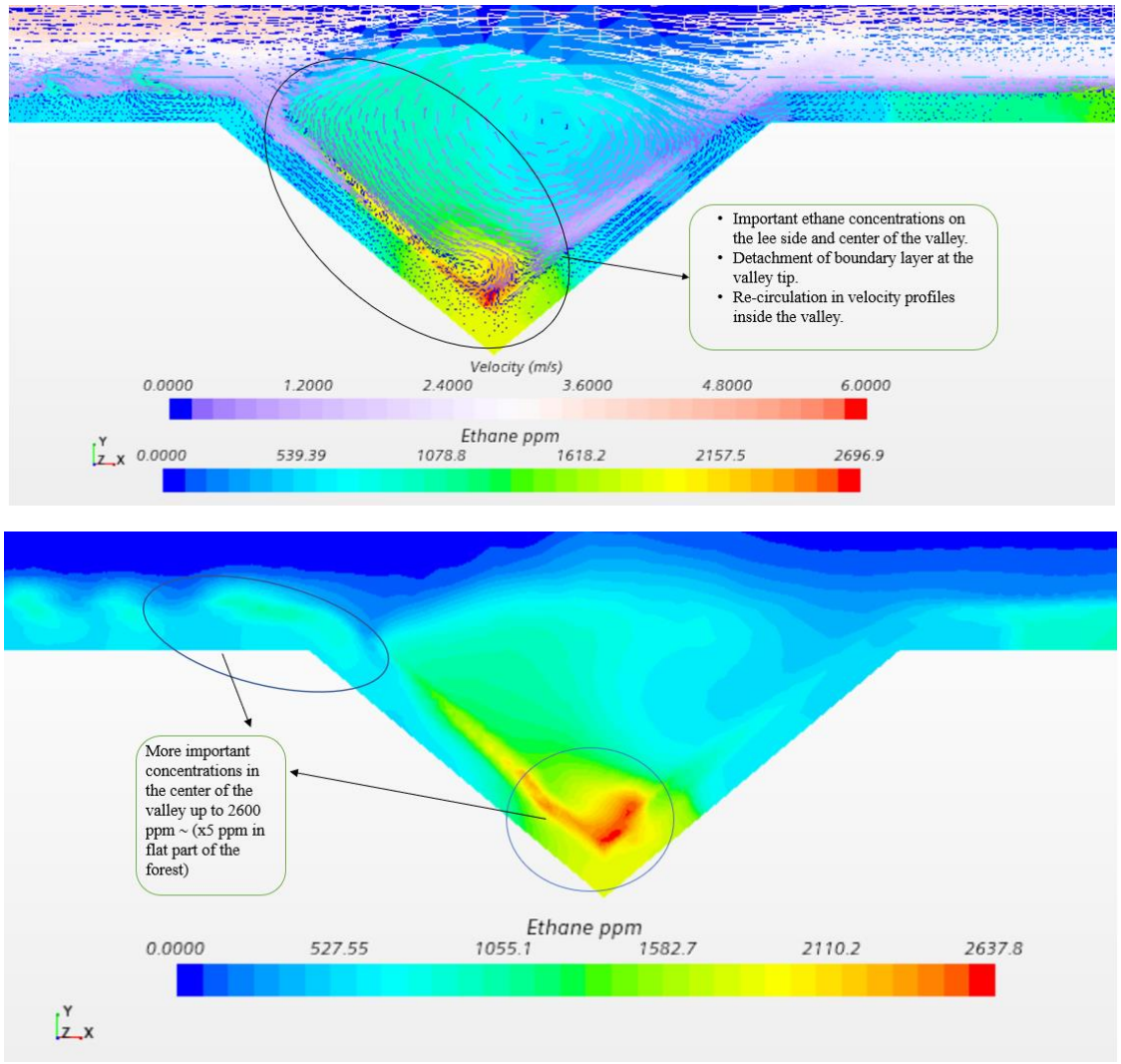

Figure II.15. Scalar scenes showing recirculation of velocity vectors (up) and ethane (C_2H_6) concentrations (down) in the valley for $\alpha = 50°$.

In the valley of $\alpha = 50°$ as the area of the flow increases the velocity decreases and the pressure gradient increases in the direction of the flow ($\frac{dp}{dx} > 0$) therefore the boundary layer detaches from the surface into the wake. The detachment of the boundary layer causes recirculation in the velocity vectors inside the valley where stagnation points are formed and C_2H_6 is concentrated remarkably on the lee side and in the center of the valley (Figure II.15) with concentrations up to ~2000 and ~ 2700 ppm, respectively. The numerical results confirmed the experimental results (*cf. Figure II.6*) and we were able to trace velocity streamlines inside the porous region and measure remarkable concentrations of C_2H_6 in places where the FID could not reach, such as the proximity of the porous region on the lee side and the center of the valley (Figure II.15). The concentrations in the center of the valley have reached 2700 ppm (Figure II.16c) about 5 times more than the concentrations inside the flat region of the forest. The recirculation of the velocity vectors was traced with the streamlines in (Figure II.15) and was confirmed by the negative values of the horizontal and vertical velocities at the three X-positions (Figure II.16). The following graphical plots represent the comparison between the

experimental and numerical values of the horizontal (U) and vertical (V) velocity magnitudes and C_2H_6 concentrations along the y-axis of the four plane sections in the valley.

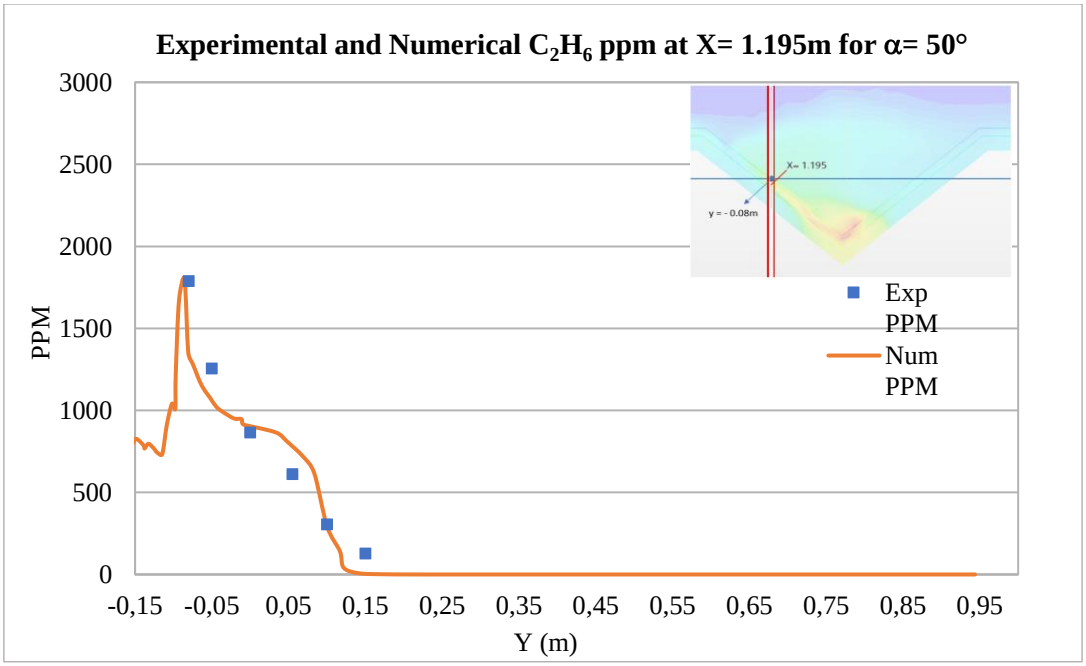

**(a). ***The best experimental measurements were at height = - 0.08m.

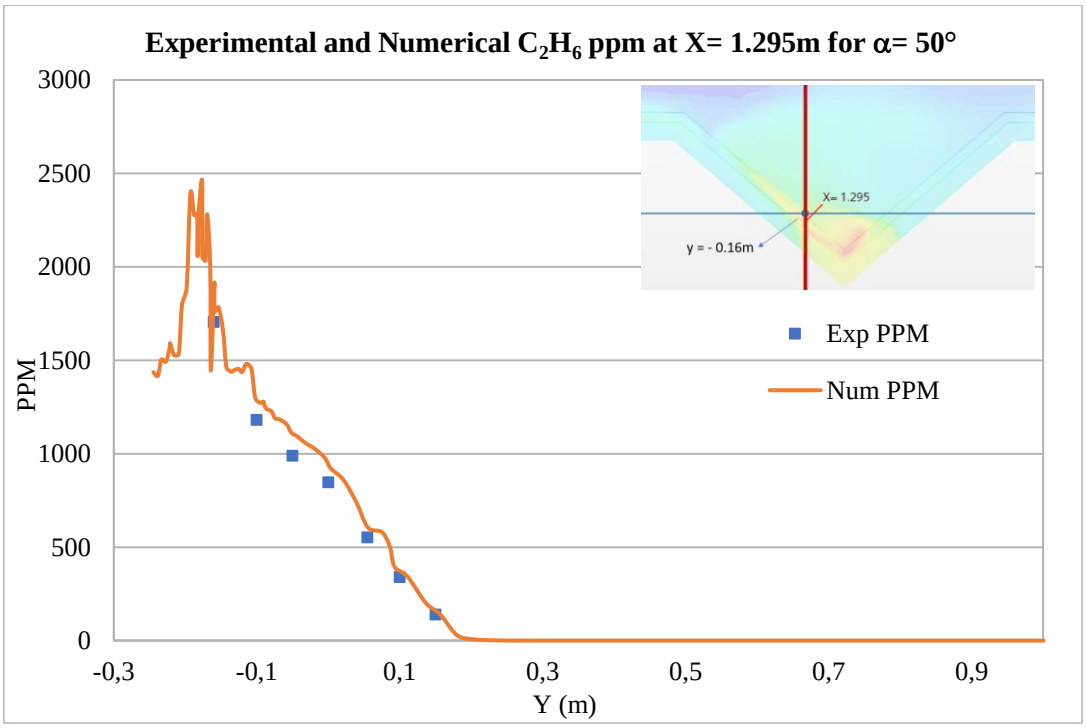

(b). *The best experimental measurements were at height = - 0.16m.

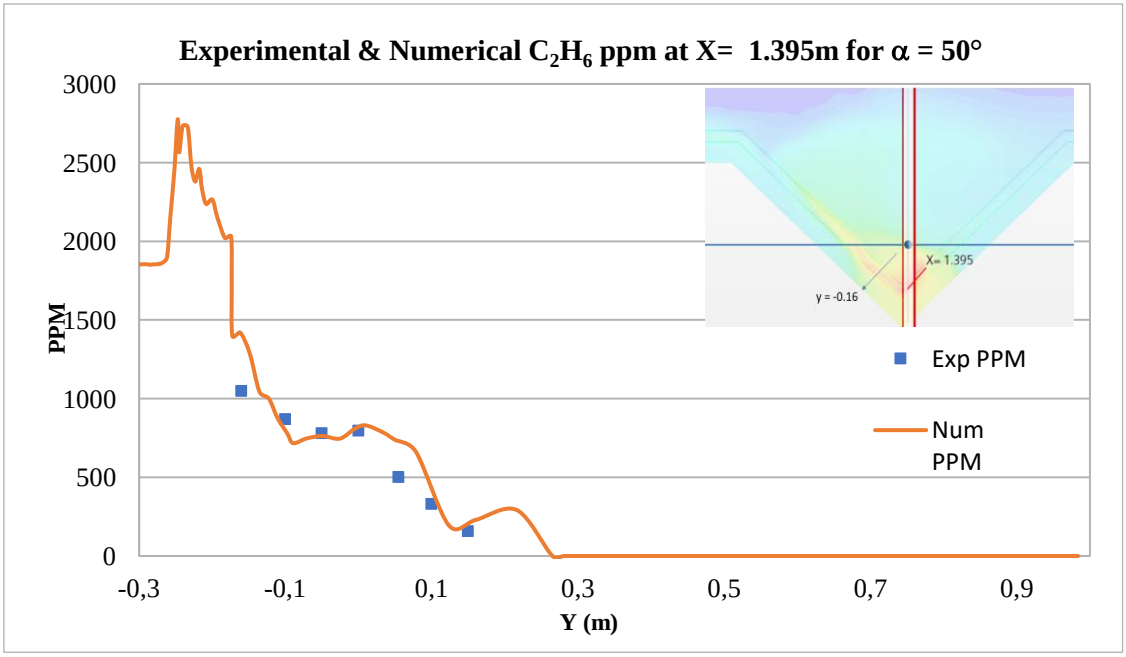

**(c). ***The best experimental measurements were at height = - 0.16m.

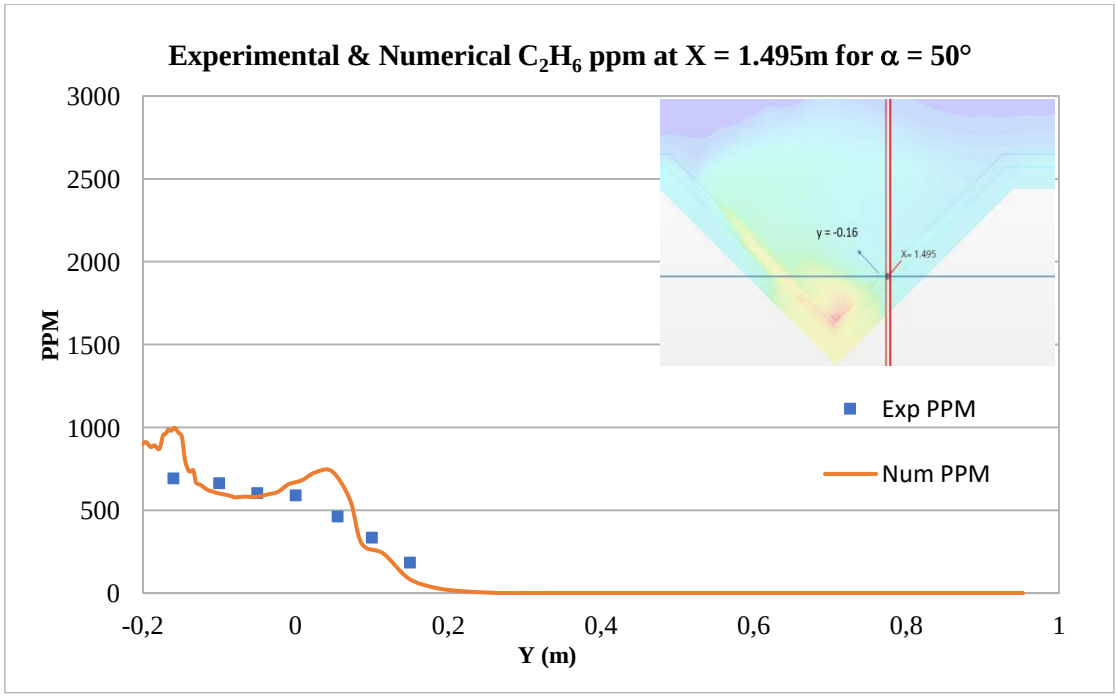

**(d). ***The best experimental measurements were at height = - 0.16m.

Figure II.16. The graphical plots of the experimental and numerical results of C_2H_6 spatial concentrations inside the valley of α = 50°. (a) X= 1.295, (b) X=1.392, and (c) X=1.495m.

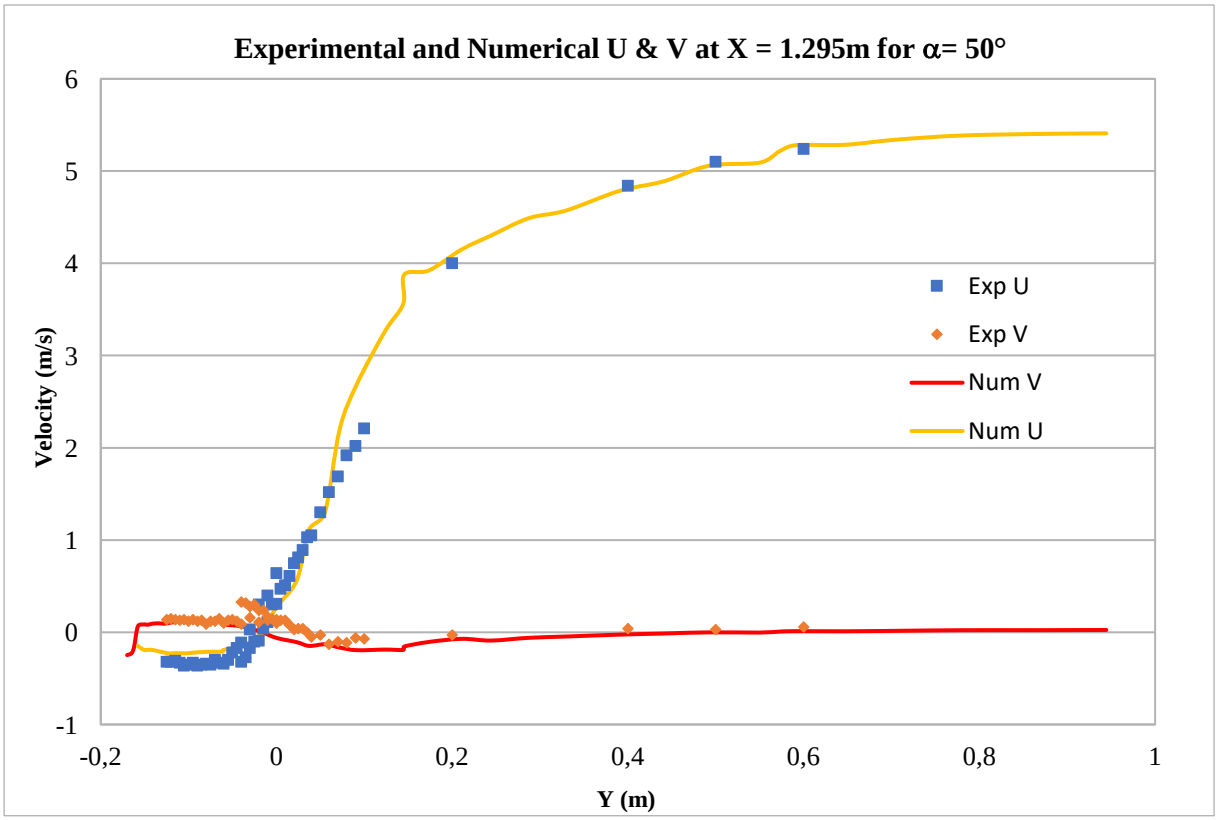
Experimental and Numerical U & V at X = 1.295m for α= 50°
Velocity (m/s)
Y (m)
Exp U
Exp V
Num V
Num U
6
5
4
3
2
1
0
-1
-0,2
0
0,2
0,4
0,6
0,8
1

(a)

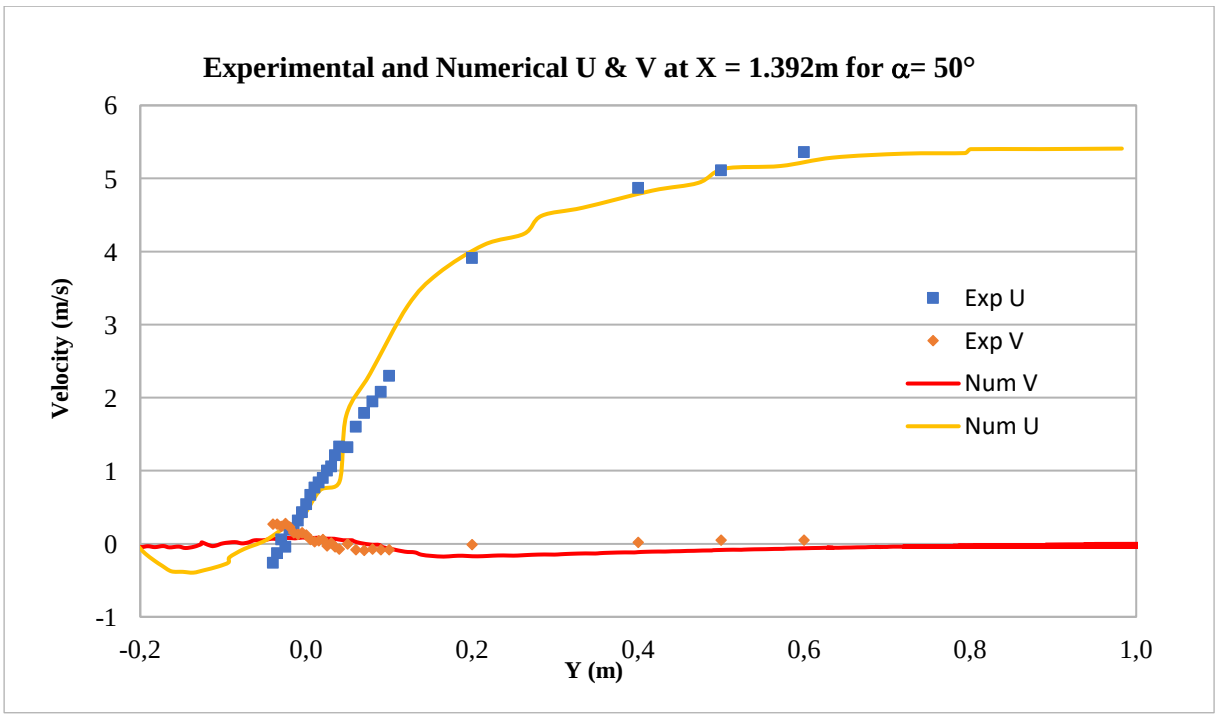
Experimental and Numerical U & V at X = 1.392m for α= 50°
Velocity (m/s)
Y (m)
Exp U
Exp V
Num V
Num U
6
5
4
3
2
1
0
-1
-0,2
0,0
0,2
0,4
0,6
0,8
1,0

(b)

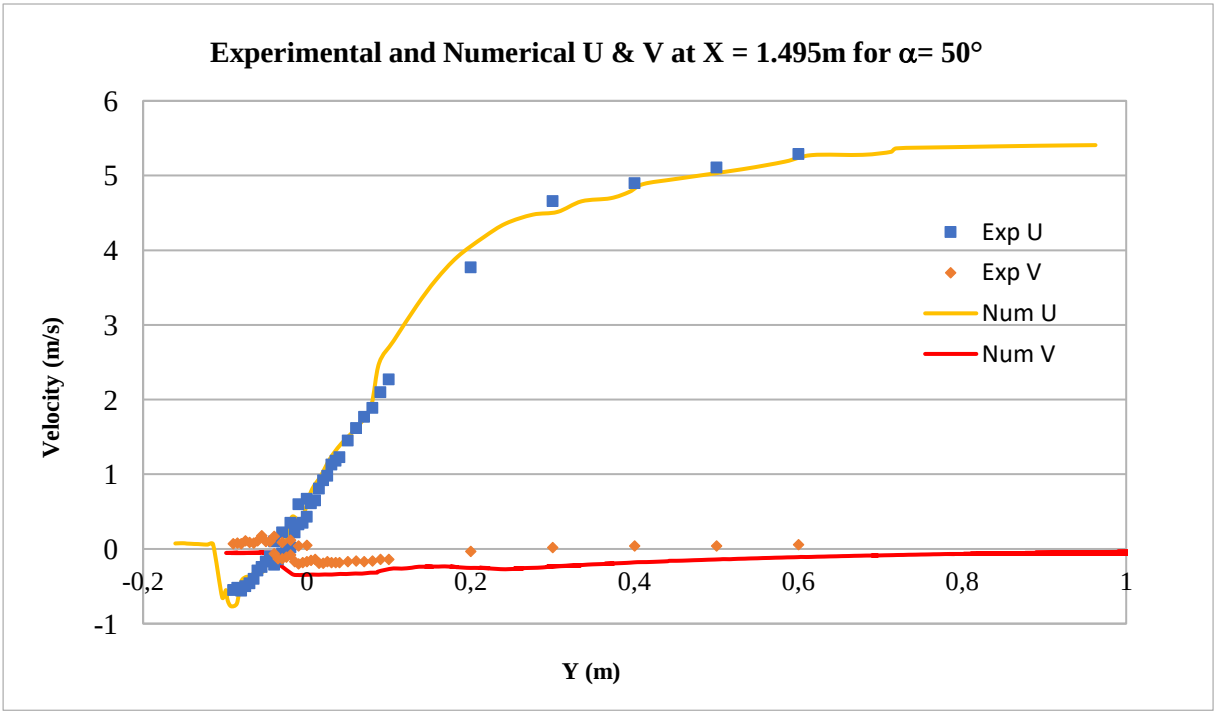

(c)

Figure II.17. The graphical plots of the experimental and numerical horizontal and vertical velocities (U & V) inside the valley of α = 50°. (a) X= 1.295, (b) X= 1.392, and (c) X= 1.495m.

4.3.1.2 α = 80°

In the valley of α = 80° there was no detachment of the boundary layer because no abrupt change has occurred in the fluid (air) velocity at the tip of the valley. However, a slight recirculation has occurred at the center of the valley explained by the negative velocity values in the graphical plots of Figure II.20, at X= 1.382 & 1.492m. Such recirculation may be the cause of visible ethane concentration (~ 1500 ppm) on the lee side of the valley (Figure II.18).

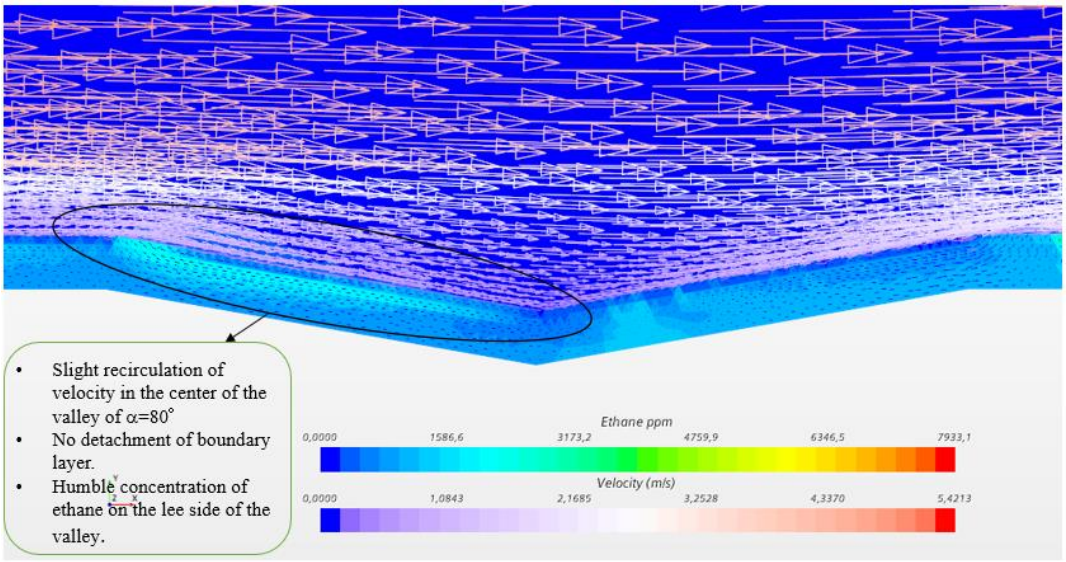

Figure II.18. Scalar scene showing slight recirculation of velocity vectors and ethane (C_2H_6) concentrations in the valley for α = 80°.

The graphical plots below show the matching experimental and numerical profiles of the velocity and ethane concentrations at the three plane sections created at three different distances along the x-axis i.e. X= 1.382, 1.492, and 1.582m on the lee side, center, and wind side of the $\alpha = 80°$ valley, respectively. C_2H_6 concentrations in the $\alpha= 80°$ valley are less important than those in $\alpha= 50°$ and are almost uniformly distributed across the valley zones (with ppm ranging from 500 to 1000 ppm) (Figure II.19) indicating better dispersion mechanisms compared to $\alpha= 50°$. C_2H_6 concentrations in the valley were almost 2 times the concentrations in the flat region of the forest prior to the valley.

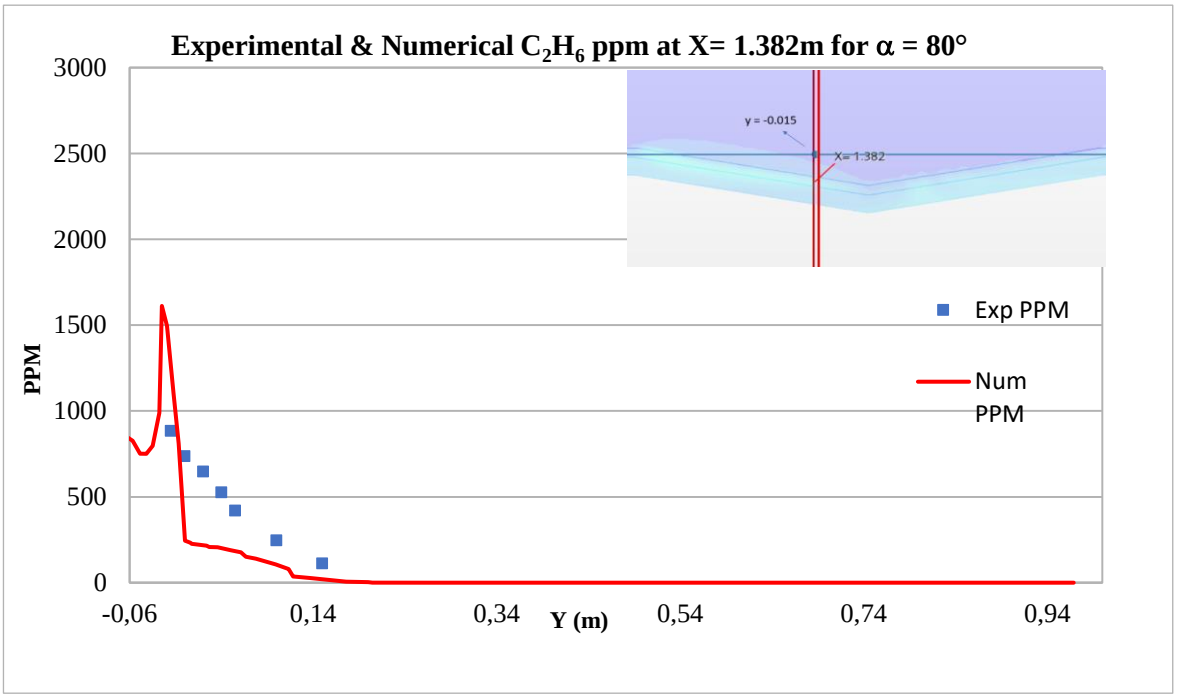

(a)

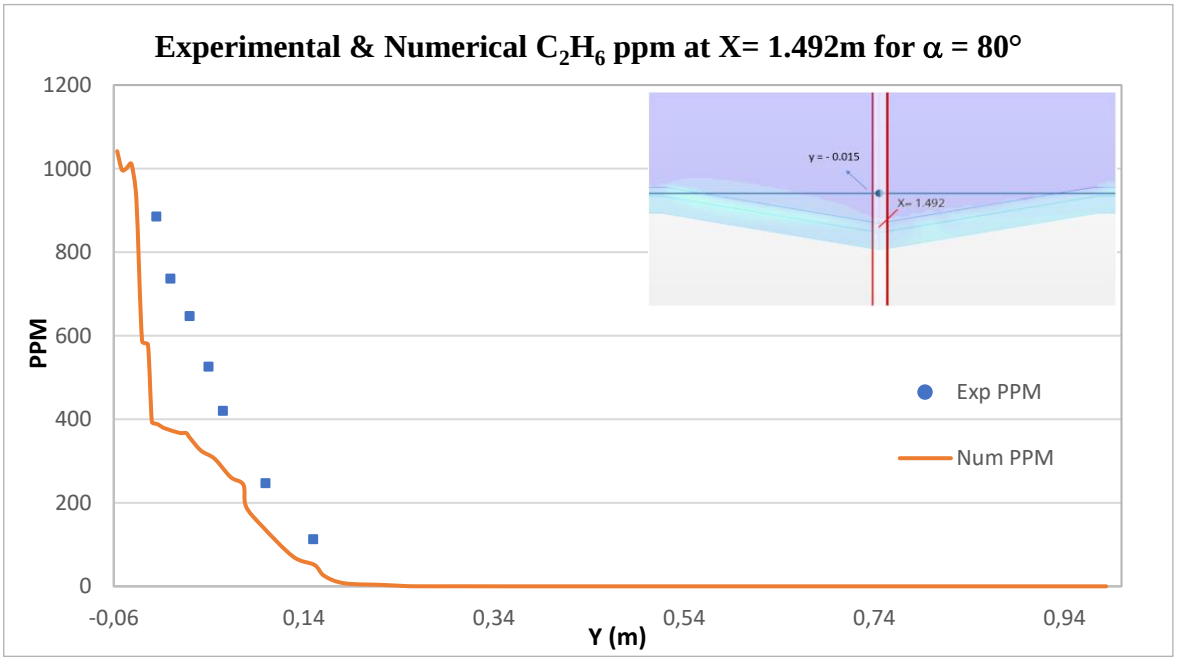

(b)

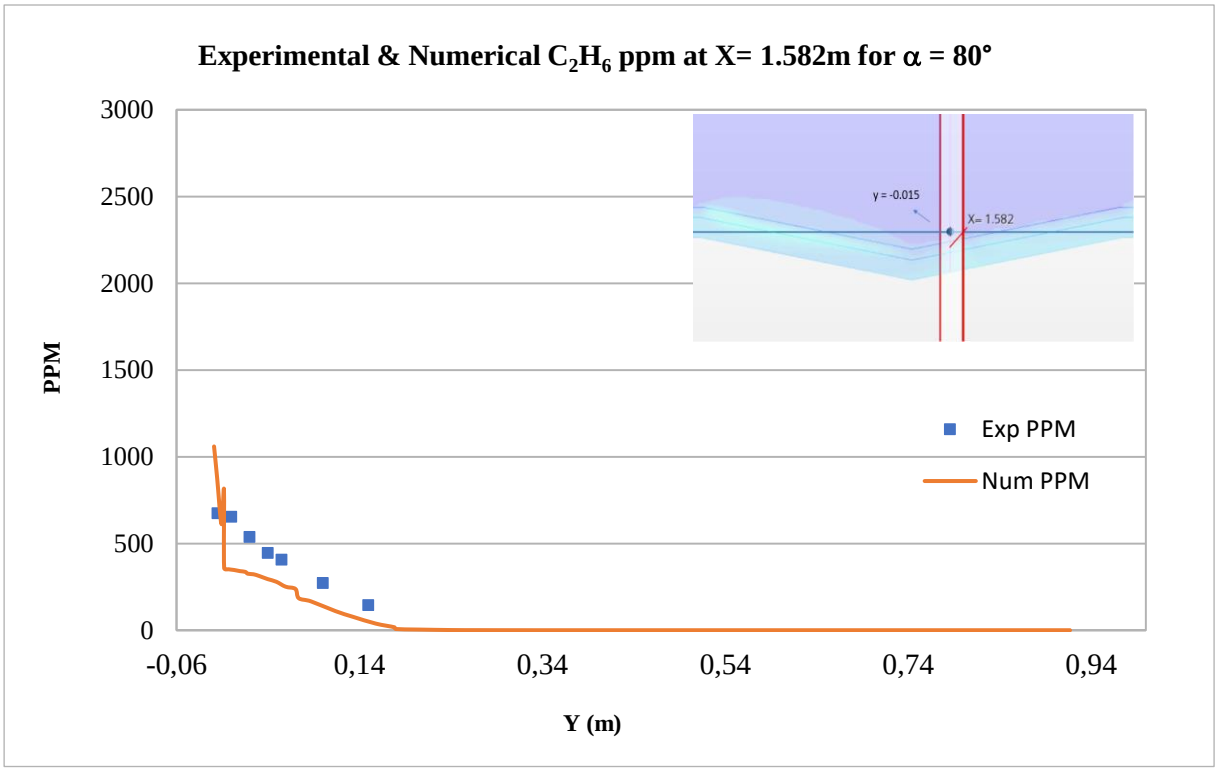

(c)

Figure II.19. The graphical plots of the experimental and numerical results of C_2H_6 spatial concentrations inside the valley of α = 80°. (a) X= 1.382, (b) X= 1.492, and (c) X= 1.582m. The best experimental measurements were at height of -0.015m.

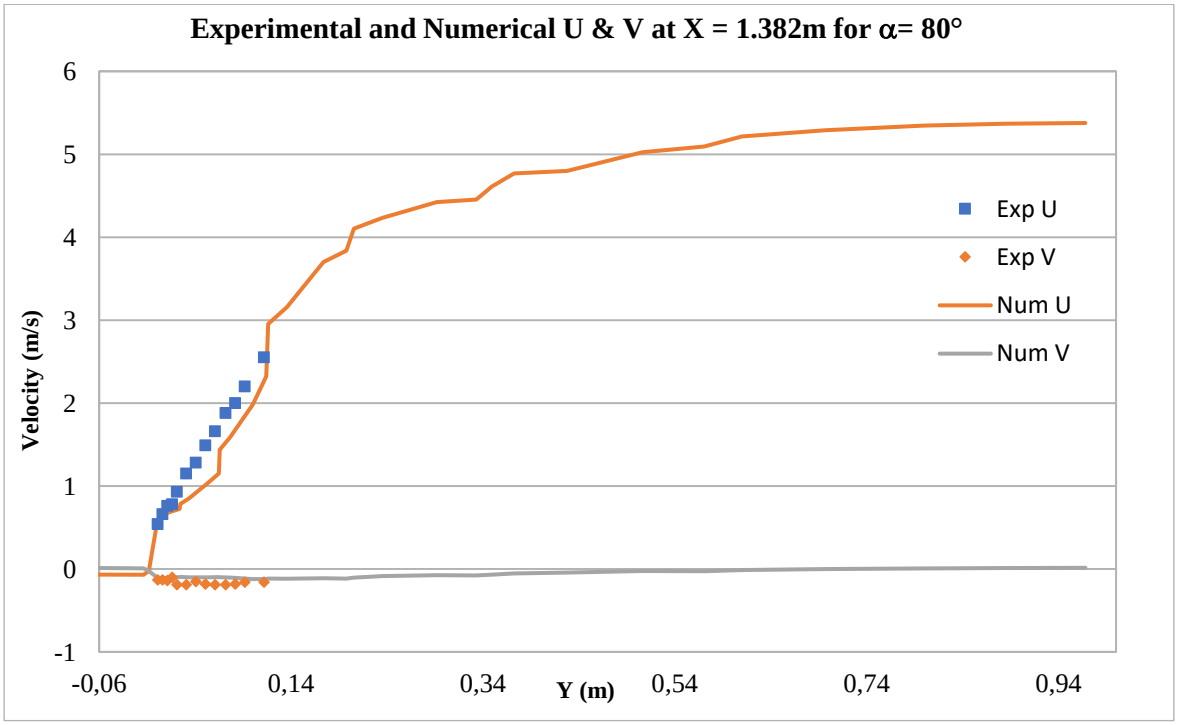

(a)

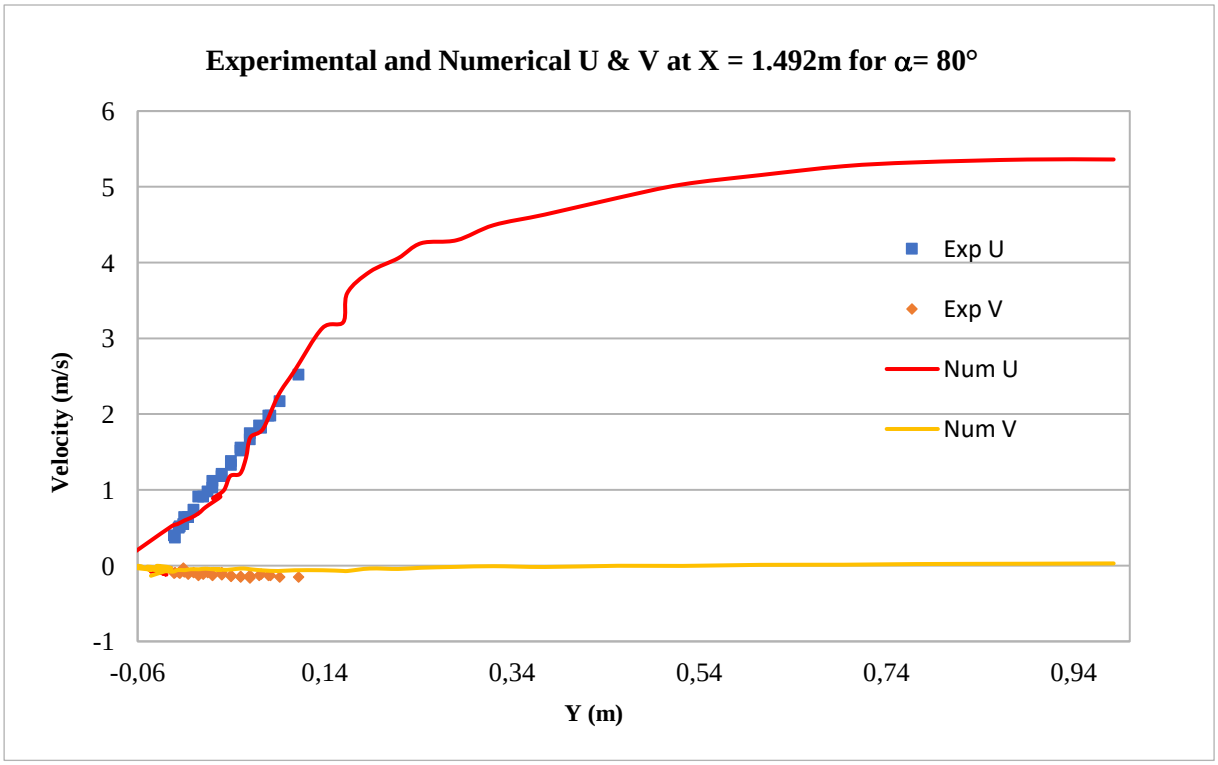

(b)

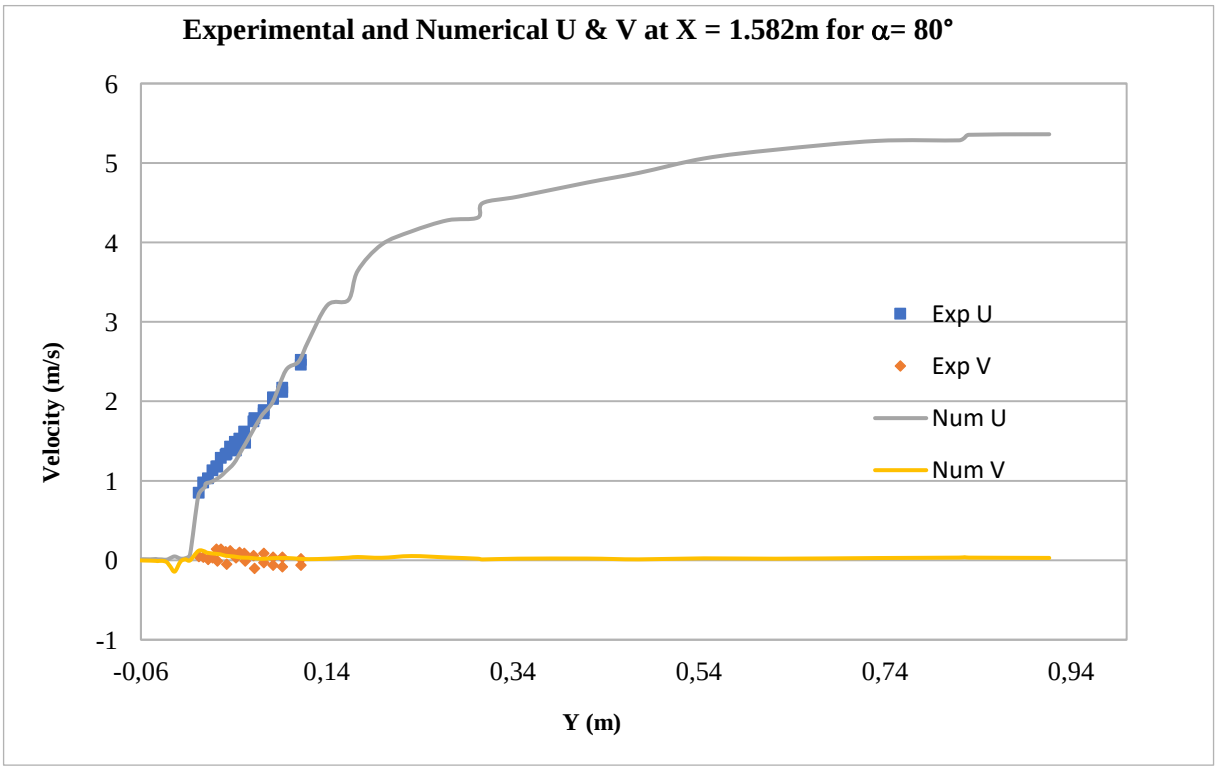

(c)

Figure II.20 The graphical plots of the experimental and numerical results of horizontal and vertical velocity (U & V) inside the valley of α = 80°. (a) X= 1.382, (b) X= 1.492, and (c) X= 1.582m.

4.4 Discussion and Analysis

Ethane density is similar to air therefore, its accumulation inside the valley can only be affected by airflow which is governed by the pressure gradients that develop against the porosity of the forest and the steepness of the valley (α). The two angles of the valley studied do not necessarily provide us a threshold of α at which the accumulations may result in a flashover phenomenon however, it is possible to conclude that valleys with sharper angles increase turbulence effects with appearance of air recirculation that favor accumulations. As STARCCM+ succeeded to reproduce the experimental results it is interesting to improve the model in order to investigate more the dispersion of the diverse VOCs emitted in a wildfire in an unsteady manner. Indeed, smoke plumes formed from vegetation in wildfires carry a wide range of VOCs (*cf. Table I.14 & I.15*). Unlike ethane, BVOCs and VOCs have densities heavier than air and with the help of the heavy particulate matter present in the plume which create a settling factor, they tend to migrate with wind at ground levels to nearby canyons forming gas pockets. Plumes containing particulates of mean diameters substantially exceeding 20 microns will have a settling component (Casal 2008). The empirical approach is that firefighters have linked strong VOC odors to eruptive fire behaviors in canyons however, the scientific approach will be to simulate numerically the emissions of the VOCs and examine their accumulations in canyons at the moment the fire front approaches the tip of the valley. If these accumulations laid within their flammability limits the risk of a flashover becomes more probable. Since our preliminary tests with ethane concluded that the concentrations will be more important for the valley of $\alpha = 50°$, it is reasonable to continue running the simulations for this particular angle, the model can be later developed to include other valley geometries and configure an angle threshold.

5 Numerical Model Improvement

5.1 Fire Modeling

In literature, fire modeling is treated with physical models that depend on the mechanisms of heat transfer to predict fire behavior (Albini 1985, Santoni and Balbi 1998), and on empirical models which do not distinguish between the heat transfer mechanisms and rely only on the principle of conservation of energy applied on a unit volume of the fuel bed ahead of the fire front (Rothermel 1972, Albini 1976). The leeward air velocity (in x-direction) in our simulations is 6 $m.s^{-1}$ therefore the vertical momentum created by the buoyant hot gases which are emitted from vegetation can be neglected, and we can for now study the dispersion of these gases under the effect of their own densities excluding the effects of fire thermal stresses. This hypothesis is supported by the work of Cai & Chow (2012) who studied the effect of wind on the dispersion of the smoke plume from a heptane pool fire under the effect of horizontal crosswind (x-axis direction) with different velocities ranging from 0 to 2.5 m. s^{-1} at atmospheric conditions. They concluded that with increasing wind velocity and consequently turbulence, the smoke plume tilted in the lateral direction (x-axis direction) carrying along the gases and particles closer to ground surface (Figure II.21). Therefore, the concentrations of gases in the fire plume are inversely proportional to wind velocities as they tend to leave the plume and concentrate closer to the ground surface. With a 6m. s^{-1} wind speed as the one used in our simulations, the plume tilt angle will tend to increase more and consequently, the densities of the gases will play an important role in their settlement regardless of the vertical momentum caused by the thermal effects. As a result, we will be using a dispersion model that does not

account for the fire thermal effects on the gaseous distribution inside the forest and the valley but rather on the densities of the various emitted gases in a wildfire.

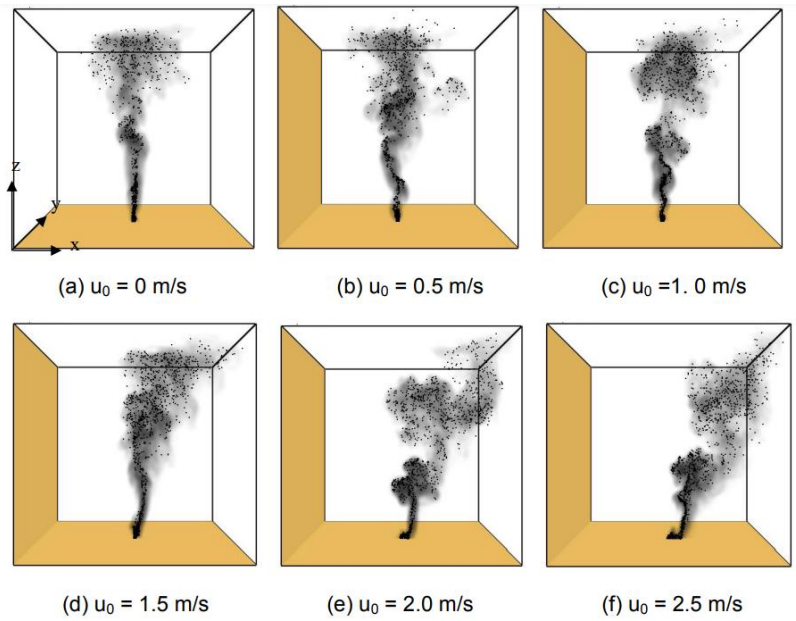

Figure II.21. Smoke and particle dispersion in lateral direction (x-axis) with different horizontal wind velocities from 0 to 2.5 m. s^{-1}, (Cai & Chow 2012).

5.2 Methodology

The presumable mixture of gases emitted from the vegetation in the forest model in a wildfire is computed by solving the set of the density-weighted conservation equations. In order to model the VOC emissions and investigate their concentrations inside the valley of $\alpha = 50°$ in our simulations, the following methodology is followed:

1. A reliable source from literature is chosen, containing data about VOC emission rates quantified as emission factors (EF) in g. kg^{-1} dry weight (dw) burnt from a documented wildfire that hit a finite inhomogeneous forest. Forests structures with similar porosity that end in developing similar wind profiles result in similar VOC distribution percentages.
2. The source contains information to predict the documented wildfire behavior (intensity, ROS, flame structure, flaming zone depth, residence time, etc.…). Such information includes the description of the fuel consumed by the wildfire (type, fuel load, moisture content, age, fire history…etc.), the atmospheric conditions that dominated during the wildfire, the global address of the wildland where the wildfire occurred (longitude and latitude), aspect, and the date of the fire.
3. Rothermel mathematical model is used to calculate the surface wildfire behavior parameters (Rothermel 1972).
4. Van Wagner criteria is used to predict the transition of a surface fire to a crown fire (Van Wagner 1977, 1989, 1993).
5. The final crown fire behavior parameters are re-calculated (reaction intensity, ROS, flaming zone depth, etc.).

6. The final fuel load (surface and crown) consumed in flaming in kg. m^{-2} is calculated and changed into kg. s^{-1} depending on the residence time and depth of the flaming zone.
7. VOC emission rates (kg. s^{-1}) in the flaming zone of the propagating fire front are scaled to fit the scale of our simulation (1/400).
8. Simulation with the same initial and boundary conditions is run and the different VOC concentrations are investigated inside the valley (α=50°) at the moment the fire-front reaches the tip of the valley.

5.3 Choice of Case Study: A Reliable Source for VOCs Emissions

5.3.1 VOC Emission Factors (EF): Prescribed Fires or Wildfires

Prescribed burning has been used to meet ecological wildland management objectives among of which interfere with wildfire management strategies to limit the risks of extreme wildfires i.e., reducing the hazardous fuel buildup (e.g. brush, shrubs and understory), implementing silviculture measures to replace the fire least resilient with the most resistant vegetation species, and more importantly to measure and identify the diverse range of the wildfire emissions with field preset measuring equipment. The first work publishing pyrogenic wildfire emissions, as emission factors (EF) for savanna and grasslands, tropical and extratropical forests (include boreal and temperate), and biofuel burning was by Andrea and Merlet 2001, which opened the doors to numerous studies collecting EFs from all types of forest fires including emissions from prescribed fires in MCR for temperate forests (Friedli et al. 2001, Akagi et al. 2013, Guérette et al. 2018), and boreal forests (Goode et al. 2000, Simpson et al. 2011). Later in 2019, the EFs from 370 publications were unified in Andrea (2019) (Table I.14). As prescribed fires are only allowed under controlled conditions (vegetation type, weather, burnt area, etc.) therefore, it is a controversy whether their emission rates can be extrapolated to real wildfires. However, the most important NMVOCs emitted in wildfires (Figure II.22), have shown more important EFs from prescribed fires (Akagi et al. 2013) when compared to wildfires (Evtyugina et al. 2013) (Table II.4) and laboratory scale fires (Yokelson et al. 2013).

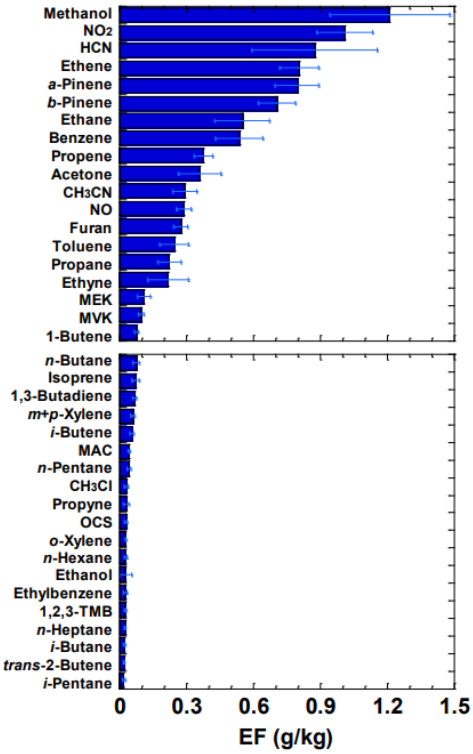

Figure II.22. EF of most important emissions (including major NMVOCs) from boreal forest fires (Simpson et al. 2011).

From the results in Table II.4, the controversy that prescribed fires underestimate the emission factors cannot be confirmed, even with similar values of MCE (~0.78 in Table II.4).

Table II.4. Emission Factors (EF) of the most common emitted compounds from wildfires and prescribed fires of mature pine trees and understory.

	EF (g. Kg^{-1})	
Compound	Wildfire [a]	Prescribed Fire [b]
α-pinene	0.2	6.2
β-pinene	0.027	0.6
Camphene	0.05	0.6
Benzene	0.6	1.7
Toluene	0.19	0.9
Isoprene	0.066	0.15
Styrene	0.005	0.101
n-Decane	0.006	0.05
p-Xylene	0.05	0.09
m-Xylene	0.05	0.5
o-Xylene	0.03	0.1

[a] (Evtyugina et al. 2013), [b] (Akagi et al. 2013)

Prescribed fire emissions especially those collected at ground level (opposite to airborne), represent critical values that can be used in studies for their role in fire propagation and extreme

fire events. Prescribed field fires have also shown more important emission percentages and diversity compared to lab scale fire emissions (Yokelson et al. 2013), (Figure II.23).

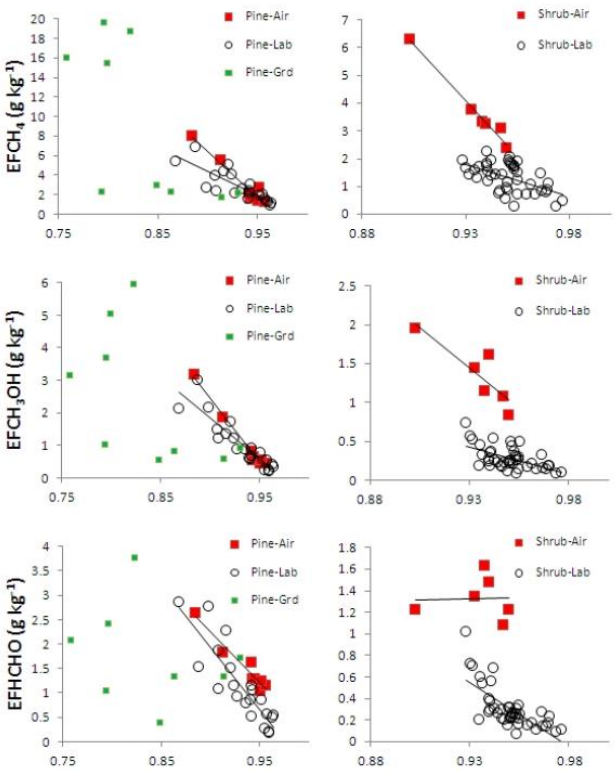

Figure II.23. Comparison of EF from the lab and the field fires for methane, methanol, and formaldehyde from pine understory (left column) and semiarid shrubland (right column). The "Grd" (green symbols) represent ground level concentrations, (Yokelson et al. 2013).

5.3.2 Prescribed Fire: Fort Jackson SC

There is still no way to rationalize the variability of EFs between prescribed and wildfires even for the same type of vegetation, except but to assume that emissions are not always vegetation type dependent but are also dependent on the environmental conditions at the event of the fire (temperature, season, wind speed, drought conditions, aspect, etc.). The advantages of using the emission factors of the trace gases from the prescribed fires in (Akagi et al. 2013) in our model are **two**:

First: their high ground-based percentages are a primary evidence that their heavy densities played a sedimentary role in their dispersion which is a trigger of flashover phenomena.

Second: the prescribed fires coordinates including the vegetation type, environmental and geological factors are all useful inputs used to estimate the fire behavior and implement it in our model.

Seven prescribed fires were investigated for their trace gases emissions in South Carolina (SC) which is an MCR dominated by a temperate climate (Akagi et al. 2013). Plume sampling was done on ground and airborne basis using land-based and airborne Fourier transform infrared spectrometer (AFTIR & LBFTIR), respectively (Akagi et al. 2013). Emission ratios calculated from ground-based smoke samples of the three Fort Jackson SC fires (Table II.5) were 3 times larger than those collected from airborne samples of the other four fires (Akagi et al. 2013).

One fire site in particular was the Fort Jackson SC that has not been subjected to fires (wild or prescribed) or to land management strategies for 50 years. Such undisturbed site has led to the development of mature pine stands with herbaceous and deciduous understory (oak, sparkleberry) and a thick litter layer of hardwood and pine needles (Akagi et al. 2013). The wind speed during the fire of Fort Jackson on October 30 was 3 to 5 m. s^{-1}, which is the closest to the wind velocity used in our simulations (6 $m.s^{-1}$). Besides, the relative humidity ratio (RH = 64%) was the lowest among the other fires (i.e., less fuel moisture content), and the age of the stand since it was last burned in 1957 (~ 55 years), is a guarantee of maturity of the longleaf pine forest for having developed a high CBD (to be defined) of 0.424 $kg.m^{-3}$ (Andreu et al. 2018) and a thick litter layer underneath thus reducing crown base height (CBH), all are factors to increase the crown fire risk. Longleaf pine needles are considered the most flammable among other pine species in the US, and the presence of common midstory pyrophytic species such as oak (e.g. *Q. laevis*), produces litter with similar flammability potential (Loudermilk et al. 2018). Such fuel model is typical for developing a high intensity surface fire which if transitioned to longleaf pine crown fire will form a precursor of extreme wildfire behaviors. The emission rates of 95 VOCs from the Fort Jackson SC fire (30 Oct), in addition to all the other documented fires are found in (Akagi et al. 2013).

Table II.5. Burning conditions for Four prescribed fires in Columbia SC. (Akagi et al. 2013)

Location	Date	Fuel Description	Temperature (° C)	%RH	Windspeed (m/s)	Atmospheric Conditions	Stand History	Latitude (° N)	Longtitude (° W)
Fort Jackson SC	30-oct	Mature Longleaf Pine	8 - 16 ° C	64	3 to 5	3.6 mm rain previous morning	Last Burned 1957	34° 1'29"	80° 52'16"
Fort Jackson SC	01-nov	Mature Longleaf Pine, sparkleberry	9 - 18 ° C	58 - 69	3 to 4	Mixing Height ~ 1650m. Clear Skies	Last Burned 1956	34° 0'15"	80° 52'37"
Fort Jackson SC	02-nov	Mature Longleaf, loblolly pine and oak	13 - 18 ° C	70	2 to 3	Mixing Height ~ 1160m. Clear Skies	Last Burned 2003	34° 5'4"	80° 46'23"
Georgetown SC	07-nov	SC Coastal grass understory	20 - 22 ° C	74	4 to 4.5	Sunny/Clear	Unknown	33° 12'9"	79° 24'6"

*The highlighted fire in brackets is the one used in our model.

The emission rates of this fire are the lowest compared to the other fires therefore, it will be interesting to investigate their dispersion and speculate their concentrations in the valley of our model as a part of future works to find a threshold of emission rates contributing to flashovers. However, our model cannot contain the 95 VOCs, therefore it will be restricted to the compounds of which their concentrations were critical in wildfire smoke plumes compared to their background air concentrations (Evtyugina et al. 2013) such as monoterpenes, benzene, toluene, methane, and others listed below in Table II.6.

Table II.6. Emission factors ($g.kg^{-1}$) of selected compounds to be implemented in numerical model. (Akagi et al. 2013)

Emitted VOCs	EF (g. kg^{-1})	Emitted VOCs	EF ($g.kg^{-1}$)
Methane	5.20	**Propane**	0.171
Acetylene	0.25	**Benzene**	0.268
Ethylene	0.89	**Toluene**	0.515
Propylene	0.40	**Monoterpenes**	5.05
Methanol	2.35	**1,3-Butadiene**	0.10
Ethane	0.503		

5.4 Surface Fire Behavior

After choosing a reliable source of wildfire emissions resulting from the flaming of the forest fuel, the EFs can now be implemented in our model. The next step will be to estimate the flame front parameters of the Fort Jackson SC fire, on Oct 30, that consumed the fuel model representing a mature longleaf pine forest. Even when the MCE of the fire is known, it is not easy to configure whether the emissions transported by the flame front are from the flaming or smoldering phase because both of the phases occur simultaneously and at close proximity. However, since ground sampling from smoke plumes is normally done at distances ranging from 10 to 150 meters downwind from flame front (Evtyugina et al. 2013, Akagi et al. 2013) therefore, when released, the emissions will be transported by the moving flaming front at a rate depending on the flaming zone parameters (fuel load/flaming zone area & residence time). Emission factors are measured in grams of VOC per kilogram of dry biomass burnt ($g.kg^{-1}$) while STARCCM+ uses the mass flow rate as kg. s^{-1} in the porous region. Therefore, it is essential to know the amount of fuel consumed by the fire front per second which consequently will result in an amount of emissions emitted per second. We have postulated that with a 6 $m.s^{-1}$ wind velocity the thermal stresses of the fire will have minimum effect on the dispersion of the VOC gases in our simulation, consequently we can use the Rothermel mathematical model to calculate the fire behavior parameters.

5.4.1 Rothermel Mathematical Model for Calculating Surface Fire Behavior

Rothermel mathematical model is quasi-empirical (steady state fire) and is the most comprehensive model since 1972. It was later developed by Albini (1976), and it is used to calculate the parameters of a surface wildfire such as: reaction intensity, forward rate of spread (ROS), burning time (residence time, τ), flame depth, etc. Any wildfire starts in the surface fuels (denoted up to 6ft or 183 cm above ground) and transition to crown fire (when applicable) if certain criteria are reached. Rothermel describes surface fire rate of spread (ROS) based on the principle of conservation of energy first proposed by (Frandsen 1971) between the flame and the fuel particles ahead of the flame front. Simply, the ROS as proposed by Rothermel is the ratio between the amount of heat provided by the flame-front and the amount received and absorbed till ignition by an effective volume of fuel ahead of it. The mathematical equations of the model require inputs of the fuel chemical and physical properties such as:

- w_0: Oven dry mass of the surface fuel per unit area (lb. ft^{-2}, $kg.m^{-2}$) of each size class of dead and live groups.
- σ: Surface area to volume ratio (ft^{-1}, m^{-1}). Fine fuels have bigger σ.
- Fuel depth (ft or m).
- ρ_f, Fuel particle density (lb. ft^{-3}, $kg.m^{-3}$).
- h, Heat content of fuel ($Btu.lb^{-1}$ or MJ. kg^{-1}).
- M_x: Moisture of extinction percentage (%), the live or dead fuel moisture content (LFMC or DFMC) at which a fuel sample will not ignite over a heating duration of 5mins.
- S_T: The non-combustible silica mineral (ash) content. High silica ash content makes the plant less flammable.
- S_e: Effective mineral content (silica free).

These descriptors are grouped under 11 fuel models which are called NFFL (Rothermel 1983), later updated by (Albini 1976) to 13 fuel models with two categories: dead and live, grouped into four general fuel community groups: 1) Grass and Grass-Dominated, 2) Chaparral and Shrub fields, 3) Timber Litter, and 4) Logging Slash (Table II.7).

Table II.7. Description of 13 fuel models used in Rothermel mathematical model. (Albini 1976)

		Dead Fuel						Live Fuel			
		Fine 1-h		Medium 10-h		Large 100-h					
		σ	w_0	σ	w_0	σ	w_0	σ	w_0		
Model Number	**Typical Fuel Complexes**	ft^{-1}	lb/ft^2	ft^{-1}	lb/ft^2	ft^{-1}	lb/ft^2	ft^{-1}	lb/ft^2	Fuel Depth ft	Moisture of Extinction $(M_x)_{dead}$ %
	Grass and Grass Dominated										
1	**Short Grass (1 ft)**	3500	0,034	-	-	-	-	-	-	1	0,12
2	**Timber (Grass and Understory)**	3000	0,092	109	0,05	30	0,23	1500	0,02	1	0,15
3	**Tall Grass (2.5 ft)**	1500	0,138	-	-	-	-	-	-	2,5	0,25
	Chaparral and Shrub fields										
4	**Chaparral (6 ft)**	2000	0,23	109	0,18	30	0,092	1500	0,23	6	0,2
5	**Brush (2 ft)**	2000	0,046	1091	0,02	-	-	1500	0,09	2	0,2
6	**Dormant Brush, Hardwood Slash**	1750	0,069	109	0,12	30	0,092	-	-	2,5	0,25
7	**Southern Rough**	1750	0,052	109	0,09	30	0,069	1550	0,02	2,5	0,4
	Timber Litter										
8	**Closed Timber Litter**	2000	0,069	109	0,05	30	0,115	-	-	0,2	0,3
9	**Hardwood litter**	2500	0,134	109	0,02	301	0,007	-	-	0,2	0,25
10	**Timber (litter and understory)**	2000	0,138	109	0,09	30	0,023	1500	0,092	1	0,25
	Logging Slash										
11	**Light Logging Slash**	1500	0,069	109	0,21	30	0,253	-	-	1	0,15
12	**Medium Logging Slash**	1500	0,184	109	0,64	30	0,759	-	-	2,3	0,2
13	**Heavy Logging Slash**	1500	0,322	109	1,06	30	1,288	-	-	3	0,25

σ: surface area to volume ratio ft^{-1}. w_0: fuel loading lb. ft^{-2}. For all models $S_t = 0.0555$, $S_e = 0.010$, h = 8000 $Btu.lb^{-1}$, $\rho_b = 32$ lb. ft^{-3}.

Dead fuel is stratified into 1 h, 10 h, and 100 h timelag classes or response times which are the time lengths required for a fuel particle to attain up to 63% of the change in its moisture content so it becomes in equilibrium with the ambient relative humidity (R.H.) (Anderson 1982). Stated differently, the moisture content of a fuel particle is related to its size, the bigger its size is the larger is the moisture content by which it will take a longer time to undergo a change in response

to an external variant. Therefore, the time lag class correlates well with the fuel particle size, as such (Albini 1976):

- 1-hr (excelsior): 0 to ¼ inch or 0 to 6.4 mm in diameter.
- 10-hr: ¼ to 1 inch or 0.6 to 2.5 cm in diameter.
- 100-hr: dead woody fuel 1 to 3 inches or 2.5 to 7.6 cm in diameter.

Only the fine size of the living fuel (< ¼ inch) is taken into consideration in fire propagation. Rothermel provides correction factors for the environmental factors (wind speeds and slopes) that affect the shape of the flame front (tilt angle) and consequently the rate at which the fuel particle ahead of the flame front loses its moisture content, releases its volatile and semi-volatile content, and ignites, Figure II.24.

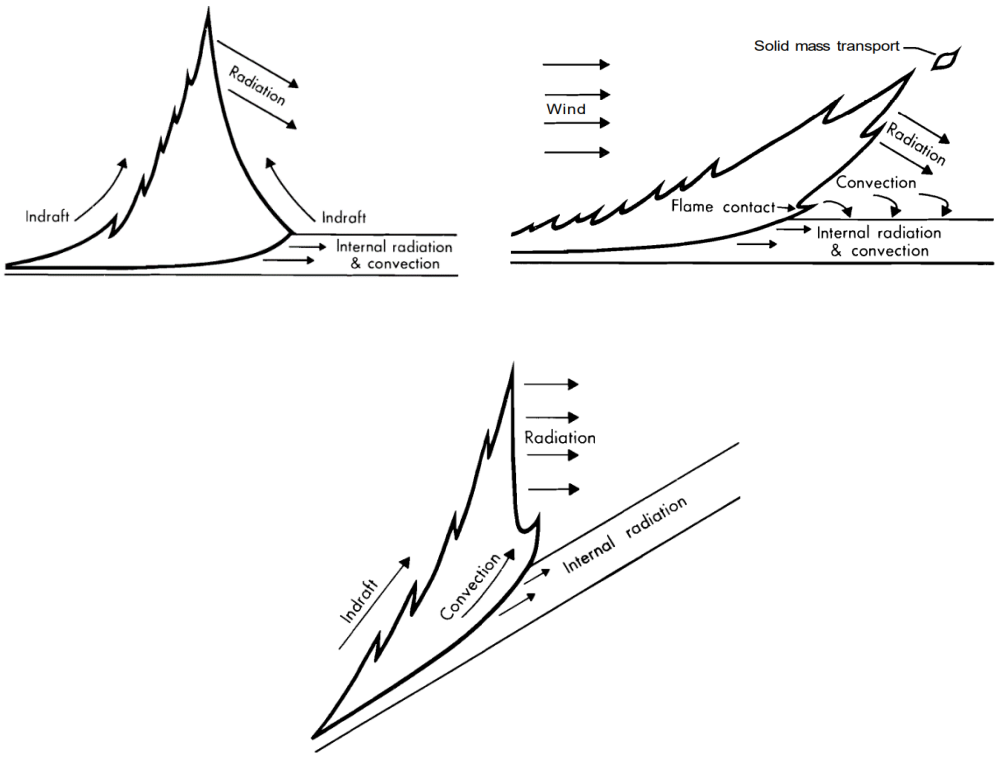

Figure II.24. Schematics of fire-front shape and thermal effects under different environmental and topographic conditions, (Rothermel 1972).

5.4.1.1 Selecting the Fuel Model

The descriptors of each fuel model are estimated to fit the circumstances leading to the most severe wildfires which threaten to pose fire control problems on firefighting teams. Anderson (1982) provides real photos of the 13 fuel models (NFFL) with their correlation to the 20 models of the American National Fire Danger Rating System (NFDRS). The plantation of Fort Jackson Sc fire was composed of mature Longleaf pine stands which were last burnt in the 1957, therefore it is expected to have a thick litter layer (timber and needles) under the pine stands. The typical fuel model which correlates with this this stand is Fuel Model 10 equivalent to

model G of the 1978 NFDRS. This fuel model is expected to provide a high intensity surface fire where crowning is highly probable, because there exists a large load of large size (3inches or 7.6 cm) dead fuels on the ground (Figure II.25). Now that the model is chosen we can proceed with computing the fire front parameters by implementing the inputs to Rothermel model. Anderson (1982), provides the output of this fuel model ROS = 0.04 m/s and flame length = 2.4 m for specified inputs of 8% of DFMC, 100% of live moisture content, and midflame height wind speed of 8 km.hr^{-1}. However, more severe wind and moisture content values will definitely lead to higher spread rates and flame length. Fire prediction models are very sensitive to the accuracy of their inputs, each fire coordinate produces different fire behavior outputs, therefore these inputs should be computed precisely given all the environmental conditions. There may exist more than one fuel model in a wildfire, given the case a fuel model occupies more than 20% of the area then the fire behavior must be weighed by the fraction of area occupied by each model (Anderson 1982).

Figure II.25. Photo representative of fuel model 10. (Anderson 1982)

5.4.1.2 Conception of Rothermel Mathematical Model

The rate of fire spread as presented by Rothermel is the ratio between a heat source and a heat sink (Equation II.16).

$$ROS = \frac{I_p}{Q_{ig}^*}, \text{ ft.min}^{-1} \qquad (II.16)$$

The numerator in Equation II.16 is called the propagating flux (I_p= f{I_R}), which is the amount of the heat released by the burning pyrolyzate gases per one-unit area of fuel bed and that is actually absorbed by the fuel in the bed ahead of the fire front. Stated differently, I_p is the rate of heat absorption by a unit area of a fuel bed per unit time (Albini 1978). The rate of heat released from the flame (burnt pyrolyzate gases) per unit area of flaming fuel bed is identified as reaction intensity (I_R, in Btu.ft^{-2}.min^{-1}), Equation II.17. It is equal to mass loss rate of the fuel which changed into pyrolyzate gases multiplied by the heat content of the fuel (h = 8000 Btu.lb^{-1} or 17 to 19 MJ. kg^{-1}) in Table II.7. It is suggested that the value of h is to be changed into h_v which represents the heat content of the pyrolyzate gases given that they represent 60% of the total combustion energy and they form about 90% of the total fuel mass (Sosutt 1982). However, we will stick with the value provided by Rothermel in his model, because he also

interpreted that the energy release rate of the fire front is from the burnt gases which result from the thermal decomposition of the solid fuels.

$$I_R = -\frac{dw}{dt} \times h, Btu.ft^{-1}.min^{-1} \qquad (II.17)$$

Where,

$\frac{dw}{dt}$, is the mass loss rate per unit area (Btu.ft^{-2}.min^{-1}).

h, is the heat content of the fuel (Btu.lb^{-1}).

However, not all of the heat released by the firefront is absorbed by the fuel bed but rather a portion of it. That is to say, the amount of heat released by the flame and is actually absorbed by the fuel bed is ξ (the propagating flux ratio), (Equation II.18). It is a fraction of the heat released (I_R) therefore, the no wind propagation flux becomes $I_p = \xi I_R$.

$$\xi = (192 + 0.2595\sigma)^{-1} exp\,[(0.792 + 0.681\,\sigma^{0.5}(\beta + 0.1)] \qquad (II.18)$$

Where, β is the packing ratio presented as the ratio of oven dry bulk density (ρ_b, lb. ft^{-1}) and fuel particle density (ρ_p, lb. ft^{-1}), $\beta = \frac{\rho_b}{\rho_p}$.

Wind and slope effects will increase the value of ξ, as the flame tilts towards the fuel bed due to wind or slope, convection and radiation effects will increase and therefore the amount of heat absorbed by the fulbed will certainly increase (Figure II.24). To account for this increase adjustment factors are added to ξ as ϕ_w and ϕ_s, i.e. the propagation flux $I_p = I_R\xi\,(1 + \phi_w + \phi_s)$.

The denominator in Equation II.16 represents the heat sink which is the heat absorbed by an effective unit volume of fuel ahead of the fire front to evaporate its moisture content, and raise its temperature from ambient to ignition. Rothermel specified a temperature range for the biomass ignition at 325°C with reference to Frandsen (1979) who claimed that only the surface of the fuel particle is required to be brought to ignition and not the whole particle volume uniformly however, Susott (1982), claimed that the temperature of ignition is reached whenever the pyrolysis process is complete i.e. 400°C. Sticking to Rothermel concept, the heat required to ignition per fuel unit mass has the following general form:

$$Q_{ig} = c_{pd}T_{ig} + M_f(c_{pw}T_B + V), Btu.lb^{-1} \qquad (II.19)$$

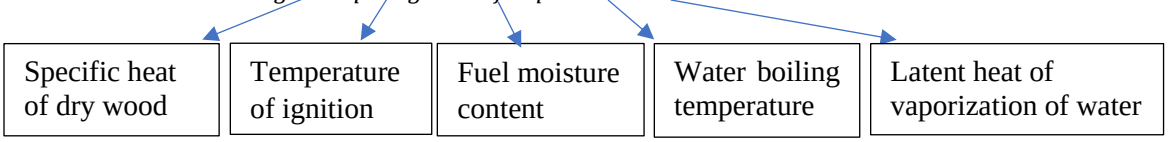

Substituting the values of each term and for T_{ig} = 325°C (Rothermel 1972, Albini 1978), gives:

$$Q_{ig} = 250 + 1116\,M_f \qquad (II.20)$$

According to Rothermel theory, only a fraction of the fuel particle is required to reach ignition which is a function of the surface area/volume ratio of the fuel particle (σ), denoted as (ε):

$$\varepsilon = exp\,(\tfrac{-138}{\sigma}) \qquad (II.21)$$

Therefore, the heat required to ignite a unit volume of fuel bed of effective bulk density (ρ_b, lb. ft^{-3}) is Q^*_{ig} calculated as:

$$Q^*_{ig} = \varepsilon \rho_b Q_{ig}\,, Btu.ft^{-3} \qquad (II.22)$$

These are the principle equation used by Rothermel to calculate the ROS of a fire with and without wind and slope effects. Rothermel does not provide any calculation of fireline intensity *I*, which is the rate of heat release per unit of length of fire front but rather it is calculated using I_R and it is called Byram fire line intensity *I* (Btu.ft^{-1}. s^{-1}) = I_RD. With the fireline intensity it will be possible to calculate the flame length $L\ (ft) = 0.45 \times (I)^{0.46}$. Other characteristics of the flame firefront are the flaming residence time (reaction zone time) $\tau_R(\text{min}) = \frac{384}{\bar{\sigma}\ (inch^{-1})}$, and the flaming zone depth (reaction zone depth) $D(ft) = \tau_R \times ROS(ft.min^{-1})$, Figure II.26.

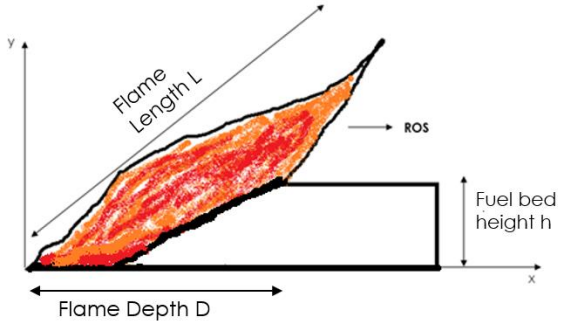

Figure II.26. Fire front flame parameters.

5.5 Case Study: Calculating Fort Jackson Sc (Oct. 30) Surface Fire Behavior

The prediction of the fire behavior through Rothermel model is illustrated in the workflow diagram (Figure II.27).

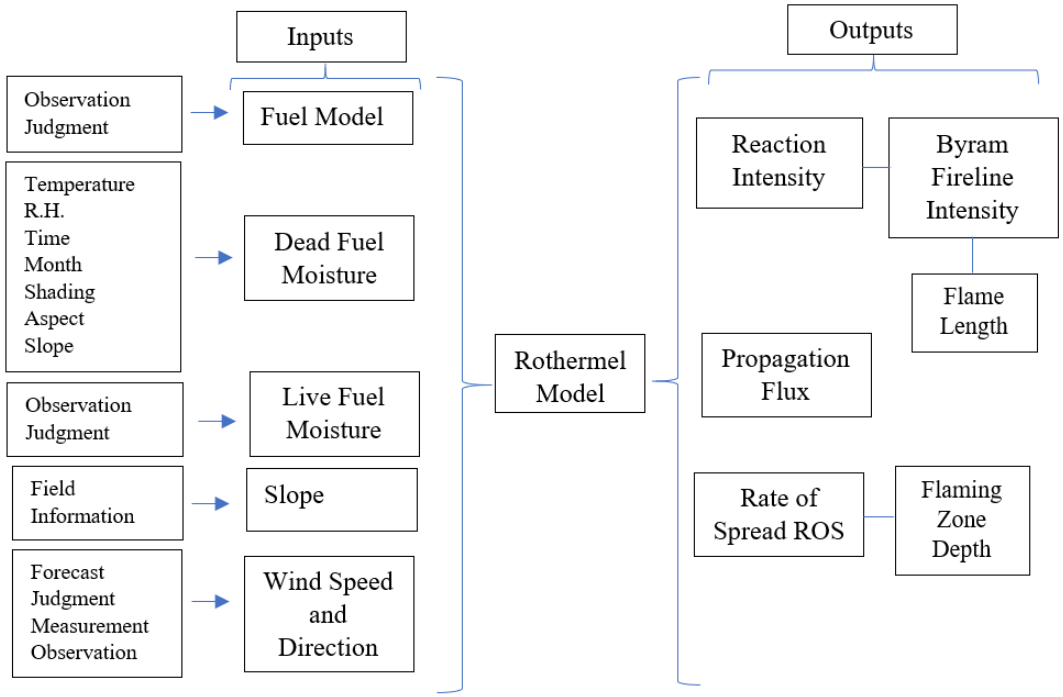

Figure II.27. Information flow of fire behavior prediction through Rothermel model.

5.5.1 Dead Fuel Moisture Content (DFMC)

Fire behavior is affected by four primary parameters, fuel, fuel moisture, wind, and slope. Fuel model 10 was selected in the previous section, the second parameter to be investigated is the fuel moisture content (dead, live, and moisture of extinction). The dead fuel moisture is verified from the exhibits and tables in (Rothermel 1983) using the values of several variables at the fire event such as temperature, humidity, date and time of the fire, shading, precipitation, etc. Those variables are defined in Table II.8 from (Akagi et al. 2013) and used with Exhibit II-2 in Rothermel (1983), to find a reference moisture content value of fine fuels (1-h) with the correction factors from tables in appendix AII.1. The moisture content of (10-h) and (100-h) are determined by adding 1 and 2% to the (1-h) value, respectively. The inputs and calculated outputs of moisture content with the correction factors according to Rothermel (1983) are listed in Table II.8. Living fuel (foliage) moisture content (LFMC) is required for fuel model 10, and it is estimated from the guidelines in Rothermel (1983) according to the stage of vegetative development between mature (100%) and dormant foliage (50%). However, since the Fort Jackson longleaf pine forest fire was sampled in the fall after a long prolonged dry summer, we will consider an LFMC of 70% from (Rothermel 1991).

Table II.8. Moisture content calculation of Fort Jackson SC Fire. (Rothermel 1983)

Daytime Fire	
Inputs	
Temperature °F	60
R.H. %	64
Shade	>50%
Aspect	North
Month	October
Time	12:00
Precipitation	3.6 mm rain from previous morning
Correction Factor[1] %	3
Precipitation Correction Factor[2] %	4
Outputs	
(1-h) Reference Moisture Content %	8
Corrected (1-h)	15
(10-h) Moisture Content %	16
(100-h) Moisture Content %	17
Living Fuel Moisture Content %	70%

[1]Correction factors based on time, aspect, elevation (Rothermel 1983).

[2] 3.6 mm rain from previous morning (Akagi et al. 2013)

5.5.2 Dead and Living Fuel Moisture of Extinction (M_X)

The moisture of extinction is determined experimentally and it is the upper limit of fuel moisture content at which the fire will no longer spread with a uniform flame front (Albini 1978, Rothermel 1983). Both dead and live fuels have upper moisture limits which are affected by several parameters related to the fuelbed type and geometry therefore, they are specific for each fuel model. It was found that the range of M_x for dead fuels is between 12 to13% for airy fuel beds (fine grasslands) and between 25 to 30% in pine litter beds (Albini 1978). However,

recent examinations have shown that a value of 30% is not appropriate, instead, a value of 40% is a better representation of the $(M_x)_{dead}$ of Mediterranean vegetation (Viegas et al. 2001, Yebra et al. 2007).

The M_x of living fuels has a lower limit of 30% (> $(M_x)_{dead}$) and is calculated according to the following formula:

$$(M_x)_{living} = 2.9 \times \left(\frac{1-\alpha}{\alpha}\right)\left[1 - \frac{10}{3}M_{f,dead}\right] - 0.226 \qquad (II.23)$$

Where, α is the ratio of the mass of living fine fuel load to the mass of the total fine fuel (dead and living) load and $M_{f,\,dead}$ is the moisture content of the dead fine fuel.

$$\alpha = \frac{w_0\ fine\ live\ fuel}{w_0\ total\ fine\ fuel} = \frac{0.092}{0.092 + 0.138} = 0.4 \qquad (II.24)$$

With $M_{f,\,dead} = 0.17$, which is the moisture content of dead fine fuel therefore the living fuel moisture of extinction is $M_{x\ living} = 1.6$.

5.5.3 Weighting Rothermel Equations by Fuel Particle Surface Area

Fuel particles with higher surface area to volume ratio (σ) that are categorized as fine fuels react the fastest to the fire because the rates of evaporation and the evolution of flammable gases are proportional to the surface area. However, it is not logical to assume that the fire behavior is mainly driven by fine fuels (< 1/8 inch) and they only should account in the prediction of the fire behavior but rather all fuel sizes should be weighted and considered. Rothermel introduced the concept of a unit fuel cell which is a representative differential volume (dv) containing all the components of the fuel bed complex (Figure II.28).

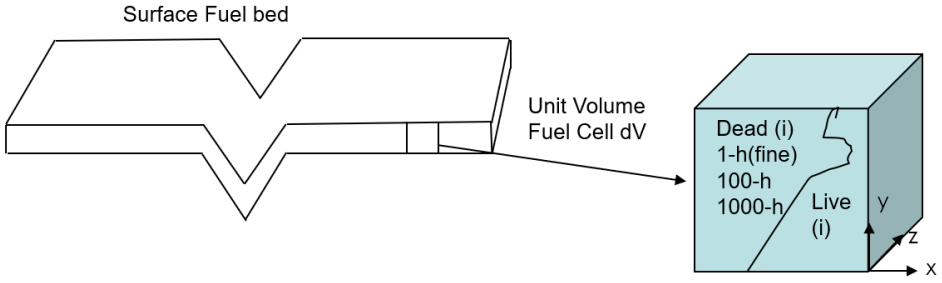

Figure II.28. Unit volume fuel cell weighted by fuel category (i) and size class (j).

The unit fuel cell contains two categories dead and live denoted by (i) and each category has a size class denoted by (j). Two weighting parameters should be used to average the inputs to the mathematical model:

- Ratio of surface area of j^{th} size class to total surface area of i^{th} category per unit fuel cell, $f_{ij} = \frac{\bar{A}_{ij}}{\bar{A}_i}$.
- Ratio of surface area of i^{th} category to total surface area per unit fuel cell, $f_i = \frac{\bar{A}_i}{A_T}$.

Where, $\bar{A}_{ij}$ is the mean total surface area per unit fuel cell of each size class within each category (Rothermel 1972, Scott and Reinhardt 2002).

$$\bar{A}_{ij} = \frac{(\bar{\sigma}_{ij})(\bar{w}_{0_{ij}})}{(\bar{\rho}_p)} \qquad (II.25)$$

Therefore, the inputs of the model (σ, w_0, & M_f) become in the form of matrices (2x3) for two categories (i) dead and live where each category includes the 3 size classes (j) (1-h, 10-h, & 100-h).

$$\begin{pmatrix} \bar{\sigma}_{11} & \bar{\sigma}_{12} & \bar{\sigma}_{13} \\ \bar{\sigma}_{21} & \bar{\sigma}_{22} & \bar{\sigma}_{23} \end{pmatrix} \begin{pmatrix} \bar{w}_{0,11} & \bar{w}_{0,12} & \bar{w}_{0,13} \\ \bar{w}_{0,21} & \bar{w}_{0,22} & \bar{w}_{0,23} \end{pmatrix} \begin{pmatrix} M_{f,11} & M_{f,12} & M_{f,13} \\ M_{f,21} & M_{f,22} & M_{f,23} \end{pmatrix}$$

And the moisture of extinction for each category, dead and live $(M_x)_i$ in (2x1) matrix;

$$\begin{pmatrix} M_{x,11} \\ M_{x,21} \end{pmatrix}$$

The input parameters to Rothermel model are weighted by the surface area and the modified equations are found from (58) to (84) in (Rothermel 1972).

5.5.4 Formulation of Rothermel Model with Python®

BEHAVE® and FARSITE® (Koo et al. 2005) are two operational models that use the Rothermel equations for fire spread behavior prediction. We've decided to model Rothermel (1972) mathematical formulations with the corrections made by Albini (1978) using Python®. The corrections brought by Albini included the combustible load (w_n) of the fuel which excludes the mineral content (S_T) from its dry weight (w_0). Albini updated the formula used by Rothermel to become $w_n = w_0 (1 - S_T)$ instead of $w_0/ (1+ S_T)$. Besides, the coefficient (A) used in the calculation of the reaction velocity (Γ') is also corrected by Albini to become $A = 133(\overline{\sigma}^{-0.7913})$.

5.5.5 Wind Adjustment Factor/Midflame wind speed

Wind exists in our model where the inlet velocity is 6 m.s^{-1} therefore, a wind correction factor (ϕ_w) should be added to the propagation flux i.e. $I_p = I_R \xi (1 + \phi_w)$, (*cf. Equation II.18*).

$$\phi_w = C U^B \left(\frac{\bar{\beta}}{\bar{\beta}_{op}}\right)^{-E} \qquad (II.26)$$

Where, U (ft. min^{-1}) is the mean wind speed at midflame height and the coefficients C, B and E are calculated using equations (82), (83), and (84) in Rothermel (1972), respectively. Most fires in surface fuels burn below 20ft height and since wind speed is slowed down by viscous effects near the surface therefore the 20ft wind speed must be adjusted to obtain a good fire prediction. The midflame height wind speed is calculated as a fraction of the wind speed at 20 ft (~ 6 m) above surface fuel bed of thickness 1 ft for fuel model 10 (Table II.7). The midflame windspeed is calculated by multiplying a wind adjustment factor to the 20 ft wind speed (Rothermel 1983). The wind adjustment factor depends on how much the surface fuels are sheltered by canopy stands and whether the stands are dense or open with less density. In our model, since the longleaf pine forest has not been burnt for more than 50 years the surface fuels are considered fully sheltered with dense mature pine stands (Ford et al. 2010) therefore, a wind adjustment factor of 0.1 should be used (Rothermel 1983). At a scale of (1/400), a 20 ft height above surface fuel bed (21ft from ground) equals 0.0525 ft (0.016 m). To obtain the mean

velocity at a height of 0.016m in the forest, a line probe section was drawn at y = 0.016 m (Figure II.29) and the mean velocity along the line probe was found to be 0.98 m. s^{-1} (192.9 ft. min^{-1}). As a result, the midflame wind speed (U) = 0.1 x 192.9 ft. min^{-1} = 19.29 ft. min^{-1} (5.82 m. min^{-1} or 0.2 mi. hr^{-1}). Fire behavior models which use Rothermel equations refer to midflame wind speed in $mi.hr^{-1}$.

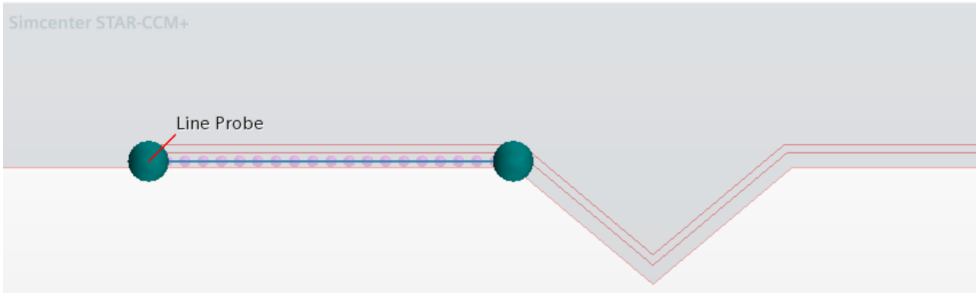

Figure II.29. Line section at y = 0.016m (21 ft height) to find the mean velocity value.

5.5.6 Inputs into Rothermel Model

The inputs of fuel model 10 into the Rothermel model written in Python are the matrices of the mean surface area to volume ratios and oven dry weight loadings from Table II.7, and the fuel moisture values and moistures of extinction (dead and live) in the order suggested in the previously (*cf. section* 5.5.3) as follows:

$$\begin{pmatrix} 2000. & 109. & 30. \\ 1500. & 0. & 0. \end{pmatrix} \quad \begin{pmatrix} 0.138 & 0.092 & 0.23 \\ 0.092 & 0. & 0. \end{pmatrix} \quad \begin{pmatrix} 0.15 & 0.16 & 0.17 \\ 0.70 & 0 & 0 \end{pmatrix}$$

$$\begin{pmatrix} 0.4 \\ 1.6 \end{pmatrix}$$

Utilizing these inputs to solve for surface fire behavior in the Rothermel code in Document.docx, gave us the surface fire behavior parameters of fuel model 10 (I_R & ROS) which enabled us to calculate the Byram fireline intensity (I), flaming zone depth (D), flame length (L) and residence time (τ) in Table II.9.

Table II.9. Fort Jackson SC (Oct 30) fire behavior parameters by Rothermel model.

Surface Fire Behavior Parameter	This Work
Reaction Intensity, IR **$Btu.ft^{-2}.min^{-1}$**	3709.5
Rate of Spread, ROS **$ft.min^{-1}$**	1.6
Byram Fireline Intensity, I **$Btu.ft^{-1}.min^{-1}$**	15579.9
Flaming Zone Depth, D **ft**	4.2
Residence Time, τ **min**	2.6
Flame Length, L **ft**	5,7

The selection of fuel models is based on the fuel stratum that best supports fire, this means that some fuel models will produce high intensities while others will produce higher rates of spread (Anderson 1982). Fuel model 10 produces higher fire reaction intensities and slower ROS unlike for example, fuel model 1 (short grass), which has less fine fuel loading (*cf. Table II.7*) that produces higher ROS and lower heat release rates per unit area (Andrews et al. 2011), (Table II.10). Given that the midflame speed in our model is as low as 0.2 mi. hr^{-1} due to porosity effects of the forest, the ROS for fuel model 10 in our work is slowed down by more than 9 folds compared to that of (Andrews et al. 2011), who calculated the ROS for a midflame speed of 5 mi. hr^{-1} and a slope of 10%. On the other hand, the Byram fireline intensity in our work for 15% DFMC was ~ 257 $Btu.ft^{-1}. s^{-1}$ compared to 344 $Btu.ft^{-1}. s^{-1}$ for DFMC of 5% (Table II.10). A 10% difference in moisture contents has led to a change of ~ 25% in the fireline intensity.

Table II.10. Fire behavior parameters of fuel models 1 &10. (Andrews et al. 2011)

Dead Fuel Moisture 5%, Live Fuel Moisture 100%, Midflame Wind speed 7 $mi.h^{-1}$

Fuel Model	ROS ft. min^{-1}	Heat Per Unit Area Btu. ft^{-2}	Fireline Intensity $Btu.ft^{-1}. s^{-1}$	Flame Length ft
1	215	92	333	6.5
10	15.5	1330	344	6.6

Now that the surface fire parameters are calculated we can proceed to verify if our surface fire will transition to a crown fire to consume the pine stands of the canopy or not. If the transition occurs, new fire behavior parameters (fireline intensity & ROS) will be calculated to proceed with implementing the moving firefront in the numerical model. Semiempirical models based on the Van Wagner criteria (Van Wagner 1977) for passive and active crown fire initiation and spread, are still the most robust models used to assess the surface fire transition to a crown fire. From the array of these models we depended on the work of Scott and Reinhardt (Scott and Reinhardt 2001) who linked the concepts of Rothermel surface and crown fire spread models (Rothermel 1972 & 1992) and Van Wagner crown fire criteria to assess the transition of a surface fire into a crown fire. In their method, Scott and Reinhardt used critical characteristics related to surface and crown fuels, site characteristics and environmental conditions in order calculate quantitively the potential of a surface fire transition to a crown fire. They also presented information about calculating the weight of the fuel consumed by the passing flame front. Scott and Reinhardt used SI units in their work while Rothermel used the US customary units, conversion tables between the two are available in appendix AII.2.

5.6 Transition of Surface Fire to a Crown Fire

As indicated in chapter one, crown fires are passive, active, and independent. The Fort Jackson SC fire has developed into an active crown fire that has consumed the longleaf pine canopy. An active fire will propagate among the crowns of the canopy with increased ROS and fire intensity than that of the surface fire, causing fire control difficulties. However, an active crown fire will not sustain without the heat coming out of the surface fire responsible for drying the crown fuels and bringing them to ignition. Therefore, it is important first to collect from literature the canopy fuel characteristics of our forest model (longleaf pines, mid, and understory) such as:

canopy bulk density (CBD), canopy base height (CBH), stand height (SH), and foliar moisture content (dead & live). Note that the terminology used to refer to these characteristics is a canopy which is a characteristic of the whole pine stand and not only a single tree which is called a crown. (Parresol 2007) and (Andreu et al. 2018) provide estimates of the median, mean, minimum, and maximum values of CBD, SH, and CBH for various coastal plain forests including the Longleaf pine with information about the date at which the stand was last burnt. The date a stand was last burnt affects the accumulations of ground litter and the maturity of the crown stands, thus CBD and CBH which interfere with crown fire potential. For example, more litter accumulations will decrease CBH and increase the crown fire potential. Midstory vegetation should not be neglected while accounting for the CBH of the crowns for example a mature longleaf pine overstory includes midstory of various deciduous oak species (O'Brien et al. 2016). The top height of midstory should not be neglected because it will definitely decrease CBH (Luo et al. 2018). Below are the summarized definitions of CBD, CBH and SH as defined in (Scott and Reinhardt 2001).

5.6.1 Canopy bulk density (CBD), (lb. ft^{-3} or kg. m^{-3})

CBD represents the amount of the canopy fuels that will be consumed in the active crown fire which includes but not restricted to fine foliage, lichen, moss and live and dead branches of thickness lower than ¼ inch (< 6mm). Some studies assume that 65% of canopy fuel (< ¼ inch) with foliar moisture content of 100% are consumed in the active crown fire flame front, however there is a risk that this percentage is overestimated (Scott and Reinhardt 2001). Canopy bulk density can be estimated from other parameters such as the leaf area index (LAI) which quantifies the amount of leaf material in the canopy (Fang and Liang 2014). CBD values are very hard to predict, for example maximum values of CBD for longleaf pine were found to be 0.424 $kg.m^{-3}$ (Andreu et al. 2018) and 0.123 $kg.m^{-3}$ (Parresol 2007) for similarly aged forests (~ 33 years). The minimum threshold of CBD for the onset of a crown fire, ranges from 0.05 to 0.10 Kg. m^{-3} (Beverly et al. 2020). The forest in our model is, a CBD of 0.123 kg. m^{-3} would be an underestimated CBD for a 55 years old longleaf forest (Ford et al. 2010) therefore, we will depend on the value estimated by (Andreu et al. 2018) as 0.424 kg. m^{-3}.

5.6.2 Canopy base height (CBH), (ft or m)

CBH is the most important canopy fuel characteristic because it identifies the minimum height above ground where sufficient canopy fuel exists to catch flames from the surface fire and propagate the fire vertically upwards. The minimum fuel load is still a controversy to define for CBH because there is no unified standard of it yet in literature. Information about the different definitions of CBH and minimum canopy fuel load in literature is presented in (Mitsopoulos and Dimitrakopoulos 2007). The mean values of CBH for longleaf pine were found 8.50 m in (Parresol 2007, Andreu et al. 2018). However, this CBH underestimates the presence of midstory vegetation therefore, a more realistic approach will be used to estimate CBH from CBD (0.424 $kg.m^{-3}$) and fuel model (FM10) according to the results of (Scott and Reinhardt 2001, Figure II.30), we attain CBH of ~ 1.6 m. This CBH is consistent with the findings of (Larry 2008) from the Native Tree Society (NTS), for a 60-80 years old longleaf pine forest.

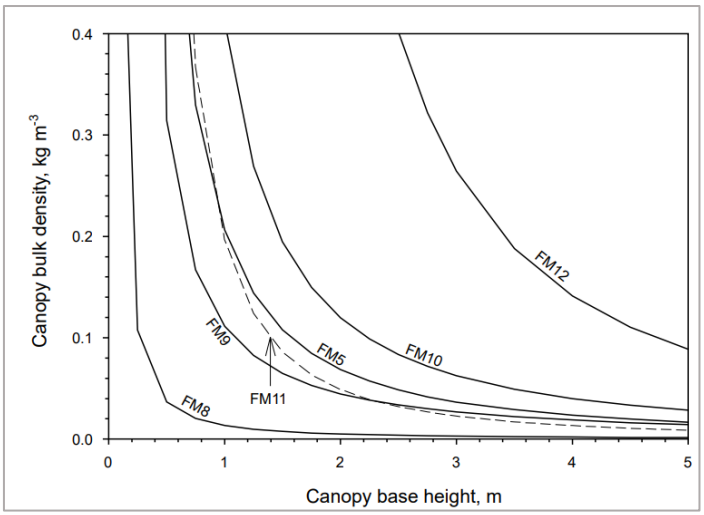

Figure II.30. Canopy bulk density (CBD) and base height (CBH) for an active crown fire behavior of different fuel models, (Scott and Reinhardt 2001).

5.6.3 Stand Height (SH), (ft or m)

SH is the average height from ground of the dominant tree layer. The maximum SH for longleaf pine were found at 28.5 m (Parresol 2007, and Andreu et al. 2018).

5.6.4 Foliar moisture content (FMC), (%)

FMC the effective foliar moisture content is affected by the percentages of the dead and live fuel in the crown. Lichen and dead fuels have the highest effect on modifying the value of the moisture content. Studies provided ranges for the live moisture content from 85% to 120% however, since the forest was subjected to a long dry hot summer (Akagi et al. 2013), the live fuel moisture content is estimated at 70% (Scott and Reinhardt 2001).

5.7 Crown Fire Initiation Criteria

The heat coming out of the surface fire flames is responsible for evaporating the moisture content of the crown fuels and bringing them to the ignition temperature. However, in order to transition to a crown fire, the surface fire behavior is required to overcome a critical intensity, I' ***initiation*** and a critical rate of spread, ROS' ***initiation***. According to Van Wagner, I' ***initiation*** depends on the crown base height CBH and foliar moisture content (FMC), (Equation II.27, SI units), (Scott and Reinhardt 2001).

$$I'_{initiation} = \left(\frac{CBH\ (460+25.9FMC}{100}\right)^{\frac{3}{2}}, KW.m^{-1} \qquad (II.27)$$

$$I'_{initiation} = \left(\frac{1.6\ \times (460 + 25.9 \times 70}{100}\right)^{\frac{3}{2}} = 219.32\ \ KW.m^{-1} \cong 63\ Btu.ft^{-1}.s^{-1}$$

$$I_{\textbf{surface fire}}\ (253\ \text{Btu. ft. s}^{-1}) > I'_{\textbf{initiation}}\ (63\ \text{Btu. ft}^{-1}\text{. s}^{-1})$$

The initiation rate of spread R' ***initiation*** depends on the surface fuel characteristics through the heat per unit area of the surface fire, HPA (Btu.ft^{-2}) = I_R (Btu.ft^{-2}.min^{-1}) × τ (min), with their values from Table II.9.

$$ROS'_{initiation} = \frac{60 \times I'_{initiaion}\ (Btu.ft^{-1}.s^{-1})}{HPA_{surface}\ (Btu.ft^{-2})}, ft.min^{-1} \qquad (II.28)$$

Therefore, for HPA **surface** = 3709.5 Btu.ft^{-1}.min^{-1} × 2.6 min = 9644.7 Btu. ft^{-2}.

$$ROS'_{initiation} = \frac{60\ \times\ 63\ (Btu.ft^{-1}.s^{-1})}{9644.7\ (Btu.ft^{-2})} = 0{,}39\ ft.min^{-1}$$

ROS **surface fire** (1.6 ft. min^{-1}) > ROS' ***initiation*** (0.39 ft^{-1}. min^{-1})

If the surface fire line intensity (I) and rate of spread (ROS **surface fire**) are greater than initiation intensity (I' ***initiation***) and initiation ROS (ROS' ***initiation***) i.e. (I > I' **initiation**) and (ROS > ROS' ***initiation***), respectively, a crown fire is likely to occur.

5.7.1 Active Crown Fire ROS

In (Scott and Reinhardt 2001) who depended on the crown fire model by Rothermel (1991), an active crown fire that consumes the crowns of a canopy will have an after active crown fire ROS (R **active**) that is equal 3.34 times the surface fire ROS of fuel model 10 (Rothermel 1972). However, in calculating the ROS of FM 10 the midflame speed should be evaluated at a rate of 40% of the 20ft open wind speed and not according to the adjustment factor we found as 0.1 (*cf. Section* 5.5.5). Therefore, the average ROS after the active crown fire (R **active**) is calculated as in Equation II.29.

$$ROS_{active}\ =\ 3.34 \times (\ ROS_{FM10})_{40\%\ of\ U_{20ft}} \qquad (II.29)$$

The foliar moisture content (FMC) will have an effect on (*R* **active**) and is accounted for in a term that is called the theoretical fuel moisture effect (FME) first defined by (Wagner 1977) and used by (Scott and Reinhardt 2001) and is calculated as:

$$FME\ =\ \left(\frac{(1.5-0.00275\ FMC)^4}{460\ +(25.9FMC)}\right) \qquad (II.30)$$

FME should be normalized before being used in Equation II.30 with a normal value FME$_0$ i.e., $\frac{FME}{FME_0}$ falls in the range between 0.714 and 1.31 depending on the value of FMC. The value of FME$_0$ is considered equal to 0.0007383 for an FMC of 100% (Scott and Reinhardt 2001) and 0.000516 for 70%. Therefore, Equation II.29 now becomes:

$$R_{\ active}\ =\ 3.34\ \left(\frac{FME}{FME_0}\right)(\ ROS_{FM10})_{@40\%\ of\ U_{20ft}} \qquad (II.31)$$

For FMC = 70%

$$FME\ =\ \left(\frac{(1.5-(0.00275\times 70))^4}{460\ +(25.9\times 70)}\right) = 0.00128$$

Therefore, $\frac{FME}{FME_0} \cong 1.7$

Running Rothermel model for a midflame windspeed equals to 40% of the wind speed at 20 ft, produces a rate of spread ($ROS_{FM10\ @\ 40\%\ of\ U20\ ft}$) equals to 17.05 ft.min^{-1}.

$$ROS_{active}\ =\ 3.34\ \times 1.7 \times 17.05\ ft.min^{-1} = 96.86 ft.min^{-1} \cong 29.5\ m.min^{-1}$$

According to Van Wagner (Wagner 1977) an active crown fire will be sustained in the canopy as long as the fire consumes a minimum crown fuel mass flow rate, S (3 kg. m^{-2}. min^{-1}), and attains an after-crown ROS (R **active**) that exceeds a critical ROS' **active**. S depends on CBD as follows,

$$S = ROS_{active} \times CBD, kg.m^{-2}.min^{-1} \qquad (II.32)$$

To check if the active crown fire developed in the longleaf pine forest will be sustained we will compare the mass flow rate consumed with the fire.

$$S = 29.5 \times 0.424 = 12.508\, kg.m^{-2}.min^{-1}$$

The critical ROS' **active** depends on the minimum fuel mass flow rate S and the CBD as follows,

$$ROS'_{active} = \frac{3.0}{CBD} = 7\, min.m^{-1} < ROS_{active}$$

ROS **active** > ROS' **active** therefore, Fort Jackson Sc fire has developed to an active crown fire that has consumed the longleaf crowns as documented by Akagi et al. (2013).

5.7.2 Final ROS and Fireline Intensity (Surface + Crown)

The uncertainty of a surface fire transition to an active crown fire strongly depends whether wind profiles are stable or not. A Torching index (TI) and a Crowning Index (CI) are used to correlate the 20ft windspeed to the crown fire initiation and active spread, respectively (Scott and Reinhardt 2001). They are related to CBH and CBD such that, a stand with higher CBH and CBD will require stronger winds to initiate crowning fire in it (TI > CI). However, in our work, wind profiles are stable and an active crown fire has actually developed in the longleaf pine forest therefore, we are only interested in finding its final behavior (surface + crown) according to the work of (Scott and Reinhardt 2001).

5.7.3 The Final ROS

$$ROS_{final} = ROS_{surface} + CFB(ROS_{active} - ROS_{surface}) \qquad (II.33)$$

Where CFB is the crown fraction burned which depends on the fuel characteristics and ranges from zero for surface fire to one for active crown fire. Several formulations are proposed for CFB in (Scott and Reinhardt 2001) however, for simplification purposes, we will consider a CFB = 1 in our model for a fully active crown fire leading to ROS **final** = ROS **active**.

$$ROS_{final} = ROS_{active} = 29.5\, m.min^{-1}$$

5.7.4 The final Fireline Intensity

The final fireline intensity (I ***final*** , Btu.ft^{-1}.s^{-1} or kW.m^{-1}), developed by the active crown fire depends on the heat per unit area of the surface fire (HPA **surface**, Btu.ft^{-2} or kJ.m^{-2}), the available canopy fuel load (W **canopy**, lb. ft^{-2} or kg.m^{-2}) and the heat content of the canopy fuel (H **canopy**, Btu.lb^{-1} or kJ.kg^{-1}), and the final rate of spread (R **final**, ft. min^{-1} or m.min^{-1}).

$$I_{final} = \frac{\left(HPA_{surface} + (W_{canopy}H_{canopy}CFB)\right)ROS_{final}}{60} \qquad (II.34)$$

HPA **surface** = 110583 kJ.m^{-2} (*cf. section* 5.7), H **canopy** = 18622 kJ.kg^{-1}, CFB = 1, ROS**final** = 29.5 m.min^{-1}, and W **canopy** (sum of crown loads) is obtained by multiplying the CBD to the difference

between stand height (SH) and CBH, (Andrews et al. 2011, Parresol 2007) i.e., W $_{canopy}$ = CBD (kg.m^{-3}) × (SH – CBH)(m) = 0.424 × (28.5 – 1.6) = 15.6 kg.m^{-2}.

$$I_{final} = \frac{(110583 + (15.6 \times 18622 \times 1)) \times 29.5}{60} = 197201\ KW.m^{-1}$$

I $_{final}$ is higher than usual since the W $_{canopy}$ is considered large considering a CBH of 1.6m. Of course, a higher CBH such as the maximum value identified in (Andreu et al. 2018) as 16.76m will lead to smaller value of I $_{final}$ but again we will be underestimating the midstory in the mature unburned longleaf forest.

5.7.5 Final Fuel Consumption by Flaming Zone

The fuel available to be consumed by the fire flaming front as it travels a distance equivalent to the depth of one reaction zone (D) in a residence time (τ_R) is referred to as W_f, (Scott and Reinhardt 2011).

$$W_f = \frac{HPA_{canopy}}{H_{canopy}}, kg.m^{-2} \qquad (II.35)$$

Where $HPA_{canopy} = \frac{I_{final}}{ROS_{final}}, kJ.m^{-2}$, with ROS $_{final}$ is in m.s^{-1} gives an HPA $_{canopy}$ value of 401086 kJ.m^{-2}. Therefore, $W_f \cong 21.5\ kg.m^{-2}\ or\ \cong 4\ lb.ft^{-2}$.

5.7.6 Reaction Zone Parameters

The time required for the fire flame front to cross the reaction zone with depth (D, m) is the residence time (τ_R, min) i.e., $D = \tau_R \times ROS_{final}$.

$$D = 29.5\ m.min^{-1} \times 2.6\ \text{min} \cong 77\ m \qquad (II.36)$$

In an area of 1 x 77 m^2 there exists 1617 kg of fuel load to be burnt in a residence time (τ_R) of 2.6min.

The crown flame length can be calculated from the fireline intensity according to (Thomas 1963) who updated Rothermel equation of surface flame length to account for higher fireline intensities of crown fires (Andrews et al. 2011).

$$L = 0.2\ (I)^{\frac{2}{3}} = 0.2 \times (57010\ Btu.ft^{-1}.s^{-1})^{\frac{2}{3}} = 296\ ft \qquad (II.37)$$

6 Running the Improved Numerical Model

6.1 Extrapolation to the Forest Model Scale

Given that the forest model used in the preliminary experimental study had a width of 1m in the Z direction (400 m in reality), the firefront ignition line will have an area of 400m x D (Figure II.30). The total W_f available for consumption in a forest area D x 400m (77 x 400 m^2) along the ignition line (Figure II.31), becomes equal to 662200 kg for 2.6 min or 4244 kg. s^{-1}. On a scale of (1/400) W_f becomes equal to 10.61 kg. s^{-1} in a depth of 0.1925 m.

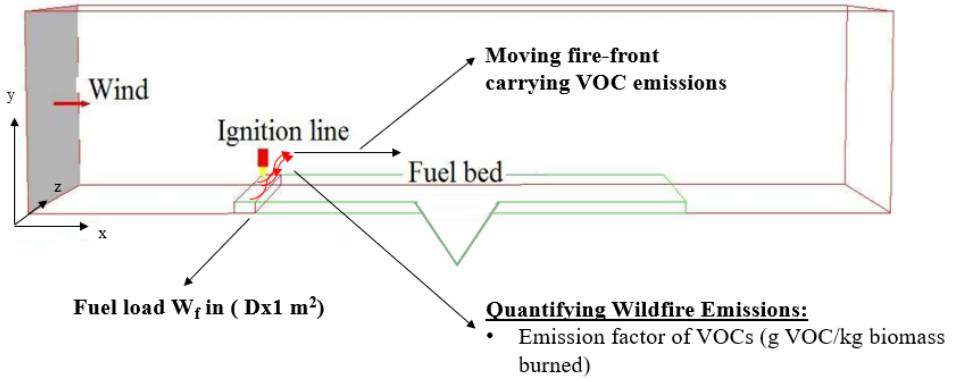

Figure II.31. Schematic of the moving firefront, consuming W_f in a reaction zone of depth D (0.033m) in the X-direction and of width (1m) along the Z-direction of the forest model.

6.1.1 VOC Emissions in the Reaction Zone of the Flamefront

In the above work we have succeeded to compute the flamefront parameters of the fire that had likely developed in the longleaf pine forest of Fort Jackson SC fire site which has the porosity characteristic of our forest model. We have also succeeded to compute the rate of the fuel load that will be consumed by the crown fire in the reaction zone (kg. s^{-1}) and accordingly we will implement the mass flow rate of the VOCs emitted from the burnt fuels in Table II.6 as EF (kg of VOC/kg of dry fuel burnt) with the scale of our forest model (1/400), Table II.11.

Table II.11. Mass flow rates of the VOCs emitted in the reaction zone of the fire flame-front.

Emitted VOCs	EF (g. kg^{-1})	Mass flow rate (kg. s^{-1})
Methane	5,2	0,0552
Acetylene	0,25	0,0027
Ethylene	0,89	0,0094
Propylene	0,4	0,0042
Methanol	2,35	0,0249
1,3-Butadiene	0,1	0,0011
Ethane	0,503	0,0053
Propane	0,171	0,0018
Benzene	0,268	0,0028
Toluene	0,515	0,0055
Monoterpenes	5,05	0,0536

6.1.2 Implementing the VOC Mass Flow Rates in the Forest Model with STARCCM+

STARCCM+ data base of chemical compounds is limited and doesn't include all the VOCs that are listed Table II.11. Therefore, the missing compounds (benzene, toluene, methanol, monoterpenes...) were added into the database and their chemical characteristics at STP conditions (density, dynamic viscosity, molecular weight, saturation and critical temperature and pressure…) were identified. Once the compounds are identified as gaseous components, STARCCM+ calculates the gaseous densities of the compounds at standard conditions. In order to avoid multiple data entries of the different monoterpenes and since α-pinene ($C_{10}H_{16}$) was the most abundant monoterpene identified in the airborne and ground-based measurements

$(2.97 \mp 3.24\ g.kg^{-1})$ (Akagi et al. 2013), it was used as a representative for all the monoterpene EF. Field functions are created for the mass flow rates of each compound using the if-else statement and the "And" logical operator to link the emissions to reaction zone time (τ_R = 2.6 mins or 156 sec) and depth (D= 0.1925m, forest model scale).

6.1.3 Field Function of VOCs EF in STARCCM+

The aim is to measure the concentrations (ppm) of the VOCs accumulating inside the valley of $\alpha = 50°$ at the three different positions (lee, center and wind side) as soon as the firefront reaches the tip of the valley. The compounds are emitted (in kg. s^{-1}) by the combusting vegetation in the reaction zone and carried by the propagating flamefront. The distance the flamefront has to cross in the horizontal forest zones (zones 1 & 2 in Figure II.3) is 1m (400 m in reality), before reaching the tip of the valley. The reaction zone depth is 0.1925m in model scale therefore, the 1m forest zone will be divided into 5 reaction zones each emitting for 2.6 mins the amounts of the different VOCs. In STARCCM+ a field function was created for the mass flow rate (kg. s^{-1}) of each compound in the 5 zones of a fixed depth and for a fixed reaction time. Such that, as the solution progresses the first zone emits from 0 to 2.6 mins (156 secs) then it stops emitting and the next zone starts emitting and so on so forth until the fire reaches the tip of the valley. At this moment, the simulation stops and the concentrations of the different compounds are evaluated inside the valley. If, however, the fire propagation continues inside the valley a different fire behavior should be calculated considering the slope effect (ϕ_s) when calculating the fire propagating flux (I_p) (Equation 80 in Rothermel 1972). An example of a field function specified for zones 1 & 2 in the porous region for ($C_{10}H_{16}$) is illustrated below (Figure II.32):

```
($Time <= 156 && $${Centroid}[0] < 0.192 ) ? 0.0536:
(
($Time > 156 && $Time <= 312 && $${Centroid}[0] > 0.192 && $${Centroid}[0]
<= 0.385)  ? 0.0536:
(
($Time > 312 && $Time <= 468 && $${Centroid}[0] > 0.385 && $${Centroid}[0]
<= 0.577)  ? 0.0536:
(
($Time > 468 && $Time <= 624 && $${Centroid}[0] > 0.577 && $${Centroid}[0]
<= 0.77)  ? 0.0536:
(
($Time > 624 && $Time <= 780 && $${Centroid}[0] > 0.77 && $${Centroid}[0]
<= 0.962)  ? 0.0536: 0
)
)
)
)
```

Figure II.32. Monoterpenes emissions represented as a field function in STARCCM+.

The same field function is defined for methane, methanol, ethane, benzene and toluene in order to know their concentrations inside the valley. These compounds were chosen given that they are among the most abundant VOCs emitted from forest fires (Figure II.22, Simpson et al. 2011) therefore, it will be important to configure their concentrations in narrow forest topographies and compare them to their flammability limits.

6.2 Results

The concentrations of the compounds chosen among the major VOCs emitted in forest fires, in the valley ($\alpha = 50°$) of our forest model were investigated. The compounds chosen are benzene, toluene, methane, ethane, methanol, and α-pinene. The spatial profiles of the accumulations inside the valley at the moment the fire reaches its tip (after 13 mins), are plotted using scalar scenes in STARCCM+ (Figure II.33). The graphical plots show the ppm concentration profiles of these VOCs distributed along the vertical axis (Y) at three different positions inside the valley at X = 1.295, 1.392, and 1.495m representing the lee side, center, and wind side of the valley, respectively, (Figure II.34).

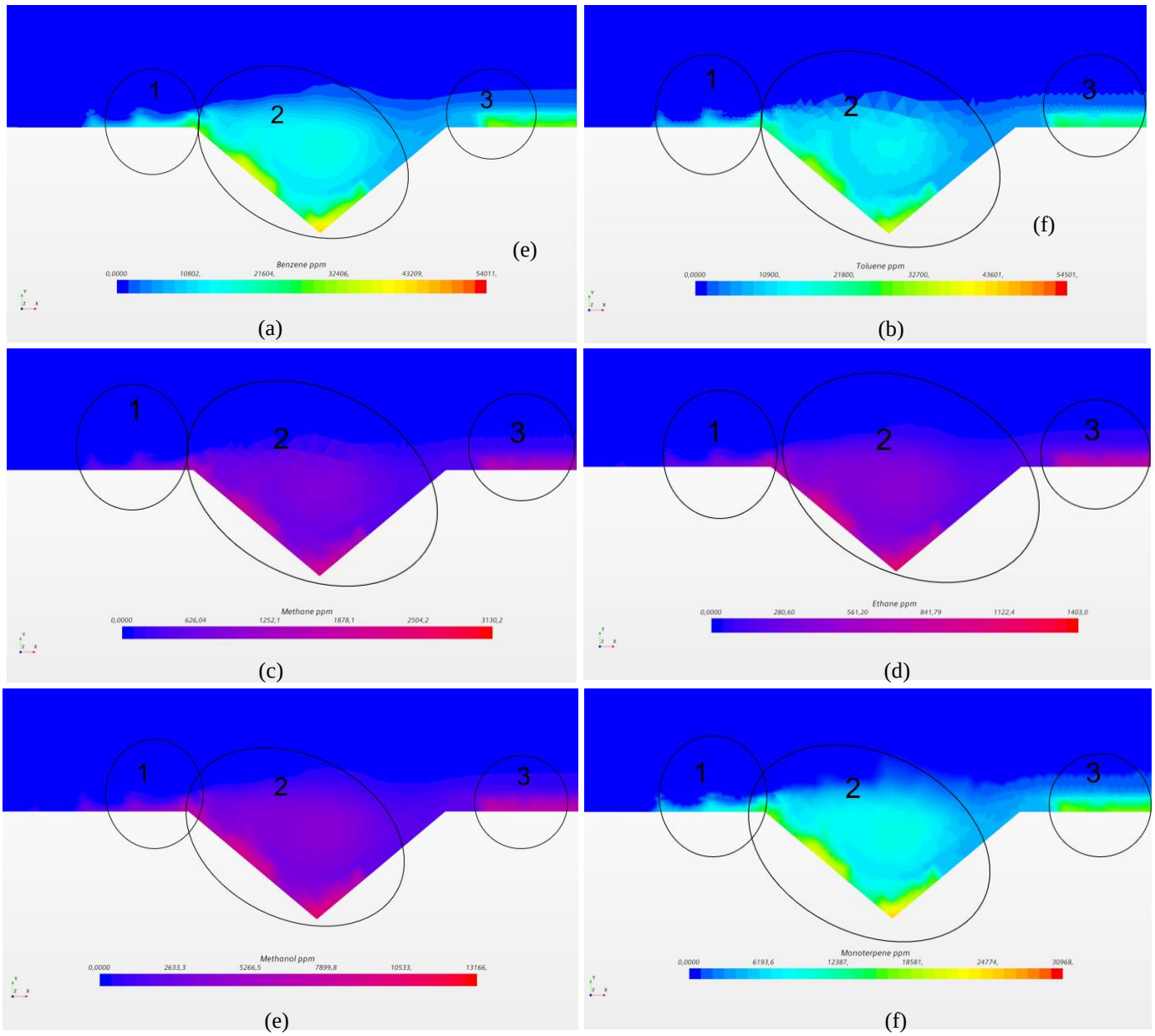

Figure II.33. Profiles of concentrations and velocity vectors in the valley of $\alpha = 50°$ after 13 mins of fire propagation till the edge of the valley for: (a). benzene (b). toluene (c). methane (d). ethane (e). methanol, and (f). monoterpenes. 1: Indication of the position of the fire-front at the tip of the valley. 2: Indication of the accumulations inside the valley at the moment the fire-front is at position 1. 3: Indication of the accumulations in the flat forest region after the vally with zero emissions.

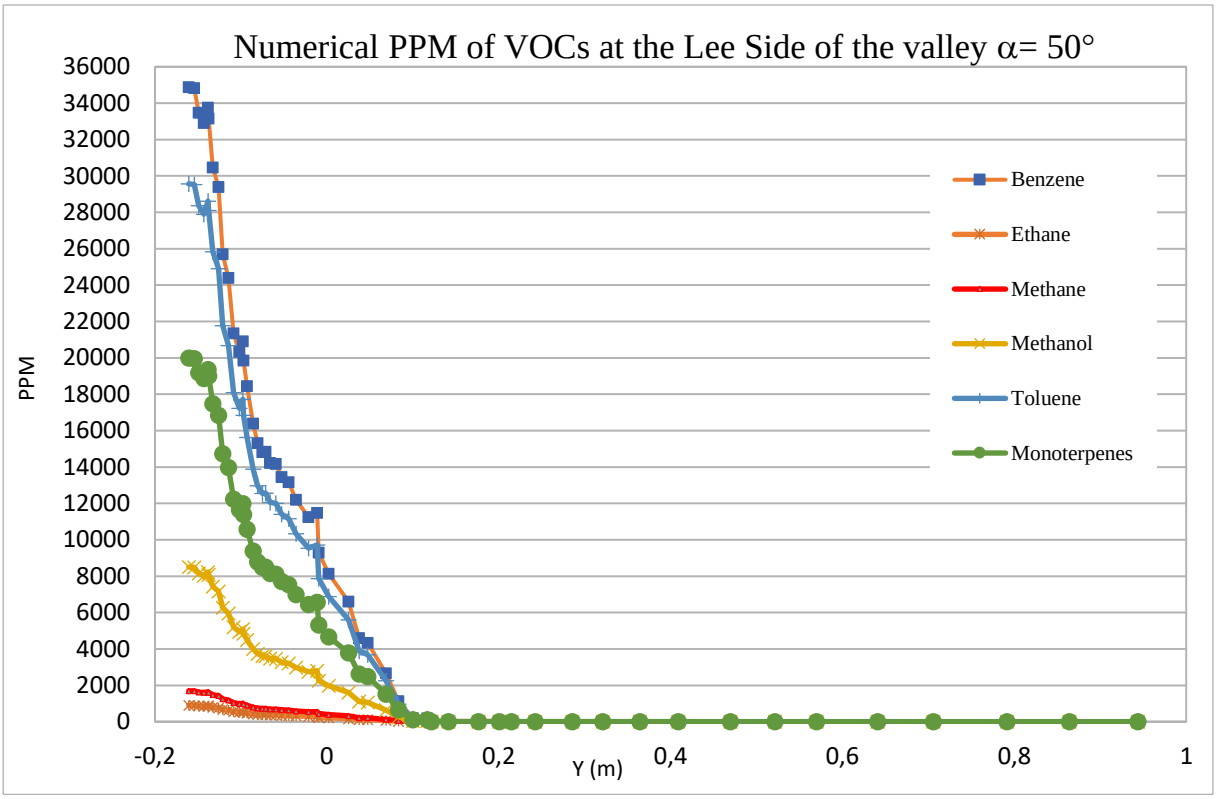
Numerical PPM of VOCs at the Lee Side of the valley α= 50°
PPM
Y (m)
Benzene
Ethane
Methane
Methanol
Toluene
Monoterpenes

(a)

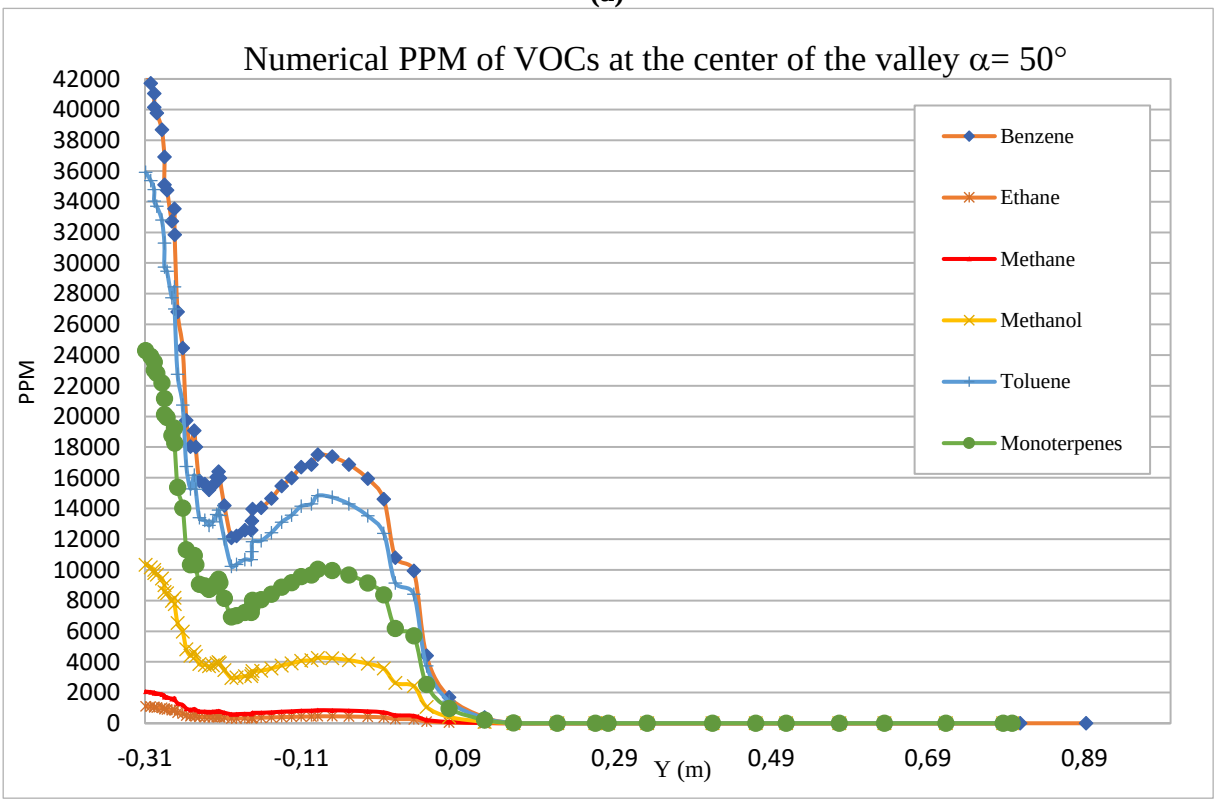
Numerical PPM of VOCs at the center of the valley α= 50°
PPM
Y (m)
Benzene
Ethane
Methane
Methanol
Toluene
Monoterpenes

(b)

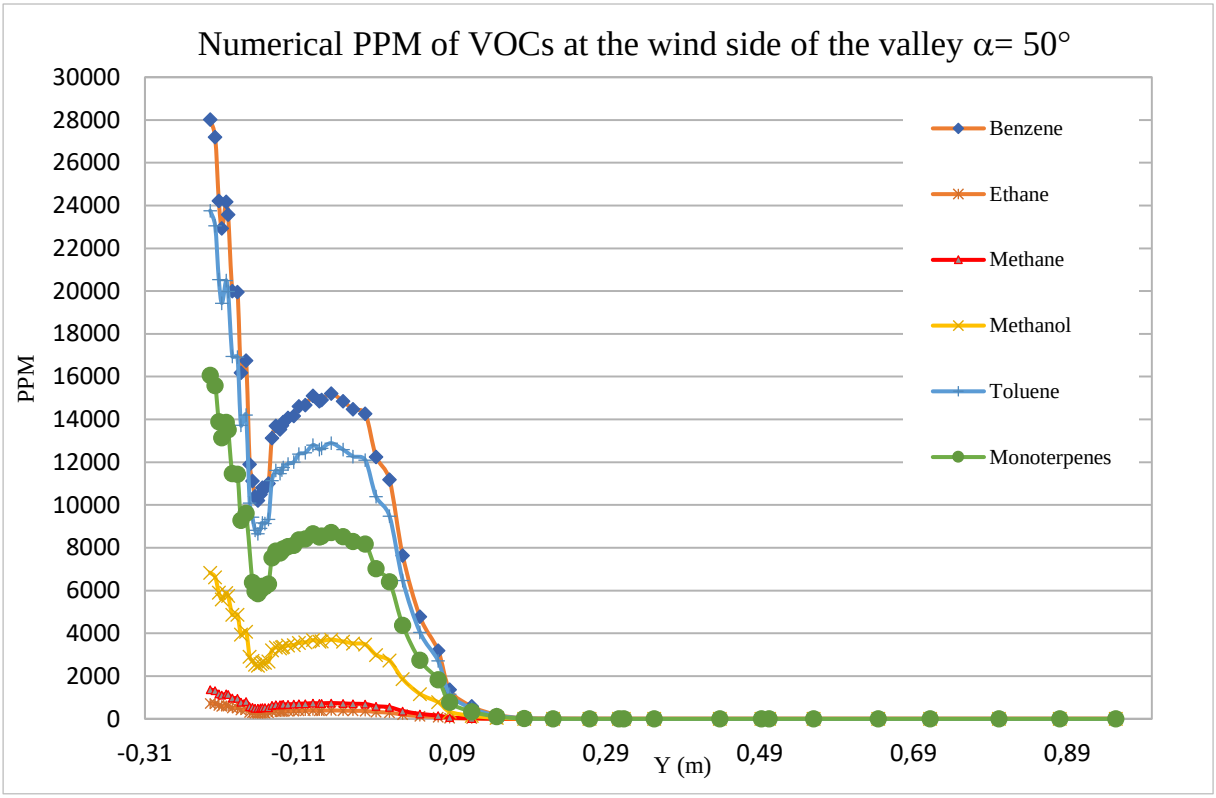

(c)

Figure II.34. The graphical plots of the numerical results of the VOCs spatial concentrations (ppm) at the three different positions inside the valley of α = 50° for different heights Y(m). (a) X = 1.295, (b) X= 1.392, and (c) X= 1.495m.

Table II.12. The max ppm and percentage by volume (%vol) of the accumulated VOCs in the valley (α= 50°) compared to their lower and upper flammability limits.

	LFL%	UFL%	Max ppm	%vol
Benzene	1.3	7.9	42355	4.2355
Toluene	1.2	7.1	35905	3.5905
a-pinene	0.8	6	24285	2.4285
Methane	4.4	16.4	2062	0.2062
Ethane	3	12.4	1100	0.11
Methanol	6	36	10325	1.0325

6.3 Discussion and Analysis

The spatial concentrations of the different compounds at the lee side and the center of the valley at the moment the fire-front reaches its tip were more critical than those at the wind side. However, their percentages at the bottom of the upslope towards the wind side remain remarkable. Their accumulations were also important in the flat forest region beyond the valley where air velocity is attenuated due to the effect of the forest porosity and where emission ratios were zero. When their ppm concentrations are compared to their flammability limits, we observed that the maximum concentrations reached by complex aromatics (benzene and

toluene) and α-pinene representing monoterpenes, laid between their flammability limits (Table II.12).

When comparing aromatic compounds i.e. benzene and toluene, we noticed that just 1% increase in the density of benzene (879 $kg.m^{-3}$) above toluene (867 $kg.m^{-3}$) (Hales and Townsend 1972) produced an increase of 0.7%vol in the deepest center of the valley although the emission rate of toluene in the forest was 2 folds that of benzene. Also, in comparison to benzene, a ~1.4% decrease in the density of α-pinene, the monoterpenes representative, (858 $kg.m^{-3}$) (Sousa & De Castro 1992), was reflected in a decrease of 1.8%vol in the valley, although the monoterpenes emission rate was higher by 18 times. The same conclusion can be drawn comparing methanol (748 $kg.m^{-3}$) and benzene, where the last is heavier than the first by 17%, but it was more concentrated in the valley by 3.1% regardless of its higher emission rate (>9 times). Therefore, we can conclude that the density of the emitted VOC compounds favors their accumulations in the valley regardless of their emission rates. According to our work, heavy compounds with their documented emission factors (Akagi et al. 2013) such as benzene, toluene, and monoterpenes have formed accumulations in a valley with an internal angle of 50°, that lay in between their lower and upper flammability limits at the moment the fire flame-front reaches the tip of the valley. These concentrations are alarming for the risk of a flashover.

7 Conclusion

Wildfire flashovers are a significant life threat that concerns firefighters especially since their direct causes remain ambiguous and controversial. Bringing new information to the debate as to whether VOC gas pockets contribute to flashovers has been the goal of our study. Our preliminary investigations involved studying the density-weighted dispersion of VOCs quantified by grams for each kg of vegetation burnt in a wildfire. The concept of transient non-steady emissions simulates their evolution and dispersal with the moving fire front in a real fire. The Rothermel model since 1972 with some adjustments from Frank Albini back in 1976, is considered a milestone of every surface fire spread model. Combining emission factors of various VOCs collected from real fires with the methods of Rothermel and Van Wagner predicting a surface fire spread transition to crown fire, can be implemented in a CFD model to simulate actual wildfire conditions. With wind speeds strong enough to overcome thermal effects, the densities of emitted VOCs play an important role in their sedimentation and accumulation in confined topographies where they are most likely to reach their flammability limits. After the experimental investigations have confirmed their accumulations in a confined valley, the numerical simulations have shown that VOCs as light as methane will accumulate while heavier compounds such as benzene, toluene, and monoterpenes will reach their flammability limits in a v-shaped valley with an internal angle of 50°. Therefore, with knowledge about forest structure i.e., porosity, topography, type and age of vegetation, and EFs of its corresponding emissions (*cf. Table I.14 & I.15 in Chapter I*) coupled with atmospheric conditions, our model can be used as a decision tool for firefighters to predict the probability of fire flashovers in wildfire prone areas, take preventive measures, and save their lives. Of course, the model still needs to incorporate thermal effects and get experimented with different wind speeds and valley angles which are considered prospects however, the debate about whether VOC accumulations will reach ignitable concentrations within the defined geometrical,

environmental, and non-thermal constraints in this study, is undoubtedly validated by our model.

CHAPTER III

****

Investigating the Flammability Characteristics of Two Mediterranean Forest Species: *Cupressus Sempervirens L.* and *Quercus Suber L.*

Résumé

Le climat méditerranéen a changé pour devenir plus sec et plus chaud en raison de sa grande sensibilité et de sa vulnérabilité au changement climatique. La tendance au réchauffement des étés des régions de climat méditerranéen (RCM) au cours des dernières décennies du XXe siècle variait entre 0,08 et 0,3 °C, et les températures en Méditerranée en particulier devraient être supérieures de 20 % à la moyenne mondiale (Drobinski et al. 2020). Des vagues de chaleur plus fréquentes et des périodes de sécheresse prolongées soulèvent des inquiétudes non seulement sur les activités économiques, la biodiversité et la santé, mais aussi sur la tendance des incendies de forêt dans les forêts de ces climats. En l'absence d'efforts sérieux pour limiter le réchauffement climatique et le changement climatique qui l'accompagne, au moins à court terme, les communautés de gestion des incendies de forêt se concentrent sur la mise en œuvre de stratégies « holistiques » de gestion du combustible qui ne se concentrent pas uniquement sur l'atténuation des incendies mais aussi sur le retardement et l'empêchement de l'allumage. Par conséquent, une détermination précise des caractéristiques d'inflammabilité de la végétation méditerranéenne est nécessaire afin de mettre en œuvre des stratégies de gestion forestière efficaces. Les descripteurs d'inflammabilité définissent l'inflammabilité, la combustibilité, la consommabilité et la durabilité de la végétation. Bien que les méthodes d'évaluation de ces descripteurs ne soient pas encore standardisées, elles sont cependant fortement liées aux réserves de COVB de la végétation en cas d'incendie (Ormeno et al. 2009, Pausas et al. 2016).

Choix de Végétation

Cupressus sempervirens var. horizontalis (cyprès) et *Quercus suber L.* (chêne-liège) sont deux espèces forestières méditerranéennes classées en fonction de leurs caractéristiques d'inflammabilité distinctives en deux catégories, résistantes au feu et résilientes au feu. Le *cyprès* est résistant au feu pour sa faible inflammabilité à l'échelle des feuilles (Della Rocca et al. 2015, 2018), et le *chêne-liège* est considéré comme résistant au feu, une caractéristique de son écorce épaisse, et aussi, il est considéré comme une espèce résiliente au feu en raison de sa capacité à repousser et à se régénérer rapidement à l'échelle de la feuille et de l'écorce, respectivement (Thompson et al. 2009, Curt et al. 2010).

***Cupressus Sempervirens var. Horizontalis* (*C.s.L.*)**

Cupressus sempervirens var. horizontalis est une espèce indigène de cyprès méditerranéen parfois appelée *Cupressus sempervirens L.* (*C.s.L.*), peut atteindre une hauteur de 30 à 35 mètres. C'est une espèce largement étudiée dans le domaine pharmaceutique en raison des caractéristiques antimicrobiennes et anti-inflammatoires de son huile essentielle (Mazari et al. 2010). De plus, il est largement utilisé dans le domaine agricole dans la RCM en raison de sa bonne qualité de bois et de sa forme caractéristique qui en fait un parfait pare-brise pour protéger les corps. Cependant, sa remarquable adaptation aux extrêmes du climat méditerranéen (sécheresse et températures extrêmes) a attiré l'attention de la communauté des feux de forêt pour évaluer son contenu volatil foliaire et sa teneur en humidité comme caractéristiques de thermo-tolérance et d'inflammabilité. Les feuilles de ce cyprès indigène méditerranéen sont recouvertes d'une épaisse couche cireuse connue sous le nom de cuticule qui limite la perte d'eau et les stomates sont disposés de manière à réduire au minimum la transpiration et la perte

d'eau. Par conséquent, leur teneur en humidité est moins affectée que d'autres familles d'arbres par périodes de sécheresse (Bianchi & Defosee 2015).

Inflammabilité de *Cupressus Sempervirens var. horizontalis*

En plus de la teneur en matières volatiles et en humidité, l'évaluation de l'inflammabilité relative des espèces végétales à l'échelle des feuilles a récemment été liée à leurs caractéristiques structurelles foliaires, c'est-à-dire le rapport surface/volume (SV, cm^{-1}), l'épaisseur des feuilles (cm) et surface foliaire spécifique (SFS $cm^2.g^{-1}$) (Ganteaume et al. 2013, Ganteaume 2018, Romero et al. 2019). Il a été prouvé dans une étude comparative entre 15 espèces forestières, dont les espèces de *Cupressaceae* et les espèces à feuilles larges (Ganteaume 2018), que la teneur en humidité jouait un rôle important dans le retardement de l'inflammation (délai d'inflammation plus long) dans les feuilles minces des espèces à feuilles larges et la litière de *cyprès*, cependant, il a aussi été remarqué que l'épaisseur des feuilles est directement proportionnelle au temps d'inflammation des feuilles vivantes du *cyprès*. Par conséquent, au niveau des particules, les épaisseurs les plus élevées, ainsi que les SV et SFS les plus petits entraînent un taux de chauffage et une diffusivité plus lente et un temps d'inflammation plus long. L'inflammabilité retardée des feuilles qui ont une longueur verticale inférieure est justifiée par le refroidissement par convection entre l'air et la surface de la feuille dû au développement d'une couche limite thermique plus courte, ce qui entraîne une moindre isolation thermique (McAllister 2022). À l'échelle des feuilles, le cyprès est classé dans la littérature comme faible à modérément inflammable (Neyişçi et Intini 2006), inflammable (Dimitrakopoulos & Papaioannou 2001), peu inflammable (vivant) et très inflammable (mort) (Ganteaume et al. 2013). À l'échelle de la litière, le cyprès est connu pour produire un lit de litière compact et profond qui entrave l'apport d'oxygène vers la matière inflammable (Ganteaume 2018) et empêche même le développement de la végétation du sous-étage en raison d'un effet allélopathique présumé (Della Rocca 2015). À l'échelle de la couronne, la structure de *C. sempervirens var. horizontalis* est importante pour retenir la chaleur radiante d'un feu qui se propage et retenir des brandons volants. Lorsqu'il est planté correctement, le *cyprès* réduira la vitesse du vent responsable de l'augmentation du taux de propagation et de l'intensité du feu. En plus de cela, si elle n'est pas taillée, cette espèce porte particulièrement un faible ratio de combustibles morts/vivants au sein de sa canopée, ce qui joue un rôle important dans la réduction de la transition verticale des incendies entre la surface et la cime. Ces trois dernières caractéristiques du cyprès soutiennent la théorie selon laquelle lorsque les barrières de cyprès sont favorisées, elles contrôlent structurellement la propagation du feu horizontalement et verticalement.

Quercus suber L. (Q.s.L.)

Les forêts sempervirentes de *Quercus suber L.* (*Q.s.L.*) sont abondantes et couvrent de vastes superficies dans la MCR, principalement au Portugal, en Algérie, en Espagne, au Maroc, en France, en Italie et en Tunisie (Dehane et al. 2017). *Q.s.L.* appartiennent au sous-genre *Cerris* du genre *Quercus*. Cette espèce s'est avérée être un émetteur non isoprénoïde (isoprène et monoterpènes) en raison de son incapacité à produire, stocker et émettre des isoprénoïdes endogènes, tandis que sa photosynthèse est inhibée à des températures > 30 °C (Loreto et al.

1998, Delfine et al. 2000). Cependant, une telle conclusion est encore contradictoire (Loreto 2002, Pio et al. 2005, Sánchez-Osorio 2019).

Inflammabilité de *Quercus suber L.*

Apparemment, *Quercus suber L.* dans la RCM (comme le Portugal et l'Italie) s'adaptent aux extrêmes du climat en produisant des monoterpènes pour survivre (Loreto et al. 2014) cependant, leur inflammabilité reste élevée par rapport aux autres espèces à feuilles larges. Les isoprénoïdes protègent les membranes thylakoïdes des feuilles et leurs réserves dans les feuilles sont également une indication d'un teneur en humidité élevé retardant ainsi l'inflammabilité. Par exemple, dans une étude comparant l'inflammabilité des espèces émettrices de monoterpènes de *Q.s.L.* et chez les conifères *Pinus halepensis*, la température au moment de l'inflammation (T_I) était positivement liée à sa teneur en humidité, ce qui signifie que plus la teneur en humidité des feuilles est élevée, plus la température d'inflammation est élevée (De Lillis 2009).

Test d'Inflammabilité à l'Aide d'ATG/ATD

La méthode traditionnelle utilisant un cône calorimètre pour évaluer l'inflammabilité des combustibles forestiers a été remplacée par l'utilisation de l'appareil ATG/ATD dans notre objectif de comparer l'inflammabilité des deux espèces forestières, *C.s.L.* et *Q.s.L.* L'application de la thermogravimétrie et de l'analyse thermique différentielle (ATG/ATD) a été normalisée par rapport à la masse pour déterminer les températures de dégradation thermique et la perte de masse des matières organiques à l'état solide, c'est-à-dire les plantes, sous atmosphères inertes ou oxydantes (Mitchelle et Knight 1965, Lopes et al. 2018). La mesure ATG est effectuée soit en fonction d'un gradient de température avec une vitesse de chauffage constante, soit en fonction du temps en considérant la perte de masse de manière isotherme (Parameshwaran et al. 2018). L'ATD mesure la différence de température (ΔT) entre un échantillon et une référence inerte en fonction du temps (t) ou de la température de chauffe (T). Le système à double balance de l'ATG permet de mesurer la perte de masse tandis que l'ATD fournira la différence de température entre l'échantillon et la référence inerte à chaque réaction endothermique et exothermique.

Critères d'Evaluation de l'Inflammabilité

L'évaluation de l'inflammabilité exploitant les résultats des deux analyses dépendra des critères suivants :

1. La perte de masse au cours du premier pic endothermique est une indication principale de la teneur en humidité (Wongsiriamnuay & Tippayawong 2010, El Sayed et al. 2014).
2. Une relation positive entre teneur en humidité et T_I (Dimitrakopoulos & Papaioannou, 2001). On estime que la teneur en humidité de 10 % augmente le temps de retard d'inflammabilité jusqu'à deux fois (Simoes et al. 2016).
3. L'inflammabilité augmente (temps d'allumage diminue) lorsque la quantité de cellulose décomposée dans la plage de température de 300° à 400°C augmente (Liodakis et al. 2002).
4. L'inflammabilité augmente (le temps d'allumage diminue) à mesure que la masse résiduelle totale après traitement thermique jusqu'à 600°C diminue (Liodakis et al. 2002).

5. L'aire de chaque pic de la courbe ATD est directement proportionnelle à la quantité de chaleur absorbée ou libérée (Berg & Egunov, 1969), ou à la variation d'enthalpie (Δh) qui représente la chaleur dégagée ou consommée au cours d'une réaction (Alastair 1975).

Objectif de ce travail

Compte tenu de tout ce qui précède, nous avons décidé d'effectuer des tests d'inflammabilité sur les deux espèces classées comme conifères et feuillus, respectivement *C.s.L* et *Q.s.L.* pour atteindre les critères suivants :

1. Comparer l'inflammabilité d'échantillons vivants et de déchets *C.s.L.* dans la même saison (sèche) pour remédier à l'effet teneur en humidité.

2. Comparez l'inflammabilité saisonnière de *C.s.L.* en effectuant des tests sur des échantillons vivants et de litière de la saison sèche (été) et de la saison des pluies (hiver).

3. Comparez l'inflammabilité de *C.s.L.* et *Q.s.L.* pour les échantillons vivants et de litière de la saison sèche.

De plus, les résultats des tests d'inflammabilité ont été couplés à des tests de pyrolyse sur des échantillons de litière de *C.s.L.* des saisons sèches et humides, également sur des feuilles de litière, des branches et des échantillons de liège de *Q.s.L.* afin d'identifier et de comparer leur contenu volatil. Les tests ATG/ATD et Py/GC-MS ont été réalisés dans le laboratoire IC2MP de l'Université de Poitiers, France.

Résultats de Ce Travail

Nous avons comparé la quantité de cellulose en décomposition avec la température de première inflammation. Nos résultats ont abouti à la conclusion que le feuillage vivant et les litières de *C.s.L.* sont moins inflammables que les *Q.s.L.* vivants et les litières, respectivement, mais ils sont plus combustibles. L'inflammabilité plus élevée du *Q.s.L.* conforme à l'augmentation de leur teneur en cellulose. Étonnamment, les critères d'évaluation de la cellulose n'ont pas fonctionné lors de la comparaison de l'inflammabilité du feuillage vivant et de la litière de la même espèce. Les feuilles vivant des *C.s.L.* et *Q.s.L.* étaient plus inflammables que leurs litières respectives mais moins combustibles, ce qui évoque un rôle du FMC dans l'augmentation de l'inflammabilité des feuilles de biomasse. Cependant, un FMC plus élevé des feuilles de cyprès (vivantes et litières) n'a pas augmenté leur inflammabilité par rapport aux feuilles de chêne (vivantes et litières). Les déchets saisonniers (saison sèche ou saison humide) de *C.s.L.* ont montré une FMC plus élevée des échantillons de saison humide par rapport à ceux de la saison sèche, les échantillons de la saison humide étaient plus inflammables avec une teneur en cellulose plus élevée. Par conséquent, les critères reliant la décomposition de la cellulose à l'inflammabilité s'appliquent uniquement aux types de biomasse similaires (par exemple, feuillage de litière ou feuillage vivant) de différentes espèces ou à la litière saisonnière de la même espèce, mais pas aux feuillages vivants ou à la litière de la même espèce. Les expériences de pyrolyse menées pour vérifier le rôle des identités des volatils émis dans l'inflammabilité avancée de *Q.s.L.* sur *C.s.L.* expliquent probablement l'inflammabilité par les quantités élevées de volatils terpéniques de *C.s.L.* qui ont été gazéifiés par distillation à des températures précoces (50°C, 80°C, 120°C) et ont continué à être émis à des températures aussi élevées que 350°C et

550°C, y compris de l'isoprène, de manière surprenante. Aucun terpénoïde n'a été émis par la pyrolyse de Q.s.L. à 350°C, 550°C ou 800°C, ce qui peut corroborer le fait qu'il s'agit d'émetteurs non isoprénoïdes, mais d'autres tests à des températures plus basses sont recommandés pour mieux étayer cette théorieLa faible teneur en cellulose du C.s.L. par rapport à Q.s.L. est soutenu par les pourcentages plus faibles d'émissions relatives provenant de la cellulose pour le C.s.L. par rapport à Q.s.L. Ce résultat confirme la faible inflammabilité du C.s.L. comparé à celui de Q.s.L. La plus grande combustibilité de *C.s.L.* par rapport à *Q.s.L.* fait probablement référence aux pouvoirs calorifiques plus élevés des terpènes émis par *C.s.L.* et non par *Q.s.L.* qui émettait principalement des phénols (par exemple à 350°C). D'autres études calculant les limites d'inflammabilité du mélange de gaz issus des deux espèces devraient être menées plus avant pour mieux comprendre leur difference d'inflammabilité. A l'échelle de la feuille, *C.s.L.* les espèces peuvent présenter une barrière retardatrice d'inflammation pour protéger *Q.s.L.* espècesconcernée par les incendies de forêt. Cependant, à l'échelle de l'arbre, des expérimentations supplémentaires devraient être menées afin de vérifier les stratégies de plantation optimales de *C.s.L.* (structure, nombre, densité, couches, etc.) afin d'obtenir une meilleure protection contre les menaces d'incendies de forêt.

1 Introduction

The Mediterranean climate has been shifting to get dryer and hotter because of its high sensitivity and vulnerability to climate change. The warming trend in the summers of the Mediterranean climate regions (MCR) in the last decades of the twentieth century ranged between 0.08 to 0.3°C, and the temperatures in the Mediterranean particularly are expected to get 20% more than the global average (Drobinski et al. 2020). More frequent heat waves and extended drought periods raise concerns not only on the economic activities, biodiversity, and health but also on the trend of wildfires in the forests of these climates. In the absence of serious efforts to limit global warming and the accompanying climate change at least on the short run, and since oxygen is always available, wildfire management communities are focusing on implementing "holistic" fuel management strategies that focus not only on easing fire suppression but also on delaying and preventing ignition. Therefore, an accurate determination of the flammability characteristics of the Mediterranean vegetation is needed in order to implement effective forest management strategies. Flammability descriptors define the vegetation ignitability, combustibility, consumability, and sustainability. Although the methods for evaluating these descriptors have not yet been standardized however, they are strongly linked to the vegetation BVOC reserves at the event of the wildfire (Ormeno et al. 2009, Pausas et al. 2016). *Cupressus sempervirens var. horizontalis* (cypress) and *Quercus suber L.* (cork oak) are two Mediterranean forest species classified based on their distinctive flammability characteristics into two categories, fire resistant and fire resilient. Cypress is fire resistant for its low ignitability on a leaf scale (Della Rocca et al. 2015, 2018), and cork oak is considered fire resistant, a characteristic of its thick bark, and also, it is considered a fire resilient species because of its ability to re-sprout and regenerate rapidly on a leaf and bark scale, respectively (Thompson et al. 2009, Curt et al. 2010). The initial growth of a forest fire occurs in the surface fuels i.e. litter beds composed mainly of foliage litter. What's more, live and dead foliage or needles in case of conifers, are the main aerial fuels responsible for crown fire transition and propagation. Of course, amongst other factors FMC is an important flammability retardant with percentages varying among dry and wet season, therefore it will be interesting to investigate its interference with foliage flammability. Given the importance of foliage in wildfire ignition and propagation, we have decided to run flammability assessment trials using thermogravimetric and differential thermal analyses (TGA/DTA) on live and litter foliage (needles in case of *C.s.L.*) from both species the coniferous *C.s.L.* and broadleaved *Q.s.L.* according to the following programs:

1. Compare the flammability of live and litter samples of *C.s.L.* in the same season (dry) season to address the FMC effect.

2. Compare the seasonal flammability of *C.s.L.* by running tests on live and litter samples from the dry season (summer) and wet season (winter).

3. Compare the flammability of *C.s.L.* and *Q.s.L.* for live and litter samples from the dry season.

Additionally, the results from the flammability tests were coupled with pyrolysis tests using Py-GC/MS analysis, on litter samples of *C.s.L.* from the dry and wet seasons, also on litter leaves, branches, and cork samples of *Q.s.L.* in order to identify and compare their volatile

contents and possibly link them to their flammability and fire resistance characteristics. The TGA/DTA and Py/GC-MS tests were conducted in the IC2MP laboratories of the University of Poitiers, France.

2 Vegetation Flammability Descriptors

Fire research still strives to define biomass fuel flammability. Research efforts since the 70s have gathered to the conclusion that flammability can be described by three important descriptors; ignitability, combustibility, and sustainability (Anderson 1970, Gill and Moore 1996, Dimitrakopoulos and Papaioannou 2001). A fourth descriptor, consumability, was later added after Anderson (1970) by Martin et al. (1993). Definitions of these descriptors are found in Table III.1.

Table III.1. Four biomass flammability descriptors and their definitions.

Descriptor	Definition
Ignitability	Time to ignition (TTI) once exposed to a heat source.
Combustibility	Rapidity of combustion after ignition.
Sustainability	Ability to sustain combustion once ignited with or without a heat source.
Consumability	Proportion of mass or volume consumed by combustion.

Experimenting each of the 5 descriptors provides different test responses. For example, ignitability testing provides data about the time to ignition (TTI) of the vegetation also referred to as induction time (Liodakis et al. 2002) in addition to the critical temperature of ignition (T_{TTI}) and the resulting heat flux. Combustibility gives information about the rate of increase in the vegetation temperature and the resulting heat release rate (HRR), whereas the consumability provides information about the mass loss rate. Till now there is no standardized method to investigate vegetation flammability neither on a field scale nor on a laboratory scale. However, the testing methods that combine the thermal gravimetric and differential thermal analysis (TGA/DTA), and pyrolysis gas chromatography/mass spectrometry (Py-GCMS) have succeeded to provide information about the flammability characteristics of vegetation matter in direct relationship with its chemical composition and volatile content.

2.1 Flammability Testing Methods: Why TGA/DTA?

The application of thermal gravimetric and differential thermal analysis (TGA/DTA) has been standardized to determine thermal degradation temperatures and mass loss of solid-state organic materials i.e. plants, under inert or oxidizing atmospheres (Mitchelle and knight 1965, Lopes et al. 2018). The TGA measurement is performed either as a function of temperature gradient with constant heating rate, or as a function of time by considering the mass loss isothermally (Parameshwaran et al. 2016). The DTA, measures the difference in temperature (ΔT) between a sample and an inert reference as function of time (t) or heating temperature (T). The base line of the TGA plots deflects from a straight line parallel to the (T) or (t) axis to form peaks and troughs at certain temperature ranges indicating physical and chemical reactions. For organic materials such as plants, troughs represent endothermic reactions such as dehydration while peaks are formed in exothermic reactions such as combustion of volatiles resulting from matter decomposition in air atmosphere. DTA can be done in an inert or air atmospheres. However, inert atmospheres allow observations such as melting and boiling points, phase transition or auto-oxidation but not combustion reactions. Since the aim of our study is to configure the

flammability characteristics of our plant specimens (i.e., ignition, HRR, consumability), our analyses were done in air atmospheres. The results of TGA/DTA methods describe the different combustion phases of the experimented vegetation specimen, starting with the drying, then volatilization (mainly terpenoids), followed by the decomposition of the hemicellulose, cellulose, and lignin to release more volatiles and tars, followed by the formation of char and mineral ash (Liodakis et al. 2002). Vegetation ignition temperature was defined by researchers in the range from 300 to 410°C (Anderson 1970), and it is rated to be a little bit higher than the temperature of its first exothermic reaction (pyrolysis) after of which the combustible gases are generated from cellulose degradation. Lower residual mass fraction left after flammability testing on vegetation specimen is associated with higher flammability rates and higher percentages of matter degradation to volatiles (Dimitrakopoulos & Papaioannou 2001, Della Rocca et al. 2017); a hypothesis that can be supported with the identification and quantification of the volatile emissions from the vegetation specimen using the Py-GC/MS analysis at the different degradation temperatures concluded from the TGA/DTA data.

2.2 Choice of Vegetation Species

Investigating vegetation flammability descriptors is a milestone in wildfire hazard assessment and forest fuel management by which fewer flammable species are favored in silviculture measures for the protection of other valuable more flammable species. Cypress species have been studied extensively for their low ignitability (longer TTI) on a leaf scale and were suggested by scientists to be planted as green barriers or fuel breaks (Dimitrakopoulos & Papaioannou 2001, Liodakis 2002, Xanthopoulos 2011, Della Rocca 2015). On the other hand, cork oak, which is a very important source of income and economical benefit in the countries of the MCR i.e., Portugal and Algeria, and regardless of its fire-resistant and regenerative barks, their forests are witnessing a major decline due to several reasons (Haenaem et al. 2017), but most importantly due to climate change and wildfires (Pausas et al. 2009, Curt et al. 2010, Dehane et al. 2017). Therefore, it is important to conserve such species and implement silvicultural measures favoring their protection with less flammable species such as cypress.

2.3 Testing Scales

Most fires begin as surface fires that may or may not transition into crown fires (passive or active) depending on certain criteria involving crown base height (CBH), and foliar (dead and live) fuel moisture content (FMC) and volatile content. Flammability within species vary according to the type of fuel tested (live or dead) however, fine fuels with the highest surface to volume ratio are the first structures consumed in a wildfire i.e., foliage and branches < 1/8 inch (Anderson 1968, Rothermel 1972) on both scales (litter and live). Therefore, it is important to estimate vegetation flammability characteristics starting from these structures. Furthermore, foliage is the primary source of volatiles emissions which are responsible for fire propagation and extreme fire behaviors (Ciccioli 2014, Materić et al. 2015). The studies linking terpenoid content in vegetation (mainly isoprene), to thermotolerance characteristics in response to abiotic stresses i.e., drought or short-term high temperature exposure are many (Yani et al. 1993, Jun-Wen & Cao 2005, De Lillis 2009, Peñuelas & Llusià 2002, Midzi et al. 2022). Nevertheless, although their quantification remains a debate, the foliar terpenoid content, especially sesquiterpenoids (ST), in relationship to vegetation flammability (particularly combustibility and sustainability), has been proven in many recent studies (Della Rocca et al.

2017, Romero et al. 2019, Della Rocca et al. 2020). However, these studies are only relevant to the leaves of the species that have special terpene storage compartments. *Quercus suber L.* are non-isoprenoid emitters (Defline et al. 2000) and their leaves lack terpene storage compartments (Niinemets & Reichstein 2002). Therefore, it will be beneficial to relatively compare the flammability characteristics of cypress and cork oak on a leaf scale, and link them to their volatile content especially terpenoids. Also, it is important to compare the seasonal (dry and wet) leaf terpene and moisture content of cypress leaves and interpret their effect on flammability. The final results can be of use in forest management strategies which favor the plantation of cypress for the protection of economically valuable species such as the cork oak. These results will also improve our understanding to vegetation auto-ignition.

3 Cupressus Sempervirens var Horizontalis

3.1 Flammability of *Cupressus Sempervirens var. Horizontalis*

Cupressus sempervirens var. horizontalis is a native Mediterranean cypress species sometimes referred to as *Cupressus sempervirens L.* (C.s.L.) that can reach a height of 30 to 35 meters. It has been an extensively studied species in the pharmaceutical field because of its essential oil's antimicrobial and anti-inflammatory characteristics (Mazari et al. 2010). Besides, it is widely used in the agricultural field in the MCR because of its good wood quality and characteristic form that makes it a perfect windshield to protect corps. However, its remarkable adaptation to the extremes of the Mediterranean climate (drought and temperature extremes) has drawn the attention of the wildfire community to assess its foliar volatile content and FMC as characteristics of thermotolerance and flammability. The leaves of this Mediterranean native cypress are covered with a thick waxy layer known as cuticle which restricts water loss and the stomata are arranged in a manner that reduces the transpiration and water loss to the minimum therefore, their moisture content is not drastically affected in periods of drought (Bianchi & Defossee 2015). In addition to volatile content and FMC, the relative flammability assessment of vegetation species on a leaf scale has recently been linked to their foliar structural characteristics i.e., surface area to volume ratio (SAV, cm^{-1}), leaf thickness (cm), and specific leaf area (SLA $cm^2.g^{-1}$) (Ganteaume et al. 2013, Ganteaume 2018, Romero et al. 2019). It was proven in a comparative study between 15 forest species including *Cupressaceae* species and broad-leaved species (Ganteaume 2018), that FMC played an important role in delaying ignition (longer time to ignition) in thin leaves of broad-leaved species and litter of cypress, however, it was the leaf thickness that was directly proportional to the time to ignition in live leaves of cypress. Therefore, on a particle level, the higher thickness also smaller SAV and SLA, result in slower heating rate and diffusivity and longer TTI. The delayed ignitability of leaves which has a lower vertical length is justified by convective cooling due to the development of shorter thermal boundary layer resulting in less heat insulation (McAllister 2022). On a leaf scale, cypress is classified in literature as low to moderately flammable (Neyişçi and Intini 2006), flammable (Dimitrakopoulos & Papaioannou 2001), and not very flammable (live) and very flammable (dead) (Ganteaume et al. 2013). On a litter bed scale, cypress is known to produce a deep compact litter bed that hinders oxygen supply to the flammable material (Ganteaume 2018) and even prevents the development of understory vegetation due to a presumed allelopathic effect (Della Rocca 2015). On a crown scale, *C. sempervirens var. horizontalis* structure is important in retaining the radiant heat of a propagating fire and flying firebrands,

and when planted properly cypress will reduce wind speeds responsible for increasing fire ROS and intensity. In addition to that, this species particularly carries a low dead-to-live fuel ratio within its canopy which is a role player in reducing surface-to-crown fire transition vertically. These last three characteristics of cypress support the theory that when cypress barriers are favored, they will structurally control fire spread horizontally and vertically.

3.2 Wildfire Case Studies: Cypress Forests

The laboratory findings and observations about cypress based on its leaf physical and chemical flammability characteristics proved its delayed ignitability. Those results were supported by field scale observations from different wildfire incidents in different countries where cypress forests and barriers were the least affected by the fire amongst the other species that were completely consumed. Researchers from Greece and Spain were the most interested in investigating cypress as green barriers to limit wildfire hazards because of their remarkable post fire field observations. Such observations have allowed us also to come out with some conclusions about the most efficient patterns of planting cypress. For instance, in Greece, where cypress trees were planted in scarce small numbers they didn't stop the fire from crossing them, however, their crowns remained intact and partly green after the fire (Fig. III. 1, 2 & 3) while all the surrounding vegetation were 90 – 100% consumed. In another observation in Spain, where cypress trees were evenly distributed in a forest, the stand was slightly affected (only 1.27% of the trees were burned, 37.09% were more or less dehydrated and 61.64% were unaffected) by a large fire that destroyed all of the surrounding vegetation represented by a *Q. ilex* community with the presence of scattered *Quercus faginea*, *Juniperus oxycedrus*, and planted *P. Halepensis* (Della Rocca et al. 2015), Figure III.4. These observations provide some evidence that cypress trees have good resistance to flammability and when planted properly in in multiple rows, they will remarkably reduce fire spread.

Figure III.1. A postfire site upslope in Greece, that occurred in June 1992. The crowns of the sparse row of cypress remained intact and partly green, while the shrubland and other vegetation species were totally consumed. (Xanthopoulos 2011).

Figure III.2. A postfire observation in June 2001, in Attica, Greece. The fire passed the unevenly planted cypress trees and consumed the majority of pine trees while the cypress crowns remained intact and evergreen. (Xanthopoulos 2011).

Figure III.3. A postfire observation upslope in Viotia, Greece in the mid-1990s. The fire again passed the scarcely planted cypress trees. The pine stands scorched entirely while the cypress trees remained intact. (Xanthopoulos 2011).

Figure III.4. A postfire observation in 2012 in Jerica, Spain. The evenly planted cypress barriers weren't affected by the fire whereas all the surrounding vegetation were totally consumed. (Della Rocca 2015).

4 Quercus Suber L.

4.1 A Non-Isoprenoid Emitter

Quercus suber L. (*Q.s.L.)* evergreen forests are abundant and cover large areas in MCR mainly in Portugal, Algeria, Spain, Morocco, France, Italy, and Tunisia (Dehane et al. 2017). *Q.s.L.* belongs to the subgenera Cerris of the genus Quercus. This species was found to be a non-isoprenoid (isoprene & monoterpenes) emitter because of its incapability of endogenous isoprenoid emission with non measurable production and storage, while its photosynthesis is inhibited at temperatures >30°C (Loreto et al. 1998, Delfine et al. 2000). However, such finding is still contradictory (Loreto 2002, Pio et al. 2005, Sánchez-Osorio 2019). The controversy lays in the difficulty to identify the purity of these species, sometimes the tested samples which emitted monoterpenes were mistaken for pure *Q.s.L.* while in fact they were hybrids of *Q. suber* and *Q. rotundifolia* (Owen et al. 2002). Also, it was proven that monoterpene production was noticed in the leaves of *Q.s.L.* due to exogenous monoterpene fumigation, even when the non-fumigated leaves were placed at a distance of 50 cm away from the fumigated leaves (Delfine et al. 2000). Therefore, mixed forests of these species with other monoterpene-emitting species such as *Q. ilex* will provoke their monoterpene emission. Monoterpene emissions in broadleaf species such as *Quercus* are light dependent because they don't have storage structures in their leaves similar to the resin ducts present in conifers knowing that the monoterpene volatilization rates in these ducts are temperature dependent. However, monoterpene reserves were observed in *Quercus suber L.* whenever their production was provoked exogenously (Defline et al. 2000, Pio et al. 2005). The controversy was settled by (Loreto 2002) who concluded that Portuguese *Quercus suber* are capable of producing isoprenoids (isoprene and monoterpenes) mainly α-pinene, β-pinene, sabinene, and limonene, and little myrcene, while the *Q. suber* in the Mediterranean basin countries are non-isoprenoid emitters.

4.2 Flammability of Quercus Suber L.

Apparently, *Quercus suber* in the MCR (such as Portugal and Italy) are adapting to the extremes of the climate by producing monoterpenes in order to survive (Loreto et al. 2014) however, their flammability remains high compared to other broadleaf species. Isoprenoids protect the

thylakoid membranes of leaves especially under heat stresses (Velikova et al. 2012), and their reserves in leaves are also an indication of high FMC thus delaying ignitability. In a study comparing the flammability of monoterpene emitting species of *Q.s.L.* and coniferous *Pinus halepensis*, the T_{TTI} was positively related to the FMC, meaning the higher the leaf moisture content the higher the temperature of ignition (De Lillis 2009). In dry conditions (FMC < 40%) relative flammability seems to depend only on the FMC, however when needles with high monoterpene content and high FMC were subjected to flame their ignition was more facilitated than when subjected to heat. Most probably because monoterpenes in conifers leaves are conserved in deep resin ducts and they take more time and higher temperatures to volatilize however, when they do volatilize they drive flammability (i.e. ignitability, combustibility) remarkably (De Lillis 2009). Therefore, for live leaves (with high FMC) the easier and earlier the isoprenoids (especially monoterpenes) are emitted from the leaves the sooner they ignite. Indeed, for the same heat flow rate monoterpenes emitted by broadleaved species may decrease the temperature of flame appearance 10 times more than comparable rates of isoprenoid emission by conifers at similar FMC, accordingly the time to ignition (TTI) is less for the former than the latter (De Lillis 2009). However, such results are no longer valid for low FMC where it becomes the flammability driver.

5 Flammability Assessment Criteria: TGA/DTA

The traditional method using cone calorimeter to assess the flammability of forest fuels, has been substituted by using the TGA/DTA apparatus in our aim to compare the flammability of the two-forest species, *C.s.L.* and *Q.s.L.* The dual balance system in the TGA enables the measurement of the mass loss while the DTA will provide the temperature difference between the sample and the inert reference at each endothermic and exothermic reaction. Flammability assessment exploiting the results of the two analyses will depend on the following criteria:

1. Mass loss during the first endothermic peak is a primary indication of the FMC (Wongsiriamnuay & Tippayawong 2010, El Sayed et al. 2014).
2. Positive relationship between FMC and TTI (Dimitrakopoulos & Papaioannou, 2001). FMC of 10% is estimated to increase the ignition delay time up to two folds (Simoes et al. 2016).
3. Ignitability increases (TTI decreases) when the amount of cellulose decomposed in the temperature range from 300° to 400°C increases (Liodakis et al. 2002).
4. Ignitability increases (TTI decreases) as the total mass residue after thermal treatment up to 600°C decreases (Liodakis et al. 2002).
5. The area (S) of each peak of the DTA curve is directly proportional to the amount of heat (Q) absorbed or liberated ($S = K \times Q$) (Berg & Egunov 1969), or the change in enthalpy (Δh) (Figure III.5) representing the heat evolved or consumed during a reaction (Alastair 1975). Berg & Egunov (1969), proposed an even simpler way to find the specific absorbed or liberated heat depending only on the deviation of the DTA curve from the zero position (Δt), i.e. ($q = S \times \frac{V}{\Delta t} \times C$), where V is the heating rate of the experiment and C is the specific heat of the sample. Šesták & Holba (2013), provided an assessment study of the different methods used for the quantitative determination of thermal effects by differential thermal analysis (DTA). In summary, the areas of the

exothermic peaks are representatives of the combustibility descriptor of the specimen flammability (Šesták & Holba 2013) while the endothermic peaks represent the quantity of heat needed to complete the first stage of degradation (dehydration and volatilization, see below).

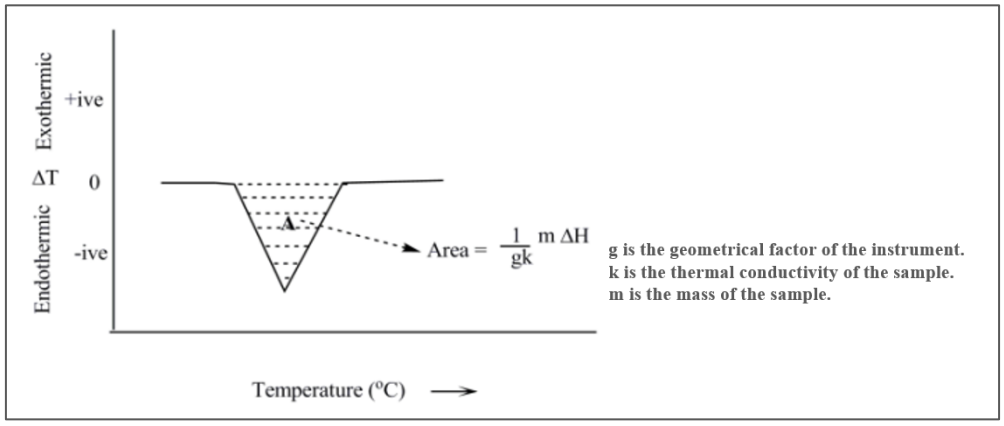

Figure III.5. The area under the peak is proportional to the enthalpy change during the endo- or exothermic reaction.

5.1 Biomass Degradation Phases in Inert vs Oxidative Atmospheres: Literature

Liodakis et el. (2002), provided very important criteria that can be used to estimate the ignitability (TTI) of vegetal biomass from TGA without the need of calorimetry. However, their tests were done in inert atmospheres. In this study, the TGA/DTA is done in oxidative atmosphere (air) to simulate the open-air fire phases undergone by the un-combusted vegetation fuel as the flaming or glowing flame front moves towards it. Therefore, in order to apply the criteria suggested by Liodakis et al. (2002) to our results, it is essential to prove the compatibility of temperature ranges for the different degradation phases between inert and oxidative atmospheres especially the cellulose degradation phase (300 – 400 °C) which is responsible for the major biomass weight loss to be correlated to ignitability. Different explanations for the TGA/DTG (Derivative Thermogravimetric) curves are available today, unfortunately less related to DTA. However, some major studies (Bilbao et al. 1997, Kumar et al. 2008, Shen et al. 2009, and Wongsiriamnuay & Tippayawong 2010) have used an identification scheme that goes along with the findings of this work. Wongsiriamnuay & Tippayawong (2010), compared the major references that used thermal gravimetric analysis to assess the effect of biomass composition on their flammability in air atmosphere. The references using the same heating rate of 10°C.min^{-1} were chosen for our compatibility study because an increase in the heating rate will increase the onset temperatures of each degradation stage (Kumar et al. 2008). However, such an increase would not affect the volatile yield at each degradation phase (Rogers et al. 1986). Kumar et al. (2008), compared the thermal degradation of corn stover in both inert and air atmosphere. Their analysis of TGA/DTG curves in air atmosphere resulted in identifying three degradation stages; stage I is dehydration (25 – 140°C), stage II is volatile combustion (220 – 400°C) and stage III is residual combustion (400 – 550°C), (Figure III.6). In inert atmosphere stage I is dehydration (25 – 110°C), stage II is active pyrolysis (250 – 420 °C) and stage III is passive pyrolysis starts at 420°C. Similar weight loss schemes for the dehydration and volatilization were observed in both atmospheres from 25 to 140°C. The second stage contributed to most of the weight loss (around 70%) with a higher rate

(10%. C°$^{-1}$) in air atmosphere, compared to 56% and < 0.7%. C°$^{-1}$ in an inert atmosphere. The third stage in air contributed to 10% of the weight loss, which was much less than the weight loss in second stage in air and third stage in inert atmospheres, (Kumar et al. 2008).

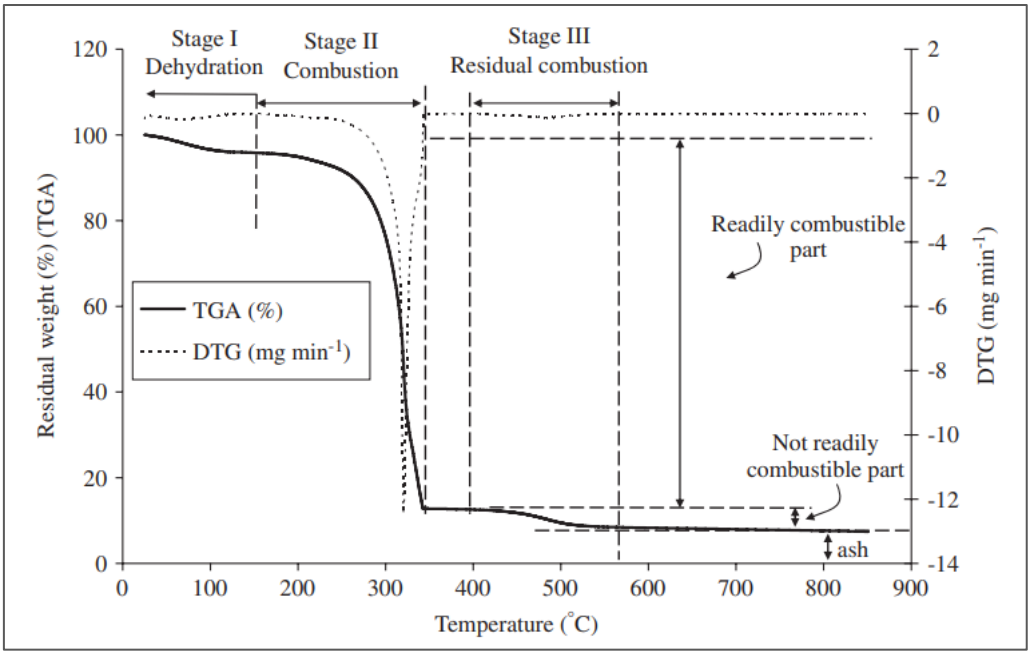

Figure III.6. The three stages of biomass (corn stover) degradation in a typical TG/DTG analyses in air atmosphere (Kumar et al. 2008).

El Sayed et al. (2014), found that the pyrolysis process of the lignocellulosic biomass can be divided into three main regions: moisture and very light volatiles components removal (<120° C), degradation of hemicellulose (220–315 °C); cellulose decomposition (315–400 °C) and lignin degradation (>450 °C). However, lignin degradation was proved to start at early stages from 180°C. Paul et al (2020), provided similar results from wheat straw pyrolysis.

Therefore, the higher volatile content of biomass volatilized under thermal stresses results in higher weight loss, higher reactivity, and lower ignition temperatures (Fatehi et al. 2019). The dominant combustion phase for most biomass is referred to as homogenous combustion of the volatiles at the surface of the particle leading to higher volatilization rates of cellulose and greater mass loss, this flame envelope prevents oxygen from reaching the particle surface however, once the homogenous combustion ends, oxygen is allowed to reach the char layer formed due to cellulose decomposition and heterogenous combustion begins normally referred to as char oxidation. This heterogenous combustion leads to the maximum lignin degradation. The primary devolatilization leads to the main weight loss and ends at 370-400 °C for biomass fuels and is followed by a slow and continuous weight loss. The secondary devolatilization, beyond 400°C, is attributed to the degradation of heavier chemical structures in the solid matrix, which were produced during the previous thermal devolatilization. The primary devolatilization forms the first peak in DTG curve is due to cellulose degradation and the second is due to lignin, Figure III.7, (Biagini et al. 2006). The DTA peaks formed in air atmosphere coincide with the DTG peaks signaling cellulose decomposition in the gas oxidation phase, Figure II.7, (Liodakis & Kakardakis 2006). Therefore, DTG and DTA peaks are different measures of the same degradation phase.

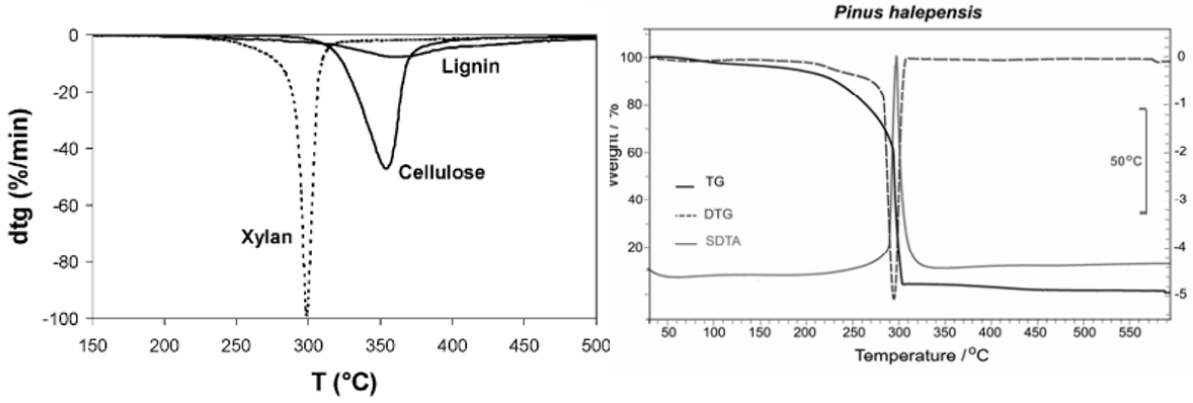

Figure III.7. Left: Peaks formed in DTG curve from biomass degradation in inert atmosphere (Biagini et al. 2006). Right: DTG peaks coincide with DTA peaks signaling cellulose degradation in air atmosphere, (Liodakis and Kakardakis 2006).

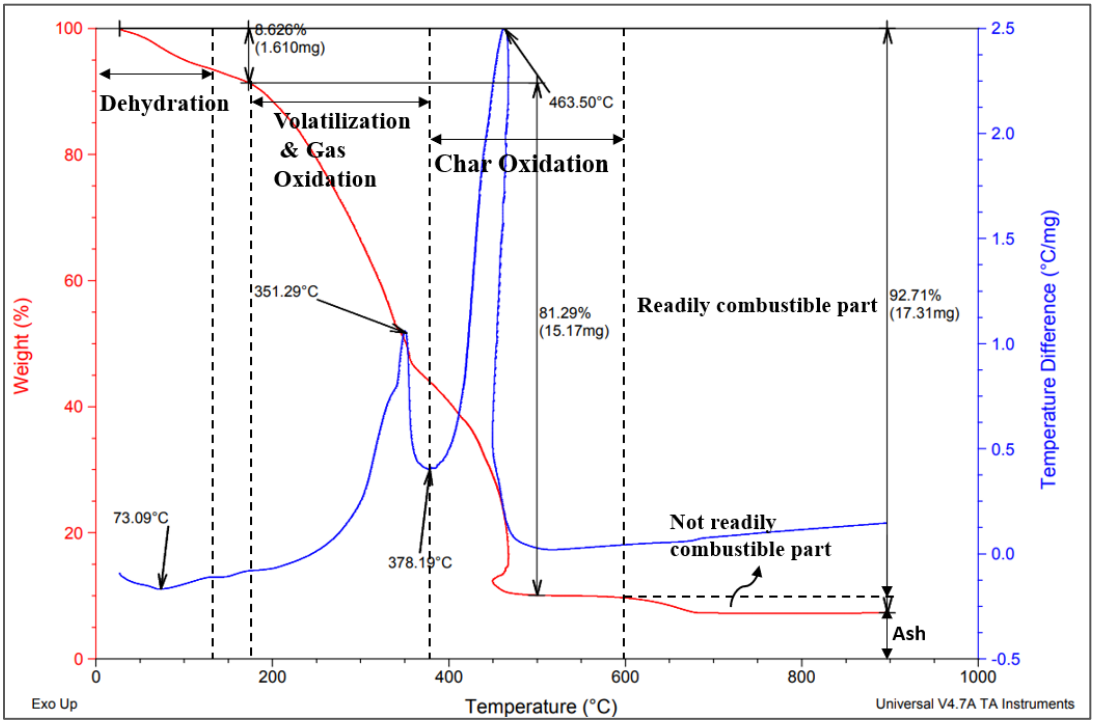

Figure III.8. The three stages of a typical TG/DT analyses for one of the tests done on *C.s.L.* litter in air atmosphere for this work.

5.2 Biomass Degradation Phases in Air Atmosphere: This Work

According to the above references the TGA/DTA curves in this work can be divided into three stages according to the scheme described in Figure III.8. The discussion of each stage follows.

5.2.1 First Stage: The dehydration phase

In the first stage, the fuel is heated by the radiative and sensible heat transfers where the biomass dehydration (FMC loss) and devolatilization of simple structure hydrocarbons (mainly terpenoids) takes place. This stage is perceived as the dehydration phase. Liodakis et al. (2002), located the dehydration from 30 to 100°C and the volatilization from 120 – 160°C in inert atmosphere. Though it is hard to differentiate between the moisture release and the

devolatilization from the TGA/DTA in air atmosphere, however Wongsiriamnuay and Tippayawong (2010), identified the dehydration phase from 30 to ~140°C and the start of volatilization from 200°C in oxidative atmosphere. The dehydration phase is accompanied by the first endothermic peak formed in the DTA curves in this work. The investigation of any volatiles released in this phase can be done with a Py/GC-MS analysis in the same temperature range.

5.2.2 Second Stage: Volatilization and Gas Phase Oxidation

Hemicellulose, cellulose and partial lignin pyrolysis occurs in this stage. In inert atmosphere with the help of DTG curve, hemicellulose pyrolysis is from 200 to 280°C, while that of cellulose is from 300 to 400 °C, lignin degradation takes place at a slower rate on a wider temperature range from 180°C and accelerates later up to 900°C (El Sayed et al. 2014). The same temperature range of cellulose degradation was found in oxygen atmosphere where a maximum weight loss of 80% was noticed until 370°C beyond of which char oxidation began and lead to rapid weight loss (Bilbao et al. 1997). Cellulose takes two paths, the first is dehydration which leads to the formation of char, and emission of CO, CO_2 and H_2O, and the second is the depolymerization which leads to the emission of volatiles and tars. When the volatiles reach a certain concentration at a certain temperature they oxidize with oxygen and ignite. However, the devolatilization process continues and the homogeneous flame envelope formed above the fuel surface during the combustion of these volatiles prevents oxygen from reaching the surface. This phase is referred to as active combustion phase (Liodakis and Kakardakis 2006) forming the first exothermic peak in the DTA curve.

5.2.3 Third Stage: Char (Fixed Carbon) Oxidation

Lignin is a more complex and thermally stable polymer than hemicellulose and cellulose. Therefore, its degradation takes a wider temperature range. Liodakis et al. (2002), referred the second peak in their DTG curve to lignin degradation in inert atmosphere in the range from 370 to 500°C. While Chen et al. (2009), referred this stage in air atmosphere to the completion of lignin degradation and the oxidation of the char residue formed from the degradation of holocellulose (hemicellulose + cellulose) in the second stage. The oxidation of the char surface is now possible because after the flaming phase of the volatiles ceased, oxygen can now contact the char surface and cause a heterogeneous exothermic combustion. Therefore, up to 370°C less cellulose is present and more char is left but it is less reactive below 370°C. Beyond 370°C char reactivity is favored and oxidation becomes significant leading to important lignin degradation (Bilbao et al. 1997). This phase leads to the formation of the second exothermic peak in the DTA curve.

Given the above findings, we can define three significant mass losses occurring simultaneously with the DTA peaks; the first endothermic peak for FMC loss, the first exothermic peak for main cellulose degradation, and the second exothermic peak for main lignin degradation. The temperature ranges from 300 to 400°C suggested by Liodakis et al. (2002) for cellulose degradation in an inert atmosphere can be adjusted to the temperatures of the first exothermic peaks in the DTA curves signaling cellulose main degradation for our samples in air atmosphere. Other criteria related to, foliage hemicellulose, lignin content, ash content, and burnout parameters can also be used to assess foliage flammability by referring to the TG/DT analyses.

6 Other Flammability Assessment Criteria

6.1 Biomass Foliar Flammability and Holocellulose

As suggested by Liodakis et al (2002), a connection exists between the amount of cellulose degraded and ignitability. Their study was done on several Mediterranean forest species including *Cupressus sempervirens L.* and depended among other parameters on the amount of cellulose degrading from 300 to 400°C in an inert atmosphere. They proved that when the amount of degraded cellulose increases ignitability increases (less TTI) and when the amount of hemicellulose from 120 to 160°C increases flammability increases; however, this last hypothesis was not well supported in their work. These observations are only related to ignition due to heat stresses simulating those coming from a fire flame front and not due to direct flame contact. Leaves with high VOC content are slower to ignite under heat stresses but they are highly ignitable when a direct contact with a flame occurs (Alam et al. 2019). According to Liodakis & Kakardakis (2006), the fuels with high ignition delay time under heat stresses have low flash point values which makes them the most ignitable fuels by direct flame contact.

6.2 Foliar Flammability and Lignin Content

The total weight loss in the third stage depends on the quantity of lignin available in the biomass i.e., the larger the mass loss the greater the lignin content. Mason et al. (2016), compared the three flammability parameters (smoke temperature, ignition temperature, and heat release rate) in relationship to dry and fresh foliar morphological and chemical traits of 30 different vegetation species including conifers by which they concluded that they were the least flammable. On morphological basis, leaves with higher thickness (higher density), have high leaf dry matter content (LDMC) which render them less flammable compared to leaves which have high perimeters (high surface area) and therefore less LDMC. On a chemical basis, conifers leaves are rich in lignin, phenols, and tannins but are also poor in cellulose, nitrogen (N) and phosphorous (P). These traits increase ignition temperatures, combustibility, and heat release rate. A surprising result for lignin, but it seems that lignin reduces leaf ignitability at the pyrolysis stage, because it is the main contributor to the production of char residue in this stage (Shen et al. 2009). However, once the leaf ignites its combustibility intensifies due to the high energy content of this complex polymer (Alam et al. 2019). Lignin rich species have the highest longevity because they poorly biodegrade due to the presence of benzene rings (Mason et al. 2016). Therefore, dry leaves of conifers will still have relatively higher lignin concentrations and possibly lower relative ignitability.

6.3 Foliar Flammability, Ash Content, and Burnout Parameters

Ash content has significant correlation with the flammability descriptors of vegetation (Della Rocca et al. 2015). The ash content of a certain species can be realized from the TGA graphs as the residual mass fraction left after the complete burnout (Figures III.7 & III.8). Higher ash fraction means there is less combustible matter in the biomass thus influencing negatively the ignitability, combustibility, sustainability and the consumability of the vegetation (Della Rocca et al. 2015, El Sayed et al. 2014). Ash content was shown to be positively correlated to TTI for *Cupressus sempervirens L.* (4.73 %) when it was compared with other Mediterranean species such as *Quercus ilex* (2.9 %) and Pinus Brutia (2.8 %) (Della Rocca et al. 2015, Liodakis et al. 2005). The burnout temperature is also an indicator of ignitability (Rostam Abadi et al. 1990). The burnout temperature is the temperature at which the mass loss rate becomes less than 1%

(El Sayed et al. 2014). Fuels with higher burnout temperatures are more difficult to burn (longer TTI), i.e. burnout temperature is negatively correlated to ignitability. Liodakis et al. (2002), defined the ash content as the mass residue left after the final degradation at 600°C. For more precision, we will depend on the mass residue at 600°C and the final mass residue after the complete burnout to compare the ignitability of our biomass.

6.4 T_{IC}, T_{DTA} and T_{MWL}

In addition to the criteria suggested above, ignitability of the vegetation specimens was also assessed depending on the onset temperatures of ignition. There are two methods to find these temperatures using the tangent lines method. The first using the TGA curve, permits the measurement of the initial combustion temperature (T_{IC}) and the other using the DTA and DTG curves to measure the temperatures of the exothermic peaks (T_{DTA}), the maximum weight loss temperature (T_{MWL}) for each peak, and the burnout temperature which is the temperature beyond at which the mass loss becomes less than 1% (T 1%.min^{-1}). T_{IC} is hard to be measured with the first method using the TGA curves when there is more than one volatilization peak (Jones et al. 2015) therefore, it is better to use the DTA curve to predict the onset temperatures of the exothermic peaks T_{DTA}. T_{DTA} of the first exothermic peaks and the T_{MWL} are used to compare the ignitability of each vegetation (Figure III.9). Grønli et al. (2002), used another method to find the onset temperatures of the hemicellulose, cellulose and lignin degradation in inert atmosphere by extrapolating the curves of mass fraction Y, and mass change (dY/dt and $\frac{d^2y}{dt^2}$).

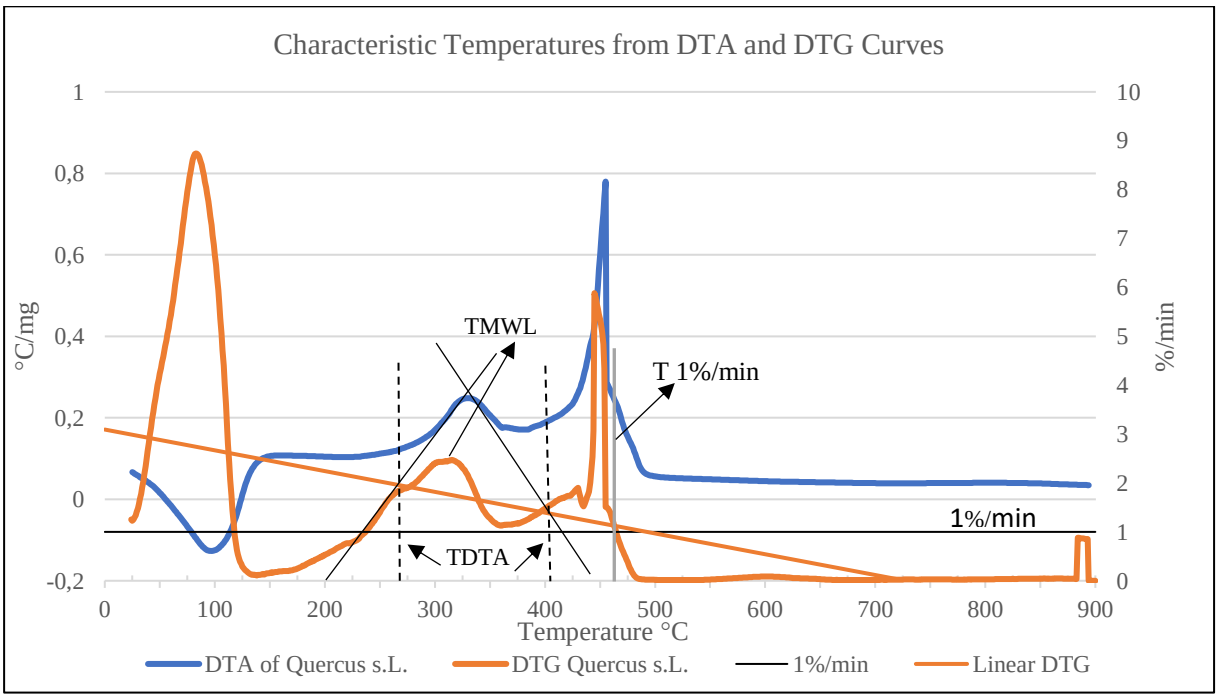

Figure III.9. Typical illustration of finding T_{DTA} (dashed lines) of the exothermic peaks, TMWL and T1%.min^{-1} (grey line). The curves represent the data of live leaves of *Q.s.L.*

7 Materials and Methods

7.1 Materials

Dry foliar samples of *C.s.L.* (*var horizontalis*) were collected and transported by airplane from under a mature tree in a Lebanese forest in the summer (dry) season in August with high average ambient temperatures from 28-30°C, and in the winter (wet) season in January with low average ambient temperatures from 5-10°C and annual rainfall from 700 to 1000 mm. Live foliar samples were obtained from irrigated cut branches of the same tree in both seasons and brought to France to be experimented in 3 days period (Figure III.10). The *Q.s.L.* litter foliar samples, branches and cork (Figure III.11), were collected randomly in the dry season from a mature *Quercus* forest in M'sila, Algeria by our collaborated research team from the University of Oran, Algeria. The live foliar of *Q.s.L.* were taken from a 1year old *Quercus* tree planted in Algeria and transported to France and were cut at the day of experimenting. All specimens were stored in the lab freezer at temperatures (-21±1°C) prior and during the experiments. Although it was not the scope of this study, the experiments allowed us to examine the fuel moisture contents between the tested litter and live samples of the two species.

Figure III.10. *C.s.L.* (*var horizontalis*) samples prepared for testing. Live (left), litter (right).

Figure III.11. *Q.s.L.* cork, branches, litter and live leaves samples prepared for testing.

7.2 Methods:

7.2.1 TGA/DTA:

The device used is SDT Q600 (DSC-TGA) (Figure III.12), equipped with a horizontal dual-balance mechanism which provides a high level of accuracy in the measurements of weight and temperature differentials. The litter and live leaves of both species were tested in an air medium at a flow rate of 50 mL.min^{-1} in a temperature range from 20 to 900°C with a heating rate of 10°C/min. The heating rate was chosen according to the recommendations of scientific evidence and trials that 10°C/min was adequate to obtain good peaks while a more rapid heating rate will cause large deviations from the thermodynamics equilibrium and produce sharp peaks (Mitchell and Knight 1965). 20 mg of fine leaf matter (leaf particle) were hardly packed in the sample cups in order to ensure complete combustion reactions, increased thermal conductivity, quicker thermocouple response, and uniformity of atmosphere in the immediate vicinity of the samples.

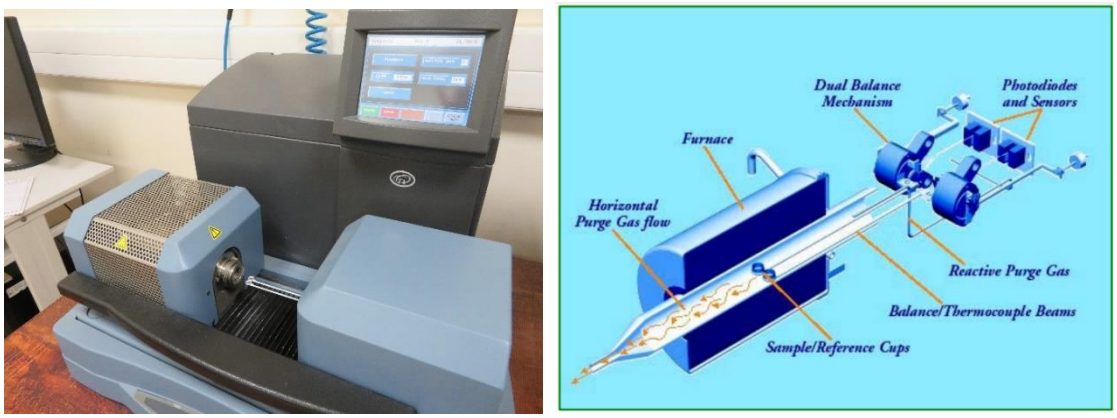

Figure III.12. SDT-Q600 equipment used for the TGA/DTA (left) with a sectional explanatory representation (right).

7.2.2 Py/GC-MS

The pyrolyzer is a Frontier Lab EGA 2020 pyrolyzer equipped with an AS-1020E auto-shot sampler coupled with a GCMS (Shimadzu QP 2010 Ultra). GC separations were done using a SLB-5MS (Supelco) capillary column (30 m long, 0.25 mm i.d, 0.25 µm phase thickness). Low- to high- temperature pyrolysis experiments were done on seasonal live and litter foliar samples of *Cupressus sempervirens L.* (*var horizontalis*), and live and litter foliar samples in addition to branches and cork samples of *Quercus suber L.* The designated pyrolysis temperatures were correlated to the TGA/DTA results which defined the different degradation temperatures of the cellulose, hemicellulose and lignin of the vegetation species. Also, we were interested to simulate the effects of the thermal stresses of the fire-front approaching the vegetation in an open forest fire. The programs of the pyrolysis tests are shown in Table III.2.

Table III.2. Pyrolysis programs with designated temperatures in (°C) of the experiments.

	Cupressus sempervirens L. (Foliar samples)	*Quercus suber L.* (Foliar, wooden, cork)
Single Shot	50 - 80 - 120 - 180	800
Double Shot	350 - 550	350 – 550
Triple Shot	120 - 350 - 550	

8 TGA/DTA Results, Analysis and Discussion

8.1 Results and Analysis

The DTG curves for all the tested vegetation are represented in Figure III.13 where they show similar weight loss behaviors (%w/w.min^{-1}) especially that the samples tested were of the same weight (20 mg). The profiles begin with dehydration followed by the successive volatilization of light compounds, holocellulose, and partial lignin and ending by secondary volatilization due to char oxidation and main lignin degradation. All tests were conducted in air atmosphere. DTG curves in Figure III.13 were offset by 5% to clarify and differentiate the results. Figure III.9 above illustrated the tangent lines method used to identify the onset temperatures of the exothermic peaks, T_{MWL} and T 1%.min^{-1}.

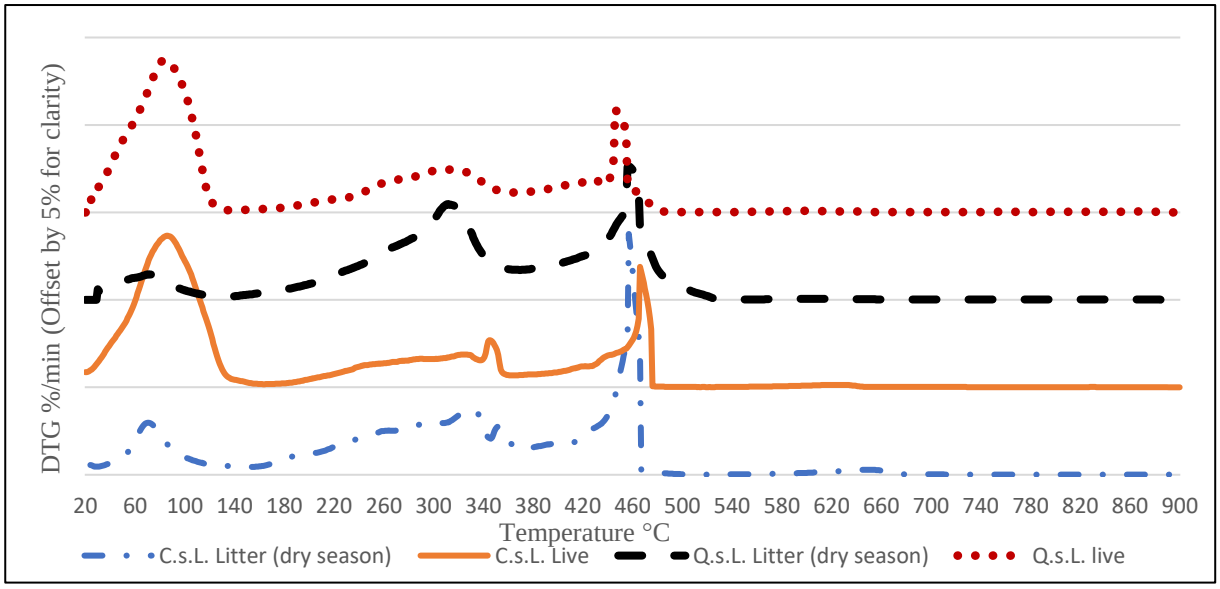

Figure III.13. DTG curves of all the tested biomass at a heating rate of 10°C.min^{-1}. Curves were offset by 5% for clarity.

8.1.1 TGA/DTA of Live Foliar *C.s.L.* vs *Q.s.L.* (Dry Season)

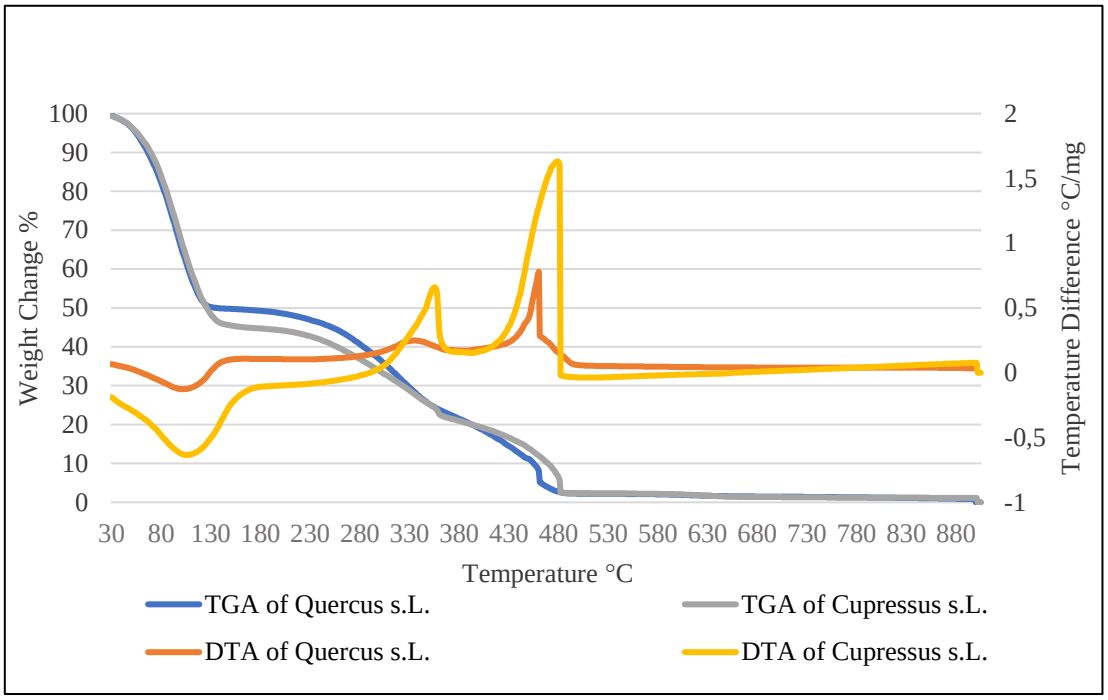

Figure III.14. TGA/DTA of live foliar samples of *C.s.L.* and *Q.s.L.* (dry season).

Table III.3a. Mass change (w/w%) and temperatures (°C) of endo- and exothermic reactions from DTA curves for live leaves of *C.sL.* and *Q.s.L.* (dry season), (Figure III.14).

Peaks ➡	**Endothermic Dehydration**		**Exothermic Gas Oxidation**		**Exothermic Char Oxidation**	
Leaves ⬇	**°C**	**% w/w**	**°C**	**% w/w**	**°C**	**% w/w**
Q.s.L. Live	30 - 130	49.59	265 - 400	24.27	413 - 480	14.05
C.s.L. Live	30 - 140	53.69	283 - 374	14.6	400 - 475	13.28

Table III.3b. Ignition evaluation data: live leaves of *C.s.L.* & *Q.s.L.* (dry season), (Figure III.14).

Criterion ➡	**Temperature °C**		**Mass Residue %w/w**	
Leaves ⬇	**Burnout**	**TMWL**	**At 600°C**	**Ash**
Q.s.L. Live	469	297	1.8	0.8
C.s.L Live	475	327	2	1.1

8.1.2 TGA/DTA of Leaf Litter *C.s.L.* vs *Q.s.L.* (Dry Season)

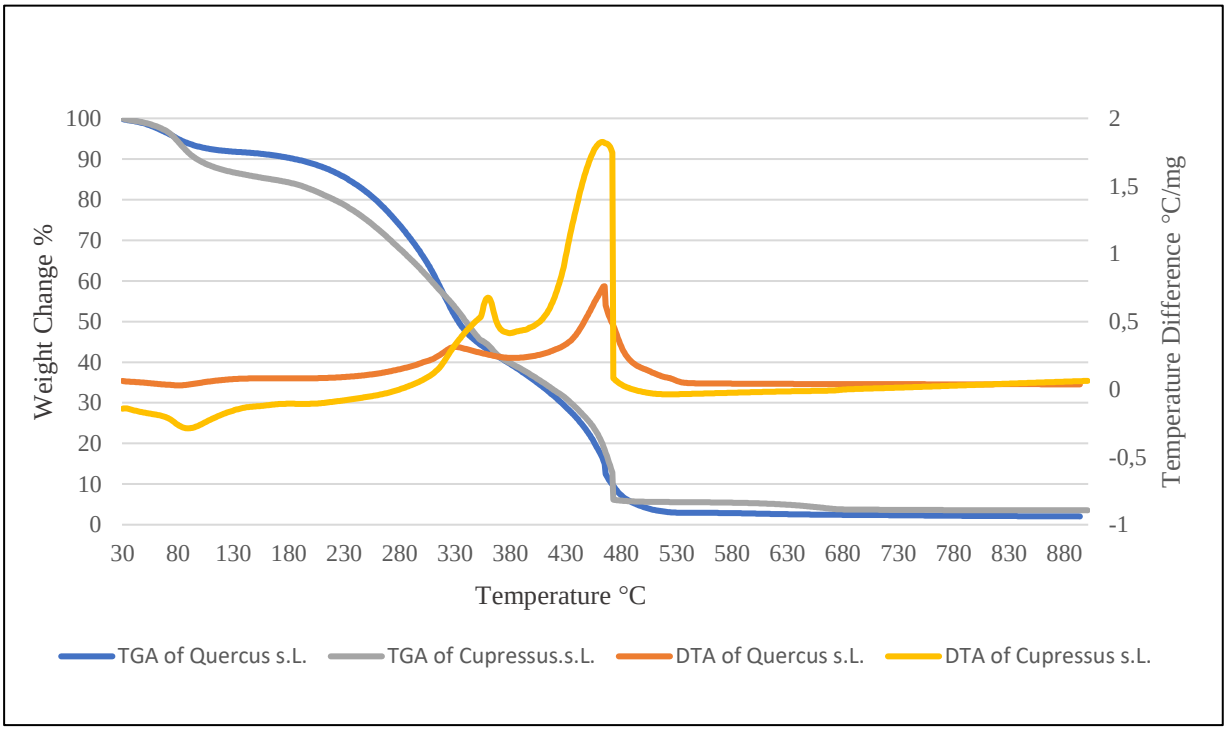

Figure III.15. TGA/DTA of litter samples of *C.s.L.* and *Q.s.L.* (dry season).

Table III.4a. Mass change (w/w%) and temperatures (°C) of endo- and exothermic reactions from DTA curves for litter leaves of *C.sL.* and *Q.s.L.* (dry season), (Figure III.15).

Peaks ➡	**Endothermic Dehydration**		**Exothermic Gas Oxidation**		**Exothermic Char Oxidation**	
Leaves ⬇	**°C**	**% w/w**	**°C**	**% w/w**	**°C**	**% w/w**
Q.s.L. Litter	30 - 90	6.61	287 - 408	37.22	423 - 493	25.68
C.s.L. Litter	30 - 100	11.27	311 - 394	20.84	394 - 465	22.84

Table III.4b. Ignition evaluation data: litter leaves of *C.sL.* and *Q.s.L.* (dry season), (Figure III.15).

Criterion ➡	**Temperature °C**		**Mass Residue %w/w**	
Leaves ⬇	**Burnout**	**TMWL**	**At 600°C**	**Ash**
Q.s.L. Litter	500	329	2.75	2.03
C.s.L Litter	476	335	5.23	4

8.1.3 TGA/DTA of Live and Litter Foliage of *C.s.L.* (Dry Season)

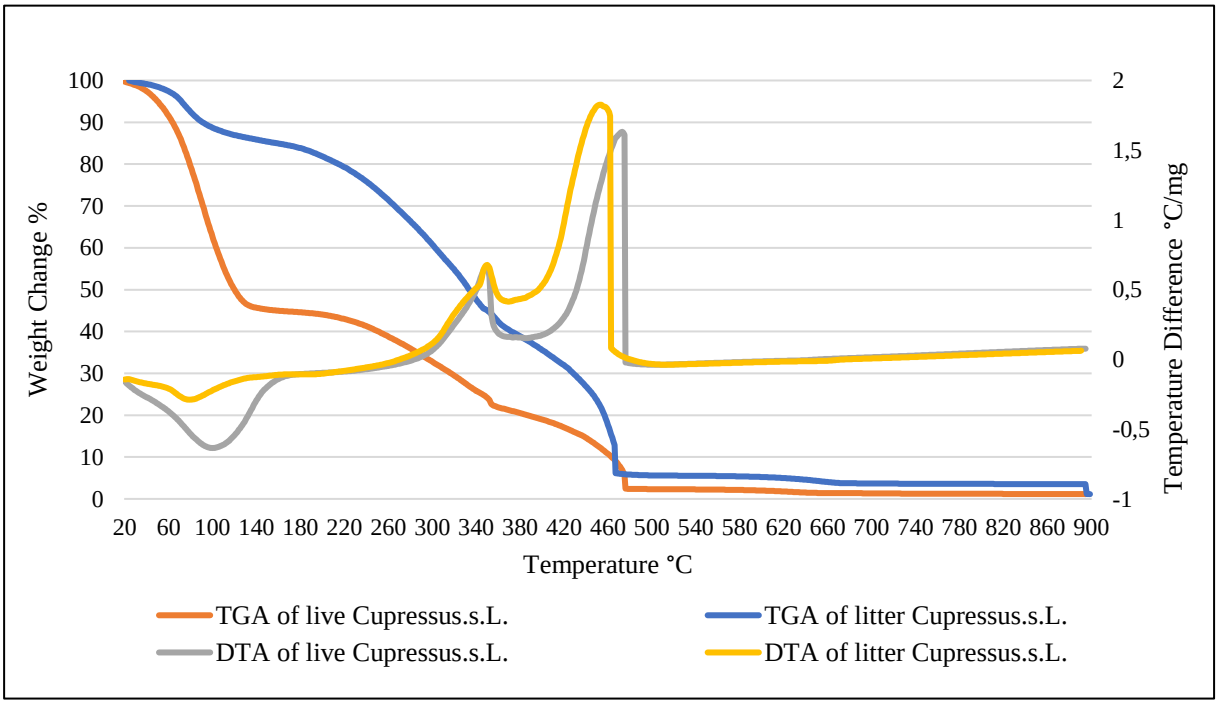

Figure III.16. TGA/DTA of live and litter foliar samples of *C.s.L.* (dry season).

Table III.5a. Mass change (w/w%) and temperatures (°C) of endo- and exothermic reactions from DTA curve for live and litter leaves of *C.s.L.* (dry season), (Figure III.16).

Peaks ➡	Endothermic Dehydration		Exothermic Gas Oxidation		Exothermic Char Oxidation	
Leaves ⬇	Temperature °C	% w/w	Temperature °C	% w/w	Temperature °C	% w/w
C.s.L. Litter	30 - 100	11.27	311 - 394	20.84	394 - 465	22.84
C.s.L. Live	30 - 140	53.69	283 - 374	14.6	400 - 475	13.28

Table III.5b. Ignition evaluation data: live and litter leaves of *C.s.L.* (dry season), (Figure III.16).

Criterion ➡	Temperature °C		Mass Residue %w/w	
Leaves ⬇	Burnout	TMWL	At 600°C	Ash
C.s.L. Litter	476	335	5.23	4
C.s.L Live	475	327	2.007	1.1

8.1.4 TGA/DTA of Live and Litter Foliage of *Q.s.L.* (Dry Season)

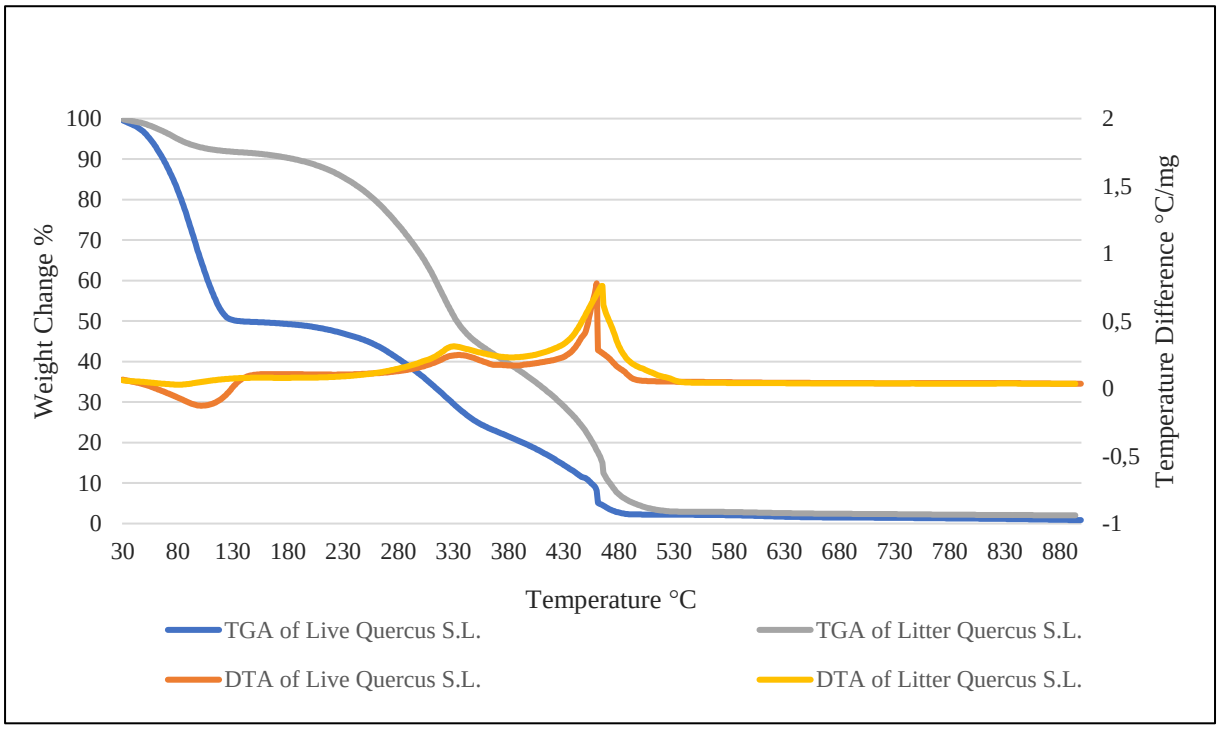

Figure III.17. TGA/TDA of litter vs live foliar samples of *Q.s.L.* (dry season).

Table III.6a. Mass change (w/w%) and temperatures (°C) of endo- and exothermic reactions from DTA curve for live and litter leaves of *Q.s.L.* (dry season), (Figure III.17).

Peaks ➡	Endothermic Dehydration		Exothermic Gas Oxidation		Exothermic Char Oxidation	
Leaves ⬇	Temperature °C	% w/w	Temperature °C	% w/w	Temperature °C	% w/w
Q.s.L. Litter	30 - 90	6.61	287 - 408	37.22	423 - 493	25.68
Q.s.L. Live	30 -130	49.59	265 - 400	24.27	413 - 480	14.05

Table III.6b. Ignition evaluation data: live and litter leaves of *Q.s.L.* (dry season), (Figure III.17).

Criterion ➡	Temperature °C		Mass Residue %w/w	
Leaves ⬇	Burnout	TMWL	At 600°C	Ash
Q.s.L. Litter	500	329	2.75	2.03
Q.s.L Live	469	297	1.89	0.8

8.1.5 TGA/DTA of Seasonal Litter Foliage of *C.s.L.* (Dry vs Wet Seasons)

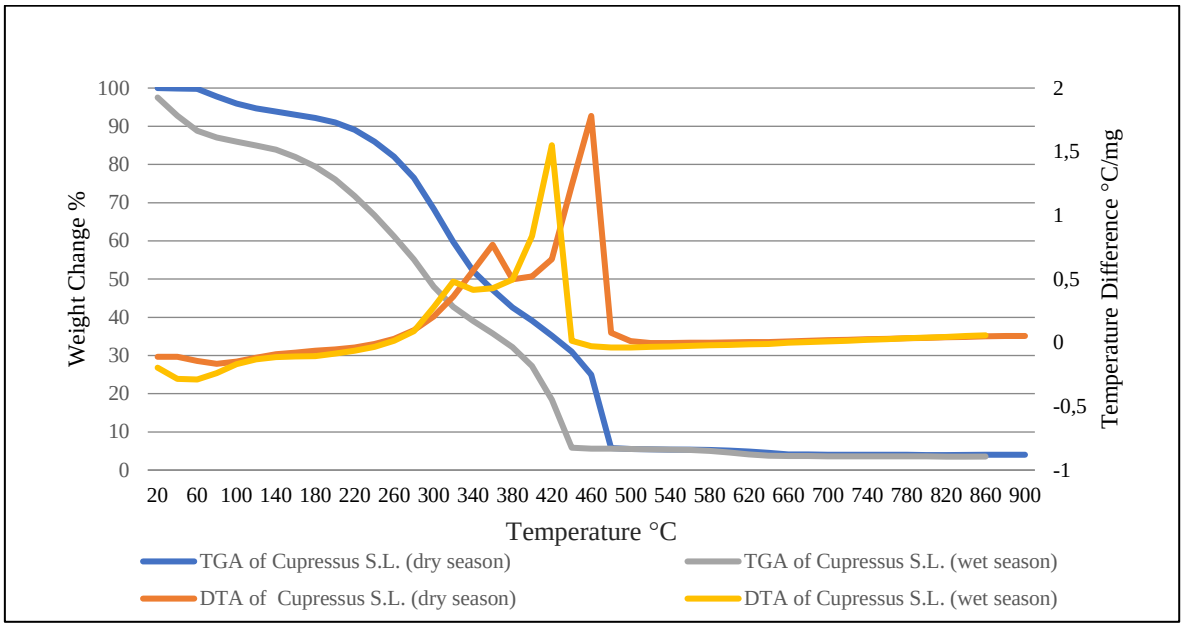

*Heating rate in this test is 20°C.min^{-1}.

Figure III.18. TGA/TDA of seasonal (dry vs wet) litter samples of *C.s. L.*

Table III.7a. Mass change (w/w%) and temperatures (°C) of endo- and exothermic reactions from DTA curve for seasonal (dry vs wet) litter leaves of *C.s.L.*, (Figure III.18).

Peaks ➡	Endothermic Dehydration		Exothermic Gas Oxidation		Exothermic Char Oxidation	
Leaves ⬇	Temperature °C	% w/w	Temperature °C	% w/w	Temperature °C	% w/w
C.s.L. (dry season)	30 - 100	11.27	311 - 390	20.84	394 - 465	22.84
C.s.L. (wet season)	30 -120	12.55	260 - 360	29.24	380 - 440	25.32

Table III.7b. Ignition evaluation data: seasonal (dry vs wet seasons) litter leaves of *C.s.L.*, (Figure III.18).

Criterion➡	Temperature °C		Mass Residue %w/w	
Leaves ⬇	Burnout	TMWL	At 600°C	Ash
C.s.L. (dry season)	476	332	5.106	4
C.s.L (wet season)	440	280	4.61	3.5

8.2 Discussion

8.2.1 Flammability Assessment

The TGA/TDA curves of the *Cupressus s. L.* and *Quercus s. L.* live and litter leaves at a heating rate of 10 °C/min in air atmosphere are shown in figures (Figure III.14, 15, 16, 17). Litter *Cupressus s.L.* (dry and wet season) in Figure III.18 were conducted at a heating rate of 20 °C.min^{-1}, their DTA curves show sharper peaks. The tables (Table III.3, 4, 5, 6 & 7) under each figure represent the proximate analysis of the different degradation phases with the corresponding temperatures and weight losses. The results represent the average values of two

tries for each sample, the reproducibility of the results was calculated to be in the margin of ~ 78%.

8.2.1.1 Live leaves of Q. s. L. vs C. s. L. (Figure III.14) & Table (III.3a, b)

The assessment of live fuel flammability is essential in estimating the surface to crown fire transition given that crown foliage are the primary morphological structures driving a crown fire. The cypress and oak live leaf samples were taken from trees cultivated in the same dry summer season in regions characterized by the same Mediterranean climate i.e. Lebanon and Algeria. However, cypress leaves had higher FMC compared to oak, 53.69 vs 49.59%, respectively. High FMC is a characteristic of cypress leaves, this means that its fuel normally requires longer exposure to heating stresses in order to evaporate its moisture content and bring it to ignition (Rothermel 1972). This delayed ignition was justified by its relatively lower cellulose decomposition percentage in the range (283 – 374°C) i.e., 14.6 % w/w compared to 24.27 % w/w for oak. Other higher values indicating higher ignition delay time of foliar live *C.s.L*. compared to live *Q.s.L.*, respectively, were also: burnout temperature (475 °C vs 469°C), fixed carbon (20.94 vs 18.41), residue at 600°C (2.007 vs 1.896 % w/w), and ash content (1.1 vs 0.8 % w/w). The qualitative observation of the endothermic and exothermic peaks in the DTA curves shows larger areas for those of cypress compared to those of oak. The endothermic peaks indicate that higher heating is required to evaporate the higher FMC of cypress. Also, as the areas of the exothermic peaks are an indication of the heat released therefore, qualitatively, live *C.s.L.* may be considered more combustible than live *Q.s.L.* The higher combustibility of the former is most probably due to its higher lignin content justified by its larger percentage of fixed carbon (20.94% vs 18.41%). The area of the second exothermic peak is also directly proportional to the lignin content of the specimen i.e., the larger the area for live *C.s.L.* indicates its relative higher lignin content compared to live *Q.s.L.* As discussed earlier higher lignin content is also an indication of reduced ignitability because its directly proportional to the ash content (Pascoa Dos Santos, 2014). This reduction of ignitability is evident in the onset temperature of the 2nd stage (gas oxidation or active combustion), 283°C compared to 265°C and TMWL 327°C compared to 297°C for *C.s.L.* and *Q.s.L.*, respectively. The higher ash content of live *C.s.L.* indicates its lower relative consumability as live fuel compared to *Q.s.L.* Finally, the burnout temperature of *Q.s.L.* is lower than that of *C.s.L.* 469°C vs 475°C, respectively meaning that former is more readily combustible than the latter. Therefore, according to these results we can conclude that live foliage of *C.s.L.* has relatively less ignitability (higher TTI), less consumability, and more combustibility than live *Q.s.L.*

8.2.1.2 Litter leaves of *Q.s.L.* vs *C.s.L.* (Figure III.10) & Table (III.4a, b)

The comparison of litter foliage of *C.s.L.* and *Q.s.L.* is beneficial in assessing the behavior of a surface wildfire that may take place in a litter bed of the two species. It has been already proven that, on a litter bed scale, the flammability of cypress litter is relatively lower because of its high FMC content that is retained and not easily evaporated due to its high compactness which also limits oxygen supply to the fuel. However, it is also important to assess litter flammability on a particle (leaf) scale. Although its litter was collected in the dry season *C.s.L.* has shown higher FMC (11.27%) compared to *Q.s.L.* litter (6.61%). Knowing that SAV of *C.s.L.* is roughly 14 cm^{-1} (Ganteaume at al. 2013) because of its high FMC content while SAV of *Q.s.L.* is 112

cm^{-1} (Essaghi et al. 2017) about eight times that of *C.s.L.* Higher SAV induces higher ignitability because there is higher surface area for water evaporation and heat exchange. Cellulose decomposed from the litter *Q.s.L.* in the temperature range 287 to 408°C is 37.22% compared to 20.84% from *C.s.L.* in the range of 311 to 390°C. The onset temperature of gas oxidation (TDTA) and TMWL for *Q.s.L.* are sooner than those of *C.s.L.* i.e., 287 vs 311 °C and 329 vs 332°C, respectively. Therefore, given these criteria we may say that *C.s.L.* litter is less ignitable than *Q.s.L.* Lignin content of *C.s.L.* litter is higher than Q.s.L. due to higher fixed carbon (37.33% vs 34.18%), higher ash content (5.1% vs 2.75%) and larger area of 2^{nd} exothermic peak indicating higher heat release rate and thus higher combustibility and less consumability of *C.s.L.* litter.

8.2.1.3 Live and Litter leaves of *C.s.L.* (dry season), (Figure III.16) & (Table III.5a, b)

It is also beneficial to compare the flammability of live and litter leaves of vegetation as a part of surface to crown fire transition assessment or for assessing the hazard of fire initiation from flying embers or firebrands. Using Liodakis et al. (2002) criteria, the amounts of cellulose decomposed of live and litter leaves of *C.s.L.* are 14.6% and 20.84%, respectively. This primary observation draws a first conclusion that litter *C.s.L.* is more ignitable than live *C.s.L.* However, the other criteria regarding T_{DTA}, TMWL, burnout temperatures, ash content, fixed carbon content and lignin content negates the first conclusion. The T_{DTA} indicating the first ignition of volatiles is lower for live leaves than for litter i.e., 283 vs 311 °C, respectively. The TMWL for cypress live is 327°C while for litter was 332°C as for their burnout temperatures they were 475 and 476 °C, respectively. Ash content and fixed carbon were higher for litter (4% & 37.73%) than for live (1.1% & 20.94%) indicating higher lignin content for litter than live. A higher lignin content results in lower ignitability of litter but higher combustibiliy (larger char combustion exo peaks). These results negate the criteria suggested by Liodakis et al. (2002), that ignitability decreases (longer TTI) when cellulose decomposition decreases since the onset of ignition for live is sooner than litter. McAllister (2022), has pointed out in her intervention that live fuels were more ignitable than dry fuels (litter in our work) because it seems that the evaporated water vapor facilitated ignition. Further investigations should be done in this regard and further confirmation of this hypothesis will follow when comparing live and litter *Q.s.L.*

8.2.1.4 Live and Litter leaves of *Q.s.L.* (dry season), (Figure III.17) & (Table III.6a, b).

Comparing live and litter leaves of *Q.s.L.* could support our previous observation with *C.s.L.* that ignitability and combustibility are respectively, positively and negatively proportional to FMC in the same vegetation species, i.e., live *Q.s.L.* is more ignitable than its litter but less combustible. Higher cellulose decomposition was observed from litter leaves of *Q.s.L.* (37.22%) compared to live leaves (24.27%) alerting that litter leaves would be more ignitable than live leaves. However, the T_{DTA}, TMWL, burnout temperatures were in the orders of 265°C & 287°C, 297°C & 329°C, and 475°C & 500°C, respectively. Ash content, and fixed carbon and consequently the respective lignin content were higher for litter than for live i.e., (2.03 vs 0.8) and (34% vs 18.4%), respectively indicating that the ignitability of live fuel of *Q.s.L.* is higher than its litter. Bearing in mind that higher lignin content delays ignitability, these results confirm once again that ignitability of live foliar of a certain species could be more than its litter. The criteria suggested by Liodakis et al. (2002) where an increase in decomposed

cellulose results in higher ignitability is skeptical when comparing the ignitability of live and litter fuels of the same species, because it seems that FMC plays a more important role. However, further investigations should be conducted to confirm these results.

8.2.1.5 Seasonal leaves of *C.s.L.* (dry vs wet season), (Figure III.18) & (Table III.7a, b).

Fires in wet seasons in the Mediterranean climate are not negligible (San-Miguel-Ayanz et al. 2022). Assessing seasonal litter flammability of *C.s.L.* during wet seasons would be important in verifying the efficiency of this species as a green barrier in different seasons. Besides, considering that leaf traits such as SAV, FMC content, volatile content, and LDMC adapt to different seasons it would be interesting to correlate them to seasonal litter flammability. Also, as litter in wet season have higher FMC (12.55%) than the dry season (11.27%), their flammability comparison will provide additional support to FMC role in increasing ignitability. Indeed, cellulose decomposed from *C.s.L.* in wet season is 29.4% from 260 to 360°C while the dry season was 20.84% from 311 to 394°C. Fixed carbon for dry season *C.s.L.* is 37.33% while the wet season litter has less percentage indicating less lignin content *C.s.L.* is 35.8% and thus more ignitability. T_{DTA} for gas ignition or oxidation and TMWL of *C.s.L.* from wet season began at a sooner temperature than the *C.s.L.* from dry season, 260 vs 311 °C and 280 vs 332°C, respectively. The less ash content which indicates more ignitability was for *C.s.L.* from wet season 3.5% vs 4% from *C.s.L.* dry season. Once again litter *C.s.L.* from dry season with less relative FMC showed larger second exothermic peaks thus higher lignin content and more combustibility than *C.s.L.* from wet season. Indeed, higher FMC reduces the LDMC and therefore lignin content (Mason et al. 2016), consequently ignitability increases. These results support our observation that FMC is an ignitability driver in the same vegetation species while the amount and perhaps the identity of the volatiles evolving from cellulose decomposition are the ignitability drivers in different vegetation species. Therefore, it is essential to identify these volatiles from both species, their diversity, and abundance using Py-GC/MS in order to configure their role in ignition.

9 Py-GC/MS Results, Analysis, and Discussion

9.1 Pyrolysis Results

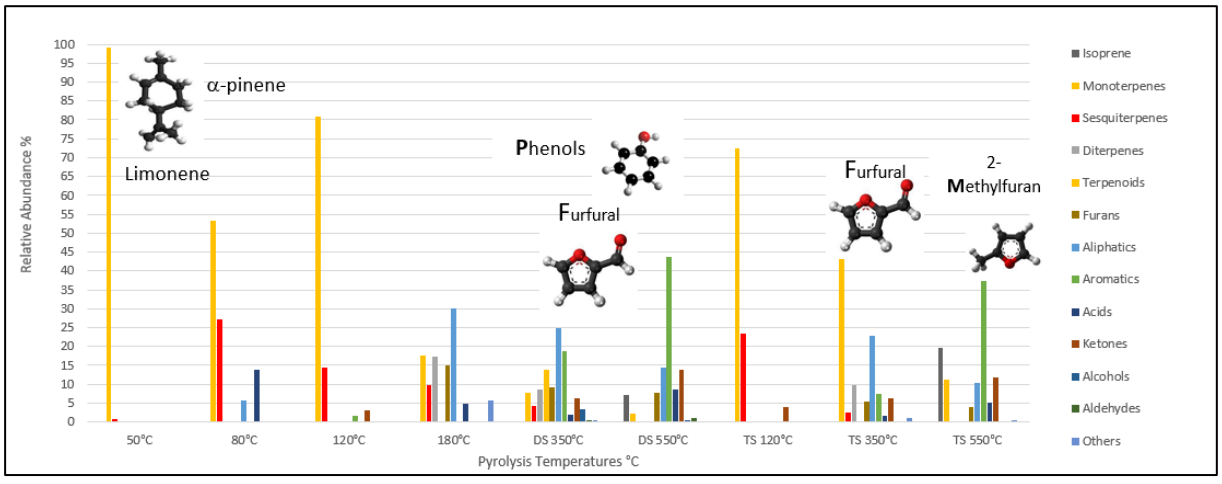

DS: Double Shot. TS: Triple Shot. LC: Long Chain.

Figure III.19. Relative abundance (%) of emissions from the pyrolysis of *Cupressus s. L.* litter leaves (dry season) at 50°C, 80°C, 120°C, 180°C, DS (350 & 550°C), and TS (120, 350 & 550°C).

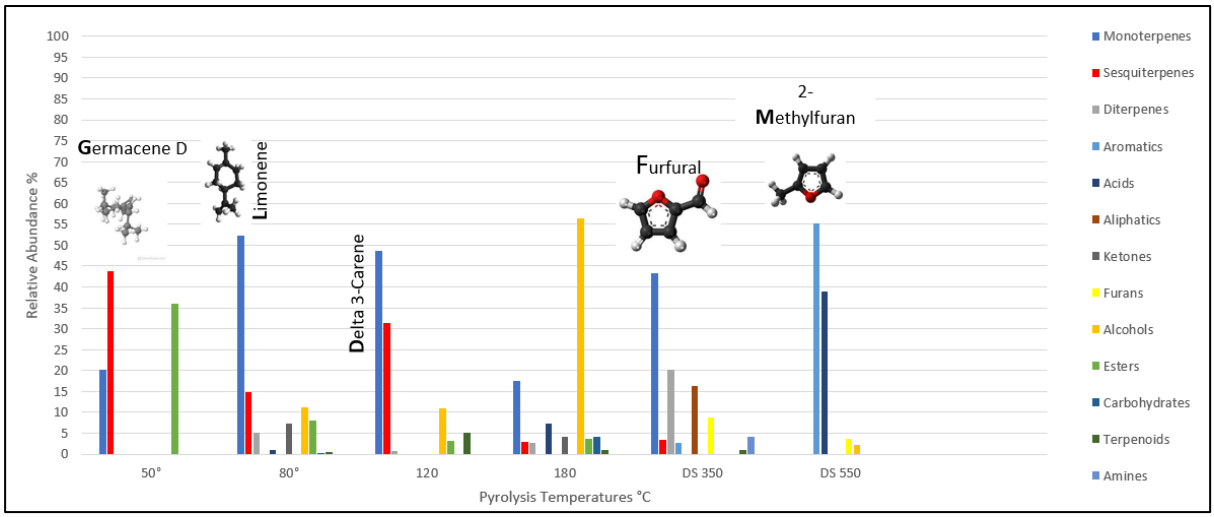

Figure III.20. Relative abundance (%) of emissions from the pyrolysis of *Cupressus s. L.* litter leaves (wet season) at 50°C, 80°C, 120°C, 180°C, and DS (350 & 550°C).

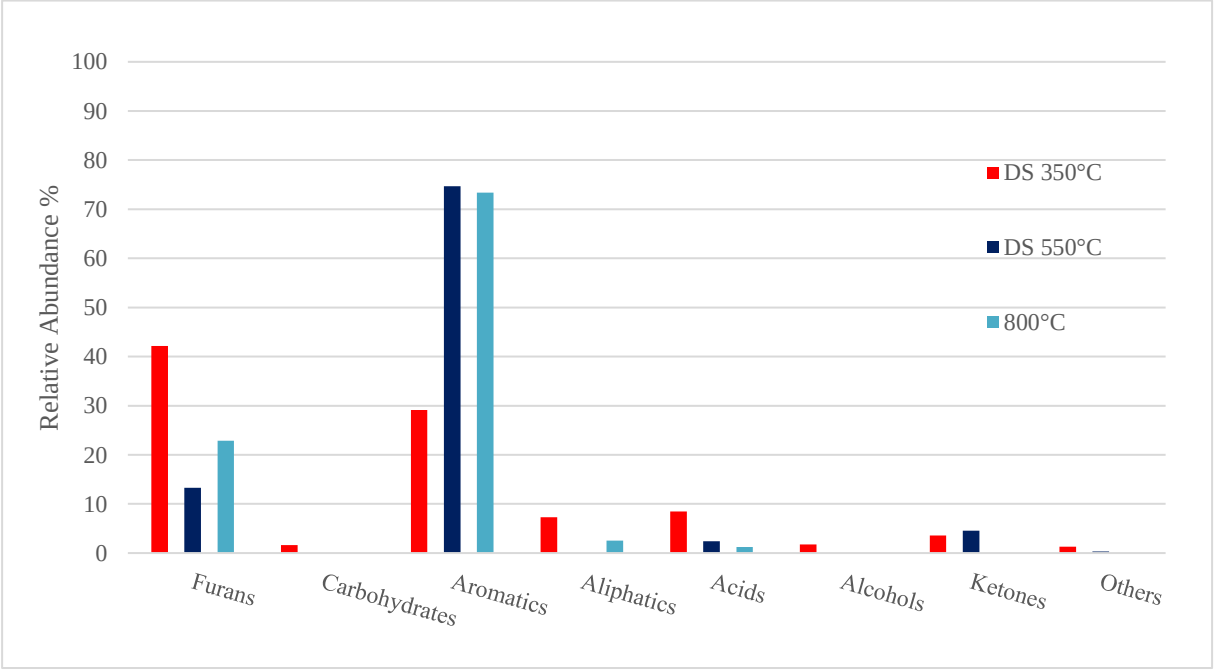

Figure III.21. Relative abundance (%) of emissions from the pyrolysis tests on *Quercus Suber L.* litter leaf samples at 800°C, and DS (350 & 550°C).

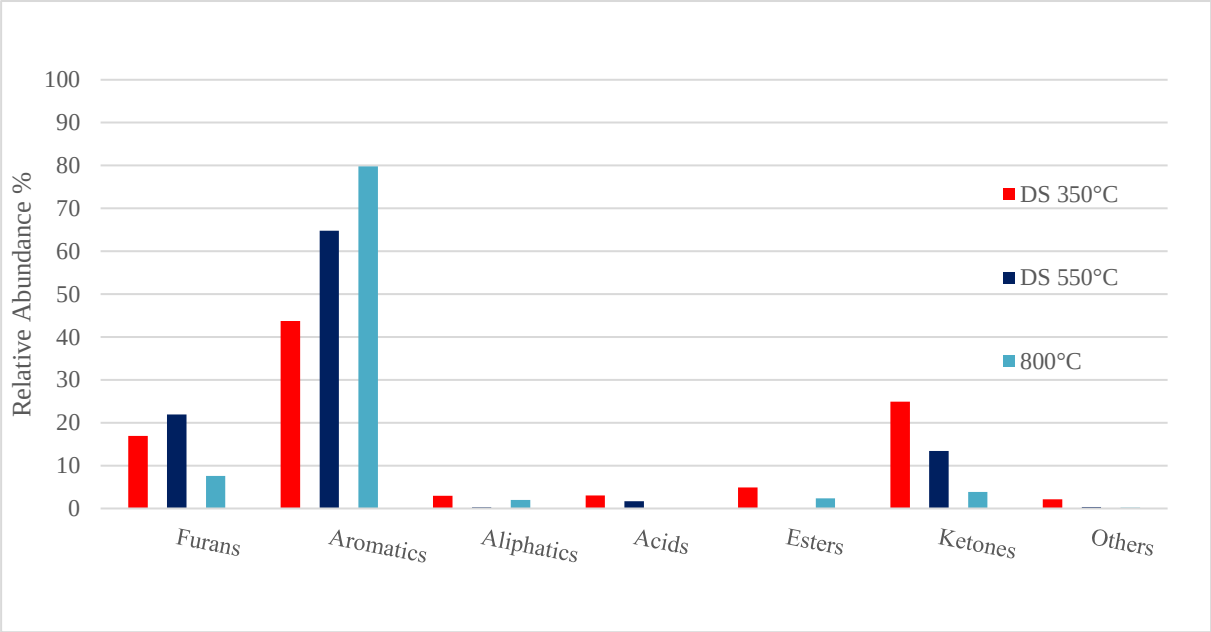

Figure III.22. Relative abundance emissions from the pyrolysis tests on *Quercus Suber L.* branch samples at 800°C, and DS (350 & 550°C).

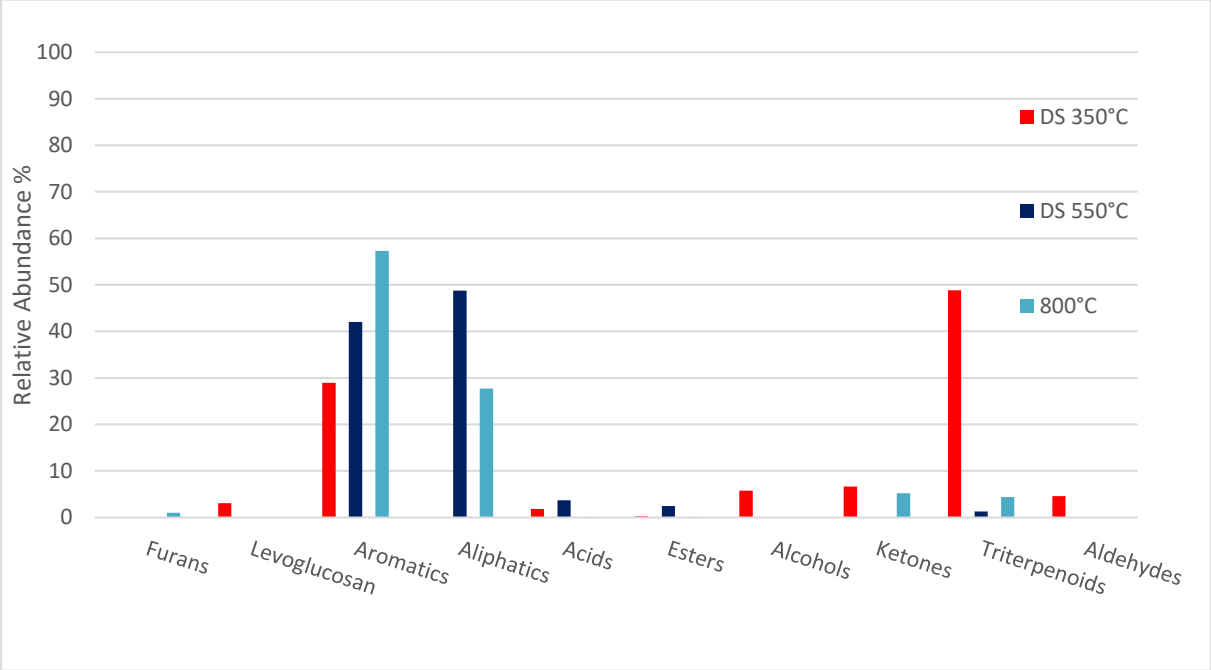

Figure III.23. Relative abundance emissions from the pyrolysis tests on *Quercus Suber L.* cork samples at 800°C, and DS (350 & 550°C).

9.2 Pyrolysis Results' Analysis

As we observed so far, live and litter *Q.s.L.* were more ignitable than those of *C.s.L.* but less combustible. Both live and litter foliage of *C.s.L.* had more FMC and less decomposed cellulose than those of *Q.s.L.* therefore, the theories relating FMC negatively and cellulose decomposition positively to ignitability, were only valid when comparing different vegetation species. However, these theories do not apply when comparing live and litter fuels from the same vegetation species from summer season, probably because FMC has overridden the role

of cellulose decomposition in driving ignitability in the same vegetation species. Live fuels of both species with higher FMC and less cellulose decomposition, were more ignitable than their litter but less combustible. However, both FMC and cellulose decomposition roughly from 300 to 400°C, have driven the ignitability in litter from wet season over the litter from the dry season for *C.s.L*. Analyzing the foliar chemical content of the two species would give more information on their distinctive flammability characteristics, especially that FMC cannot be considered a flammability driver by itself so probably the volatiles (mainly terpenes) carried by the evaporating moisture provide a better explanation. Despite the fact that studies linking terpene content and flammability are limited in comparison to those dealing with the impact of FMC or other leaf traits, there must be a role in ignition played by the volatiles emitted during the dehydration and devolatilization stages, as shown in Figure III.24, (Riaza et al. 2017).

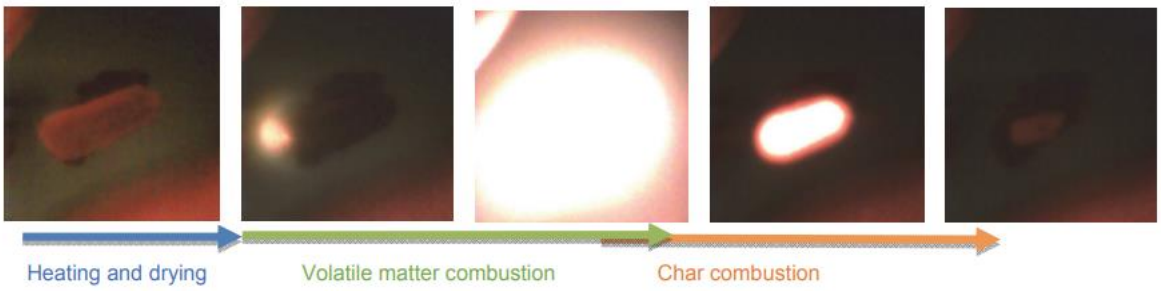

Figure III.24. Sequential steps of the combustion of a biomass particle in air atmosphere, (Riaza et al. 2017).

The ignition lays between the preignition and the combustion stage. The preignition phase where low molecular weight molecules (terpenes) are volatilized and carried away by evaporating FMC, get overlapped by the volatiles emerging from holocellulose depolymerization before they reach their flammability limits at a certain temperature and pressure (normally atmospheric pressure) and ignite. Many studies related biomass foliar ignitability to FMC, however few related them to their volatile content, especially terpenes (Romero et al. 2019, Della Rocca et al. 2017). These researchers have compared the flammability of live and litter biomass only, however, none have investigated seasonal litter flammability although our experiments showed higher ignitability of litter from wet season compared to dry season. A recent study addressed seasonal foliar FMC and terpene content of Mediterranean species including Cupressus sempervirens and related them to their flammability characteristics (Ganteaume et al. 2021). Figures III.19 & 20, illustrate the percentages of the different volatiles emitted from pyrolyzing *C.s.L*. litter from dry and wet seasons, respectively. Starting at low temperatures in order to configure the identity of volatiles emitted in the preignition phase where dehydration and volatilization occur (50 to 180°C), cellulose decomposition at 350°C and lignin decomposition at 550°C. The double shot (DS), at 350 and 550°C were done in order to simulate cellulose and lignin consecutive decomposition, while the triple shot (TS) at 120, 350, and 550°C were done in order to simulate volatilization, cellulose and lignin decomposition bearing in mind that these processes overlap over such temperature ranges. Figures III.21, 22 & 23, illustrate the percentages of volatiles evolving from *Q.s.L*. foliar litter, branches, and cork, respectively.

9.3 Discussion

9.3.1 *C.s.L.* (dry & wet seasons) Volatilization at Low Temperatures 50, 80 & 120°C & Flammability

The pyrolysis of *C.s.L.* litter in both seasons resulted in a wide range of terpenes, furans, aliphatic, aromatics, alcohols, ketones, and acids. Esters and terpenoids were emitted solely from wet season *C.s.L.* Terpene emissions started from temperatures as low as 50°C until 350°C for wet season (winter) and 550°C for dry season (summer). However, the relative percentages of monoterpenes were higher from *C.s.L.* (dry season) than from wet season probably because their reserves increase in foliage under abiotic stresses before falling. The dehydration phase (preignition) in the range from 40 to 100°C for dry season and from 40 to 120°C in wet season has resulted in terpenes devolatilization. Notably, esters (i.e., terpinyl acetate) were emitted from wet season *C.s.L.* with relative percentages of 35.8% at 50°C, 7.9% at 80°C, 3.2% at 120°C, and 3.6% at 180°C. Although esters at these low temperatures can be considered products of hemicellulose or early lignin degradation, no esters were emitted by *C.s.L.* litter from dry season. The flammability parameters of *C.s.L.* litter were poorly correlated to terpenes content when FMC was not considered, however when FMC was included as independent variable, combustibility and sustainability decreased while consumability increased with terpene content (Della Rocca et al. 2017). This probably explains the higher consumability but less combustibility of *C.s.L.* from wet season with higher FMC especially that higher FMC reduced the LDMC. Taking FMC as an independent factor, sesquiterpenes content is linked to higher ignitability (less TTI) and higher consumability while monoterpenes decrease ignitability and consumability (Della Rocca et al. 2017). This may explain the higher relative ignitability and consumability (less ash content) of *C.s.L.* from wet season compared to *C.s.L.* from dry season, given that the first had higher sesquiterpene relative abundance in the preignition phase (43.8%, 14.8%, & 31.3% at 50°C, 80°C, and 120°C) compared to the second (0.8%, 27%, &14.8% at 50°C, 80°C, and 120°C). Winter *C.s.L.* showed more diversity in sesquiterpene content compared to the summer season (5 vs 3, respectively) which agrees with the findings of Ganteaume et al. (2021). Monoterpene relative emissions were also higher from the *C.s.L.* of dry season at low temperatures (99.1%, 53.3%, & 80.81% at 50°C, 80°C, and 120°C) compared to their emissions from *C.s.L.* from wet season (20.3%, 52.2%, & 48.5% at 50°C, 80°C, and 120°C). High monoterpene diversity was detected from *C.s.L.* (dry season) where 11 monoterpenes were identified including α-pinene, 2-thujene, β-myrcene, 3-carene, limonene, γ-terpinene, and sabinene, while only 5 monoterpenes were detected from the *C.s.L.* (wet season) which may be an indication that abiotic stresses such as high summer temperatures and drought tend to increase monoterpene production and reserves in certain Mediterranean species such as *Cypress* (Llusià and Peñuelas 1998, Ormeño et al. 2007). Therefore, their litter in dry season are richer in monoterpenes than in wet season. FMC content and leaf thickness were linked to biomass fuel time to ignition (positive effect) however the higher FMC will mean higher volatilization rate of the stored volatiles especially if the volatiles are not stored deeply inside the leaves such as the sub-epidermal glands in *C.s.L.* (Romero et al. 2019). Similar results of higher temperatures to ignition for summer *C.s.L.* compared to winter *C.s.L.* were also found by Ganteaume et al. (2021). Diterpenes were also related negatively to flammability i.e.; higher total diterpene content excluding totarol increases TTI (Ganteaume et al. 2021). This is evident

in our results because the relative abundance of diterpenes in samples from dry season which showed higher temperatures to ignition (delayed ignition), were higher than their relative abundance from the samples of the wet season which ignited more readily. Concerning the diversity of diterpenes, 7 different diterpenes were emitted from summer season samples while 5 were emitted from the wet season, these results agree with the findings of Ganteaume et al. (2021), who found 7 diterpenes from *C.s.L*. in winter and 8 in summer. One differing diterpene, totarol, was found to enhance flammability (decrease TTI) (Ganteaume et al. 2021), was emitted from *C.s.L*. winter samples at temperatures as low as 80°C while it was emitted at 350°C from C.s.L. of dry season. Overall, the major difference between the emissions of *C.s.L*. litter (wet season) and *C.s.L*. litter (dry season) which may be correlated to the pronounced ignitability of the first over the second, is the significant relative abundance of the sesquiterpenes emitted in the preignition stages at temperatures as low as 50°C from the first compared to the second. Of course, further evidence should be pursued in order to confirm the correlation between FMC and sesquiterpenes and their role in driving the ignitability of litter leaves of *C.s.L*.

9.3.2 *C.s.L*. Leaf Litter (dry season) Pyrolysis at High Temperatures, 180°C, DS (350-550°), and TS (120-350-550°C)

Low pyrolysis temperatures break down the chemical bonds between the monomers of holocellulose and lignin polymers in the leaves leading to the emissions of VOCs and rearrangement of the chemical bonds existing in the matrix of the residual fixed carbon. Early depolymerization traces (furans, acids, and some phenols) emerged at 180°C which may originate from hemicellulose or lignin, were noticed to overlap with cellulose decomposition at 350°C through the emergence of 5-hydroxymethylfurfural. The main components from cellulose decomposition at double shot (DS) 350°C, are furans such as furfural, 2,3-dihydrobenzofuran and ketones such as 2-2-methylpropylidene-cyclohexanone. However, there were no traces of anhydrosugar derivatives like levoglucosan or levoglucosenone, which normally emerge from hemicellulose pyrolysis at 250 °C or cellulose pyrolysis at ~350°C (Chen et al. 2019). The primary products of lignin degradation are phenols and aldehydes. Bearing in mind that lignin decomposition covers a wider range that starts slowly at 138°C and accelerates from 370°C towards 700°C (Chen et al. 2019). However, the main pyrolytic products of lignin were the aromatic hydrocarbons, phenolics (2-methoxy-4-vinylphenol & phenol-2-methoxy-3-2-propenyl), and hydroxy-phenolics (pyrocatechol & creosol) at DS 350°C. Other lignin degradation compounds at DS 350°C were also aldehydes (citral, and 2,3-dihydroxybenzaldehyde) and ketones (Cyclohexanone, 2-(2-methylpropylidene)-) whereas those originating from lipid were free fatty acids such as tetradecanoic acid (C14) and pentadecanoic acid (C15) and long chain aliphatics (n-alkanes) from C27 to C35 originated from epicuticular waxes (cutin). Monoterpenes (sabinene), sesquiterpenes (cedrene & alpha-cubebene), and diterpenes (trans-totarol & ferruginol) were emitted from C.s.L. (dry season) at DS 350°C as a result of distillation and not pyrolysis. Cellulose decomposition decreases at DS 550°C after its torrefaction at DS 350°C, especially that furfural no longer exists and 5.3% of 2-methylfuran is detected, presumably from the conversion of furfural (Chen et al. 2019). The release of oxygenated compounds at DS 350°C increases the percentage of the fixed carbon formed (char). Therefore, temperature of DS 550°C, breaks down the bonds in char as aromatization takes place to release phenol (7.9%), unsubstituted aromatics such as toluene

(4.5%) and xylene (3.8%), and polycyclic aromatic hydrocarbons (PAH) in less amounts such as naphthalene, 2,6-dimethyl- (0.5%). Temperatures higher than 550°C are most likely to increase the amounts of PAH. More compounds indicating lignin degradation at DS 550°C, are ketones as 1,2-benzenediol, 4-methyl- (4.14%), phenol derivatives as isoeugenol (0.6%), and aldehydes as benzaldehyde, 2,4,6-trimethyl- (0.4%). Macrocyclic lactones such as oxacycloheptadec-8-en-2-one (ambrettolide) was also detected at a percentage of 6.2%. A very important observation was the detection of isoprene at DS 550°C with a high relative abundance of 7.2% which may be an indication of degradation under high temperature stresses as there are no particular structures to store isoprene in leaves. On the other hand, the triple shot (TS) pyrolysis allows to study the effect of torrefaction at 120°C on the stability of cellulose and lignin thermal degradation (fragmentation and depolymerization) at higher temperatures 350 and 550°C. While observing the results, it looks like the TS120°C had no effect on cellulose decomposition especially that the relative content of furfural has increased by 1% at the TS 350°C compared to the DS 350°C i.e., 5.5% vs 4.5%, respectively. Aromatics relative percentages at TS 350°C (7.3%) were less than those detected at DS 350°C (18.8%), presumably because of the higher monoterpenes detected from the leaves at the TS (43%) compared to the DS (7.8%) at 350°C. Although the relative abundance of monoterpenes detected at TS 120°C was relatively high (72%) it seems that such a thermal stress has induced some kind of cellular damage that lead to the release of more monoterpenes at TS 350°C. Isoprene detected at TS 550°C was of a higher relative abundance (19.7%) compared to DS 550°C, probably because the thermal stresses were applied two times at 120 and 350°C prior to 550°C. Finally, although the total aromatics detected at TS 550°C were less than those detected at DS 550°C the phenolics detected from lignin degradation at TS 550°C such as phenol, phenol- 2-methoxy, and phenol-3-methyl were more pronounced than those detected at DS 550°C. Neither esters nor carbohydrates, were detected from *C.s.L.* litter leaves (dry season) throughout the whole pyrolysis temperatures.

9.3.3 C.s.L. Leaf Litter (wet season) Pyrolysis at High Temperatures, 180°C and DS (350-550°)

The first observation from C.s.L. (wet season) pyrolysis at 180°C is the high relative abundance of oxygenated compounds such as alcohols and ketones. The elimination of these oxygenated compounds leads to the formation of double bonds $C = C$, which are responsible for the evolution of furan rings in the cellulose char (Collard & Blin 2014). Anhydrosugars (4H-pyran-4-one, 2,3-dihydro-3,5-dihydroxy-6-methyl-) signaling cellulose decomposition (Ojha & Vinu 2015) were also detected with a relative percentage of 4.08% at 180°C. Surprisingly, similar monoterpenes abundance was detected from *C.s.L.* wet season compared with dry season, 17.4% at 180°C. The DS 350 and 550°C pyrolysis, also showed different composition of the compounds detected for example percentages of monoterpenes and diterpenes were higher (compared to dry season) at DS 350°C, 43.3%, and 20.2%, respectively. Furans, furfural from cellulose degradation and 2-furanmethanol from lignin degradation were also detected at 350°C, however aromatics presumably from lignin degradation, are very low (2.7%). DS 550° was the temperature of major lignin degradation as aromatics (mainly phenols) were detected at 55.3% and fatty acids methyl esters (FAME) produced from the pyrolysis of lipid and lignin mixtures in the leaf litter i.e., 9,12-octadecadienoic acid (Z, Z)-methyl ester at 33.7%. Fatty acid methyl esters are the most important constituents of biodiesel (Babinszki et al. 2022) therefore,

their important abundance from litter leaves of *C.s.L.* in wet seasons makes these last very important lipid-containing lignocellulosic biomass structures that could be considered in renewable energy resources. Although the exact degradation mechanism is still lacking however, a DS 350 – 550°C using Py-GC-MS is a beneficial start to configure the detailed degradation process.

9.3.4 Q.s.L. Leaf Litter Pyrolysis at High Temperatures DS (350-550°C) and 800°C

When observing the compounds emerging from *Q.s.L.* litter at DS 350°C, furans some from cellulose decomposition (furfural, 2-5-methyl-furancarboxaldehyde) and others from lignin (2,3-dihydro- benzofuran) formed about 42.13% of the total emissions. Furan derivatives from *Q.s.L.* cellulose alone (22.84%) exceeded those resulting from *C.s.L.* (dry season) (9.05%) therefore, a higher percentage of cellulose decomposing from *Q.s.L.* may support their higher ignitability, presumably the criteria of Liodakis et al. (2002) applies. Moreover, cellulose decomposition continues to occur at the higher temperature of the double shot (550°C) with furan derivatives forming 13.29% which still exceed those emerging from cypress (7.78%). Lignin decomposition overlaps that of cellulose at DS 350° through a relative abundance of 29.10% of aromatics mainly phenols (13% of phenol & 5.65% of 2-methoxy-4-vinylphenol) and 19.29% of 2,3-dihydro-benzofuran, compared to a relative abundance of 19.4% of aromatics (11.46% of pyrocatechol) from *C.s.L.* Lignin decomposition increases rapidly at DS 550°C as the relative abundance of aromatics reaches a high of 74.67% (24.28% of phenol, and 13.04% of toluene) compared to 43.61% (7.9% of phenol & 4.5% of toluene) for *C.s.L.* The same percentage of aromatics emerge at 800°C from *Q.s.L.* On the other hand, aliphatics (n-alkanes) emerging from *Q.s.L.* at DS 350 and 550°C (7.31% and 0.32%) are very low compared to those emerging from *C.s.L.* (24.2% and 14.5%) probably because the cuticular waxes are more abundant in cypress leaves. Aliphatic compounds were almost null at DS 550°C from *Q.s.L.* litter leaves except for the steroid hydrocarbon stigmastan-3,5-diene. No terpenes seemed to be detected from *Q.s.L.* at all temperatures, which may support the theory that *Quercus suber L.* are non-isoprenoid emitters and have no terpene storage compartments in their foliage however, further confirmation is probable through pyrolysis testing should at low temperatures where terpene volatilization is maximized with moisture evaporation. Finally, the higher combustibility of *C.s.L.* as opposed to *Q.s.L.* in both decomposition phases (Figure III.15) can be explained by the emission of terpenes from the first and their absence in the second, because terpenes have higher calorific values (avg. 1480 kcal/mol) compared to for example phenols (729 kcal/mol), (Hawkins & Eriksen 1954). The higher ignitability of *Q.s.L.* however, could be explained by the hypothesis that the mixtures of gases evolving in the preignition phase have lower flammability limits than those evolving from *C.s.L.*

9.3.5 *Q.s.L.* Branch Pyrolysis at High Temperatures DS (350-550°C) and 800°C

Furan derivatives originating from cellulose decomposition in branches are of considerable percentages compared to leaves starting from 16.95% at DS350°C and reaching a maximum of 21.91% at the second shot (550°C), probably because of the different inherent structures and chemical nature of cellulose in branches that increase wood thermal stability, in contrast to foliage. Besides, higher lignin content indicates a higher thermal stability of biomass structures which is evident from lignin derived aromatics such as phenols (12.25% of phenol, 9.98% of 2-methoxy-phenol) form about 43.71% of the emissions at DS 350 and about 64.7% at DS

550°C. The degradation of the higher molecular weight compounds at 350°C results in an increase in the amount of aromatic compounds at 550°C. This is why the percentages of 2-Methoxy-4-vinylphenol for example decreases from 6.87% at 350°C to 4.91% at 550°C while those of phenol and 2-methoxy-phenol increased from 5.85% to 12.25% and from 0% to 9.89%, respectively. Toluene was emitted at a percentage of 6.68% at the second shot 550°C, however its percentage was 4.5 times higher at SS 800°C (30.16%). Given that toluene percentages have only doubled for leaves between 550°C after the first shot 350°C, and the SS 800°C.

9.3.6 *Q.s.L.* Cork Pyrolysis at High Temperatures DS (350-550°C) and 800°C

Extractives are low or medium molecular weight molecules that are readily removed from biomass by solvent extraction without affecting its cellular structure (Pereira 2007). These compounds are divided into lipophillic (triterpenes, fatty acids, n-alkanes, ...) and polar (phenolics and sugars). Cork contains more extractives than wood, mainly triterpenes from the families of friedelan, by which the triterpenoid ketone friedelan-3-one (friedelin) forms about 1% if its weight (Pereira 2007). This extractive formed the majority of the compounds detected at DS 350°C from cork with a relative abundance of 43.86% in addition to phenolics such as 2-methoxy-4-vinylphenol (14.98%). Ketones such as 1-(4-hydroxy-3-methoxyphenyl)- 2-propanone at 350°C, was seperated from triterpenoids because it originates from lignin depolymerization.Vanillin, a value-added chemical, represents a major constituent of the volatiles produced from the thermal degradation of lignin in cork at low reaction temperatures (Chen et al. 2019) was released at a percentage of 4.96% at DS 350°C. No vanillin was detected at higher temperatures DS 550°C or SS 800°C. Levoglucosan from cork cellulose degradation was detected at a percentage of 3.10% at 350°C. One third of extractives that form about 5 – 8% of cork include triterpenes, n-alkanes (from C25 to C35), n-alkanols (C16 to C36) and long chain fatty acids, whereas, phenolics form about 6 – 9% of cork (Pereira 2007). Aliphatics from cork are null at the first shot of 350°C, but they increase significantly at the second shot 550°C (48.75%), however they are only 27.2% at SS 800°C. This may support the theory suggested by Collard and Blin (2014), that at temperatures higher than 300°C, most of the C–C bonds within and between the alkyl chains become unstable and react to release more aliphatics (Collard & Blin 2014). Besides, formation of oxygenated compounds from the breakage of ether bonds of lignin at low temperatures (i.e., 350°C) permits the release of aromatics at higher temperatures (550°C), which explains the increase of aromatics from cork from 28.9% to 42.04%. However, aliphatics and aromatics may be originating from another source in cork, suberin. While cellulose and lignin form an average of 22% and 12% of cork, respectively, suberin accounts for more than 45% forming more than half of the cork solid material while lignin forms a one third, (Pereira 2007). Its high thermal stability provides an insulation characteristic of *Quercus suber L.* at the bark level. Chemically, suberin is a complex lipid polymer consisting of a fatty acid-derived domain (aliphatic suberin) that is cross-linked by ester bonds to a polyaromatic lignin-like domain (aromatic suberin), (Yao et al. 2012). Aliphatic suberin is normally quantified by the aliphatic compounds released during depolymerization (Pereira 2007) however, the differentiation between lignin and the suberin-associated polyphenolic moiety remains a hardship in scientific research. Py seems not to be an efficient method to simultaneously differentiate between the compounds emitted from suberin or lignin, however a study done by Costa (2019), identified the compounds from cork lignin and suberin

of three different oak provenances and found that the compounds emerging from suberin were fatty acids, alkenes, alkanes & alkadienes while the compounds emerging from lignin were of phenol, guaiacol, and syringol types. Therefore, it is safe to consider that the relative abundance of aliphatics and fatty acids from cork at DS (350°C – 550°C) and SS 800°C originate solely from suberin. Zero aliphatics and 1.84% of fatty acids at 350°C and respective 27.72% and 0.14% at 800°C, prove the high thermal resistance of suberin.

9.3.7 Emissions by Source from *C.s.L.* and *Q.s.L.* Leaf Litter (Dry Season) at DS (350 – 550°C)

The compounds emitted from the leaf litter of *C.s.L.* and *Q.s.L* (dry season) are categorized according to the source they derive from, Figure III.25. Literature was used to categorize the compounds that derive from cellulose, lignin, and cuticular wax (in *C.s.L.*), lipid and cutin (in *Q.s.L.*). The categorization aims at understanding better the relationship between the polymer decomposition and litter ignitability, especially cellulose as suggested by Liodakis et al. (2002). Cellulose compounds were mainly furan derivatives, anhydro-sugars, ketones, esters, aldehydes, alcohols, and if applicable acetic acid (Chen et al. 2019, Ojha &Vinu 2015, Marques et al. 2007), lignin compounds are mainly of phenol guaiacol, syringol, catechol types (Chen et al. 2019b) in addition to mono- and polycyclic aromatic hydrocarbons (Shen et al. 2023), and n-hexadecanoic acid, whereas cuticular wax and lipids were long chain n-alkanes, n alkanols, alkadienes, alkenes, triterpenoids, and fatty acids (Costa 2019, Marques et al. 2006, Gupta et al. 2007). Terpenes (isoprene, mono, sesqui and diterpenes) were not attributed to any source as they are volatilized by distillation process rather than pyrolysis.

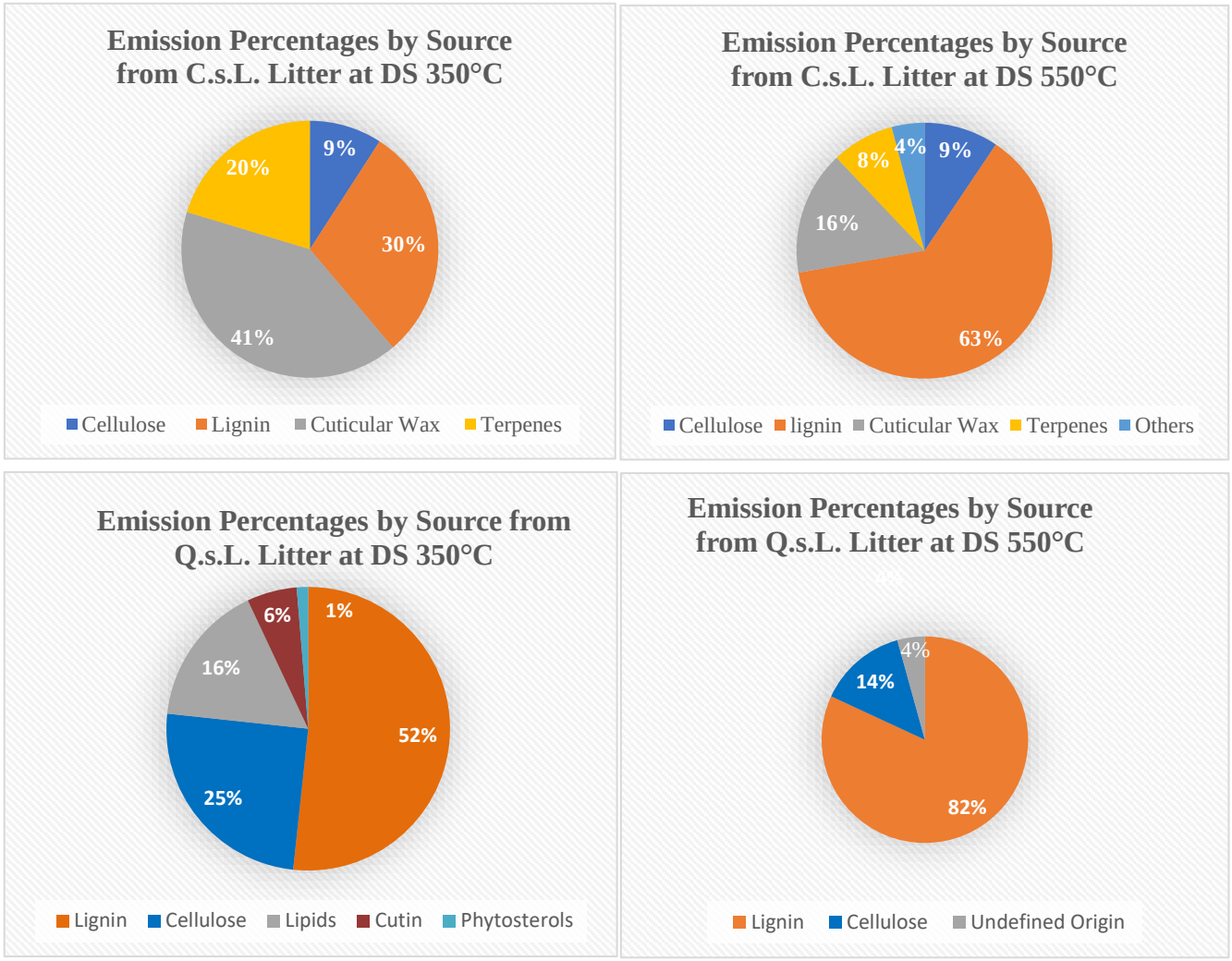

Figure III. 25. Identified compounds from Py of *C.s.L.* and *Q.s.L.* leaf litter according to source at DS 350 and 550°C.

As expected the amounts of cellulose decomposed from *C.s.L.* at both shots of the DS 350-550°C were both less than those of *Q.s.L.* which may explain their lower ignitability presumably the criteria of Liodakis et al. (2002) applies. Lignin decomposition on the other hand, was higher from *Q.s.L.* at both temperatures although the lignin percentages in *C.s.L.* are of high values as well. This can be referred to the higher FMC of *C.s.L.* that results in less LDMC and thus less lignin percentages (Alam et al. 2019) however, these percentages remain only relative. Indeed, *C.s.L.*, are conifers which are poor in cellulose and rich in lignin (Mason et al. 2016). Unfortunately, the hypothesis suggested by Mason et al. (2016) that biomass with higher lignin percentages thus richer in phenols, combust at higher temperatures was not verified by our results. For instance, phenols from lignin in *C.s.L.* formed a total relative abundance of 18% while phenol alone from *Q.s.L.* formed 24.28% at DS 550°C. On the other hand, the higher combustibility of *C.s.L.* explained by their larger 2nd exothermic peak areas, is probably referred to their higher terpene emissions and cuticular wax derivatives at both temperatures (350°C & 550°C). All the identified compounds from *C.s.L.* leaf pyrolysis and *Q.s.L.* leaf, branch, and cork pyrolysis (Py) can be found in appendix AIII.1 and AIII.2, respectively.

10 Conclusion

Several biomass flammability assessment criteria including, FMC, the amount of cellulose decomposition, the ash content, the burnout temperature, the lignin content, and others, have been utilized throughout this work to verify and compare the flammability descriptors of two important Mediterranean forest species; *Cupressus sempervirens L.* (cypress) and *Quercus suber L.* (oak). These species are categorized by the forest fire management community as fire resistant at different scales; cypress on leaf scale, and oak on bark scale. However, since foliage (fresh and litter) are considered the primary structures consumed by surface and crown forest fires, it was important to compare the flammability of the two species based on; the ease of their foliage to ignite, their heat of combustion indicating their combustibility, and how much of the biomass is consumed in combustion indicating their consumability. *Q. suber L.* is considered a valuable forest species for its economic value however, it is widely consumed in wildfires occurring in MCR. On the other hand, *C. sempervirens L.* has survived devastating wildfires around the world and it could be used as a silviculture measure to protect the fire endangered *Q.s.L.* species. We have compared the amount of cellulose decomposing with the temperature of the first ignition. Our findings have ended in the conclusion that live and litter foliage of C.s.L. are less ignitable than live and litter Q.s.L., respectively however, they are more combustible. The higher ignitability of Q.s.L. conformed with the increase in their cellulose decomposition amount. Surprisingly, the cellulose assessment criteria didn't work when comparing the ignitability of the live and litter foliage of the same species. Live C.s.L. and live Q.s.L. were more ignitable than their respective litter but less combustible, which evokes a role of FMC in increasing the ignitability of biomass leaves. However, a higher FMC of cypress leaves (live and litter) didn't increase their ignitability over oak leaves (live and litter). Seasonal (dry vs. wet season) litter of C.s.L. has shown a higher FMC of the wet vs. the dry season samples, the samples from the wet season were more ignitable with higher cellulose content. Therefore, the criteria relating cellulose decomposition to ignitability only applies to similar biomass types (e.g. litter foliage or live foliage) of different species or seasonal litter of the same species but not to live vs. litter foliage of the same species. The pyrolysis experiments conducted to verify the role of the identities of emitted volatiles in the advanced ignitability of *Q.s.L.* over *C.s.L.* is probably explained by the high amounts of terpene volatiles from *C.s.L.* which were gasified by distillation at early temperatures (50°C, 80°C, and 120°C) and continued to be emitted at temperatures as high as 350°C and 550°C including isoprene, surprisingly. No terpenoids were emitted from the pyrolysis of *Q.s.L.* at 350°C, 550°C or 800°C which may support the fact that they are non-isoprenoid emitters, however other tests at lower temperature ranges are recommended to support this theory better. Lower cellulose content of *C.s.L.* compared to *Q.s.L.* is supported by the lower percentages of relative emissions deriving from cellulose from the first compared to the second, which support their respective lower and higher ignitability, respectively. The higher combustibility of *C.s.L.* when ignited compared to *Q.s.L.* is probably referred to the higher calorific values of terpenes emitted by *C.s.L.* and not by *Q.s.L.* which mainly emitted phenols (e.g. at 350°C). Further studies calculating the flammability limits of the mixture of gases evolving from both species should be further conducted to understand better their ignitability variance. On a leaf scale, *C.s.L.* species can present an ignitability delaying barrier to protect *Q.s.L.* species in wildfires however, on a tree scale further experimentation should be done in order to verify the optimal plantation strategies

of *C.s.L*. (structure, number, density, layers, …etc.) in order to achieve better protection from wildfires threats.

CHAPTER IV

*****

Influence of Hydric Stress on VOC Emissions Under Thermal Stresses from Mediterranean Shrub Species: *Rosmarinus Officinalis* and *Cistus Albidus*

Résumé

Stress abiotiques et émissions de la végétation

Le changement climatique, accompagné de périodes de sécheresse prolongées et de températures extrêmes, augmente les risques d'initiation et de propagation des incendies. Selon un article récent publié dans « The Guardian » en février 2022, on s'attend à ce que les incendies de forêt qui ont frappé la Californie, l'Australie et la Sibérie deviennent 50 % plus fréquents d'ici la fin du siècle, le changement climatique étant le principal facteur de changement. D'après nos études et la littérature, il est évident qu'une relation existe entre les descripteurs d'inflammabilité de la végétation, leurs contenu volatil, leurs taux d'émission. Il a également été constaté que la présence ou l'absence de réservoirs de stockage de terpènes dans les espèces végétales interfère avec les modèles d'émissions volatiles, à l'example des terpènes. Cependant, la controverse est de savoir s'ils affectent ou non leurs taux d'émission (Llusià *et al.* 2009, Ormeño *et al.* 2007). La certitude est que lorsque ces zones de stockage sont endommagées par des facteurs externes tels que des incendies, les taux d'émission sont modifiés de manière remarquable. *Cistus albidus* (*Cistaceae*) et *Rosmarinus officinalis* (*Lamiaceae*), sont deux espèces de bois arbustif largement consumées par les feux de forêt et elles sont parmi les premières à émerger après un feu de forêt (Serbouti *et al.* 2022). Ce sont à la fois des espèces stockant des terpènes avec des compartiments de stockage différents, des poils glandulaires foliaires pour le premier et des organes sécrétoires, tels que les trichomes glandulaires pour le second. À mesure que les taux de photosynthèse et la conductance stomatique diminuent en réponse à la sécheresse, les taux d'émissions de COVB des ces espèces diminuent considérablement et, par conséquent, leurs réserves de terpènes devraient être maintenues. Notamment, les émissions de terpènes ont diminué et leurs réserves (à l'exception des sesquiterpènes) se sont avérées minimes chez *C. albidus* après un traitement à court terme par sécheresse induite (Llusià & Peñuelas 1998) et des sécheresses saisonnières (Llusià et al. 2009) à moins qu'elles ne soient bien irriguées avant la saison sèche. Les monoterpènes émis par *C. albidus* proviennent directement de la synthèse *de-novo* tandis que les sesquiterpènes sont plus susceptibles de provenir des bassins de stockage (Ormeno *et al.* 2007). Quant à *R. officinalis*, certaines études n'ont trouvé aucun effet du stress hydrique sur leurs émissions de monoterpènes et ils ont été attribués à des espèces résistantes bien adaptées à la sécheresse, d'autant plus que leurs émissions de monoterpènes ne reflétaient aucune inhibition photosynthétique sous stress hydrique (Peñuelas & Llusià 1997). Différents résultats ont été trouvés par Nogues *et al.* (2015), où les émissions de monoterpènes ont augmenté sous des stress légers et diminué sous des stress de sécheresse sévères (Nogués *et al.* 2015). Il semble que les émissions de monoterpènes des espèces de *Lamiaceae* dépendent de la sévérité de la sécheresse.

Objectif de ce travail

Notre objectif est d'investiguer expérimentalement les identités et les taux d'émission des COV des deux espèces : *Rosmarinus officinalis L.* et *Cistus albidus*, sous stress thermique après les avoir soumis à des périodes de forte sécheresse sous serre. Les stress thermiques ont été réalisés à l'échelle de la plante et à l'échelle de la feuille. À l'échelle de la plante, des plantes stressées et non stressées hydriquement de chaque espèce ont été placées face à un panneau radiant

jusqu'à atteindre 200°C, et les émissions ont été collectées à l'aide de tubes adsorbants (Chemisorbers) pour être thermodesorbées et analysées par Py-GC/MS dans une atmosphère inerte. À l'échelle des feuilles, des échantillons de feuilles ont été prélevés sur des plantes stressées et non stressées hydriquement pour chaque espèce et leurs émissions ont été analysées à une température de 180°C à l'aide d'une analyse Py-GC/MS sous atmosphère inerte. Des analyses physiologiques ont également été réalisées à l'échelle des feuilles témoins et stressées hydriquement pour chaque espèce végétale afin de comparer leurs mécanismes d'adaptation aux sécheresses sévères. Cette étude vise à mieux comprendre ces espèces et la relation entre la sécheresse, leur teneur en COV et leur inflammabilité, d'autant plus qu'elles sont largement consumées par les incendies de forêt dans de nombreuses RCM et pourraient contribuer aux 'Flashovers' observés pendant les incendies de forêt.

Rosmarinus Officinalis L.

Parmi les arbustes méditerranéens indigènes (maquis), le romarin (*Rosmarinus officinalis L.*) a de fortes capacités d'adaptation au stress hydrique et sont capable de survivre à une teneur en eau relative (en anglais : RWC) aussi faible que 35 % (Munne-Bosch *et al.* 2002). Les *R. officinalis* sont d'arbustes persistant et sont les espèeces pricipales avec les ajoncs méditerranéens après un incidents après un incendie (Baeza *et al.* 2002). En plus des constituants actifs de ses huiles essentielles, tels que le 1,8-cinéole, le camphre, l'α-pinène, le β-pinène et le bornéol, *R. officinalis* est riche en composés phénoliques qui se répartissent en trois groupes : les diterpènes phénoliques, les flavonoïdes et les acides phénoliques (Yeddes *et al. 2019*, Sarmoum *et al.* 2019). Les émissions de sesquiterpènes de *R. officinalis* diminuent considérablement en cas de stress hydrique (Ormeño *et al.* 2007b).

Cistus albidus

Cistus albidus, le ciste blanc, fait partie de la famille des Cistaceae. Similaire à *R. officinalis*, c'est aussi un arbuste persistant qui germe souvent après feu donc c'est une espèce pyrophyte pionnière ce qui signifie que sa croissance est stimulée par les feux (Le Houérou 1973). Ses feuilles sont couvertes de poils glandulaires qui leur donnent une couleur jaune pâle, et sont capables de protéger la plante du soleil et du vent, et de retenir l'humidité absorbée de l'air. Les substances volatiles émises par les feuilles de *C. albidus* sont dominées par les monoterpènes, par exemple le limonène et par les sesquiterpènes, par exemple le β-caryophyllène, le α-cadinol, le camphre de genévrier, le germacréne D et le spathulénol (Maccioni et al. 2006, Llusià & Peñuelas 2000).

Le stress hydrique

Vingt plants de 1 an de chaque espèce ; *R. officinalis* et *C. albidus*, ont été cultivés dans un mélange en pot de terre et de vermiculite. Chacune des deux espécesa été divisée en deux lots de 10 plantes placées en serre, 10 ont été bien arrosées et considérées comme plantes témoins, tandis que 10 autres ont été privées d'arrosage pendant 16 jours consécutifs de la mi-mai au 1er de juin. Les températures moyennes variaient de 22,5°C à 30°C et la photopériode pendant la période de test était de 16 h de lumière et de 8 h d'obscurité. En raison du confinement du COVID-19 et de l'infestation d'insectes, certaines plantes de la serre ont été perdues, nous avons donc dû mener nos expériences sur cinq plantes de *R. officinalis*. Et quatre plantes de *C. albidus*.

Le Stress Thermiques

Des feuilles des plants *R. officinalis* et *C. albidus* qui ont été ou non (témoins) soumises à un stress hydrique ont été prélevées pour etre chauffées à l'aide d'une Py-GC/MS. Le but de cette étape était d'étudier et de comparer la composition des émissions des feuilles sous contrainte thermique avec ou sans stress hydrique. Les plantes soumises au stress hydrique chez les deux espèces, c'est-à-dire RHS1 à RHS5 et CHS1 à CHS4, ont été soumises à des stress thermiques à l'échelle de la plante où elles ont été entièrement stressées thermiquement à l'aide d'un panneau radiant placé latéralement pour être au plus proche de l'arrivée d'un front de flamme. Des plants de *R. officinalis* et *C. albidus* frais supplémentaires (20 de chaque) ont également été expérimentés à des fins de comparaison. Ces expériences ont été réalisées dans une enceinte hermétique (1,2 m^3) en Siporex recouverte de panneaux de silicate de calcium de l'intérieur, équipée d'un panneau de chaleur radiant et d'un vitrage résistant à la chaleur utilisé pour l'observation. Le panneau radiant (48 x 48 cm2) a la capacité de fournir une puissance radiative équivalente à 83 $kW.m^{-2}$.

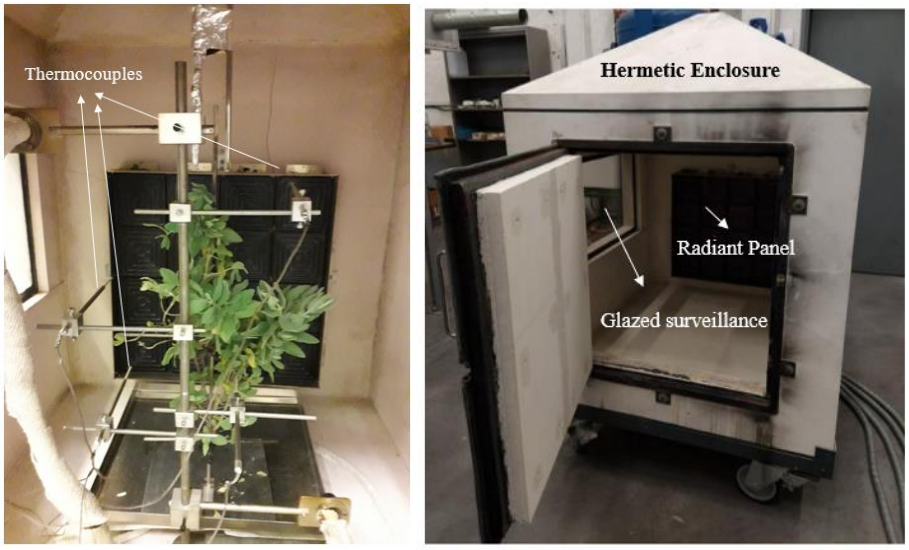

Figure. Les thermocouples se trouvent avec une plante de *C. albidus* attachée à un autre support situé devant le panneau radiant (à gauche). Enceinte hermétique équipée d'un panneau radiant (à droite).

Résultats de ce travail

Adaptation physiologique des feuilles au stress hydrique

Le stress hydrique pendant 16 jours a diminué modérément et pas sévèrement le potentiel hydrique (en anglais : LWC inférieur) dans les feuilles de *R. officinalis* (16 %) et *C. albidus* (15 %) ; une réponse d'une réduction de 60% de SVWC. La teneur en chlorophylle est fortement réduite de plus de 50% pour les deux plantes, un indicateur clair de l'inhibition de la photosynthèse due à une diminution de l'absorption de CO2 causée par la fermeture stomatique, c'est-à-dire une conductance stomatique réduite. L'analyse anatomique des feuilles des deux plantes a montré des caractéristiques d'adaptation remarquables au stress hydrique, conférant à ces plantes la caractéristique d'espèces arbustives méditerranéennes tolérantes à la sécheresse. Par exemple, l'evapo-transpiration a été réduite, ce qui a été expliqués par le changement de la structure de l'épiderme abaxial (ridé) chez les plantes stressées par la sécheresse. La modification de la taille et de la structure de la cuticule est également une stratégie développée

par les plantes pour limiter la transpiration non stomatique en réduisant la conductance épidermique. La diminution de l'espace aérien intercellulaire sous stress hydrique est suggérée pour interférer avec l'assimilation du CO2 nécessaire à la photosynthèse (Olmos *et al.* 2007). Par conséquent, les chloroplastes sont considérablement réduits en tant que mécanisme de protection contre le déficit hydrique. Les petites cellules épidermiques sont 20 fois plus résistantes à l'effondrement que les plus grandes, donc cela pourrait aussi être un mécanisme d'adaptation à la sécheresse car les cellules épidermiques ont augmenté en nombre comme dans le cas de *C. albidus*. Un plus grand nombre de cellules épidermiques par unité de surface foliaire reflète un meilleur contrôle de la perte d'eau par transpiration cuticulaire (Lorente et al. 2020). Enfin, la modification des cellules palissadiques du mésophylle (Pp) et des glandes sécrétoires des trichomes glandulaires de *R. officinalis*, sites actifs de production de COV (Midzi et al. 2022), est sûrement le reflet d'une production compromise de COV par ces feuilles. Enfin, il est évident que le stress hydrique a exercé une charge plus importante sur les feuilles de *R. officinalis* que sur *C. albidus*, expliquée par les modifications anatomiques et physiologiques plus importantes chez les premières par rapport aux secondes. Ceci soulève la conclusion que *C. albidus* est une espèce arbustive plus résistante au stress hydrique que *R. officinalis*.

Analyses des émissions de COV sous stress thermiques

Afin de vérifier l'efficacité d'adsorption des tubes adsorbants (chimisorbeur), nous avons décidé de comparer les émissions à l'échelle de la plante dans l'enceinte hermétique adsorbées par le chimisorbeur avec celles obtenues par chauffe des feuilles à 180°C, de la même plante *R. officinalis* stressée par la sécheresse. La gamme de terpènes (monoterpènes) adsorbés par le chimisorbeur était inférieure à celle acquise par la pyrolyse des feuilles et l'abondance relative était remarquablement plus petite car une gamme plus élevée d'hydrocarbures à longue chaîne était adsorbée. Les chimisorbeurs semblent avoir une meilleure adsorption des composés lourds que les hydrocarbures à longue chaîne (C_{25} - C_{33}). La dominance des triterpénoïdes et des alcanes dans les émissions de *R. officinalis* stressé par la sécheresse peut être liée à la cire cuticulaire formée à la surface des feuilles en réponse à la sécheresse. La formation de cire cuticulaire sur les structures végétales la protège des stress abiotiques comme la sécheresse en isolant les feuilles afin de limiter la transpiration. La prévalence de paraffines impaires de *R. officinalis* telles que C_{27}, C_{29}, C_{31} et C_{33} est conforme aux résultats de Scognamiglio et al. (2022). Outre les alcanes à longue chaîne, les triterpènes tels que la β-amyrénone (14,65 %) et les triterpénoïdes tels que la β-amyrone (15,12 %) et la β-amyrine (2,12 %), étaient les deuxièmes les plus abondants provenant également de la cire cuticulaire recouvrant les feuilles de *R. officinalis*. Les monoterpènes, les sesquiterpènes et les cétones arrivent en troisième position des émissions. Par exemple, le β-pinène avait une abondance relative de 13,6 % à partir de feuilles pyrolysées stressées par la sécheresse, contre 0,12 % à partir de feuilles fraîches soutenant la teneur élevée en terpènes de *R. officinalis* après les stress de sécheresse. En conclusion, les climats méditerranéens sont caractérisés par de longs étés secs qui exercent des stress abiotiques sévères sur les espèces végétales les poussant à modifier leurs mécanismes physiologiques pour survivre. La thermotolérance est un caractère, donné aux espèces végétales capables de s'adapter physiologiquement aux stress abiotiques environnementaux. Parmi ces adaptations, on observe un contenu en COVB plus important qui, lorsqu'ils sont altérés par le feu, alimentent les incendies de forêt et augmentent le risque de 'Flashovers'. *Rosmarinus*

officinalis et *Cistus albidus* ont été testés pour leur thermotolérance, leur adaptation au stress hydrique et leurs réserves conséquentes en COVB à l'échelle des feuilles et des plantes. Nos résultats ont montré une adaptation remarquable de ces espèces arbustives méditerranéennes à 16 jours de stress hydrique autant au niveau physiologique qu'au niveau de leur contenu en COVB. La photosynthèse a été limitée chez les deux espèces après que la teneur en chlorophylle de leurs feuilles ait été réduite de près de moitié, conséquence d'une moindre absorption de CO_2 en raison de leur conductance stomatique réduite. Cependant, *C. albidus* a montré une plus grande résistance à la sécheresse que *R. officinalis*, une conclusion tirée en fonction de la sévérité des changements anatomiques observés dans les feuilles de C. albidus. Le contenu volatil des deux espèces a augmenté relativement. Notamment, la teneur en terpènes de *C. albidus* était proche de zéro dans les feuilles témoins et stressées par la sécheresse, à l'exception des faibles concentrations de sesquiterpènes (par exemple le caryophyllène) notées dans les feuilles témoins. Au contraire, la teneur en terpènes de *R. officinalis* était importante dans le contrôle et augmentait remarquablement dans les feuilles stressées par la sécheresse, en particulier la concentration de monoterpènes oxygénés et non oxygénés. D'autre part, le stress hydrique a augmenté les concentrations végétales d'acides gras, d'alcools, d'esters et d'alcanes à longue chaîne chez les deux espèces. Bien sûr, ces émissions particulières proviennent des cires cuticulaires sécrétées par les plantes comme mécanisme de protection contre les stress hydriques. Les émissions des feuilles témoins et stressées hydriquement ont été récupérées à l'échelle des feuilles par pyrolyse à l'aide d'un appareil Py-GC/MS. Les émissions à l'échelle de la plante ont été réalisées par dégradation thermique sous exposition à la chaleur radiative dans une enceinte hermétique où la technologie d'adsorption/désorption utilisant un extracteur en phase solide (chimisorbeur) a été mise en œuvre avec un échantillonnage continu actif des émissions. Les principaux résultats sur les émissions de *R. officinalis* sont apparus satisfaisants et ont confirmé les émissions par pyrolyse avec une reproducibilité acceptable. Malheureusement, la technologie n'a pas pu être utilisée avec *C. albidus* pour des problèmes techniques qui nécessitent de futures expérimentations. D'autre investigations devraient être menées avec une espèce non méditerranéenne pour observer les différences physiologiques et des émissions. D'autres investigations pourraient également être réalisées sur les caractéristiques d'inflammabilité des mélanges d'émissions identifiés afin de connaître les composés qui rendent les mélanges les plus inflammables et qui pourraient donc contribuer le plus aux flashovers de feux de forêt pendant les saisons estivales sèches de la MCR.

1 Introduction

Climate change creates local prolonged drought periods and high temperatures, increase fire initiation and spread risks, but also reduces soil moisture content and consequently affects vegetation volatiles (especially terpenes) synthesis and emission rates. According to a recent article published in "The Guardian" on February 2022, it is expected that the wildfires which have hit California, Australia, and Siberia will become 50% more frequent by the end of the century, with climate change being the primary game changer. From our studies and literature, it is evident that a relationship exists between vegetation volatile content, emission rates, and their flammability descriptors (i.e. ignition, flammability…), *(cf. Chapter III, section 9.3)*. It's also found that the presence or absence of terpene storage pools in vegetation species interfere with the patterns of volatile emissions such as terpenes however, the controversy is whether or not they affect their emission rates (Ormeno et al. 2007, Llusià et al. 2009). The certainty is that when these pools are damaged by external factors such as fires, emission rates are presumably to be modified remarkably. *Cistus albidus* (Cistaceae) and *Rosmarinus officinalis* (Lamiaceae), are two shrub-wood species that are largely consumed by wildfires and they are among the first to emerge post a wildfire (Serbouti et al. 2022). They are both terpenes storing species with different storage compartments, foliar glandular hairs for the first and secretory organs e.g. glandular trichomes for the second (*cf. Chapter I, section 3.3*). As photosynthetic rates and stomatal conductance decrease in response to drought (*cf. Chapter I, section 3.4.2*), the volatile emission rates of these species decrease dramatically and consequently their terpene reserves are expected to be sustained. Notably, terpene emissions decreased and their reserves (except for sesquiterpenes) were found to be minimal in C. albidus after short-term induced drought treatment (Llusià & Peñuelas 1998) and seasonal droughts (Llusià et al. 2009) unless they were well irrigated before the drought season. The monoterpenes emitted from *C. albidus* originate directly from *de-novo* synthesis while the sesquiterpenes are more likely to originate from the storage pools (Ormeno et al. 2007b). As for *R. officinalis*, some studies found no effect of drought stress on their monoterpene emissions and they were ascribed as resistant well-adapted species to drought especially since their monoterpene emissions didn't reflect any photosynthetic inhibition under drought stresses (Peñuelas & Llusià 1997). Different results were found by Nogues et al. (2015), where monoterpene emissions have increased under mild stresses and decreased under severe drought stresses. It seems that monoterpene emissions from *Lamiaceae* species are dependent on the severity of drought. Our aim was to confirm these results by examining the volatile emissions from both species under thermal stresses after subjecting them to severe drought periods in a greenhouse. As far as our knowledge, literature hasn't studied yet the effect of an approaching fire front on the emissions of plants. Therefore, thermal stresses were conducted on a plant-scale facing radiant panels with incremental temperature raise where emissions were collected using adsorbent tubes (chemisorbers) and correlated to plant ignition in air atmosphere. On a leaf-scale using Py-GC/MS in an inert atmosphere. Stomatal conductance and other leaf morphological traits were examined throughout the hydric stresses performed on potted plants from both species.

2 Climate Change Induced Hydric Stresses

2.1 *Forest Scale: Hydraulic Failure Hypothesis*

"Desertification is the Mediterranean invisible enemy", an article I recently read alarming the serious threat climate change is causing to the forest wealth in MCR. Precipitation rates are decreasing, temperatures and sea levels are increasing, consequently increasing soil salinity and causing plant mortality. Scientific explanations of the exact mechanisms of plant mortality in response soil moisture depletion are still lacking but are essential for predicting future mortality rates especially that climate change is a worsening situation. The information available to date suggest that drought and high temperatures deplete soil moisture content and impose high evaporative demands on the vegetation, respectively. These factors raise a hydraulic failure hypothesis, which implies that drought increases an individual tree's water stress to the point that water transport system that supplies its leaves is impaired. This occurs when the water column in xylem conduits breaks or cavitates in result of excessive negative xylem pressure therefore, less water is transported to the plant organs and tissues so they eventually dehydrate and die (Anderegg et al. 2011). Measuring xylem pressure during drought stress is another indication of hydraulic failure intensity.

2.2 *Forest Mortality: Carbon Starvation Hypothesis*

Hydraulic failure is accompanied by carbon starvation which is caused when stomatal conductance is altered as turgor pressure is lost in foliage due to moisture depletion, suppressing photosynthesis and increasing transpiration. Transpiration is the inverse of photosynthesis where the plants use their carbohydrates reserves with oxygen to produce the energy necessary for their survival (Anderegg et al. 2011). This imbalance between carbon uptake and carbon consumption (loss) results in a negative carbon balance (McDowell et al. 2008).

Mortalities in forest stands change canopy structures by increasing the empty spaces among them allowing for more heat to access the understory litter beds and over-dry them, besides of increasing the litter/live ratio in canopy and litter beds, all of these changes were predicted to have increased wildfire ROS by 30%, (Nolan et al. 2020). As canopies become less dense, light and heat can access understory allowing for flammable shrubs and midstory vegetation which are able to endure drought to survive and populate thus increasing the risks of wildfires. It's important to point out that biotic agents, such as insects and pathogens infestations, can amplify or be amplified by both carbon starvation and hydraulic failure.

2.3 *Plant Scale: Drought, Photosynthesis and BVOC Emissions*

Photosynthesis decreases after stomatal closure as a response to the chemicals released (e.g. abscisic acid) due to dehydration at plant root level. Drought limits photosynthesis due to a decline in Rubisco enzyme activity and an increase in the action of its binding inhibitors (Farooq et al. 2009). In short, dehydration causes cell shrinkage that results in a decrease in cellular volume and an increase in cytoplasmic solute concentration. This leads to an increase in cellular content viscosity where the resulting toxicity affects the function of the enzymes e.g. Rubisco, which is responsible for CO_2 fixation by photosynthesis (Farooq et al. 2009). Inhibited photosynthesis reduces carbon and energy supply necessary for the production of constitutive BVOCs (mainly isoprene and monoterpenes) however, the controversy in literature is that some studies have found that drought sometimes increases BVOC emissions, while others found a

decreasing effect or even increasing followed by decreasing effect on BVOC emissions, all depending on the vegetation type, the identity of the BOVC, and drought severity (mild to severe), (Simpraga et al. 2011). For instance, mild drought stress doesn't affect isoprene and monoterpene emissions because it only affects mildly the stomatal openness and foliar carbon fixation, and not the photosynthetic electron transport responsible for the supply of isoprene production precursors; IPP and DMAPP (Niinemets et al. 2010). On a separate note, mild heat stresses activate isoprene and monoterpene synthase in a competing endeavor for photosynthetic electrons and carbon uptake against this latter fixation therefore, increasing their production remarkably (Loreto et al. 2006).

3 Climate Change Induced Heat Stresses

3.1 *Plant Scale: BVOC Emissions*

It is surprising to know that plants are the major hydrocarbon emitters on this planet, isoprene alone exceeds the total global methane emissions (Sharkey et al. 2008). Although the effects of drought on Mediterranean plant emissions is conflicting, there are studies that suggest an increase of BVOC emissions from plants suffering water deficit (Loreto & Sharkey 1993, Ormeno et al. 2007). Drought in the MCR regions is accompanied by summer temperatures averaging above 50°C, subjecting the vegetation covers to severe heat stresses that also affect among others, the BVOC emissions (Singsaas & Sharkey 2000, Loreto et al. 2006). For example, isoprene emissions from most Mediterranean vegetation species are temperature dependent and they are found to be inhibited beyond 35 – 40°C. However, photosynthesis and stomatal conductance seem not to affect isoprene emissions from leaves. The fact that isoprene is not stored in leaves, because its emission is highly dependent on light and temperature, the stomatal closure may falsely be considered to enhance the blockage of isoprene in the intercellular airspace, apparently this is not the case (Singsaas & Sharkey 2000). The partial pressure of these compounds creates a resistance against stomatal closure (Loreto & Schnitzler 2010). Therefore, isoprene emission is clearly an indication of its synthesis rate and its synthesis rate is strongly dependent on photosynthesis. Same conclusion can be drawn for monoterpenes. In normal conditions, 2% of fixed carbon from photosynthesis was used to synthesize isoprene while 50% were used under abiotic stresses (Ormeno et al. 2007). Isoprene emission increased during the first 10 mins at high leaf temperature (35 – 45°C), but decreased beyond that and never recovered back to its initial values therefore, thermotolerance characteristic of isoprene works only under short term heat stresses (Singsaas & Sharkey 2000). Prolonged heat stresses are suspected to cause irreversible isoprene synthetic enzyme denaturation rather than messing with its regulation, and thermotolerance is played by other mechanisms e.g., heat-shock proteins production (Singsaas & Sharkey 2000). The patterns followed by isoprene synthesis under abiotic stresses are similarly followed by other terpenes (i.e. monoterpenes and sesquiterpenes). However, the vegetation which have special compartments (glands or ducts) store high quantities of terpenes (mono- & sesqui-) but are tightly separated by impermeable cell layers therefore, unless the storage pools are altered by external factors such as strong winds, or fires, the emission under high heat stresses remain moderate. On the other hand, plants that do not store BVOCs into specialized structures (Figure IV.1), have small temporary pools in the leaf mesophyll and are easily emitted under heat stresses, however oxygenated VOCs (e.g. methanol, C6 aldehydes, and alcohols) are harder to transition to gaseous phase and therefore

are not easily emitted, especially if stomatal closure due to accompanied drought took place (Loreto & Schnitzler 2010). Similar to isoprene, *de novo* emissions of monoterpenes have decreased after subjecting terpene storing vegetation species to prolonged heat stresses above 45°C without any clear post-stress recovery (Kleist et al. 2012).

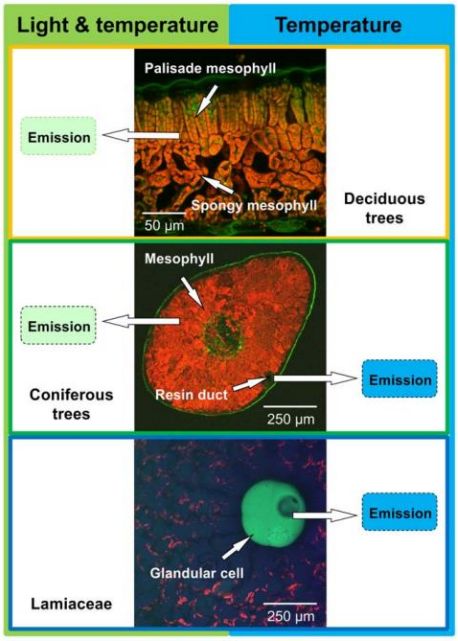

Figure IV.1. Origin of volatile terpene emissions from different leaf types (Loreto & Schnitzler 2010).

4 Vegetation Choice

The vegetation species used in our hydric and thermal stresses studies were chosen relevant to their abundance in the MCR regions that have been consumed vastly by wildfires. They were also related to extreme wildfire behaviors such as flashovers, i.e., the emissions of *R. officinalis* were found to reach flammability limits alarming a flashover (Chetehouna et al. 2014) and *C. albidus* was the main maquis species consumed by the *Palasca* fire in 2000 (Dold et al. 2009). Both species possess drought adaptive characteristics therefore, studying their volatile reserve and emission responses to abiotic stresses common to the Mediterranean climate will be an added value to the fire fighting and wild fuel management strategies.

4.1 *Rosmarinus Officinalis L.*

Among native Mediterranean shrubs (maquis), rosemary (*Rosmarinus officinalis L.*), (Figure IV.2), has strong drought stress adaptation capabilities and is able to survive at relative water content (RWC) as low as 35% (Munne-Bosch et al. 2002). *R. officinalis* are referred to as shrub obligate seeder and are dominantly found as Mediterranean gorse shrub species post-fire incidents (Baeza et al. 2002). In addition to active constituents of its essential oils e.g.,1,8-cineole, camphor, α-pinene, β-pinene and borneol, *R. officinalis* are rich in phenolic compounds which are divided into three groups: phenolic diterpenes, flavonoids and phenolic acids (Yeddes et al. 2019, Sarmoum et al. 2019). Sesquiterpenes emissions from *R. officinalis* were found to decrease substantially under drought stresses (Ormeno et al. 2007).

Figure IV.2. A fresh (left) and stressed (right) samples of *R. officinalis* experimented in this study.

4.2 *Cistus Albidus*

Cistus albidus (Figure IV.3), the white cistus, is part of the *Cistaceae* family. Similar to *R. officinalis*, it is also a shrub obligate seeder that often germinates post-fire therefore, it's a pioneer pyrophyte species which means that its growth is stimulated by fires (Le Houérou 1973). This evergreen shrub grows at an average height of 30-100 cm, with leathery and long leaves (3 to 5 cm), its flowers have an average life span of 12 and 24 h (Blasco & Mateu 1995). Native to the west of the Mediterranean basin, it is found in Portugal, southern Spain, in the Balearic Islands, Morocco, Algeria, southern France, in northern and central Italy, and in Sardinia (Tison & De Foucault 2014, Pignatti et al., 2017). Their leaves are covered with glandular hairs which gives them a pale-yellow color, are able to protect the plant from the sun and wind and retain moisture absorbed from the air. The volatiles emitted from C. albidus leaves are dominated by monoterpenes e.g. limonene, and sesquiterpenes e.g. caryophyllene, α-cadinol, juniper camphor, germacrene D, and spathulenol (Maccioni et al. 2006, Llusià & Peñuelas 2000). Monoterpenes were found to be the major emissions affected by prolonged water stresses on *C. albidus* by a negative effect, (Ormeno et al. 2007b). The emissions and storage rates of terpenes are strongly related to seasonality (Llusià & Peñuelas 2000, Llusià et al. 2009).

Figure IV.3. A fresh (left) and stressed (right) samples of C. albidus experimented in this study.

5 Materials and Methods

5.1 *Hydric Stress*

5.1.1 Materials

Twenty, 1-year old plants of each species; *R. officinalis* and *C. albidus*, were cultivated in potted mixture of soil and vermiculite (3/1, v/v) of volumes 5.02 cm^3 and 2.41 cm^3, respectively. R. officinalis were ascribed by the letter R, and C. albidus by the letter C. Each set of the plants was equally divided into two batches (10 x 10) and placed in a greenhouse, 10 were well watered and considered as control plants, while 10 others were deprived from irrigation for 16 consecutive days from mid-May till the 1st of June and donated the suffix (HS) referring to hydric stress. The average temperatures ranged from 22.5°C to 30°C and the photoperiod during the test period was 16 h of light and 8 h of darkness. Due to COVID-19 confinement and insect infestation, some plants in the greenhouse were lost, therefore, we had to conduct our experiments on five R. officinalis plants numbered as RHS1 to RHS5 and four *C. albidus* numbered from CHS1 to CHS4. Same applies on well-watered (control) *R. Officinalis* and *C. albidus* used for analysis, they were five (CR1 to CR5) and four (CC1 to CC4), respectively. Although, studying the effect of herbivores on the plants could have been an addition but it wasn't the scope of this study. Hydric stress is sometimes referred to as drought stress in the context of this chapter.

5.1.2 Methods

5.1.2.1 Soil Moisture Measurement

The available soil volumetric water content (SVWC) measurements were made by inserting a 12 cm long probe of a digital measuring device (Soil Moisture Meter TDR 150; Spectrum®) into the substrates in the pots before and after the stress phase, (Figure IV.4). Attempts were intended to measure the salinity of the substrate in the pots in decisiemens (dS/m), unfortunately, we couldn't proceed efficiently with this method due to confinement restrictions.

Figure IV.4. Digital soil volumetric water content measuring device.

5.1.2.2 Leaf Water Content (LWC)

Leaf water contents (LWC) was measured according to the following formula:

$$LWC\ (\%) = \frac{LFW - LDW}{LFW} \times 100 \quad (1)$$

Where LFW is the weight of the leaf (control and stressed) measured before applying oven drying. LDW is the dry weight measured after oven-drying the leaves at 80°C for 24 hours.

Previous studies have shown that SVWC and LWC are linearly related (Zhou et al. 2021). The leaves used for LWC measurements were randomly picked as the fully expanded leaves from almost the middle height of the plants. Unlike the upper level leaves, lower level leaves are the most prone to water loss when encountering drought therefore, in order to avoid extremes in measuring LWC, we picked the most fully expanded leaves from the middle heights of the plants (Zhou et al. 2021). Physiological analyses were made on 15 leaves by species and by culture conditions to get consistent results.

5.1.2.3 Leaf Chlorophyll Content

Chlorophylls a and b (Ca, Cb) in leaves, were measured before and after applying the hydric stresses as important indicators about plant growth and photosynthetic rates. Leaf samples were taken separately from each plant species before and after hydric stress to compare their chlorophyll contents. The leaves were then crushed using a mortar and a pestle. The paste was then soaked for 15 mins in 15 ml of acetone in addition to CaCO2 and NaSO4 which were intended to neutralize and stabilize the extract. Then, the mixture was centrifuged in a (Sigma3-16Kl) for 5 min at 4000 g. About 10ml of the supernatant liquid was collected and stored at 4°C for 24 h, after which an analysis using spectrophotometry was performed. The spectrophotometric analysis of the solution was made from 400 to 700 nm in spectrophotometer (JENWAY 6320D®) at the following wavelengths: 645, 652 and 663 nm. The measurements of chlorophyll a and chlorophyll b were carried out according to the method of Mackinney (Mackinney 1941), which is based on Beer-Lambert law that relates the concentration of a sample to the attenuation of light as it passes through it as follows:

$$OD = \varepsilon \times c \times l \quad (2)$$

Where, OD is the optic density is used to estimate the level of cellular concentration and pigment levels such as chlorophyll in the biomass when a specific wavelength corresponds to the chromophore absorption. ε is the attenuation coefficient, c is the concentration in the sample, and l is the pathlength. According to the values of OD at the different wavelengths the chlorophyll a and b were calculated according to the following formulas:

$$C_a = 0.0127OD_{663} - 0.00269OD_{645} \quad (3)$$

$$C_b = 0.0229OD_{645} - 0.00468OD_{663} \quad (4)$$

And the total chlorophyll $C_t = C_a + C_b$. It was also possible to find the OD at a wavelength of 652 nm as follows;

$$DO_{652} = 34.5 \times (C_a + C_b) \quad (5)$$

5.1.3 Anatomy Analysis: Cellular/Microscopic Level

Leaf morphological adaptations to hydric stresses were examined under microscopy by comparing small leaf pieces from control and drought-stressed. After sampling, leaves were

immediately fixed at 4°C in a mixture (%v/v) of 2% paraformaldehyde, and 5% glutaraldehyde, buffered with 0.05 M sodium phosphate buffer (1 h, pH 7.2). The samples were then washed three times for 20 mins each in 0.2 M sodium phosphate (pH 7.2) supplemented with 7.5% sucrose followed by a post-fixation step in 1% osmium tetroxide for 5 mins. The leaf segments were later dehydrated in an alcohol series, before getting infiltrated and embedded in hydrophilic acrylic resin (LR White) according to Fleurat-Lessard et al. (2016). Cross sections of leaves (several µm thick) were made using a microtome (EMUC6, Leica, Wetzlar ®), stained with 1% toluidine blue O in borax and examined with Zeiss photomicroscope (Axioplan ®).

5.2 *Thermal Stress*

5.2.1 Materials

The *R. officinalis L.* and *C. albidus* plants that were and weren't (control) subjected to hydric stresses were pyrolyzed on leaf scales using Py-GC/MS. The aim of this step was to investigate and compare the identity of their volatile content in an inert atmosphere similar to the pyrolysis phase. The plants subjected to hydric stresses in both species i.e., RHS1 to RHS5 and CHS1 to CHS4, were subjected to thermal stresses on a plant scale where they were exposed wholly to radiant heat fluxes. Additional fresh *R. officinalis* and *C. albidus* (20 of each) were also experimented for comparison purposes. These experiments were conducted in a hermetic enclosure (1.2 m^3) made of Siporex layered with calcium silicate boards from the inside, equipped with a radiative heat panel, and a heat-resistant glazing used for surveillance. The radiant panel (48 x 48 cm^2) has the capacity of supplying a radiative power equivalent to 83 $kW.m^{-2}$ (Figure IV.5). The aim of these experiments was to simulate the radiant heat fluxes experienced by the plant from an approaching fire front and to identify the emerging volatiles. The emerging emissions from the stressed plants were collected and analyzed with adsorption/desorption techniques using a solid phase extractor; Magic Chemisorber™®. In order to measure the temperatures at the plant level inside the hermetic enclosure, we used thermocouples type K (Alumel, Chromel) of a diameter equivalent to 200µm specifically designed for sensing temperatures in turbulent flows that involve convection and radiation (Arlaud & Lalizel, 2016).

5.2.2 Methods

5.2.2.1 Leaf scale: Py-GC/MS

Pyrolysis experiments were conducted on stressed and unstressed (control) leaves from both plant species in order to compare their volatile content as a result of continuous and interrupted irrigation. A multi-shot Pyrolyzer EGA/PY-3030-D (Frontier lab) coupled with a QP2010 Ultra (Shimadzu) GC/MS was used. The pyrolysis products were carried by a helium gas flow $1ml.min^{-1}$ to the GC and separated on a TR5-MS capillary column (30 m, 0.25 mm internal diameter, 0.25 µm phase thickness). The injector was set to 250°C with a 50/1 split ratio. The temperature of the GC oven was programmed from 60°C (1 min isotherm) to 300°C (11 min isotherm) with a $5°C.min^{-1}$ rate. The interface temperature was set to 280°C. The mass spectrometer (MS) used to detect the ionized molecules separately was a quadrupole analyser, the ionization mode was electron impact (70 eV) and the temperature of the source was set to 200°C. The acquisition was realized in full scan mode from m/z 50 to 600 at 0.2 amu. s^{-1}. The pyrolysis experiments were conducted on 15 mg of leaf samples heated isothermally at 180°C

for 1 min ensuring the volatilization of most terpenes. The temperature choice was further to the experiments of Chetehouna et al. (2014) who found that the temperatures responsible for maximum emission rates from *R. officinalis* were between 172°C and 202°C.

5.2.2.2 Plant Scale: Hermetic Enclosure with Radiant Panel

The plants intended for testing were cut from the stem, fixed on a stand with a branching pattern similar to the original plant, and situated directly in front of the radiant panel (Figure IV.5). The thermocouples were situated behind the plant and extended forward in order to measure the temperatures at the plant level. The radiant panel was initially programmed to attain an initial temperature of 30°C inside the compartment. Once the temperature reached 30°C the plants were inserted and placed at a distance of 30 cm in front of the radiant panel. The radiant panel had a ramp of 10 °C.min^{-1} while the heating rate inside the compartment at the plant level started slow at ~ 2 °C.min^{-1} then accelerated after one minute from 6 to 10 °C.min^{-1} therefore, the plant remained in the compartment for a testing period ranging from 20 - 30 mins. The Chemisorber was installed inside a grooved probe at the top of the enclosure (Figure IV.6). A suction pump was installed on the other side of the probe to ensure continuous flow of the emitted volatiles at a rate of 2.6 l.min^{-1} through the Chemisorber. A separate gas analyzer (ECOM J2KN PRO) for continuous monitoring of light gases (e.g. CO, O_2, CO_2, CH_4) was also used throughout the tests of each plant. Due to their small sizes, some plants were superimposed to form an adequate size proportion compared to the others. A digital scale was used to monitor plant weigh loss during the experiment, however it was damaged by the high temperatures developing inside the compartment. Instead, plants were weighed before and after the end of each experiment to estimate weight loss mainly due to dehydration and devolatilization (30 – 200°C), (Figure IV.6).

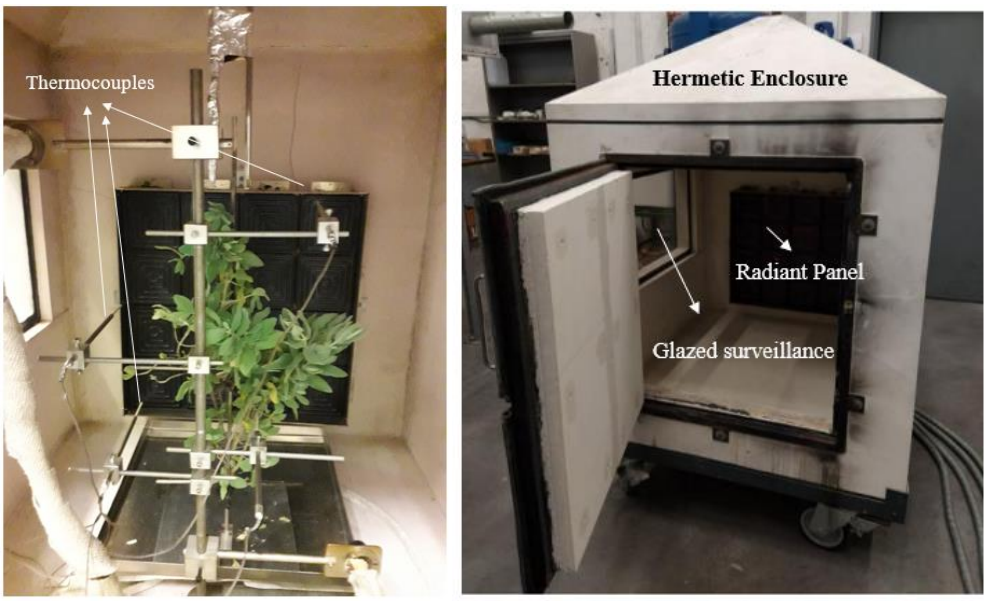

Figure IV.5. Hermetic enclosure equipped with a radiant panel (right). The thermocouples stand with a *C. albidus* plant attached to another stand situated in front of the radiant panel (left).

Figure IV.6. Two examples of drought-stressed *C. albidus* (left) and *R. officinalis* (right) residue left after degradation (plant scale).

5.2.2.3 Magic Chemisorber Adsorption and Desorption

Chemisorbers' adsorption efficiency was tested for the best position among three in the apparatus i.e., the first on the floor, the second in the probe extending down inside the hermetic compartment just above the plant, and the third in the probe at the top of the ceiling of the compartment (Figure IV.7). The latter position provided the best adsorption techniques compared to the others as they presented the risks of contamination and melting caused by the high temperatures reached inside the compartment. The chemisorbers were collected inside a sterilized glass tube and refrigerated (5°C) until their thermal desorption. As recommended by the manufacturer, the thermal desorption was done thermally using a double-shot pyrolyzer. After several trials, the best desorption technique was to initially set the pyrolizer at 150°C then the temperature was raised at a rate of 20°C.min^{-1} and then fixed at 180°C for 10 mins hold for the GC/MS run. The peaks of the attained pyrograms were then analyzed and the compounds emerging were identified for each thermal stressing trial.

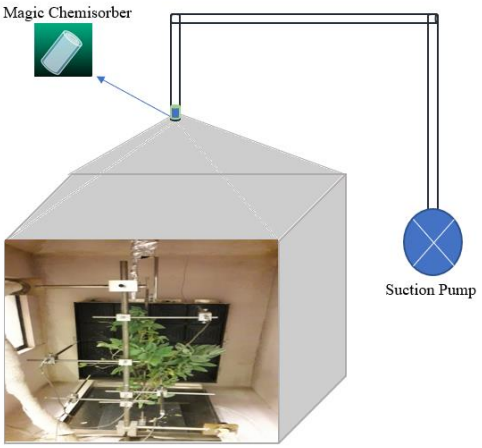

Figure IV.7. Placement of Magic Chemisorber in the probe outside the compartment.

6 Hydric Stress Results and Discussion

6.1 *LWC and SVWC*

One set of each plant species were subjected to hydric stress by depriving them from irrigation for 16 days, while the other two sets (control) were watered daily (*cf. section* 5.1.1). Before the beginning of the stress period, both sets of each group were watered equally and regularly. SVWC was found to be 90% for well-watered (control) plants of *R. officinalis* and *C. albidus*, while the stressed plants of both species had an SVWC of 30%. On the other hand, the leaf

water content (LWC) was 73% ± 7 and 70% ± 5 in control *C. albidus* and *R. officinalis*, respectively. These values decreased by 15% and 16%, respectively after 16 days of declined irrigation. Therefore, the final LWCs for drought-stressed plants were 62% ± 4 and 59% ± 3, respectively, (Table IV.1).

	Control (No Water Stress)		**Water Stressed**	
	R. Officinalis	*C. Albidus*	*R. Officinalis*	*C. Albidus*
SVWC%	*90*	*90*	*30*	*30*
LWC %	*70 ± 5*	*73 ± 7*	*59 ± 3*	*62 ± 4*

6.2 *Leaf Physiology and Anatomy*

6.2.1 Chlorophyll Content

Chlorophyll a (C_a) and chlorophyll b (C_b) were measured for both plant species in control and drought-stressed plants. For the control plants, the total chlorophyll content ($C_a + C_b$) of *R. officinalis* was found to be 5.64 ± 1.38 mg. g^{-1} dw (Figure IV.8), while that of *C. albidus* was 4.84 ± 0.72 mg. g^{-1}. dw, (Figure IV.9). Direct measurements of total chlorophyll contents at 652 nm were slightly lower and higher than the previous values of (C_a + C_b) for control *R. officinalis* and *C. albidus*, respectively. The stressed plants showed lower chlorophyll contents for both *R. officinalis* and *C. albidus*. For instance, the total chlorophyll content (C_a + C_b) for the former was reduced by 51% while that of the latter was reduced by 52%. Also, the total chlorophyll contents measured directly at 652 nm were reduced by 56% and 44% for *R. officinalis* and *C. albidus*, respectively. Also, total chlorophyll contents measured directly at 652 nm for stressed *R. offcinalis* and *C. albidus* were respectively lower and higher than the values of (C_a+ C_b), (Table IV.2).

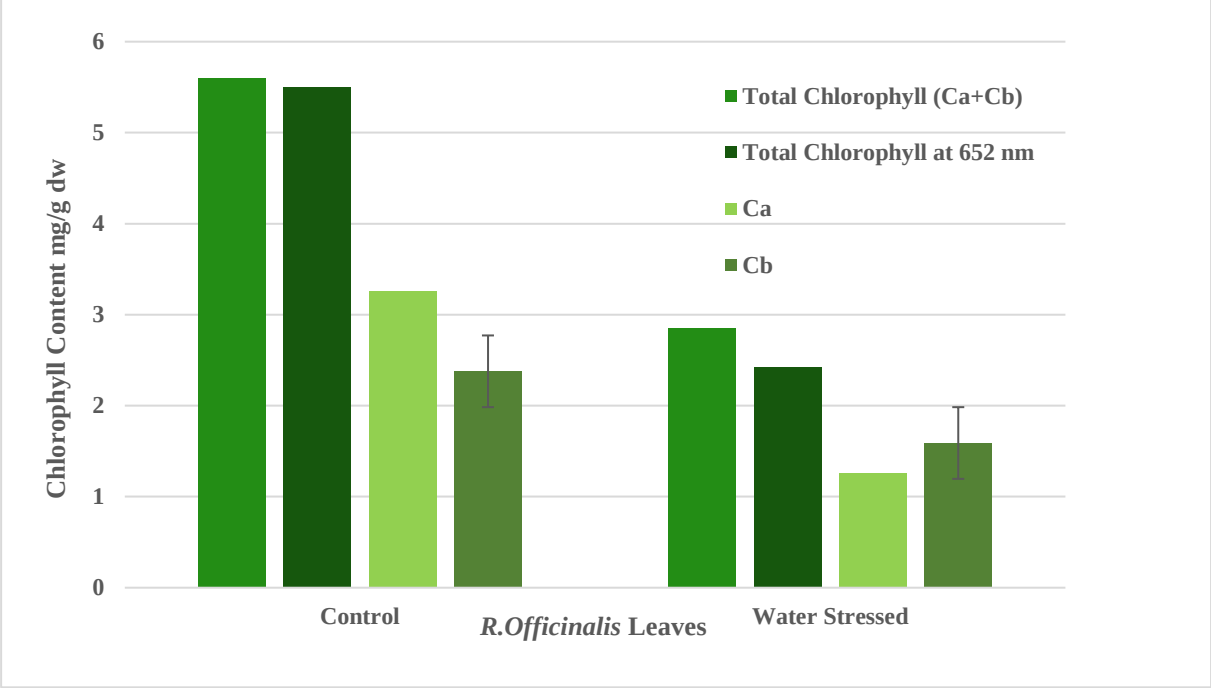

Figure IV.8. Chlorophyll a (C_a) and chlorophyll b (C_b), total chlorophyll (C_a + C_b), and total chlorophyll content measured directly at a wavelength of 652 nm of *R. officinalis* (control and stressed).

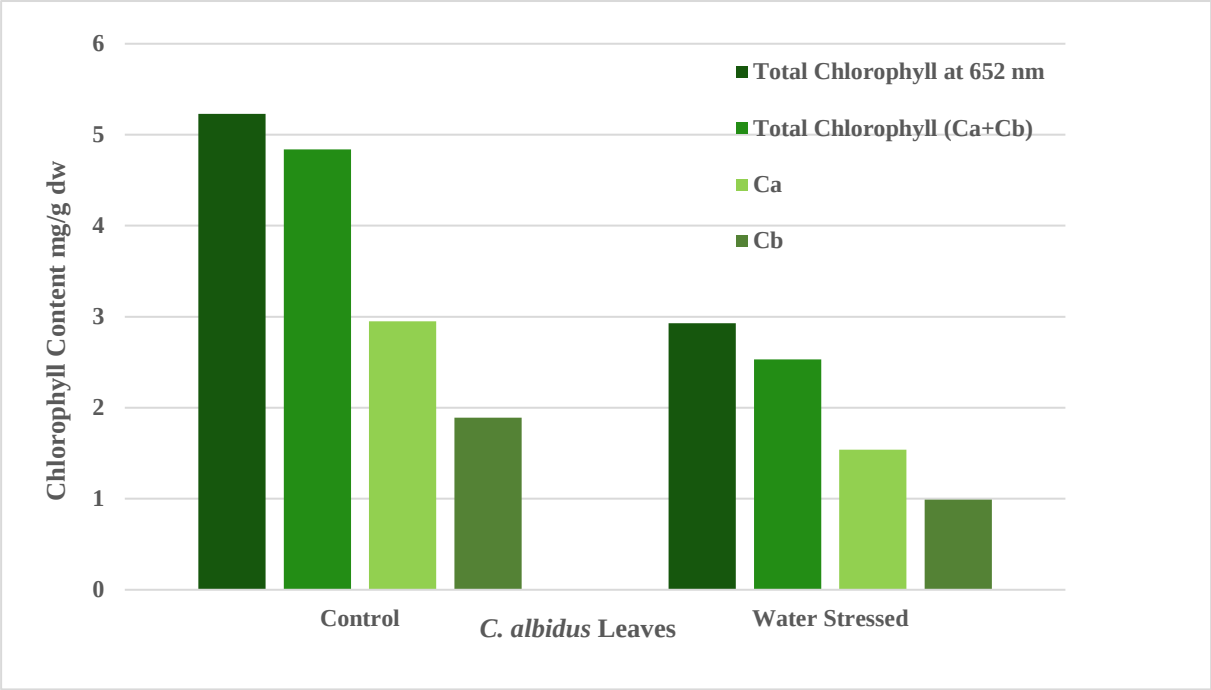

Figure IV.9. Chlorophyll a (Ca) and chlorophyll b (Cb), total chlorophyll (Ca + Cb), and total chlorophyll content measured directly at a wavelength of 652 nm for *C. albidus* (control and stressed).

Table IV. 2. Chlorophyll content of control and drought-stressed *R. officinalis* and *C. albidus* plants.

	R. Officinalis		***C. Albidus***	
Chlorophyll Content mg. g^{-1} dw	**Control**	**Drought-stressed**	**Control**	**Drought-stressed**
Ca	3,26	1,26	2,95	1,54
Cb	2,38	1,59	1,89	0,99
Total Chlorophyll (Ca+Cb)	5,6	2,85	4,84	2,53
Total Chlorophyll at 652 nm	5,5	2,42	5,23	2,93

6.2.2 Leaf Anatomy: Control vs Drought-stressed

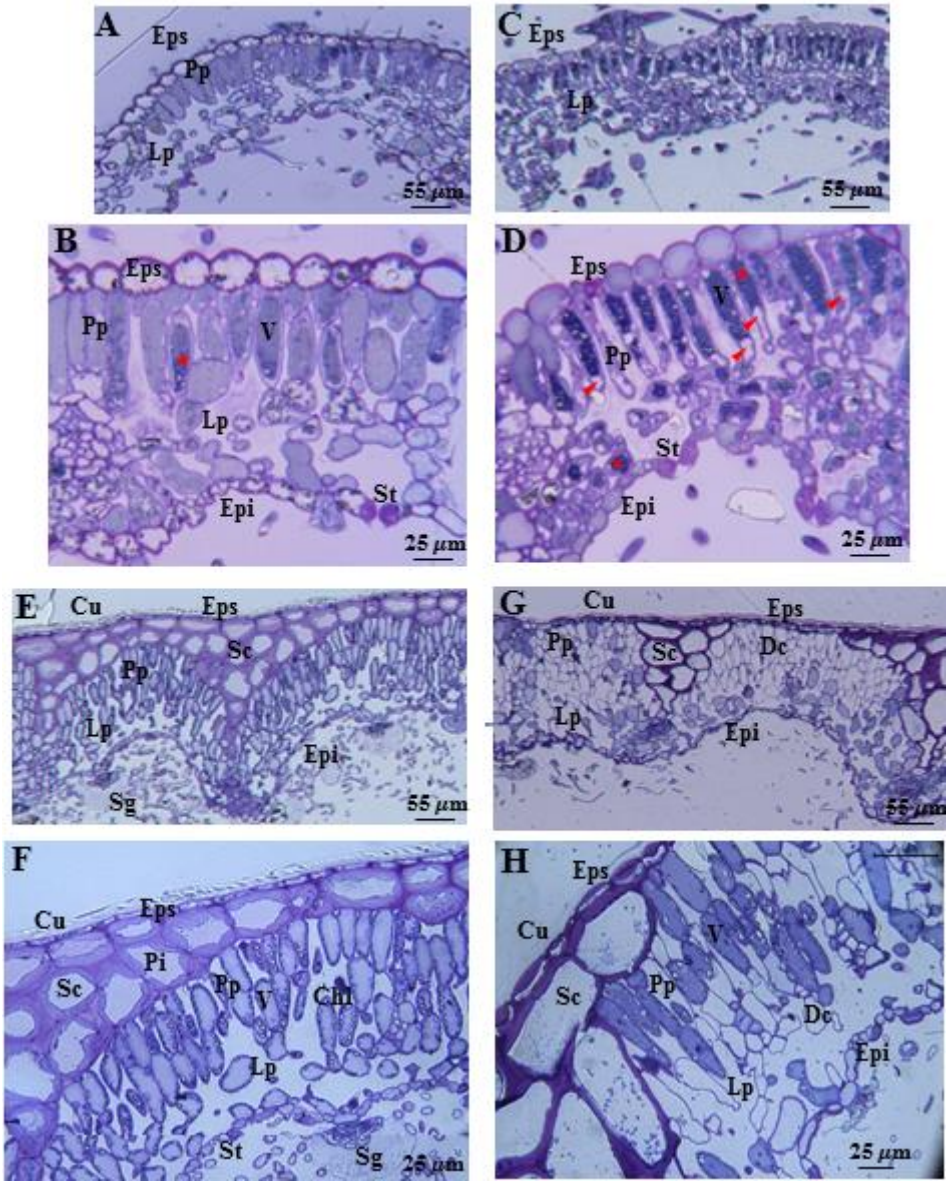

Figure IV.10. Leaves' cross sections showing comparative leaf anatomy of *C. albidus* (A-D) and *R. officinalis* (E- H). Control leaves (A&B) and drought-stressed leaves (C&D) of *C. albidus*. Control leaves (E&F) and drought-stressed leaves (G&H) of *R. officinalis*. Cu: cuticle. Eps: superior epidermis (adaxial). Epi: inferior epidermis (abaxial). Sc : Sclerenchyma. Pi : pit. Pp : Palisade parenchyma. Lp : lacunar parenchyma. Chl: Chloroplast. V: vacuole. St: stomata. Sg: Secretory gland. Dc: Dead cell. Tanins (asterisk) and Cell plasmolysis (arrow).

The capacity of *R. officinalis* and *C. albidus* to adapt to drought stress depends on the severity of changes occurring on their anatomic and ultrastructure cellular levels i.e. the more the modifications the more adaptive they are. The anatomic investigations on the leaf sections of drought-stressed *R. officinalis* and *C. albidus* have shown an increase in cell density and decrease in cell size (Figure IV.10). Also, the inferior epidermis, Epi (abaxial) appeared wrinkled and its cells appear to have developed cuticle in their internal epidermal cell wall (**D, G, &H**). The cellular area occupied by these abaxial epidermal cells has reduced greatly with cuticle developing inside the internal epidermal cell wall in drought-stressed leaves (**D, G**).

There is also a reduction in the cellular size of the superior epidermis, Eps (adaxial), in drought-stressed leaves (**D**, **H**). The sclerenchyma cells (Sc) have lignified by developing a very dense body and increasing in size in *R. officinalis* stressed leaves therefore, occupying a very large percentage of the stroma (**H, G**). The intercellular spaces in the mesophyll have decreased significantly in drought-stressed leaves of both plants. The percentage and density of palisade parenchyma (Pp) increased in drought-stressed *R. officinalis* leaves, and the adaxial epidermis cells have reduced in size (**G, H**). For example, the Pp which was composed of one and two layers in the control leaves of *C. albidus* (**A, B**) and R. officinalis (**G**, **H**), respectively, have increased to two (**C**, **D**), and three even four (**G, H**) in the drought-stressed leaves of these species, respectively. The (Pp) have plasmolyzed in the drought-stressed leaves (**D**, **H**), which is evident in their acquired heterogeneity compared to their homogenous aspect in control leaves (**B**, **F**). What's more, the stomata are smaller in size (l x w) in drought-stressed leaves (**B** vs **D**). The cuticle (Cu) has been modified in size and structure under drought stress in R. officinalis leaves, i.e.; it became thicker (**G**, **H**). The size and shape of the secretory gland (Sg), resembling a glandular trichome, that appears in control leaf of R. officinalis (**F**) are different than those of the Sg appearing in the stressed leaf (**H**), as it seems to have collapsed and the cuticle that surrounds the gland in control (**F**) contrarily seems disrupted in the stressed leaves. Absence of chloroplasts in stressed leaves of R. officinalis (**F** vs **H**). Also, in drought-stressed leaves, the cytoplasm of palisade parenchyma cells (Pp), frequently contained small lipid bodies (**G**). The central vacuole (V) in Pp which appeared normal in control leaves was filled with dense matter in drought-stressed leaves (**D, H**). Finally, the number of dead cells in *R. officinalis* stressed leaves (**G**) are more than those appearing in *C. albidus* (**C**).

6.3 *Discussion*

The drought stress for 16 days has decreased moderately and not severely the water potential (lower LWC) in the leaves of *R. officinalis* (16%) and *C. albidus* (15%); a response of a 60% reduction in SVWC. The chlorophyll content is highly reduced by more than 50% for both plants a clear indicator of photosynthesis inhibition due to a decrease in CO2 uptake caused by the stomatal closure i.e., reduced stomatal conductance. The leaf anatomic analysis of both plants has shown remarkable adaptation characteristics to drought stress, giving these plants the characteristic of drought-tolerant Mediterranean shrub species. For example, reduced transpiration rates and thereby reduced water loss were explained by the change in the structure of the abaxial epidermis (wrinkled) in the drought-stressed plants. The modification in the cuticle size and structure is also a strategy developed by plants to limit non-stomatal transpiration by reducing epidermal conductance. The decrease in the intercellular air space under drought stress is suggested to interfere with CO2 assimilation necessary for photosynthesis (Olmos et al. 2007) therefore, chloroplasts are significantly reduced as a protective mechanism against water deficit. A greater number of cells (small epidermal cells) is 20 times more resistant to collapse than larger ones, therefore this could also be a mechanism of adaptation to drought as the epidermal cells increased in number as in the case of *C. albidus* (Figure IV.10. C). A greater number of epidermal cells per leaf surface unit area reflects better control over water loss through cuticular transpiration (Lorente et al. 2020). Last but not least, the modification of the palisade mesophyll cells (Pp) and the secretory glands of the glandular trichomes of R. officinalis, which are active sites of VOC production (Midzi et al. 2022), is

surely a reflection of a compromised VOC production by these leaves. Finally, it's evident that drought stress has exerted a greater load on R. officinalis leaves than *C. albidus* explained by the higher anatomical and physiological modifications in the first compared to the second. This raises the conclusion that *C. albidus* is a more resistant shrub species to drought stress than *R. officinalis*.

7 Thermal Stress: Py Leaf Scales

The control and drought-stressed leaves from both species were subjected to pyrolysis testing at 180°C for 1 min where their emissions were identified. The choice of temperature was taken according to our findings on the degradation of cypress and oak foliage where the volatilization of terpenes was most likely to occur, partly during and mainly after the dehydration (100°C), and before the degradation of hemicellulose (200°C). Indeed, the experiments of Chetehouna et al. (2009) on *R. officinalis*, have shown that 180°C was the temperature of maximum terpenes volatilization. We thank Mr. Axel Rigoulet, an internship Masters student for conducting the pyrolysis experiments.

7.1 *Rosmarinus Officinalis*

The pyrolysis emissions from control and drought-stressed leaves of *R. officinalis* showed important reproducibility results. The emissions of control leaves from three different R. officinalis plants (RC 1.1, RC1.2, & RC1.3) are shown in Figure IV.11, while the reproducibility of drought-stressed leaves from the same R. officinalis plant (RHS2.1, RHS2.1b, & RHS2.2) are shown in Figure IV.12. Even a leaf sample that has been placed in a freezer at -20°C and retested after a week (RHS 2.1b), reproduced the same emission compounds of leaf 2.1.

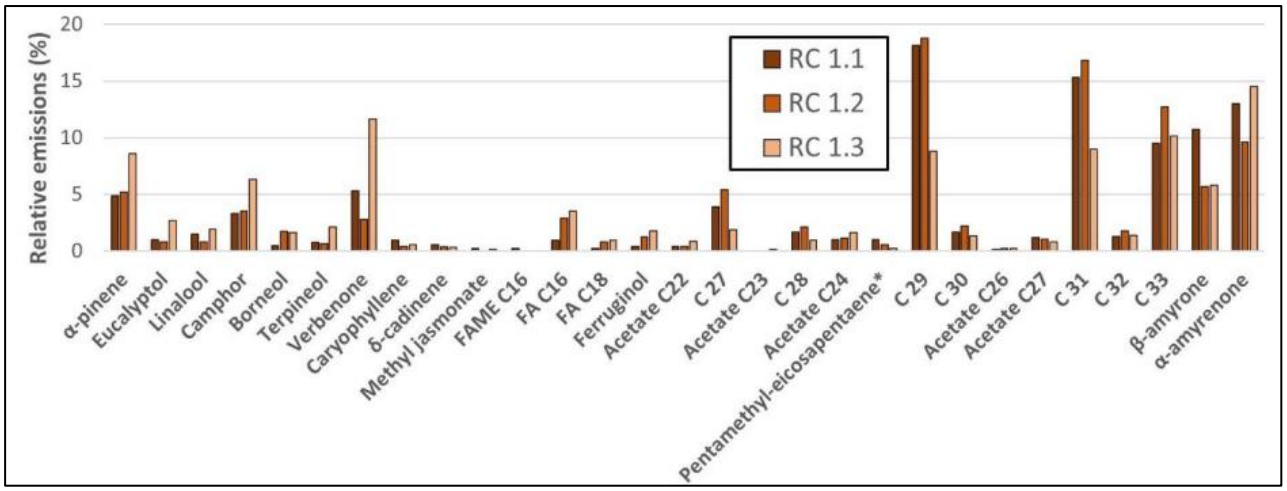

Figure IV.11. Reproducibility of control leaves from three different *R. officinalis* plants.

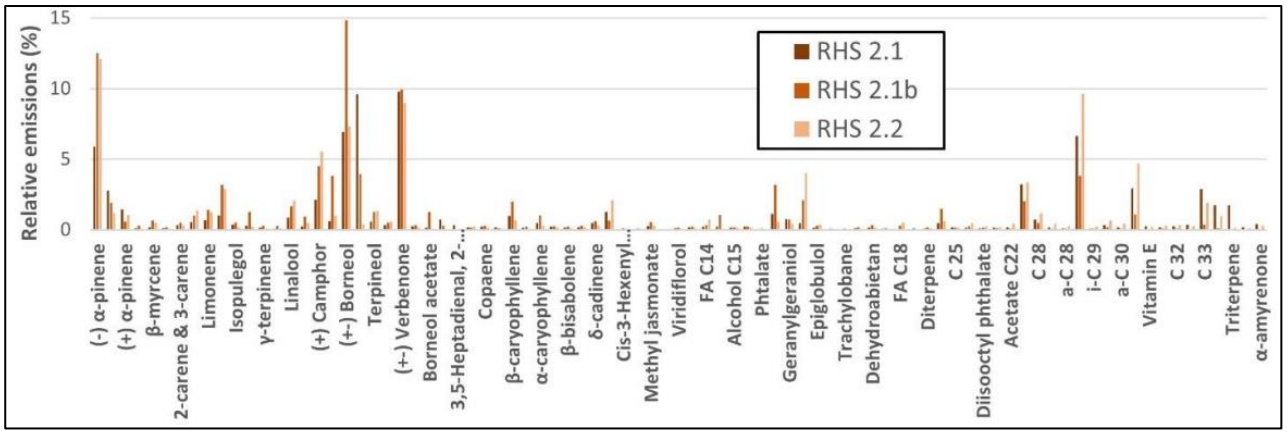

Figure IV.12. Reproducibility of emissions of two different leaves from the same plant of drought-stressed *R. officinalis*. 2.1b: leaf sample (leaf 2.1) placed in a freezer (-20°C) for a week before retesting.

The relative abundance (%) of emissions (average of tries) from drought-stressed and control leaves of *R. officinalis* are shown in Figure IV.13. As predicted, the major compounds emitted from the pyrolysis of *R. officinalis* at 180°C were terpenes, more precisely monoterpenes (Figure IV.12). Indeed, terpenes accounted for 78.85% and 92.2% of the total emissions from control and drought-stressed leaves, respectively with monoterpenes representing 70.76% and 83.76% of them. The major terpenes emitted and were common among control and stressed leaves were: (-) α-pinene, eucalyptol, linalool, borneol, and verbenone. Long-chain alkanes (C_{25} – C_{33}), were also emitted at relative percentages of 5.61% and 16.87% from control and drought-stressed leaves, respectively. Phthalates were emitted solely from drought-stressed leaves. Fatty alcohols (C_{15}, C_{16}, and C_{18}) from stressed leaves exceeded those from control leaves. The same goes for C_{22} and C_{24} acetates, with increased emissions from stressed leaves. Finally, saturated and unsaturated fatty acids were only emitted by drought-stressed leaves and they ranged C_{12} to C_{18} (even carbon numbers only).

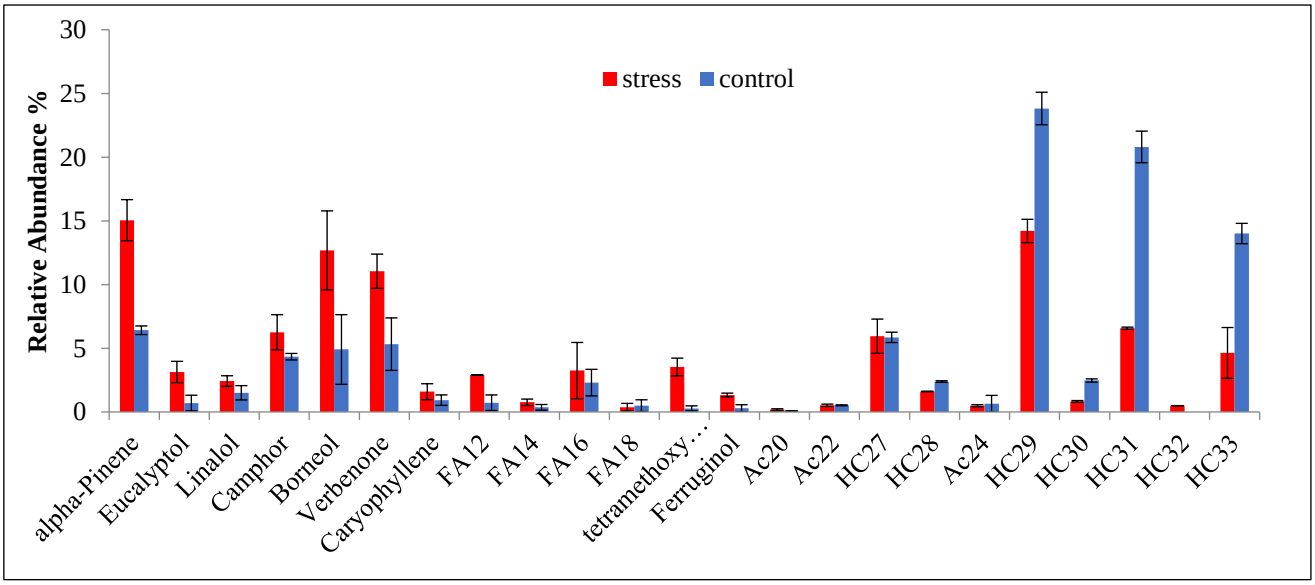

Figure IV.13. Relative abundance (%) of emissions from pyrolyzing drought-stressed and control leaves of *R. officinalis*. FAn: Fatty Acid, Acn: Acetate, HCn: Hydrocarbon, n: number of Carbon atoms.

The main emitted fatty acids were dodecanoic acid (1.34%) and hexadecenoic acid (2.19%). The relative abundance of total emissions from both control and drought-stressed leaves of R. officinalis are identified and categorized in appendix AIV.1.

7.2 *Cistus Albidus*

The emissions from control and drought-stressed leaves of *C. albidus* have also shown very good reproducibility results. The relative abundance (%) of emissions from leaves of three different control *C. albidus* plants (CC1, CC2, and CC3) are shown in Figure IV.14. Whereas the relative abundance (%) for the emissions from two leaf samples of two different drought-stressed *C. albidus* (CHS2 & CHS3) are shown in Figure IV.15. The very good reproducibility results allowed us to take an average of the relative abundance (%) for the emissions from control and drought-stressed *C. albidus* leaves. The major emissions from *C. albidus* were long-chain alkanes representing 85.39% of the total emissions from the control leaves versus 67.92% from drought-stressed leaves. These alkanes ranged from C_{23} to C_{32} from control samples and from C_{19} to C_{33} for the stressed ones. Bearing in mind that odd carbon numbered alkanes were dominant among these emissions and C_{19} to C_{22} were only observed from drought-stressed leaves. A notable increase in the emissions of fatty acids such as $C_{9,}$ C_{12}, C_{14}, $C_{16,}$ & linoleic and linolenic C_{18} acids were detected from stressed *C. albidus* plants, in addition to a rise in the percentage of alcohols from stressed leaves.

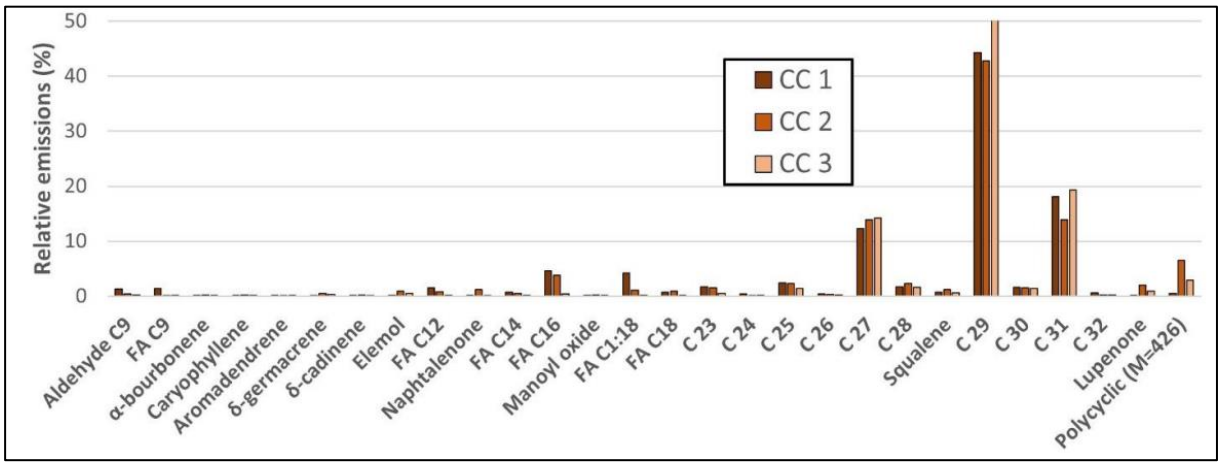

Figure IV.14. Reproducibility of emissions from leaves of three different control *C. albidus* plants.

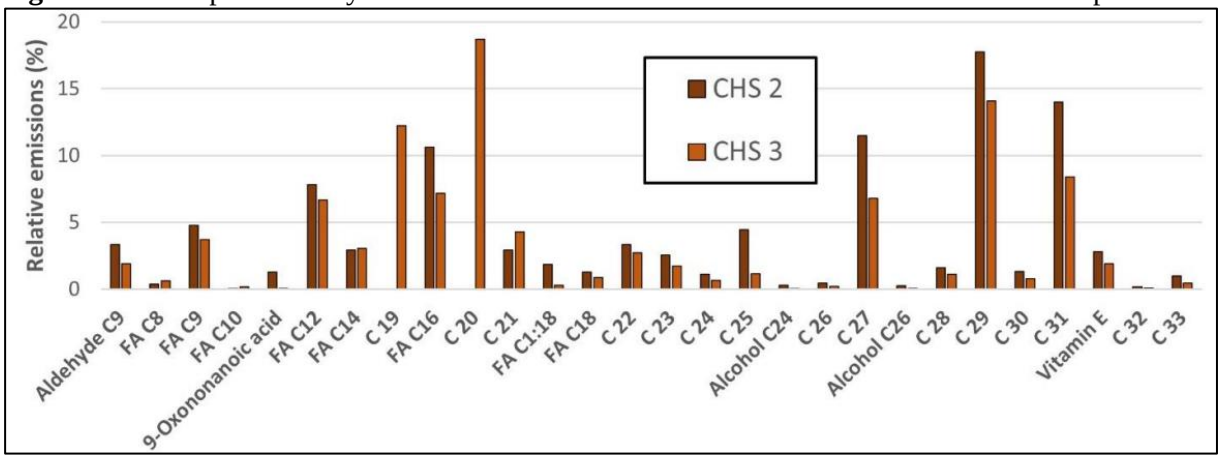

Figure IV.15. Reproducibility of emissions from leaves of two different drought-stressed *C. albidus* plants.

Terpenes were only emitted by control leaves, they accounted for 3.12% of the total emissions, and included sesquiterpenes, diterpenes and triterpenes. Alcohols (C_{24} & C_{26}) were only identified from stressed leaves. Notably, the relative emissions of fatty acids increased by a factor of 5 between control and stressed leaves i.e., 5.3% to 26.8% of the total emissions. Remarkably, out of these fatty acids, octanoic, decanoic, and 9-oxononanoic acids were only emitted from stressed leaves while dodecanoic acid relative emission from stressed leaves doubled its emission from control leaves. The relative abundances (%) of the whole range of emitted compounds from control versus stressed leaves are listed in appendix AIV.2.

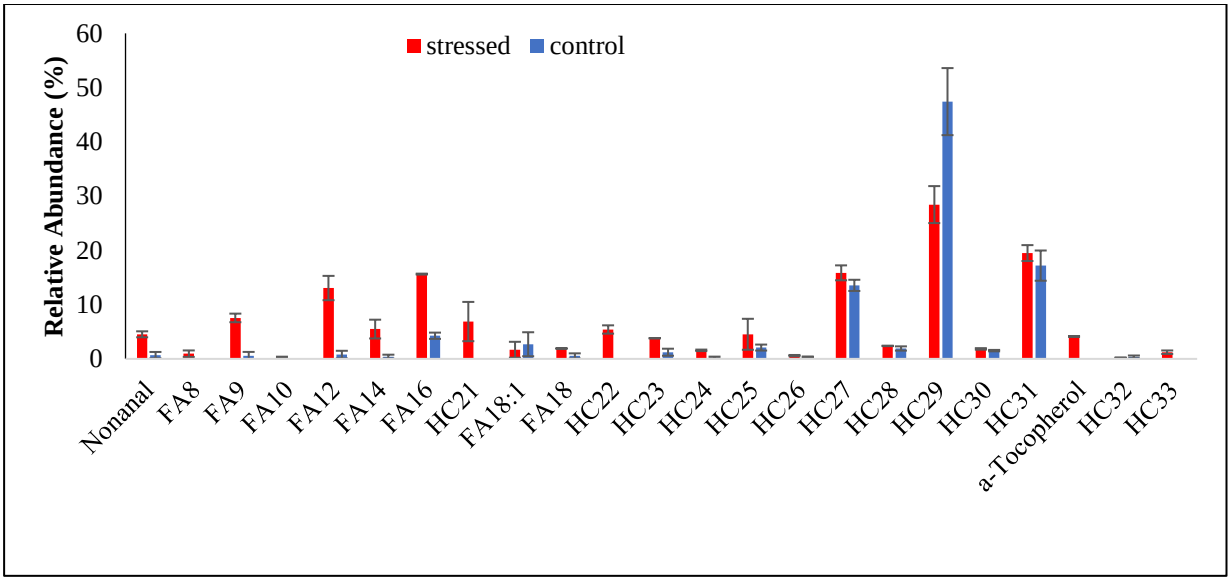

Figure IV.16. Relative abundance (%) of emissions from control vs drought-stressed *C. albidus* leaves. FAn: Fatty Acid, Acn: Acetate, HCn: Hydrocarbon, n: number of Carbon atoms.

7.3 *Discussion*

When comparing the pyrolysis emissions from control and drought-stressed leaves of both plant species we notice the presence of terpenes (mainly monoterpenes) stored in *R. officinalis* and their absence in *C. albidus* as they were emitted from the first but not from the second (control and drought-stressed). The absence of monoterpenes content in *C. albidus* plants can be referred to their storage sites i.e., foliar glandular hairs which are not deep enough to prevent the most volatile terpenes such as α-pinene and even less volatile terpenes such as limonene, from getting stored. These results confirm the findings of Llusià & Peñuelas (2000), that *C. albidus* emit terpenes (mainly under temperature stresses) more than storing them. Another study has shown that *C. albidus* under well irrigated conditions store only the sesquiterpene caryophyllene (Llusià & Peñuelas 1998). Non-terpenoid VOC emissions such as medium-chained aldehydes which are normally produced in the cuticular layers of plant leaves (Peñuelas & Llusià 2001), e.g. nonanal (C_9) was emitted in higher concentrations from stressed *C. albidus* leaves than from well-watered (control) leaves signaling to damaged lipid membranes (Copolovici & Niinemets, 2016). On the other hand, significant emissions of long-chain hydrocarbons and fatty acids were emitted probably from the thick adaxial cuticle layer formed in response to drought stress (Viros et al. 2020). The release of free polyunsaturated fatty acids such as C_{12}, C_{14}, C_{16} & C_{18} are induced by the damage occurring to plant tissues which triggers the hydrolytic cleavage of complex membrane lipids by lipases, followed by a subsequent cleavage

of lipid hydroperoxide that gives rise to the emission of alcohols (Midzi et al. 2022). On the contrary, emissions from drought-stressed *R. officinalis* were dominated by non-oxygenated monoterpenes (e.g. α-pinene), and oxygenated monoterpenes (e.g. camphor, borneol). However, their increased percentages from drought-stressed leaves of *R. officinalis* indicate their higher reserves, a result that conforms with the findings of Nogués et al. (2015). Terpenes are stored in storing plant species in higher percentages under drought stresses due to reduced stomatal conductance, but also as a strategy used by the plant in order to strongly defend itself from biotic attacks and increase their toxicity to herbivores (Viros et al. 2020). The increased fatty acids emissions from stressed leaves may originate from the glandular trichomes in *R. officinalis* leaves in response to water deficit. Finally, vitamin E emissions from drought-stressed *R. officinalis* is a drought adaptation root secretion technique (root exudates) that permit a better water and nutrients uptake from the soil (Danish & Zafar-ul-Hye 2019).

8 Thermal Stress: Plant Scale

The tests conducted on a plant scale inside the hermetic enclosure have faced some technical difficulties. The ECOM analyzer that was supposed to analyze the total hydrocarbons emitted from the tested plant, in addition to CO, CO_2, O_2 and H_2O, has malfunctioned during the tests and we weren't able to collect correct emission recordings. H_2O percentages have been summed from the first detection till the first emissions of CH_4 indicating the beginning of volatilization stage. This is why the Chemisorbers were used to adsorb the emissions to be further analyzed with Py. The desorption mechanisms were hard to be figured out and the supplier's information were limited so we had to improvise and conduct several trials before figuring out the best desorption technique as described in section 5.2.2.3. The thermal stress trials in the hermetic enclosure on drought-stressed, and live (fresh) plants of *R. officinalis* and *C. albidus* are scheduled in appendix AIV.3 and AIV.4, respectively. ImageJ® software was used to measure the area of each plant for normalization purposes. In certain trials, a number of plants were combined together in order to increase the surface area facing the radiant panel.

8.1 *R. officinalis*

8.1.1 ECOM Results

The first observations from the information collected by ECOM (Appendix AIV.3) when applicable, for *R. officinalis* have shown that, emissions of methane gas (CH_4) started at higher temperatures for drought-stressed plants, with higher maximal values than live plants denoted as fresh. Same applies to CO emissions which started at higher temperatures with higher values and shorter emission periods for stressed compared to fresh. CO emissions were also more than those of CH_4 in both fresh and stressed plants. The dehydration phase was identified from the emergence of the first H_2O% until the first recording of CH_4 ppm indicating the beginning of volatilization phase of light compounds. CO emissions in oxygen atmosphere cannot be verified if they originate from cellulose decomposition (Liodakis et al. 2002b), or from the reactions of released VOCs with oxygen under thermal stresses (Greenberg et al. 2006). CO emissions begin to be released from live fresh *R. officinalis* at temperatures as low as 17°C compared to > 100°C for stressed plants with lower periods of emission. Information on their H_2O percentages were not sufficient to conclude on FMC as the ECOM failed to record them for stressed plants.

8.1.2 Magic Chemisorber

Glowing was noticed on the *R. officinalis* fresh plants and therefore we have decided to use chemisorbers before and after glowing in order to configure the nature of emissions involved before and after the glowing. The emissions from pre- and post-glowing are identified in appendix AIV.5. No major differences were noticed between the two phases except that sesquiterpenes such as α- and β- caryophyllene, γ-muurolene, and δ-cadinene, in addition to anhydrosugars such as 1,6-anhydro-D-galactose and furans such as coumaran were identified in the pre-glowing but not in the after glowing emissions. Hydrocarbons from C_{25} to C_{35} were common with similar concentrations between the two phases. Syringol and guaiacol lignin derived compounds were emitted in the pre-glowing phase but were absent after glowing. In the absence of sufficient O_2 percentages inside the compartment (19%) to support flaming combustion; glowing combustion may be a result of char oxidation formed from cellulose depolymerization. As discussed in chapter I (*cf. section 4.2*), when char > tar, glowing occurs where char oxidizes with O_2 to produce CO which later oxidizes to CO_2. As soon as the compartment door opened to allow access of air, the plant burst into flames due to abundance of O_2. No monoterpenes were detected in the compounds desorbed from the Chemisorbers from pre- and post-glowing as the desorption was made at a heating rate of 500°C.min^{-1}. However, at a heating rate of 50°C.min^{-1}, terpenes were well desorbed as will be shown in the following section.

8.1.3 Emissions Collected by Pyrolysis (Leaf Scale) vs Magic Chemisorber (Plant Scale)

In order to verify the adsorption efficiency of the Magic Chemisorbers, we've decided to compare the emissions from the plant scale in the hermetic enclosure adsorbed by the Chemisorber with those gained by leaf pyrolysis Py, from the same drought-stressed *R. officinalis* plant (Figures IV.17 and IV.18).

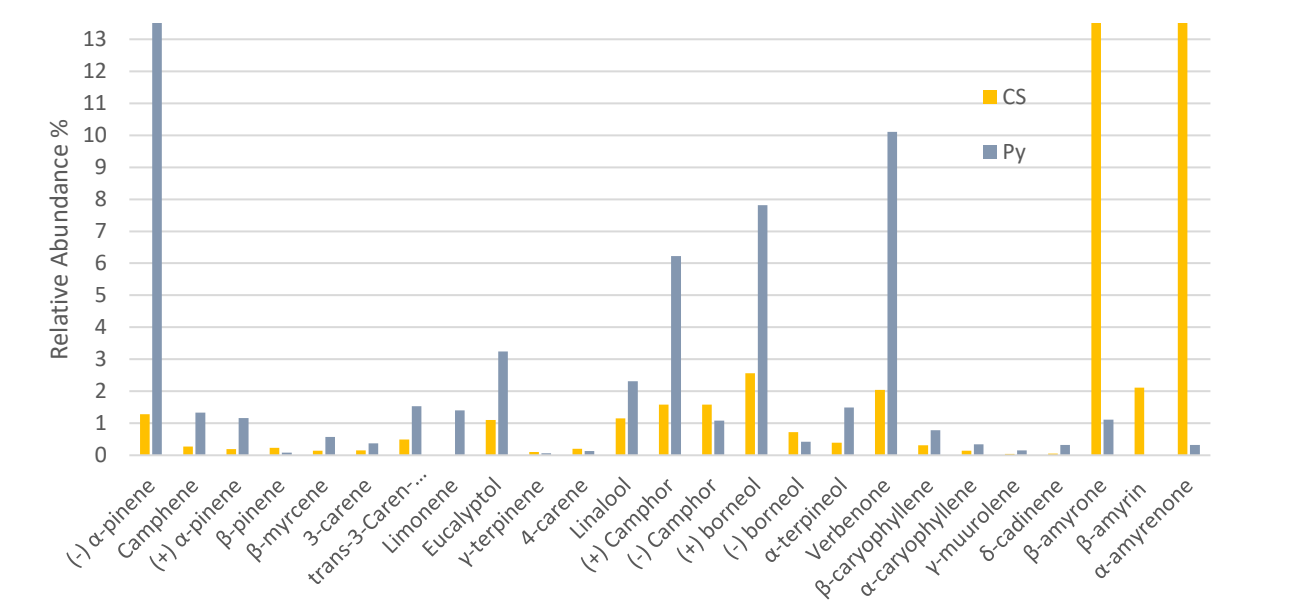

Figure IV.17. Relative abundance (%) of terpenes and terpenes derivatives amongst the total emissions from leaf scale pyrolysis (Py) vs plant scale thermal degradation using Magic Chemisorber (CS) for drought-stressed *R. officinalis* (RHS2).

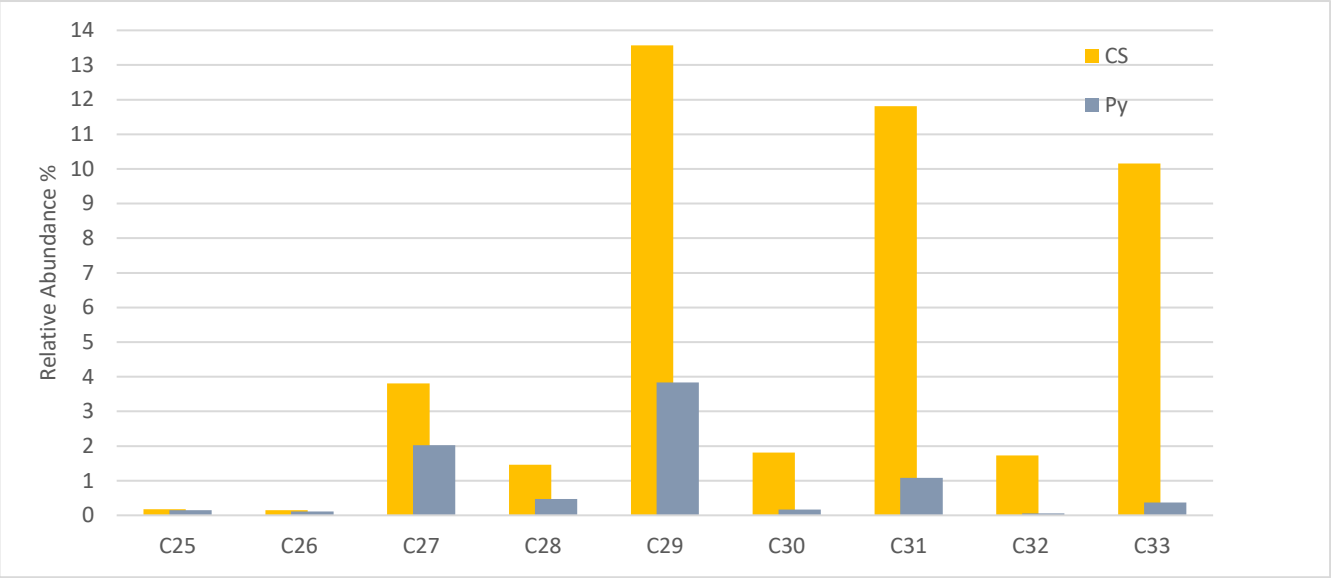

Figure IV.18. Relative abundance (%) of long-chain hydrocarbons amongst the total emissions from leaf scale pyrolysis (Py) vs plant scale thermal degradation using Magic Chemisorber (CS) for drought-stressed *R. officinalis* (RHS2).

The range of terpenes (monoterpenes) adsorbed by the Chemisorber was lower than that gained by leaf pyrolysis and the relative abundance was remarkably smaller as a higher range of long-chain hydrocarbons was adsorbed. Magic Chemisorbers seem to have better adsorption of heavy compounds as long-chain hydrocarbons (C_{25} - C_{33}). The dominance of triterpenoids and alkanes in the emissions of drought-stressed *R. officinalis*, can be related to the cuticular wax formed on the surface of leaves as a response to drought. Cuticular wax formation on plant structures protects it from abiotic stresses such as drought by insulating the leaves in order to limit transpiration. The prevalence of odd paraffins from *R. officinalis* such as C_{27}, C_{29}, C_{31}, and C_{33} conform with the results of Scognamiglio et al. (2022). In addition to long-chain alkanes, triterpenes such as α-amyrenone (14.65%) and triterpenoids such as β-amyrone (15.12%) and β-amyrin (2,12%), were the second most abundant also originating from the cuticular wax covering *R. officinalis* leaves. Monoterpenes, sesquiterpenes and ketones come at the third place of emissions. For example, α-pinene had a relative abundance of 13.6% from pyrolyzed drought-stressed leaves compared to 0.12% from fresh leaves supporting the elevated terpene content of *R. officinalis* post drought stresses.

8.2 *C. albidus*

The plant scale thermal degradation tests on *C. albidus* didn't go as planned because of major problems encountered with the ECOM analyzer, the Chemisorbers and the compartment structure. However, the primary information we could get from the ECOM is that methane gas (CH_4) emissions from drought-stressed *C. albidus* started at earlier plant temperatures (141°C & 171°C) for longer durations (up to 30 mins) compared to fresh *C. albidus* (187°C & 211°C) for shorter durations (up to 26 mins). No information of emissions from these tests could be harvested using Chemisorbers therefore, we depended on the information gained by leaf pyrolysis to compare the emissions of fresh and drought-stressed *C. albidus* in (*cf. section* 7.2).

9 Conclusion

Mediterranean climates are characterized by long dry summers that exert severe abiotic stresses on the vegetation species driving them to change their physiological mechanisms in order to survive. Thermotolerance is a character, donated to vegetation species that are able to adapt physiologically to environmental abiotic stresses. Amongst of these adaptations is their increased reservoirs of volatile content which when altered by fire will feed wildfires and increase the risk of flashovers. Two physiologically different shrub species; *Rosmarinus officinalis* and *Cistus albidus,* were tested for their thermotolerance, their adaptation to drought stress, and their consequent volatile reserves on leaf and plant scales. Our results have shown the remarkable adaptation of these Mediterranean shrub species to 16 days of drought stress on both levels; physiological traits and volatile content. Photosynthesis was restricted in both species after their leaf chlorophyll contents were reduced by almost half, a consequence of less CO2 uptake due to their reduced stomatal conductance. However, *C. albidus* showed higher resistance to drought than *R. officinalis,* a conclusion drawn according to the severity of the anatomical changes observed in the leaves of *C. albidus*. The volatile content of both species has increased relatively. Notably, the terpene content of *C. albidus* was close to null in control and drought-stressed leaves except for the humble concentrations of sesquiterpenes (e.g. β-caryophyllene) noted in control leaves. On the contrary, the terpene content of *R. officinalis* was big in control and increased in drought-stressed leaves remarkably, especially the concentration of oxygenated and non-oxygenated monoterpenes. On the other hand, the drought stress increased the plant concentrations of fatty acids, alcohols, esters, and long-chain alkanes in both species. Of course, these particular emissions originate from the cuticular waxes secreted by plants as a protective mechanism against drought stresses. The emissions from control and drought-stressed leaves were recovered on a leaf scale by pyrolysis using Py-GC/MS apparatus. The plant scale emissions from fresh and drought-stressed plants of both species were done by thermal degradation under radiant heat exposure in a hermetic enclosure where the adsorption/desorption technology using a solid phase extractor (Magic Chemisorber) was implemented with active continuous emissions sampling. The desorption process of the Chemisorbers was challenging and still demands reproducibility experimentation however, the primary results on *R. officinalis* emissions came satisfying and confirmed the emissions by pyrolysis with an acceptable precision. Unfortunately, the technology couldn’t be used with *C. albidus* for technical problems which calls for future experimenting. Normalization methods were hard to be achieved as the continuous weight loss monitoring scales were damaged by heat effects during plants' thermal degradation experiments. Finally, further investigations should be run to relate the flammability characteristics of the identified emission mixtures to their probable contribution to wildfire flashovers in the dry summer seasons of the MCR.

CHAPTER V

*****

Investigating the Flammability Limits of β-Caryophyllene

Résumé

Les sesquiterpènes $C_{15}H_{24}$

Les sesquiterpènes (C15-terpènes) sont des COVB produits par les plantes, à partir de 3 précurseurs (Isopentényl diphosphate (IPP)), proche de l'isoprène, pour devenir $C_{15}H_{24}$. Parmi leurs dérivés (sesquiterpénoïdes) figurent les alcools oxygénés ($C_{15}H_{22}O$), les aldéhydes ($C_{15}H_{24}O$) et les cétones ($C_{15}H_{26}O$) (Helmig *et al.* 2003). Les sesquiterpènes sont synthétisés et émis par les plantes comme formes de protection contre les herbivores, attractifs pour les pollinisateurs et responsables du parfum des plantes (*cf. Tableau I.6*). Des teneurs plus élevées en sesquiterpènes dans la végétation ont été liées à leur inflammabilité accrue (Della Rocca *et al. 2017*), une observation qui a été confirmée par nos études sur *Cupressus sempervirens L.* (*cf chapitre III, section 10.3.1*). Les sesquiterpènes communs tels que le α-humulène et le β-caryophyllène ont une volatilité modérée dans des conditions ambiantes (25°C), où leurs constantes de loi de Henry (K_h, $Pa.m^3.mol^{-1}$) sont respectivement de 3410 et 2731, par rapport aux monoterpènes pour exemple α-pinène (13590 $Pa.m^3.mol^{-1}$), (*cf. Tableau I.8*). Par conséquent, leurs taux d'évaporation sont très retardés. Pour éviter leur cytotoxicité, les sesquiterpènes sont stockés dans des environnements hydrophobes profondément à l'intérieur des structures végétales telles que les conduits de résine et les trichomes glandulaires loin des tissus mésophylles aqueux où la photosynthèse a lieu (Delatte *et al.* 2018). Par conséquent, les émissions des plantes ne sont déclenchées que lorsque ces tissus végétaux sont endommagés et fissurés par distillation sous effets thermiques ou par une attaque externe d'herbivores. Bien que les sesquiterpènes aient une courte durée de vie dans l'atmosphère et qu'ils s'oxydent de manière significative pour former des aérosols organiques secondaires (AOS) (Ciccioli *et al.* 2014), leurs taux d'émission (principalement β-caryophyllène) parmi les COVB dans les incendies de végétation méditerranéenne (par exemple, les conifères mixtes), viennent directement après les monoterpènes (Hatch et al. 2019).

β-caryophyllène

Parmi tous les sesquiterpènes, le β-caryophyllène est le plus abondant émis par les conifères, les pins, les arbres à feuilles caduques (Gao *et al.* 2022, Chen *et al.* 2023) et aussi les arbustes indigènes, par exemple, *Manuka, C. albidus*, et *R. officinalis* (Bernardes *et al.* 2010, Alsaud *et al. 2020*). En raison de leur point éclair plus élevé, les sesquiterpènes ont une volatilité moins grande que, par exemple, les monoterpènes (par exemple, 33 °C pour les données Sigma-Aldrich du α-pinène), mais leurs taux d'émission dans les incendies de végétation, en particulier pour le β-caryophyllène, ont atteint des niveaux relativement élevés parmi les autres émissions de terpènes (62% de *P. halepensis*, 32,4% de *P. pinaster*, 31,2% de *P.pinea*, 5,2% de *C. albidus*, 13,6% de *C. laurifolius*), (Ormeno *et al.* 2009).

Objectif de ce Travail

Comme les sesquiterpènes font partie des mélanges gazeux émis lors des incendies de forêt, il serait important d'obtenir des informations concrètes sur leurs limites inférieure et supérieure d'inflammabilité afin de prédire correctement leur probabilité d'inflammation. Pour déterminer les limites d'inflammabilité des sesquiterpènes, nous avons trouvé important de déterminer les

pressions de vapeur et les limites d'inflammabilité de l'un des sesquiterpènes les plus couramment identifiés dans les incendies de forêt ; β-aryophyllène. Les tests de limites d'inflammabilité sont effectués conformément aux normes internationales ASTM et EN, en particulier la norme anglaise EN 1839 : 2017, où deux méthodes de test sont suivies : la méthode T (méthode du tube) et la méthode B (méthode de la bombe). La méthode B sera adaptée tout au long de ce travail pour la disponibilité de l'appareil de test dans nos laboratoires. D'après Catoire et Naudet (Chetehouna *et al.* 2014), et la réaction de combustion équilibrée du β-caryophyllène avec l'air, on peut en déduire sa limite d'inflammabilité à son point d'ébullition et à la pression atmosphérique. Ces conditions ont été choisies pour simuler la température d'évaporation du β-caryophyllène de la végétation lors d'un feu de forêt à pression atmosphérique. Des tentatives expérimentales ont été menées pour mesurer les pressions de vapeur du β-caryophyllène dans la chambre Tension Vapeur Saturante (TVS) dans les laboratoires à l'institut PPRIME. L'objectif était de confirmer les pressions de vapeur expérimentales du β-caryophyllène à différentes températures jusqu'à son point d'ébullition, cependant, comme le manomètre capacitif à haute température a une pression limite de 110 mbar, nous n'avons pas pu mener d'expériences de pression de vapeur à des températures dépassant 200°C.

Limites d'inflammabilité et pression de vapeur de β-caryophyllène

Les limites d'inflammabilité inférieure (LLI) et supérieure (LIS) du carburant dans l'air dépendent de la température, c'est-à-dire que la LII diminue tandis que la LSI augmente avec l'augmentation de la température initiale du mélange. D'autre part, les LII des vapeurs ne sont pas affectées par les variations de pression sauf si la pression était inférieure à 50 mm Hg (66.6 mbar) où la flamme peut se propager plus longtemps. Au contraire, la LSI augmentera avec l'augmentation de la pression, ce qui augmentera considérablement la plage d'inflammabilité. Selon les normes OSHA, les limites d'inflammabilité inférieure et supérieure du β-caryophyllène sont respectivement de 2 et 12 %. En préparation des travaux expérimentaux, les résultats théoriques pour trouver les limites d'inflammabilité du β-caryophyllène dans un bomb sphérique sont abordés tout au long de ce chapitre. Des tests préliminaires ont été menés sur du décane pour tester l'efficacité de l'appareil puis des tests ont été menés sur β-caryophyllène à différentes températures. Les deux résultats étaient satisfaisants et confirmés avec les pressions de vapeur de la littérature. Les perspectives futures peuvent être d'augmenter la capacité du manomètre à mesurer la pression de vapeur du β-caryophyllène à sa température d'ébullition et d'effectuer les tests de limites d'inflammabilité.

1 Introduction

Sesquiterpenes (C15-terpenes) are BVOCs produced by plants, consist of 3 isoprene units to become $C_{15}H_{24}$. Among their derivatives are, oxygenated alcohols ($C_{15}H_{22}O$), aldehydes ($C_{15}H_{24}O$), and ketones ($C_{15}H_{26}O$), (Helmig et al. 2003). Sesquiterpenes are synthesized and emitted by plants as forms of protection against herbivores, attractant to pollinators, and responsible for plant fragrance (*cf Table I.6*). High sesquiterpenes contents in vegetation have been linked to their increased ignitability (Della Rocca et al. 2017), an observation that was confirmed by our studies on Cupressus sempervirens L. (*cf. Chapter III, Section 9.3.1*). Common sesquiterpenes such as α-humulene and β-caryophyllene have moderate volatility in ambient conditions (25°C), where their Henry's constants (Kh, Pa. m^3. mol^{-1}) are 3410 and 2731, respectively, in comparison to monoterpenes for example β-pinene (13590), (*cf. Chapter I, Table I.8*). Therefore, their evaporation rates are highly delayed. To avoid their cytotoxicity, sesquiterpenes are stored in hydrophobic environments deeply inside plant structures such as resin ducts, and glandular trichomes away from the aqueous mesophyll tissues where photosynthesis takes place (Delatte et al. 2018). Therefore, their emissions from plants are only triggered when such plant tissues are damaged and cracked open by distillation under thermal effects or by an external attack from herbivores. Although sesquiterpenes have a short atmospheric lifetime and they oxidize significantly to form secondary organic aerosol (SOA) (Ciccioli et al. 2014), their emission rates (mainly β-caryophyllene) among BVOCs in wildfires of Mediterranean vegetation (e.g. mixed conifers), come directly after monoterpenes (Hatch et al. 2019). As sesquiterpenes will be part of the gaseous mixtures emitted in wildfires it would be important to get concrete information about their lower and upper flammability limits in order to predict their ignition probability correctly. With humble efforts paid by the scientific community to determine the flammability limits of sesquiterpenes, we found it important to determine the vapor pressures and flammability limits of one of the most commonly identified sesquiterpenes in wildfires; β-caryophyllene. Since pure sesquiterpenes will be addressed in this work we will refer to them as hydrocarbons of the form (C_xH_y) throughout this chapter.

2 Lower and Upper Flammability Limits of Hydrocarbons

As discussed in chapter I (*cf. section 6.3.3.3*), the lower flammability limit (LFL) of a fuel vapor in an oxidizing atmosphere e.g. air, is its minimum concentration expressed in volume percentage (%vol) below at which it doesn't ignite with a mediated ignition source whereas the upper flammability limit (UFL) is the maximum concentration beyond of which the gas will no longer ignite or permit a flame propagation. Therefore, below the LFL (%) there is not enough fuel vapor in air to ignite and above the UFL (%) there is no enough oxygen in the air/vapor volume for the vapor to ignite. There is also the possibility to measure the lower flammability limit of a mixture of gases in air following *Le Chatelier's* law as shown in chapter 1 *(cf. equation 19*) given that the individual LFLs (%) of each constituent are known.

2.1 LFL and UFL and Stoichiometric Concentration

The best way to determine flammability limits is experimentally however, literature provided empirical equations to measure lower and upper flammability limits. The equation of Jones

which depends on the stoichiometric concentration (C_{est}) of the flammable hydrocarbon to undergo complete combustion in air (Hristova & Tchaoushev 2006). Air is considered as oxidizer oxygen in the combustion reaction as follows,

$$C_mH_xO_y + zO_2 \rightarrow mCO_2 + \frac{x}{2}H_2O$$

$$LFL = 0.55C_{est} \quad (1)$$

$$UFL = 3.5C_{est} \quad (2)$$

$$LFL(\%) = \frac{0.55(100)}{4.76m + 1.19x - 2.38y + 1} \quad (3)$$

$$UFL(\%) = \frac{3.50(100)}{4.76m + 1.19x - 2.38y + 1} \quad (4)$$

2.2 LFL and UFL and Enthalpy of Combustion

Other empirical equations are available for the prediction of flammability limits depending on the heat liberated from complete combustion of the gas in air (Albahri 2003), as follows:

$$LFL \times (-\Delta H_{comb}) = 4.354 \times 10^3 \quad (5)$$

Where, ΔH_{comb} is the heat of combustion in kJ.mol^{-1}.

Another method to determine lower flammability limits is the one suggested by Dalmazzone et al. (2001).

$$LFL(\%) = \frac{100MC_1}{(\Delta H^{\circ}_{Ci})_{298K} - (MM_i - M) \times C_1} \quad (6)$$

Where, i refers to the compound of which its LFL% is calculated, $(\Delta H^{\circ}_{Ci})_{298K}$ is its enthalpy of combustion at 298K, MM_i is its molecular mass in g.mol^{-1}. M is the molar mass of air (28.84 g.mol^{-1}), and C_1= - 0.345.

2.3 LFL, UFL, and Flash Point

The lower flammability limit for a gas at its flash point temperature is related to the vapor pressure of the gas at this temperature according to the following formula (Hristova & Tchaoushev 2006);

$$LFL_i(\%) = \frac{P^{sat}_{i,fp}(@T_f)}{P} \quad (7)$$

Where, LFL_i is the lower flammability limit of the flammable gas in air. And $P^{sat}_{i,fp}(T_f)$ is the saturation vapor pressure of the flammable gas at flash point temperature, and P is the atmospheric pressure.

It should be noted however, that flash points concentrations depend on the downward propagation of the flame to the surface of a flammable liquid inside a cup where it forms a flash whereas the lower flammability limits cited in literature are mostly measured in spherical apparatus and depend on the upward propagation of flame (Prugh 2008). Since the upward propagation of flame facilitated by thermal buoyancey is easier than downward propagation, it is suggested that the concentrations for flash point are bigger than LFLs. The above equations

provide calculation methods of flammability limits normally at 25°C however, flammability limits can be measured at various temperature ranges and there are few equations, four to our knowledge, that can be used to calculate the flammability limits in relationship to temperature.

2.4 LFL and UFL Dependence on Temperature

Lower and upper flammability limits of fuel in air are temperature dependents i.e., LFL decreases while UFL increases with the increase of the initial mixture temperature. Therefore, these limits change with every temperature and corresponding formulas exist to find them. When expressed in terms of mass per cubic meter, the lower flammability limit (LFL) based on the molecular weight M ($g.mol^{-1}$) of the hydrocarbon and temperature T(K) and the LFL (%) according to (Prugh 2008) becomes,

$$LFL\ (g.m^{-3}) = {}^{100}\Big/\left[\left\{{}^{12200M}\Big/_{[52(T+273)]}\right\}+1\right] vol\% \qquad (8)$$

Another formula is the one provided by Catoire and Naudet (2005), to measure the lower flammability limit of compounds containing C, H or O atoms.

$$LFL\ \%\ (T) = 519.957 \times X^{0.70936} \times n_C^{-0.197} \times T^{-0.51536} \qquad (9)$$

Where $X = \frac{1}{1+5n_C+\frac{5}{4n_H}-5/2n_O}$, is the stoichiometric mole fraction of the hydrocarbon in the compound/air mixture, n_C, n_H, and n_O are the number of carbons, hydrogen, and oxygen atoms, respectively, and T is the temperature in K.

Two other formulas that take experimental values of LFL as a reference for finding the numerical ones at different temperatures are Burgess-Wheeler, and Britton-Furip laws (Rowley et al. 2011, Mendiburu et al. 2017). The upper flammability limit UFL of a vapor can also be calculated depending on the temperature T (°C) and the net heat of combustion ΔH_c (Kcal.mole^{-1}), if its UFL value at 25°C is known according to the modified law of Burgess-Wheeler (Wu et al. 2018) as follows,

$$UFL_T = UFL_{25} + \frac{0.75}{\Delta H_c}(T-25) \qquad (10)$$

This formula is also valid for LFL with a change in sign.

$$LFL_T = LFL_{25} - \frac{0.75}{\Delta H_c}(T-25) \qquad (11)$$

2.5 LFL and UFL Dependence on Pressure

The LFLs of vapors are not affected by pressure variations unless the pressure was less than 50mm Hg where flames no longer propagate (Zhao 2011, Zhao 2023). Contrarily UFL will increase with pressure increase significantly, thus increasing the flammability range.

$$UFL_p(\%) = UFL + 20.6(\log P + 1) \qquad (12)$$

Where, UFL is the upper flammability limit in (% vol of air fuel mixture at atmospheric pressure, 1 atm). P is the initial pressure and UFL_p is the upper flammability limit at pressure P.

2.6 Volume Occupied by BVOC at LFL in Space

The volume occupied by the flammable gas (e.g. terpene) reaching its LFL in a fire plume can be calculated using the following formula (Chen et al. 2023);

$$V_{space} = \frac{W_{loading} \times C_{volatileoil} \times \rho_{volatileoil} \times 1000}{LFL_{terpene}} \quad (13)$$

Where, V_{space} is the volume occupied by the flammable terpene in m^3, $W_{loading}$ is the quantity of fuel (dead and/or live) possibly emitting the flammable compound per hectare in t. ha^{-1}, $C_{volatileoil}$ is the concentration of the terpene in an oil form available in the fuel (dead and/or live) in $mL.kg^{-1}$ and $\rho_{volatile}$ is the density of the volatile at atmospheric condition (25°C and 100kPa) in $g.mL^{-1}$. Guerrero et al. (2022), provides methods for finding the volatile oil concentrations in live/dead biomass.

3 Experimental Methods for Testing Flammability Limits

Flammability limits tests are run according to international ASTM and EN standards, one of particular is the English Norm EN 1839:2017, where there are two testing methods followed: Method T (tube method), and Method B (spherical bomb method). Method B will be adapted throughout this work for the availability of the testing apparatus in our labs.

3.1 Test Method B (Spherical Bomb Method)

3.1.1 Principle

The sesquiterpene (liquid) is admitted to a spherical vessel equipped with an ignition source. The characterization of the flammability limits consists of determining at what quantity of fuel admitted to the vessel there won't be an ignition in air atmosphere. Experiments should be initiated at atmospheric pressure and the ignition is monitored using two methods; pressure rise and spark monitoring. The amount of test substance in the test mixture is varied in increments until the LFL or UFL is determined, or until the absence of a flammable range is established.

3.1.2 Spherical Bomb

The bomb is a spherical vessel made of catalytic non-reactive stainless steel to avoid corrosion and is equipped with glazing to monitor flame propagation after ignition. The test vessel is also equipped with pressure transducers to measure overpressure after ignition. The vessel, valves, joints, pressure transducers, and all accessories should be designed to sustain a pressure of 15bars. The internal volume of the vessel must be greater or equal to 0.005 m^3 (5 dm^3). The larger the volume of the bomb the closer are the flammability limit values to open atmospheres, (Barbosa et al. 2021).

3.1.3 Ignition Source

The ignition is allowed through tinned copper fuse wires located in the center of the vessel in a way not to obstruct the flame in case of ignition. An electric arc is generated by passing an electric charge using an isolation transformer through a fuse wire connected between the two metal rods of diameter between 1.5 and 5mm. The energy supply should be in the range of 10 to 20J to avoid any significance effect on flammability limits accuracy. Such a range will be attained if the isolation transformer power is maintained between 0.7 to 3.5 kW. The stainless-steel rods should be coincident and separated by a distance of (5±1 mm) and the fuse wire (NiCr) with a diameter between 0.05 to 0.2 mm soldered to the ends of the two rods (Gieras et

al. 2006). The electric wires connecting the transformer to the rods should have a surface area of 2.5 to 7mm^2 and the length should be less than 5m.

3.1.4 Overpressure Measurement

The pressure after ignition will increase until reaching a maximum value beyond of which it decreases when heat is dissipated through the walls of the vessel. The pressure transducer should operate at a frequency of 10kHz. A typical pressure criterion for ignition would be when the pressure is equal or greater than the overpressure created by the ignition source alone in air plus 5 ± 0.1% of initial operating pressure. The pressure readings are then traced as a function of time P = f(t). Several types of pressure-time curves will emerge depending whether the flame is propagating upward or downward (growing or extinguishing), governed by the burning velocity of the vapor and the bulk buoyancy velocity of the rising burnt gases (Crowl & Jo 2009). A typical pressure-time curve where the concentration of vapor is in the flammable range (above LFL and below UFL) and the upward and downward propagation limits is shown in Figure V.1, other curves for different flammability scenarios are found in (Crowl & Jo 2009). In Figure V.1, after ignition the flame kernel goes upward and the pressure rise rate accelerates where it appears concave until the flame touches the top of the vessel and goes down to extinguish in its way down forming a convex curve.

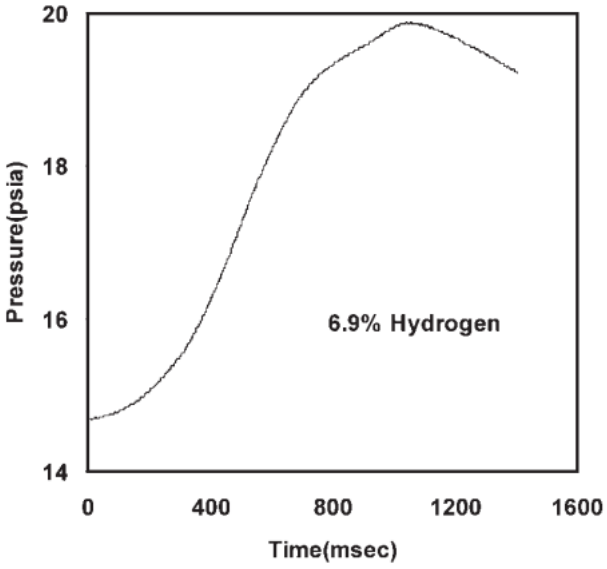

Figure V.1. Pressure-time curve of hydrogen igniting in air in a spherical vessel, (Crowl & Jo 2009)

3.1.5 Flammable Compound

Flammable sesquiterpene should be well prepared and added to the vessel with care to avoid leakage or contamination. The whole apparatus must be heated to the same temperature of evaporation in order to avoid condensation in any of its parts. Accuracy must be taken into consideration when simulating the theoretical values of partial pressures, temperatures and equivalence ratio (Air/Fuel, A/F). The tested liquid should be of a purity not less than 99.8%. The liquid should be injected at a lower pressure than its vapor pressure in order to ensure its complete evaporation. The liquid vapor pressure and the corresponding number of moles is found experimentally at the designated temperature. Synthetic air is added to the vessel to the designated experimenting pressure (e.g. atmospheric pressure 101kPa) in compliance to the A/F

ratio. The partial pressures are monitored by a feedback control from normally a high precision pressure transducer. It should be noted that all apparatus parts should be heated in order to avoid any forms of condensation of the flammable gas inside the vessel.

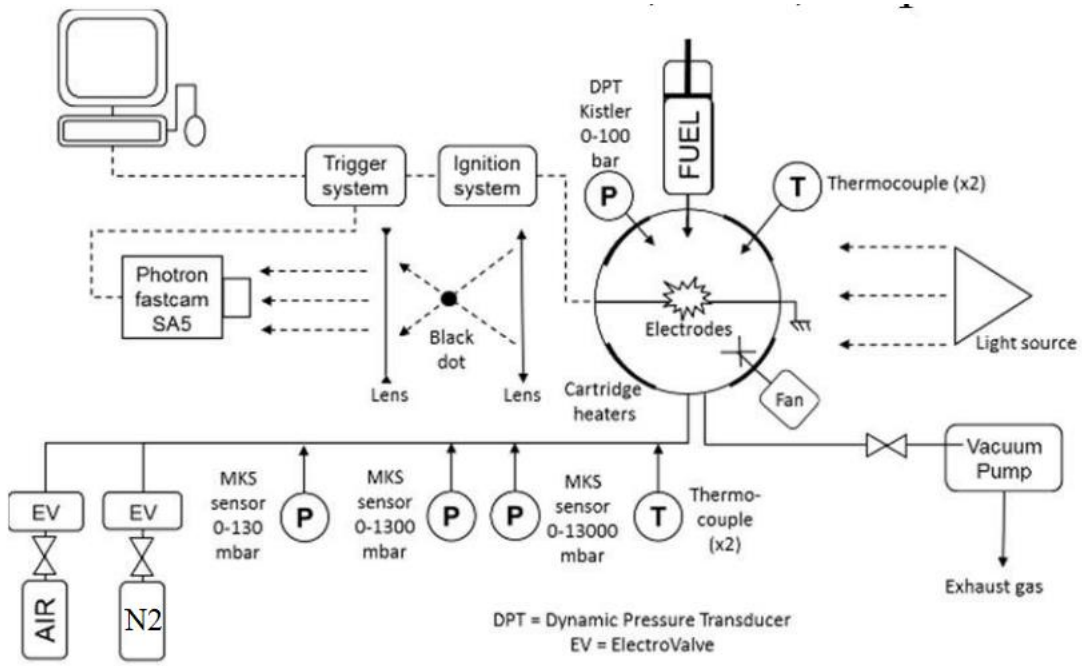

Figure V.2. Typical experimental apparatus used for determining flammability limits of chemical compounds, (Le Dortz et al. 2017).

4 Sesquiterpenes and Flammability

4.1 Sesquiterpenes and Vegetation Flammability

Several studies including ours (*cf. chapter III, section* 9.3) correlated the flammability descriptors (particularly ignitability and combustibility) to vegetation (mainly litter) terpene content. More profoundly monoterpenes and sesquiterpenes. For example, mono- and sesquiterpenes emissions from *P. halepensis* and *R. officinalis* litter under thermal stresses have enhanced their flammability characteristics (Romero & Ganteaume 2021). Their comparative study on two species of pine i.e., *P. halepensis* and *P. sylvestris* showed the dominance of sesquiterpenes among the terpene emissions of both species. Among about 17 different identified sesquiterpenes and sesquiterpenoids, β-caryophyllene was the most abundant with a percentage of 28.5% among the other terpenes from *P. halepensis*. In contrast to monoterpenes, sesquiterpenes have enhanced the flammability of *P. halepensis* shoots (Figure V.3). A relevance between sesquiterpenes and induced flammability was also found by Ganteaume et al. (2021). Whether positive or negative is the role played by sesquiterpenes on flammability, their abundance in gaseous mixtures emitted from Mediterranean vegetation in fire events demands investigating experimentally their flammability limits in order to link them to flashovers.

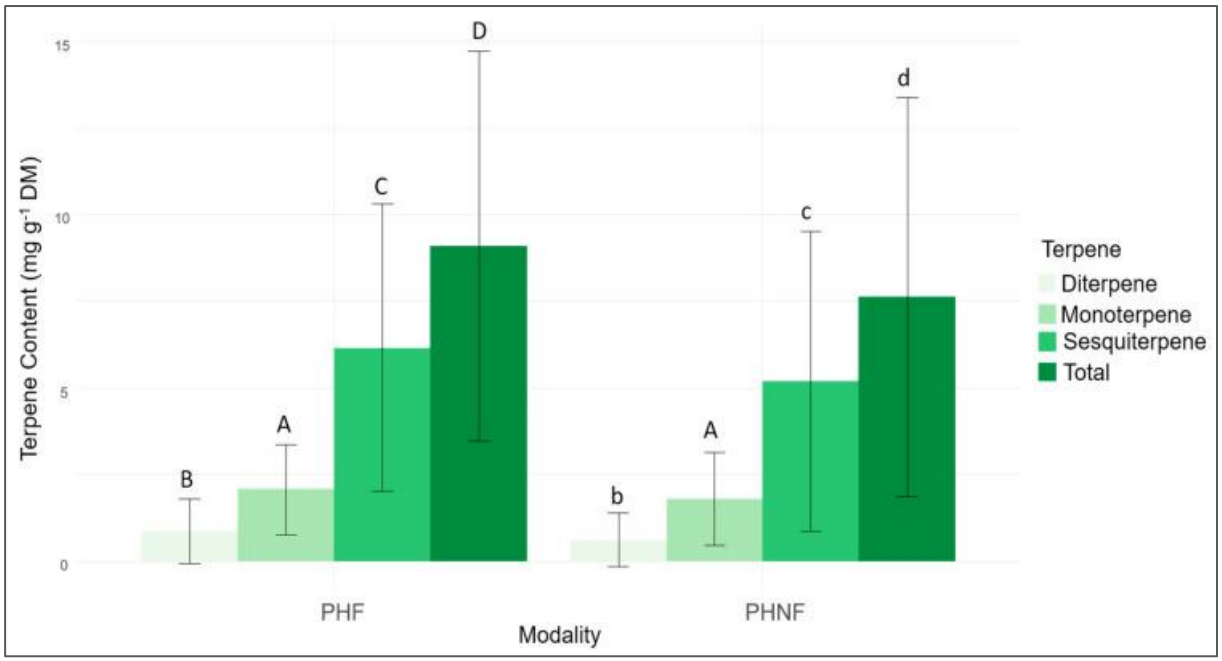

Figure V.3. Dominance of sesquiterpenes in the total terpene content of *P. halepensis* emissions in two fire modalities; PHF & PHNF, (Romero & Ganteaume 2021).
PHF: *P. halepensis* fire modality. PHNF: *P. halepensis* no fire modality.

4.2 Physical Properties of Common Sesquiterpenes

Literature provides humble records about the flammability characteristics of sesquiterpenes, nevertheless their contribution to vegetation flammability is inevitable and undeniable. Table V.1, contains physical properties of common sesquiterpenes and sesquiterpenoids emitted by pines during a fire event (Romero & Ganteaume 2021). Information lacking on thermochemical properties of sesquiterpenes, i.e., flammability limits or vapor pressures, demands the need to investigate them experimentally. Although sesquiterpenes are less volatile than monoterpenes however, they are equally important.

Table V.1. Physical properties of common sesquiterpenes emitted from *P. halepensis* litter fire (Romero & Ganteaume 2021).

Compound	Chemical Formula	Boiling Point (°C) at 1 atm	LFL % (25°C)	UFL % (25°C)	Flash Point (°C)	Saturation Vapor Pressure (Kpa)		Source
Sesquiterpenes						25°C	75°C	
B-Cadinene	C15H24	273 - 276	---	---	106.67	1.4e-03	---	TGSC Information System
α-Muurolene	C15H24	271.5	---	---	106.5	1.4e-03	---	TGSC Information System
D-Germacrene	C15H24	280	---	---	111.67	9.3e-04	---	TGSC Information System
Valencene	C15H24	274	---	---	100	1.4e-03	---	Sigma-Aldrich SDS
α-Humulene	C15H24	267	---	---	90	9.23e-04	7.48e-02	Helmig et al. 2003
β-Caryophyllene	C15H24	263	2	12	105.5	1.35e-03	9.79e-02	Helmig et al. 2003, OSHA HCS
γ Cadinene	C15H24	271 - 276	---	---	106.67	1.3e-03	---	VIGON SDS
Ylangene	C15H24	248 - 249	---	---	105	5.06e-03	---	TGSC Information System
β-Elemene	C15H24		3.5	15	98.30	3.67e-03	---	TGSC Information System

B Bourbonene	C15H24	255 - 256	---	---	104	3.3e-03	---	TGSC Information System
α Copaene	C15H24	246 - 251	---	---	42.78	2.19e-03	1.37e-01	TGSC Information System, Helmig et al. 2003
α Cubebene	C15H24	245 - 246	---	---	100	1.8E-03	---	TGSC Information System
Aromadendrene	C15H24	262	---	---	---	1.07e-03	8.32e-02	Helmig et al. 2003
Sesquiterpenoids								
Elemol	C15H26O	289 - 290	---	---	98.89	3.19e-05	---	TGSC Information System
τ Cadinol	C15H26O	302 - 304	---	---	128.33	---	---	TGSC Information System
α Bisabolol	C15H26O	314	---	---	93.3	5.30e-05	1.01e-02	VIGON SDS
α Cadinol	C15H26O	303.4 ± 31	---	---	128 ± 17.1	0.186	---	ChemSrc

5 Flammability Limit of β-Caryophyllene

5.1 β-Caryophyllene

Among all the sesquiterpenes, β-Caryophyllene is the most abundantly emitted from coniferous, pines, deciduous trees (Gao et al. 2022, Chen et al. 2023) and also indigenous shrubs, for example, *Manuka*, *C. albidus*, and *R. officinalis* (Bernardes et al. 2010, Alsaud et al. 2020). Owing to their higher flash points, sesquiterpenes have less volatility compared to, for example, monoterpenes (e.g. 33°C for α-pinene Sigma-Aldrich data) however, their emission rates in wildfires from vegetation especially for β-Caryophyllene have reached high relative abundance among other terpene emissions (62% from *P. halepensis*, 32.4% from *P. pinaster*, 31.2% from *P.pinea*, 5.2% from *C. albidus*, 13.6% from *C. laurifolius*), (Ormeno et al. 2009). According to OSHA standards, lower and upper flammability limits of β-caryophyllene are found to be 2 and 12%, respectively.

5.2 Theoretical Stoichiometric Air (A/F) of β-Caryophyllene

It is the minimum concentration of air required to complete the combustion of a hydrocarbon (e.g. sesquiterpenes, $C_{15}H_{24}$). The complete combustion results in the complete transformation of carbon to CO_2, and hydrogen to H_2O. The theoretical stoichiometric ratio represents the amount of air required to burn an amount of fuel completely. The stoichiometric air is also referred to as air to fuel ratio (A/F) and is found by the solving for the balanced chemical combustion reaction. The stoichiometric air for β-caryophyllene becomes;

$$C_{15}H_{24} + a(O_2 + 3.76N_2) \rightarrow bCO_2 + cH_2O + dN_2$$

Where,

C: b = 15 O: 2b + c = 2a, a = 21

H: c = 12 N: d = 3.76a, d = 78.96

The balanced reaction becomes:

$$C_{15}H_{24} + 21(O_2 + 3.76N_2) \rightarrow 15CO_2 + 12H_2O + 78.96N_2$$

Therefore, the air fuel ratio (A/F) of the above combustion reaction on a mass basis will be:

$$\frac{A}{F} = \frac{m_{air}}{m_{fuel}} = \frac{(NM)_{air}}{(NM)_C + (NM)_{H_2}}$$
$$= \frac{21(4.76kmol)(28.84kg.kmol^{-1})}{1(15kmol)(12\ kg.kmol^{-1}) + 1(12kmol)(2kg.mol^{-1})}$$
$$= 14.13\ kg\ air\ /\ kg\ fuel$$

Theoretically, 14.13 kg of air are required to burn each kilogram of β-caryophyllene.

5.3 Equivalence Ratio

Ideal A/F ratios are never achieved in combustion experiments, because experimenters opt to use excess air in order to increase the chances of attaining complete combustion. The amount of the air excess is usually expressed in a percentage of the stoichiometric air, for example, a 30% excess air is 130% of the stoichiometric air. This amount is expressed in terms of an equivalence ratio (Φ). The equivalence ratio (Φ), is the fraction of the actual to the stoichiometric fuel to air mass ratios. The importance of the equivalence ratio is in its role in the flame stabilization once established. It also interferes with the displacement speed of pre-mixed flames (Palies 2020).

$$\Phi = \frac{(A/F)_{stoichiometric}}{(A/F)_{actual}} = \frac{(F/A)_{actual}}{(F/A)_{stoichiometric}} \qquad (14)$$

A fuel-rich mixture will have Φ > 1 however, if Φ < 1 the mixture is considered a fuel-lean mixture. Therefore, for a given equivalence ratio the combustion balance reaction of β-caryophyllene becomes;

$$\Phi C_{15}H_{24} + 21(O_2 + 3.76N_2) \rightarrow 15\Phi CO_2 + 12\Phi H_2O + 21[(1-\Phi)O_2 + 3.76N_2]$$

The mass fraction of $C_{15}H_{24}$ becomes:

$$Y_{C_{15}H_{24}} = \frac{\Phi(15W_C + 24W_H)}{\Phi(15W_C + 24W_H) + 21[2W_O + 2 \times 3.76W_N]}$$

The mass faction of CO_2 becomes:

$$Y_{CO_2} = \frac{15\Phi(W_C + 2W_O)}{12\Phi(2W_H + W_O) + 15\Phi(W_C + 2W_O) + 21[(1-\Phi)2W_O + 2 \times 3.76W_N]}$$

The mass fraction of H_2O becomes:

$$Y_{H_2O} = \frac{12\Phi(2W_H + W_O)}{12\Phi(2W_H + W_O) + 15\Phi(W_C + 2W_O) + 21[(1-\Phi)2W_O + 2 \times 3.76W_N]}$$

The mass fractions of β-caryophyllene, H_2O, CO_2, N_2, and O_2 for different values of equivalence ratios Φ are listed in Table V.2.

Table V.2. Mass fractions at various equivalence ratios Φ for combustion of β-caryophyllene ($C_{15}H_{24}$) with air.

Φ	**0,5**	**0,6**	**0,7**	**0,8**	**0,9**	**1**	**1,1**	**1,2**
$C_{15}H_{24}$ - Air								
Y_{C15H24}	0,034	0,154	0,176	0,196	0,215	0,233	0,251	0,267

Y_{CO2}	0,111	0,129	0,146	0,163	0,178	0,193	0,207	0,220
Y_{H2O}	0,036	0,043	0,050	0,057	0,063	0,070	0,076	0,083
Y_{O2}	0,225	0,223	0,222	0,220	0,219	0,217	0,216	0,215
Y_{N2}	0,741	0,736	0,731	0,726	0,721	0,716	0,712	0,707

5.4 Lower Flammability Limit Calculation

According to Catoire and Naudet (2005) in Chetehouna et al. (2014), and the balanced combustion reaction of β-caryophyllene with air, we can deduce its flammability limit at its boiling point and atmospheric pressure. These conditions were chosen to simulate the evaporation temperature of β-caryophyllene from the vegetation in a forest fire at atmospheric pressure.

$$C_{15}H_{24} + 21(O_2 + 3.76N_2) \rightarrow 15CO_2 + 12H_2O + 78.96N_2$$

The lower flammability limit (LFL%) of β-caryophyllene at its boiling temperature (T= 263°C, Table V.1) using Equation 9, and its mole fraction in the stoichiometric air X= 0.01, becomes:

$$LFL\ \%\ (263°C) = 519.957 \times 0.01^{0.70936} \times 15^{-0.197} \times (263 + 273)^{-0.51536} = 0{,}4\%$$

6 β-Caryophyllene Vapor Pressure

Investigating the flammability limits of a certain compound (e.g. β-caryophyllene), requires information about its vapor pressure with its respective volume at the designated temperature. Our aim is to study the flammability limits of β-caryophyllene at its boiling point and atmospheric pressure, i.e., 263°C and 1atm.

6.1 Theoretical Investigation of β-caryophyllene Vapor Pressure

The vapor pressures of β-caryophyllene at different temperatures are investigated theoretically according to the work of Carissa Nelson (2018), who used chromatographic methods to investigate the vapor pressures and evaporation enthalpies of sesquiterpenes, e.g. α-humulene, β-caryophyllene, and α-bergamotene. Their studies allowed them to find a relationship between the vapor pressure and the temperature as follows;

$$\ln\left(\frac{P}{P^{\circ}}\right) = A_s + B_s\left(\frac{1}{T}\right) + C_s\left(\frac{1}{T}\right)^2$$

Where, P (Pa) is the vapor pressure at temperature T in (K), P° is the atmospheric pressure 101325Pa, and A_s, B_s, and C_s (Table V.3) are the vapor pressure constants evaluated by several experimental trials and compared with literature standards.

Table V.3. Vaporization enthalpies (ΔH) and vapor pressure constants of common sesquiterpenes, (Nelson 2018).

	ΔH (KJ.mol^{-1})	As	Bs (K)	Cs (K^2)
β-Caryophyllene	65.9±2.1	11.139±0.004	-5180.0±3.2	376356±584
α-Humulene	67.5±2.1	11.381±0.005	-5363.5±3.8	376853±693
α-Bergamotene	69.5±2.0	12.025±0.004	-5545.1±2.9	385490±521
Z-Caryophyllene	66.0±2.0	11.200±0.0045	-5171.1±0.004	375861±548

Vapor pressures of β-caryophyllene using the method suggested by Nelson (2018), which proved to provide the most consistent results with literature, are listed in Table V.4. β-caryophyllene vapor pressure at its boiling temperature (536K) is 119481,338 Pa (1,194813383 bar). Therefore, the pressure in the testing vessel should not overcome this value in order to avoid condensation inside of it.

TableV.4. Vapor pressures (Pa) of β-caryophyllene at different temperatures including its boiling temperature (536K).

Temperature (K)	Pressure (Pa)	Pressure (bar)
298.15	2.879	2.87915E-05
310	7.684	7.68381E-05
320	16.481	0.000164815
330	33.520	0.0003352
340	64.983	0.000649826
350	120.638	0.00120638
360	215.340	0.0021534
370	370.909	0.003709094
380	618.419	0.006184189
390	1000.884	0.010008839
400	1576.344	0.015763439
410	2421.302	0.024213015
420	3634.467	0.036344668
430	5340.742	0.053407417
440	7695.366	0.076953657
450	10888.138	0.108881377
460	15147.622	0.151476222
470	20745.250	0.207452505
480	27999.228	0.279992276
490	37278.163	0.372781634
500	49004.355	0.49004355
510	63656.655	0.63656655
520	81772.876	0.817728759
530	103951.689	1.039516894
536*	119481.338	1.194813383
540	130853.993	1.308539929
550	163203.728	1.632037285
560	201788.148	2.017881484

*Boiling temperature of β-caryophyllene.

6.2 Experimental Investigation of β-caryophyllene Vapor Pressure

Experimental investigations of β-caryophyllene were also conducted using an experimental apparatus TVS (Chambre Tension Vapeur Saturante), (Figure V.4). The experimental setup consisted of a perfectly sealed metallic chamber (volume = 2.830e-03 m^3), rolled from the outside with a protected resistance to sustain a heated environment in the inside. Vapor pressure inside the chamber is measured using a high temperature capacitance manometer (Baraton®, type 631C), that operates at a temperature up to 200°C and has a full pressure range of 1000torr

with an accuracy of 0.50% of reading. Pressure readings are displayed in mbar using a digital LCD display type PR4000A. The heat generating resistance wire is uniformly rolled around the testing chamber in order to ensure steady and uniform heating of the hydrocarbon sample inside it and avoid any form of condensation. Temperature are regulated using a digital thermometer getting the signals from thermocouples inserted tightly into the interior lining of the chamber to wall to measure accurate temperature values. A suction pump is used to depressurize the chamber and maintain ensure vacuum conditions prior to each test.

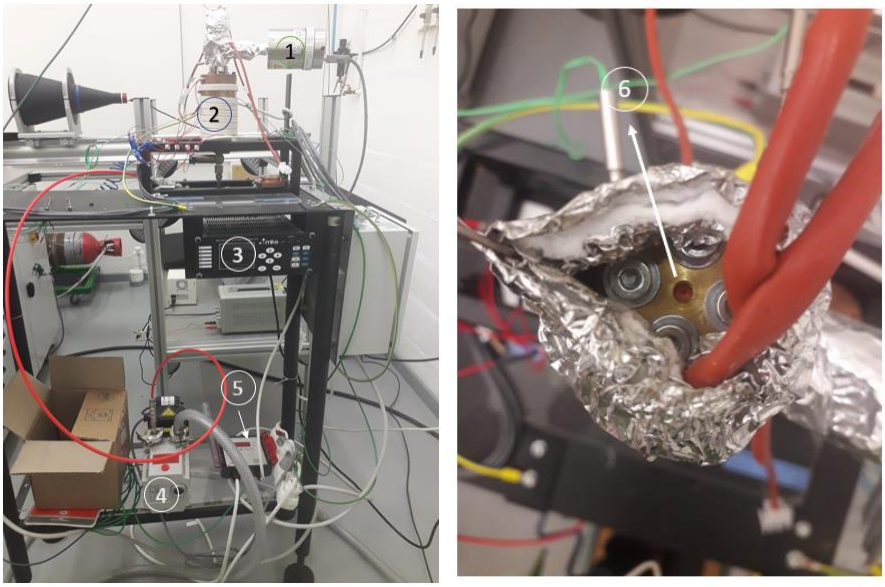

Figure V.4. TVS apparatus. 1) High temperature capacitance Manometer, 2) Heated chamber, 3) Digital power supply and readout 4) Vacuum pump 5) Digital thermostat 6) Sealed sample access to the vapor pressure testing chamber.

6.2.1 Testing Protocol

6.2.1.1 Material Handling

β-Caryophyllene was ordered from Sigma Aldrich®, Merck Group. The purity of the ordered compound is ≥ 98% transported and conserved in a cooled atmosphere (≅ 4°C) to avoid any forms of thermal degradation under heat effects. A graded syringe was used to sample the compound and inject it in the testing chamber. β-Caryophyllene is a very heavy compound with a density that is equal to 0.9 $g.mL^{-1}$ therefore, it was hard for us to do the suction sampling using a syringe with a volume of less than 500µL with minor graduations of 50µL. Syringes with less volumes were not able to aspire the liquid. β-Caryophyllene should be handled according to the indications listed in the compound safety datasheet.

6.2.1.2 Equipment Preparation

- All wires, electrical connections, thermocouples, tubes and flexibles should be examined to verify their structure and avoid any short circuits or leakages in the system.
- The pump exhaust duct should be connected to the main air exhaust ducts in the testing room.

- Regulate the thermometer to the temperatures required to perform the tests in order to allow temperature stabilization and uniformity inside the chamber. The maximum temperature should not pass 200°C.
- Turn on the system equipment (regulation, acquisition, and synchronization instruments) to allow them to reach a stable state for about 2 hours prior to performing the tests.

6.2.1.3 Running the Tests

- Vacuum is maintained inside the chamber in order to perform leakage tests and ensure emptying the chamber from any residuals left from previous tests.
- Before conducting each experiment, a leakage test should be run in order to ensure there is no major gas leakage of vapors in the testing chamber. Close the valve on the pipe connecting the chamber to the suction pump and record the vacuum pressure. Variations in vacuum pressure inside the chamber recorded prior to all tests showed a tolerable 0.13mbar/30secs. Keep the suction pump on during the tests.
- Sample the liquid in the needle with volumes consistent with the volumes of a perfect gas behavior at the designated temperature.
- Inject the sampled liquid inside the testing chamber and allow its complete vaporizations for 1 min and record the pressure reached on the digital readout display.
- Continue injecting the liquid until reaching the saturation pressure at the designated temperature, while keeping a register of the volumes injected with the corresponding pressures.
- At the end of each test, open the valve in order to empty the chamber from β-Caryophyllene vapor and rerun the above steps for the following temperature programs.

On a separate note it's preferable to start an ascending temperature program while conducting the tests. Our tests on vapor pressure of β-caryophyllene were run successively at 150, 160, 170 and 200°C. Unfortunately, the testing equipment were not designed to sustain a temperature > 200°C and a pressure > 110 mbar therefore, we couldn't test β-caryophyllene vapor pressure at its boiling temperature of 263°C.

6.3 Results and Discussion

Before conducting the vapor pressure experiments on β-Caryophyllene, preliminary tests were undergone to test the vapor pressures of decane ($C_{10}H_{22}$) at arbitrary chosen temperatures. The purpose of these preliminary tests was to test the efficiency of the experimental apparatus, to reduce the costs of material purchase as β-caryophyllene is very expensive, and finally to practice on using the apparatus equipment. The vapor pressures of decane and β-caryophyllene were measured and compared to perfect gas behavior and saturation pressure relevant to the tested volumes of the compound and the temperatures. The full range of the manometer is 110 mbar therefore, the vapor pressures that exceeded this limit at higher temperatures were unfeasible.

6.3.1 Vapor Pressures of Decane

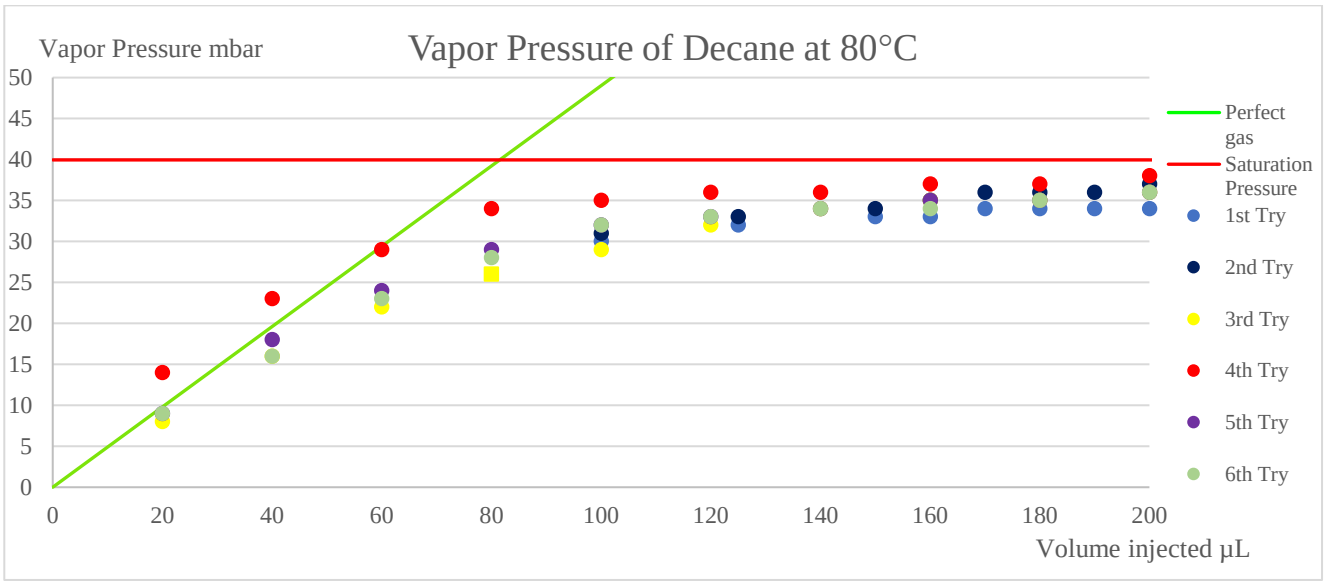

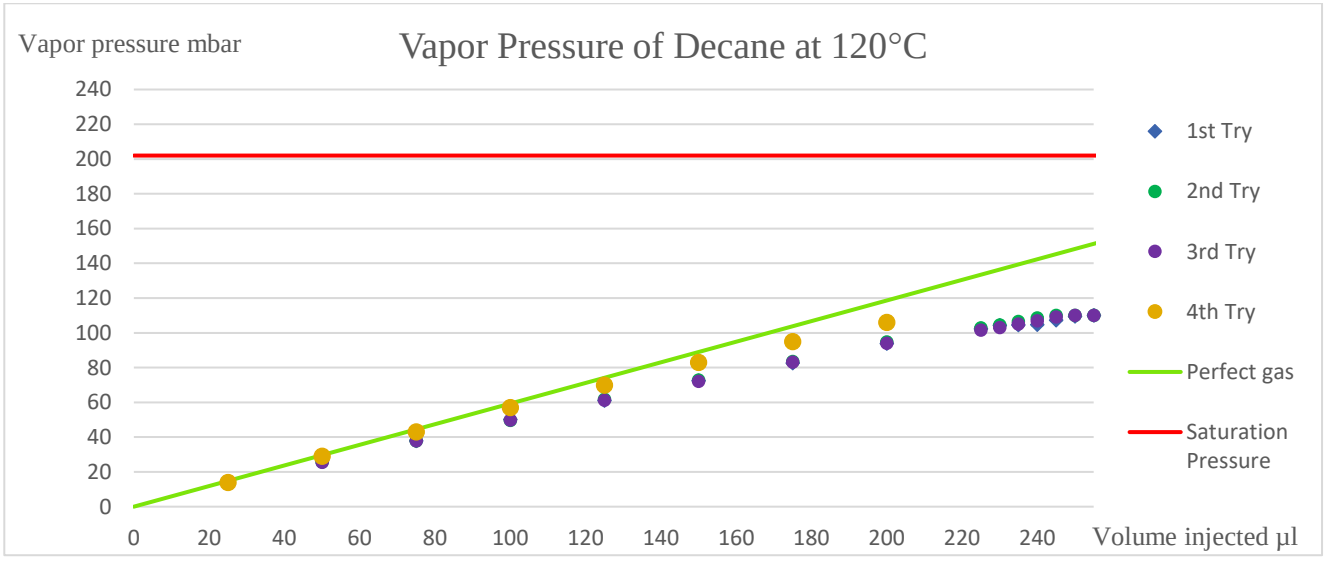

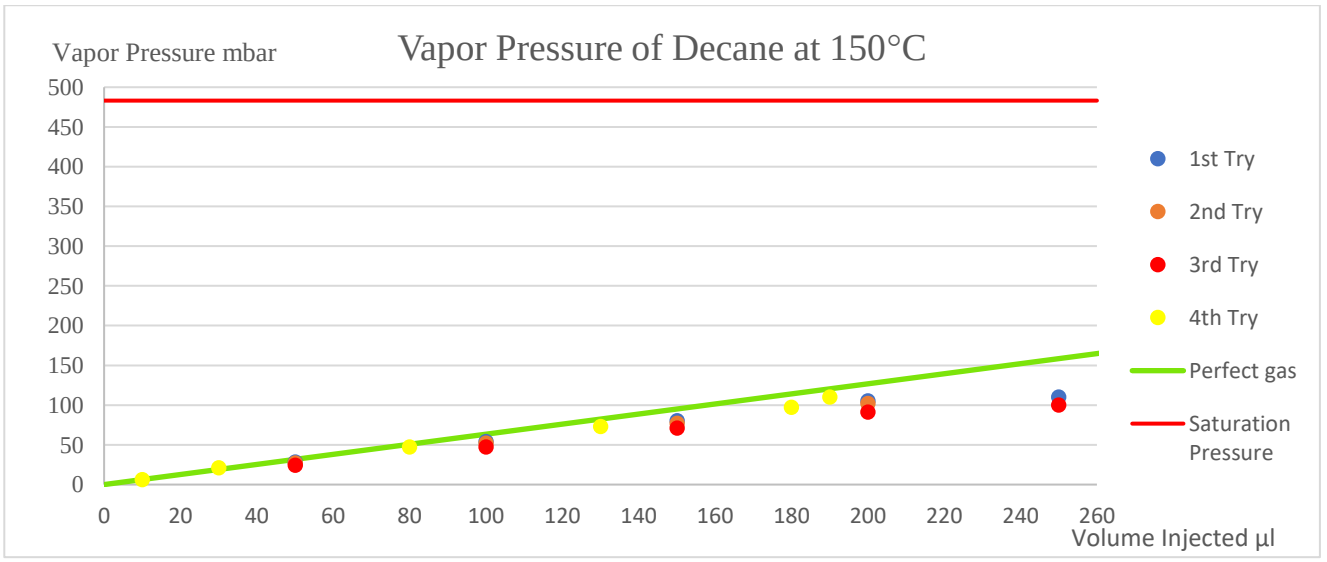

Figure V.5. Vapor pressures of decane ($C_{10}H_{22}$) tested using the TVS at 80°C, 120°C & 150°C.

The experimental tests conducted on decane were useful to predict the accuracy of the testing apparatus, (Figure V.5). The results came with a good repeatability with a pooled relative standard deviation of 25%. Therefore, we've decided to proceed with testing the vapor pressures of β-caryophyllene.

6.3.2 Vapor Pressures of β-Caryophyllene

The experimental vapor pressure profiles came compatible with the theoretical vapor pressures calculated using the methods suggested by Nelson (2018) and other sources in the literature.

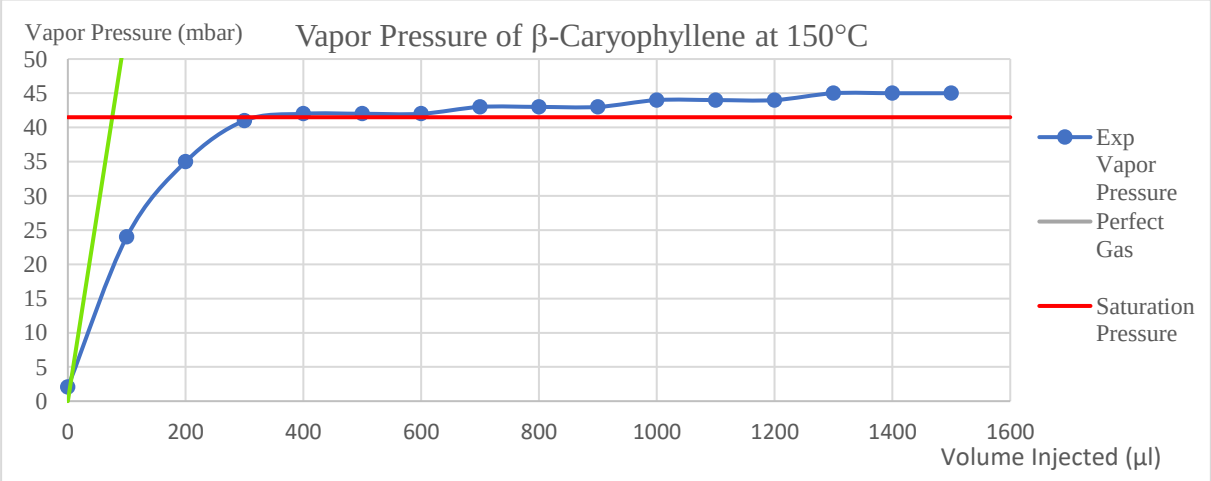

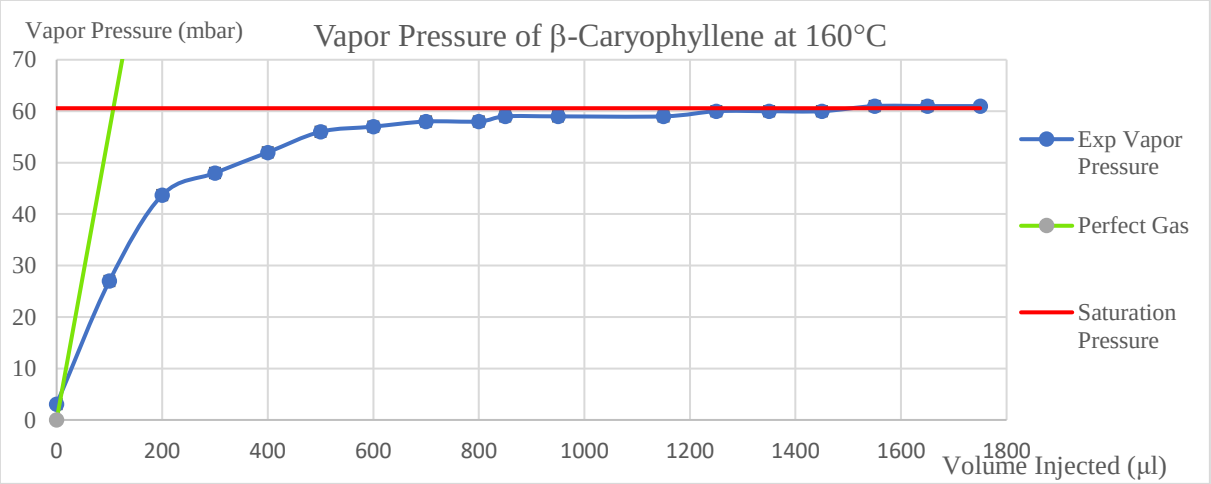

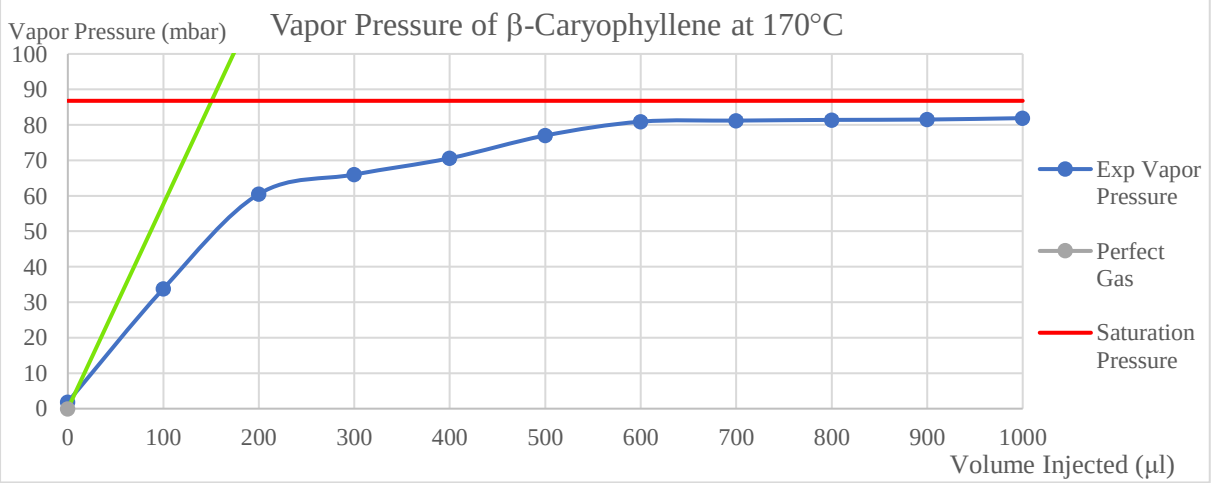

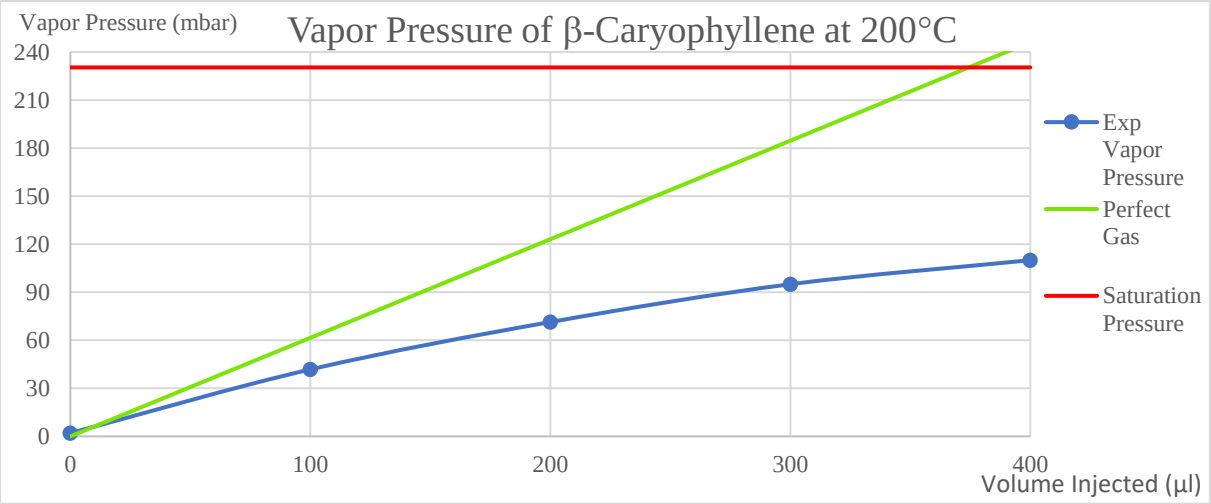

Figure V.6. Vapor pressures of β- caryophyllene tested using the TVS at 150°C, 160°C, 170°C & 200°C.

Table V.5. Vapor pressures P (mbar) of β-Caryophyllene at different temperature from this work compared to literature.

Sesquiterpene		**β-Caryophyllene**		
Density (kg.m^-3)		905		
Purity (%)		>99		
Supplier		Sigma-Aldrich		
T (°C)	**T(K)**	**P/(mbar) (This work)**	**P/(mbar) (Literature)**	
			Ref a*	Ref b*
150	423	42	41,4	43,1
160	433	61	60,5	70,8
170	443	81	86,7	100,3
200	473	>110	227,3	243,13

a* Orf et al. 2021. b* Yao et al. 2019.

The vapor pressures of β-cayophyllene at the tested temperatures came compatible to the values found in literature, except for the temperature of 200°C where the vapor pressure overcome the limit of the manometer used in the setup (Figure V.6 & TableV.5). The experimental results showed a standard deviation of less than 3 mbar. Therefore, it's safe to consider that such an apparatus is efficient in testing vapor pressures of BVOC compounds i.e., sesquiterpenes. Of course, the manometer should be adjusted to calculate higher vapor pressures exceeding 110 mbar at high temperatures.

7 Conclusion

Little information is provided in the literature about the flammability characteristics of sesquiterpenes. We were able to build and operate an experimental setup to investigate the vapor pressures of hydrocarbons including β-caryophyllene as preliminary tests to further investigate their flammability limits in a bomb vessel. Unfortunately, for budget reasons the manometer used in our setup had an upper limit of 110 mbar which restricted the range of operating temperatures less than 200°C. However, for temperatures less than 200°C, vapor

pressures of the compounds tested were compatible to the values found in literature with a standard deviation <3 mbar. Future prospects are to perform vapor pressure testing at higher temperatures reaching the boiling points of β-caryophyllene, and continuing to test experimentally its lower and upper flammability limits using the bomb vessel apparatus at its boiling temperature and atmospheric pressures. Knowing such limits can further assist to predict the potential of sesquiterpene emissions from vegetation in wildfires to concentrate and contribute to flashovers.

General Conclusions and Future Propects

****

General Conclusions

The work executed in this thesis aims towards providing the fire and rescue services and forest management communities, with a more real-time information necessary for configuring and understanding the most controversial forms of extreme wildfire behaviors; the wildfire flashovers. Flashovers associated with confined topographies of the Mediterranean climate wildlands, have harvested vast areas of vegetation communities and the lives of hundreds of humans, and continue to form a major threat to the Mediterranean climate ecosystems especially if they are left unconfigured. The controversy is whether gas pockets or accumulations favored by topography and dense VOC mixtures emitted from burning plants, will reach a flammable range and burst out in a sudden and extremely violent form resembling a lake of fire that will overwhelm the firefighting crews and increase the fire intensities and rates of spread vigorously. Physical and chemical aspects should be considered in a decision support tool in order for it to be successful and efficient for the fire and rescue service to predict and possibly obviate flashover incidents. The chemical part of our work focused on the VOC emissions from Mediterranean forest and shrub species, how their rates and synthesis mechanisms are affected by the climate change stressors (drought and temperatures), and to what extent is their influence on the vegetation flammability. The physical part addressed the possibility of these VOCs to accumulate in a confined topography and whether their accumulations will lay within their flammability limits range and consequently burn when in contact with an ignition source. In a summarized cotext the outcomes of the work in this thesis are as follows:

- *The Mediterranean climate regions are the primary hosts of the wildfire flashover incidents due to the highest frequencies of annual wildfire outbreaks in these regions, and the fact that the vegetation species covering the wildlands of these regions are rich in BVOC content. These BVOCs are emitted in large proportions during wildfires and are subjected to thermal degradation to produce various aromatic and aliphatic hydrocarbons which, amongst other factors (e.g. atmospheric and topography), are directly related to wildfire propagation and violent behaviors.*
- *Porous regions in STARCCM+ produce accurately the effect of forest trees on the atmospheric boundary layer. The region inside the porous region is dominated by the local effect of the forest whereas the one above is representative of an atmospheric boundary layer developing on a very rough surface.*
- *Rothermel mathematical equations for solving surface fire propagation coupled with Van Wagner criteria for transition to a crown fire, proved to produce accurate steady state firefront propagating in the forest.*
- *Emission factors of VOCs measured in gVOC/kg of biomass burned can be used to simulate unsteady emission rates integrated in a moving firefront with ROS ($m.s^{-1}$), flame depth (D), and residence time (τ).*

- *Neglecting the thermal effects at a wind speed of 6 $m.s^{-1}$, densities of heavy aromatics (benzene and toluene) and monoterpenes (α-pinene) favored their accumulations in a sharp-angled valley with an internal angle $\alpha = 100°$. Their concentrations laid between their lower and upper flammability limits. Within the constraints of our numerical investigations, flashovers are highly probable.*
- *TGA/DTA used to assess the flammability descriptors such as ignitibility, combustibility, and consumability from, cellulose content, lignin content, ignition and onset temperatures of endo- and exo-thermic peaks, ash content, and peak areas, proved that live and litter leaves of Cupressuss sempervirents var Horizontalis L. are less ignitable than live and litter leaves of Quercus suber L. However, the FMC of live and litter leaves of the same species provided contradicting results with their cellulose content as ignitability assessment citeria i.e., live leaves of C.s.L. are more ignitable than its litter and likewise for live and litter leaves of Q.s.L. Therefore, regardless of the leaves' cellulose contents, higher FMC of leaves from the same species augmented their ignitability. However, comparing litter from dry and wet seasons for C.s.L. showed higher relative ignitability for C.s.L. from wet season than the dy season, with agreement between the two criteria indicating higher ignitability under heating effect i.e., higher FMC and cellulose amounts.*
- *Many conclusions have been drawn on the relationship between foliar VOC content and flammability in direct contribution to fire propagation and extreme behaviors. The most important are, higher and lower relative abundance of monoterpene and sesquiterpene emissions, respectively from litter leaves of C.s.L. (dry season) compared to those from wet season. Sesquiterpenes content were linked to ignitability and consumability (positive effect) while monoterpenes had a negative effect on both descriptors.*
- *Higher cellulose and lignin percentages in Q.s.L. leaf litter than C.s.L. leaf litter were proved by the higher relative abundance of the emissions deriving from those polymers in the former compared to the latter. The compounds deriving from cuticular wax in the cypress leaf litter dominated the emissions at 350°C. Cupressus sempervirens L. could be used in silviculture measures in forest management to protect more fire vulnerable species such as Quercus suber from the heat of an approaching firefront.*
- *Adaptation to prolonged drought periods of the Mediterranean climate is a trait developed by Mediterranean shrubs with dissimilar percentages. Cistus albidus showed better resistance to drought on a leaf morphological level compared to Rosmarinus officinalis.*
- *Different BVOCs storage sites in vegetation leaves affect their percentages after being subjected to abiotic stresses. The deeper the storage sites the better content of BVOCs at which their evaporation will be harder to take place. Storing BVOCs under drought stresses is a defense mechanism adapted by shrub species such as R. officinalis against abiotic and biotic threats as well.*
- *Flammability limits of sesquiterpenes are not thoroughly addressed in literature although their contribution to vegetation flammability is undeniable. β-caryophyllene is one of the most abundant sesquiterpene emitted by most of the Mediterranean forest*

and shrub species. Our aims to investigate its flammability limits starting with measuring its vapor pressures at different tempeatures were successful.

Future Prospects

The outcomes of the works executed in this thesis in the aim to investigate the Mediterranean climate regions vegetation, their flammability characteritics, their adaptation to the adverse effects of the climate change, and their VOC emissions, all in favor of investigating wildfire flashovers, have been very promising and convincing. However, several possible prospects are able to improve and complete the current approaches as follows:

- *The numerical model investigating the density weighted dispersion of VOCs may include the thermal effects of a realistic propagating fire front in order to account for buoyancy effects on the dispersion of VOCs. These last should follow a reactive chemical profile. Such an improvement can be done with implementing a reacting flame propgation model using reactive chemical species of biomass degradation* with the "*Flamlet" model in STARCCM+. It's recommended to use the JP10 reactive reactions library for biomass fuel.*
- *Further experimental testing on the two distinctively flammable species C.s.L. and Q.s.L. should be done in order to reproduce the results we had from our works. It will be interesting also to investigate the resistance of C.s.L. on a canopy level i.e., investigating the structural characteristics of C.s.L. stands, and their plantation patterns to provide fire resistant walls similar to fire breaks.*
- *As the criteria used in our study proves the relative resistance of C.s.L. on a foliar level to heat stresses simulating an approaching firefront however, it would be interesting to compare the resistance of this species to direct flame as well.*
- *Investigating the morphological adaptation mechanisms and VOC emission rates from R. officinalis and C. albidus under drought and thermal stresses was fruitful. However, it's necessary to rerun the flammability testing on a plant scale in air atmosphere and collect and analyze the VOC emissions using our methods with adsorbtion/desorption, and investigate the autoignition of plants facing a radiant panel simulating real wildfire conditions.*
- *Space is always open to experiment more vegetation species consumed by the wildfires hitting the Mediterranean climate regions. These species can be forest species such as Aleppo pine, Pinus halepensis, Holm oak, or chaparral shrubs such as Brachypodium retusum, Ulex parviflorus … etc.*
- *Flammabiltiy limits testing on β-caryophyllene and possibly other sesquiterpenes in a bomb vessel apparatus is a good support to literature and to the investigations of VOC accumulations favoring flashovers. Of course, the TVS equipment should be improved to measure vapor pressures of sesuiterpenes boiling temperatures.*

References

A.-C Genard-Zielinski, C Boissard, Christian Fernandez, C Kalogridis, J Lathi`ere, et al (2015). Variability of BVOC emissions from a Mediterranean mixed forest in southern France with a focus on Quercus pubescens. Atmospheric Chemistry and Physics, European Geosciences Union,15, pp.431-446.

Abatzoglou, John & Williams, Alton & Barbero, Renaud. (2019). Global Emergence of Anthropogenic Climate Change in Fire Weather Indices. Geophysical Research Letters. 46.

Acácio, V., Holmgren, M., Rego, F., Moreira, F., & Mohren, G. M. J. (2008). Are drought and wildfires turning Mediterranean cork oak forests into persistent shrublands? Agroforestry Systems, 76(2), 389–400.

Akagi, S. K., Yokelson, R. J., Burling, I. R., Meinardi, S., Simpson, I., Blake, D. R., ... & Weise, D. R. (2013). Measurements of reactive trace gases and variable O 3 formation rates in some South Carolina biomass burning plumes. Atmospheric Chemistry and Physics, 13(3), 1141-1165.

Akagi, S. K., Yokelson, R. J., Wiedinmyer, C., Alvarado, M. J., Reid, J. S., Karl, T., ... & Wennberg, P. O. (2011). Emission factors for open and domestic biomass burning for use in atmospheric models. Atmospheric Chemistry and Physics, 11(9), 4039-4072.

Alam, Md Azharul; Wyse, Sarah V.; Buckley, Hannah L.; Perry, George L. W.; Sullivan, Jon J.; Mason, Norman W. H.; Buxton, Rowan; Richardson, Sarah J.; Curran, Timothy J.; Gilliam, Frank (2019). Shoot flammability is decoupled from leaf flammability, but controlled by leaf functional traits. Journal of Ecology, 1365-2745.13289.

Alastair Nicol, W. (1975). Physicochemical Methods of Mineral Analysis || Thermal Analysis. 10.1007/978-1-4684-2046-3(Chapter 10), 389–420.

Albahri, T. A. (2003). Flammability characteristics of pure hydrocarbons. Chemical Engineering Science, 58(16), 3629–3641.

Albini, F. (1976). Estimating wildfire behavior and effects. USDA Forest Service, Intermountain Forest and Range Experiment Station, General Technical Report INT-30, 92.

Albini, F. A. (1985) "A model for fire spread in wildland fuels by radiation," Combustion Science and Technology, vol. 42, pp. 229–258.

Alexander M. & Cruz, M. (2010). Assessing crown fire potential in coniferous forests of western North America: a critique of current approaches and recent simulation studies. International Journal of Wildland Fire, 19(4) 377–398.

Alsaud, Noor & Shahbaz, Kaveh & Farid, Mohammed. (2020). Evaluation of deep eutectic solvents in the extraction of β-caryophyllene from New Zealand Manuka leaves (Leptospermum scoparium). Chemical Engineering Research and Design. 166.

Anderegg, W. R. L., Berry, J. A., Smith, D. D., Sperry, J. S., Anderegg, L. D. L., & Field, C. B. (2011). The roles of hydraulic and carbon stress in a widespread climate-induced forest die-off. Proceedings of the National Academy of Sciences, 109(1), 233–237.

Anderson HE (1970) Forest fuel ignitibility. Fire Technology 6, 312–319, 322.

Anderson, H. E. (1968), "Sundance Fire: An Analysis of Fire Phenomena," USDA Forest Service Research Paper INT-56, Intermountain Forest and Range Experiment Station 39 pp.

Anderson, H. E. (1982). Aids to determining fuel models for estimating fire behavior. USDA, Forest Service, General Technical Report INT-122 Ogden, UT: Intermountain forest and range Experiment Station, 4–16 pp.

Andreae, M. O. (2019). Emission of trace gases and aerosols from biomass burning–an updated assessment. Atmospheric Chemistry and Physics, 19(13), 8523-8546.

Andreae, M. O. and Merlet, P. (2001). Emission of trace gases and aerosols from biomass burning, Global Biogeochem. Cy., 15, 955–966.

Andreu Anne G., Blake John I., Zarnoch Stanley J. (2018) Estimating canopy fuel characteristics for predicting crown fire potential in common forest types of the Atlantic Coastal Plain, USA. International Journal of Wildland Fire **27**, 742-755.

Andrews, Patricia & Heinsch, Faith & Schelvan, Luke. (2011). How to Generate and Interpret Fire Characteristics Charts for Surface and Crown Fire Behavior. USDA Forest Service - General Technical Report RMRS-GTR.

Aragão, Luiz & Anderson, Liana & Fonseca, Marisa & Rosan, Thais Michele & Vedovato, Laura & Wagner, Fabien & Silva, Camila & Silva-Junior, Celso & Arai, Egidio & Aguiar, Ana Paula & Barlow, Jos & Berenguer, Erika & Deeter, Merritt & Domingues, Lucas & Gatti, Luciana & Gloor, Manuel & Malhi, Yadvinder & Marengo, Jose & Miller, John & Saatchi, Sassan. (2018). 21st Century drought-related fires counteract the decline of Amazon deforestation carbon emissions. Nature Communications. 9. 536.

Arlaud H. and Lalizel G. (2016). 'Caractérisation spectrale de µthermocouples K de 7, 6 µm de diamètre pour une application aux mesures de fluctuations de température dans des écoulements anisothermes turbulents.', Congr. Fr. Therm. Toulouse, Fr. 2016 31 Mai to 3 June.

Auburn, S., Leitl, B., (2004). Development of an improved physical modelling of a forest area in a wind tunnel. Atmos. Environ. 38, 2797–2801.

Babinszki, Bence & Jakab, Emma & Terjék, Viktor & Sebestyén, Zoltán & Czirok, István & Bozi, János & Attanatho, Lalita & Thanmongkhon, Yoothana & Czégény, Zsuzsanna. (2022). In situ formation of fatty acid methyl esters via thermally assisted methylation by lignin during torrefaction of oil palm biomass. Journal of Analytical and Applied Pyrolysis. 168.

Bäck, J., Hari, P., Hakola, H., Juurola, E., & Kulmala, M. (2005). Dynamics of monoterpene emissions in Pinus sylvestris during early spring. Boreal Environment Research, 10(5), 409.

Baeza, M., De Luís, M., Raventós, J., & Escarré, A. (2002). Factors influencing fire behaviour in shrublands of different stand ages and the implications for using prescribed burning to reduce wildfire risk. Journal of Environmental Management, 65(2), 199–208.

Baines PG (1990) Physical mechanisms for the propagation of surface fires. Mathematical and Computer Modelling 13(12), 83–94.

Baranovskiy, N., & Demikhova, A. (2019). Mathematical modeling of heat transfer in an element of combustible plant material when exposed to radiation from a forest fire. Safety, 5(3), 56.

Barboni, Toussaint & Chiaramonti, Nathalie & Leoni, Eric & Desjobert, Jean-Marie & Santoni, Paul-Antoine. (2006). Analysis of smoke during prescribed fire. 10.1109/ISEIMA.2006.345041.

Barbosa, J. A., Coronado, C. J. R., Tuna, C. E., Silva, M. H., Mendiburu, A. Z., Carvalho Junior, J. A., & de Andrade, J. C. (2021). Experimental determination of lower flammability limits of Synthesized Iso-Paraffins (SIP), jet fuel and mixtures at atmospheric and reduced pressures with air. Fire Safety Journal, 121, 103276.

Basu, P. (2018). *Biomass gasification, pyrolysis and torrefaction: practical design and theory*. Academic press.

Berg L. G.; Egunov V. P. (1969). Quantitative thermal analysis, I Mathematical problems of quantitative differential thermal analysis. 1(1), 5–13.

Bernardes WA, Lucarini R, Tozatti MG, Flauzino LG, Souza MG, Turatti IC, Andrade e Silva ML, Martins CH, da Silva Filho AA, Cunha WR, 2010. Antibacterial activity of the essential oil from Rosmarinus officinalis and its major components against oral pathogens. Z Naturforsch C J Biosci; 65(9-10) :588-93.

Beverly, Jennifer L., Sonja E. R. Leverkus, Hilary Cameron, and Dave Schroeder. (2020). "Stand-Level Fuel Reduction Treatments and Fire Behaviour in Canadian Boreal Conifer Forests" Fire 3, no. 3: 35.

Biagini, E., Barontini, F., & Tognotti, L. (2006). Devolatilization of Biomass Fuels and Biomass Components Studied by TG/FTIR Technique. Industrial Engineering Chemistry Research, 45(13), 4486–4493.

Bianchi, Lucas & Defosse, Guillermo. (2015). Live fuel moisture content and leaf ignition of forest species in Andean Patagonia, Argentina. International Journal of Wildland Fire. 24. 340-348.

Bilbao, R., Mastral, J. F., Aldea, M. E., & Ceamanos, J. (1997). Kinetic study for the thermal decomposition of cellulose and pine sawdust in an air atmosphere. Journal of Analytical and Applied Pyrolysis, 39(1), 53-64.

Blasco, S. and Mateu, I. (1995) 'Flowering and fruiting phenology and breeding system of Cistus albidus L.', Acta Botanica Gallica, 142(3), pp. 245–251.

Bonora L, Conese C, Lampin C, Martin P, Martı´nez J, Molina D, Salas J (2002) Towards methods for investigating on wildland fire causes. Euro-Mediterranean wildland fire laboratory, a ''wall-less'' laboratory for wildland fire sciences and technologies in the Euro-Mediterranean Region. Deliverable D-05-02.

Bosabalidis, A. M., & Kofidis, G. (2002). Comparative effects of drought stress on leaf anatomy of two olive cultivars. Plant Science, 163(2), 375–379.

Bota, Josefina & Medrano, Hipolito & Flexas, Jaume. (2004). Is photosynthesis limited by decreased Rubisco activity and RuBP content under progressive water stress? New Phytol. New Phytologist - NEW PHYTOL. 162.

Bowman, D. M. J. S., Balch, J., Artaxo, P., Bond, W. J., Cochrane, M. A., D'Antonio, C. M., … Swetnam, T. W. (2011). The human dimension of fire regimes on earth. Journal of Biogeography, **38**(12), 2223– 2236.

Bracho-Nunez, A., Welter, S., Staudt, M., & Kesselmeier, J. (2011). Plant-specific volatile organic compound emission rates from young and mature leaves of Mediterranean vegetation. Journal of Geophysical Research: Atmospheres, 116(D16).

Brebu, Mihai & Vasile, Cornelia. (2010). Thermal degradation of lignin – A Review. Cellulose Chemistry and Technology. 44. 353-363.

Burton, C., Betts, R.A., Jones, C.D. and Williams, K., 2018. Will fire danger be reduced by using Solar Radiation Management to limit global warming to 1.5° C compared to 2.0° C? Geophysical Research Letters, 45(8), pp.3644-3652.

Butler, B. W., Anderson, W. R., & Catchpole, E. A. (2007). Influence of slope on fire spread rate. The fire environment innovations, management, and policy, 75-83.

Butler, B. W., Bartlette, R. A., Bradshaw, L. S., Cohen, J. D., Andrews, P. L., Putnam, T., & Mangan, R. J. (1998). Fire Behavior Associated with the 1994 South Canyon Fire on Storm King Mountain, Colorado. Research Paper RMRS-RP-9, Ogden, UT, USDA, Forest Service, Rocky Mountain Research Station, 82 p.

Butler, B. W., Finney, M. A., Andrews, P. L., & Albini, F. A. (2004). A radiation-driven model for crown fire spread. Canadian Journal of Forest Research, 34(8), 1588-1599.

Byram GM (1959) Combustion of forest fuels. In: Davis KP (ed) Forest fire: control and use. McGraw-Hill, New York, pp 61–89.

Cai N, Chow WK. (2012). Wind effect on spread of fire and smoke. Paper presented at International Conference on Advances in Wind and Structures.

Calfapietra, C., Fares, S., Manes, F., Morani, A., Sgrigna, G., & Loreto, F. (2013). Role of Biogenic Volatile Organic Compounds (BVOC) emitted by urban trees on ozone concentration in cities: A review. Environmental polluion, 183, 71-80.

Camia, A., Durrant Houston, T., San-Miguel-Ayanz, J., (2010). The European Fire Database: Development, Structure and Implementation. In: D.X. Viegas (Ed.) Proceedings VI International Conference on Forest Fire Research, Coimbra, Portugal.

Camia, A., Durrant, T., & San-Miguel-Ayanz, J. (2014). The European fire database: technical specifications and data submission. EUR 26546 EN. Luxemburg (Luxemburg), Publications Office of the European Union.

Carbonell, G., Monet, J. P., Dusserre, G., & Sauvagnargues-Lesage, S. (2004) Embrasement generalisé éclair en feu de forêt. Rapport EMA-SDIS 13, 153.

Casal, J., (2008). Evaluation of the effects and consequences of major accidents in industrial plants, chapter 6 atmospheric dispersion of toxic or flammable clouds. Ind. Saf. Ser. 8, 195-248.

Cashdollar, K. L., A. Zlochower, I., Green, G. M., Thomas, R. A., & Hertzberg, M. (2000). Flammability of methane, propane, and hydrogen gases. Journal of Loss Prevention in the Process Industries, 13(3-5), 327–340.

Catoire L., V. Naudet, (2005). Estimation of temperature-dependent lower flammability limit of pure organic compounds in air at atmospheric pressure, Process Saf. Prog. 24, 130–137.

Cengel, Y.A. and Cimbala, J.M. (2006) Fluid Mechanics. Vol. 1, Tata McGraw-Hill Education, New York.

Chan, C. Y., Engling, G., Sang, X., & Zhang, T. (2011). Biofuel Combustion Emissions-Chemical and Physical Smoke Properties (pp. 978-953). ISBN.

Chas-Amil, Marisa & Touza, Julia & García, Eduardo. (2013). Forest fires in the wildland-urban interface: A spatial analysis of forest fragmentation and human impacts. Applied Geography. 43. 127-137.

Chatelier, Henri & Boudouard, O. (2005). On the flammable limits of gas mixtures. Process Safety Progress - PROCESS SAF PROG. 24. 3-5. 10.1002/prs.10062.

Chatelon, F. J., Sauvagnargues, S., Dusserre, G., & Balbi, J. H. (2014). Generalized Blaze Flash, a" flashover" behavior for forest fires-Analysis from the firefighter's point of view. Open Journal of Forestry, 4(5), 547-557.

Chatzivasileiou, A. O., Ward, V., Edgar, S. M., & Stephanopoulos, G. (2019). Two-step pathway for isoprenoid synthesis. Proceedings of the National Academy of Sciences, 116(2), 506-511.

Chen C., Ma, X., & Liu, K. (2011). Thermogravimetric analysis of microalgae combustion under different oxygen supply concentrations. Applied Energy, 88(9), 3189–3196.

Chen H., Xu, G., Xiao, C., Bi, Y., & Hu, J. (2019b). Fast Pyrolysis of Organosolv Lignin: Effect of Adding Stabilization Reagents to Extraction Process. Energy & Fuels.

Chen, Feng, Liqing Si, Fengjun Zhao, and Mingyu Wang. (2023). "Volatile Oil in Pinus yunnanensis Potentially Contributes to Extreme Fire Behavior" Fire 6, no. 3: 113.

Chen, J., Tang, J., & Yu, X. (2020). Environmental and physiological controls on diurnal and seasonal patterns of biogenic volatile organic compound emissions from five dominant woody species under field conditions. Environmental Pollution, 259, 113955.

Chen, W.-H., Wang, C.-W., Ong, H. C., Show, P. L., & Hsieh, T.-H. (2019). Torrefaction, pyrolysis and two-stage thermodegradation of hemicellulose, cellulose and lignin. Fuel, 258, 116168.

Chetehouna K, Courty L, Garo JP, Viegas DX, Fernandez-Pello C., (2014). Flammability limits of biogenic volatile organic compounds emitted by fire-heated vegetation (Rosmarinus officinalis) and their potential link with accelerating forest fires in canyons: A Froude-scaling approach. Journal of Fire Sciences. 32(4):316-327.

Chetehouna, K., Barboni, T., Zarguili, I., Leoni, E., Simeoni, A., & Fernandez-Pello, A. C. (2009). Investigation on the Emission of Volatile Organic Compounds from Heated Vegetation and Their Potential to Cause an Accelerating Forest Fire. Combustion Science and Technology, 181(10), 1273–1288.

Chetehouna, K., Courty, L., Garo, J. P., Viegas, D. X., & Fernandez-Pello, C. (2014). Flammability limits of biogenic volatile organic compounds emitted by fire-heated vegetation (Rosmarinus officinalis) and their potential link with accelerating forest fires in canyons: A Froude-scaling approach. Journal of fire sciences, 32(4), 316-327.

Christian, T. & Kleiss, B. & Yokelson, R. & Holzinger, Rupert & Crutzen, Paul & Hao, W. & Saharjo, B. & Ward, D. (2003). Comprehensive laboratory measurements of biomass-burning emissions: 1. Emissions from Indonesian, African, and other fuels. Journal of Geophysical Research, v.108 (2003).

Chuvieco, E., Cocero, D., Riano, D., Martin, P., Martınez-Vega, J., De La Riva, J., & Pérez, F. (2004). Combining NDVI and surface temperature for the estimation of live fuel moisture content in forest fire danger rating. Remote Sensing of Environment, 92(3), 322-331.

Ciccioli, P., Centritto, M., & Loreto, F. (2014). Biogenic volatile organic compound emissions from vegetation fires. Plant, cell & environment, 37(8), 1810-1825.

Ciccioli, P., Brancaleoni, E., Frattoni, M., Cecinato, A., & Pinciarelli, L. (2001). Determination of volatile organic compounds (VOC) emitted from biomass burning of Mediterranean vegetation species by GC-MS. Analytical Letters, 34(6), 937-955.

Ciccioli, Paolo & Centritto, Mauro & Loreto, Francesco. (2014). Biogenic volatile organic compound emissions from vegetation fires. Plant, cell & environment. 37.

Collard, F.-X., & Blin, J. (2014). A review on pyrolysis of biomass constituents: Mechanisms and composition of the products obtained from the conversion of cellulose, hemicelluloses and lignin. Renewable and Sustainable Energy Reviews, 38, 594–608.

Conan, B, Auburn, S, Coudour, B., Chetehouna, K., Garo, J.P., (2015). Contribution of coherent structures to momentum and concentration fluxes over a flat vegetation canopy modelled in a wind tunnel. Atmos. Environ. 107, 329–341.

Copolovici, L. O., & Niinemets, Ü. (2005). Temperature dependencies of Henry's law constants and octanol/water partition coefficients for key plant volatile monoterpenoids. Chemosphere, 61(10), 1390-1400.

Copolovici, L., & Niinemets, Ü. (2015). Temperature dependencies of Henry's law constants for different plant sesquiterpenes. Chemosphere, 138, 751-757.

Copolovici, L., & Niinemets, Ü. (2016). Environmental Impacts on Plant Volatile Emission. Deciphering Chemical Language of Plant Communication, 35–59.

COPPER, F. I., & MOUNTAIN, C. (1980). Specialists' Workshop on Fast Pyrolysis of Biomass Proceedings-NREL.

Costa, R. A. R. (2019). Chemical Composition of Cork Phloem and Xylem of Quercus Suber L. from Different Provenances (Doctoral dissertation, Universidade de Lisboa (Portugal)).

Coudour, Bruno & Chetehouna, Khaled & Conan, Boris & Auburn, Sandrine & Garo, J.P. (2014). Experimental investigation of the influence of geometry on gas accumulation using a V-shape forest model. Advances in Forest Fire Research. 10.14195/978-989-26-0884-6_21.

Crowl, Daniel & Jo, Young-Do. (2009). A Method for Determining the Flammable Limits of Gases in a Spherical Vessel. Process Safety Progress. 28. 227 - 236.

Curt T., Bertrand R., Borgniet L., Ferrieux T., Marini E. (2010). The impact of fire recurrence on populations of Quercus suber in southeastern France. VI International Conference on Forest Fire Research. Coimbra, Portugal. 10 p. ffhal-00583408f.

Dalmazzone, D. ; Laforest, J.C; Petit, J.P. (2001). Application of thermochemical energy hazard criteria to the prediction of lower flammability limits of hydrocarbons in air. Oil Gas Sci. Technol.56, 365–372.

Danish, S., Zafar-ul-Hye, M., (2019) Co-application of ACC-deaminase producing PGPR and timber-waste biochar improves pigments formation, growth and yield of wheat under drought stress. Sci Rep **9**, 5999.

De Groot, W. J., Flannigan, M. D., & Cantin, A. S. (2013). Climate change impacts on future boreal fire regimes. Forest Ecology and Management, 294, 35–44.

De Lillis, Manuela; Bianco, Pietro Massimiliano; Loreto, Francesco (2009). The influence of leaf water content and isoprenoids on flammability of some Mediterranean woody species. International Journal of Wildland Fire, 18(2), 203.

Dehane Belkheir, Hernando Carmen, Guijarro Mercedes, Madrigal Javier. (2017). Flammability of some companion species in cork oak (Quercus suber L.) forests. Annals of Forest Science. 74 (3), pp.60.

Dehane, B.; Madrigal, J.; Hernando, C.; Bouhraoua, R.; Guijarro, M. (2015). New bench-scale protocols for characterizing bark flammability and fire resistance in trees: Application to Algerian cork. Journal of Fire Sciences, 33(3), 202–217.

Delatte TL, Scaiola G, Molenaar J, de Sousa Farias K, Alves Gomes Albertti L, Busscher J, Verstappen F, Carollo C, Bouwmeester H, Beekwilder J. (2018). Engineering storage capacity for volatile sesquiterpenes in Nicotiana benthamiana leaves. Plant Biotechnol J. 16(12):1997-2006.

Delfine, S., Csiky, O., Seufert, G., & Loreto, F. (2000). Fumigation with exogenous monoterpenes of a non-isoprenoid-emitting oak (Quercus suber): Monoterpene acquisition, translocation, and effect on the photosynthetic properties at high temperatures. New Phytologist, 146(1), 27-36.

Della Rocca G, Danti R, Hernando C, Guijarro M and Madrigal J (2018) Flammability of Two Mediterranean Mixed Forests: Study of the Non-additive Effect of Fuel Mixtures in Laboratory. Front. Plant Sci. 9:825.

Della Rocca G, Hernando C, Madrigal J, Danti R, Moya J, Guijarro M, Pecchioli A, Moya B. (2015). Possible land management uses of common cypress to reduce wildfire initiation risk: a laboratory study. J Environ Manage. 159 :68-77.

Della Rocca G, Madrigal J, Marchi E, Michelozzi M, Moya B, Danti R (2017). Relevance of terpenoids on flammability of Mediterranean species: an experimental approach at a low radiant heat flux. iForest 10: 766-775.

Della Rocca, G.; Danti, R.; Hernando, C.; Guijarro, M.; Michelozzi, M.; Carrillo, C.; Madrigal, J. (2020) Terpenoid Accumulation Links Plant Health and Flammability in the Cypress-Bark Canker Pathosystem. Forests, 11, 651.

Diebold, J. P. (1980, October). Ablative pyrolysis of macroparticles of biomass. In Proceedings of the Specialists Workshop on the Fast Pyrolysis of Biomass, Copper Mountain, Co (p. 237).

Dimitrakopoulos AP, Papaioannou KK (2001) Flammability assessment of Mediterranean forest fuels. Fire Technology 37, 143–152.

Dold, J. W. (2010). Flow attachment in eruptive fire growth. In Proceedings of the 6th International Conference on Forest Fire Research.

Dold, J. W., & Zinoviev, A. (2009). Fire eruption through intensity and spread rate interaction mediated by flow attachment. Combustion Theory and Modelling, 13(5), 763-793.

Dold, John & Simeoni, A. & Zinoviev, Anna & Weber, R. (2009). The Palasca fire, September 2000: Eruption or Flashover?

Dold, John & Weber, R. & Gill, Malcolm & McRae, Rick & Cooper, Neil. (2005). Unusual phenomena in an extreme bushfire.

Domingos, X.V., Albert, S., Gavriil, X., Carlos, R.J., Mario, R.L., Paulo, P.L., Darko, S., Anna, Z., Rodney, W., John, D.C., David, C., & Jesus, S.M. (2009). Recent Forest Fire Related Accidents in Europe.

Dowdy AJ (2018) Climatological variability of fire weather in Australia. Journal of Applied Meteorology and Climatology **57**, 221–234.

Drobinski, P., Da Silva, N., Bastin, S. et al. How warmer and drier will the Mediterranean region be at the end of the twenty-first century. Reg Environ Change **20**, 78 (2020).

El-Sayed S. A. Mostafa M. E, (2014). Pyrolysis characteristics and kinetic parameters determination of biomass fuel powders by differential thermal gravimetric analysis (TGA/DTG) Energy Convers. Manage. 85:165–172.

EN 1839, Determination of explosion limits of gases and vapors, 2003, (European standard).

Essaghi, Salaheddine & Hachmi, M'hamed & Yessef, Mohammed & Dehhaoui, Mohammed & Sesbou, Abdessadek. (2017). Spatial and Seasonal Response of the Surface Area-to-Volume Ratio to Changes in Moisture Content in Some Dominant Mediterranean Forest Fuels. International Journal of Applied Engineering Research. 12. 10676-10692.

Evtyugina, M., Calvo, A. I., Nunes, T., Alves, C., Fernandes, A. P., Tarelho, L., ... & Pio, C. (2013). VOC emissions of smouldering combustion from Mediterranean wildfires in central Portugal. Atmospheric Environment, 64, 339-348.

Fang, H., & Liang, S. (2014). Leaf Area Index Models. Reference Module in Earth Systems and Environmental Sciences.

FAO (1990). Fire as a forest management tool. An international journal of forestry and forest industries – Vol. 41 -1990/3, Paris.

Fares, S., Schnitzhofer, R., Jiang, X., Guenther, A., Hansel, A., & Loreto, F. (2013). Observations of diurnal to weekly variations of monoterpene-dominated fluxes of volatile organic compounds from Mediterranean forests: implications for regional modeling. Environmental science & technology, 47(19), 11073-11082.

Farooq M., Wahid A., Kobayashi N., D. Fujita S.M.A. Basra, (2009). Plant drought stress: effects, mechanisms and management. Agronomy for Sustainable Development. 29 (1), pp.185-212.

Fatehi, Hesam & Weng, Wubin & Costa, Mário & Li, Zhongshan & Rabaçal, Miriam & Aldén, Marcus & Bai, Xue-Song. (2019). Numerical simulation of ignition mode and ignition delay time of pulverized biomass particles. Combustion and Flame. 206. 400.

Faubert, P. (2010). Responses of Non-Methane Biogenic Volatile Organic Compound Emissions to Climate Change in Boreal and Subarctic Ecosystems. Itä-Suomen yliopisto.

Flannigan, M., Cantin, A. S., de Groot, W. J., Wotton, M., Newbery, A., and Gowman, L. M. (2013). Global wildland fire season severity in the 21st century, Forest Ecol. Manage., 294, 54–61.

Fleurat-Lessard P, Béré E, Lallemand M, Dédaldéchamp F, Roblin G (2016) Co-occurrence of tannin and tannin-less vacuoles in sensitive plants. Protoplasma 253, 821–834.

Fons, Wallace L. (1946). Analysis of fire spread in light forest fuels. Journal of Agricultural Engineering Research. 72(3): 93–121.

Ford, Chelcy & Minor, Emily & Fox, Gordon. (2010). Long-term effects of fire and fire-return interval on population structure and growth of longleaf pine (Pinus palustris). Canadian Journal of Forest Research. 40. 1410-1420.

Frandsen, William H.; Andrews, Patricia L. 1979. Fire behavior in non-uniform fuels. Res. Pap. INT-232. Ogden, UT: U.S. Department of Agriculture, Forest Service, Intermountain Research Station. 34 p.

Friedli, H. R., Atlas, E., Stroud, V. R., Giovanni, L., Campos, T., & Radke, L. F. (2001). Volatile organic trace gases emitted from North American wildfires. Global biogeochemical cycles, 15(2), 435-452.

Fukui, Y. & Doskey, P. V. (2000). Identification of nonmethane organic compound emissions from grassland vegetation. Atmos. Environ., 34(18), 2947-2956.

Furukawa, Y., Inubushi, K., Ali, M. et al. Effect of changing groundwater levels caused by land-use changes on greenhouse gas fluxes from tropical peat lands. Nutr Cycl Agroecosyst **71**, 81–91 (2005).

Ganteaume A, Jappiot M, Lampin C, Guijarro M, Hernando C. (2013). Flammability of some ornamental species in wildland-urban interfaces in southeastern France: laboratory assessment at particle level. Environ Manage. 52(2) :467-80.

Ganteaume A. (2018). Does plant flammability differ between leaf and litter bed scale? Role of fuel characteristics and consequences for flammability assessment. International Journal of Wildland Fire. 27 (5), pp.342-352.

Ganteaume, A., Romero, B., Fernandez, C., Ormeño, E., & Lecareux, C. (2021). Volatile and semi-volatile terpenes impact leaf flammability: differences according to the level of terpene identification. Chemoecology, 31(4), 259–275.

Ganteaume, A., Syphard, A.D., 2018. Ignition Sources.

Ganteaume, Anne & Romero, Bastien & Ormeño, Elena & Lecareux, Caroline & Fernandez, Catherine. (2021). Does Seasonality of Leaf Terpene Content and Moisture Content Trigger Leaf Flammability Seasonal Variation.

Gao X, Gao F, Liu D, Zhang H, Nie X, Yang C (2016) Engineering the methylerythritol phosphate pathway in cyanobacteria for photosynthetic isoprene production from CO_2. Energy Environ Sci 9:1400–1411.

Gao, L., Song, J., Mohr, C., Huang, W., Vallon, M., Jiang, F., Leisner, T., and Saathoff, H. (2022): Kinetics, SOA yields, and chemical composition of secondary organic aerosol from β-caryophyllene ozonolysis with and without nitrogen oxides between 213 and 313 K, Atmos. Chem. Phys., 22, 6001–6020.

Gauquelin, Thierry & Michon, Genevieve & Joffre, Richard & Duponnois, Robin & Genin, Didier & Fady, B. & Bou Dagher Kharrat, Magda & Arezki, Derridj & Slimani, Said & Badri, Wadi & Alifriqui, Mohamed & Auclair, Laurent & Simenel, Romain & Mohammed, Aderghal & Baudoin, Ezékiel & Galiana, Antoine & Prin, Yves & Sanguin, Hervé & Fernandez, Catherine & Baldy, Virginie. (2016). The Mediterranean region under climate change : a scientific update, 339.

Geron, C. D., Guenther, A. B., & Pierce, T. E. (1994). An improved model for estimating emissions of volatile organic compounds from forests in the eastern United States. Journal of Geophysical Research, 99(D6), 12773.

Ghirardo, A., Koch, K., Taipale, R., Zimmer, I., Schnitzler, J.-P., & Rinne, J. (2010). Determination of de novoand pool emissions of terpenes from four common boreal/alpine trees by CO2 labelling and PTR-MS analysis. Plant, Cell & Environment.

Gieras, M., Klemens, R., Rarata, G., & Wolański, P. (2006). Determination of explosion parameters of methane-air mixtures in the chamber of 40dm3 at normal and elevated temperature. Journal of Loss Prevention in the Process Industries, 19(2-3), 263–270.

Gill AM, Moore PHR (1996) Ignitibility of leaves of Australian plants. CSIRO Plant Industry, Centre for Plant Biodiversity Research. (Canberra).

Gimenez, Carmen & Gallardo, M. & Thompson, R.B. (2013). Plant–Water Relations.

Goode, J. G., Yokelson, R. J., Ward, D. E., Susott, R. A., Babbitt, R. E., Davies, M. A., and Hao, W. M.: Measurements of excess O3, CO2, CO, CH4, C2H4, C2H2, HCN, NO, NH3, HCOOH, CH3COOH, HCHO, and CH3OH in 1997 Alaskan biomass burning plumes by airborne Fourier transform infrared spectroscopy (AFTIR), J. Geophys. Res., 105, 22 147–22 166.

Greenberg, J. P., Friedli, H., Guenther, A. B., Hanson, D., Harley, P., and Karl, T., (2006): Volatile organic emissions from the distillation and pyrolysis of vegetation, Atmos. Chem. Phys., 6, 81–91.

Grønli, M. G., Várhegyi, G., & Di Blasi, C. (2002). Thermogravimetric Analysis and Devolatilization Kinetics of Wood. Industrial & Engineering Chemistry Research, 41(17), 4201–4208.

Grumstrup, Torben P.; McAllister, Sara S.; Finney, Mark A. 2017. Qualitative flow visualization of flame attachment on slopes. Presented at the 10th U. S. National Combustion Meeting Organized by the Eastern States Section of the Combustion Institute; April 23-26, 2017; College Park, MD. Pittsburgh, PA: The Combustion Institute. 6 p.

Guérette, E. A., Paton-Walsh, C., Desservettaz, M., Smith, T. E., Volkova, L., Weston, C. J., & Meyer, C. P. (2018). Emissions of trace gases from Australian temperate forest fires: emission factors and dependence on modified combustion efficiency. Atmospheric Chemistry and Physics, 18(5), 3717-3735.

Guerrero, Fabián, Camilo Carmona, Carla Hernández, Mario Toledo, Andrés Arriagada, Lorena Espinoza, Jan Bergmann, Lautaro Taborga, Karen Yañez, Yulián Carrasco, and Ariel A. Muñoz. 2022. "Drivers of Flammability of Eucalyptus globulus Labill Leaves: Terpenes, Essential Oils, and Moisture Content" Forests 13, no. 6: 908.

Guo, Fei; Wu, Fengchang; Mu, Yunsong; Hu, Yan; Zhao, Xiaoli; Meng, Wei; Giesy, John P.; Lin, Ying (2016). Characterization of organic matter of plants from lakes by thermal analysis in a N2 atmosphere. Scientific Reports, 6(1), 22877.

Gupta, N. S., Briggs, D. E. G., Collinson, M. E., Evershed, R. P., Michels, R., Jack, K. S., & Pancost, R. D. (2007). Evidence for the in situ polymerisation of labile aliphatic organic compounds during the preservation of fossil leaves: Implications for organic matter preservation. Organic Geochemistry, 38(3), 499–522.

Haenaem Kim & Hye Jin & Myeong-Ja Kwak & Khaine, Inkyin & You, Hana & Lee, Taeyoon & Ahn, Tai & Woo, Su-Young. (2017). Why does Quercus suber species decline in Mediterranean areas. Journal of Asia-Pacific Biodiversity.

Hales J.L; Townsend R (1972). Liquid densities from 293 to 490 K of nine aromatic hydrocarbons. 4(5), 763–772.

Hammer, R. B., Radeloff, V. C., Fried, J. S., & Stewart, S. I. (2007). Wildland–urban interface housing growth during the 1990s in California, Oregon, and Washington. International Journal of Wildland Fire, 16(3), 255-265.

Harley, P. C. (2013). “The roles of stomatal conductance and compound volatility in controlling the emission of volatile organic compounds from leaves,” in Biology, Controls and Models of Tree Volatile Organic Compound Emissions, eds U. Niinemets and R. K. Monson (Berlin: Springer), 181–208.

Hatch, L. E., Jen, C. N., Kreisberg, N. M., Selimovic, V., Yokelson, R. J., Stamatis, C., ... & Barsanti, K. C. (2019). Highly speciated measurements of terpenoids emitted from laboratory and mixed-conifer forest prescribed fires. Environmental Science & Technology, 53(16), 9418-9428.

Hawkins, J. E., & Eriksen, W. T. (1954). Physical and Thermodynamic Properties of Terpenes. II. The Heats of Combustion of Some Terpene Hydrocarbons. Journal of the American Chemical Society, 76(10), 2669–2671.

Helmig, D., Revermann, T., Pollmann, J., Kaltschmidt, O., Hernández, A. J., Bocquet, F., & David, D. (2003). Calibration system and analytical considerations for quantitative sesquiterpene measurements in air. Journal of Chromatography A, 1002(1-2), 193-211.

Hirsch KG, Fuglem P (Tech Cords) (2006) Canadian wildland fire strategy: background syntheses, analyses, and perspectives. Natural Resources Canada, Canadian Forest Service, Northern Forestry Centre. (Edmonton, AB).

Holopainen, J. K. (2004). Multiple functions of inducible plant volatiles. Trends in plant science, 9(11), 529-533.

Howell, J. R., & Mengüç, M. P. (2011). Radiative transfer configuration factor catalog: A listing of relations for common geometries. Journal of Quantitative Spectroscopy and Radiative Transfer, 112(5), 910-912.

Hristova, Mariana & Tchaoushev, Stilijan. (2006). Calculation of Flash Points and Flammability Limits of Substances and Mixtures. 41. 291-296.

Igini Martina (2022). Top 12 Latgest Wildfires in History. Retrieved from https://earth.org/largest-wildfires-in-history/.

Iijima, Yoko. (2014). Recent Advances in the Application of Metabolomics to Studies of Biogenic Volatile Organic Compounds (BVOC) Produced by Plant. Metabolites. 4. 699-721.

Ijaz, A. (2021). High-resolution molecular characterization of complex environmental mixtures: Aquatic dissolved organic matter and wildfire-influenced aerosol (Doctoral dissertation, Michigan Technological University).

Innes, A., & Innes, J. (2011). Flame retardants. In Applied plastics engineering handbook (pp. 469-485). William Andrew Publishing.

Jones, J.M.; Saddawi, A.; Dooley, B.; Mitchell, E.J.S.; Werner, J.; Waldron, D.J.; Weatherstone, S.; Williams, A. (2015). Low temperature ignition of biomass. Fuel Processing Technology, 134(), 372–377.

Jun-Wen, C., Cao, Kf. Plant VOCs emission: a new strategy of thermotolerance. Journal of Forestry Research **16**, 323–326 (2005).

Katyal, A., & Morrison, R. D. (2007). FORENSIC APPLICATIONS OF CONTAMINANT TRANSPORT MODELS IN THE SUBSURFACE. Introduction to Environmental Forensics, 513–575.

Keeley, J. E., Syphard, A. D., & Fotheringham, C. J. (2013). The 2003 and 2007 Wildfires in Southern California. Natural Disasters and Adaptation to Climate Change, 42–52.

Keeley, J.E., Bond, W.J., Bradstock, R.A., Pausas, J.G., Rundel, P.W. (2012). Fire in Mediterranean climate ecosystems: ecology, evolution and management. Univ. of Cambridge Press, Cambridge, UK,515 pp.

Keeling, Christopher & Bohlmann, Jörg. (2006). Diterpene resin acids in conifers. Phytochemistry. 67. 2415-23.

Kganyago, Mahlatse, and Lerato Shikwambana. 2020. "Assessment of the Characteristics of Recent Major Wildfires in the USA, Australia and Brazil in 2018–2019 Using Multi-Source Satellite Products" Remote Sensing 12, no. 11: 1803.

Kleist, E., Mentel, T. F., Andres, S., Bohne, A., Folkers, A., Kiendler-Scharr, A., ... & Wildt, J. (2012). Irreversible impacts of heat on the emissions of monoterpenes, sesquiterpenes, phenolic BVOC and green leaf volatiles from several tree species. Biogeosciences, 9(12), 5111-5123.

Koo, E. & Pagni, P. & Stephens, S. & Huff, J. & Woycheese, J. & Weise, David. (2005). A Simple Physical Model for Forest Fire Spread Rate. Fire Safety Science. 8. 851-862. 10.3801/IAFSS.FSS.8-851.

Kornakova, M., & Glavovic, B. (2018). Institutionalising wildfire planning in New Zealand: Lessons learnt from the 2009 Victoria bushfire experience. Australasian journal of disaster and trauma studies, 22, 51-61.

Krawchuk, Meg & Moritz, Max & Parisien, Marc-André & Van Dorn, Jeff & Hayhoe, Katharine. (2009). Global Pyrogeography: The Current and Future Distribution of Wildfire. PloS one. 4. e5102. 10.1371/journal.pone.0005102.

Kumar Ajay; Wang Lijun; Dzenis Yuris A; Jones David D.; Hanna Milford A. (2008). Thermogravimetric characterization of corn stover as gasification and pyrolysis feedstock. 32(5), 460–467.

Lambert Karel (2013). Backdraft: fire science and firefighting, a literature review.

Lampin-Maillet, C., Jappiot, M., Long, M., Bouillon, C., Morge, D., & Ferrier, J.-P. (2010). Mapping wildland-urban interfaces at large scales integrating housing density and vegetation aggregation for fire prevention in the South of France. Journal of Environmental Management, 91(3), 732–741.

Laothawornkitkul, J., Taylor, J. E., Paul, N. D., & Hewitt, C. N. (2009). Biogenic volatile organic compounds in the Earth system. New Phytologist, 183(1), 27–51.

Larry 2008, Native Tree Society, accessed 7th of September 2022, < http://www.nativetreesociety.org/species/sp_gallery/longleaf/longleaf_pines1.htm >.

Lawson, S.J. & Keywood, Melita & Galbally, Ian & Gras, J. & Cainey, Jill & Cope, Martin & Krummel, P. & Fraser, Paul & Steele, L. & Bentley, S. & Meyer, C. & Ristovski, Zoran & Goldstein, A. (2015). Biomass burning emissions of trace gases and particles in marine air at Cape Grim, Tasmania. ATMOSPHERIC CHEMISTRY AND PHYSICS. 15. 13393-13411.

Le Dortz Romain, Marc Bellenoue, Laurence Bonneau, Ekaterina Mazanchenko, Julien Sotton, et al. Laminar Burning Velocities and Markstein Lengths of Jet Fuel Surrogate/Air Mixtures in a Spherical Chamber. 8th european combustion meeting, Apr 2017, Dubrovnik, Croatia. ffhal-01537768f.

Le Houérou, H.N., 1973. Fire and vegetation in the Mediterranean basin (pp. 237-277). Rome, Italy : FAO.

Lemieux, P. M., Lutes, C. C., & Santoianni, D. A. (2004). Emissions of organic air toxics from open burning: a comprehensive review. Progress in Energy and Combustion Science, 30(1), 1-32.

Liodakis, S. & Bakirtzis, D. & Lois, Evripidis. (2002). TG and autoignition studies on forest fuels. Journal of Thermal Analysis and Calorimetry, 69(2), 519-528.

Liodakis, S., Bakirtzis, D., & Dimitrakopoulos, A. (2002b). Ignition characteristics of forest species in relation to thermal analysis data. Thermochimica Acta, 390(1-2), 83–91.

Liodakis, S., Katsigiannis, G., & Kakali, G. (2005). Ash properties of some dominant Greek forest species. Thermochimica Acta, 437(1-2), 158–167.

Liodakis, Stylianos & Kakardakis, Tilemachos. (2006). Measuring the Particle Flammability of Forest Species from Wildland/Urban Inter-face (WUI) near Athens by Thermal Analysis. 2006 1st International Symposium on Environment Identities and Mediterranean Area, ISEIM. 24 - 28.

Llusià, J., & Peñuelas, J. (1998). Changes in terpene content and emission in potted Mediterranean woody plants under severe drought. Canadian Journal of Botany, 76(8), 1366–1373.

Llusià, J., Peñuelas, J., Alessio, G. A., & Estiarte, M. (2006). Seasonal contrasting changes of foliar concentrations of terpenes and other volatile organic compound in four dominant species of a Mediterranean shrubland submitted to a field experimental drought and warming. Physiologia Plantarum, 127(4), 632-649.

Llusià, J., Peñuelas, J., Ogaya, R., & Alessio, G. (2009). Annual and seasonal changes in foliar terpene content and emission rates in Cistus albidus L. submitted to soil drought in Prades forest (Catalonia, NE Spain). Acta Physiologiae Plantarum, 32(2), 387–394.

Llusia` J, Peñuelas J (2000) Seasonal patterns of terpene content and emission from seven Mediterranean woody species in field conditions. American Journal of Botany, 87(1),133–140.

Lobert, J. M., & Warnatz, J. (1993). Emissions from the combustion process in vegetation. Fire in the Environment, 13, 15-37.

Lopes, Fernanda & Pereira, Janainna & Tannous, Katia. (2018). Thermal decomposition kinetics of guarana seed residue through thermogravimetric analysis under inert and oxidizing atmospheres. Bioresource Technology. 270.

Lorente, B., Zugasti, I., Ortuño, M. F., Nortes, P., Bañón, S., Hernández, J. A., & Sánchez-Blanco, M. J. (2020). Substrate composition affects the development of water stress and subsequent recovery by inducing physiological changes in Cistus albidus plants. Plant Physiology and Biochemistry, 158, 125-135.

Loreto F. & Sharkey T.D. (1993) On the relationship between isoprene emission and photosynthetic metabolites under different environmental conditions. Planta 189, 420–424.

Loreto Francesco (2002). Distribution of isoprenoid emitters in the Quercus genus around the world: chemo-taxonomical implications and evolutionary considerations based on the ecological function of the trait. 5(3), 0–192.

Loreto, F., & Fineschi, S. (2014). Reconciling functions and evolution of isoprene emission in higher plants. New Phytologist, 206(2), 578–582.

Loreto, F., & Schnitzler, J. P. (2010). Abiotic stresses and induced BVOCs. Trends in plant science, 15(3), 154-166.

Loreto, F., Barta, C., Brilli, F., & Nogues, I. (2006). On the induction of volatile organic compound emissions by plants as consequence of wounding or fluctuations of light and temperature. Plant, cell & environment, 29(9), 1820 – 1828.

Loreto, F., Centritto, M., Chartzoulakis, K., 2003. Photosynthetic limitations in olive cultivars with different sensitivity to salt stress. Plant Cell Environ. 26, 595–601.

Loreto, F., Ciccioli, P., Brancaleoni, E., Valentini, R., Manuela De Lillis, Csiky, O., & Seufert, G. (1998). A Hypothesis on the Evolution of Isoprenoid Emission by Oaks Based on the Correlation between Emission Type and Quercus Taxonomy. Oecologia, 115(3), 302–305. 0

Loudermilk, E. Louise; Hiers, J. Kevin; O'Brien, Joseph J. (2018). The role of fuels for understanding fire behavior and fire effects. In: L. Katherine Kirkman and Steven B. Jack, Ecological restoration and management of longleaf pine forests. CRC Press, Taylor & Francis Group. 107-122. 16 p.

Lowden, L. A., & Hull, T. R. (2013). Flammability behaviour of wood and a review of the methods for its reduction. Fire Science Reviews, 2, 1-19.

Luo L, Zhai Q, Su Y, Ma Q, Kelly M, Guo Q. (2018). Simple method for direct crown base height estimation of individual conifer trees using airborne LiDAR data. Opt Express. 26(10): A562-A578.

Lüpke M, Leuchner M, Steinbrecher R, Menzel A., (2016). Impact of summer drought on isoprenoid emissions and carbon sink of three Scots pine provenances. Tree Physiol. 36(11):1382-1399.

Maccioni, S., Baldini, R., Cioni, P. L., Tebano, M., & Flamini, G. (2006). In vivo volatiles emission and essential oils from different organs and pollen ofCistus albidus from Caprione (Eastern Liguria, Italy). Flavour and Fragrance Journal, 22(1), 61–65.

Mackinney, G. (1941). Absorption of Light By Chlorophyll Solutions. Journal of Biological Chemistry, 140(2), 315–322.

Mansfield TJ, Atkinson CJ (1990) Stomatal behavior in water stressed plants. In: Stress Responses in Plants: Adaptation and Acclimation Mechanisms, Alscher RG, Cumming JR (Eds), Wiley-Liss, New York. pp. 241–264.

Marcenò, C., Guarino, R., Loidi, J., Herrera, M., Isermann, M., Knollová, I., … Chytrý, M. (2018). Classification of European and Mediterranean coastal dune vegetation. Applied Vegetation Science.

Marques, A. V., Pereira, H., Rodrigues, J., Meier, D., & Faix, O. (2006). Isolation and comparative characterization of a Björkman lignin from the saponified cork of Douglas-fir bark. Journal of Analytical and Applied Pyrolysis, 77(2), 169–176.

Marques, G., Gutiérrez, A., & del Río, J. C. (2007). Chemical characterization of lignin and lipophilic fractions from leaf fibers of curaua (Ananas erectifolius). Journal of agricultural and food chemistry, 55(4), 1327-1336.

Martin R.E., Gorden D.A., Gutierrez M.E., Lee D.S., Molina D.M., Schroeder R.A., Sapsis D.A., Stephens S.L., and Chambers M., (1993). Assessing the flammability of domestic and wildland vegetation. Author-produced version of the article published in International Journal of Wildland Fire, 2014, 23, 8, 1061-1075. The original publication is available “In Proceedings of the 12th Conference on Fire and Forest Meteorology, 26–28, pp.130-137.

Mason, Norman W. H.; Frazao, Cyril; Buxton, Rowan P.; Richardson, Sarah J. (2016). Fire form and function: evidence for adaptive flammability in the New Zealand flora. Plant Ecology, 217(6), 645–659.

Materić D, Bruhn D, Turner C, Morgan G, Mason N, Gauci V, (2015). Methods in plant foliar volatile organic compounds research. Applications in Plant Science. 15; 3(12).

Mazari, Khadidja & Bendimerad, Nassima & Bekhechi, C. & Fernandez, Xavier. (2010). Chemical composition and antimicrobial activity of essential oils isolated from Algerian Juniperus phoenicea L. and Cupressus sempervirens L. Journal of Medicinal Plants Research. 4. 959-964.

McAllister S. (2022). Experiments to understand physical processes in wildland fire behavior. IX International Conference on Forest Fire Research. Coimbra, Portugal. November, 2022.

McDowell, N., Pockman, W. T., Allen, C. D., Breshears, D. D., Cobb, N., Kolb, T., … Yepez, E. A. (2008). Mechanisms of plant survival and mortality during drought: why do some plants survive while others succumb to drought? New Phytologist, 178(4), 719–739.

Mendiburu, A. Z., Coronado, C. R., & de Carvalho Jr, J. A. (2020). Difficulties on the determination of the flammability limits of fuel mixtures by the Law of Le Chatelier. Process Safety and Environmental Protection, 142, 45-55.

Mendiburu, Andrés & Carvalho, Joao & Coronado, Christian J. R & Roberts, Justo. (2017). Flammability limits temperature dependence of pure compounds in air at atmospheric pressure. Energy. 118. 414-424.

Michaletz, S. T., & Johnson, E. A. (2007). How forest fires kill trees: a review of the fundamental biophysical processes. Scandinavian Journal of Forest Research, 22(6), 500-515.

Midzi, J.; Jeffery, D.W.; Baumann, U.; Rogiers, S.; Tyerman, S.D.; Pagay, V. (2022). Stress-Induced Volatile Emissions and Signaling in Inter-Plant Communication. Plants, 11, 2566.

Miranda, A. I., Borrego, C., Martins, H., Martins, V., Amorim, J. H., Valente, J., & Carvalho, A. (2009). Forest fire emissions and air pollution in southern Europe. Earth Observation of Wildland Fires in Mediterranean Ecosystems, 171-187.

Mitchell, B. D., & knight, A. H. (1965). The Application of Differential Thermal Analysis to Plant Materials. Journal of Experimental Botany, 16(46), 1–15.

Mitsopoulos, I. D., & Dimitrakopoulos, A. P. (2007). Canopy fuel characteristics and potential crown fire behavior in Aleppo pine (Pinus halepensis Mill.) forests. Annals of Forest Science, 64(3), 287–299.

Moreira, F., Ascoli, D., Safford, H., Adams, M. A., Moreno, J. M., Pereira, J. M., ... & Fernandes, P. M. (2020). Wildfire management in Mediterranean-type regions: paradigm change needed. Environmental Research Letters, 15(1), 011001.

Morsdorf, F., Mårell, A., Koetz, B., Cassagne, N., Pimont, F., Rigolot, E., & Allgöwer, B. (2010). Discrimination of vegetation strata in a multi-layered Mediterranean forest ecosystem using height and intensity information derived from airborne laser scanning. Remote Sensing of Environment, 114(7), 1403-1415.

Müller, M. M., Vacik, H., Diendorfer, G., Arpaci, A., Formayer, H., & Gossow, H. (2013). Analysis of lightning-induced forest fires in Austria. Theoretical and Applied Climatology, 111, 183-193.

Munne-Bosch, S., Lopez-Carbonell, M., Alegre, L., & van Onckelen, H. A. (2002). Effect of drought and high solar radiation on 1-aminocyclopropane-1-carboxylic acid and abscisic acid concentrations in Rosmarinus officinalis plants. Physiologia Plantarum, 114(3), 380–386.

Myers, N., Mittermeier, R. A., Mittermeier, C. G., Da Fonseca, G. A., and Kent, J. (2000). Biodiversity hotspots for conservation priorities. Nature 403, 853–858.

Nash, C. H., & Johnson, E. A. (1996). Synoptic climatology of lightning-caused forest fires in subalpine and boreal forests. Canadian Journal of Forest Research, 26(10), 1859-1874.

Nath, A., & Nath, R. (2019). Identification of Black Dragon forest fire in Amur River Basin Using Satellite Borne NDVI Data and Its Impact on Long Range Transport of Pollutants: A Case Study. Journal of Atmospheric Science Research, 2(3), 6-10.

Naudts K, Chen Y, McGrath MJ, Ryder J, Valade A, Otto J, Luyssaert S. Europe's forest management did not mitigate climate warming. Science. 2016 Feb 5;351(6273):597-600.

Nelson, C. R. (2018). Investigation of Vaporization Enthalpies and Vapor Pressures of Organic Compounds by Correlation Gas Chromatography. University of Missouri-Saint Louis.

Neyişçi, T., and M. Intini. 2006. The use of cypress barriers for limiting fires in mediterranean countries. In proceedings of the " Il cipresso e gli incendi " workshop, June 14-16, 2006, Valencia, Spain. Interreg IIIB MEDOCC, Project MedCypre. Florence, Italy: 3-18.

Niinemets, Ü. (2010). Mild versus severe stress and BVOCs: thresholds, priming and consequences. Trends in Plant Science, 15(3), 145–153.

Niinemets, Ü., Kännaste, A., & Copolovici, L. (2013). Quantitative patterns between plant volatile emissions induced by biotic stresses and the degree of damage. Frontiers in Plant Science, 4, 262.

Niinemets, U¨., and M. Reichstein, (2002). A model analysis of the effects of nonspecific monoterpenoid storage in leaf tissues on emission kinetics and composition in Mediterranean sclerophyllous Quercus species, Global Biogeochem. Cycles, 16(4), 1110.

Nogués, I., Muzzini, V., Loreto, F., & Bustamante, M. A. (2015). Drought and soil amendment effects on monoterpene emission in rosemary plants. Science of the Total Environment, 538, 768-778.

Nolan, R. H., Blackman, C. J., de Dios, V. R., Choat, B., Medlyn, B. E., Li, X., ... & Boer, M. M. (2020). Linking forest flammability and plant vulnerability to drought. Forests, 11(7), 779.

O'Brien, Joseph & Loudermilk, Louise & Hiers, John & Pokswinski, Scott & Hornsby, Benjamin & Hudak, AT & Strother, Dexter & Rowell, Eric & Bright, Benjamin. (2016). Canopy-Derived Fuels Drive Patterns of In-Fire Energy Release and Understory Plant Mortality in a Longleaf Pine (Pinus palustris) Sandhill in Northwest Florida, USA. Canadian Journal of Remote Sensing. 42. 00-00.

Ojha, D. K., & Vinu, R. (2015). Fast co-pyrolysis of cellulose and polypropylene using Py-GC/MS and Py-FT-IR. RSC Advances, 5(82), 66861–66870.

Olmos, E., Sánchez-Blanco, M. J., Ferrández, T., & Alarcón, J. J. (2007). Subcellular Effects of Drought Stress inRosmarinus officinalis. Plant Biology, 9(1), 77–84.

Olson DM, Dinerstein E (2002) The global 200: priority ecoregions for global conservation. Ann Missouri Bot Gard 89 :199–224.

Orf, Megan & Kurian, Manu & Nelson, Carissa & Simmons, Dan & Espinosa, Lorna & Chickos, James. (2021). Correlation Gas Chromatographic Study of the Vaporization Enthalpies and Vapor Pressures of the Major Sesquiterpene Hydrocarbons in Patchouli Oil. Journal of Chemical & Engineering Data, 66(6), 2538-2549.

Ormeño, E., Baldy, V., Ballini, C., & Fernandez, C. (2008). Production and diversity of volatile terpenes from plants on calcareous and siliceous soils: effect of soil nutrients. Journal of chemical ecology, 34, 1219-1229.

Ormeno, E., Cespedes, B., Sanchez, I. A., Velasco-García, A., Moreno, J. M., Fernandez, C., & Baldy, V. (2009). The relationship between terpenes and flammability of leaf litter. Forest Ecology and Management, 257(2), 471-482.

Ormeño, Elena & Mévy, Jean-Philippe & Vila, Bruno & Bousquet-Mélou, Anne & Greff, Stephane & Bonin, G & Fernandez, Catherine. (2007). Water deficit stress induces different monoterpene and sesquiterpene emission changes in Mediterranean species. Relationship between terpene emissions and plant water potential. Chemosphere. 67. 276-84.

Ormeño, E., Fernandez, C., Bousquet-Mélou, A., Greff, S., Morin, E., Robles, C., Vila, B., Bonin, G., (2007b). Monoterpene and sesquiterpene emissions of three Mediterranean species through calcareous and siliceous soils in natural conditions. Atmos. Environ. 41, 629–639.

Ottmar, R. D. (2014). Wildland fire emissions, carbon, and climate: Modeling fuel consumption. Forest Ecology and Management, 317, 41–50.

Owen, S. M., Boissard, C., & Hewitt, C. N. (2001). Volatile organic compounds (VOCs) emitted from 40 Mediterranean plant species: Atmospheric Environment, 35(32), 5393–5409.

Owen, S., Boissard, C., Street, R.A., Duckham, S.C., Csiky, O., Hewitt, C.N., (1997). The BEMA Project: screening of 18 Mediterranean plant species for volatile organic compound emissions. Atmospheric Environment 31 (S1), 101–118.

Owen, S.M., Harley, P., Guenther, A., Hewitt, C.N., (2002). Light dependency of VOC emissions from selected Mediterranean plant species. Atmospheric Environment 36, 3147–3159.

Page, W. G., Freeborn, P. H., Butler, B. W., & Jolly, W. M. (2019). A review of US wildland firefighter entrapments: trends, important environmental factors and research needs. International journal of wildland fire, 28(8), 551-569.

Palies, P. (2020). Premixed swirling flame stabilization. Stabilization and Dynamic of Premixed Swirling Flames, 105–158.

Parameshwaran, R., Sarı, A., Jalaiah, N., & Karunakaran, R. (2018). Applications of Thermal Analysis to the Study of Phase-Change Materials. Handbook of Thermal Analysis and Calorimetry, 6, 519-572.

Parente, J., Amraoui, M., Menezes, I., & Pereira, M. G. (2019). Drought in Portugal: Current regime, comparison of indices and impacts on extreme wildfires. Science of The Total Environment, 685, 150-173.

Parresol, Bernard, (2007). Estimating canopy fuel parameters for Atlantic Coastal Plain forest types. Report to the US Forest Service Savannah River. USDA Forest Service, Southern Research Station, Asheville, NC, 28804, 35.

Pascoa Dos Santos, M. (2014). Pyrolysis and thermogravimetric analysis of wood and its components (Dissertation). Retrieved from http://urn.kb.se/resolve?urn=urn:nbn:se:kth:diva-158618.

Paul, A. S., Panwar, N. L., Salvi, B. L., Jain, S., & Sharma, D. (2020). Experimental investigation on the production of bio-oil from wheat straw. Energy Sources, Part A: Recovery, Utilization, and Environmental Effects, 1–16.

Pausas JG, Pereira JS, Aronson J (2009) The tree. In: Aronson J, Pereira JS, Pausas JG (eds) Cork oak woodlands on the age. Island Press, Washington DC, pp 11–23.

Pausas, J. G., & Keeley, J. E. (2009). A burning story: the role of fire in the history of life. BioScience, 59(7), 593-601.

Pausas, J. G., Alessio, G. A., Moreira, B., and Segarra-Moragues, J. G. (2016). Secondary compounds enhance flammability in a Mediterranean plant. Oecologia 180, 103–110.

Pausas, J. G., Llovet, J., Rodrigo, A., & Vallejo, R. (2008). Are wildfires a disaster in the Mediterranean basin? A review. International Journal of wildland fire, 17(6), 713-723.

Pellizzaro, G., Cesaraccio, C., Duce, P., Ventura, A., & Zara, P. (2007). Relationships between seasonal patterns of live fuel moisture and meteorological drought indices for Mediterranean shrubland species. International Journal of Wildland Fire, 16(2), 232-241.

Peñuelas, J. and Llusià, J. (2002), Linking photorespiration, monoterpenes and thermotolerance in Quercus. New Phytologist, 155: 227-237.

Peñuelas, J. and Staudt, M. (2010) BVOCs and Global Change, Trends in Plant Science, 15, 133-144.

Peñuelas, J., & Llusià, J. (2001). Seasonal patterns of non-terpenoid C6–C10 VOC emission from seven Mediterranean woody species. Chemosphere, 45(3), 237–244.

Peñuelas, J., Llusià, J., (1997). Effects of carbon dioxide, water supply and seasonality on terpene content and emission by Rosmarinus officinalis. J. Chem. Ecol. 23, 979–994.

Pereira, Helena (2007). The chemical composition of cork, Cork Biology Production and Uses 55–99. https://doi.org/10.1016/B978-044452967-1/50005-4.

Peuch, E (2007) Wild fire safety: feed back on sudden ignitions causing fatalities. 4th International Wildland Fire Conference. Seville, Spain.

Pignatti, S., Guarino R. and La Rosa, M. (2017) 'Flora d'Italia, vol. 2', pp. 1047–1048.

Pio C.A.; Silva P.A.; Cerqueira M.A.; Nunes T.V. (2005). Diurnal and seasonal emissions of volatile organic compounds from cork oak (Quercus suber) trees. 39(10), 1817–1827.

Pivello, V. R. (2011). The use of fire in the Cerrado and Amazonian rainforests of Brazil: past and present. Fire ecology, 7, 24-39.

Plucinski, M. P. (2012). A review of wildfire occurrence research. Bushfire Cooperative Research Centre.

Preston, B. L., & Jones, R. N. (2006). Climate change impacts on Australia and the benefits of early action to reduce global greenhouse gas emissions (p. 41). Canberra: CSIRO.

Prugh, Richard. (2008). The relationship between flash point and LFL with application to hybrid mixtures. Process Safety Progress. 27. 156 - 163.

Puigdefábregas, J., & Mendizabal, T. (1998). Perspectives on desertification: western Mediterranean. Journal of Arid Environments, 39(2), 209–224.

Pyne, S. J. (1989). The Great Black Dragon Fire: a Chinese Inferno. BioScience, 39(10), 732+.

Radeloff, V. C., Helmers, D. P., Kramer, H. A., Mockrin, M. H., Alexandre, P. M., Bar-Massada, A., ... & Stewart, S. I. (2018). Rapid growth of the US wildland-urban interface raises wildfire risk. Proceedings of the National Academy of Sciences, 115(13), 3314-3319.

Retana, Javier & Espelta, Josep & Habrouk, Abdessamad & Ordóñez, José & Solà-Morales, Faustina. (2002). Regeneration patterns of three Mediterranean pines and forest changes after a large wildfire in NE Spain. Ecoscience. 9, 89-97.

Riaza, Juan; Ajmi, Muhammad; Gibbins, Jon; Chalmers, Hannah (2017). Ignition and Combustion of Single Particles of Coal and Biomass under O2/CO2 Atmospheres. Energy Procedia, 114(), 6067–6073.

Rick, T., Ontiveros, M. Á. C., Jerardino, A., Mariotti, A., Méndez, C., & Williams, A. N. (2020). Human-environmental interactions in Mediterranean Climate Regions from the Pleistocene to the Anthropocene. Anthropocene, 31, 100253.

Rivoal, A., Fernandez, C., Lavoir, A. V., Olivier, R., Lecareux, C., Greff, S., ... & Vila, B. (2010). Environmental control of terpene emissions from Cistus monspeliensis L. in natural Mediterranean shrublands. Chemosphere, 78(8), 942-949.

Rogan, J., & Franklin, J. (2001). Mapping Wildfire Burn Severity in Southern California Forests and Shrublands Using Enhanced Thematic Mapper Imagery. Geocarto International, 16, 89-99.

Rogers, J. M., Susott, R. A., & Kelsey, R. G. (1986). Chemical composition of forest fuels affecting their thermal behavior. Canadian Journal of Forest Research, 16(4), 721–726.

Romero B, Ganteaume A. Effect of Fire Frequency on the Flammability of Two Mediterranean Pines: Link with Needle Terpene Content. Plants (Basel). 2021 Oct 12 ;10(10) :2164.

Romero, B., Fernandez, C., Lecareux, C., Ormeño, E. and Ganteaume, A., 2019. How terpene content affects fuel flammability of wildland–urban interface vegetation. International journal of wildland fire, 28(8), pp.614-627.

Rostam-Abadi M.; Debarr J.A.; Chen W.T. (1990). Combustion studies of coal derived solid fuels by thermogravimetric analysis: III. Correlation between burnout temperature and carbon combustion efficiency. 166(none), 351–356.

Rothermel, R. C. (1991). Predicting behavior and size of crown fires in the Northern Rocky Mountains. Res. Pap. INT-438. Ogden, UT: U.S. Department of Agriculture, Forest Service, Intermountain Forest and Range Experiment Station. 46 p

Rothermel, R. C., & Anderson, H. E. (1966). Fire spread characteristics determined in the laboratory (Vol. 30). Intermountain Forest & Range Experiment Station, Forest Service, US Department of Agriculture.

Rothermel, R.C. (1972) A Mathematical Model for Predicting Fire Spread in Wildland Fuels, Vol. 115. Intermountain Forest & Range Experiment Station, Forest Service, US Department of Agriculture, Ogden.

Rothermel, Richard C. (1983). How to predict the spread and intensity of forest and range fires. Gen. Tech. Rep. INT-143. Ogden, UT: U.S. Department of Agriculture, Forest Service, Intermountain Forest and Range Experiment Station. 161 p.

Rowley, J. R., Rowley, R. L., & Wilding, W. V. (2011). Estimation of the lower flammability limit of organic compounds as a function of temperature. Journal of Hazardous Materials, 186(1), 551–557.

Ruffault, J., Curt, T., Martin-StPaul, N. K., Moron, V., & Trigo, R. M. (2018). Extreme wildfire events are linked to global-change-type droughts in the northern Mediterranean. Natural Hazards and Earth System Sciences, 18(3), 847-856.

Safdari, Saeed & Rahmati, Mahmood & Amini, Elham & Howarth, Joel & Berryhill, Jansen & Dietenberger, Mark & Weise, David & Fletcher, Thomas. (2018). Characterization of pyrolysis products from fast pyrolysis of live and dead vegetation native to the Southern United States. Fuel. 229. 151-166.

Safford, H. D., & Vallejo, V. R. (2019). Ecosystem management and ecological restoration in the Anthropocene: integrating global change, soils, and disturbance in boreal and Mediterranean forests. In Developments in Soil Science (Vol. 36, pp. 259-308). Elsevier.

Salim, Salim M. & Cheah, S.C. (2009). Wall y+ Strategy for Dealing with Wall-bounded Turbulent Flows. Lecture Notes in Engineering and Computer Science. 2175.

Sánchez-Osorio Israel, López-Pantoja Gloria, Tapias Raúl, Pareja-Sánchez Evangelina, Domínguez Luis. (2019). Monoterpene emission of Quercus suber L. highly infested by Cerambyx welensii Küster. Annals of Forest Science. 76 (4), pp.98.

Sandhyavitri, A., Amri, R., & Fermana, D. (2016, June). Development of Underground Peat Fire Detection. In Int. Conf. on Technology, Innovation, and Society (ICTIS2019) (pp. 439-444).

San-Miguel-Ayanz, J., Durrant, T., Boca, R., Maianti, P., Libertá, G., Artés-Vivancos, T., Oom, D., Branco, A., de Rigo, D., Ferrari, D., Pfeiffer, H., Grecchi, R., Onida, M., Löffler, P. 2022. Forest Fires in Europe, Middle East and North Africa 2021, Publications Office of the European Union, Luxembourg, 2022,

Santoni, P.A. & Balbi, J.H. (1998). Modelling of two-dimensional flame spread across a sloping fuel bed. Fire Safety Journal. 31. 10.1016/S0379-7112(98)00011-3.

Sarmoum, Radhia, Soumia Haid, Mohamed Biche, Zahreddine Djazouli, Bachar Zebib, and Othmane Merah. (2019). "Effect of Salinity and Water Stress on the Essential Oil Components of Rosemary (Rosmarinus officinalis L.)" Agronomy 9, no. 5: 214.

Saunier A, Ormeño E, Wortham H, Temime-Roussel B, Lecareux C, Boissard C and Fernandez C (2017) Chronic Drought Decreases Anabolic and Catabolic BVOC Emissions of Quercus pubescens in a Mediterranean Forest. Front. Plant Sci. 8:71.

Schnitzler, J. P., Graus, M., Kreuzwieser, J., Heizmann, U., Rennenberg, H., Wisthaler, A., and Hansel, A., (2004). Contribution of Different Carbon Sources to Isoprene Biosynthesis in Poplar Leaves, Plant Physiol., 135, 152–160.

Schröder, V. (2016). Calculation of Flammability and Lower Flammability Limits of Gas Mixtures for Classification Purposes (pp. 1-17). Bundesanstalt für Materialforschung und-prüfung (BAM).

Scognamiglio, Mariarosa, Lucia Baldino, and Ernesto Reverchon. (2022). "Fractional Separation and Characterization of Cuticular Waxes Extracted from Vegetable Matter Using Supercritical CO_2" Separations 9, no. 3: 80.

Scott JH, Reinhardt ED (2001). Assessing crown fire potential by linking models of surface and crown fire behavior. Research paper RMRS-RP-29. USDA, Forest Service, Rocky Mountain Research Station, Fort Collins, p 59.

Scott, Joe H. 2006. Comparison of crown fire modeling systems used in three fire management applications. Res. Pap. RMRS-RP-58. Fort Collins, CO: U.S. Department of Agriculture, Forest Service, Rocky Mountain Research Station. 25 p.

Scott, Joe H.; Reinhardt, Elizabeth D. 2002. Estimating canopy fuels in conifer forests. Fire Management Today. 62(4): 45-50.

Serbouti, S., Abbas, Y., Ettaqy, A., Boukcim, H., Achiban, H., Abderrazzak, B., & Ghachtouli, N. E. (2022). Evolution of wildfires, burned areas, and affected species in Middle Atlas forests (Morocco) from 2000 to 2020. Trees, Forests and People, 10, 100319.

Šesták, Jaroslav & Holba, Pavel. (2013). Heat inertia and temperature gradient in the treatment of DTA peaks. Journal of Thermal Analysis and Calorimetry. 113.

Sharkey D. Thomas, Wiberley E. Amy, Autumn R. Donohue (2008). Isoprene Emission from Plants: Why and How, Annals of Botany, Volume 101, Issue 1, Pages 5–18.

Sharkey TD, Singsaas EL. (1995). Why plants emit isoprene. Nature. 374:769.

Sharkey TD. Isoprene synthesis by plants and animals. Endeavor. 1996; 20:74–78.

Sharples, J. J., Cary, G. J., Fox-Hughes, P., Mooney, S., Evans, J. P., Fletcher, M. S., ... & Baker, P. (2016). Natural hazards in Australia: extreme bushfire. Climatic Change, 139, 85-99.

Sharples, J. J., Lewis, S. C., & Perkins-Kirkpatrick, S. E. (2021). Modulating influence of drought on the synergy between heatwaves and dead fine fuel moisture content of bushfire fuels in the Southeast Australian region. Weather and Climate Extremes, 31, 100300.

Sharples, Jason & Gill, A & Dold, John. (2010). The Trench Effect and Eruptive Wildfires: Lessons from the King's Cross Underground Disaster. Proceedings AFAC 2010.

Shen D.K.; Gu S.;. Luo K.H;. Bridgwater A.V; Fang M.X. (2009). Kinetic study on thermal decomposition of woods in oxidative environment. 88(6), 1024–1030.

Shen, Tianhao, Fengxia Zhang, Shiliang Yang, Hua Wang, and Jianhang Hu. (2023). "Investigation of Pyrolysis Kinetic Triplet, Thermodynamics, Product Characteristics and Reaction Mechanism of Waste Cooking Oil Biodiesel under the Influence of Copper Slag" Energies 16, no. 5: 2137.

Silva, J. S., & Catry, F. (2006). Forest fires in cork oak (Quercus suber L.) stands in Portugal. International Journal of Environmental Studies, 63(3), 235-257.

Simoes, Goncalo & Magalhaes, Duarte & Rabaçal, Miriam & Costa, Mário. (2016). Effect of gas temperature and oxygen concentration on single particle ignition behavior of biomass fuels. Proceedings of the Combustion Institute. 36.

Šimpraga, M., Ghimire, R. P., Van Der Straeten, D., Blande, J. D., Kasurinen, A., Sorvari, J., ... & Kivimäenpää, M. (2019). Unravelling the functions of biogenic volatiles in boreal and temperate forest ecosystems. European Journal of Forest Research, 138, 763-787.

Šimpraga, M., Verbeeck, H., Demarcke, M., Joó, É., Pokorska, O., Amelynck, C., … Steppe, K. (2011). Clear link between drought stress, photosynthesis and biogenic volatile organic compounds in Fagus sylvatica L. Atmospheric Environment, 45(30), 5254–5259.

Simpson, I. J., Akagi, S. K., Barletta, B., Blake, N. J., Choi, Y., Diskin, G. S., Fried, A., Fuelberg, H. E., Meinardi, S., Rowland, F. S., Vay, S. A., Weinheimer, A. J., Wennberg, P. O., Wiebring, P., Wisthaler, A., Yang, M., Yokelson, R. J., and Blake, D. R. (2011). Boreal forest fire emissions in fresh Canadian smoke plumes: C_1-C_{10} volatile organic compounds (VOCs), CO_2, CO, NO_2, NO, HCN and CH_3CN, Atmos. Chem. Phys., 11, 6445–6463.

Singsaas, E. & Sharkey, Thomas. (2000). The effects of high temperature on isoprene synthesis in oak leaves. Plant Cell and Environment - PLANT CELL ENVIRON. 23. 751-757.

Solomon, K. A. (2019). Chemistry of Natural Products. MJP Publisher.

Sonobe, T., & Worasuwannarak, N. (2008). Kinetic analyses of biomass pyrolysis using the distributed activation energy model. Fuel, 87(3), 414–421.

Sonwani, S., Saxena, P., and Kulshrestha, U. (2016). "Role of global warming and plant signaling in BVOC emissions," in Plant Responses to Air Pollution, eds Ulshrestha, U., and Saxena, P. (Singapore: Springer), 45–57.

Sousa, Ana & Nieto de Castro, Carlos. (1992). Density of α-pinene, B-pinene, limonene, and essence of turpentine. International Journal of Thermophysics - INT J THERMOPHYS. 13. 295-301.

Stauffer, E., Dolan, J. A., & Newman, R. (2008). Chemistry and Physics of Fire and Liquid Fuels. Fire Debris Analysis, 85–129.

Stewart, S. I., Radeloff, V. C., Hammer, R. B., & Hawbaker, T. J. (2007). Defining the wildland–urban interface. Journal of Forestry, 105(4), 201-207.

Stocks B.J., Mason J.A., Todd J.B., Bosch E.M., Wotton B.M. Amiro B.D., et al. 2003. Large forest fires in Canada, 1959–1997. J. Geophys. Res. D: Atmospheres, 108 (D1): FFR 5–1-FFR 5-12.

Susott Ronald A., Characterization of the Thermal Properties of Forest Fuels by Combustible Gas Analysis, Forest Science, Volume 28, Issue 2, June 1982, Pages 404–420.

Thierry Gauquelin, Geneviève Michon, Richard Joffre, Robin Duponnois, Didier Genin, et al.. Mediterranean forests, land use and climate change: a social-ecological perspective. Regional Environmental Change, 2018, 18 (3), pp.623-636.

Thomas, P.H. 1963.The size of flames from natural fires. In: Proceedings, 9th International Symposium on Combustion; 1962; Ithaca, NY: Academic Press: 844-859.

Thompson, I., Mackey, B., McNulty, S., Mosseler, A. (2009). Forest Resilience, Biodiversity, and Climate Change. A synthesis of the biodiversity/resilience/stability relationship in forest ecosystems. Secretariat of the Convention on Biological Diversity, Montreal. Technical Series (Vol. 43, No. 1, pp. 1-67).

Tison, J.-M. and de Foucault, B. (2014) Flora gallica : flore de France. Biotope.

Trabaud L. (1981). Man, and fire: Impacts on mediterranean vegetation. In: di Castri F., Goodall D.W.and Specht R.L. (eds), Mediterranean-type shrublands. Elsevier, Amsterdam, pp. 523-538.

Turco, M., Llasat, M.-C., von Hardenberg, J., & Provenzale, A. (2014). Climate change impacts on wildfires in a Mediterranean environment. Climatic Change, 125(3-4), 369–380.

Úbeda, X., & Sarricolea, P. (2016). Wildfires in Chile: A review. Global and Planetary Change, 146, 152-161.

Ucla 2006. Retreived from https://news.mongabay.com/2006/10/methane-from-peat-bogs-may-worsen-global-warming.

Van Wagner, C. E. 1974. A spread index for crown fires in spring. Inf. Rep. PI-X-55. Canadian Forest Service, Petawawa Nat. For. Inst. Van Wagner, C. E. 1977. Conditions for the start and spread of crown fire. Canadian Journal of Forest Research. 7: 23–34.

Van Wagner, C. E. 1977. Conditions for the start and spread of crown fire. Canadian Journal of Forest Research. 7: 23–34.

Van Wagner, C. E. 1989. Prediction of crown fire behavior in conifer stands. In: D. C. MacIver, D. C.; Auld, H.; Whitewood, R., eds. Proceedings of the 10th conference of fire and forest meteorology; 1989 April 17–21, Ontario, Canada. Environment Canada, Forestry Canada: 207–212.

Van Wagner, C. E. 1993. Prediction of crown fire behavior in two stands of jack pine. Canadian Journal of Forest Research. 23: 442–449.

Velikova V, Sharkey TD, Loreto F. (2012). Stabilization of thylakoid membranes in isoprene-emitting plants reduces formation of reactive oxygen species. Plant Signal Behav;7(1):139-41.

Viegas D, Simeoni A, Xanthopoulos G, Rossa C, Ribeiro L, Pita L, Stipanicev D, Zinoviev A, Weber R, Dold J, Caballero D, San-Miguel-Ayanz J, authors Viegas D, editor (2009). Recent Forest Fire Related Accidents in Europe. EUR 24121 EN. Luxembourg (Luxembourg): Publications Office of the European Union. JRC56107.

Viegas DX (2005) A mathematical model for forest fires blow-up. Combustion Science and Technology 177, 1–25.

Viegas, D. X. (2004). A Mathematical Model for Forest Fire Blowup. Combustion Science and Technology, 177, 27-51.

Viegas, D. X., & Simeoni, A. (2011). Eruptive behaviour of forest fires. Fire technology, 47, 303-320.

Viegas, D.X. ed. (2009) Recent forest fire related accidents in Europe. European Commission Joint Research Centre Scientific and Technical Reports, European Communities

Viegas, Domingos & J, Piñol & MT, Viegas & R, Ogaya. (2001). Estimating live fine fuel moisture content using meteorologically-based indices. International Journal of Wildland Fire.

Viegas, Domingos & Pita, Luis & Ribeiro, Luis & Palheiro, P. (2005). Eruptive Fire Behaviour in Past Fatal Accidents.

Viegas, Domingos & Pita, Luis. (2004). Fire spread in canyons. International Journal of Wildland Fire. 13. 10.1071/WF03050.

Viegas, Domingos & Rossa, Carlos & Caballero, David & Pita, Luis & Palheiro, P. (2006). Analysis of accidents in 2005 fires in Portugal and Spain. Forest Ecology and Management - FOREST ECOL MANAGE. 234.

Viegas, Domingos & Stipanicev, Darko & Ribeiro, Luis & Pita, Luis & Rossa, Carlos. (2008). The Kornati fire accident - Eruptive fire in relatively low fuel load herbaceous fuel conditions. WIT Transactions on Ecology and the Environment. 119. 365-375.

Vilagrosa, Alberto & Bellot, Juan & Vallejo, Ramon & Pelegrín, Eustaquio. (2003). Cavitation, stomatal conductance, and leaf dieback in seedlings of two co-occurring Mediterranean shrubs during an intense drought. J Exp Bot. Journal of experimental botany. 54. 2015-24.

Viola, F. M., Paiva, S. L. D., & Savi, M. A. (2010). Analysis of the global warming dynamics from temperature time series. Ecological Modelling, 221(16), 1964–1978.

Viros J., Fernandez C., Wortham H., Gavinet J., Lecareux C., Ormeno E., (2020). Litter of mediterranean species as a source of volatile organic compounds. Atmospheric Environment, 242, 117815.

Wane MingYu ; Li Tao ; Ren YunMao ; Shu Lifu ; Zhao FengJun ; Tian XiaoRui, (2009). Research advances in forest fire behavior and special forest fire behaviors. World Forestry Research 2009, Vol.22 No.2 pp.45-49 ref.42.

Werth Paul, Potter Brian, Clements Craig, Finney Mark, Goodrick Scott, Martin Alexander, Miguel Cruz, Jason Forthofer, and Sara McAllister (2011). "Synthesis of Knowledge of Extreme Fire Behavior: Volume I for Fire Managers" Faculty Publications, Meteorology and Climate Science

Williams, A. P., Abatzoglou, J. T., Gershunov, A., Guzman-Morales, J., Bishop, D. A., Balch, J. K., & Lettenmaier, D. P. (2019). Observed impacts of anthropogenic climate change on wildfire in California. Earth's Future.

Williams, Caroline (2007). Ignition impossible. 195(2615), 38–40.

Williamson R, Banwell C, Calear AL, LaBond C, Leach LS, Olsen A, Walsh EI, Zulfiqar T, Sutherland S, Phillips C. Bushfire Smoke in Our Eyes: Community Perceptions and Responses to an Intense Smoke Event in Canberra, Australia. Front Public Health. 2022 Feb 24; 10:793312.

Wolfe BT, Sperry JS, Kursar TA. (2016). Does leaf shedding protect stems from cavitation during seasonal droughts? A test of the hydraulic fuse hypothesis. New Phytologist 212: 1007– 1018.

Wongsiriamnuay Thanasit; Tippayawong Nakorn (2010). Thermogravimetric analysis of giant sensitive plants under air atmosphere. 101(23), 9314–9320.

Wu, M., Shu, G., Tian, H., Wang, X., & Liu, Y. (2018). The thermal theory-based equation for correlation between temperature and flammability limits of hydrocarbons. Fuel, 214, 55–62.

Xanthopoulos, G. (2011). Cypress (Cupressus sempervirens) and forest fires. Cypress and forest fire: a practical manual, reports of the training school held in Florence (Italy), 23-27.

Yani ; G. Pauly ; M. Faye ; F. Salin ; M. Gleizes (1993). The effect of a long-term water stress on the metabolism and emission of terpenes of the foliage of Cupressus sempervirens. Plant, Cell, and Environment, 16(8), 975–981.

Yao, Guangyan; Wang, Linlin; Chen, Xiaopeng; Liao, Dankui; Wei, Xiaojie; Liang, Jiezhen; Tong, Zhangfa (2019). Measurement and correlation of vapor–liquid equilibrium data for binary and ternary systems composed of (−)-β-caryophyllene, p-cymene and 3-carene at 101.33 kPa. The Journal of Chemical Thermodynamics, 128(), 215–224.

Yao, S., Cao, J., Zhang, K., Jiao, K., Ding, H., & Hu, W. (2012). Artificial bacterial degradation and hydrous pyrolysis of suberin: Implications for hydrocarbon generation of suberinite. Organic Geochemistry, 47, 22–33.

Yebra, M., Aguardo, I., Garcia, M., Nieto, H., Chuvieco, E. et Salas, J. (2007). Fuel moisture estimation for fire ignition mapping, Wildfire 2007. Sevilla, Spain, May 2007.

Yeddes, W., Chalghoum, A., Aidi-Wannes, W., Ksouri, R., & Saidani Tounsi, M. (2019). Effect of bioclimatic area and season on phenolics and antioxidant activities of rosemary (Rosmarinus officinalis L.) leaves. Journal of Essential Oil Research, 31(5), 432-443.

Yokelson, R. J., Burling, I. R., Gilman, J. B., Warneke, C., Stockwell, C. E., de Gouw, J., … Weise, D. R. (2013). Coupling field and laboratory measurements to estimate the emission factors of identified and unidentified trace gases for prescribed fires. Atmospheric Chemistry and Physics, 13(1), 89–116.

Zhao, F. J., Shu, L. F., Wang, Q. H., Wang, M. Y., & Tian, X. R. (2011). Emissions of volatile organic compounds from heated needles and twigs of Pinus pumila. Journal of Forestry Research, 22(2), 243-248.

Zhao, F. (2011). Inert gas dilution effect on flammability limits of hydrocarbon mixtures (Vol. 73, No. 06).

Zhao, Fuman. (2023). Experimental measurements and modeling prediction of flammability limits of binary hydrocarbon mixtures. Doctoral Dissertation, Texas A & M University.

Zhou, H., Zhou, G., He, Q., Zhou, L., Ji, Y., & Lv, X. (2021). Capability of leaf water content and its threshold values in reflection of soil–plant water status in maize during prolonged drought. Ecological Indicators, 124, 107395.

Appendix II

AII.1. Exhibit 2 for fuel moisture content calculation (Rothermel 1983).

REFERENCE FUEL MOISTURE

DAY TIME 0800-1959

Dry Bulb Temperature (°F)	RELATIVE HUMIDITY (PERCENT)																				
	0 ↓ 4	5 ↓ 9	10 ↓ 14	15 ↓ 19	20 ↓ 24	25 ↓ 29	30 ↓ 34	35 ↓ 39	40 ↓ 44	45 ↓ 49	50 ↓ 54	55 ↓ 59	60 ↓ 64	65 ↓ 69	70 ↓ 74	75 ↓ 79	80 ↓ 84	85 ↓ 89	90 ↓ 94	95 ↓ 99	100
10 - 29	1	2	2	3	4	5	5	6	7	8	8	8	9	9	10	11	12	12	13	13	14
30 - 49	1	2	2	3	4	5	5	6	7	7	7	8	9	9	10	10	11	12	13	13	13
50 - 69	1	2	2	3	4	5	5	6	6	7	7	8	8	9	9	10	11	12	12	12	13
70 - 89	1	1	2	2	3	4	5	5	6	7	7	8	8	8	9	10	10	11	12	12	13
90-109	1	1	2	2	3	4	4	5	6	7	7	8	8	8	9	10	10	11	12	12	13
109+	1	1	2	2	3	4	4	5	6	7	7	8	8	8	9	10	10	11	12	12	12

DEAD FUEL MOISTURE CONTENT CORRECTIONS

FEBRUARY MARCH APRIL/AUGUST SEPTEMBER OCTOBER

		EXPOSED – LESS THAN 50% SHADING OF SURFACE FUELS																			
		0800 →			1000 →			1200 →			1400 →			1600 →			1800 →				
		B	L	A	B	L	A	B	L	A	B	L	A	B	L	A	B	L	A		
N	0-30%	3	4	5	1	2	3	1	1	2	1	1	2	1	2	3	3	4	5		
	31%+	3	4	5	3	3	4	2	3	4	2	3	4	3	3	4	3	4	5		
E	0-30%	3	4	5	1	2	3	1	1	1	1	1	2	1	2	3	3	4	5		
	31%+	3	3	4	1	1	1	1	1	1	1	2	3	3	4	5	4	5	6		
S	0-30%	3	4	5	1	2	2	1	1	1	1	1	1	1	2	3	3	4	5		
	31%+	3	4	5	1	2	2	0	1	1	0	1	1	1	2	2	3	4	5		
W	0-30%	3	4	5	1	2	3	1	1	1	1	1	1	1	2	3	3	4	5		
	31%+	4	5	6	3	4	5	1	2	3	1	1	1	1	1	1	3	3	4		
	SHADED – GREATER THAN OR EQUAL TO 50% SHADING OF SURFACE FUELS																				
N	0%+	4	5	6	4	5	5	3	4	5	3	4	5	4	5	5	4	5	6		
E	0%+	4	5	6	3	4	5	3	4	5	3	4	5	4	5	6	4	5	6		
S	0%+	4	5	6	3	4	5	3	4	5	3	4	5	3	4	5	4	5	6		
W	0%+	4	5	6	4	5	6	3	4	5	3	4	5	3	4	5	4	5	6		

NOTE: A = 1000'-2000' above site
L = ±1000' of site location
B = 1000'-2000' below site

TABLE D

DAYTIME 0800-1959

AII.2. Conversion tables of units from English to metric system, multiplication factors (Scott and Reinhardt 2002).

Weight							
From	to=>	g	oz	lb	kg	ton	Mg
g		1	0.035	0.002205	0.001	0.000001102	0.000001
oz		28.35	1	0.06251	0.02835	0.00003125	0.00002835
lb		453.6	16	1	0.4536	0.0005	0.0004536
kg		1000	35.30	2.205	1	1.10E-03	0.001
Mg		1.E+06	3,53E+04	2205	1000	1.102	1

Distance										
from	to=>	mm	cm	inch	feet	yard	meter	chain	km	mile
mm		1	0.1	0.03937	0.003281	0.001094	0.001	0.00004971	1.E-06	0.0006214
cm		10	1	0.3937	32.81	10.94	0.01	0.4971	1.E-05	0.006214
inch		25.40	2.540	1	0.08333	0.02778	0.02540	0.001	0.0254	0.01578
feet		304.8	30.48	12	1	0.3333	0.3048	0.01515	0.3048	0.1894
yard		914.4	91.44	36	3	1	0.9144	45.45	0.9144	0.5682
meter		1000	100	39.37	3.281	1.094	1	0.04971	0.001	0.6214
chain		2,01E+07	2,01E+06	7,92E+05	66	22	20.12	1	20.12	12.5
km		1.E+06	1.E+05	3,94E+07	3,28E+06	1,09E+06	1000	49.71	1	0.6214
m ile		1,61E+09	1,61E+08	6,34E+07	5280	1760	1,61E+06	80	1.609	1

Area										
from	to=>	cm 2	in2	ft2	yd2	m 2	acre	ha	km 2	mi2
cm 2		1	0.1550	1,08E+03	0.1196	0.0001	0.00002471	0.00000001	0.0000000001	0.00000003861
in2		6.452	1	6,94E+03	0.7716	0.6452	0.0001594	0.00006452	0.0000006452	0.0000002491
ft2		929.0	144	1	0.1111	0.09290	0.02296	0.00929	0.0000929	0.00003587
yd2		8361	1296	9	1	0.8361	0.2066	0.08361	0.0008361	0.0003228
m 2		1.E+04	1550	10.76	1.196	1	0.2471	1.E-04	0.000001	0.0003861
acre		4,05E+10	6,27E+09	4,36E+07	4840	4047	1	0.4047	4,05E+03	1,56E+03
ha		1.E+08	1,55E+10	1,08E+08	1,20E+07	1.E+04	2.471	1	0.010000045	3,86E+03
km 2		1.E+10	1,55E+12	1,08E+10	1,20E+09	1.E+06	247.1	100	1	0.3861
m i2		2,59E+13	4,01E+12	2,79E+10	3,10E+09	2,59E+09	640.0	259.0	2.590	1

Rate of Spread ROS										
from	to=>	ft/min	ch/hr	cm/s	m/min	km/hr	ft/sec	mi/hr	knot	m/sec
ft/min		1	0.9091	0.5080	0.3048	0.01829	0.01667	0.01136	9.875E-03	5.080E-03
ch/hr		1.100	1	0.5588	0.3353	0.02012	0.01833	0.01250	0.01086	5.588E-03
cm/s		1.968	1.790	1	0.6000	0.03600	0.03281	0.02237	0.01944	0.01
m/min		3.281	2.983	1.667	1	0.06000	0.05468	0.03728	0.03240	0.01667
km/hr		54.68	49.71	27.78	16.67	1	0.9113	0.6214	0.5400	0.2778
ft/sec		60	54.55	30.48	18.29	1.097	1	0.6818	0.5925	0.3048
mi/hr		88	80	44.70	26.82	1.609	1.467	1	0.8690	0.4470
knot		101.3	92.06	51.44	30.87	1.852000037	1.688	1.151	1	0.5144
m/sec		196.8	179.0	100	60	3.6	3.281	2.237	1.944	1

Bulk Density						
from	to=>	ton/(ac.ft)	kg/m3	ton/(ac-in)	lb/ft3	gm/cm3
ton/(ac-ft)		1	0.7355	0.08333	0.04591	7.355E-04
kg/m3		1.360	1	0.1133	0.06243	0.001
ton/(ac-in)		12	8.826	1	0.5510	8.826E-03
lb/ft3		21.78	16.02	1.815	1	0.01602
gm/cm3		1360	1000	113.3	62.43	1

Area Intensity					
from	to=>	kJ/(m2.min)	kW/m2	BTU/(ft2.s)	cal/(cm2.s)
kJ/(m2-min)		1	0.01667	1.469E-03	3.984E-04
kW/m2		60	1	0.08811	0.02390
BTU/(ft2-s)		680.9	11.35	1	0.2712
cal/(cm2-s)		2510	41.84	3.687	1

Heat Content				
from	to=>	kJ/kg	BTU/lb	cal/gm
kJ/kg		1	0.4303	0.2390
BTU/lb		2.324	1	0.5555
cal/gm		4.184	1.800	1

Appendix III

AIII.1. Chemical Composition of the volatile gases resulting from the pyrolysis tests on Cupressus sempervirens var. horizontalis litter leaves (wet & dry Season) from low to high temperature profiles (50°C, 80°C, 120°C, 180°C, DS350 - 550°C, TS 120-350-550°C).

C.s.L. (Wet season)			
SS 50°C			
Compound	**Area %**	**RT (min)**	**Chemical Formula**
Limonene	2.77	8.0	C10H16
Camphene	9.68	14.3	C10H16
Terpinyl Acetate	35.88	16.8	C12H20O2
α Cubebene	14.53	19.9	C15H24
Germacrene D	29.28	20.1	C15H24
(E)-β-Ocimene	7.84	44.3	C10H16
SS 80°C			
α Pinene	10.22	5.6	C10H16
β Pinene	3.32	6.5	C10H16
δ-3-Carene	10.79	7.5	C10H16
Limonene	27.88	8.0	C10H16
Trans-p-Mentha-2,8-dienol	0.41	10.7	C10H16O
4H-Pyran-4-one, 2,3-dihydro-3,5-dihydroxy-6-methyl-	0.01	11.9	C6H8O4
Cyclohexanol, 2-methylene-5-(1-methylethenyl) -	4.52	12.7	C10H16O
(E)-3(10) -Caren-4-ol	2.43	13.9	C10H16O
Terpinyl Acetate	7.95	16.8	C12H20O2
Germacrene D	14.89	20.1	C15H24
Nerolidol	8.27	22.1	C15H26O
α Bisabolol	2.26	25.3	C15H26O
8-Cedren-13-Ol	0.39	26.9	C15H24O
Cupressene	0.22	30.0	C20H32
n-Hexadecanoic acid	0.19	31.0	C16H32O2
Hibaene	1.32	31.3	C20H32
16-Kaurene	2.76	34.5	C20H32
Sclareol	0.37	36.3	C20H36O2
Trans-Totarol	1.63	37.5	C20H30O
SS 120°C			
α Pinene	12.23	5.6	C10H16
β Pinene	8.04	6.5	C10H16
δ-3-Carene	22.92	7.5	C10H16
Limonene	3.07	8.0	C10H16
Terpinolene	2.29	9.2	C10H16
Copaene	3.89	16.6	C15H24
Terpinyl Acetate	3.22	16.8	C12H20O2
Germacrene D	24.31	20.1	C15H24
α Bergamotene	3.14	20.8	C15H24
Germacrene D-4-ol	10.91	22.7	C15H26O
Cupressene	0.27	30.0	C20H32
Hibaene	0.54	31.3	C20H32
16-Kaurene	5.15	34.5	C20H32
SS 180°C			
α Pinene	4.38	5.6	C10H16
β Pinene	1.03	6.5	C10H16
δ-3-Carene	3.42	7.5	C10H16
Limonene	8.63	8.0	C10H16
Trans-p-Mentha-2,8-dienol	1.47	10.7	C10H16O
4H-Pyran-4-one, 2,3-dihydro-3,5-dihydroxy-6-methyl-	4.09	11.9	C6H8O4
Cyclohexanol, 2-methylene-5-(1-methylethenyl) -	1.09	12.7	C10H16O
(E)-3(10) -Caren-4-ol	1.71	13.9	C10H16O
Terpinyl Acetate	3.67	16.8	C12H20O2
Germacrene D	2.84	20.1	C15H24
Elemol	0.68	22.0	C15H26O

Nerolidol	2.00	22.1	C15H26O
α Bisabolol	3.02	25.3	C15H26O
8-Cedren-13-Ol	1.07	26.9	C15H24O
Cupressene	0.48	30.0	C20H32
Biformen	2.21	30.3	C20H32
n-Hexadecanoic acid	4.14	31.0	C16H32O2
Sclareol	33.48	36.3	C20H36O2
Trans-Totarol	17.34	37.5	C20H30O
Kauran-18-al, 17-(acetyloxy)-, (4,beta,)-	3.27	40.0	C22H34O3
DS 350°C			
Furfural	3.36	3.1	C5H4O2
2-Furanmethanol	5.42	3.8	C5H6O
Monoterpene	5.32	4.7	C10H16
α pinene	6.72	5.6	C10H16
β pinene	2.38	6.5	C10H16
δ-4-Carene	7.82	7.0	C10H16
Limonene	16.52	8.0	C10H16
Terpinolene	0.45	9.2	C10H16
β Ocimene	0.96	9.5	C10H16
Phenol, 2-methoxy-	1.01	9.8	C10H12O2
Cyclohexane, 1,3-butadienylidene-	0.70	11.2	C10H14
(E)-3(10) -Caren-4-ol	1.00	13.9	C10H16O
3,10-Dioxatricyclo [4.3.1.0(2,4)] dec-7-ene	1.07	14.2	C8H10O2
Copaene	0.44	16.6	C15H24
Terpinyl Acetate	3.14	16.8	C12H20O2
Germacrene D	3.04	20.1	C15H24
Alkane	0.71	22.1	
Alkane	0.80	25.3	
Cupressene	3.25	30.0	C20H32
Resorcinol, 4-[(2-hydroxy-5-methyl-3-pyridyl) azo] -	2.42	32.5	C12H11N3O3
Kaur-16-ene	1.85	34.5	C20H32
Androstan-17-one, 3-ethyl-3-hydroxy-, (5. Alpha.) -	1.90	35.9	C20H32
Sclareol	7.02	36.3	C20H34O2
Trans Totarol	5.20	37.5	C20H32O
Alkane	0.83	45.7	
Alkane	2.28	48.3	
Alkane	9.41	51.0	
Alkane	1.65	54.6	
Alkane	0.59	55.5	
DS 550°C			
Phenol	22.26	7.0	C6H6O
Trans-3-Caren-2-ol	2.12	7.9	C10H16O
Methyl cyclopentenolone	2.94	8.1	C6H8O2
Phenol, 2-methyl-	4.31	8.8	C7H8O
Phenol, 3-methyl-	15.24	9.4	C7H8O
Phenol, 2-methoxy-	8.53	9.8	C10H12O2
Phenol, 2-methoxy-4-methyl-	4.98	12.5	C8H10O2
Benzofuran, 2,3-dihydro-	3.67	13.4	C8H8O
Ac16:2	2.22	30.4	
9,12-Octadecadienoic acid (Z, Z) -, methyl ester	33.74	37.9	C19H34O
C.s.L. (Dry season)			
SS 50°C			
α Pinene	6.64	5.6	C10H16
β Myrcene	4.04	7.1	C10H16
δ-3-Carene	24.46	7.5	C10H16
Limonene	57.00	8.0	C10H16
Monoterpene	6.98	8.4	C10H16
Copaene	0.87	16.6	C15H24
SS 80°C			
α Pinene	30.09	5.6	C10H16
2-Thujene	4.46	6.7	C10H16

δ-3-Carene	18.76	7.5	C10H16
Copaene	8.71	16.6	C15H24
α Cubebene	18.38	19.9	C15H24
Trans-4-(Hexyloxy)chalcone	13.75	36.5	
Tritriacontane (C33)	5.84	51.0	
SS 120°C			
α Pinene	24.87	5.7	C10H16
2-Thujene	18.90	6.6	C10H16
β Myrcene	3.19	7.0	C10H16
δ-3-Carene	26.58	7.5	C10H16
Limonene	4.69	8.0	C10H16
γ Terpinene	0.83	8.8	C10H16
δ-2-Carene	1.76	9.6	C10H16
Copaene	3.32	16.6	C15H24
α Cubebene	10.69	19.9	C15H24
Benzene, 1-(1,5-dimethyl-4-hexenyl) -4-methyl-	0.90	20.2	C15H22
α Bergamotene	0.66	20.7	C15H24
Germacrene	0.51	22.5	C15H24
Rimuen	3.10	35.0	C20H32
SS 180°C			
α Pinene	5.15	5.6	C10H16
2-Thujene	2.55	6.6	C10H16
δ-3-Carene	4.67	7.5	C10H16
Limonene	3.04	8.0	C10H16
γ Terpinene	1.29	8.8	C10H16
Terpinolene	0.77	9.2	C10H16
Copaene	3.31	16.6	C15H24
α Cubebene	6.41	19.9	C15H24
Cupressene	7.31	30.0	C20H32
Resorcinol, 4-[(2-hydroxy-5-methyl-3-pyridyl) azo] -	5.30	32.5	C12H11N3O3
Kaur-16-ene, (8, beta,13, beta,) -	10.05	33.7	C20H32
2-Furancarboxamide, N-(4-amino-2-methoxyphenyl) -	15.10	35.3	C12H12N2O3
Benzenamine, N-(3-methylphenyl) -2,4-dinitro-	0.33	35.8	C13H11N3O4
Trans-4-(Hexyloxy)chalcone	4.75	36.5	C21H24O2
Alkane	14.76	42.9	CH27
Alkane	15.20	45.6	CH29
DS 350°C			
Furfural	4.55	3.1	C5H4O2
Sabinene	7.80	6.2	C10H16
Cyclohexanone, 2-(2-methylpropylidene) -	0.09	11.4	C10H16O
2,3-Dihydroxybenzaldehyde	0.15	11.6	C7H6O3
Creosol	0.17	12.4	C8H10O2
Pyrocatechol	11.46	12.8	C6H6O2
Benzofuran, 2,3-dihydro-	1.01	13.4	C8H8O
5-Hydroxymethylfurfural	3.49	13.6	C6H6O3
Naphthalene, 2,6-bis(1,1-dimethylethyl) -	0.33	14.4	C18H24
Naphthalene, 1,2,3,4,4a,5,6,7-octahydro-4a-methyl-	0.21	15.0	C11H18
Benzenemethanol, 4-(1-methylethyl) -	0.79	15.2	C10H14O
Carvacrol	0.34	15.5	C10H14O
2-Methoxy-4-vinylphenol	1.44	15.8	C9H10O2
Phenol, 2-methoxy-3-(2-propenyl) -	3.33	16.7	C10H12O2
Citral	0.41	16.9	C10H16O
α Cubebene	1.71	19.9	C15H24
Cedrene	2.89	23.2	C15H24
2-Cyclohexen-1-one, 4-(3hydroxybutyl) -3,5,5-trimethyl-	0.64	25.0	C10H14O
Cis-Nuciferol	2.24	25.5	C15H22O
Tetradecanoic acid	1.80	25.9	C13H22O2
Phenanthrene, 7-ethenyl-1,2,3,4,4a,5,6,7,8,9,10,10a-dodecahydro-	2.64	26.6	C20H32
Hibaene	1.22	31.3	C20H32
Kaur-16-ene, (8, beta,13, beta,) -	2.06	33.7	C20H32
Podocarp-7-en-3-one, 13, beta, -methyl-13-vinyl-	1.49	34.0	C20H30O

Trans-4-(Hexyloxy)chalcone	0.41	36.5	C21H24O2
Ferruginol	1.43	37.1	C20H32
Trans-Totarol	0.95	37.5	C20H32
HC25	3.24	37.7	
HC26	3.92	39.0	
HC27	0.54	41.4	
HC28	1.18	42.9	
HC29	1.27	44.3	
HC31	1.03	45.7	
Triterpene 396 (297)	0.47	48.4	
Ketone C29	2.37	48.5	
HC32	2.94	49.0	
HC33	4.30	49.6	
Ketone C31	1.01	51.1	
Ox triterpene	13.95	51.5	
HC34	1.03	52.3	
HC35	4.77	52.7	
Ketone C33	2.86	54.7	
DS 550°C			
1,3-Pentadiene, (Z)-	7.29	1.6	C5H8
Furan, 2-methyl-	5.36	1.9	C5H6O
4-Methyl-2-pentyne	0.86	2.1	C6H10
1,3,5-Heptatriene, (E, E) -	0.66	2.8	C7H10
Toluene	4.53	3.0	C7H8
2-Cyclopenten-1-one	1.35	3.8	C5H6O
M-Xylene	3.88	4.5	C8H10
1-Phenylethanol	0.22	4.9	C8H10O
1,2-Cyclopentanedione	2.05	5.5	C5H6O2
Cis-2,6-Dimethyl-2,6-octadiene	0.63	5.9	C10H18
1,3,6-Heptatriene, 2,5,6-trimethyl-	0.12	6.0	C10H16
D-Limonene	1.36	6.3	C10H16
3-Ethyltoluene	1.92	6.4	C9H12
Cyclohexanone, 4-methylidene-	0.66	6.7	C7H10O
Phenol	7.99	6.9	C6H6O
4-Cyclooctene-1-methanol	0.60	7.0	C9H16O
1,5-Heptadiene, 3,3,5-trimethyl-	1.51	7.1	C10H18
Benzene, 1,2,3-trimethyl-	0.68	7.2	C9H12
Cis-2,6-Dimethyl-2,6-octadiene	1.44	7.3	C10H18
1,3,6-Heptatriene, 2,5,6-trimethyl-	0.54	7.6	C10H16
(+) -Carvomenthene	1.13	7.8	C10H18
Benzene, 1,4-diethyl-	2.64	7.9	C10H14
O-Cresol	1.89	8.8	C7H8O
P-CRESOL	5.55	9.3	C7H8O
Mequinol	2.61	9.7	C7H8O2
Undecane	0.59	9.9	C11H24
Cosmene	0.55	10.3	C10H14
Phenol, 2-ethyl-	0.34	11.0	C8H10O
Phenol, 2,4-dimethyl-	1.37	11.3	C8H10O
1H-Indene, 1-methyl-	0.33	11.5	C10H10
Phenol, 4-ethyl-	1.70	11.8	C8H10O
Phenol, 2,3-dimethyl-	0.81	11.9	C8H10O
1-Dodecene	0.39	12.4	C12H24
Phenol, 2-methoxy-4-methyl-	2.05	12.5	C8H10O2
1,2-Benzenediol	5.38	13.0	C6H6O2
Benzofuran, 2,3-dihydro-	1.51	13.4	C8H8O
Naphtho[2,3-b] furan-4,9-dione, 2-isopropyl-	0.92	14.5	C15H12O3
Phenol, 4-ethyl-2-methoxy-	1.57	14.9	C9H12O2
1-Tridecene	0.36	15.2	C13H26
Tridecane	0.77	15.4	C13H28
1,2-Benzenediol, 4-methyl-	4.14	15.4	C7H8O2
2-Methoxy-4-vinylphenol	1.37	15.8	C9H10O2

Phenol, 4-(2-propenyl) -	0.25	16.6	C9H10O
Ethanone, 1-(3-methoxyphenyl) -	1.21	17.0	C9H10O2
Phenol, 2-methoxy-4-propyl-	0.36	17.3	C10H14O2
(1-Methylpenta-1,3-dienyl) benzene	0.20	17.4	C12H14
1,2,3-Trimethylindene	0.13	17.6	C12H14
1-Tetradecene	0.31	17.8	C14H28
Tetradecane	0.38	18.0	C14H30
1-Oxetan-2-one, 4,4-diethyl-3-methylene-	0.26	18.2	C8H12O2
Benzaldehyde, 2,4,6-trimethyl-	0.41	18.4	C10H12O
Naphthalene, 2,6-dimethyl-	0.55	18.7	C12H12
Germacrene B	0.13	18.8	C15H24
Isoeugenol	0.66	19.4	C10H12O2
3-(4-Isopropylphenyl) -2-methylpropionaldehyde	0.70	19.7	C13H18O
1-Pentadecene	0.35	20.3	C15H30
Pentadecane	0.36	20.5	C15H32
But-3-enal, 2-methyl-4-(2,6,6-trimethyl-1-cyclohexenyl) -	0.11	20.7	C14H22O
Cyclopentan-1-al, 4-isopropylidene-2-methyl-	0.07	21.0	C10H16O
1-Ethynyl-3,5-dimethyladamantane	0.13	21.8	C14H20
1H-Naphthalen-2-one, 3,4,5,6,7,8-hexahydro-4a,8a-dimethyl-	0.12	22.2	C12H20O
3-(2-Methyl-propenyl) -1H-indene	1.05	22.7	C13H14
Hexadecane	0.15	22.9	C16H34
Tetradecanoic acid	0.88	26.8	C14H28O2
2-Hexadecene, 3,7,11,15-tetramethyl-, [R- [R*, R*-(E)]] -	0.17	28.3	C20H40
Pentadecanoic acid	0.20	28.8	C15H30O2
Oxacycloheptadecan-2-one	1.13	30.2	C16H30O2
Phenanthrene, 2,5-dimethyl-	0.86	32.4	C16H14
Oxacycloheptadec-8-en-2-one	6.28	37.9	C16H28O2
Stigmastan-3,5-diene	0.94	48.5	C29H48
TS 120°C			
α Pinene	11.28	5.0	C10H16
δ-3-Carene	8.91	7.5	C10H16
Limonene	28.61	8.0	C10H16
Terpinen-4-Ol	1.51	12.0	C10H18O
α Terpinene	23.75	16.7	C10H16
α Cubebene	17.75	19.9	C15H24
β Bisabolene	5.71	22.1	C15H24
α Bisabolol	2.47	25.0	C15H26O
TS 350°C			
Furfural	5.55	3.1	C5H4O2
Thujene	2.07	4.9	C10H16
α Pinene	7.61	5.1	C10H16
Sabinene	1.03	6.2	C10H16
β Myrcene	1.29	6.6	C10H16
δ-3-Carene	11.35	7.5	C10H16
Limonene	17.83	8.0	C10H16
γ Terpinene	1.27	8.8	C10H16
Terpinolene	0.94	9.2	C10H16
2-Methoxy-4-vinylphenol	1.12	15.8	C9H10O2
Copaene	0.43	16.6	C15H24
Phenol, 2-methoxy-4-(1-propenyl)	0.63	19.4	C20H24O4
α Cubebene	1.19	19.9	C15H24
Cedrene	0.95	25.0	C15H24
2-Cyclohexen-1-one, 4-(3-hydroxybutyl) -3,5,5-trimethyl-	0.97	25.4	C13H22O2
Tetradecanoic acid	0.67	26.6	C14H28O2
Phytol	0.46	28.1	C20H40O
Cupressene	2.55	30.0	C20H32
Biformen	0.29	30.3	C20H32
Resorcinol, 4-[(2-hydroxy-5-methyl-3-pyridyl) azo] -	2.65	32.5	C12H11N3O3
Kaur-16-ene, (8, beta,13, beta,) -	2.94	33.7	C20H32
Androstane-3,7,17-triol, (3, beta, 5, beta,7, alpha,17, beta,)-	2.97	34.0	C19H32O3
Trans-Totarol	3.71	37.5	C20H32

alkane C27	0.64	42.9	
alkane C29	1.09	45.7	
alkane C31	1.63	48.4	
Stigmastan-3,5-diene	3.73	48.5	C29H48
ketone C29	0.82	48.7	
alkane C33	11.46	51.1	
ketone C31	2.30	51.5	
Oxygenated triterpene	0.95	52.3	
alkane C34	0.66	52.7	
alkane 35	3.60	54.7	
ketone C33	2.07	55.4	
ketone C35	0.70	60.9	
TS 550°C			
1,3-Pentadiene, (Z)-	19.70	1.6	C5H8
Toluene	7.67	3.0	C7H8
M-Xylene	5.22	4.5	C8H10
2-Butenal, 2-ethyl-	1.64	5.5	C6H10O
Phenol	9.26	7.0	C6H6O
Limonene	11.20	8.0	C10H16
Phenol, 3-methyl-	1.97	9.4	C7H8O
Phenol, 2-methoxy-	7.15	9.8	C7H8O2
Phenol, 2-methoxy-4-methyl-	2.49	12.5	C8H10O2
1,2-Benzenediol	6.87	12.8	C6H6O2
Benzofuran, 4,7-dimethyl-	0.66	13.1	C10H10O
Benzofuran, 2,3-dihydro-	1.67	13.4	C8H8O
4-Amino-5,7-dinitrobenzofurazan	1.63	14.4	C6H3N5O5
Phenol, 4-ethyl-2-methoxy-	1.21	14.9	C9H12O2
1,2-Benzenediol, 4-methyl-	2.91	15.2	C7H8O2
2-Methoxy-4-vinylphenol	0.88	15.8	C9H10O2
3-Cyclohexene-1-carboxaldehyde, 4-methyl-	0.38	16.3	C10H16O
Phenol, 2-methoxy-3-(2-propenyl) -	0.63	16.7	C14H13N3O
Benzenemethanamine, N-(1,3-benzodioxol-5-ylmethylidene) -	0.81	17.1	C15H13NO2
1-Tetradecene	0.53	17.7	C14H28
Tetradecane	0.57	18.0	C14H30
Naphthalene, 1,7-dimethyl-	0.96	18.6	C12H12
Phenol, 2-methoxy-4-(1-propenyl) -	0.29	19.3	C10H12O2
Guaia-3,9-diene	0.18	20.9	C15H24
Naphthalene, 1,4-dihydro-2,5,8-trimethyl-	0.16	21.1	C13H16
Azulene, 4,6,8-trimethyl-	0.28	21.3	C13H14
Dodecanoic acid	0.43	22.1	C12H24O2
Naphthalene, 2,3,6-trimethyl-	2.54	22.7	C13H14
Eudalene	0.44	24.6	C14H16
Tetradecanoic acid	0.69	26.5	C14H28O2
2-Propenoic acid, 3-(4-methoxyphenyl) -	0.63	26.9	C10H10O3
Phenanthrene, 1,2,3,4,4a,9,10,10a-octahydro-1,1,4a-trimethyl-	0.38	29.0	C17H24
Anthracene, tetradecahydro-	0.18	29.5	C14H24
10,18-Bisnorabieta-8,11,13-triene	0.44	29.8	C18H26
Anthracene, tetradecahydro-	0.20	30.0	C14H24
Cis-9-Hexadecenoic acid	1.94	30.5	C16H30O2
n-Hexadecanoic acid	0.31	30.6	C16H32O2
Phenanthrene, 2,5-dimethyl-	1.74	32.3	C16H14
HC 21	0.41	33.1	C21H44
Oxacycloheptadec-8-en-2-one	1.06	37.3	C16H28O2
HC 28	0.99	42.9	
HC 29	0.40	44.3	
HC 30	0.27	45	

AIII. 2. Chemical Composition of the volatile gases resulting from the pyrolysis tests on quercus suber L. litter leaves (dry Season), branch and cork samples at high temperature profiles DS (350 – 550°C) and 800°C.

Pyrolysis Temperature: DS 350°C					
			Wood	**Leaves**	**Cork**
Family	**Compound**	**RT (min)**	**Area %**	**Area %**	**Area %**
Furan	Furfural	3.23	2.91	20.31	
Furan	2-Furancarboxaldehyde. 5-methyl-	6.09		2.53	
Ketone	Cyclopentanone. 2-methyl-	5.43	4.82		
Aromatic	Phenol	7.13	5.85	13.00	
Ketone	3-cyclobuten-1.2-dione.3.4 dihydroxy	7.49	8.69		
Aromatic	Phenol-methoxy	9.76	3.18	1.56	4.69
Ketone	2-Cyclopenten-1-one. 3-ethyl-2-hydroxy-	10.65		0.53	
Carbohydrate	4H-Pyran-4-one. 2.3-dihydro-3.5-dihydroxy-6-	11.57		1.59	
Furan	Benzofuran. 2.3-dihydro-	14.02	12.52	19.29	
Vanillin Aldehyde	3.4-Dihydroxyacetophenone	15.26	0.58		
Aromatic	Indole	15.99		2.05	
Aromatic	2-Methoxy-4-vinylphenol	16.21	6.87	5.65	14.98
Aromatic	Phenol. 2-methoxy-4-(2-propenyl)-	17.17			0.62
Aromatic	Phenol. 2.6-dimethoxy-	17.30	6.22	1.70	
Aromatic	Phenol. 2-methoxy-3-(1-propenyl)-	18.60	0.40		
Phenolic	Vanillin	18.77			4.56
Phenolic	4-Hydroxy-2-methoxybenzaldehyde	18.79	0.57		
Aromatic	1.2.4-Trimethoxybenzene	19.68	0.96	0.44	
Aromatic	Phenol. 2-methoxy-4-(1-propenyl)-	19.82	5.99	1.76	6.67
Phenol	Ethanone. 1-(4-hydroxy-3-methoxyphenyl)-	20.88			2.02
Armatic	Benzene. 1.2.3-trimethoxy-5-methyl-	21.52	1.19	0.50	
Ketone	2-Propanone. 1-(4-hydroxy-3-methoxyphenyl)-	21.89	2.21		2.46
Levoglucosan	.beta.-D-Glucopyranose. 1.6-anhydro-	22.52			3.10
Ketone	3'.5'-Dimethoxyacetophenone	22.69	8.71	3.04	
Aromatic	Phenol. 2.6-dimethoxy-4-(2-propenyl)-	25.86	8.28	2.44	
Benzoic acid	Methyl-(2-hydoxy-3-ethoxy-benzyl)ether	24.79	0.77		1.85
Aldehyde	Benzaldehyde. 4-hydroxy-3.5-dimethoxy-	25.11	0.55		
Ketone	Ethanone. 1-(4-hydroxy-3.5-dimethoxyphenyl)-	26.63	0.46		
Aromatic	4-((1E)-3-Hydroxy-1-propenyl)-2-	27.00	0.80		
Aromatic	3.4-Dimethoxy-6-amino toluene	27.35	3.41		
Alcohol	Tetramethyl-hexadecenol	28.02	0.41		
Aliphatic	Eicosyne	28.91		1.58	
Ester	Dibutyl phthalate	30.93	2.52		
Acid	n-Hexadecanoic acid	31.10	1.67	3.60	
Ester	Hexadecanoic acid. ethyl ester	31.31	0.78		
Ester	octadecanoic acid-methyl ester	33.80			0.22
Acid	Octadecadienoic acid	34.29	0.61	4.88	
Ester	Linoleic acid ethyl ester	34.45	0.92		
Ester	Ethyl octadecatrienoate	34.59	0.66		
	Unidentified	37.41	0.34.		
Alcohol	Alcohol	40.07			5.74
Aliphatic	Alkane	42.92	0.45		
Alcohol	Alcohol	43.12		1.77	
Furans	7-(3,4 méthylènedioxy)tétrahydrobenzofuranone.	43.29	1.52		
Aliphatic	AlkaneC29	45.72	2.52	3.63	
Aliphatic	Alkane C30	47.05		0.56	
Aliphatic	Alkane C31	48.32		1.53	
Steroid Aliphatic	Stigmastadiene	48.67		0.15	
	Vitamin E	49.06		0.98	
phytosterol	Sitosterol	52.13	0.04	0.18	
Steroid ketone	Stigmasta-3.5-dien-7-one	53.92			0.47
Steroid ketone	Stigmast-4-en-3-one	54.76			3.76
Triterpenoid	Friedelan-3-one	57.60			43.86
Triterpenoid	3.12-Oleandione	62.01			4.98

Pyrolysis Temperature: DS 550°C			Wood	Leaves	Cork
		RT (min)	Area %	Area %	Area %
Aromatic	Toluene	2.97	6.68	13.04	4.43
Aliphatic	1-Octene	3.09			2.08
Aliphatic	Octane	3.21			1.02
Acid	Pyrrolidin-1-acetic acid	3.54	1.72		
Furan	Furan.dimethyl-	3.94	3.27	1.70	
Furan	Furan.methyl-	4.02	2.84		
Furan	Furanmethanol	4.37	1.24	0.88	
Aliphatic	1-Nonene	4.63			1.15
Aliphatic	Nonane	4.78			0.96
Aromatic	Styrene	4.91	0.65	1.41	
Aromatic	Benzene. 1.3-dimethyl-	4.92			0.88
Ketone	2-Cyclopenten-1-one. 2-methyl-	5.24		0.60	
Furan	2(5H)-Furanone	5.81	5.49	2.49	
Furan	2(3H)-Furanone. 5-methyl-	6.09	8.62	3.71	
Furan	2-Furancarboxaldehyde. 5-methyl-	6.54		0.84	
Alkene	1-Decene	6.82			0.99
Alkane	Octane. 4-ethyl-	7.01			0.86
Aromatic	Phenol	7.37	12.25	24.28	
Ketone	2-Cyclopenten-1-one. 2-hydroxy-3-methyl-	8.58	5.15	2.19	
Aromatic	Phenol. 2-methyl-	9.24	1.51	1.15	
Alkene	1-Undecene	9.47			0.89
Alkane	Undecane	9.66			0.78
Aromatic	Phenol. 3-methyl-	9.78		8.92	
Aromatic	Phenol. 2-methoxy-	9.98	9.89	4.73	10.42
Aromatic	Phenol. 2.4-dimethyl-	11.75		0.68	
Alkene	1-Dodecene	12.27			0.71
Aromatic	Phenol. 4-(methoxymethyl)-	12.33		1.70	
Alkane	Dodecane	12.46			0.88
Aromatic	Phenol. 2-methoxy-4-methyl-	12.83	4.95	3.17	7.09
Ketone	1.2-Benzenediol	13.94	3.49		
Aromatic	Dimethoxytoluene	14.03	0.17		
Furan	Benzofuran. 2.3-dihydro-	14.09	0.45	3.68	
Ketone	1.2-Benzenediol. 3-methoxy-	14.93		1.78	
Alkene	1-Tridecene	15.05			0.83
Aromatic	Phenol. 4-ethyl-2-methoxy-	15.12	3.29	1.89	5.83
Aromatic	Indolizine	16.03		1.43	
Aromatic	2-Methoxy-4-vinylphenol	16.27	4.91	5.97	12.49
Aromatic	Phenol. 2.6-dimethoxy-	17.40	9.83	3.29	
Aliphatic	1-Tetradecene	17.73			0.97
Aliphatic	Tetradecane	17.89			1.03
Aromatic	1.2.4-Trimethoxybenzene	19.76	5.19	2.17	
Aromatic	Phenol. 2-methoxy-4-(1-propenyl)-	19.83	1.35		0.91
Aliphatic	1-Pentadecene	20.28			1.08
Aliphatic	Pentadecane	20.42			1.12
Aromatic	Benzene. 1.2.3-trimethoxy-5-methyl-	21.58	2.40	0.85	
Acid	3-tert-Butyl-4-hydroxyanisole	22.62		1.49	
Aliphatic	Hexadecene	22.70			0.97
Ketone	3'.5'-Dimethoxyacetophenone	22.72	4.79		
Aliphatic	hexadecane	22.83			1.03
Aliphatic	1-Heptadecene	24.99			0.96
Aliphatic	heptadecane	25.11			1.00
Aromatic	Phenol. 2.6-dimethoxy-4-(2-propenyl)-	25.85	1.70		
Aliphatic	1-Octadecene	27.18			1.07
Aliphatic	Octadecane	27.28			1.13
Aliphatic	1-Nonadecene	29.26			1.20
Aliphatic	Nonadecane	29.35			1.22
Acid	n-Hexadecanoic acid	31.11		0.92	
Aliphatic	1.19-Eicosadiene	31.14			1.08
Aliphatic	Alkene C20	31.25			1.76
Aliphatic	Tritetracontane	31.33			1.48
Aliphatic	Alkene C21	33.16			3.17
Aliphatic	Heneicosane	33.22			2.19
Aliphatic	Alkene C22	34.97			5.75
Aliphatic	Docosane	35.02			1.21

Aliphatic	1-Tricosene	36.68			1.47
Aliphatic	Tricosane	36.73			1.31
Aliphatic	Tetracosene	38.29	0.29		
Aliphatic	Alkene C24	38.36			2.59
Aliphatic	Alkene C24	38.49			0.57
Ester	Methyl 18-methylicosanoate	39.02			0.27
Ester	13-Docosenoic acid. methyl ester. (Z)-	40.60			2.18
Acid	Erucic acid	40.96			2.02
Aliphatic	17-Pentatriacontene	41.48			0.91
Acid	Tetracosenoic acid	43.94			1.65
Aliphatic	Alkene C28	48.27			1.02
Aliphatic	Alkene C28	48.44			0.21
Steroid Aliphatic	Stigmastan-3.5-diene	48.81	0.36	0.32	0.11
Aliphatic	Alkene C29	49.25			0.10
Steroid Ketone	Stigmast-4-en-3-one	55.03			0.49
Triterpenoid	Friedelan-3-one	57.94			0.66
Triterpenoid	3.12-Oleandione	62.43			0.15

Pyrolysis temperature: 800°C			**Wood**	**Leaves**	**Cork**
		RT (min)	**Area %**	**Area %**	**Area %**
Aromatic	Toluene	2.88	30.16	23.93	21.43
Aliphatic	Octene	3.03			4.04
Fatty acid	Pyridine. 2-methyl-	3.77		0.68	
Furan	Furan. 2.5-dimethyl-	3.90			1.04
Furan	Furfural	3.91		7.75	
Furan	Dimethyl furan	3.92	4.70		
Furan	Methyl furan	4.00	1.97		
Aromatic	Ethylbenzene	4.23	4.07	5.44	5.32
Furan	2-furanmethanol	4.33		0.58	
Aromatic	P-xylene	4.41	3.34	2.34	7.23
Fatty acid	Pyridine. 3-methyl-	4.56		0.52	
Aliphatic	Nonene	4.58			1.93
Aromatic	Styrene	4.88	4.98	5.81	7.52
Aromatic	Benzene. propyl-	6.13		0.79	1.08
Aromatic	Benzene. trimethyl-	6.30			0.86
Furan	2-furancarboxaldehyde. 5-methyl-	6.57		1.29	
Aliphatic	Decadiene	6.63			0.92
Aliphatic	1-decene	6.81		0.46	1.92
Aromatic	Benzene ethenyl-methyl-	7.24		0.73	2.30
Aromatic	Phenol	7.32	14.53	20.73	3.31
Aromatic	Benzene. propenyl-	7.37			1.13
Aromatic	Benzene. 1-ethenyl-4-methyl-	8.07	0.24		
Ketone	1.2-cyclopentanedione. 3-methyl-	8.44	1.11		
Protein	Indene	8.65	1.96	1.56	3.00
Aromatic	Phenol. 2-methyl-	9.21	2.97	1.47	1.47
Aliphatic	Undecadiene	9.28			0.79
Aliphatic	Undecene	9.47			1.08
Aromatic	Phenol. 3-methyl-	9.89		7.33	2.97
Aromatic	Methoxy phenol	9.96	6.67		
Ester	3-hydroxypyridine monoacetate	10.82	2.38		
Aliphatic	1h-Indene. Methyl-	11.55		0.24	0.58
Aliphatic	Dodecadiene	12.08			0.72
Aliphatic	Dodecene	12.28		0.29	0.68
Aromatic	Phenol. 3-ethyl-	12.45	1.67		
Aromatic	Phenol. 4-ethyl-	12.46		3.11	
Aromatic	Azulene	12.75	1.95	1.70	
Aromatic	Naphthalene	12.76			2.93
Furan	Benzofuran. 2.3-dihydro-	14.19	0.89	13.26	

Ketone	Benzenediol	13.86			4.78
Ketone	1.2-benzenediol	13.98	2.75		
Aromatic	2-isopropoxyphenol	14.30	7.61		
Aliphatic	Tridecadiene	14.88			1.02
Aliphatic	Tridecene	15.06			0.69
Aldehyde	1.4-benzenedicarboxaldehyde. 2-methyl-	15.16	0.22		
Aromatic	Naphthalene. 2-methyl-	15.83	0.57		0.93
Aromatic	Phenol. 4-(2-propenyl)-	15.96	1.06		0.59
Ketone	Benzenediol. -methyl-	16.39			0.42
Aliphatic	1h-Indene Hexamethyl Hexahydro	17.34			1.36
Aliphatic	Tetradecadiene	17.57			0.73
Aliphatic	Tetradecene	17.74			0.68
Aliphatic	Pentadecadiene	20.13			0.57
Aliphatic	Pentadecene	20.28			0.71
Aliphatic	Hexadecadiene	22.57			0.78
Aliphatic	Hexadecene	22.70			0.49
Aliphatic	Heptadecadiene	24.87			0.64
Aliphatic	Heptadecene	24.99			0.33
Aliphatic	Octadecadiene	27.07			0.55
Aliphatic	Octadecene	27.17			0.36
Aliphatic	Nonadecadiene	29.16			0.37
Aliphatic	Nonadecene	29.25			0.30
Aliphatic	Eicosadiene	31.15			0.45
Aliphatic	Eicosene	31.23			0.39
Aliphatic	Heneicosene	33.13			0.60
Aliphatic	Docosene	34.94			0.55
Aliphatic	Tricosene	36.66			0.10
Aliphatic	Tetracosene	38.33			0.39
Fame	Docosenoic acid. methyl ester	40.54			0.11
Acid	Erucic acid	40.90			0.14
Pentacyclic triterpenoid	Friedelanone	57.63			4.35
Pentacyclic triterpenoid	Oleandione	62.00			0.04

APPENDIX IV

AIV.1. Relative abundance (%) of pyrolysis emissions identified and categorized from control and drought-stressed leaves of *R. officinalis* at 180°C for 1 min. N.I.: Not Identified.

Compound	Relative Abundance %		
	Family	**Control**	**Drought-stressed**
(-) α-pinene	Monoterpene	17.50	10.17
Camphene	Monoterpene	1.68	1.95
(+) α-pinene	Monoterpene	0.39	1.02
β-pinene	Monoterpene	1.03	0.16
β-myrcene	Monoterpene	1.28	0.45
α-phellandrene	Monoterpene	0.38	0.11
3-carene	Monoterpene	0.95	0.39
trans-3-Caren-2-ol	Monoterpene	0.42	0.97
Limonene	Monoterpene	2.08	1.11
Eucalyptol	Monoterpene	5.32	2.35
Isopulegol	Monoterpene	N.I.	0.35
Monoterpene / Mw = 154	Monoterpene	N.I.	0.59
Dehydroabietan	Diterpene	0.14	0.19
Octadecanol	Fatty alcohol	N.I.	0.08
Octadecanoic acid	Fatty acid	N.I.	0.27
Kaurene	Diterpene	N.I.	0.06
Diterpene	Diterpene	N.I.	0.12
Cupressene	Diterpene	0.06	N.I.
Phytol	Diterpene	0.21	N.I.
Viridiflorol	Diterpene	0.05	N.I.
Podocarpa-6,8,11,13-tetraen-12-ol, 13-isopropyl-, acetate	Diterpene	0.07	N.I.
Ferruginol	Diterpene	0.59	0.87
Pentacosane	Alkane	0.08	0.15
Diterpene	Diterpene	N.I.	0.28
Diisooctyl phthalate	Phtalate	N.I.	0.16
Trans-totarol	Diterpene	0.14	N.I.
Hexacosane	Alkane	0.06	0.14
Docosyl acetate	Acetate	0.06	0.23
Heptacosane	Alkane	1.25	2.85
Octacosane	Alkane	0.37	0.78
Tetracosyl acetate	Acetate	0.12	0.23
Squalene	Diterpene	0.06	N.I.
1-methylheptacosane	Branched alkane	0.05	0.14
Nonacosane	Alkane	2.76	6.70
2-methyloctacosane	Branched alkane	N.I.	0.13
Triacontane	Alkane	0.11	0.38
1-methylnonacosane	Branched alkane	N.I.	0.24
Hentriacontane	Alkane	0.70	2.90
Vitamin E	Others	N.I.	0.17
2-methyltriacontane	Branched alkane	N.I.	0.17
Dotriacontane	Alkane	0.04	0.22
1-methyhentriacontane	Branched alkane	N.I.	0.22
Tritriacontane	Alkane	0.28	1.73
β-amyrone	Triterpene	1.87	0.94
Triterpene	Triterpene	N.I.	0.63
1-methyltritriacontane	Branched alkane	N.I.	0.10
α-amyrenone	Triterpene	1.40	0.24
γ-terpinene	Monoterpene	0.70	0.15

4-tujanol	Monoterpene	0.21	N.I.
4-carene	Monoterpene	1.18	0.16
Linalool	Monoterpene	3.82	1.53
Monoterpene / Mw = 154	Monoterpene	N.I.	0.54
Chrysantenone	Monoterpene	0.33	N.I.
(+-) Camphor	Monoterpene	13.43	5.87
(+-) Borneol	Monoterpene	12.31	9.69
(-) endo & iso-borneol	Monoterpene	N.I.	4.65
Pinocamphone	Monoterpene	2.35	N.I.
Terpineol	Monoterpene	2.62	1.05
Isobornyl formate	Monoterpene	N.I.	0.47
(+-) Verbenone	Monoterpene	13.74	9.57
(-) cis-myrtanol	Monoterpene	N.I.	0.24
Borneol acetate	Monoterpene	1.80	0.50
4-Vinylguaiacol	Monoterpene	N.I.	0.34
3,5-Heptadienal, 2-ethylidene-6-methyl-	Monoterpene	N.I.	0.13
Eugenol	Monoterpene	N.I.	0.18
Copaene	Monoterpene	N.I.	0.22
Methyl eugenol	Monoterpene	0.24	0.11
β-caryophyllene	Sesquiterpene	1.21	1.22
α-bergamotene	Sesquiterpene	0.22	0.14
α-caryophyllene	Sesquiterpene	0.61	0.59
γ-muurolene	Sesquiterpene	0.17	0.20
α-cadinene	Sesquiterpene	0.08	N.I.
β-bisabolene	Sesquiterpene	0.14	0.17
γ-cadinene	Sesquiterpene	0.19	0.21
δ-cadinene	Sesquiterpene	0.41	0.46
Dodecanoic acid	Fatty acid	N.I.	1.34
(Z)-3-Hexenyl Benzoate	Others	0.21	0.05
Caryophyllen alcohol	Sesquiterpene	0.06	N.I.
Caryophyllene oxide	Sesquiterpene	0.05	0.05
Methyl jasmonate	Others	0.77	0.36
α-cadinol	Sesquiterpene	0.03	0.03
Viridiflorol	Sesquiterpene	N.I.	0.10
α-bisabolol	Sesquiterpene	0.15	0.17
Tetradecanoic acid	Fatty acid	N.I.	0.43
Ascabiol	Sesquiterpene	N.I.	0.44
Pentadecanol	Fatty alcohol	0.25	0.15
Unsaturated fatty acid	Fatty acid	N.I.	0.20
Diisobutyl phtalate	Phtalate	N.I.	0.04
Hexadecanol	Fatty alcohol	0.27	1.64
Geranylgeraniol	Sesquiterpene	0.38	0.64
Hexadecanoic acid	Fatty acid	N.I.	2.19
Epiglobulol	Sesquiterpene	0.07	0.26
Hibaene	Diterpene	0.04	0.04
Trachylobane	Diterpene	0.04	0.04
Unsaturated fatty acid	Fatty acid	N.I.	0.10

AIV.2. Relative abundance (%) of emissions from control vs drought-stressed leaves of *C. albidus*.

Compound		Relative Abundance (%)	
	Family	Control	Drought-stressed
Nonanal	Aldehyde	0.69	2.62
Octanoic acid	Fatty acid	N.I.	0,50
Nonanoic acid	Fatty acid	0,54	4,23
Decanoic acid	Fatty acid	N.I.	0,11
α-bourbonene	Sesquiterpene	0,11	N.I.
β-Caryophyllene	Sesquiterpene	0,12	N.I.
Aromadendrene	Sesquiterpene	0,05	N.I.
δ-germacrene	Sesquiterpene	0,34	N.I.
9-Oxononanoic acid	Fatty acid	N.I.	0,65
δ-cadinene	Sesquiterpene	0,14	N.I.
Elemol	Sesquiterpene	0,46	N.I.
Dodecanoic acid	Fatty acid	0,78	7,26
Nonacosane	Alkane	N.I.	6,12
4a,8a-dimethyl-7-propan-2-yl-5,6,7,8-tetrahydro-1H-naphthalen-2-one	Ketone	0,47	N.I.
Tetradecanoic acid	Fatty acid	0,41	2,99
Hexadecanoic acid	Fatty acid	2,96	8,89
Manoyl oxide	Diterpenoid	0,07	N.I.
Heicosane	Alkane	N.I.	9,36
Heneicosane	Alkane	N.I.	3,63
Oleic acid	Fatty acid	1,80	1,08
Octadecanoic acid	Fatty acid	0,54	1,09
Docosane	Alkane	N.I.	3,02
Tricosane	Alkane	1,22	2,16
Tetracosane	Alkane	0,22	0,91
Pentacosane	Alkane	2,07	2,81
Tetracosanol	Fatty alcohol	N.I.	0,16
Hexacosane	Alkane	0,34	0,35
Heptacosane	Alkane	13,47	9,14
Hexacosanol	Fatty alcohol	N.I.	0,14
Octacosane	Alkane	1,91	1,36
Squalene	Triterpene	0,84	N.I.
Nonacosane	Alkane	47,18	15,92
Triacontane	Alkane	1,51	1,06
Hentriacontane	Alkane	17,11	11,23
Vitamin E	Others	N.I.	2,35
Dotriacontane	Alkane	0,36	0,12
Tritriacontane	Alkane	N.I.	0,73
Lupenone	Triterpene	0,99	N.I.
Polycyclic (M=426)	Others	3,31	N.I.

AIV.3. Comparative study between fresh and drought-stressed *R. officinalis* subjected to thermal stresses on a plant scale. Emissions collected by ECOM gas analyzer include methane gas (CH_4), CO and H_2O.

	R. Officinalis Fresh (RF)					
Criteria	RF1	RF2	RF3	RF 19&13	RF 9&15	RF 7&12
ImageJ Area cm^2	NA	NA	NA	321.876	357.63	368.551
Initial Weight (grams)	NA	75,77	81,66	59,77	60,08	68,9
Final Weight (grams)	NA	9,31	18,503	14,2	11,5	11,8
Weight Loss %	NA	87,71	77,34	76,24	80,86	82,87
Dehydration (H_2O) %	1.2	0.45	1.8	1.44	1.62	0.36
Time of Dehydration (mins)	10	12	8	15	22	11
Methane Gas Emissions (C_xH_y)						
CH_4 Max (ppm)	62	80	26	NA	26	34
Duration of Emissions (mins)	33	24	17	NA	21	38
Tgas (°C) Initial	57	58	65	NA	39.7	117
Tgas (°C) Final	74	80,7	74	NA	67	129
Tplant (°C) Initial	55	160	180	NA	199	207
Tplant (°C) Final	160	200	220	NA	217	219
CO Emissions						
CO Max (ppm)	1107	2118	NA	76	424	402
Duration of Emission (mins)	53	40	NA	15	41	33
Tgas (°C) Initial	24	31	NA	45	19	39.5
Tgas (°C) Final	75	72	NA	60.8	67	63
Tplant (°C) Initial	28	17	NA	152	24	125
Tplant (°C) Final	220	210	NA	215	218	211

	R. Officinalis Hydric Stressed (HS)				
Criteria	RHS4	RHS5	RHS2	RHS1	RHS3
ImageJ Area cm^2	238,013	359,853	117,963	303	259,144
Initial Weight (grams)	53,2	73,96	37,8	69,16	37,8
Final Weight (grams)	14,16	19,66	5	26,7	9,8
Weight Loss %	73,38	73,42	86,77	61,39	74,07
Dehydration (H_2O) %	0.3	0.4	NA	NA	NA
Time of Dehydration (mins)	2	17	NA	NA	NA
Methane Gas Emissions (C_xH_y)					
CH_4 Max (ppm)	84	90	NA	NA	NA
Duration of Emissions (mins)	23	22	NA	NA	NA
Tgas (°C) Initial	109	120	NA	NA	NA
Tgas (°C) Final	139	147	NA	NA	NA
Tplant (°C) Initial	167	210	NA	NA	NA
Tplant (°C) Final	252	221	NA	NA	NA
CO Emissions					
CO Max (ppm)	1034	1697	878	NA	NA
Duration of Emission (mins)	10	16	13	NA	NA
Tgas (°C) Initial	141	62	126	NA	NA
Tgas (°C) Final	141	142	144	NA	NA
Tplant (°C) Initial	139	160	206	NA	NA
Tplant (°C) Final	141	216	215	NA	NA

Tgas: Temperature of gases emitted as recorded by ECOM.

Tplant: Temperature at plant level as recorded by the thermocouples inside the compartment.

H_2O (%): The percentage of H_2O recorded by ECOM.

Dehydration Stage: Defined from the first recording of H_2O until the first recording methane CH_4. This last signaling volatilization.

NA: Not applicable: ECOM Failure.

AIV.4. Comparative study between fresh and drought-stressed *C. albidus* subjected to thermal stresses on a plant scale. Emissions collected by ECOM gas analyzer include methane gas (CH_4), CO and H_2O.

C. Albidus Fresh (CF)			
Criteria	CF1	CF2	CF3
Initial Weight	58,3	69,33	80,06
Final Weight	0	22,3	24,08
Weight Loss %	100,00	67,83	69,92
Dehydration (H_2O) %	0.43	0.26	0.46
Time of Dehydration (mins)	16	11	13
Methane Gas Emissions (CH_4)			
CH_4 Max (ppm)	NA	34	44
Duration of Emissions (mins)	NA	10	26
Tgas (°C) Initial	NA	12.4	126
Tgas (°C) Final	NA	13.7	130
Tplant (°C) Initial	NA	187	211
Tplant (°C) Final	NA	226	226
CO Emissions			
CO Max (ppm)	20	132	824
Duration of Emissions (mins)	4	9	15
Tgas (°C) Initial	16	13.6	126
Tgas (°C) Final	19	21	60
Tplant (°C) Initial	16	181	79
Tplant (°C) Final	203	218	219
C. Albidus Hydric Stressed (HS)			
Criteria	CHS4	CHS1	CHS2+CHS3
Initial Weight	85	65	70
Final Weight	29,44	18,16	25,2
Weight Loss %	65,36	72,06	64
Dehydration (H2O) %	0.5	0.5	0.6
Time of Dehydration (mins)	11	12	8
Methane Gas Emissions (CH_4)			
CH_4 Max (ppm)	39	33	29
Duration of Emissions (mins)	24	23	30
Tgas (°C) Initial	49	65	67
Tgas (°C) Final	58	68	60
Tplant (°C) Initial	141	211	171
Tplant (°C) Final	186	241	200
CO Emissions			
CO Max (ppm)	NA	NA	NA
Duration of Emissions (mins)	NA	NA	NA
Tgas (°C) initial	NA	NA	NA
Tgas (°C) Final	NA	NA	NA
Tplant (°C) Initial	NA	NA	NA
Tplant (°C) Final	NA	NA	NA

Tgas: Temperature of gases emitted as recorded by ECOM.

Tplant: Temperature at plant level as recorded by the thermocouples inside the compartment.

H_2O (%): The percentage of H_2O recorded by ECOM.

Dehydration Stage: Defined from the first recording of H_2O until the first recording of CH_4. This last signaling volatilization.

NA: Not applicable: ECOM failure.

AIV.5. Emissions during the pre- and post-glowing phases of fresh *R. officinalis* under thermal stresses, on plant level, in the hermetic enclosure using the adsorption/desorption techniques with Magic Chemisorber.

		Pre-Glowing	**Post-Glowing**
Compound Name	**RT (min)**	**%**	**%**
m-cresol	9,268	0,11919	
Heptanoic acid	9,334	0,13104	
Mequinol	9,456	0,20281	
3-Pyiridinol	10,757	0,18099	
Camphor	10,82	0,30756	
Terpineol	11,712	3,29612	
Verbenone	12,886	0,89522	
Coumaran	13,378	0,79735	
4-Vinylguaiacol	15,773	1,1282	
Syringol	16,765	1,06959	
β-Caryophyllene	18,582	0,48267	
Methylsyringol	19,228	0,24625	
Isoeugenol	19,319	0,33416	
α-caryophyllene	19,452	0,33123	
γ-muurolene	19,988	0,13892	
1,6-Anhydro-D-Galactose	20,32	1,17533	
δ-cadinene	21,122	0,35162	
3,4,5-Trimethoxytoluene	21,183	0,66452	
Guaiacylacetone	21,356	0,48769	
3',5'-Dimethoxyacetophenone	22,136	1,00199	
Methoxyeugenol	25,238	0,55477	
Homosyringic acid	26,798	0,7012	
3,7,11,15-Tetramethyl-2-hexadecenol (2^{nd} isomer)	28,028	1,15396	
3,7,11,15-Tetramethyl-2-hexadecenol (1^{st} isomer)	28,907	0,88603	
Hexadecanoic acid	30,532	0,762	
N.I.	32,5	0,38759	
Phytol	33,391	1,09009	
N.I.	36,68	1,89164	
Ferruginol	37,303	1,93724	1,13501
Sugiol	38,052	0,14956	0,48165
N.I.	38,233	0,38677	
N.I. (m/z = 298)	39,095	0,18829	
N.I. (m/z = 296)	39,238	0,26325	
Pentacosane (C25)	39,802	1,06535	0,59275
13-Isopropylpodocarpen-12-ol-20-al	40,53	0,43989	0,28403
Phtalate	40,628	0,82308	0,46255
Hexacosane (C26)	41,328	0,63676	0,34544
N.I. (m/z = 310)	41,487	0,15958	
N.I. (m/z = 298)	42,027	0,62979	
2-methylhexacosane	42,261	0,20431	0,10013
N.I. (m/z = 296)	42,54	0,04924	

Heptacosane (C27)	42,803	9,62018	3,87986
1-methylheptacosane	43,855	0,38128	0,17079
Octacosane (C28)	44,218	2,13366	0,90105
Tetracosyl acetate	44,409	0,25493	
Squalene	44,683	0,27056	0,19362
2-methyloctacosane	45,092	1,43308	0,5543
1-methyloctacosane	45,245	0,08808	
Nonacosane (C29)	45,607	21,32253	7,98345
2-methylnonacosane	46,436	0,14134	
1-methylnonacosane	46,585	1,87334	0,75742
Triacontane (C30)	46,925	1,34726	0,52041
2-methyltriacontane	47,739	1,5257	0,59989
1-methyltriacontane	47,892	0,21098	
Hentriacontane (C31)	48,221	11,5111	4,22691
β-sitostreol acetate	48,426		0,16229
Vitamin E	48,836	1,89949	0,98882
2-methylhentriacontane	49,007	0,13883	
1-methylhentriacontane	49,154	1,83171	0,76674
Dotriacontane (C32)	49,485	1,03025	0,416
2-methyldotriacontane	50,341	1,17367	0,51062
1-methyldotriacontane	50,516	0,20987	
Tritriacontane (C33)	50,891	8,05408	3,24919
β-amyrone	51,807	1,67316	3,78256
1-methyltritriacontane	52,089	0,94611	0,03114
α-amyrenone	52,576	1,27726	2,73437
Pollinastanol	52,735	0,35461	0,10516
α-amyrin	53,04	0,02863	0,19124
Lupenone	54,249	0,01907	0,01225
Pentatriacontane (C35)	54,449	0,18345	0,0608
N.I.	57,058	0,31248	

N.I. Not Identified.

RT: Retention Time.

*Empty cells mean compound not detected.